Polymer-Based Advanced Functional Composites for Optoelectronic and Energy Applications

Polymer-Based Advanced Functional Composites for Optoelectronic and Energy Applications

Edited by

NITHIN KUNDACHIRA SUBRAMANI

Asst Professor, Dept. of Chemistry, and Coordinator (Centre for Research and Development), The National Institute of Engineering, Mysuru, India

H. SIDDARAMAIAH†

Vice-Chancellor of JSS Science and Technology University, Mysuru, India

JOONG HEE LEE

Vice President of Jeonbuk National University, Republic of Korea



ELSEVIER

† Deceased.

Elsevier
Radarweg 29, PO Box 211, 1000 AE Amsterdam, Netherlands
The Boulevard, Langford Lane, Kidlington, Oxford OX5 1GB, United Kingdom
50 Hampshire Street, 5th Floor, Cambridge, MA 02139, United States

Copyright © 2021 Elsevier Inc. All rights reserved.

No part of this publication may be reproduced or transmitted in any form or by any means, electronic or mechanical, including photocopying, recording, or any information storage and retrieval system, without permission in writing from the publisher. Details on how to seek permission, further information about the Publisher's permissions policies and our arrangements with organizations such as the Copyright Clearance Center and the Copyright Licensing Agency, can be found at our website: www.elsevier.com/permissions.

This book and the individual contributions contained in it are protected under copyright by the Publisher (other than as may be noted herein).

Notices
Knowledge and best practice in this field are constantly changing. As new research and experience broaden our understanding, changes in research methods, professional practices, or medical treatment may become necessary.

Practitioners and researchers must always rely on their own experience and knowledge in evaluating and using any information, methods, compounds, or experiments described herein. In using such information or methods they should be mindful of their own safety and the safety of others, including parties for whom they have a professional responsibility.

To the fullest extent of the law, neither the Publisher nor the authors, contributors, or editors, assume any liability for any injury and/or damage to persons or property as a matter of products liability, negligence or otherwise, or from any use or operation of any methods, products, instructions, or ideas contained in the material herein.

Library of Congress Cataloging-in-Publication Data
A catalog record for this book is available from the Library of Congress

British Library Cataloguing-in-Publication Data
A catalogue record for this book is available from the British Library

ISBN: 978-0-12-818484-4

For information on all Elsevier publications
visit our website at https://www.elsevier.com/books-and-journals

Publisher: Matthew Deans
Acquisitions Editor: Edward Payne
Editorial Project Manager: Mariana C.Henriques
Production Project Manager: Poulouse Joseph
Cover Designer: Greg Harris

Typeset by SPi Global, India



In Memoriam of H. Siddaramaiah

In loving memory of beloved professor Dr. Siddaramaiah, Vice Chancellor, JSS Science and Technology University, Mysuru.



Dear meastre,

Words are often incapable of expressing the heart's language. However, within the limits of the lexicon, we, the proud alumni of Dr. polymer's lab, express our sincere pranams to our beloved Siddu, for all that we are today and will be in times to come. As someone rightly quoted, "When someone you love becomes a memory, that memory becomes a treasure." You are one of our most loved ones and an invaluable treasure. Going forward, we truly believe that "Death may end one's life and part his body from the other, but never a genuine relationship or collaborative thought, for that matter."

You were, you are, and you will always be our pride meastre.

Dedication

We humbly bow our heads and dedicate this book to God Almighty for giving us the perseverance to complete this work. We also dedicate this contribution to our beloved family members (both personal and professional) for their unconditional support and blessings throughout our lives.

Dr. Nithin Kundachira Subramani
Dr. H. Siddaramaiah[†]
Dr. Joong Hee Lee

[†] Deceased.

Contents

Contributors xv
Foreword by Dong Won Kim. xix
Foreword by Sudhanva. xxi
Preface xxiii
Acknowledgments xxv

Chapter 1 Polymer-based smart composites and/or nanocomposites for optical, optoelectronic, and energy applications: A brief introduction. 1
K.S. Nithin, S. Sachhidananda, K.N. Shilpa, S. Sandeep, C.S. Karthik, B.M. Jagajeevan Raj, and H. Siddaramaiah†

1.1 Introduction 1
1.2 Classification of PBSCs 3
1.3 Important types of stimuli-responsive PBSCs: Properties and related applications 3
1.4 Conclusions and future directions 22
References 23

Chapter 2 Conjugated polymer-based smart composites for optoelectronics and energy applications 31
Smitha V. Kamath, Kanakaraj Aruchamy, and Nataraj Sanna Kotrappanavar

2.1 Introduction 31
2.2 Importance of optoelectronic materials. 32
2.3 Various types of materials used in optoelectronic devices 34
2.4 Working principle of optoelectronic materials 36
2.5 Smart materials for optoelectronic and energy applications . . 37

† Deceased.

2.6 Conclusions and future directions 46
Acknowledgment 46
References 46

Chapter 3 Metal oxide nanofillers introduced polymer-based composites with advanced optical, optoelectronic, and electrical energy storage functionalities 51
S. Sachhidananda, B.K. Sarojini, K.S. Nithin, K.N. Shilpa, B.M. Jagajeevan Raj, K.A. Muthappa, H. Siddaramaiah†, and A. Sahaya Anselin Nisha,

3.1 Introduction 51
3.2 What is nanotechnology? 52
3.3 History of nanotechnology 53
3.4 Operating at the nanoscale 53
3.5 Polymers as advanced functional matrices 54
3.6 Functional additives and/or fillers 56
3.7 Polymer nanocomposites 67
3.8 Conclusions and future directions 80
References 81

Chapter 4 Tools and techniques toward characterizing polymer-based smart composites for optical, optoelectronic, and energy-related applications 91
K.S. Nithin, K.N. Shilpa, Rohini Thimmaiah, B.M. Jagajeevan Raj, S. Sachhidananda, and H. Siddaramaiah†

4.1 Introduction 91
4.2 Tools and techniques adopted for the characterization of polymer-based smart composites of optical, optoelectronic and electrical interest 92
4.3 Conclusions and future directions 111
References 111

† Deceased.

Chapter 5 Mechanically flexible and visibly transparent polymer-based nanocomposites for UV-protective applications 117
B.M. Jagajeevan Raj, K.S. Nithin, K.N. Shilpa, S. Sachhidananda, S. Sandeep, H. Siddaramaiah† and K. Pushpalatha
5.1 Introduction 117
5.2 Classification of polymer-based UV-protective materials 119
5.3 Imperative requirements toward developing mechanically flexible and visibly transparent UV protective materials 126
5.4 Surface engineering and in-situ polymerization approaches toward developing mechanically flexible and visibly transparent polymer-based UV protective materials 130
5.5 Conclusions and future directions 130
References 131

Chapter 6 Photo-active polymer nanocomposite layer for energy applications 135
Arul Varman Kesavan and Praveen C. Ramamurthy
6.1 Introduction 135
6.2 Polymer-zero dimensional material composites 136
6.3 Polymer one-dimensional material composites 144
6.4 Polymer two-dimensional material composites 146
6.5 Conclusions and future directions 152
References 153

Chapter 7 Shape memory polymers (SMP's) in optoelectronic devices 157
K. Anand and Vaishak Nambiathody
7.1 Introduction 157
7.2 Polymer as a material 157

† Deceased.

7.3 Solar cells 158
7.4 Shape memory polymers as a substrate for optoelectronics 160
7.5 Conclusions and future directions 163
References 164

Chapter 8 π-Stacking, conjugated, polymer-supported carbon nanotubes (CNTs) composite materials for light-emitting diode (LED) application 169
V. Ramkumar, I.P. Bincy, D. Santhanaraj, M. Gopiraman, and Sellamuthu N. Jaisankar

8.1 Introduction 169
8.2 π-Stacking and conjugation of polymers 170
8.3 The molecular photochemistry and photophysics 171
8.4 The internal conversion and intersystem crossings. 173
8.5 Fluorescence and phosphorescence 173
8.6 The electron transfer reactions. 174
8.7 Determination of bandgap energy 175
8.8 Carbon nanotubes 176
8.9 CNT-polymer nanocomposites 177
8.10 Optoelectronic devices 178
8.11 CNT-PNCs in optoelectronics 180
8.12 Polymer-CNT composite in LED application 182
8.13 CNT-PNCs as a stretchable electrode material 182
8.14 CNT-PNCs as an anode material. 185
8.15 CNT-PNCs as HTL and ETL 186
8.16 CNT-PNCs as an emissive layer 188
8.17 Conclusion 192
Acknowledgment 192
References 192

Chapter 9 Advances in polymer-based composites for solar energy conversion to chemical fuels 195
Anupma Thakur, Praveen Kumar, R.K. Sinha, and Pooja Devi
9.1 Introduction 195
9.2 Fundamentals of solar energy conversion to chemical fuel . . 198
9.3 Advances in polymer-based composites as photoactive materials for clean-energy fuel systems 203
9.4 Conclusions and future directions 209
References 209

Chapter 10 Polymer nanocomposites for energy-related applications 215
Haradhan Kolya, Tapas Kuila, Nam Hoon Kim, and Joong Hee Lee
10.1 Introduction 215
10.2 Preparation of polymer nanocomposites 217
10.3 Energy-related applications of polymer nanocomposites 219
Acknowledgments 241
References 241

Chapter 11 Influence of polymers on carbon-based composites in energy storage applications 249
Manu Patel U.M.
11.1 Introduction 249
11.2 Polymer-based binders for a Li-ion battery 253
11.3 Polymer-based binders for an Li-S battery 255
11.4 Conductive polymer/carbon composites in Li-S cathode electrode 257
11.5 Conclusions and future directions 260
References 260
Further reading 264

Chapter 12 Recent advances in conjugated polymers for lithium-ion and supercapacitor applications 265
U.T. Uthappa, Ho-Young Jung, and Mahaveer D. Kurkuri
12.1 Introduction 265
12.2 Operating principles of conjugated polymers. 266
12.3 Applications of conjugated polymers 267
12.4 Conclusions and future directions 282
Acknowledgments 283
References 283

Chapter 13 Polymer-based electro-active smart composites as stretchable strain sensors 291
K.S. Nithin, K.R. Prakash, V. Ravi Kumar, M.V.S. Deepak, B.J. Kishen Karumbaiah, S. Sachhidananda, K.N. Shilpa, B.M. Jagajeevan Raj, and H. Siddaramaiah†
13.1 Introduction 291
13.2 Classification of polymer-based strain sensors based on operating mechanism 292
13.3 Factors validating the suitability of materials for stretchable strain sensing and their related performance metrics 300
13.4 Stretchable elastomer-based conductive polymer composites 306
13.5 Material selection for stretchable strain sensors and their related applications 307
13.6 Factors affecting the strain sensing performance of polymer-based conductive composites. 312
13.7 Conclusions and future directions 313
Acknowledgment 313
References 313

† Deceased.

Chapter 14 Nanotechnology-enabled polymer-based flexible electronics and their potential applications 321
B.J. Kishen Karumbaiah, K.S. Nithin, K.R. Prakash, V. Ravi Kumar, K.N. Shilpa, T. Basava, P. Shruthi, and S. Sachhidananda
14.1 Introduction 321
14.2 Polymer-based electro-active smart composites 322
14.3 Applications of nanotechnology-enabled polymer smart composite-based flexible electronics. 323
14.4 Skin-inspired electronics. 329
14.5 Conclusions and future directions 330
Acknowledgment. 334
References 334

Index 341

Contributors

K. Anand Department of Basic Sciences, Amal Jyothi College of Engineering, Kanjirapally, Kerala, India

Kanakaraj Aruchamy Centre for Nano and Material sciences, Jain University, Bangalore, India

T. Basava Department of Mechanical Engineering, Sri Dharmasthala Manjunatheshwara Institute of Technology, Ujire, India

I.P. Bincy Department of Physics, MES College, Nedumkandam, Kerala, India

M.V.S. Deepak Department of Mechanical Engineering, ATME College of Engineering, Mysuru, India

Pooja Devi Academy of Scientific and Innovative Research (AcSIR), Ghaziabad; CSIR-Central Scientific Instruments Organisation, Chandigarh, India

M. Gopiraman Department of Applied Bioscience, College of Life and Environment Science, Konkuk University, Seoul, South Korea

B.M. Jagajeevan Raj Department of Chemistry, The National Institute of Engineering, Mysuru, India

Sellamuthu N. Jaisankar Department of Polymer Science and Technology, Council of Scientific and Industrial Research (CSIR), Central Leather Research Institute (CLRI), Chennai, Tamilnadu, India

Ho-Young Jung Department of Environment and Energy Engineering, Chonnam National University, Buk-gu, Gwangju, Republic of Korea

Smitha V. Kamath Centre for Nano and Material sciences, Jain University, Bangalore, India

C.S. Karthik Department of Chemistry, Sri Jayachamarajendra College of Engineering, JSS Science and Technology University, Mysuru, India

Arul Varman Kesavan Department of Materials Engineering, Indian Institute of Science, Bangalore, India

Nam Hoon Kim Department of Nano Convergence Engineering, Jeonbuk National University, Jeonju, Jeonbuk, Republic of Korea

B.J. Kishen Karumbaiah Department of Mechanical Engineering, Coorg Institute of Technology, Ponnampet; Department of Mechanical Engineering, Sri Dharmasthala Manjunatheshwara Institute of Technology, Ujire, India

Haradhan Kolya Department of Nano Convergence Engineering, Jeonbuk National University, Jeonju, Jeonbuk, Republic of Korea

Tapas Kuila Surface Engineering and Tribology Division, CSIR-Central Mechanical Engineering Research Institute, Durgapur, India

Praveen Kumar School of Materials Science, Indian Association for the Cultivation of Science, Kolkata, India

Mahaveer D. Kurkuri Centre for Nano and Material Sciences, Jain University, Jain Global Campus, Bengaluru, Karnataka, India

Joong Hee Lee Department of Nano Convergence Engineering; Carbon Composite Research Centre, Department of Polymer-Nano Science and Technology, Jeonbuk National University, Jeonju, Jeonbuk, Republic of Korea

K.A. Muthappa Department of Electronics and Communication Engineering, Sathyabama Institute of Science and Technology, Chennai, Tamilnadu, India

Vaishak Nambiathody Technical Consultancy Division, Rubber Research Institute of India, Kottayam, Kerala, India

K.S. Nithin Department of Chemistry, The National Institute of Engineering, Mysuru, India

K.R. Prakash Department of Mechanical Engineering, The National Institute of Engineering, Mysuru, India

K. Pushpalatha Department of Chemistry, The National Institute of Engineering, Mysuru, India

Praveen C. Ramamurthy Department of Materials Engineering, Indian Institute of Science, Bangalore, India

V. Ramkumar Department of Polymer Science and Technology, Council of Scientific and Industrial Research (CSIR), Central Leather Research Institute (CLRI), Chennai, Tamilnadu, India

V. Ravi Kumar Department of Mechanical Engineering, The National Institute of Engineering, Mysuru; Department of Mechanical Engineering, Amrita School of Engineering, Amrita Vishwa Vidyapeetham, Bengaluru, India

S. Sachhidananda Department of Polymer Science and Technology, Sri Jayachamarajendra College of Engineering, JSS Science and Technology University, Mysuru, India

A. Sahaya Anselin Nisha Department of Electronics and Communication Engineering, Sathyabama Institute of Science and Technology, Chennai, Tamilnadu, India

S. Sandeep Department of Chemistry, Sri Jayachamarajendra College of Engineering, JSS Science and Technology University, Mysuru, India

Nataraj Sanna Kotrappanavar Centre for Nano and Material sciences, Jain University, Bangalore, India

D. Santhanaraj Department of Chemistry, Loyola College, Chennai, India

B.K. Sarojini Department of Industrial Chemistry, Mangalore University, Mangaluru, India

K.N. Shilpa Department of Polymer Science and Technology, Sri Jayachamarajendra College of Engineering, JSS Science and Technology University, Mysuru, India

P. Shruthi Department of Chemistry, The National Institute of Engineering, Mysuru, India

H. Siddaramaiah[†] Vice-Chancellor of JSS Science and Technology University, Mysuru, India

R.K. Sinha CSIR-Central Scientific Instruments Organisation, Chandigarh; Department of Applied Physics, Delhi Technological University, Bawana Road, Delhi, India

Anupma Thakur Academy of Scientific and Innovative Research (AcSIR), Ghaziabad; CSIR-Central Scientific Instruments Organisation, Chandigarh, India

Rohini Thimmaiah Department of Chemistry, Coorg Institute of Technology, Ponnampet, India

Manu Patel U.M. Scientist, Hollingsworth and Vose, Mysuru, India

U.T. Uthappa Centre for Nano and Material Sciences, Jain University, Jain Global Campus, Bengaluru, Karnataka, India; Department of Environment and Energy Engineering, Chonnam National University, Buk-gu, Gwangju, Republic of Korea

[†] Deceased.

Foreword by Dong Won Kim

As the President of the Jeonbuk National University, where Professor Joong Hee Lee serves, I am very proud and honored to introduce this important compilation of recent research in the field of polymer-based composite materials.

It is increasingly clear that multifunctional and high-performance materials with advanced end properties will play a significant role in meeting the world's future needs. As the pressure for such materials to bridge the gap from lab to market grows, the field matures and fixes its sights on new goals. Most recently, the advanced materials research community has begun to tackle the possibilities and challenges inherent in polymer-based smart composite materials with combinatorial and synergistic functionalities. The editors of this book, Prof. Joong Hee Lee, Prof. M.R. Siddaramaiah, and Dr. Nithin K.S., have well-deserved reputations as leaders in the field, with each having been published in well-regarded international journals and having obtained several patents related to their specific expertise. I have no doubt that they have brought their best efforts as editors to bear in successfully bringing this volume to life.

My appreciation extends to Elsevier, which has once again proved its commitment to publishing vital, enriching, and research-centric books that are critical to the research and development cycle.

This book focuses on the various applications of polymer-based advanced functional composites. Accordingly, it opens with an introduction to polymer-based smart composites for optoelectronic and energy applications, and covers tools and techniques adopted for characterizing polymer-based smart composites. It also offers comprehensive coverage on optical, optoelectronic, electrical, and energy-related applications of polymer-based advanced functional composites and/or nanocomposites.

As a considerable compilation of advanced research findings, this book would serve as a comprehensive survey of the state of the field that may be of significant interest to academicians, scientists, researchers, upper-level undergraduates, and graduates as well as engineers or technologists working with polymer-based composite materials or in related areas.

Dong Won Kim, Ph.D.
President of Jeonbuk National University, Jeonju-Si, Republic of Korea

Foreword by Sudhanva

Dr. Nithin is a talented young researcher and has done innovative work. I have enjoyed my association with him at the National Institute of Engineering. I wish him all the very best. In a time when the world is seeking multifunctional and high-performance materials with advanced end properties, the materials research community has started to bank on the composite approach, which enables the effective mining of combinatorial and synergistic functionalities. Polymer-based smart composite-based advanced material research is one such domain aimed at futuristic material needs. Elsevier has yet again proved its commitment to publishing such need-based and knowledge-enriching research-centric books. This book focuses on polymer-based smart composite applications in optical and sensor development in the first half while the final section focuses on energy conservation and harvesting. The editors of this book, Prof. Nithin K.S., Prof. Joong Hee Lee, and Prof. M.R. Siddaramaiah, are known to me and are professional researchers in this domain. They have proven expertise in this area, having published a number of research findings in reputed international journals while also filing and publishing several patents related to the said field of expertise. Also, I firmly believe that the editors are contributing their best in bringing out this futuristic book.

This book, with a considerate compilation of imperative advanced research findings in polymer-based functional materials for optical, optoelectronic, and energy applications, would serve as comprehensive literature for academicians, scientists, researchers, upper-level undergraduates, and graduates as well as engineers and technologists working in the same or allied areas.

D. Sudhanva
NIE Management Committee, Mysore, India
Excelsoft Technologies Pvt. Ltd., Mysore, India
Confederation of Indian Industry, Mysore, India

Preface

From household appliances to flexible electronics, advanced functional materials are continuously revolutionalizing the material world. However, to keep pace with accelerated market growth and amplified consumer desires, the current material research and innovation initiatives are aimed at taking advantage of combinatorial and/or synergistic material property mining. The said approach involves a thoughtful combination of different materials with diverse end properties to realize multiple functionalities.

One such material research domain focuses on thoughtfully combining dopant-dependent material property engineerable polymers with functional nanoparticles, thereby enabling smart functionalities. This contribution attempts to summarize the imperative research exercises on optical, optoelectronic, and energy applications of polymer-based smart composites.

This book opens with an introductory chapter on polymer-based smart composites for optoelectronic and energy applications, followed by conjugated polymer-based smart composites. Going forward, it also presents imperative tools and techniques adopted toward characterizing polymer-based smart composites of optical, optoelectronic, and energy significance. Finally, it gives comprehensive coverage on optical, optoelectronic, and energy-related applications of polymer-based smart composites, including luminescent downshifting materials for UV shielding, photo-active materials for energy applications, shape-memory materials for optoelectronic devices, conjugated polymer-supported carbon nanotubes for light-emitting diode applications, polymer-carbon composites for energy applications, conjugated polymer composites for lithium-ion and supercapacitor applications, flexible electronics, and at length electro-active smart composites for strain-sensing applications.

Dr. Nithin Kundachira Subramani
Dr. H. Siddaramaiah[†]
Dr. Joong Hee Lee

[†] Deceased.

Acknowledgments

This book has been kept on track and been seen through to completion with the support and encouragement of a number of people, including our learned authors, who have contributed their vast scientific knowledge to strengthen this contribution; the Elsevier team, Edward Payne, Mariana C. Henriques, Poulouse Joseph, Jagannathan Subramaniam, Sheela Bernardine Josy, Greg Harris, who guided us throughout the publication process; our parent institutions, The National Institute of Engineering (Centre for Research and Development), Mysuru, India, Sri Jayachamarajendra College of Engineering, JSS Science and Technological University, Mysuru, India, and Jeonbuk National University, South Korea, for their incessant support; and our beloved research scholars Sachhidananda Shivanna and Jagajeevan Raj B.M. This contribution would never have been possible without their unconditional support.

Dr. Nithin Kundachira Subramani
Dr. H. Siddaramaiah[†]
Dr. Joong Hee Lee

[†] Deceased.

1

Polymer-based smart composites and/or nanocomposites for optical, optoelectronic, and energy applications: A brief introduction

K.S. Nithin[a], S. Sachhidananda[b], K.N. Shilpa[b], S. Sandeep[c], C.S. Karthik[c], B.M. Jagajeevan Raj[a], and H. Siddaramaiah[d,†]

[a]Department of Chemistry, The National Institute of Engineering, Mysuru, India, [b]Department of Polymer Science and Technology, Sri Jayachamarajendra College of Engineering, JSS Science and Technology University, Mysuru, India, [c]Department of Chemistry, Sri Jayachamarajendra College of Engineering, JSS Science and Technology University, Mysuru, India, [d]Vice-Chancellor of JSS Science and Technology University, Mysuru, India

1.1 Introduction

Polymer-based smart composites (PBSCs) are essentially mechanically flexible stimuli-responsive composites with an ability to respond selectively and reversibly to an external stimulus. The nature of stimuli varies from temperature to humidity, pH to chemical compounds, and wavelength or intensity of light to electrical or magnetic fields. While, the nature of response varies from color switching to changes in light-transmitting abilities, alteration in conductivity to changes in material shape and material wettabilities [1–3]. For illustration, electro-chromic and thermo-chromic PBSCs display appreciable color switching when subjected to appropriate amounts of electric and thermal potentials, respectively. The observed changes in the material properties of stimuli-responsive PBSCs result from external stimuli-induced changes in secondary forces such as hydrogen bonding and other related electrostatic interactions. Further, the degree or extent of response depends on the intensity of applied stimulus.

† Deceased.

Polymer-Based Advanced Functional Composites for Optoelectronic and Energy Applications
https://doi.org/10.1016/B978-0-12-818484-4.00011-2
Copyright © 2021 Elsevier Inc. All rights reserved.

PBSCs may be successfully developed via considerate introduction of stimuli-responsive functional fillers (fillers with a dynamic response to external stimulus) into particle stabilizing polymers [4–7]. Plus, if the size of the introduced filler is in the nanometric scale, it leads to the development of polymer-based smart nanocomposites. Accordingly, various researchers have successfully developed and demonstrated diverse PBSCs through significant inspirations drawn from some of the important naturally occurring stimuli-responsive practices (Fig. 1.1). Also, the wide diversity in the nature of the stimulus and related responsivities has enabled PBSCs for numerous techno-commercial applications. Some of the commercial exploits of such PBSCs are in the fields of optical and optoelectronic devices, biomedical applications involving diagnosis and imaging, energy-related applications and catalysis, industrial automation and robotics, and so forth [8–10].

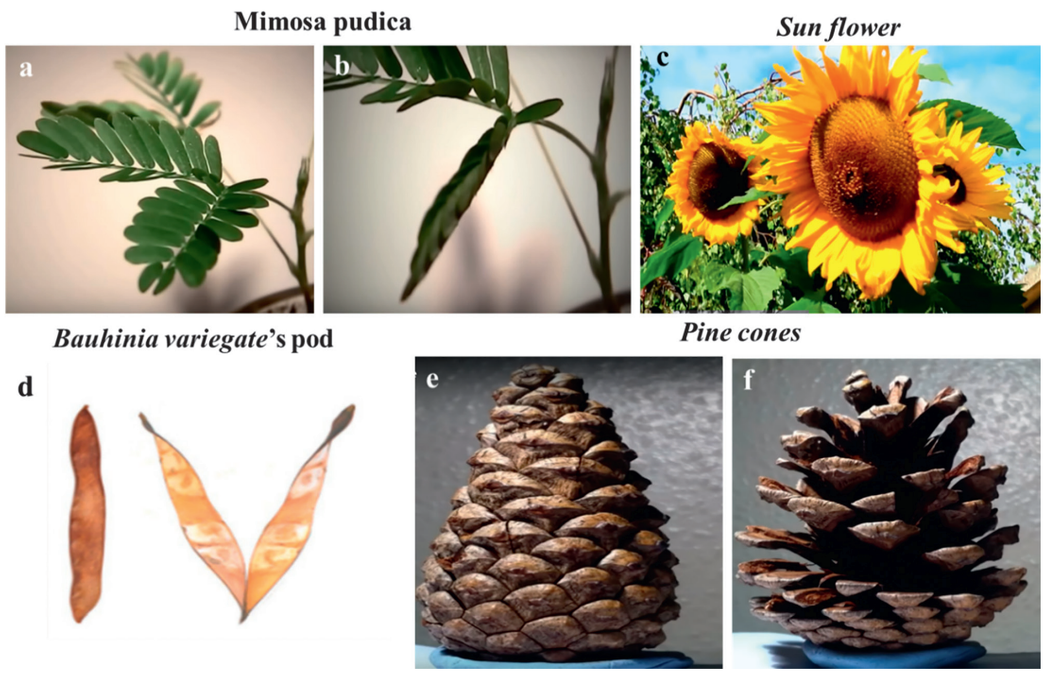


Fig. 1.1 Some of the important naturally occurring stimuli-responsive practices. (A and B) Touch-sensitive opening and closing of *Mimosa pudica* leaves; (C) tropistic motion bending of sunflowers in the direction of sunlight; (D) a closed *Bauhinia variegate*'s pod under a wet environment (left) and an opened seed pod in a dry environment; (E) closed pine cone, when wet; and (F) opened pine cone, when dried.

1.2 Classification of PBSCs

Stimuli-responsive PBSCs are grouped into different types based on four important criteria: the nature of the stimulus they respond to, the number of stimuli they respond to, the actual stimulus they respond to, and finally their (PBSCs) relative architecture.

Based on the nature of the stimulus they respond to, PBSCs are classified as physical, chemical, or biological stimuli-responsive PBSCs.

Based on the actual stimulus they respond to, physical stimuli-responsive PBSCs are further classified as temperature-responsive, light-responsive, magnetic field-responsive, or electric field-responsive PBSCs. While, chemical stimuli-responsive PBSCs are further classified as pH-responsive, redox reaction-responsive, and solvent-responsive PBSCs. Biological stimuli-responsive PBSCs are further classified as glucose-responsive and enzyme-responsive PBSCs. Table 1.1 presents some of the important classes of stimuli-responsive polymer-based materials, their synthetic techniques, and related applications [42].

Based on the number of stimuli they respond to, PBSCs are classified as single, dual, or multiple stimuli-responsive PBSCs. Going forward, dual stimuli-responsive PBSCs are further classified as heat- and light-responsive, heat- and pH-responsive, and so forth. While, multiple stimuli-responsive PBSCs are further classified as responsive to heat, light, and pH; responsive to heat, light, and redox reaction; and so forth.

Finally, based on the relative architecture of PBSCs, they may be classified as hydrogels, interpenetrating networks (IPNs), graft copolymers, and so forth [43]. Table 1.2 presents various types of PBSCs based on dual classification criterion, that is, the actual stimuli they respond to and their corresponding responses.

1.3 Important types of stimuli-responsive PBSCs: Properties and related applications

Physical, chemical, and biological stimulus are the three major categories of external factors that may draw appreciable smart responses in PBSCs. Physical stimuli such as light, heat, and electrical or magnetic fields may lead to reversible changes in the chain dynamics of polymer composites, thereby inducing stimuli-responsive behaviors. Whereas, chemical stimuli such as oxidizing or reducing agents, solvents, and other related factors aid to modulate the molecular interactions between the polymer host and the introduced filler, thereby enabling smart functionalities. Finally, biological stimuli such as enzymes and related receptors will work to reversibly transform the physicochemical properties of the polymer composites and thereby enable smart behaviors.

Table 1.1 Some of the important stimuli-responsive polymer-based materials, their synthetic techniques, and related applications.

Actual stimulus	Polymer-based stimulus responsive material	Synthesis technique	Related applications
Physical stimuli-responsive			
Temperature	PNiPAAm [11, 12]	Living radical polymerization	Tissue adhesion prevention material
	PNVC [13]	Living radical polymerization	Thermo-sensitive hydrogel at any temperature
	PLLA/PEG/PLLA [14]	Ring open polymerization	Potential anticancer drug carrier
	PEO–PPO–PEO [15]	Cross-linking the ethoxysilane cap	Drug carrier
Electric field	PT [16]	Electrochemical synthesis	Drug release and cancer chemotherapy
	PSS [17]	Emulsion polymerization	Drug carrier
Light	Azobenzene or spiropyran-containing		
	PAA [18, 19]	Copolymerization	Photo-chromic polymer
	PHPMAm [20, 21]		Sensor
	PNIPAM [22, 23]		Photodegradation material
Chemical stimuli-responsive			
pH	Chitosan [24]	Biosynthesis	Drug release
	Albumin [25]		Enzyme immobilization
	Gelatin [26]		Immunoassay
	PAAc/chitosan IPN [27]	UV irradiation	Wound dressing material and drug release
	P(MAA-g-EG) [28, 29]	Free-radical and solution photo-polymerization	Controlled insulin delivery
	PEI [30]	Solution polymerization	pH-sensitive controlled release systems
	PDAAEMA PL [31, 32]	Biosynthesis	Vectors for gene delivery
Ion-responsive			
Redox reactions	Polyanhydrides [33, 34]	Melt condensation polymerization	Potential oral drug delivery systems
	PLGA [35]	Double emulsion solvent evaporation	Controlled delivery systems

Table 1.1 Some of the important stimuli-responsive polymer-based materials, their synthetic techniques, and related applications—cont'd

Actual stimulus	Polymer-based stimulus responsive material	Synthesis technique	Related applications
	PbAEs [36]	Addition solution polymerization	Efficient carrier for cytotoxic agents
	Poly (NiPAAm-coRu(bpy)3) [37]	Living radical copolymerization	Artificial muscles
Biological stimuli-responsive			
Glucose	GOx conjugated chitosan [38, 39]	Carbodiimide chemistry	Self-regulated insulin delivery
Enzyme	DEXS/chitosan [40]	Layer-by-layer assembly	Local and sustained drug release
	Azoaromatic cross-linked hydrogel [41]	Copolymerization	Specific delivery of peptides and proteins

Reproduced from reference E. Cabane, X. Zhang, K. Langowska, C.G. Palivan, W. Meier, Stimuli-responsive polymers and their applications in nanomedicine, Biointerphases 7 (2012) 9–10 with permission of Springer.

Table 1.2 Types of PBSCs based on the actual stimuli they respond to and their corresponding responses.

Response → / Stimulus ↓	Electrical	Magnetic	Optical	Thermal	Mechanical
Electrical			1. Electro-chromic 2. Electro-luminescent 3. Electro-optic	1. Thermoelectric	1. Piezoelectric 2. Electrostrictive
Magnetic			1. Magneto-optic		1. Magnetostrictive
Optical	1. Photoconductive		1. Photo-chromic		
Thermal			1. Thermo-chromic 2. Thermo-luminescent		1. Shape memory materials
Mechanical	1. Piezoelectric 2. Electrostrictive	1. Magnetostrictive	1.Mechano-chromic		1. Negative Poisson ratio materials

1.3.1 Thermo-responsive PBSCs

Thermo-responsive PBSCs are those polymer composite-based stimuli-responsive materials that respond to heat. Such heat-sensitive PBSCs have attracted significant technological interest, owing to their stimuli-sensitive and recordable changes in physicochemical properties (solubility, volume, and conformation) and hence, the resultant material properties (optical, electrical, and other related factors).

Such thermo-responsive PBSCs are further grouped into three important categories:

1. Lower critical solution temperature (LCST)-type or upper critical solution temperature (UCST)-type PBSCs.
2. Temperature-induced shape memory-type PBSCs.
3. Temperature-induced color switching-type PBSCs [44].

1.3.1.1 LCST and UCST-type PBSCs

The thermo-responsive properties in the LCST-type and/or UCST-type PBSCs arise from differences in the solubility response (in a particular solvent) of materials with temperature (Fig. 1.2). Consequently, both LCST-type and UCST-type PBSCs exhibit temperature-dependent solvated-desolvated transitions.

LCST-type PBSCs are inherently hydrophilic and remain extended or swollen at temperatures below LCST. However, at higher solution temperatures (temperatures above LCST), they display reversible transitions from an extended state (hydrophilic) to a collapsed state (hydrophobic) via the adequate omission of solvent molecules (Fig. 1.2). Poly(*N*-alkyl substituted acrylamides) and poly(*N*-vinylalkylamides),

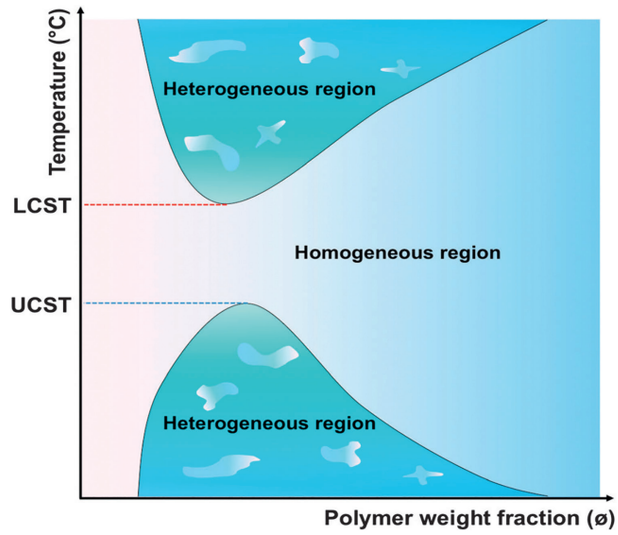


Fig. 1.2 Dispersion in temperature of LCST- and UCST-type polymer-based thermo-responsive materials, as a function of their weight fraction (phase diagram of LCST and UCST-type polymer aqueous solutions). Reproduced from reference Y.J. Kim, Y.T. Matsunaga, Thermo-responsive polymers and their application as smart biomaterials, J. Mater. Chem. B RSC. 5 (2017) 4307–4321 with permission of The Royal Society of Chemistry.

as well as copolymers such as poly(L-lactic acid)-poly(ethylene glycol)-poly(L-lactic acid) (PLLA-PEG-PLLA), poly(ethylene oxide)-poly(propylene oxide)-poly (ethylene oxide) (PEO-PPO-PEO), and their composites are the most extensively studied LCST-type PBSCs. This is owing to the fact that these polymeric matrices present LCST close to the human physiological temperature (30–35°C). It is this operating temperature range that enables the possible applications of LCST-type PBSCs as temperature-regulating smart fabrics.

UCST-type PBSCs, on the other hand, display phase separation upon cooling. That is to say, UCST-type PBSCs tend to swell when the solvent temperature exceeds UCST and collapse when the solution temperature is below UCST [44]. Polyacrylamide (PAAm), polyacrylic acid (PAAc), and their composites are some of the most established UCST-type PBSCs, which display strong hydrogen bonding at temperatures lower than UCST, but instantaneously dissociate at temperatures above UCST.

Further, LCST-type PBSCs are often homogeneously clear and transparent at temperatures below LCST. While, UCST-type PBSCs are heterogeneously cloudy and opaque below UCST.

This observed switching in the solvation tendency of PBSCs with temperature may be because of the temperature-dependent bonding and debonding of the secondary interactions (such as hydrogen bonding and other related effects), which facilitate the effective formation of thermodynamically favorable systems.

Given that, the critical solution temperatures (CSTs) of PBSCs may be considerately regulated by varying the nature and content of nanofillers. Choe et al. fabricated thermo-sensitive colorimetric sensors by decorating gold nanoparticles (Au NPs) on poly(*N*-isopropylacrylamide) (PNIPAm) microgels [45], which were thoughtfully embedded into PAAm hydrogels. The said LCST-type thermo-responsive smart composites were reported to exhibit reversible and strain-insensitive color switching (between red and grayish violet) in response to changes in temperature. The observed color switching was because of the collapsing of the sensor from its initial raspberry shape (upon increasing the temperature beyond the LCST of PNIPAm), which in turn led to the microgel solvation state modulated plasmon coupling within the PBSC (Fig. 1.3). Moving forward, the same team also demonstrated proof of concepts of the said thermo-responsive PBSC as a smart colorimetric patch for temperature scanning and as a colorimetric thermometer for thermo-responsive actuator applications (Fig. 1.4).

Herein, the pNIPAm-Au microgels are the Ref and counterparts with 0.1 M and 0.2 M NaCl are N1 and N2. Also, 1 mM SDS and 2 mM SDS are S1 and S2 with different LCSTs of 32, 31.5, 29, 33.5, and 37°C, respectively. Further, *red-dotted boxes* indicate the positions of the co-PNIPAM films while the *red arrows* indicate a specific finger exhibiting actuation and color change [45].

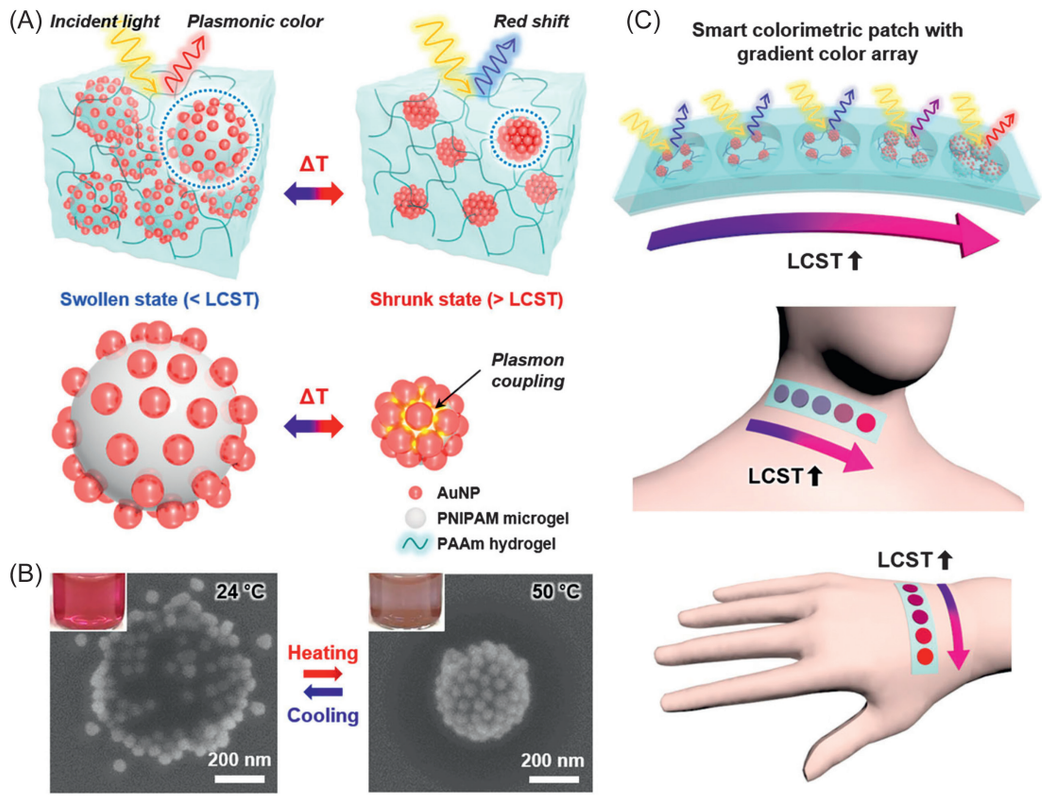


Fig. 1.3 The operating principle of LCST-type thermo-responsive PBSC. (A) Schematic depiction of plasmonic microgels (PNIPAm-Au) in a PAAm hydrogel under swollen and shrunken states; (B) scanning electron microscopic (SEM) images of microgels, under a swollen state at 24°C (left) and under a shrunken state at 50°C (right) (inset: pictorial depiction of plasmonic microgel dispersions under the above-cited conditions); and (c) schematics of wearable sensor array patches attached to human skin at various places [45].

1.3.1.2 Temperature-induced shape memory-type PBSCs

The second important category of thermo-responsive PBSCs is the temperature-induced shape memory type, which displays temperature-dependent variations in their dimension and shape.

Polymer-based shape memory composites are those stimuli-responsive materials with an inherent potential to memorize their geometry, be programmed to take one or more temporary shapes (upon exposure to an external stimulus), and return to the original shape (upon removal of stimulus).

Fig. 1.5 presents the thermo-mechanical cycle to evaluate the shape memory effect (SME) of one such polymer-based shape memory composite made of Ni particle introduced polyurethane (PU). The SEM images validating the shape recovery cycle in the said temperature-induced shape memory-type PBSCs are given in Fig. 1.6 [46].

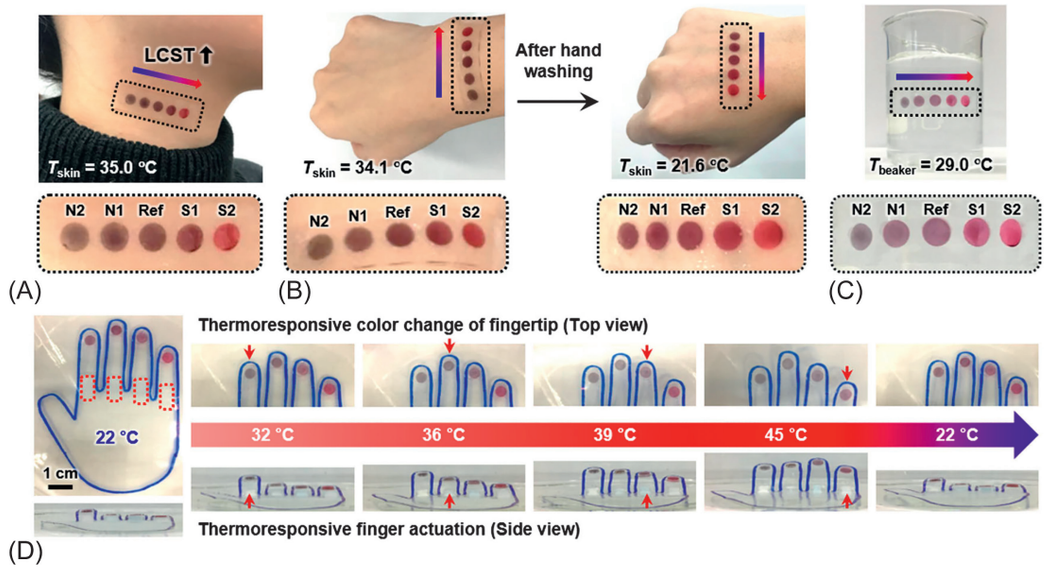


Fig. 1.4 Proof-of-concept demonstration for a thermo-responsive smart colorimetric patch. (A) Photographs of the color array patch attached to the neck; (B) hand, before washing (left) and after washing (right); (C) beaker filled with water (pictures were recorded 5 s after attachment of the patches); and (D) hand-shaped actuator with plasmonic comicrogel film on fingertips and co-PNIPAM films on finger joints, placed in a water bath at different temperatures for 1 min. From A. Choe, J. Yeom, R. Shanker, M.P. Kim, S. Kang, H. Ko, Stretchable and wearable colorimetric patches based on thermoresponsive plasmonic microgels embedded in a hydrogel film, NPG Asia Mater. 10 (2008) 912–922.

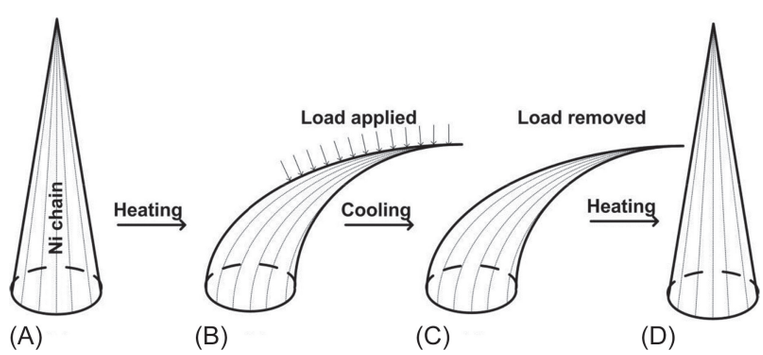


Fig. 1.5 Illustration of a thermo-mechanical cycle to evaluate the shape memory effect in Ni particle introduced PU composites. (A) Initial shape; (B) predeformed shape; (C) flattened shape; and (D) recovered shape. Reproduced from reference X. Lan, W. Huang, J. Leng, Shape memory effect in micro-sized shape memory polymer composite chains, Appl. Sci. 9 (2019) 2919–2920 with permission of MDPI.

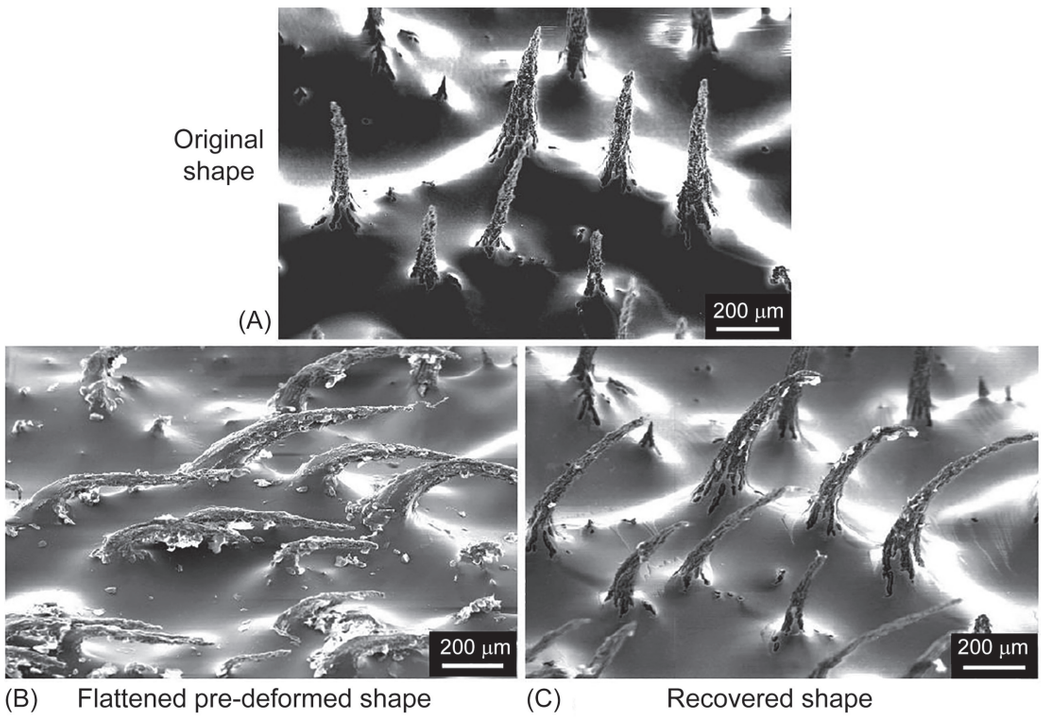


Fig. 1.6 SEM images supporting the shape recovery cycle of shape memory PU/nickel (SMPU/Ni) chains (2 vol% Ni). (A) Original shape; (B) flattened predeformed shape; and (C) recovered shape. Reproduced from reference X. Lan, W. Huang, J. Leng, Shape memory effect in micro-sized shape memory polymer composite chains, Appl. Sci. 9 (2019) 2919–2920 with permission of MDPI.

The phenomenon by which PBSCs prompt a recovery from the fixed shape to the initial one is termed the shape memory effect (SME). While, the ability to take up a temporary shape and the extent to get back to the original shape is called the shape fixity ratio (R_f) and the shape recovery ratio (R_r), respectively [47]. This SME in PBSCs may be linked to temperature-induced changes in their amorphous (soft segment) or crystal (hard segment) mobilities. Further, the temperature corresponding to the shape switching is expressed as the switching temperature (T_s), which depends on the ratio of the soft to hard segments and the extent of cross-linking.

Consequently, when the T_s of PBSCs is less than the actual or operating temperature, the cross-linked PBSC networks begin to deform. Hence, the elastic modulus of the cross-linked PBSC decreases. Finally, upon cooling, the entropy of the PBSCs lessens and as a consequence, the polymer networks revert to their original shape.

Furthermore, excellent structural versatility, low manufacturing cost, processing ease, high elastic deformation, and low recovery

temperature [45] have all contributed to increasing research interest in polymer-based shape memory materials.

Virgin polymer-based shape memory materials are very advantageous over conventional shape memory alloys. They often suffered from low mechanical strength and shape recovery stress, which in turn, paved way for polymer-based shape memory composites and/or nanocomposites. Moreover, polymer-based composite materials are those multicomponent hybrids that are essentially developed via the thoughtful combination of diverse materials with different physical and chemical properties, so as to realize advanced materials with improved performance [48–50]. Besides, the fact that the addition of even very small amounts of functional fillers may aid the shape recovery stress of polymer-based composites and/or nanocomposites also renders them as the most sought after materials for numerous techno-commercial applications [51–53]. Furthermore, the introduced fillers may either enable combinatorial properties or induce entirely new properties via synergistic effect [54–57]. Accordingly, Ma et al. developed a dual responsive (temperature and pH), color and shape tunable PBSC actuator made of composite layers of pH-responsive perylene bisimide functionalized hyper branched polyethylenimine (PBI-HPEI) and thermo-responsive GO (graphene oxide)-pNIPAm hydrogel [58]. A detailed description of the significance of polymer composites and/or nanocomposite technology towards enabling smart functionalities (with special emphasis on the considerate peddling of optical, optoelectronic, and energy storage functionalities of polymers (using various nanofillers) is presented in the chapter that follows.

1.3.1.3 Temperature-induced color switching-type PBSCs

Temperature-induced color switching-type PBSCs are those PBSCs that change their optical behaviors (show visible light color switching) in response to phonons or heat. Such temperature-dependent color switching may arise either due to heat-induced phase transformations or temperature-modulated changes in the structure of the chromic species [59].

Accordingly, Carotenuto et al. developed thermo-chromic optical switches made of reversibly color switching (dark brown to light yellow) PBSCs consisting of silver/polystyrene (PS) NCs [60]. Hyungwoo Kim et al. reported temperature-responsive reversible color switching (opaque orange (25°C) to transparent yellow (120°C)) with an organo gel fiber-embedded polymer composite film (Fig. 1.7) [59]. Further, Moriyuki Sato et al. developed temperature-responsive yellow light-emitting poly(*N*-vinylcaprolactam) (VCL)-cosodium acrylate (SA) NCs loaded with surface-modified (PEGylated) ZnO NPs. They also reported that the size of the as-developed NCs showed

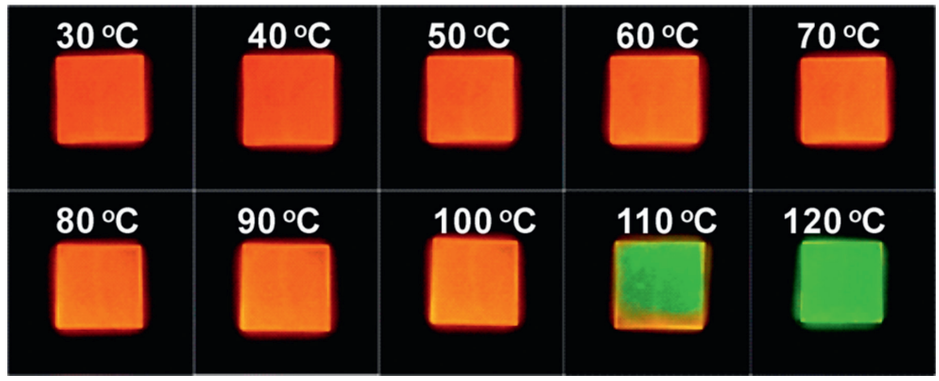


Fig. 1.7 Digital photographs of organo gel fiber-embedded EGDMA film (under 365 nm irradiation) at temperatures ranging from 30 to 120°C. From H. Kim, J.Y. Chang, Reversible Thermochromic polymer film embedded with fluorescent organogel nanofibers, Langmuir: ACS J. Surf. Colloids 30 (2014) 13673–13679.

thermo-responsive behaviors (a drastic reduction in size with temperature) in the range of 20–35°C. The said effect was owed to the introduction of steric hindrance and the relative enhancement of the hydrophilic PEG chain concentrations (within the NC networks) [61]. Moving forward, Toommee et al. developed polydiacetylene (PDA)/zinc oxide (ZnO) NCs, which showed reversible thermo-chromism in a solution medium at various temperatures (Fig. 1.8) [62]. While, Xygkis et al. demonstrated thermo-chromic VO_2/poly-vinyl-pyrrolidone (PVP) NCs that served to regulate the internal temperature of concrete structures [63]. Further, such reversibly thermo-chromic PBSCs that

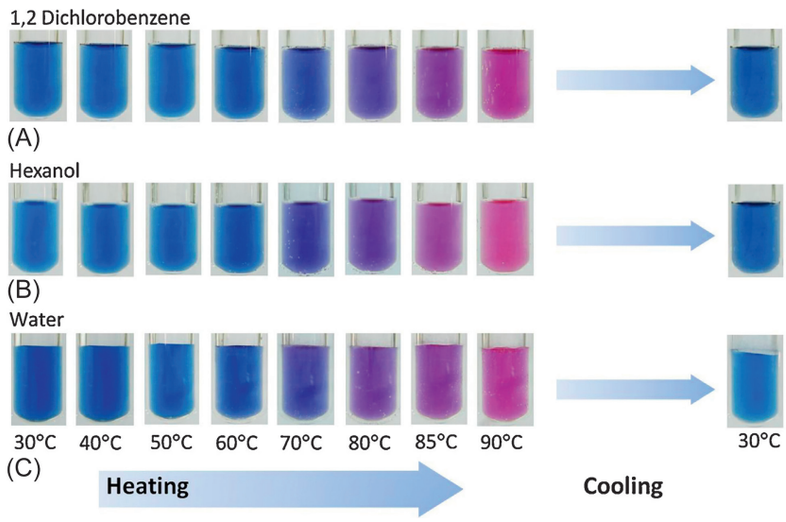


Fig. 1.8 Digital photographs of PDA/ZnO NC suspensions (temperature ranging from 30 to 90°C) in (A) 1,2-dichlorobenzene; (B) hexanol; and (C) water. Reproduced from reference S. Toommee, R. Traiphol, N. Traiphol, High color stability and reversible thermochromism of polydiacetylene/zinc oxide nanocomposite in various organic solvents and polymer matrices, Colloids Surf. A 468 (2015) 252–261 with permission of Elsevier.

display temperature-responsive color switching are of considerable interest as mechanically flexible temperature sensors.

1.3.2 Photo-responsive PBSCs

Photo-responsive PBSCs are essentially polymer composite-based light- or photon-responsive materials.

Of all the stimuli available for actuation, light has attracted significant interest because of its numerous attractive characteristics, including localized delivery (light can be easily and directly delivered to the desired material surface), engineerable or tunable stimuli related functionalities (exposure wavelength, light intensity, spot radius, exposure time, and polarization direction) and on-demand pausing and resuming of actuation. Subsequently, photo-responsive PBSCs may offer prospective solutions to scores of pressing technological problems, especially where a noncontact form of stimulation and control is desired [64].

Such photo-responsive smart composites operate either via applied photon-induced reversible changes in their chemical structures (photo-isomerization), or their physical properties (photo-chromism, photo-conductivity, light-induced changes in the viscosity of polymeric solutions, light-induced changes in the gas permeability of polymer films, and so forth). Besides, photo-responsive polymer-based materials are often developed either using a polymer containing photo-responsive functional group or via combination of a polymer with a photo-responsive compound (wherein, the polymer serves the template or carrier role) [65].

Accordingly, most polymer-based photo-responsive materials are either composed of light-sensitive organic chromophores (azobenzene groups [66, 67], spiropyran groups [68, 69], and other related functional groups) or light-sensitive fillers (plasmonic metal derivatives or nanostructured semiconductors) [65, 70]. Also, photo-responsive polymers with azo-based chromophores display light-induced reversible isomerization of the azo bond (between thermally stable *trans* form and meta-stable *cis* form). Those polymers with spiropyran derivatives display light-induced reversible transformation from hydrophobic spiro conformation to hydrophilic zwitterionic merocyanine conformation. Such photo-responsive smart materials offering a reversible control over their overall physicochemical and optoelectronic properties are of considerable interest toward photo-switching applications, including sensing and actuation, biomedical imaging and diagnosis, self-healing, energy harvesting, and many more.

On the other hand, a photo-responsive PBSC developed via thoughtful introduction of photo-sensitive fillers into a tailored polymer surrounding is one of the most well-established strategies for

transferring effects from the molecular level into macroscopically visible functionalities. Such an arrangement allows the freedom of extracting unique material functionalities using various polymer-filler combinations [71–75]. It is this filler-polymer combination controlled optical functionalities, their unique photo-physics and largest nonresonant optical effects with fastest response time, which renders PBSCs as one of the most important classes of advanced photonic materials [76–79].

Consequently, Nithin et al. developed a reversibly photo-chromic PVA/Cs_2ZnO_2 based UV sensing smart composite. The said smart composite displayed an appreciable color switching (white to yellow green) upon changing the light source from lesser energy visible light to higher energy UV (Fig. 1.9). The same group opined that those PBSCs are of considerable interest as luminescent downconverting materials towards augmenting the solar energy harvesting efficacies of PV cells. Moving forward, the same group also developed a multifunctional photo-responsive PNC-based PV converter [IP-3570-IN-17181077-NPA-2019], which converted light energy from the sun into usable voltage. While, Sachhidananda et al. extracted UV photon-induced bright orange-red fluorescence using PVA/Na_2ZnO_2 NCs, which exhibited reversible photo-chromic behavior upon altering the light source from visible to UV [80]. Further, Han et al. prepared a PNIPAm-introduced AuNP hydrogel actuator that exhibited a peristaltic crawling motion in a photo-controllable manner [81].

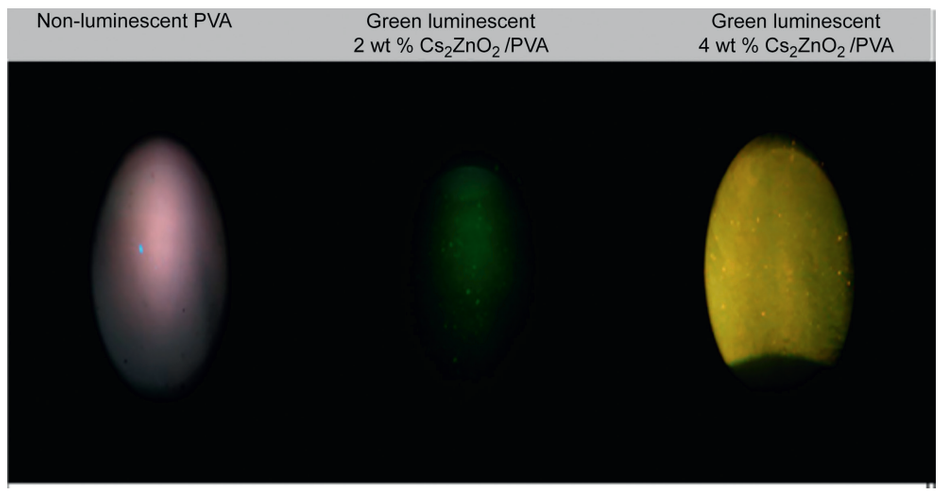


Fig. 1.9 Fluorescent microscopic images of PVA/Cs_2ZnO_2 NC thick films (under UV illumination). Reproduced from reference K.S. Nithin, Siddaramaiah, Opto-electrical characteristics of poly (vinyl alcohol)/cesium zincate nanodielectrics, J. Phys. Chem. C 119 (2015) 20244–20255 with permission of The American Chemical Society.

Besides, the nanoworld offers equal and exciting opportunities to both science and engineering disciplines and is being increasingly investigated as a multidisciplinary research domain. Nanotechnology offers smarter materials that are better built, highly durable, and relatively safe to be employed in various industrial sectors, such as optical communications, biomedical and drug delivery applications, energy conversion and storage, and other related sectors [82–85].

Consequently, the forthcoming chapters of this book will focus on the significance of PNC technology towards the effective development of PBSCs, tools and techniques adopted toward their successful fabrication and characterization; nanotechnology-enabled smart behaviors in PBSCs (with special emphasis on optical, optoelectronic, and energy allied functionalities); and their related applications.

1.3.3 Electro-responsive PBSCs

Electro-responsive PBSCs are those polymer composite-based stimuli-responsive materials that respond to an external electric field [86, 87].

Such electric field-responsive smart materials have garnered significant technological interest, owing to the inherent convenience of applying the stimulus and its fine tunability (magnitude of electric field, duration of electrical pulse, and intervals between the pulses). Further, electro-responsive PBSCs are either conducting polymer-based or semiconducting and/or insulating polymers filled with electro-responsive filler-based soft materials [88–90]. Such electro-responsive PBSCs display a measurable change in their material functionalities (structural, morphological, optical, and mechanical) with electrical stimulus [91–93].

Besides, PBSCs that exhibit a large amount of deformation (while sustaining large forces) upon applying an adequate electric field are the most preferred for robotic applications (which demand considerable linear movement). While, PBSCs that produce a voltage output upon being flexed are the most sought after for self-powered electronics applications [94].

1.3.3.1 Classification of electro-responsive PBSCs

Electro-responsive PBSCs are mainly grouped into two important categories:

1. Ionic-type electro-responsive PBSCs.
2. Electronic-type electro-responsive PBSCs.

A comparative account of the advantages, disadvantages, and related applications of two important classes of electro-responsive PBSCs is presented in Table 1.3.

Table 1.3 Summary of the comparative advantages, disadvantages, and related applications of two major types of electro-responsive PBSCs and their subclasses.

Electro-responsive PBSCs		
Ionic-type electro-responsive PBSCs		
Actual type	**Advantages**	**Disadvantages**
Conducting polymer-based	**1.** Excellent chemical stability. **2.** Improved scope for miniaturization. **3.** Facile fabrication process. **4.** Can adopt multiple forms (sheet-like, film-like, tube-like, and many more).	**1.** Inadequate adhesion onto substrate. **2.** Fragile upon mechanical and thermal loading.
Ionic polymer metal composite-based	**1.** High sensitivity to large bending deformation. **2.** Improved scope to work in wet environment. **3.** Light weight and biocompatible.	**1.** Slow response. **2.** Moisture- and temperature-sensitive hysteresis. **3.** Operation limited only to low temperature, owing to liquid-like electrolyte.
Applications **1.** Catheters **2.** Automotives devices **3.** Prosthetic devices **4.** Active noise and vibration reduction materials **5.** 5. Pristaltic pumps		
Electronic-type electro-responsive PBSCs		
Actual type	**Advantages**	**Disadvantages**
Dielectric elastomer-based	**1.** Large sensing range. **2.** High cycle stability. **3.** Ability to display self-sensing actuation.	**1.** Highly defect-sensitive. **2.** Nonsensitive to compression in normal direction. **3.** Performance may be affected by temperature.
Liquid-crystal elastomer-based	**1.** Potential to sense high strain changes. **2.** Excellent sensitivity.	**1.** Complex synthetic and/or fabrication techniques.

Table 1.3 Summary of the comparative advantages, disadvantages, and related applications of two major types of electro-responsive PBSCs and their subclasses—cont'd

Electronic-type electro-responsive PBSCs		
Actual type	**Advantages**	**Disadvantages**
Piezoelectricpolymer-based	**1.** Wide bandwidth. **2.** Improved electro-mechanical response. **3.** Relatively low power requirements. **4.** High generative forces.	**1.** Relatively low output performance, owing to charge dissipation. **2.** Certain materials need to be stretched and poled to gain higher output.

Applications

Actuation-related

1. Haptic feedback for portable consumer electronics.
2. Overear headphones.

Sensor-related

1. Strain sensing devices.
2. Smart containers and smart mats.
3. Energy generating and energy harvesting devices.

Adapted from T. Wang, M. Farajollahi, Y.S. Choi, I.T. Lin, J.E. Marshall, N.M. Thompson, S. Kar-Narayan, J.D.W. Madden, S.K. Smoukov, Electroactive polymers for sensing, Interface Focus, 2016.

Ionic-type electro-responsive PBSCs Ionic type electro-responsive PBSCs are those PBSCs activated by the electrically induced transport of ions or molecules. These ionic-type PBSCs (that encompass conducting polymer-based, ionic polymer gel-based, electro-rheological fluid-based, and ionic-polymer metal composites (IPMCs)) often operate under wet conditions and with low actuation voltages (1–5 V) [95].

Electro-responsive PBSC gels PBSC gels are those electro-responsive gels that either swell or shrink in response to applied electric fields. Such PBSC gels, which are lighter, softer, mechanically flexible, and able to generate biomimetic motions (without the aid of any mechanical parts), are of significant interest as biomimetic actuators and/or artificial muscles.

Accordingly, Yang et al. reported an rGO/poly(AAm-*co*-2-acrylamido-2-methylpropane sulfonic acid) composite hydrogel that exhibited reversible unidirectional actuation (owing to the DC current-induced generation of osmotic pressure) upon alternating the electric field [96]. Jiang et al. reported a bidirectional actuator made of PAAc-*co*-*N*,*N*-dimethylacrylamide NC hydrogel with $Al(OH)_3$ NPs as cross-linkers [97]. Such PBSC gels are extensively employed in drug

delivery systems, robotic hands, transporting devices, and so forth. Also, the observed smart behaviors in such matrices arise from possible phase transitions induced by secondary forces such as hydrogen bonding, coulombic forces, and van der Waals interactions [98]. The said effects pave the way to effectively control the overall material behaviors of PBSCs via considerate engineering of their external physicochemical conditions.

Electro-responsive conducting PBSCs Electro-responsive conducting PBSCs include either intrinsically conductive polymers (ICPs) with alternating single and double bonds or polymers introduced with conducting fillers.

In the case of ICPs, the desired electronic properties arise from their π-conjugated systems. However, in the case of polymers introduced with conducting fillers, they arise from polymer/filler combinatorial and/or synergistic effects. Of all ICPs, polyaniline (PANI), polypyrrole (PPy), and poly(3,4-ethylenedioxythiphene) (PEDOT) are of considerable interest in sensing and actuation, owing to their excellent electrical conductivity, good thermal stability, and facile process abilities [99–101].

Consequently, Uh et al. reported camphor sulfonic acid-doped PANI microfibers that converted absorbed electrical energy (triggered by current) to thermal energy, and in turn expanded and bent [102]. Xue et al. reported an electro-active ammonia sensor capable of rapidly and reversibly detecting ammonia gas with an ultralow detection limit of 0.05 ppb [100]. Nanda et al. reported electro-active shape memory composites made of a shape memory polyurethane (PU) block copolymer containing multiwalled carbon nanotubes (MWCNTs) and polypyrrole (PPy) [103]. Also, such electro-responsive PBSCs are widely employed to detect humidity, volatile organic compounds, mechanical strain, and other related functionalities.

Electro-responsive ionic polymer-metal composites Electro-responsive IPMCs are usually made of a thin ionomeric membrane (polyelectrolyte membrane) consisting of noble metal electrodes plated on its surface. They further present a perfect balance of charges (cations and anions), which are covalently fixed to the polymer backbone.

Consequently, when IPMCs are hydrated, the cations may migrate to the cathodic site (under the influence of an electric field), while the anions stay put in the polymer backbone. This ion migration often leads to alternating swelling and shrinking in the cathodic and anodic sites, which in turn results in the bending of IPMCs. Additionally, the fact that IPMCs exhibit both reversible mechanical deformation (i.e., bend, upon applying external voltage) and generate a small voltage (upon being bent) makes them highly suitable for both sensing and actuation applications. Besides, IPMCs also present numerous advantages over conventional electro-responsive materials, which includes modest operating voltage (1–2 V), fast response rates (tenths of Hz), large bending displacements (up to 10% of the gauge length),

lightweight, compact design, and the ability to operate both in liquid medium or in open air.

Accordingly, IPMCs show great promise for various biomimetic applications, including robotic fingers and grippers for planetary missions, catheter tips for intravascular neurosurgery, dust wipers used in a nanorover camera window, and so forth [104, 105].

Electronic-type electro-responsive PBSCs Electronic-type electro-responsive PBSCs are those PBSCs that are activated by an external electric field or by coulombian forces. The electronic types (that includes piezoelectric polymer-based, electrostrictive polymer-based, and dielectric elastomer (DE)-based) operate under dry conditions and often require the application of high voltage [95].

Piezoelectric PBSCs Piezoelectric (PE) PBSCs are those polymer-based composite materials that operate via the thoughtful conversion of applied stress into usable electrical charge (direct PE effect) or convert an applied electrical potential to mechanical strain (inverse PE effect).

Such PE-PBSCs are essentially polymer-based composites in which the application of an electric field reverses the direction of spontaneous polarization. These composite materials are either made of a PE base polymer or made of polymers reinforced with PE fillers. Consequently, PE-PBSCs are extensively tried for both sensing- and actuation-related applications, including structural health monitoring devices, energy harvesting and storage units, and other related domains.

Further, in PBSCs operating via the direct piezoelectric effect, the application of mechanical stress disrupts the orientation of electric dipoles and the realigning of it (as they were during polarization with the applied electric field) brings about a net polarizatio that in turn creates a potential difference across the PBSC. It is this voltage drop that allows the charge to flow between either poles (in order to realign the dipoles), thus generating current [94]. Although PE effects were mostly encountered in ceramic materials, conventional peizo-ceramics often suffered from tribulations related to their mechanical performance. Hence, they are less preferred, especially toward wearable sensor applications.

Thus, PE-PBSCs have gained substantial scientific interest and various researchers have reported different polymer/filler combinations with appreciable PE effects. Gullapalli et al. fabricated mechanically flexible PEs by successfully embedding zinc oxide (ZnO) NPs in cellulose fibers [106]. Chen et al. reported PDMS-based $PbTiO_3$ nanowires (PTNWs)/graphene nanocomposites (NCs) (fabricated via the layer-by-layer approach) with higher sensitivity and a rapid response time [107]. Park et al. adopted a sandwich approach and successfully developed a PE mat of electrospun (poly(vinylidenefluoride-*co*-trifluoroethylene)) nanofiber sandwiched between two sheets of elastomer. Such an approach was found to yield highly sensitive PE-PBSCs with improved microstrain measurement characteristics [108, 109].

Dielectric elastomer-based smart composites Dielectric elastomer-based smart composites are essentially variable capacitors that can generate large strains. These electro-responsive materials are often made of a sheet of rubbery natured PBSC, either coated on both sides with compliant electrode materials or sandwiched between two compliant electrodes. Thus, the application of an external electric field leads to electrostatic attraction (between opposing charges) or repulsion (between like charges) induced (within the compliant electrode) electrostatic pressure that causes the elastomer to deform (contract in thickness and expand in area) [110, 111]. It finally returns to its original position upon removal of the external electric field.

Such dielectric PBSCs are highly versatile biomimetic smart materials empowered with high strain, variable stiffness, and noiseless operation. Additionally, owing to the fact that they share many similarities in mechanical properties to living muscles, they often find quite a natural niche in biomedical engineering. Further, of all the polymer composites explored, PU-based dielectric elastomers are of significant interest for biomedical applications, owing to their dopant-dependent large electrical field strains, high chemical and abrasion resistance, ease of processing, and increased biocompatibilities.

Such dielectric PBSCs with large strain and relatively high energy density (nearly unmatched in comparison with other electro-active smart materials such as ferroelectrics and PEs) are extensively used as soft sensors and/or actuators. Besides, those dielectric PBSCs with low elastic modulus that are subjected to a high electric field often exhibit large deformations. Hence, they are the most commonly tried soft sensors and actuators toward diaphragm blood pumps, surgical robotics training, rehabilitation orthotics, soft robots that can walk, crawl, hop, and fly [112, 113], and other related applications.

1.3.4 Magneto-responsive PBSCs

Magneto-responsive PBSCs are those polymer composite materials with magnetic field-responsive smart behaviors. Such magneto-responsive PBSCs may be obtained via the successful merger of mechanically flexible polymeric matrices with magnetically active smart fillers or dopants. Besides, these smart hybrids have garnered intense research interest because the magnetic actuation provides many unique capabilities, that is, they can be spatially and temporally controlled and also be operated externally (via a noninvasive approach). Accordingly, magneto-responsive PBSCs are extensively employed for biomedical (drug delivery, tissue engineering, and active diagnosis), smart clothing (smart textiles and fibers), and microelectronic (actuators and electro-mechanics) applications. Besides, magnetically ac-

tive fillers, when loaded to various particle stabilizing polymers, may enable the successful development of diverse magneto-responsive PBSCs (Fig. 1.10).

Further, to perfectly anticipate and induce the desired properties in magneto-responsive PBSCs, many important factors have to be adequately engineered. Additionally, the amplitude of the desired magneto response in such PBSCs is governed by the geometrical parameters (size, shape, surface/volume ratio, and aspect ratio) of the fillers and nature and/or the composition of the resulting composite (extent of magnetic material loading, filler-polymer compatibilities, and other related factors). A summary of the same is presented in Table 1.4.

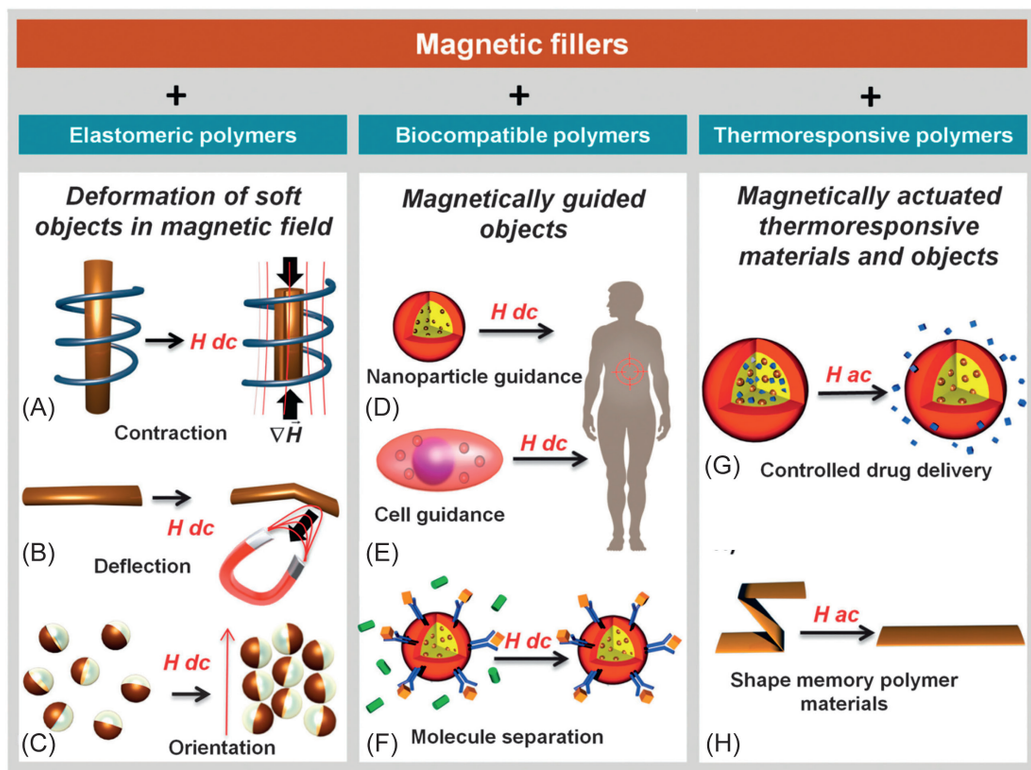


Fig. 1.10 Schematics depicting various classes of magnetic-responsive PBSCs obtained via the thoughtful doping of polymers with magnetic particles, and the illustration of their corresponding response when exposed to a static magnetic field (H dc) (or) to an alternating magnetic field (H ac). Reproduced from reference J. Thévenot, H. Oliveira, O. Sandre, S. Lecommandoux, Magnetic responsive polymer composite materials, Chem. Soc. Rev. 42 (2013) 7099–7116 with permission of The Royal Society of Chemistry.

Table 1.4 Summary of major filler and polymer-related factors to be controlled so as to enable the desired magneto-responsive PBSCs for various target applications.

Target Applications ⟹	Magneto-elastic deformations-based	Magnetic guidance and magnetic separation-based	Alternating magnetic field-induced thermal phase or shape transition-based
Magnetic fillers	1. Controlled size **For ferrogels:** magnetic core size or clusters size superior to gel mesh-size **For silicones:** micrometric size that induces particle chaining when submitted to a DC magnetic field	1. Higherfiller loading to reach high magnetization 2. Biocompatible magnetic materials (surface passivation is desired when magnetic NPs are not made of pure iron oxide so as to shield from the toxicity of "hard" nanomagnets)	1. Homogeneous distribution in particular polymer matrix 2. High specific absorption rate (SAR) to maximize the heating source
Polymer matrix	1. Softer matrices so as to optimizethe magneto-elastic ratio (balance of magnetization vs. mechanical strength)	1. Engineerable surface properties so as to fine tune their interactions with biostructures (depending on the target application) 2. High porosity to suit ecological purposes (remediation)	**For drug delivery:** 1. Tunable transition temperatures (40–45°C), so as to address the biological constraints 2. Controllable physicochemical mechanisms leading to drug release (permeability vs. degradation) **For shape memory devices:** 1. Minimized the reduce surface-to-volume ratio forcontrolled heat dissipation

Reproduced from reference J. Thévenot, H. Oliveira, O. Sandre, S. Lecommandoux, Magnetic responsive polymer composite materials, Chem. Soc. Rev. 42 (2013) 7099–7116 with permission of The Royal Society of Chemistry.

1.4 Conclusions and future directions

Although PBSCs have been explored for decades, the true techno-commercial potential of such materials is still emerging. We give all credit to the rapid advancements in the field of nanotechnology, catalyzed by the development of novel synthetic and characterization tools. These technological advancements have led to the successful development of new erudite nanofiller synthesizing approaches, a comprehensive understanding of the responsive polymer/filler moiety interactions, and the effective fabrication and characterization of advanced PBSCs with engineerable material properties. Further, the fact that the end functionalities of PBSCs can be successfully tuned by using various filler/matrix combinations (through either combinatorial or synergistic effects) has enabled different researchers to develop diverse stimuli-responsive smart materials with

unique physicochemical behaviors. This in turn has paved the way for emerging applications of such mechanically flexible smart materials in sensors, actuators, self-healing coatings, miniaturized electronic devices, and other related areas.

To sum up, we believe that in the future, the commercial success of PBSCs in various imperative applications (household, industrial, medicinal, and environmental) would require a transdisciplinary research approach. That demands successful collaboration among researchers from diverse areas of science, engineering, and technology. So, in the near future, there could be many more interesting stories on the research and commercialization of such PBSCs.

References

[1] M.W. Urban (Ed.), Handbook of Stimuli-Responsive Materials, John Wiley & Sons, 2011.
[2] L. Brunsveld, B.J.B. Folmer, E.W. Meijer, R.P. Sijbesma, Supramolecular polymers, Chem. Rev. 101 (2001) 4071–4098.
[3] D. Roy, J.N. Cambre, B.S. Sumerlin, Future perspectives and recent advances in stimuli–responsive materials, Prog. Polym. Sci. 35 (2010) 278–301.
[4] H. Koerner, G. Price, N.A. Pearce, M. Alexander, R.A. Vaia, Remotely actuated polymer nanocomposites stress–recovery of carbon–nanotube–filled thermoplastic elastomers, Nat. Mater. 3 (2004) 115–120.
[5] C.Y. Lai, B.G. Trewyn, D.M. Jeftinija, K. Jeftinija, S. Xu, S. Jeftinija, V.S.Y. Lin, A mesoporous silica nanosphere-based carrier system with chemically removable CdS nanoparticle caps for stimuli-responsive controlled release of neurotransmitters and drug molecules, J. Am. Chem. Soc. 125 (2003) 4451–4459.
[6] S.K. Nagaraj, S. Shivanna, N.K. Subramani, H. Siddaramaiah, Revisiting powder X-ray diffraction technique: a powerful tool to characterize polymers and their composite films, J. Mater. Sci. 4 (2016) 1–5.
[7] M.V. Bhavya, D.V. Gowda, S. Praveen, N.K. Subramani, H. Siddaramaiah, Cosmetics: polymers, in: Encyclopedia of Polymer Applications, first ed., T&F, 2018.
[8] K.S. Nithin, S. Kasargod Nagaraj, S. Shivanna, H. Siddaramaiah, Yellow–green luminescent poly (vinyl alcohol) nanocomposite thick films as effective spectral manipulators, J. Appl. Polym. Sci. 135 (2018) 46854–46855.
[9] K.S. Nithin, Polymer nanocomposites as luminescent down shifting layers, Res. Rev.: J. Mater. Sci. 4 (3) (2016) 6.
[10] S. Sandeep, A.S. Santhosh, N.K. Swamy, G.S. Suresh, J.S. Melo, K.S. Nithin, Electrochemical detection of L-DOPA using crude polyphenol oxidase enzyme immobilized on electrochemically reduced RGO-Ag nanocomposite modified graphite electrode, Mater. Sci. Eng. B Solid-State Mater. Adv. Technol. 232 (2018) 15–21.
[11] L. Zhang, T. Xu, Z. Lin, Controlled release of ionic drug through the positively charged temperature-responsive membranes, J. Membrane Sci. 281 (2006) 491–499.
[12] Y. Liu, L. Meng, X. Lu, L. Zhang, Y. He, Thermo and pH sensitive fluorescent polymer sensor for metal cations in aqueous solution, Polym. Adv. Technol. 19 (2008) 137–143.
[13] S. Ohya, H. Sonoda, Y. Nakayama, T. Matsuda, The potential of poly (N-isopropylacrylamide)(PNIPAM)-grafted hyaluronan and PNIPAM-grafted gelatin in the control of post-surgical tissue adhesions, Biomaterials 26 (2005) 655–659.

[14] S. Kazuo, K. Morishita, A. Kishida, M. Akashi, Synthesis and functionalities of poly (N-vinylalkylamide). V. Control of a lower critical solution temperature of poly (N-vinylalkylamide), J. Polym. Sci. Polym. Chem. 35 (1997) 3087–3094.
[15] K. Na, K.H. Lee, D.H. Lee, Y.H. Bae, Biodegradable thermo-sensitive nanoparticles from poly (L-lactic acid)/poly (ethylene glycol) alternating multi-block copolymer for potential anti-cancer drug carrier, Eur. J. Pharm. Sci. 27 (2006) 115–122.
[16] D.P. Jones, J.L. Carlson, P.S. Samiec, P. Sternberg Jr., V.C. Mody Jr., R.L. Reed, L.A. Brown, Glutathione measurement in human plasma: evaluation of sample collection, storage and derivatization conditions for analysis of dansyl derivatives by HPLC, Clin. Chim. Acta 275 (1998) 175–184.
[17] P.M. Mendes, Stimuli–responsive surfaces for bio-applications, Chem. Soc. Rev. 37 (2008) 2512–2529.
[18] Y. Li, X. Jia, M. Gao, H. He, G. Kuang, Y. Wei, Photoresponsive nanocarriers based on PAMAM dendrimers with a o-nitrobenzyl shell, J. Polym. Sci. Part A Polym. Chem. 48 (2020) 551–557.
[19] M. Czaun, L. Hevesi, M. Takafuji, H. Ihara, A novel approach to magneto–responsive polymeric gels assisted by iron nanoparticles as nano cross–linkers, Chem Commun. Apr. 28 (2008) 2124–2126.
[20] D. Szabó, G. Szeghy, M. Zrínyi, Shape transition of magnetic field sensitive polymer gels, Macromolecules 31 (1998) 6541–6548.
[21] B.D. Korth, P. Keng, I. Shim, S.E. Bowles, C. Tang, T. Kowalewski, K.W. Nebesny, J. Pyun, Polymer-coated ferromagnetic colloids from well-defined macromolecular surfactants and assembly into nanoparticle chains, J. Am. Chem. Soc. 128 (2006) 6562–6563.
[22] A. Marin, M. Muniruzzaman, N. Rapoport, Acoustic activation of drug delivery from polymeric micelles: effect of pulsed ultrasound, J. Control. Release 71 (2001) 239–249.
[23] P. Norris, M. Noble, I. Francolini, A.M. Vinogradov, P.S. Stewart, B.D. Ratner, J.W. Costerton, P. Stoodley, Ultrasonically controlled release of ciprofloxacin from self–assembled coatings on poly(2-hydroxyethyl methacrylate) hydrogels for Pseudomonas aeruginosa biofilm prevention, Antimicrob. Agents Chemother. 49 (2005) 4272–4279.
[24] K.S. Soppimath, A.R. Kulkarni, T.M. Aminabhavi, Chemically modified polyacrylamide-g-guar gum-based crosslinked anionic microgels as pH-sensitive drug delivery systems: preparation and characterization, J. Control. Release 75 (2001) 331–345.
[25] M.Y. Abdelaal, E.A. Abdel-Razik, E.M. Abdel-Bary, I.M. El-Sherbiny, Chitosan-based interpolymeric pH–responsive hydrogels for in vitro drug release, J. Appl. Polym. Sci. 103 (2007) 2864–2874.
[26] H.Y. Park, I.H. Song, J.H. Kim, W.S. Kim, Preparation of thermally denatured albumin gel and its pH-sensitive swelling, Int. J. Pharm. 175 (1998) 231–236.
[27] M. Kurisawa, N. Yui, Gelatin/dextran intelligent hydrogels for drug delivery: dual-stimuli-responsive degradation in relation to miscibility in interpenetrating polymer networks, Macromol. Chem. Phys. 199 (1998) 1547–1554.
[28] J.W. Lee, S.Y. Kim, S.S. Kim, Y.M. Lee, K.H. Lee, S.J. Kim, Synthesis and characteristics of interpenetrating polymer network hydrogel composed of chitosan and poly(acrylic acid), J. Appl. Polym. Sci. 73 (1999) 113–120.
[29] K. Nakamura, R.J. Murray, J.I. Joseph, N.A. Peppas, M. Morishita, A.M. Lowman, Oral insulin delivery using P(MAA-g-EG) hydrogels: effects of network morphology on insulin delivery characteristics, J. Control. Release 95 (2004) 589–599.
[30] J. Zhang, N.A. Peppas, Synthesis and characterization of pH- and temperature-sensitive poly(methacrylic acid)/poly(N-isopropylacrylamide) interpenetrating polymeric networks, Macromolecules 33 (2000) 102–107.

[31] Z. Sideratou, D. Tsiourvas, C.M. Paleos, Quaternized poly(propylene imine) dendrimers as novel pH-sensitive controlled-release systems, Langmuir 16 (2000) 1766–1769.
[32] S.E. Burke, C.J. Barrett, pH-responsive properties of multilayered poly(L-lysine)/hyaluronic acid surfaces, Biomacromolecules 4 (2003) 1773–1783.
[33] K. Szczubiałka, M. Jankowska, M. Nowakowska, Smart polymeric nanospheres as new materials for possible biomedical applications, J. Mater. Sci. Mater. Med. 14 (2003) 699–703.
[34] K.W. Leong, B.C. Brott, R. Langer, Bioerodible polyanhydrides as drug-carrier matrices. I: Characterization, degradation, and release characteristics, J. Biomed. Mater. Res. 19 (1985) 941–955.
[35] E. Mathiowitz, J.S. Jacob, Y.S. Jong, G.P. Carino, D.E. Chickering, P. Chaturvedi, C.A. Santos, V. Kavita, M. Sean, B. Michael, M. Craig, Biologically erodable microspheres as potential oral drug delivery systems, Nature 386 (1997) 410–414.
[36] S. Cohen, T. Yoshioka, M. Lucarelli, L.H. Hwang, R. Langer, Controlled delivery systems for proteins based on poly(lactic/glycolic acid) microspheres, Pharm. Res. Off. J. Am. Assoc. Pharm. Sci. 8 (1991) 713–720.
[37] S. Matsumoto, R.J. Christie, N. Nishiyama, K. Miyata, A. Ishii, M. Oba, H. Koyama, Y. Yamasaki, K. Kataoka, Environment-responsive block copolymer micelles with a disulfide cross-linked core for enhanced siRNA delivery, Biomacromolecules 10 (2009) 119–127.
[38] Y. Qiu, K. Park, Environment-sensitive hydrogels for drug delivery, Adv. Drug Deliv. Rev. 53 (3) (2001) 321–339.
[39] R. Yoshida, T. Yamaguchi, E. Kokufuta, New intelligent polymer gels: a self-oscillating gel with pacemaking and actuating functions, J. Artif. Organs 2 (1999) 135–140.
[40] T.F. Vandamme, A. Lenourry, C. Charrueau, J.C. Chaumeil, The use of polysaccharides to target drugs to the colon, Carbohydr. Polym. 48 (2002) 219–231.
[41] Y. Itoh, M. Matsusaki, T. Kida, M. Akashi, Enzyme-responsive release of encapsulated proteins from biodegradable hollow capsules, Biomacromolecules 7 (2006) 2715–2718.
[42] H. Meng, G. Li, A review of stimuli–responsive shape memory polymer composites, Polymer 54 (2013) 2199–2221.
[43] V.A. Ganesh, A. Baji, S. Ramakrishna, Smart functional polymers—a new route towards creating a sustainable environment, RSC Adv. 4 (2014) 53352–53364.
[44] Y.J. Kim, Y.T. Matsunaga, Thermo-responsive polymers and their application as smart biomaterials, J. Mater. Chem. B RSC 5 (2017) 4307–4321.
[45] A. Choe, J. Yeom, R. Shanker, M.P. Kim, S. Kang, H. Ko, Stretchable and wearable colorimetric patches based on thermoresponsive plasmonic microgels embedded in a hydrogel film, NPG Asia Mater. 10 (2008) 912–922.
[46] X. Lan, W. Huang, J. Leng, Shape memory effect in micro-sized shape memory polymer composite chains, Appl. Sci. 9 (2019) 2919–2920.
[47] W.M. Huang, Y. Zhao, C.C. Wang, Z. Ding, H. Purnawali, C. Tang, J.L. Zhang, Thermo/chemo-responsive shape memory effect in polymers: a sketch of working, mechanisms, fundamentals and optimization, J. Polym. Res. 19 (2012) 1–34.
[48] S. Prashanth, K.M. Subbaiah, K.S. Nithin, S. Sachhidananda, Fiber reinforced composites—a review, J. Mater. Sci. Eng. 6 (2017) 341–342.
[49] B. Suresha, R. Hemanth, K.S. Nithin, Automotive Applications: Reinforced Material Components, Encyclopedia of Polymer Applications, CRC Press, 2018.
[50] B. Suresha, K. Adappa, N.K. Subramani, Mechanical and tribological behaviours of epoxy hybrid composites reinforced by carbon fibers and silicon carbide whiskers, Mater. Today: Proc. 5 (2018) 16658–16668.

[51] S. Pradhan, R. Lach, H.H. Le, W. Grellmann, H.J. Radusch, R. Adhikari, Effect of filler dimensionality on mechanical properties of nanofiller reinforced polyolefin elastomers, ISRN Mater. Sci. 2013 (2013).
[52] H. Meng, G. Li, A review of stimuli-responsive shape memory polymer composites, Polymer 54 (2013) 2199–2221.
[53] A.M.N. Saeed, M.Q.A. Al-Gunaid, N.K. Subramani, B.S. Madhukar, S. Basavarajaiah, Effect of cesium aluminate nanofiller on optical properties of polyvinyl pyrrolidone nanocomposite films, Polym. – Plast. Technol. Eng. 57 (2008) 1188–1196.
[54] L. Hu, Q. Zhang, X. Li, M.J. Serpe, Stimuli-responsive polymers for sensing and actuation, Mater. Horiz. 6 (2019) 1774–1793.
[55] D. Roy, N.J. Cambre, B.S. Sumerlin, Future perspectives and recent advances in stimuli-responsive materials, Prog. Polym. Sci. 35 (2010) 278–301.
[56] K.S. Nithin, S. Shivanna, S.K. Nagaraj, H. Siddaramaiah, Refractive index engineering of poly(vinylalcohol)/Li_2ZnO_2 nanocomposites: effect of filler content and annealing temperature, AIP Conf. Proc. 1943 (2018) 020127–020128.
[57] C.A. Finch, Polyvinyl Alcohol: Developments, Wiley, 1992.
[58] C.X. Ma, W. Lu, X.X. Yang, J. He, X.X. Le, L. Wang, J.W. Zhang, M.J. Serpe, Y.J. Huang, T. Chen, Bioinspired anisotropic hydrogel actuators with on-off switchable and color-tunable fluorescence behaviors, Adv. Funct. Mater. 28 (2018) 1704568–1704569.
[59] H. Kim, J.Y. Chang, Reversible thermochromic polymer film embedded with fluorescent organogel nanofibers, Langmuir: ACS J. Surf. Colloids 30 (2014) 13673–13679.
[60] G. Carotenuto, G. La Peruta, L. Nicolais, Thermo-chromic materials based on polymer-embedded silver clusters, Sensors Actuators B Chem. 114 (2006) 1092–1095.
[61] M. Sato, K. Yuzo, M. Shigekazu, Y. Isao, F. Yasuhisa, Visible light-emitting and temperature-sensitive copolymer gel/ZnO nanocomposites loaded with surface-modified ZnO nanoparticles having polyethylene glycol chains, Eur. Polym. J. 48 (2012) 1177–1185.
[62] S. Toommee, R. Traiphol, N. Traiphol, High color stability and reversible thermochromism of polydiacetylene/zinc oxide nanocomposite in various organic solvents and polymer matrices, Colloids Surf. A 468 (2015) 252–261.
[63] M. Xygkis, E. Gagaoudakis, L. Zouridi, O. Markaki, E. Aperathitis, K. Chrissopoulou, G. Kiriakidis, V. Binas, Thermochromic behavior of VO_2/polymer nanocomposites for energy saving coatings, Coatings 9 (2019) 163–164.
[64] G. Stoychev, A. Kirillova, L. Ionov, Light-responsive shape-changing polymers, Adv. Opt. Mater. 7 (2019) 1900067–1900068.
[65] S. Shivanna, N.K. Subramani, S.K. Nagaraj, J.R.B. Mutturaj, S. Basavaraj, Patina-green coloured light emitting polycarbonate films: a synergistic extraction of improved UV endurance and considerate spectral down-conversion, J. Lumin. 210 (2019) 276–284.
[66] K. Ichimura, S.K. Oh, M. Nakagawa, Light-driven motion of liquids on a photoresponsive surface, Science 288 (2000) 1624–1626.
[67] K. Ichimura, Y. Suzuki, T. Seki, A. Hosoki, K. Aoki, Reversible change in alignment mode of nematic liquid crystals regulated photochemically by command surfaces modified with an azobenzene monolayer, Langmuir 4 (1988) 1214–1216.
[68] S. Wang, Y. Song, L. Jiang, Photoresponsive surfaces with controllable wettability, J. Photochem. Photobiol. C 8 (2007) 18–29.
[69] M. Yoshida, J. Lahann, Smart nanomaterials, ACS Nano 2 (2008) 1101–1107.
[70] B.M. Jagajeevanraj, S. Sachhidananda, K. Pushpalatha, K.S. Nithin, Nanostructured $Al_{0.2}Y_{1.8}O_3$ semiconductor assisted enhancement in PVOH forti-

tude to withstand high energy UV photons: an opto-mechanical study, Optik 182 (2019) 598–604.
[71] K.S. Nithin, Siddaramaiah, Opto-electrical characteristics of poly (vinyl alcohol)/cesium zincate nanodielectrics, J. Phys. Chem. C 119 (2015) 20244–20255.
[72] K.S. Nithin, S. Kasargod Nagaraj, S. Shivanna, H. Siddaramaiah, Highly flexible and visibly transparent poly (vinyl alcohol)/calcium zincate nanocomposite films for UVA shielding applications as assessed by novel ultraviolet photon induced fluorescence quenching, Macromolecules 49 (2016) 2791–2801.
[73] C. Sci, Poly (vinyl alcohol) decorated lithium doped stannous oxide nanocomposites as highly flexible UVA shieldants, Chem. Sci. J. 7 (2016) 121–122.
[74] K.N. Shilpa, K. Subramani, S. Sachhidananda, B.S. Madhukar, Visibly transparent PVA/sodium doped dysprosia ($Na_2Dy_2O_4$) nano composite films, with high refractive index: an optical study, J. Alloys Compd. 694 (2017) 884–891.
[75] N. Kundachira Subramani, S. Shivanna, S. Kasargod Nagaraj, B. Suresha, B.M. Jagajeevan Raj, H. Siddaramaiah, Optoelectronic behaviours of UV shielding calcium zirconate reinforced polycarbonate nanocomposite films: an optical view, Mater. Today Proc. 5 (8 Part 3) (2018) 16626–16632.
[76] S. Sachhidananda, G.R. Suma, K.S. Nithin, S.V. Satyanarayana, Siddaramaiah, Tuning the electrical and thermal functionalities of mechanically flexible poly (vinyl alcohol) nanocomposites: effect of cerium zirconate nanofiller content, Int. J. Eng. Sci. 1 (2019) 8–14.
[77] T. Champa, S. Sachhidananda, K.N. Shilpa, K.S. Nithin, Siddaramaiah, Optoelectronic behaviors of reversibly stretchable $Na_{0.8}Mn_{0.8}O_2$ reinforced poly(vinyl alcohol) nanocomposites, Int. J. Eng. Sci. Comput. 7 (2017) 14875–14879.
[78] G.R. Suma, K.S. Nithin, B.V. Latha, S.K. Nagaraj, S. Shivanna, S.V. Sathyanarayana, Gent to refractive index engineering of strontium doped zirconium oxide (SZO) reinforced poly vinyl pyrrolidone composite films: effect of dopant content and annealing temperature, Int. J. Eng. Sci. Comput. 6 (2016) 5703–5709.
[79] G.R. Suma, K.S. Nithin, K.N. Shilpa, S. Sachhidananda, S.V. Satyanarayana Siddaramaiah, Effect of $Ce_{0.5}Zr_{0.5}O_2$ nano fillers on structural and optical behaviors of poly(vinyl alcohol), J. Mater. Sci. Mater. Electron. 28 (2017) 10707–10714.
[80] S. Shivanna, K.S. Nithin, S. Kasargod Nagaraj, H. Siddaramaiah, Orange-red fluorescent polymer nanocomposite films with large stokes shift: an opto-electronic exercise, J. Lumin. 208 (2019) 488–494.
[81] L. Han, Y. Zhang, X. Lu, K. Wang, Z. Wang, H. Zhang, Polydopamine nanoparticles modulating stimuli-responsive PNIPAM hydrogels with cell/tissue adhesiveness, ACS Appl. Mater. Interfaces 42 (2016) 29088–29100.
[82] K.N. Shilpa, H.B. Patil, P. Karthik, K. Mallikarjun, B.M. JagajeevanRaj, S. Sharon, K.S. Nithin, Removal of Cu(II) from water using hydrothermally synthesized strontium doped zirconium oxide nano adsorbents, J. Mater. Sci. Eng. 1 (2016) 252–256.
[83] H.B. Vasanth Patil, K.S. Nithin, S. Sachhidananda, Siddaramaiah, K.T. Chandrashekara, B.Y. Sathish Kumar, Mycofabrication of bioactive silver nanoparticle: photo catalysed synthesis and characterization to attest its augmented bio-efficacy, Arab. J. Chem. 12 (2019) 4596–4611.
[84] K.N. Shilpa, S.R. Urs, H.B. Patil, H.P. Jayadevappa, B.V. Latha, K.S. Nithin, S. Sachhidananda, Adsorptive removal of Cu(II) from aqueous solution using nanostructured lithium zincate, Int. J. Eng. Sci. Comput. 6 (2016) 8463–8468.
[85] P. Sivadasu, D.V. Gowda, N.K. Subramani, B.M. Vishweshwaraiah, S. Shivanna, S. Hatna, Direct brain targeted nanostructured lipid carriers for sustained release of schizophrenic drug: formulation, characterization and pharmacokinetic studies, Indian J. Pharm. Educ. Res. 54 (2020) 73–84.

[86] G.R. Suma, N.K. Subramani, S. Sachhidananda, S.V. Satyanarayana, Siddaramaiah, Nanotechnology enabled *E. coli* sensors: an opto-electronic study, Mater. Today Proc. 4 (10) (2017) 11300–11304.
[87] K.M. Mahesha, K.S. Subbaiah, B.M.J. Nithin, S. Raj, Shivanna, highly flexible and conducting polymer nanocomposite films for selective gas sensing applications, Mater. Today Proc. 9 (2019) 515–521.
[88] M.Q.A. Al-Gunaid, A.M.N. Saeed, K.S. Nithin, B.S. Madhukar, Siddaramaiah, Optical parmeters, electrical permittivity and I-V characterstics of PVA/Cs_2CuO_2 nanocomposite films for opto-electronic applications, J. Mater. Sci.: Mater. Electron. 28 (2017) 8074–8086.
[89] M. Tirumali, B. Kandasubramanian, A. Kumaraswamy, N.K. Subramani, B. Suresha, Fabrication, physicochemical characterizations and electrical conductivity studies of modified carbon nanofiber-reinforced epoxy composites: effect of 1-butyl-3-methylimidazolium tetrafluoroborate ionic liquid, Polym. Plast. Technol. Eng. 57 (2018) 218–228.
[90] K.S. Nithin, Nanotechnology enabled electrode materials for rechargeable sodium-ion batteries: an ideal resolution to global energy crisis, Res. Rev. J. Mater. Sci. 4 (4) (2016) 3.
[91] Y. Zhao, L. Cao, L. Li, W. Cheng, L. Xu, X. Ping, L. Pan, Y. Shi, Conducting polymers and their applications in diabetes management, Sensors 16 (2016) 1787–1788.
[92] P.J. Glazer, M. van Erp, A. Embrechts, S.G. Lemay, E. Mendes, Role of pH gradients, in the actuation of electro-responsive polyelectrolyte gels, Soft Matter 8 (2012) 4421–4426.
[93] H. Jiang, L. Fan, S. Yan, F. Li, H. Li, J. Tang, Tough and electro-responsive hydrogel actuators with bidirectional bending behaviour, Nanoscale 11 (2019) 2231–2237.
[94] N.K. Subramani, K.N. Shilpa, S. Sachhidananda, B.M. Jagajeevan Raj, H. Siddaramaiah, Chapter 6: Advances in polymer-based piezoelectric systems, in: Emergent Research on Polymeric and Composite Materials, IGI Global, Hershey, PA, 2018, pp. 139–157.
[95] F. Raju, D. Sakthi Kumar, Biomedical Applications of Polymeric Materials and Composites, first ed., Wiley-VCH Verlag GmbH & Co. KGaA, 2017.
[96] C. Yang, Z. Liu, C. Chen, K. Shi, L. Zhang, X.J. Ju, W. Wang, R. Xie, L.Y. Chu, Reduced graphene oxide-containing smart hydrogels with excellent electro-response and mechanical properties for soft actuators, ACS Appl. Mater. Interfaces 9 (2017) 15758–15767.
[97] H. Jiang, L. Fan, S. Yan, F. Li, H. Li, J. Tang, Tough and electro-responsive hydrogel actuators with bidirectional bending behaviour, Nanoscale 11 (2019) 2231–2237.
[98] M. Shingo, H. Yusuke, Y. Ryo, H. Shuji, Active polymer gel actuators, Int. J. Mol. Sci. 11 (2010) 52–66.
[99] C.O. Baker, X. Huang, W. Nelson, R.B. Kaner, Polyaniline nanofibers: broadening applications for conducting polymers, Chem. Soc. Rev. 46 (2017) 1510–1525.
[100] M. Xue, F. Li, D. Chen, Z. Yang, X. Wang, J. Ji, High-oriented polypyrrole nanotubes for next-generation gas sensor, Adv. Mater. 28 (2016) 8265–8270.
[101] D.S. Shin, Z. Matharu, J. You, C. Siltanen, T. Vu, V.K. Raghunathan, G. Stybayeva, A.E. Hill, A. Revzin, Sensing conductive hydrogels for rapid detection of cytokines in blood, Adv. Healthc. Mater. 5 (2016) 659–664.
[102] K. Uh, B. Yoon, C.W. Lee, J.M. Kim, An electrolyte-free conducting polymer actuator that displays electrothermal bending and flapping wing motions under a magnetic field, ACS Appl. Mater. Interfaces 8 (2016) 1289–1296.
[103] G.S. Nanda, Y.C. Jung, J.W. Cho, Electroactive shape memory effect of polyurethane composites filled with carbon nanotubes and conducting polymer, Mater. Manuf. Process. 22 (2007) 419–423.

[104] J.W. Paquette, K.J. Kim, Ionomeric electroactive polymer artificial muscle for naval applications, IEEE J. Ocean. Eng. 29 (2004) 729–737.
[105] Y. Bar-Cohen, S.P. Leary, A. Yavrouian, K. Oguro, S. Tadokoro, J.S. Harrison, J.G. Smith, J. Su, Challenges to the application of IPMC as actuators of planetary mechanisms, Proc. SPIE 3987 (2000) 40–41.
[106] H. Gullapalli, V.S. Vemuru, A. Kumar, A. Botello-Mendez, R. Vajtai, M. Terrones, S. Nagarajaiah, P.M. Ajayan, Flexible piezoelectric ZnO-paper nanocomposite strain sensor, Small 6 (2010) 1641–1646.
[107] Z. Chen, Z. Wang, X. Li, Y. Lin, N. Luo, M. Long, N. Zhao, J.B. Xu, Flexible piezoelectric-induced pressure sensors for static measurements based on nanowires/graphene heterostructures, ACS Nano 11 (2017) 4507–4513.
[108] S.H. Park, H.B. Lee, S.M. Yeon, J. Park, N.K. Lee, Flexible and stretchable piezoelectric sensor with thickness-tunable configuration of electrospun nanofiber mat and elastomeric substrates, ACS Appl. Mater. Interfaces 8 (2016) 24773–24781.
[109] L. Persano, C. Dagdeviren, Y. Su, Y. Zhang, S. Girardo, D. Pisignano, Y. Huang, J.A. Rogers, High performance piezoelectric devices based on aligned arrays of nanofibers of poly (vinylidenefluoride-co-trifluoroethylene), Nat. Commun. 4 (2013) 1633–1634.
[110] K.J. Yoon, S. Shin, H.C. Park, N.S. Goo, Design and manufacture of a lightweight piezocomposite curved actuator, Smart Mater. Struct. 11 (2002) 163–168.
[111] P. Brochu, Q. Pei, Advances in dielectric elastomers for actuators and artificial muscles, Macromol. Rapid Commun. 31 (2010) 10–36.
[112] E. Biddiss, T. Chau, Dielectric elastomers as actuators for upper limb prosthetics: challenges and opportunities, Med. Eng. Phys. 30 (2008) 403–418.
[113] G. Kovacs, P. Lochmatter, M. Wissler, An arm-wrestling robot driven by dielectric elastomer actuators, Smart Mater. Struct. 16 (2007) 306–317.

2

Conjugated polymer-based smart composites for optoelectronics and energy applications

Smitha V. Kamath, Kanakaraj Aruchamy, and Nataraj Sanna Kotrappanavar
Centre for Nano and Material sciences, Jain University, Bangalore, India

2.1 Introduction

Effective energy management in an ever expanding digital world with a continuously increasing consumer population requires a new set of smart energy conversion and storage devices. In the age of portable devices, finding suitable energy conversion and storage devices has become a bottleneck situation to try and fulfill the demand of energy resources to the world [1]. Accepting the prevalence of the energy crisis and working towards addressing it are among the main steps toward solving that bottleneck. It is further assumed that the best solution toward addressing the ongoing energy conversion and storage problems may well come from the new class of materials known as smart materials or intelligent materials. These are multifunctional in nature, easy to adapt to different conditions and processes, and can be applied to work as a system that apparently uses its own functionalities intelligently, depending on the varying conditions of the device. These materials also behave smartly with the environmental changes and offer a longer shelf life [2].

Conjugated polymer-based smart materials have attracted much deserved attention in many fields, owing to their tunable properties, particularly for use in flexible electronics. Most of the conjugated polymers can also be converted into flexible plastics known as thermoplastics, which bear special interest in optoelectronics and energy storage devices because of their excellent combination of mechanical, optical, electronic, and structural properties [3]. Further, progress in nanotechnology procedures and methods has enabled conjugated polymers to attain exceptional properties when combined with other conventional optoelectronic and energy materials. To exploit these

Polymer-Based Advanced Functional Composites for Optoelectronic and Energy Applications
https://doi.org/10.1016/B978-0-12-818484-4.00005-7
Copyright © 2021 Elsevier Inc. All rights reserved.

synergic effects, researchers working in almost every field have taken advantage of composite conjugated polymer-based materials, which may result from a thoughtful combination of conjugated polymer/conjugated polymer, conjugated polymer/hybrid inorganic material, and conjugated polymer/nanomaterial [4].

Moreover, augmented demand from both industrial sectors and the innovating community has induced significant interest toward converting conventional conjugated polymer-based composites into smart materials via the appropriate intrinsic property engineering of its constituents. The as-developed smart conjugated polymer composites may possess an interesting ability to respond and adjust to the external environment and conditions where they have been applied, including stress, temperature, pH, light, chemical environment, magnetic and electrical fields, and so forth [5].

Smart conjugated polymer composites, which are extensively used in telecommunication services, such as plastic optical fibers (POFs) are an attractive transmission medium for network systems and office automation systems, as they can be easily connected with light sources in portable as well as fixed locations [6]. Smart conjugated polymer composites will also be able to bear harsh radiation conditions when exposed to near-infrared (near-IR) optical sources. Such materials are used in optical communication systems due to the special functionality that exists in the conjugated polymer backbone [7, 8]. In the recent past, organic materials have also shown excellent potential for nonlinear optical devices because of their large optical nonlinearity and fast response time. Conjugated polymeric thin films, which exhibit a third-order optical nonlinearity with good processabilities, have also been investigated, and are expected to have many useful applications in integrated optics such as optical stability and optical data processing [9].

On the other hand, energy conversion and storage devices extensively use smart conjugated polymer composites as the main component of the device. Smart conjugated polymer composites with high tunable electronic and ionic conductivity, flexibility, storage capacity, ion/charge transport ability, and mechanical agility are increasingly suitable for energy applications [10, 11]. Consequently, conjugated polymer composite hydrogels have been extensively used as polyelectrolytes in batteries, supercapacitors, and fuel cells [12, 13]. Self-healing conjugated polymer systems have been tried as media for flexible energy storage devices [14].

2.2 Importance of optoelectronic materials

The quest for high performance, lower cost, and complex functionality has led to a fast-emerging technology called optoelectronics, which, since its debut in the early 1960s, has transformed the lives

of humankind. The transformational changes in communication technologies, which deal with applying electronic devices to the sourcing, detection, and control of light (particularly designed to optimize light absorption and emission), have resulted in the high conversion efficiency of signals from one form into another, thereby leading to a telecommunication revolution [15, 16]. With the help of optoelectronic devices, one can generate, modulate, detect, and switch photons in a way that is analogous to electrons in an electrical circuit [17]. The main reason why optoelectronic devices are so prevalent in the modern era is because most people depend greatly on vision to observe the world around them. Because of this, manipulating light to be transformational in its existence becomes extremely useful. The capability of an optoelectronic material that translates light into multiple forms has allowed us to see at night as well as to record images and videos of things we observe while easily sharing such information with others.

Beyond that, there are many other important optoelectronic applications such as laser technology, transistors, light-emitting diodes (LEDs), solar cells, sensors, photo-refractive devices, and so forth [18–20] (Fig. 2.1). Because photons are not limited by problematic parameters such as channel length, width, capacitance, etc., it is inevitable that we will move toward optoelectronics, at least for the foreseeable future.

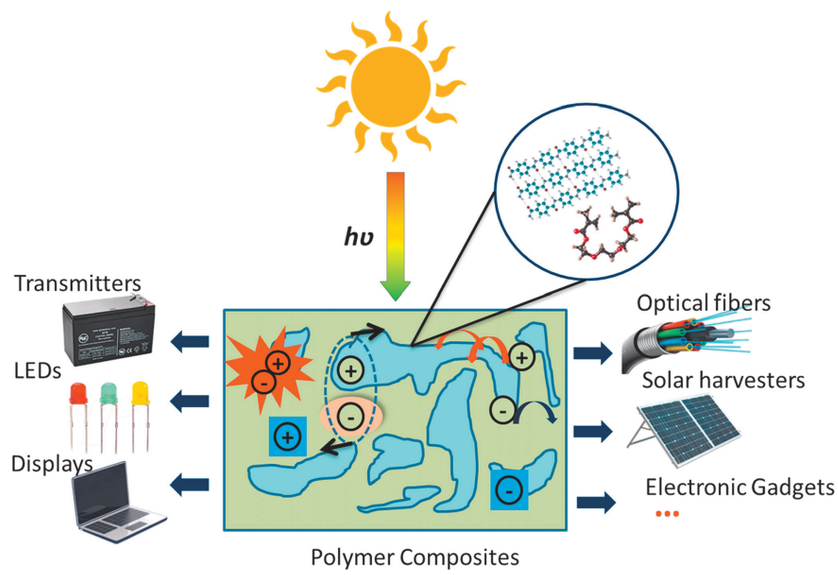


Fig. 2.1 Schematic representation of various applications of optoelectronic materials. From O. Ostroverkhova, Organic optoelectronic materials: mechanisms and applications, Chem. Rev.116 (2016) 13279–13412.

2.3 Various types of materials used in optoelectronic devices

Various newly synthesized materials have become critical components of emerging technologies. In order to optimize the performance of optoelectronic devices, several theoretical and experimental studies have been performed. Improving the material efficiency is one such ongoing study. Optoelectronic components are fabricated from a wide range of materials. The selection of material for optoelectronic and energy-related application is based on a number of factors, including optical properties such as the refractive index, absorption and emission characteristics, electrical properties such as mobility and conductivity, and other factors such as stability and process compatibilities [21, 22].

In fact, the choice of material for optoelectronic and energy-related purposes depends on the nature of the device chosen. As waveguides, the optoelectronic materials should exhibit very low absorption or scattering loss while optical modulators and switches rely on those materials with high electro-optic coefficients. On the other hand, LEDs and lasers require materials with large radiative emission efficiencies while detectors require those materials that show appreciable absorptions at the desired wavelengths. Further, batteries and other energy storage and conversion devices demand materials with a higher surface area and good electrical conductivities [23]. Such optoelectronic materials are mainly grouped into three categories: inorganic, organic, and hybrid materials. Those classifications are diagrammatically represented in Fig. 2.2.

2.3.1 Inorganic materials

In conventional optoelectronics, the functional materials employed are inorganic semiconductors, which are known for their long-term stability under various mechanically, electrically, and environmentally stressed environments. Various inorganic catalytic materials such as metal oxides, metal nanoparticles, and nonoxide materials, which exhibit different morphologies, surface structures, and physical and chemical properties, are being continuously explored. They also possess very good processing compatibility with existing infrastructures that are used for deposition, crystallization, doping, and other related processes [24]. Among various inorganic materials, semiconductors in particular have experienced tremendous growth. Their unique band structures give them superior electrical and optical properties suitable for a wide range of electronics and energy-related applications. However, the main drawback of these materials is that the rigid form of inorganic optoelectronic and energy storage devices renders them

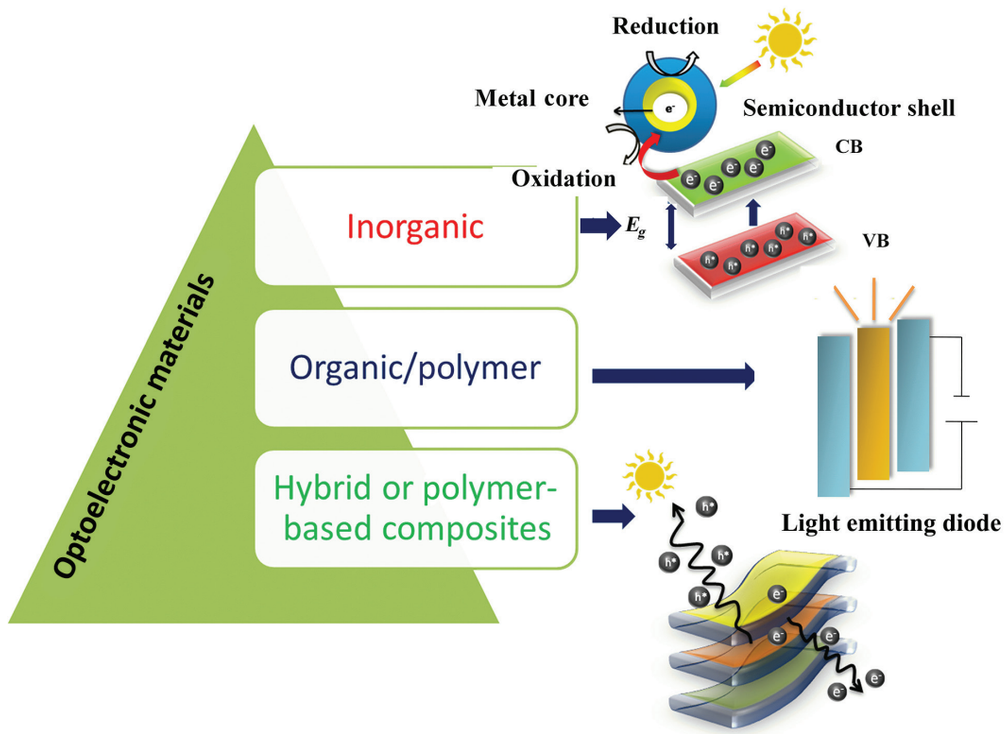


Fig. 2.2 Different categories of optoelectronic materials.

difficult to be employed in many applications. In contrast to the above problem, mechanically flexible optoelectronic devices and systems can enable a much broader range of applications than that offered by the rigid materials [25].

2.3.2 Organic materials

Previously, organic materials were considered to be insulators and were commonly used in applications such as coating as well as containers, insulating support, and so forth. Nevertheless, the discovery of conductive conjugated polymers gave a new impulse to the field of organic electronics [26]. Organic materials can easily address the limitations of inorganic materials by providing the required mechanical flexibility to optoelectronic devices, along with the additional advantages of being economical, compatible with various flexible substrates, and able to be manufactured on a large scale [23]. However, there are certain problems associated with the use of organic materials, as they suffer from oxidation, recrystallization, and temperature-induced degradation, which can greatly affect the device performance. Among various organic electronic

and optoelectronic devices, organic LEDs (OLEDs), organic field-effect transistors (OFETs), and organic photovoltaic devices (OPVs) have been the subjects of current research interest and development.

2.3.3 Hybrid materials

Hybrid materials are composite forms that consist of two constituents mixed either at the nanometer or molecular level. Commonly, one of these constituents is inorganic and the other is organic in nature. The hybrids of conjugated polymer/organic material-based optoelectronic devices have drawn significant attention from both the academic and industrial research communities. This is due to the increased potential of such materials to offer a low-cost, large-area, processable technology alternative to conventional inorganic optoelectronics [27].

In most cases, the inorganic component of the hybrid provides mechanical strength and an overall structure to the composite while the organic component is involved in ensuring bonding between the inorganic building blocks. These hybrid designer materials are also associated with multifunctional properties. Mixing diverse materials, physically and/or chemically, results in a composite formation that exhibits advantageous properties of both components in the hybrid [28]. Some of the advantages of hybrid materials are:

(a) Specific optical and electronic properties can be easily incorporated into the organic conjugated polymer matrix.

(b) In contrast to pure inorganic materials that often require a high temperature for processing, hybrid materials exhibit polymer-like handling because of the large organic content or due to the crosslink formation of inorganic networks in the conjugated polymer matrix [29].

(c) Light scattering in such a homogeneous hybrid material can be avoided, therefore the optical transparency of the composite material can be achieved [30].

2.4 Working principle of optoelectronic materials

The basic working principle of optoelectronic materials can be described as follows.

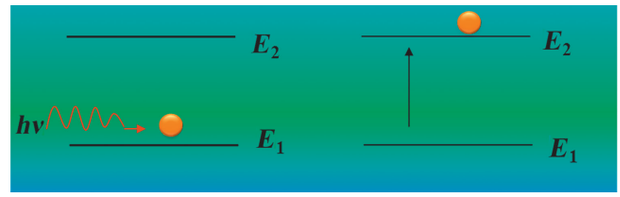
2.4.1 Radiative transitions

Basically, there are three processes occurring during the interaction between a photon and an electron in a solid: absorption, spontaneous emission, and stimulated emission.

2.4.1.1 Absorption

When a photon of energy equal to the energy difference between the ground state and the excited state falls on a material, an atom in the ground state E_1 absorbs the photon and gets excited to E_2. This is the absorption process and it constitutes an important step in the working of most optoelectronic materials. The process of absorption is diagrammatically represented in Fig. 2.3.

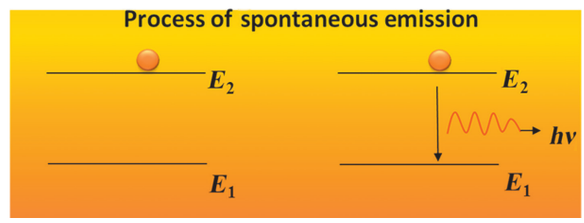
Fig. 2.3 Mechanistic view of photon absorption and subsequent electron excitation.



2.4.1.2 Spontaneous emission

Because the excited state of an electron is unstable, the electron stays there for a short period of time and then makes a transition back to the ground state, emitting the excess energy in the form of photons. The above process is termed spontaneous emission. This process is found to be responsible for light emission in LEDs. The above process is represented diagrammatically in Fig. 2.4.

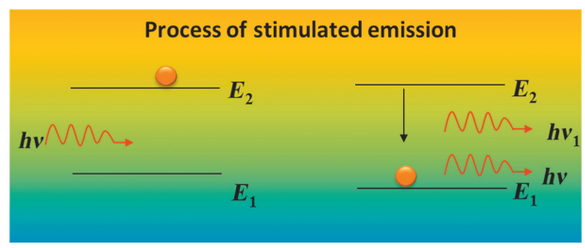
Fig. 2.4 Mechanistic view of spontaneous emission.



2.4.1.3 Stimulated emission

When the atom is in the excited state, if a photon of energy, $h\nu$, impinges on it, the electron gets stimulated to make a transition to the ground state by emitting the excess energy in the form of a photon of energy, $h\nu_1$, which is in phase with the incident photon $h\nu$. This type of process is used in laser diodes. The above process is diagrammatically represented in Fig. 2.5.

Fig. 2.5 Mechanistic view of stimulated emission.



All the above processes constitute the working principle of optoelectronic materials [31].

2.5 Smart materials for optoelectronic and energy applications

With increasing advancements in the fabrication and monitoring of electronic devices, various novel materials, in particular smart materials, that offer versatile and dynamically tunable material properties have been continuously developed and explored. Such vigorous research and development activities have enabled various interesting

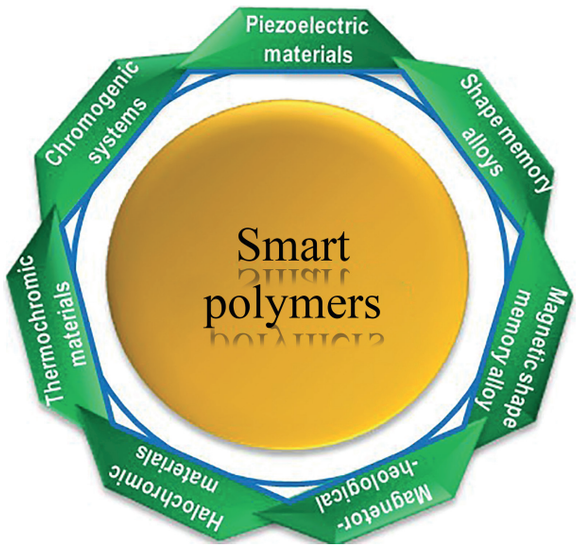


Fig. 2.6 Various application domains of polymer-based smart materials.

applications using such polymer-based smart materials (Fig. 2.6).

Smart polymer-based materials are those intelligent matrices that are essentially designed to exhibit external stimuli-dependent material property engineering [32]. Lately, functional or intelligent conjugated polymer-based materials have been continuously tried for a wide range of advanced applications [33]. In their various forms, these materials have been continuously explored as sensors and actuators for diverse optoelectronic applications [34].

2.5.1 Carbon-based materials

For the past few decades, zero-dimensional (fullerenes), one-dimensional (carbon nanotubes, (CNTs)), and two-dimensional (graphene) carbon nanomaterials have drawn significant research attention. This is due to their unique optical, electronic, thermal, mechanical, and chemical properties. Earlier studies have supported that these properties of carbon materials could enable high performance in selected applications. However, with recent advances concerning synthesis, sorting, and assembly techniques, carbon nanomaterials are experiencing renewed interest for optoelectronic applications [35].

Carbon is an important optoelectronic material, owing to its ability to exist in various allotropic forms, as shown in Fig. 2.7. Moreover, in recent years, an emerging class of carbon-based luminescent nanomaterial, that is, carbon quantum dots (CQDs), has shown increasing potential for optoelectronic applications. This is due to its inherent unique material behaviors, which include tunable fluorescence emission, broad emission wavelengths, high thermal stability, and low cytotoxicity. In 2010, graphene sheets were converted into blue luminescent CQDs for the first time via the hydrothermal route, which expanded the application of carbon-based materials into the field of optoelectronics such as photovoltaic devices, LEDs, photo detectors, photo catalysis, and so forth [36].

2.5.2 Conjugated polymers

Traditional conjugated polymers have been engineered in such a way that materials with low density, mechanical strength, and environmental stability have been enabled. Intelligent conjugated polymers are engineered in such a way that they respond to the external stimuli in a manner that enhances the performance. Fig. 2.8 sheds

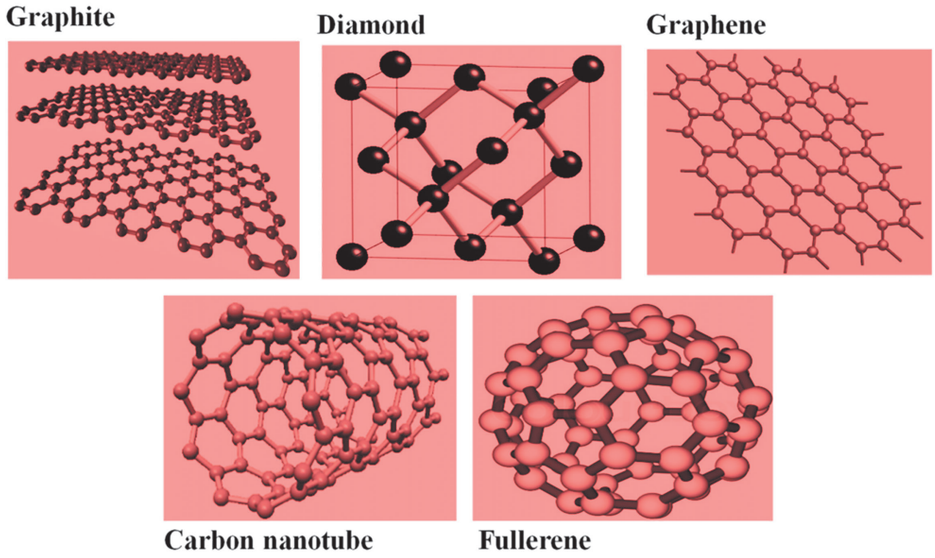


Fig. 2.7 Structural differences in various allotropes of carbon.

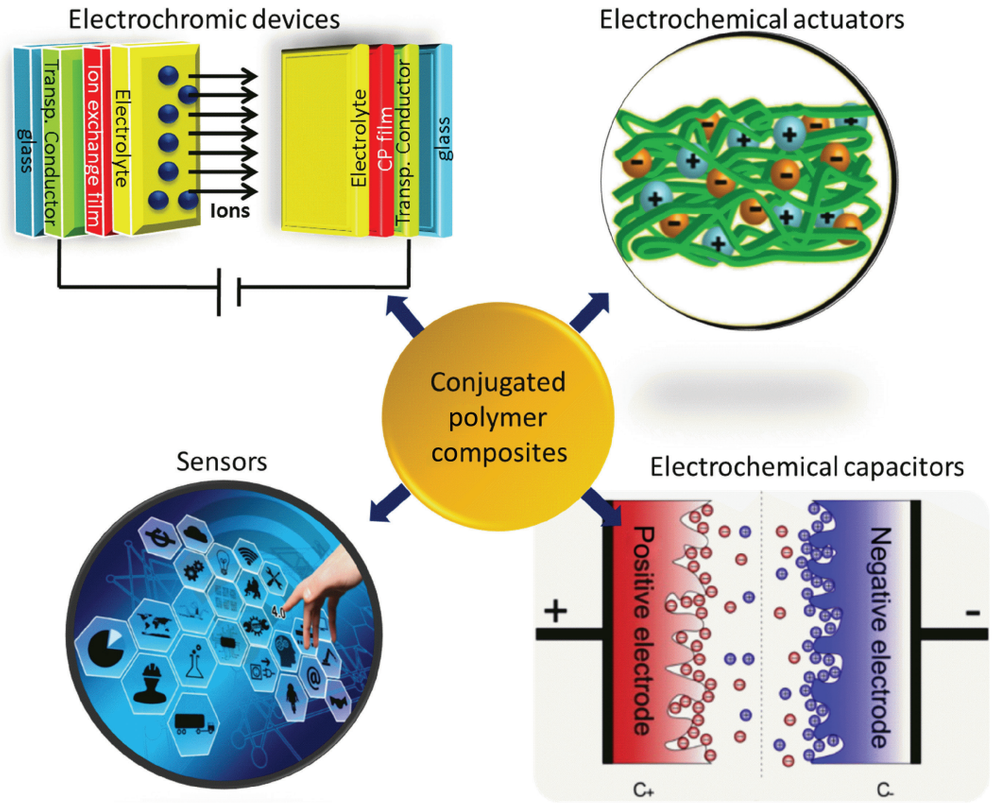


Fig. 2.8 Smart conjugated polymer composites for optoelectronics and energy-related applications.

light on some of the important techno-commercial applications involving such materials.

Unlike traditional conjugated polymers, intelligent conjugated polymers are not electronic insulators and conduct electricity. Moreover, they have dynamic structures, unlike traditional conjugated polymers that have a static structure. Besides, the stimuli-dependent properties of such matrices depend on the oxidation state of the structure, which in turn is dependent on the external environment [37]. Also, intelligent conjugated polymers have the ability of sensing, processing information, and actuating responses. Further, in order to implement these functions, energy is required, so therefore energy conversion/storage capabilities are desirable.

Low-cost conjugated polymer-based optoelectronic materials are being used in the fabrication of optical devices such as waveguides, photonic display devices, photo-chromic windows, and so forth. Those applications are because of their unique material behaviors, including high optical transmission, good plasticity, and excellent mechanical stability. In addition to those properties, conjugated polymer-based materials are associated with excellent compatibility, which allows them to be combined with other materials to extract a synergistic response. Due to the high electro-optic (EO) coefficients, high thermal stability, good flexibility, and low dielectric constant of the conjugated polymer materials, they are also widely used for high-efficiency organic electro-optical modulation devices as well as in flexible electronic circuits [38].

Extensive studies in the fields of optoelectronics and energy have shown that organic materials in their solid state exhibit a variety of interesting optical, electrical, photo-electric, and magnetic properties. In recent years, organic materials that are photo-active and electro-active have been the subject of extensive research interest. Such materials include organic semiconductors, photoconductors, organic photo-active materials for solar cells, organic metals including superconductors, organic nonlinear optical materials, organic ferromagnets, photo-chromic and electro-chromic organic materials, liquid crystals, and others. Among the various materials explored, liquid crystals, organic photoconductors, and resist materials have been used as photoreceptors in electro-photography, display devices, and lithographic processes for the production of semiconductor devices. In addition to the above-mentioned applications, organic optoelectronic materials have received great attention due to their potential use in optoelectronic and electronic devices such as sensors, organic electroluminescent devices, plastic batteries, solar cells, optical data storage, switching devices, frequency doublers, and many others [39]. The technological advantages of using conjugated polymer-based materials include their cost effectiveness

and the possible room-temperature deposition of conjugated polymers from solution onto a large-area and/or flexible substrates. Due to their advantageous features such as large-area device fabrication, they have enabled not only single-component devices (such as conjugated polymer TFTs) with high performance but also devices that use composite forms of conjugated polymers with different functionalities, such as bulk heterojunction (BHJ) solar cells and small molecule conjugated polymer-based TFTs. Recent advances in the field of conjugated polymer design, synthesis, and processing have led to remarkable progress in conjugated polymer-based device performance [23]. Triphenylamine (TPA) is one of the emerging organic materials used for optoelectronic purposes, due to its excellent thermal and morphological stability, high oxidizability, and high stability of the corresponding radical cation. Triphenylamine-based conjugated polymers are prepared by the incorporation of TPA into the conjugated polymer backbone, which makes the resulting structure highly rigid due to strong intermolecular interactions. This causes it to have a high glass transition temperature and lower solubility in organic solvents. Such properties are extremely beneficial for the fabrication of large area, thin film optoelectronic devices. Therefore, the above-mentioned properties of TPA-based conjugated polymers make them applicable for wide use in optoelectronic devices such as photoconductors, light emitters, electro-chromics, and especially in hole transporting materials in organic LEDs, solar cells, organic field-effect transistors, and photo-refractive materials [40].

Similarly, there are several other optoelectronic materials being studied. One such promising candidate is found to be azulene, which has a unique electronic structure and unusual physical properties that make it applicable for various optical and electronic purposes. These are increasingly used in organic field-effect transistors (OFETs) and solar cells. Thus, high-performance conjugated polymer materials are synthesized by incorporating azulene derivatives into the conjugated polymer backbone [41]. Conjugated polymer LEDs (PLEDs) are one of the optoelectronic devices currently on the rise that are based on the conjugated polymer, poly (2-methoxy-5-(2-ethyl-hexoxy) 1,4-phenylene vinylene), abbreviated as PPV. In comparison to the inorganic or organic materials for LEDs, conjugated polymer-based LEDs have quick response times, the ability to uniformly cover large areas, and low operating voltages while many of its optical and electrical properties can be tuned according to the needs [42]. Several techniques have been proposed to improve the performance of such conjugated PLEDs [43–45]. One such method is the chemical modification of the conjugated polymer with bulky phenyl side groups or PPV-based alternating copolymers. One disadvantage of using low molecular weight conjugated polymers is that they are subject to

easier chain motion under device operation, which reduces the device performance. Thus, the selection of conjugated polymers of suitable molecular weight becomes a necessity [46].

Conducting conjugated polymers such as transparent conducting electrodes (TCE) have been used in organic LED devices with reasonably good performance. In conventional OLEDs, indium tin oxide (ITOs) glass has been used as the anode, and provides good transparency and conductivity. But the main drawback associated with using ITOs is that they are not flexible. Thus, ITOs in conventional OLEDs are now replaced by conjugated polymers such as poly (3,4-ethylenedioxythiophene) polystyrene sulfonate and polyaniline (PANI) with excellent mechanical stability, flexibility, and, more importantly, good conductivity and transparency [47].

π-Conjugated polymers such as polyfluorenes, fluorene-thiophenepolymers, polyphenylenes, polythiophenes, and polycarbazoles and their derivatives have been extensively investigated for their potential applications in optoelectronics, including photovoltaic cells, thin-film transistors, light-emitting devices, electro-chromic devices, and switches. Polythiophenes and thiophene containing conjugated polymers are promising materials, particularly for photovoltaic applications. Soluble fluorene-thienothiadiazole copolymers possess a low bandgap and high electron affinity while exhibiting reversible electro-chromic behaviors. These properties are of interest for various electro-chromic and photovoltaic applications [48].

Another class of conjugated polymers is the polymer that is emerging as a promising material for understanding and controlling processes that are associated with both photovoltaic energy conversion and light-emitting devices. The increasing interest in using block copolymers for optoelectronic purposes originates not only from their potential technological advantages, but also from their ability to self-assemble into periodic ordered nanostructures, thereby developing idealized morphologies. The incorporation of these self-organized block copolymer materials into optoelectronic device fabrication processes or directly into devices will lead to new insights into structure-property relationships and perhaps ultimately increase device efficiency [49].

Besides, in optoelectronic device fabrication, plastic materials are also of special interest because of their handling ease. Plastic optical fiber (POF) is one such plastic material that is an attractive transmission medium for use in local area network systems and office automation systems because of its ease of connectivity with the light sources. The development of highly efficient nonlinear optical materials is expected for optical signal processing systems. Organic materials with large optical nonlinearity and fast response time have good potential for nonlinear optical applications [38]. Further, polyimides are one of

the most important classes of conjugated polymers used in microelectronics and photo-electronics because of their high thermal stability, improved chemical resistance, and good mechanical and electrical properties. Recently, aliphatic and alicyclic polyimides have found applications in optoelectronics, due to their good transparencies and low dielectric constants. Constant research efforts have been exerted in the development of aliphatic polyimide with increased thermal and mechanical stabilities while maintaining their transparencies and low dielectric constants by the incorporation of rigid moieties [50].

Also, blending conjugated polymers has been practiced to engineer their physical properties. The conjugated polymer blend can be designed in such a way as to combine the attractive features of both components. Sometimes, the blend may possess new properties not present in either of the components. In the field of conjugated polymer electronics, blending is an attractive approach to optimize the device function, where conjugated polymers are processed from solution to form the active semiconducting layer of an LED or photovoltaic (PV) device [51].

2.5.3 Conjugated polymer-based composites

The origin of hybrid research has initiated a new class of materials with promising properties for different applications. Recently, increasing interest has been devoted to the use of inorganic/organic materials as hosts to create potential supramolecular structures to enhance their performance and/or to create new application routes [52]. Organic/inorganic nanocomposites are generally conjugated polymer composites with one of the components as a nanoscale building block, which has been extensively studied for a long time. The composite form acquires the properties of both the organic and inorganic components. It possesses the properties of both organic and inorganic components combined or may enable entirely new functionalities arising from synergistic effects [53]. Several nanosized materials exhibit interesting physical properties. When these materials are incorporated into a matrix, it leads to unexpected performance, which makes them attractive for applications in different fields. In comparison to individual components, a composite must possess enhanced properties that allow it to be used for a particular application. Thus, it must be capable of replacing more than one material, which would be required to obtain similar properties for a particular application [54]. The material properties of these hybrids can be tuned by modifying the composition at the molecular scale, so as to enable smart functionalities [55].

Besides, polymer-based smart materials are also required for those applications that involve energy conversion and storage. Accordingly, advances in stationary power systems, portable electronic devices, and

hybrid electric vehicles have created enormous demand for nontoxic, easily manufactured, and low-cost alternatives to conventional solar cells [56]. Also, there are different modification techniques used to alter the complex properties of hybrid materials, which allows perfect control over size, composition, and functionality [57]. The progress in the field of dielectric conjugated polymer nanocomposites has been accelerated and has been witnessing exciting outcomes. The properties of conjugated polymer nanocomposites are greatly improved compared to those of a conjugated polymer matrix because the dielectric properties of these materials can be thoughtfully engineered. Accordingly, the energy density of conjugated polymer nanocomposites could be greatly improved via the judicious combination of a conjugated polymer matrix and functional nanoparticles [58]. Further, depending on the manner in which the organic and inorganic components are associated, one can distinguish two types of composites. The first type includes composites made up of inorganic materials embedded in a conjugated polymer matrix (organic-inorganic composites). The second type includes composites made of a conjugated polymer deposited in an inorganic template (inorganic-organic composites).

2.5.3.1 Organic-inorganic composites

This composite type generally includes inorganic nanoparticles of oxides or semiconductors, which are incorporated into a matrix of a conjugated polymer solution in a controlled manner [59]. In order to allow a uniform distribution of particles in the conjugated polymer matrix, modification of the surface may be necessary without modifying the intrinsic properties of the crystal. For example, the treatment of CdSe nanocrystals by pyridine, an organic ligand, is seen to allow uniform distribution of the particles in the conjugated polymer matrix of poly (3-hexylthiophene-2,5diyl) [60]. One advantage of this type of composite is that the precise determination of the composition of the composite is possible. Therefore, it is possible to have better control of their optical properties. Other advantages of using conjugated polymer composites include good processability (thin films of controlled size and thickness), lighter weight, and higher flexibility [61]. The composite form has a combination of unique physical properties (light scattering, emission, and absorption and magnetic response) of the inorganic components, with the relevant chemical features derived from the morphology and microstructure of conjugated polymer chains. These all play a key role in the development of highly functional nanocomposites [57]. In order to obtain the desired properties, the choice of nanoparticle size and nanoparticle type, the nature of the conjugated polymer, and the extent of the compatibilities between inorganic and organic components are of significant interest. On the other hand, the enhancement of the stability of the organic matrix is

due to the presence of inorganic particles [62]. The main drawback of this type of composite film preparation is the nonhomogeneous nature of the film due to the aggregation of particles during the deposition process, which may greatly modify its properties [63].

2.5.3.2 Inorganic-organic composites

In this type of composite, the inorganic component is used as a template in which the organic component is deposited. The preparation of these composite materials involves the use of metal oxides such as silica or alumina containing nanopores as substrates and the composites are obtained by filling these pores with conjugated polymers [64]. Herein, the nature of the interactions between the organic and inorganic components affects the overall electro-chemical properties of the composites. Such a type of material with tunable electro-chemical properties is increasingly explored for energy-related applications, such as the fabrication of batteries. However, if the substrate has a largely porous nature, the diffusion of conjugated polymer chains into such a host structure may lead to composites with higher potential to be used for optoelectronic applications [65].

Besides, conjugated polymer composites are an attractive means to exploit the unique properties of carbon structures such as single-walled CNTs and graphene. This is particularly of importance in photonic and optoelectronic applications, where a number of devices have already been demonstrated that include electro-luminescent and photovoltaic devices, transparent conductors, and saturable absorbers [66]. Numerous works have been carried out in using composite materials with exciting properties for novel application in the field of optoelectronics. One such novel material for molecular optoelectronic application is the composite of poly (m-phenylenevinylene-co-2,5-dioctoxy-p-phenylenevinylene) and CNTs [67]. Further, the need to develop alternative molecular-scale electronic materials becomes a necessity as the recent trend progresses toward smaller and more efficient devices. Thus, the integrated fabrication of electronic components from organics has been recognized theoretically as the ultimate goal. Besides, electrochemically synthesized conducting conjugated polymer composites are being increasingly tried for various electronics, optoelectronics, and energy storage applications. This is due to the possible control over electrical conductivity of such composites, over the range from the insulating to the highly conducting state. Consequently, conducting conjugated polymer-based composite materials are used in solar energy conversion devices, photo-conducting materials, colored LEDs, and so forth [68, 69]. They are capable of replacing traditional LCDs, which are limited to a small size. Commercial signboards, time tables in airports and railway stations, calculators, and clocks are known to make use of solid-state electro-chromic cells

[70]. In the near future, the increasing worldwide demand for economic fuel and a pollution-free environment can be met through energy applications. These include the use of rechargeable batteries and supercapacitors that make use of conducting conjugated polymers as electrode materials [71, 72]. Devices such as ultracapacitors store and release energy like batteries, but in comparison to batteries, they have vastly longer lives and can unload their energy 10–100 times faster. These new devices may be used in electrical vehicles, exhibiting superior performance.

2.6 Conclusions and future directions

Conjugated polymers, a unique class of organic materials characterized by a carbon backbone of alternating single and double bonds, presents a wide range of applications in interesting optoelectronic and energy applications. A number of conducting conjugated polymer-based materials have been successfully synthesized and their optoelectronic and energy-related performances validated. Yet, as of now, it is quite unclear as to how successful these materials would be when efficiency, large-scale production, and commercialization are taken into consideration.

Acknowledgment

The authors thank DST, the government of India, for nanomission project funding (SR/NM/NT-1073/2016).

References

[1] M.G. Molina, Energy storage and power electronics technologies: a strong combination to empower the transformation to the smart grid, Proc. IEEE 105 (2017) 2191–2219.
[2] F. Guo, Z. Guo, Inspired smart materials with external stimuli responsive wettability: a review, RSC Adv. 6 (2016) 36623–36641.
[3] Z.L. Wu, Y.N. Qi, X.J. Yin, X. Yang, C.M. Chen, J.Y. Yu, J.C. Yu, Y.M. Lin, F. Hui, P.L. Liu, Y.X. Liang, Polymer-based device fabrication and applications using direct laser writing technology, Polymers 11 (2019) 553.
[4] J.H. Koo, Conjugated Polymer Nanocomposites, McGraw-Hill Professional Publication, 2006.
[5] T. Manouras, M. Vamvakaki, Field responsive materials: photo-, electro-, magnetic-and ultrasound-sensitive conjugated polymers, Polym. Chem. 8 (2017) 74–96.
[6] Y.J. Liu, X. Lan, H.B. Lu, J.S. Leng, Recent progresses in conjugated polymeric smart materials, Int. J. Mod. Phys. B 24 (2010) 2351–2356.
[7] T. Ishigure, E. Nihei, Y. Koike, C.E. Forbes, L. LaNieve, R. Straff, H.A. Deckers, Large-core, high-bandwidth conjugated polymer optical fiber for near infrared use, IEEE Photon. Technol. Lett. 7 (1995) 403–405.

[8] E. Perzon, F. Zhang, M. Andersson, W. Mammo, O. Inganas, M.R. Andersson, A conjugated polymer for near infrared optoelectronic applications, Adv. Mater. 19 (2007) 3308–3311.
[9] S.K. Yesodha, C.K.S. Pillai, N. Tsutsumi, Stable conjugated polymeric materials for nonlinear optics: a review based on azobenzene systems, Prog. Polym. Sci. 29 (2004) 45–74.
[10] Y. Shi, G. Yu, Designing hierarchically nanostructured conductive conjugated polymer gels for electrochemical energy storage and conversion, Chem. Mater. 28 (2016) 2466–2477.
[11] C. Yang, H. Wei, L. Guan, J. Guo, Y. Wang, X. Yan, X. Zhang, S. Wei, Z. Guo, Polymer nanocomposites for energy storage, energy saving, and anticorrosion, J. Mater. Chem. A 3 (2015) 14929–14941.
[12] C.X. Guo, M. Wang, T. Chen, X.W. Lou, C.M. Li, A hierarchically nanostructured composite of MnO2/conjugated polymer/graphene for high-performance lithium ion batteries, Adv. Energy Mater. 1 (2011) 736–741.
[13] S. Ghosh, O. Inganas, Conducting conjugated polymer hydrogels as 3D electrodes: applications for supercapacitors, Adv. Mater. 11 (1999) 1214–1218.
[14] X. Cheng, J. Pan, Y. Zhao, M. Liao, H. Peng, Gel polymer electrolytes for electrochemical energy storage, Adv. Energy Mater. 8 (2018), 1702184.
[15] M. Filka, Optoelectronics: for Telecommunications and Informatics, Optokon Co., Ltd., & Methode Electronic Inc, Dallas, Texas, United States of America, 2009.
[16] S.L. Chuang, Physics of Optoelectronic Devices, Wiley, 1995.
[17] T. Ouchi, Integrated Optoelectronic Device, and Integrated Circuit Device, Google Patents, 2002.
[18] R. Soref, Applications of silicon-based optoelectronics, MRS Bull. 23 (1998) 20–24.
[19] C. Bryson, Interferometric sensor system for security applications, in: Tenth International Conference on Optical Fibre Sensors. International Society for Optics and Photonics, 1994.
[20] G.P. Smestad, Optoelectronics of Solar Cells, SPIE Press, 2002.
[21] A.D. Rakic, A.B. Djurisic, J.M. Elazar, M.L. Majewski, Optical properties of metallic films for vertical-cavity optoelectronic devices, Appl. Opt. 37 (1998) 5271–5283.
[22] N. Tessler, D.J. Pinner, V. Cleave, P.K.H. Ho, R.H. Friend, G. Yahioglu, P. Le Barny, J. Gray, M. De Souza, G. Rumbles, Properties of light emitting organic materials within the context of future electrically pumped lasers, Synth. Met. 115 (2000) 57–62.
[23] O. Ostroverkhova, Organic optoelectronic materials: mechanisms and applications, Chem. Rev. 116 (2016) 13279–13412.
[24] Z. Ma, D. Liu, Inorganic Flexible Optoelectronics: Materials and Applications, John Wiley & Sons, 2019.
[25] D.H. Kim, J. Xiao, J. Song, Y. Huang, J.A. Rogers, Stretchable, curvilinear electronics based on inorganic materials, Adv. Mater. 22 (2010) 2108–2124.
[26] P. Mueller, H.E. Riel, W. Riess, H. Vestweber, International Business Machines Corp, Organic Opto-Electronic Devices, U.S. Patent 6,316,786, 2001.
[27] G. Kickelbick, Hybrid materials–past, present and future, Hybrid Mater. 1 (2014) 39–51.
[28] C. Sanchez, B. Lebeau, F. Chaput, J.P. Boilot, Applications of hybrid organic–inorganic nanocomposites, J. Mater. Chem. 15 (2005) 559–3592.
[29] I.Y. Jeon, J.B. Baek, Nanocomposites derived from conjugated polymers and inorganic nanoparticles, Materials 3 (2010) 3654–3674.
[30] L.L. Beecroft, C.K. Ober, Nanocomposite materials for optical applications, Chem. Mater. 9 (1997) 1302–1317.
[31] P. Bhattacharya, L.Y. Pang, Semiconductor Optoelectronic Devices, Prentice Hall, NJ, 1997.

[32] M.R. Aguilar, J.S. Roman, Smart Conjugated Polymers and Their Applications, Woodhead Publishing, 2019.
[33] A. Kumar, S. Akshay, I.Y. Galaev, B. Mattiasson, Smart conjugated polymers: physical forms and bioengineering applications, Prog. Polym. Sci. 32 (2007) 1205–1237.
[34] F.D. Jochum, P. Theato, Temperature and light-responsive smart conjugated polymer materials, Chem. Soc. Rev. 42 (2013) 7468–7483.
[35] T. Yuan, T. Meng, P. He, Y.X. Shi, Y. Li, X. Li, L. Fan, S. Yang, Carbon quantum dots: an emerging material for optoelectronic applications, J. Mater. Chem. C 7 (2019) 6820–6835.
[36] X. Li, M. Rui, J. Song, Z. Shen, H. Zeng, Carbon and graphene quantum dots for optoelectronic and energy devices: a review, Adv. Funct. Mater. 25 (2015) 4929–4947.
[37] G.G. Wallace, P.R. Teasdale, G.M. Spinks, L.A. Kane-Maguire, Conductive Electroactive Polymers: Intelligent Materials Systems, CRC Press, 2002.
[38] T. Kaino, Y. Katayama, Conjugated polymers for optoelectronics, Polym. Eng. Sci. 29 (1989) 1209–1214.
[39] Y. Shirota, Organic materials for electronic and optoelectronic devices basis of a presentation given at materials chemistry discussion, University of Nottingham, UK, J. Mater. Chem. 10 (2000).
[40] H.J. Yen, G.S. Liou, Design and preparation of triphenylamine-based conjugated polymeric materials towards emergent optoelectronic applications, Prog. Polym. Sci. 89 (2018).
[41] H. Xin, C. Ge, X. Jiao, X. Yang, K. Rundel, C.R. McNeill, X. Gao, Incorporation of 2, 6 connected azulene units into the backbone of conjugated polymers: towards high-performance organic optoelectronic materials, Angew. Chem. Int. Ed. 57 (2018) 1322–1326.
[42] X. Gong, M.R. Robinson, J.C. Ostrowski, D. Moses, G.C. Bazan, A.J. Heeger, High-efficiency polymer-based electrophosphorescent devices, Adv. Mater. 14 (2002) 581–585.
[43] T.H. Han, Y. Lee, M.R. Choi, S.H. Woo, S.H. Bae, B.H. Hong, J.H. Ahn, T.W. Lee, Extremely efficient flexible organic light-emitting diodes with modifiedgraphene-anode, Nat. Photonics 6 (2012) 105.
[44] S.H. Jin, M.S. Jang, H.S. Suh, H.N. Cho, J.H. Lee, Y.S. Gal, Synthesis and characterization of highly luminescent asymmetric poly (p-phenylene vinylene) derivatives for light-emitting diodes, Mater. Chem. 14 (2002) 643–650.
[45] J. Huang, G. Li, E. Wu, Q. Xu, Y. Yang, Achieving high efficiency polymer white light emitting devices, Adv. Mater. 18 (2006) 114–117.
[46] Z.K. Chen, N.H.S. Lee, W. Huang, Y.S. Xu, Y. Cao, New phenyl-substituted PPV derivatives for polymer light-emitting diodes—synthesis, characterization and structure-property relationship study, Macromolecules 36 (2003) 1009–1020.
[47] J. Lewis, S. Grego, B. Chalamala, E. Vick, D. Temple, Highly flexible transparent electrodes for organic light-emitting diode-based displays, Appl. Phys. Lett. 85 (2004) 3450–3452.
[48] V. Cimrova, I. Kminek, D. Vyprachticky, Novel soluble fluorene–thienothiadiazole and fluorene–carbazole coconjugated polymers for optoelectronics, in: Macromolecular Symposia, Wiley Online Library, 2010.
[49] I. Botiz, S.B. Darling, Optoelectronics using block coconjugated polymers, Mater. Today 13 (2010) 42–51.
[50] A.S. Mathews, I. Kim, C.S. Ha, Synthesis, characterization, and properties of fully aliphatic polyimides and their derivatives for microelectronics and optoelectronics applications, Macromol. Res. 15 (2007) 114–128.
[51] C.R. McNeill, N.C. Greenham, Conjugated-conjugated polymer blends for optoelectronics, Adv. Mater. 21 (2009) 3840–3850.
[52] K.S. Nithin, Siddaramaiah,Opto-electrical characteristics of poly (vinyl alcohol)/cesium zincate nanodielectrics, J. Phys. Chem. C 119 (2015) 20244–20255.

[53] K.S. Nithin, K.N. Shilpa, S. Shivanna, J. Raj, H. Siddaramaiah, Advances in polymer-based piezoelectric systems, in: Emergent Research on Polymeric and Composite Materials, IGI Global, 2018.
[54] N. Hu, Composites and Their Properties, InTech, 2012. BoD–Books on Demand.
[55] M.V. Gandhi, B. Thompson, Smart Materials and Structures, Springer Science & Business Media, 1992.
[56] A.C. Arango, L.R. Johnson, V.N. Bliznyuk, Z. Schlesinger, S.A. Carter, H.H. Horhold, Efficient titanium oxide/conjugated polymer photovoltaics for solar energy conversion, J. Adv. Mater. 12 (2000) 1689–1692.
[57] S.H. Mir, L.A. Nagahara, T. Thundat, P. Mokarian-Tabari, H. Furukawa, A. Khosla, Organic-inorganic hybrid functional materials: an integrated platform for applied technologies, J. Electrochem. Soc. 165 (2018) B3137–B3156.
[58] R. Sengupta, M. Bhattacharya, S. Bandyopadhyay, A.K. Bhowmick, A review on the mechanical and electrical properties of graphite and modified graphite reinforced polymer composites, Prog. Polym. Sci. 36 (2011) 638–670.
[59] S. Li, M. Meng, M.S. Lin, D.K. Toprak, M.M. Kim, Nanocomposites of polymer and inorganic nanoparticles for optical and magnetic applications, Nano Rev. 1 (2010) 5214.
[60] I. Lokteva, N. Radychev, F. Witt, H. Borchert, J. Parisi, J. Kolny-Olesiak, Surface treatment of CdSe nanoparticles for application in hybrid solar cells: the effect of multiple ligand exchange with pyridine, J. Phys. Chem. 114 (2010) 12784–12791.
[61] L. Mohammed, M.N. Ansari, G. Pua, M. Jawaid, M.S. Islam, A review on natural fiber reinforced polymer composite and its applications, Int. J. Polym. Sci. 2015 (2015).
[62] H. Althues, J. Henle, S. Kaskel, Functional inorganic nanofillers for transparent conjugated polymers, Chem. Soc. Rev. 36 (2007) 1454–1465.
[63] S. Fu, Z. Sun, P. Huang, Y. Li, N. Hu, Some basic aspects of polymer nanocomposites: a critical review, Nano Mater. Sci. 1 (2019) 2–30.
[64] L. Fu, Q. Qu, R. Holze, V.V. Kondratiev, Y. Wu, Composites of metal oxides and intrinsically conducting polymers as supercapacitor electrode materials: the best of both worlds? J. Mater. Chem. A 7 (2019) 14937–14970.
[65] D.R. Paul, L.M. Robeson, Conjugated polymer nanotechnology: nanocomposites, Polymer 49 (2008) 3187–3204.
[66] T. Hasan, V. Scardaci, P.H. Tan, F. Bonaccorso, A.G. Rozhin, Z. Sun, A.C. Ferrari, Nanotube and graphene polymer composites for photonics and optoelectronics, in: Molecular and Nano-Tubes, Springer, Boston MA, 2011.
[67] S.A. Curran, P.M. Ajayan, W.J. Blau, D.L. Carroll, J.N. Coleman, A.B. Dalton, A.P. Davey, A. Drury, B. McCarthy, S. Maier, A. Strevens, A composite from poly (m-phenylenevinylene-co-2, 5-dioctoxy-p-phenylenevinylene) and carbon nanotubes: a novel material for molecular optoelectronics, J. Adv. Mater. 10 (1998) 1091–1093.
[68] M. Berggren, O. Inganas, G. Gustafsson, J. Rasmusson, M.R. Andersson, T. Hjertberg, O. Wennerström, Light-emitting diodes with variable colours from polymer blends, Nature 372 (1994) 444–446.
[69] P.K. Ho, D. Stephen, R.H. Friend, N. Tessler, All-polymer optoelectronic devices, Science 285 (1999) 233–236.
[70] P.M. Beaujuge, J.R. Reynolds, Color control in π-conjugated organic conjugated polymers for use in electrochromic devices, Chem. Rev. 110 (2010) 268–320.
[71] G.A. Snook, P. Kao, A.S. Best, Conducting-conjugated polymer-based supercapacitor devices and electrodes, J. Power Sources 196 (2011) 1–12.
[72] K. Gurunathan, A.V. Murugan, R. Marimuthu, U.P. Mulik, D.P. Amalnerkar, Electrochemically synthesised conducting polymeric materials for applications towards technology in electronics, optoelectronics and energy storage devices, Mater. Chem. Phys. 61 (1999) 173–191.

3

Metal oxide nanofillers introduced polymer-based composites with advanced optical, optoelectronic, and electrical energy storage functionalities

S. Sachhidananda[a], B.K. Sarojini[c], K.S. Nithin[b], K.N. Shilpa[a], B.M. Jagajeevan Raj[b], K.A. Muthappa[d], H. Siddaramaiah[e,†], and A. Sahaya Anselin Nisha[d]

[a]Department of Polymer Science and Technology, Sri Jayachamarajendra College of Engineering, JSS Science and Technology University, Mysuru, India, [b]Department of Chemistry, The National Institute of Engineering, Mysuru, India, [c]Department of Industrial Chemistry, Mangalore University, Mangaluru, India, [d]Department of Electronics and Communication Engineering, Sathyabama Institute of Science and Technology, Chennai, Tamilnadu, India, [e]Vice-Chancellor of JSS Science and Technology University, Mysuru, India

3.1 Introduction

The advent of nanotechnology has led to the design/discovery and fabrication of various inorganic nanostructures with important cooperative physical phenomena. Yet, they often suffer from tribulations related to their further shaping, which is vital for real-time operational applications [1, 2]. Nevertheless, the thoughtful introduction of such functional nanomaterials into a rational host polymer, enables high-performance novel materials with advanced/smart material functionalities (arising from combinatorial and/or synergistic effects) [2, 3]. Accordingly, the field of polymer nanocomposite (PNC) technology is at the forefront of vigorous research and developmental activities owing to the early suggestions that these multifunctional hybrids would revolutionalize the materials world.

[†] Deceased.

Polymer-Based Advanced Functional Composites for Optoelectronic and Energy Applications
https://doi.org/10.1016/B978-0-12-818484-4.00002-1
Copyright © 2021 Elsevier Inc. All rights reserved.

3.2 What is nanotechnology?

Delving into the depths of nanoscale science and nanotechnology demands a clear understanding of terminologies such as "nanoscale," "nanoscience," and "nanotechnology."

The prefix "nano" is essentially derived from the Greek term "nannos," meaning "very short man" [4]. In the metric system, the prefix "nano" denotes one-billionth (1×10^{-9}) of the base unit. It is essentially that scale in the metric system at which nanometric material/nanotechnology operates. For a system to operate at the nanoscale, the size of the system in at least one dimension must be within 100 nm.

Going forward, the term nanotechnology is best defined by the National Nanotechnology Initiative (NNI) as the understanding and controlling of matter at dimensions of roughly 1–100 nm. This may in turn lead to unique material properties and hence, advanced functional applications [5]. In simpler terms, nanotechnology is an effective blend of science and technology that involves the engineering of material functionalities at molecular levels (within 100 nm), so as to enable advanced material properties [6–9]. The said effects may be owed to a higher surface area to volume ratio of particles with lesser size. In turn, this leads to the availability of a greater proportion of particles at the surface and hence, higher reactivity. As a consequence,

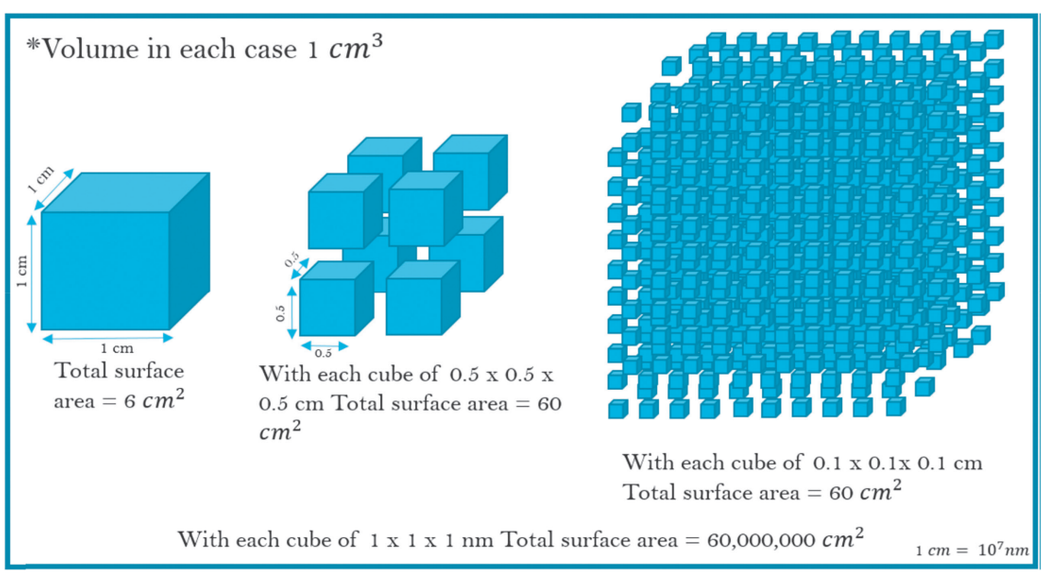


Fig. 3.1 Pictorial representation of the increase in surface area with miniaturization of the same volume. Reproduced from reference C. Paladiya, A. Kiani, Nano structured sensing surface: significance in sensor fabrication, Sensor Actuat. B-Chem. 1 (2018) 494–511 with permission of Elsevier.

materials that may be inert in their bulk forms are highly reactive, when produced in the nanosize. Fig. 3.1 illustrates how smaller size supports increased reactivity.

3.3 History of nanotechnology

Although the science of nanostructured materials has seen momentous growth only in recent years, nanoscale science is not all that new. That is, long before the origin of the nano era, the human race came across various nano-sized systems and practiced different nanolevel processes. However, this was without a clear understanding of the nature of these materials and processes. Many times, the secrets behind the production of such materials were passed on to the successive generation without the actual reasons as to why the derived product exhibited unique properties (in contrast to bulk).

However, the modern history related to the origin of nanostructured materials can be traced back to 1857 when Michael Faraday reported the aqueous dispersions of gold (Au) nanoparticles (NPs) and characterized their optical behaviors [10]. In 1959, in his speech at the California Institute of Technology called "There's Plenty of Room at the Bottom." While, it was Richard Feynman, who described the principles involved in miniaturization, without violating the established laws of physics [11]. However, the term nanotechnology was first used in 1974 by Norio Taniguchi in an article called the "Basic Concept of Nanotechnology." This was essentially a compilation of Feynman's thoughts in detail and presented a conceptual image of nanotechnology in materials processing. Norio Taniguchi further added that "nanotechnology is an art in production technology to obtain additional accuracy and ultrafine dimensions" [12]. In 1987, in his book "Engines of Creation: The Coming Era of Nanotechnology" [13], Eric Drexler gave new insight to the world of nanostructured materials, based on molecular assemblers. This allowed placing atoms in almost any reasonable arrangement and facilitated the formation of almost anything in accord with the laws of nature.

However, it was only in 2000 that the United States introduced the National Nanotechnology Initiative. This aimed to promote research interest in nanometric materials and to develop the science and technology of nanostructured materials as a major research thrust of the 21st century.

3.4 Operating at the nanoscale

Rapid advancements in the field of nanotechnology, catalyzed by the advent of novel synthetic and characterization techniques, have enabled the human race to perceive further and deeper into the roots of nanoscience. However, many of the tools and techniques employed in nanotechnology borrow insights from recent advances in the field of physics [14].

Moreover, with every passing minute, our understanding of the world of nature and the laws governing it changes radically, as we have moved from classical mechanics to quantum theory and from Galilean relativity to general relativity. Electron microscopes (scanning electron microscope (SEM), transmission electron microscope (TEM), and atomic force microscopy (AFM)) stand tall as imperative tools to understand the physicochemical phenomenon operating at the nanoscale. Various other tools such as Fourier transform infrared (FTIR) spectroscopy, powder X-ray diffraction (P-XRD), and dynamic light scattering (DLS) techniques have all escalated the research outcomes in nanotechnology [14].

Generally, nanotechnology involves the synthesis of nano-sized materials via thoughtful manipulations at the atomic level. The resultant unique material behaviors of nanomaterials may be owed to their ultrafine dimensions and high specific surface areas [15–18]. Also, at the nanoscale, quantum effects become more significant in determining the overall material characteristics [3]. It is these unique features of nanomaterials that have garnered significant research interest from almost all branches of science and technology.

Further, the nanoworld offers equal and exciting opportunities to both science and engineering disciplines, and it is being increasingly investigated as a multidisciplinary research domain. Nanotechnology offers smarter materials that are better built, highly durable, and relatively safe to be employed in various industrial sectors. This involves optical communications, biomedical and drug delivery, energy conversion and storage, and other related sectors (Fig. 3.2) [19–21].

However, one of the greatest challenges faced by the human race in the 21st century is the fast-depleting energy sources and exponentially expanding energy demands. Consequently, in 2002–03, Nobel laureate Richard Smalley developed a list of the top 10 global challenges, with energy topping the list. Since then, various researchers across the globe have developed and demonstrated the excellent potential of materials in the nanometric range to be the key towards a sustainable energy future.

Besides, cutting edge research and development in nanotechnology may open up the possibilities of introducing new cost-effective, environmentally benign, and highly efficient energy storage technologies. In general, technological innovations in nanoresearch may have considerable impact on each and every fragment of the value-added chain, a propos to optoelectronic and energy sectors.

3.5 Polymers as advanced functional matrices

Polymers are those wonder materials that have existed in nature since the beginning of life on Earth. Since then, the human race has

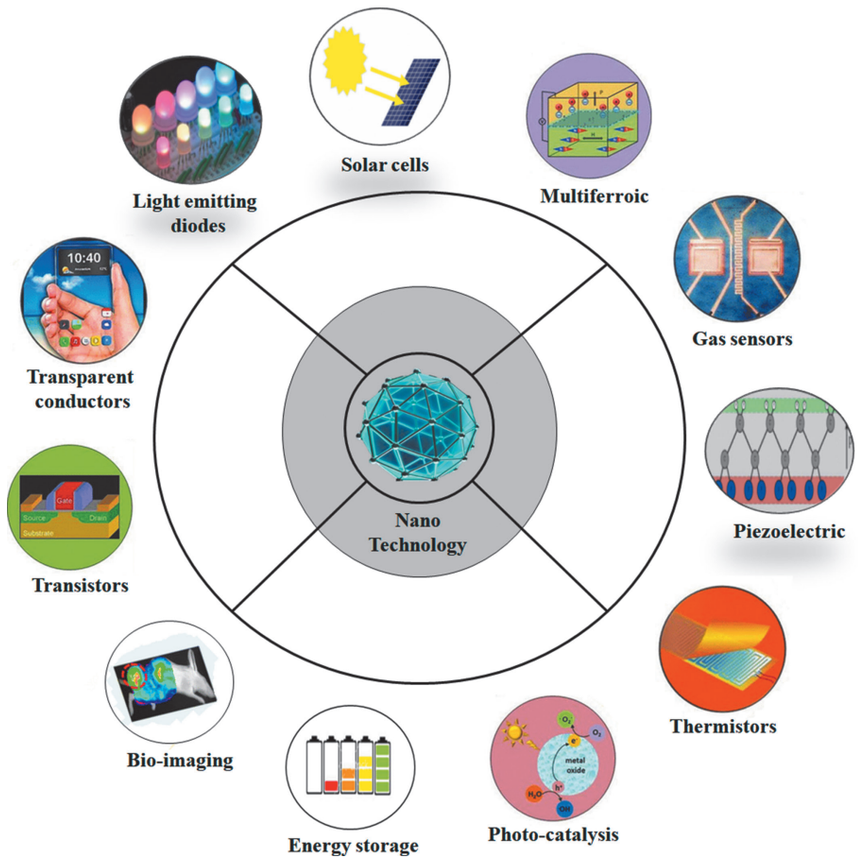


Fig. 3.2 Pictorial representation of some important application areas of nanomaterials.

taken advantage of a number of naturally occurring macromolecules for various domestic and commercial applications [22]. Nevertheless, the origin of the current state-of-the-art polymer industry dates back to the early 19th century. During that time, significant work was done on the modification of certain natural polymers.

However, it was Thomas Hancock who first gave insight into modifying natural rubber (NR) via blending. Charles Goodyear improved the properties of NR by vulcanizing it with sulfur. The first synthetic polymer (Bakelite) was produced in 1909, followed by synthetic fiber (Rayon) in 1911. However, the systematic study of polymeric materials was pioneered by Herman Staudinger, who redefined polymers and established that high molecular mass compounds were made of long chain molecules that are covalently bonded.

Polymers are those unique macromolecular systems that are regularly applied in almost every field, owing to their excellent process abilities and unique chemistry. Although polymers may be used without any additives/fillers, more often they are loaded with organic/inorganic fillers to cut costs and/or to enhance the material performance toward multifunctional applications [23, 24]. Further, polymers are mostly insulators [25–28]. However, in recent years, conjugated and inherently conducting polymers (ICPs) have been continuously reported. The application of polymer-based materials in electronics originated with the discovery of conducting polymers [29], which was soon followed by the discovery of electroluminescent poly (*p*-phenylene vinylene) (PPV) in 1990 [30]. In 2002, Philips (The Netherlands) was the foremost company to launch polymer-based light-emitting products that operated on the principle of electroluminescence. In recent years, the need for newer photovoltaic (PV) technologies, together with vast opportunities in the field of plastic-based electronics, has contributed to momentous research interest in polymer-based flexible electronics [31]. Besides PV applications, plastic solar cells are also expected to revolutionalize the area of polymer-based electronics. Additionally, polymer-based soft materials are also being explored in the field of photonics, which includes transparent conducting films (TCFs), light emitting diode (LED) encapsulates, antireflecting coatings, luminescent downshifting (LDS) layers, transparent solar concentrators, and so forth [20, 32–34].

3.6 Functional additives and/or fillers

The dopant-dependent material property engineering in polymer-based materials offers immense scope for the successful development of polymer-based composites and/or nanocomposites [35, 36].

Such composites materials are essentially made of two major categories of constituent materials, namely the matrix and reinforcement or fillers. The matrix offers a supporting role by surrounding the reinforcing system so as to aid the retention of their relative positions. The functional reinforcements or fillers act to improve the overall material properties (optical, electrical, mechanical, and so forth). Besides, a synergistic filler-matrix combination may also enable entirely new functionalities that are otherwise unavailable from their individual constituents.

A summary of the role of various functional additives on the overall performance of the host polymer is presented in Table 3.1.

3.6.1 Nanofillers

The term nanofiller emphasizes the dimensional significance of fillers with no particular definition. However, when the geometric size of the reinforcement is within (lesser than or equal to) 100 nm, it is collectively addressed as nanofiller.

Table 3.1 Effect of additives/fillers/reinforcements on the overall performance of the host polymer.

Additive/filler/reinforcement type	Actual materials	Effects on polymer properties	References
Reinforcing fibers	Carbon, fibrous minerals, glass, and kevlar	• Increases tensile strength • Increases flexural modulus • Resists shrinkage and warpage	[37–39]
Coupling agents	Silanes and titanates	• Improves interface bonding between the polymer matrix and introduced fibers	[38, 39]
Plasticizers	Monomeric liquids and low-molecular-weight plasticizers	• Improves melt flow properties • Enhances flexibility	[40]
Extender fillers	Calcium carbonate, silica, and clay	• Reduces overall material cost	[38, 41]
Conductive fillers	Aluminum powders, carbon-based materials, and graphite	• Improves electrical and thermal conductivity	[38, 42]
Flame retardants	Chlorine, bromine, phosphorus, and metallic salts	• Reduces the occurrence and spread of combustion	[43]
Colorants (pigments and dyes)	Metal oxides, bromates, and other organic colorants	• Provides color fastness • Protects from thermal and UV degradation (with UV shielding metal oxides)	[43, 44]
Blowing agents	Gas, azo compounds, and hydrazine derivatives	• Generates a cellular form to obtain low-density materials	[45]

These nanofillers may be thoughtfully introduced into the polymer matrix so as to enable the improved material performance of the resultant nanocomposite. However, the composite performance depends on the size and morphology of the introduced nanofiller, together with their (filler) relative dispersions [46] in the host polymer. Also, the filler-matrix interfacial compatibilities play a very crucial role to achieve the ideal material performance [47].

Nanometric fillers are very unique when compared to bulk materials, owing to their extremely large surface areas. This in turn quantifies the interfacial area between the host polymer and the introduced nanofiller. It is this interfacial area that is instrumental in defining the overall composite properties and their related applications [48].

The proportion of the interfacial region is, however, dependent on the filler size and is found to show a dramatic increase for fillers with nanometric size [34]. In short, a larger polymer-filler interfacial region can be a deciding factor that settles the overall material properties of PNC systems.

3.6.1.1 Classification of nanofillers

Nanofillers may be classified into different types based on various classifying metrics or criteria. Based on their origin, nanofillers are broadly classified as natural nanofillers or synthetic nanofillers. Based on their chemical composition, they are classified as organic (carbonaceous) and inorganic (noncarbonaceous) nanofillers. While, on the basis of their role or functionality, they are classified as optically functional, electrically functional, biomedically functional, and structurally functional nanofillers. Based on their geometry, they are grouped into one-, two-, and three-dimensional nanofillers (Table 3.2).

Table 3.2 Geometrical classifications of nanofillers and their representative examples.

Nanofiller type	Schematic depiction	Characteristic feature	Representative examples
One-dimensional		One dimension < 100 nm	Layered materials (sheet like): Graphite nanoplatelets, ZnO nanodiscs, carbon nanowalls, and so forth
Two-dimensional		Two dimensions < 100 nm	Fibrous materials (tube/filament like): carbon nanotubes (CNTs), boron nitride nanotubes, carbon nanofibers, Au nanowires, and so forth
Three-dimensional		All dimensions < 100 nm	Particulate materials (sphere/cube like): NPs of metals, nanosilica, nanoalumina, quantum dots, and so forth

Inorganic nanofillers

Various kinds of nanosized inorganic fillers have been synthesized and studied so far\ [15, 16, 49]. Of the available lot, a few potential inorganic filler varieties, their characteristic properties, and representative examples are listed in Table 3.3.

Inorganic nanofillers combine superior mechanical and thermal properties (i.e., modulus, strength, hardness, thermal stability, and low thermal expansion) of inorganic materials together with the large surface area offered by nanometric dimensions.

In addition to appreciable enhancement in their thermal and/or mechanical properties, various other unique material (optical, electrical, and magnetic) properties can also be realized using appropriate inorganic nanofillers. However, the selection of the appropriate additive (or) filler (towards the performance enhancement of polymer composites and/or nanocomposites) depends on the desired property enhancement and target applications.

Metal oxide nanofillers

Ceramic powders that include oxides, nitrides, and silicates have attracted significant technological interest, owing to their superior phase homogeneities and lower densification temperatures.

Further, metals form a large diversity of oxides that can adopt varied structural geometries with unique electronic band structures [82–84]. Accordingly, metal oxides are being increasingly investigated for wide varieties of technological applications, including the fabrication of electronic circuits, sensors, piezoelectric devices, dielectric capacitors, and so forth.

Bulk oxides are mostly robust and stable materials with well-defined crystal lattices. However, in the case of nanostructured oxides, the reduction in particle size induces considerable crystallographic changes leading to structural transformations [85, 86]. Additionally, with the decrease in particle size, the so-called quantum confinement effect also occurs. Quantum confinement may be defined as the quantization of energy levels of nanomaterials with decreasing particle size. It is this quantization that leads to the particle size-dependent material properties of nanosized metal oxides [82, 83].

Zinc oxide nanofillers Among various metal oxide nanofillers that have been investigated so far, ZnO is one of the most important semiconductor metal oxides that has attracted considerable scientific interest toward optical, optoelectronic, and energy storage applications. ZnO nanofillers are also of particular interest as potential additives to realize advanced polymer-based photonic NCs, owing to their inherent abilities to show size- and morphology-dependent optical properties [16, 87].

Additionally, ZnO is one of the primary wide bandgap semiconductors with large exciton binding energy, direct bandgap absorption, and

Table 3.3 Some of the important inorganic nanofillers, their characteristic properties, and representative examples.

Type of nanofiller		Characteristic properties	Representative examples	References
Layered silicates		a. Excellent gas barrier properties b. Appreciable optical clarity c. Increased flame retardancy	Kaolinite, halloysite, montmorillonite, and so forth	[50, 51]
Particulate fillers	Metals	a. Improved catalytic activity b. Excellent antibacterial properties at the surface	Gold	[52]
		a. Higher compression resistance b. Improved microhardness	Aluminum (Al)	[53]
		a. Improved mechanical property b. Excellent antimicrobial activity c. Excellent wear resistance	Copper (Cu)	[54, 55]
		a. Excellent antimicrobial activity b. Improved electrical conductivity	Silver (Ag)	[56, 57]
	Metal oxides	a. Novel light-emitting properties b. Excellent UV shielding behaviors c. Improved charge storage d. Enhanced dielectric properties	Zinc oxide (ZnO)	[58]
		a. Effective UV screens b. Peroxide sensors c. Dental adhesives d. Antimicrobial coatings	Titanium dioxide (TiO_2)	[59]
		a. Barrier coatings b. Improved mechanical properties c. Transparent conducting films	Alumina (Al_2O_3)	[60, 61]
		a. Improved thermal behaviors b. Enhanced magnetic properties c. Biomedical imaging	Iron oxide (Fe_2O_3)	[62]
		a. Excellent UV shielding properties b. Increased electrical energy storage c. Improved catalytic activity	Cerium oxide (CeO_2)	[63, 64]
		a. Appreciable breakdown strength b. Augmented dielectric constant	Zirconium tungstate (ZrW_2O_8)	[65]
		a. Increased electrical conductivity b. Improved catalytic activity	Zirconium oxide (ZrO_2)	[66]
		a. Increased dielectric constant b. Enhanced energy storage aptitudes c. Improved piezoelectric coefficients	Barium titanate ($BaTiO_3$)	[67, 68]
		a. Improved electrochemical performance b. Increased dielectric constant	Silica (SiO_2)	[69, 70]
		a. Enhanced energy storage density b. Increased piezoelectricity	Lead titanate ($PbTiO_3$)	[71]
		a. Increased electrical conductivity b. Polymer solar cells	Copper oxide (CuO)	[72, 73]

Table 3.3 Some of the important inorganic nanofillers, their characteristic properties, and representative examples.—cont'd

Type of nanofiller		Characteristic properties	Representative examples	References
	Metal sulphides	a. Nonlinear optical properties b. Photoluminescence c. Improved thermal properties	Cadmium sulphide (CdS) and zinc sulphide (ZnS)	[74–76]
	Metal selenides	a. Improved dielectric response b. Fluorescent emission	Zinc selenide (ZnSe) and cadmium selenide (CdSe)	[77, 78]
Other nanofillers	Layered double hydroxides	a. Permanent anion-exchange ability b. Adsorption aptitudes c. Improved thermal properties	$\left[M^{2+}_{1-x}M^{3+}_{x}(OH)_2\right]^{x+}\left(A^{n-}\right)_{x/n}\cdot mH_2O$ Here, M^{2+} and M^{3+} are di- and tri-valent metal cations; A^{n-} is the interlayer guest ion with $n-$ valency and the values of x vary between 0.22 and 0.33	[79–81]

intrinsic structural defect induced exciton emissions [16, 28, 88, 89]. Consequently, ZnO with its wurtzite structure and strong UV absorbing properties is being continuously employed as a UV-blocking agent in sunscreen lotions as well as for use as photo catalysts, in solar cells, and also in nonlinear optical systems [90, 91].

ZnO can also adopt diverse morphologies (nanorings, nanorods, nanohelices, and so forth) depending on the synthetic conditions [92]. It is also known to exhibit surface and quantum size effects that enable unique material functionalities. Further, ZnO nanofillers with Zn-O linkage are associated with high electron mobility, higher thermal conductivity, direct bandgap electronic transitions, and large exciton binding energies, which also widen their application window [93].

Metal oxide nanofiller synthetic techniques

Numerous synthetic routes have been proposed and adopted to produce inorganic nanofillers; these may be collectively generalized into bottom-up and top-down approaches [49].

The bottom-up approach makes use of liquid-phase chemical reactions such as sol-gel synthesis [16], the hydrothermal growth process

[15], and the intercalation technique for clay minerals [94], which allows precise control over the chemical compositions and reaction conditions. The top-down technique involves milling and pulverization approaches in which the particle size control is relatively tougher.

Further, the physicochemical properties and the material functionalities of the resulting nanostructures are dependent on the synthetic route employed and are very crucial in tuning the stoichiometry (composition), structure, and morphology of the desired product.

Hydrothermal growth process Although the hydrothermal technique has established itself as one of the most versatile approaches toward the synthesis of inorganic nanofillers, there is no unanimous definition for this technique.

The term hydrothermal refers to heterogeneous reactions carried out under high temperature and pressure. It essentially involves the recrystallization of the desired particle from high temperature aqueous solutions at elevated pressures [15].

The origin of the hydrothermal technique dates back to the formation of a majority of minerals in the presence of water molecules at elevated temperature and under pressure [95]. Nevertheless, the commercial significance of the hydrothermal growth process was only realized with the development of single crystals of quartz and zeolites [96].

The term "hydrothermal" is of geological origin with geologists/mineralogists having continuously studied hydrothermal phase separations [97]. However, the desired crystal growth in the hydrothermal process depends on the effective solubilities of minerals in hot aqueous solutions under elevated pressure.

In a typical synthetic route, the nutrient solution maintained in an autoclave is subjected to a temperature gradient between the two opposite ends of the growth chamber. Then, the nutrient solution dissolves in the hotter end of the growth chamber while crystal growth occurs in the cooler end [15, 34]. A pictorial depiction of the typical hydrothermal growth process is presented in Fig. 3.3.

Additionally, the hydrothermal method as a nanofiller synthesis technique allows the effective realization of various unique morphologies in the desired product (by varying the reactions conditions), so as to obtain tailor-made material properties. Such a technique is extremely efficient and highly competent toward the production of nanostructured materials with crystalline phases so as to harness unique material functionalities (structural, optical, electrical, optoelectronic, and so forth).

Sol-gel technique The sol-gel technique is yet another bottom-up approach that involves the formation of inorganic nanostructures via the effective gelation of inorganic sol (colloidal suspension) so as to form a continuous network in the liquid phase. The pictorial representation of the sol-gel synthesis technique is given in Fig. 3.4.

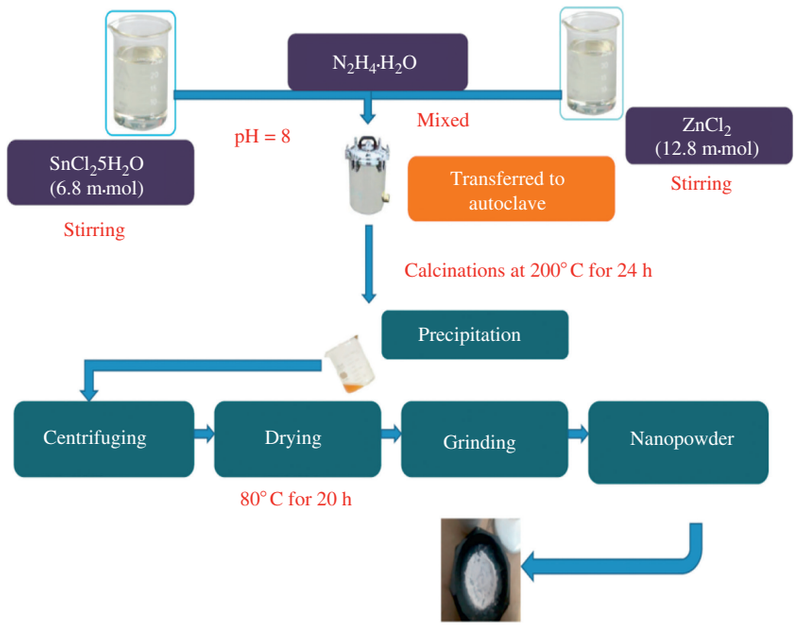


Fig. 3.3 Schematic representation of the synthesis of zinc stannate NPs via the hydrothermal growth process. Reproduced from reference L. Joseph, J.E. Allwin, M.M. Jeronsia, Jaculine, S.J. Das, Investigations on structural and optical properties of hydrothermally synthesized Zn_2SnO_4 nanoparticles, Phys. Res. Int. 2016.

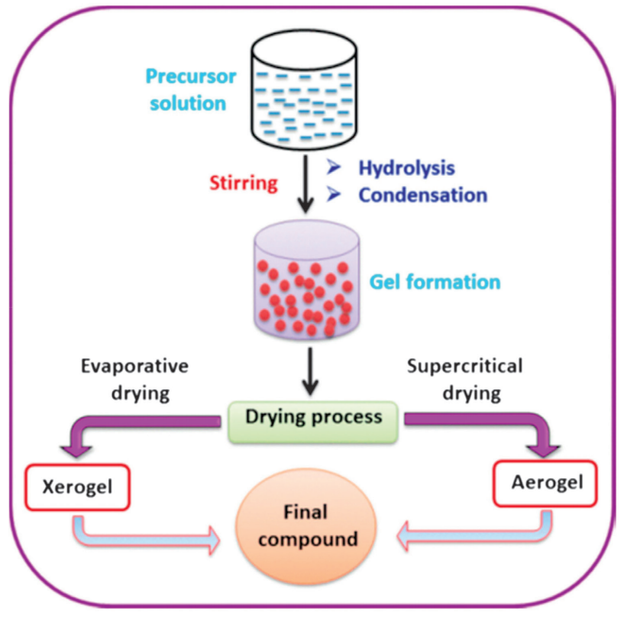


Fig. 3.4 Schematic representation of the sol-gel technique adopted toward the synthesis of metal oxide nanomaterials. Reproduced from reference G. Rao, D. Bolla, Mukherjee, B.M. Reddy, Novel approaches for preparation of nanoparticles (chapter), in: Nanostructures for Novel Therapy, 2017, pp. 1–36 with permission of Elsevier.

Further, the sol-gel technique utilizes metal/metalloid (precursors) bounded by reactive ligands, which are suitably processed to form the dispersive oxides (in the presence of water/dilute acids). The water/acid content is then removed from the processed sol to yield the gel, which on calcination confers the desired metal oxide. Often, the sol-gel transition involves the hydrolysis and condensation of metal alkoxide ($M(OR)_x$) precursors as presented below:

$$M-OR+H_2O \rightarrow M-OH+RO-(\text{Hydrolysis})$$

$$M-OH+RO-M \rightarrow M-O-M+R-OH(\text{Condensation})$$

Solution combustion technique Combustion synthesis, also called self-propagating high temperature synthesis (SHS), is an effective low-cost technique for synthesizing highly pure and homogeneous nanocrystalline powders.

Solution combustion synthesis (SCS) is a versatile process that allows the successful synthesis of a wide range of nano-sized ceramic materials. A pictorial depiction of the same (SCS) is given in Fig. 3.5.

A typical SCS involves a heat-initiated self-sustained reaction between the oxidizer (metal nitrate) and the fuel (glycine/urea/sucrose), leading to the formation of fine powders. Various factors such as heat content and the temperature of the flame generated during combustion have a direct influence on the physical behaviors (crystallite size and surface area) of solution combusted powders [3, 15]. SCS is also governed by the nature of fuel and the effectiveness of the fuel-to-oxidizer ratios [3, 16]. The fuel-to-oxidizer ratios are, however, computed by scheming the total oxidizing and reducing valences of the fuel and the oxidizer by a standard technique proposed by Jain et al. [98]. Nevertheless, SCS is a high-temperature process that involves the production of thermodynamically stable phases only.

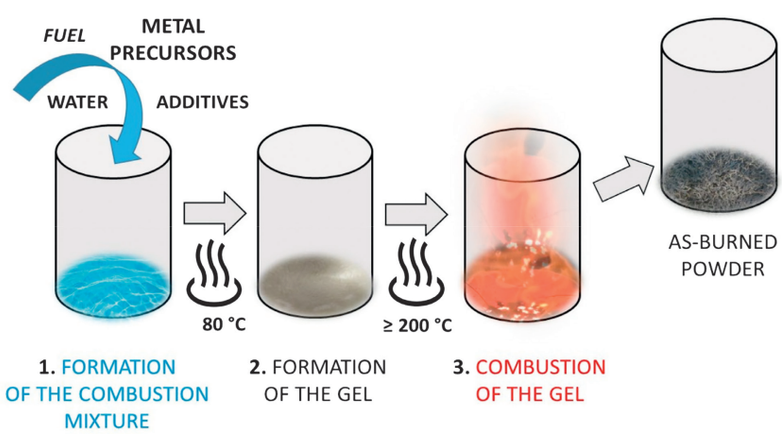


Fig. 3.5 Schematic description of the three major steps involved in SCS. From F. Deganello, Nanomaterials for environmental and energy applications prepared by solution combustion based-methodologies: role of the fuel, Mater. Today 4 (4 Part E) (2017) 5507–5516.

3.6.1.2 Properties and applications of nano-sized metal oxides

Properties of nano-sized metal oxides The current state-of-the-art research on oxide materials affirms that their physicochemical properties display acute dependence on particle size. Further, oxide materials are known to exhibit exceptional physicochemical and optoelectronic functionalities, owing to their limited size and high density of edge surface sites.

Additionally, the particle size of metal oxides is expected to influence two basic material properties, namely the structural characteristics and the electronic properties. In turn, these drive the third imperative behavior, that is, the physical and chemical properties.

Bulk oxide materials are highly robust and thermodynamically stable systems with well-defined crystal geometries. However, the changes in their surface free energy and inherent stress associated with the size reduction process may disturb the thermodynamic stability [99, 100]. Consequently, phases with low thermodynamic stability in bulk systems can be quite stable in their nanodimensional forms and the same has been reported in nanostructures of aluminum, titanium, molybdenum, and other related oxides.

The second imperative effect of size reduction is, however, related to the electronic properties of the system under consideration. Generally, nanostructured materials are said to be associated with the alleged quantum confinement effect arising from the presence of discrete atom-like electronic states. Further, electronic effects are found to have appreciable influence on exciton levels (energy shift) and hence, the optical bandgaps. Moreover, in their bulk states, most metal oxides are associated with wide bandgaps and relatively low reactivity. Nevertheless, the reduction in particle size brings about a substantial alteration in the magnitude of the bandgap and hence, the electronic band structure and chemical reactivity of nanostructured materials [15, 16].

Applications of nano-sized metal oxides Rapid advancements in nanotechnology together with the availability of novel synthetic methods and newer characterization tools have all resulted in the escalated utilization of nanostructured metal oxides for vivid technological applications [99].

Consequently, semiconductor metal oxides such as TiO_2, ZnO, WO_3, and other related oxides, which present a strong oxidizing ability and an improved ease of hydroxyl radical (OH) formation, are effective photo-catalysts.

The finer powders of ZnO and TiO_2 with relatively higher coefficients of photonic absorption are ideal UV shields [101, 102].

Besides, nano-sized metal oxides are also potential antimicrobial agents, antibiotic carrier vehicles, and excellent anticancerous

materials [103, 104]. Similarly, particle size-dependent microbial inhibition and the inherent ability to prevent biofilm formation make nanostructured metal oxides (Fe_3O_4, TiO_2, CuO, and ZnO) ideal for skin care products, biomedical devices, optical sensors, and food-additive applications.

Nevertheless, one of the greatest challenges faced by the human race in recent decades is the fast-depleting energy sources and exponentially expanding energy demands. As a consequence, the scientific community has continuously explored the potential of nanometric materials for various energy-related applications. The nanostructured semiconductor metal oxides with high carrier mobility and low recombination rates show immense potential toward the development of diverse energy harvesting and storage devices. This includes batteries [21, 105], photo-voltaic (PV) converters [106], fuel cells [107], electronic transistors [108], and other related systems.

Of all the available metal oxides for energy-related applications, transition metal oxides with intrinsic abilities to exhibit variable oxidation states and relatively higher capacitance (than conventional carbon-based materials) are the most studied for supercapacitor applications. However, their low electrical conductivities and restricted faradaic reactions (occurring only at the surface of metal oxides) often limit their real-time operational abilities.

As a consequence, nanostructured porous materials have attracted considerable scientific interest, with nanosized $CuCo_2O_4$-based anode materials exhibiting exceptionally high energy storage ability and increased cycle stability (~ 5000 continuous cycles) [109]. However, in recent years, molybdates and lithium-based metal oxides have been the most frequently tried electrode materials for supercapacitor applications [21, 110]. Of all lithium insertion metal oxides studied, the spinel-type $LiMn_2O_4$ is the most cost-effective and environmentally benign. Its long-term operational stability was further promoted by Hwang et al., who tried chromium substitution on $LiMn_2O_4$ (Cr-substituted $LiMn_2O_4$) and established that the cycling stability of $LiMn_2O_4$ improved with the partial substitution of Mn^{3+} by Cr^{3+}. Similarly, Jayalakshmi et al. bettered the electrical performance of ZnO and Fe_2O_3 (for rechargeable Li-batteries) with carbon additives [111]. Nevertheless, the ideal electrode materials for supercapacitor applications must present extremely narrow particle size distribution together with exceptionally high surface areas.

Further, nanostructured metal oxides are also of significant interest in energy conversion devices such as catalysts for artificial photosynthesis, electrode materials in fuel cells, photovoltaic devices, and so forth. Self-doped $SrTiO_3$ nanostructures brought about a considerable enhancement in artificial photosynthetic ability for methanol production. Boron-doped zinc oxide (B-doped ZnO) nanomaterials

exhibited the highest catalytic activity toward H_2 evolution. Further, Y_2O_3 stabilized ZrO_2 (YSZ), $LaCoO_3$, $Ce_{0.6}Mn_{0.3}Fe_{0.1}O_2$, $La_{0.8}Sr_{0.2}Ga_{0.8}Mg_{0.15}Co_{0.05}O_3$, $Sm_{0.5}Sr_{0.5}CoO_3$, and CeO_2 are some of the most studied oxide materials for solid oxide fuel cell applications [112]. TiO_2, ZnO, and MoO_3 nanostructures are the most preferred for solar and electrical energy harvesting and storage applications.

3.7 Polymer nanocomposites

PNCs are essentially polymer-based composite materials with one or more nanometric components loaded in the host polymer. They represent a new generation of hybrids, in which, the introduced nanofiller can bring about significant changes to the overall material functionalities of the polymer host [113, 114].

Although PNC hybrids have been known for decades, the lack of effective characterization tools had limited the total understanding of their material behaviors and hence, narrowed their application domains. Nevertheless, the pioneering work towards understanding and establishing nanofiller-induced changes in the material properties of PNC system dates back to 1993, when Kojima et al. published their research findings on polyamide filled nanoclay. They established that even a very small loading (< 5 vol%) of nanoclay increased the modulus of nylon-6 by a factor of ~ 3 units, while the heat deflection temperature improved by 80 K [115]. Inspired by these revelations, the scientific community started exploring the chemistry between various combinations of nanofillers and polymers, in addition to analyzing the crucial physics, that leads to property enhancement. Consequently, the field of PNCs is currently a billion-dollar global industry, with products ranging from packaging materials to automotive components and being explored in diverse fields such as aerospace, energy, electronics, and cosmetics [116]. Some of the representative PNCs and their commercial exploits are listed in Table 3.4.

It is often observed that, the introduced nanofiller does not alter the fundamental polymer characteristics, but rather enables new functionalities without affecting the inherent process ability of the host polymer. The basic notion behind the development of PNCs was to employ materials with nanometric dimensions, so as to develop advanced composite hybrids that offer excellent mechanical performance in conjunction with enhanced material properties [118].

Additionally, the physicochemical properties of PNCs are often different from their individual components. That is, PNC systems either display combinatorial behaviors or synergistic effects depending on the nature of the polymer-filler interface. Generally, the interface pedals the degree of interactions between the introduced nanofiller

Table 3.4 Some of the representative PNCs of commercial significance [3, 47, 57, 89, 117].

Polymeric matrix	Nanofiller	Property enhancement	Related application
Thermoplastic polyolefin	Exfoliated clay	Stiffness/strength	Exterior step assist
Polyamide	Exfoliated clay	Stiffness	Timing belt cover
Polyisobutylene	Exfoliated clay	Permeability barrier	Tennis balls, tires, and soccer balls
Natural rubber	Silver	Antimicrobial	Latex gloves
Nylon	Exfoliated clay	Barrier	Beverage containers
SBR rubber	Carbon nanofibers	Improved tire performance in winter	Winter tires
Nylon 6,6	Exfoliated clay	Barrier	Auto fuel systems
Epoxy	Carbon nanotubes	Strength/stiffness	Tennis rackets/hockey sticks
PVA	Cs_2ZnO_2	UV to visible down conversion	Mechanically flexible UV sensors
PMMA	ZnO	UV shielding	Contact lens
PVA	Na_2ZnO_2	Spectral manipulators	Luminescent solar concentrators
PVA	ZnO	Dielectric behaviors	Dielectric capacitors
Polyimide	TiO_2	Barrier	Gas separation
PC	SiO_2	Wear	Dental applications and abrasion-resistant coatings
PMMA	SiO_2	Luminescence	Optical display devices
PC	ZnO	Selective optical transmission	Band pass filters
PVA	$Al_{0.2}Y_{1.8}O_3$	Improved UV shielding	Mechanically flexible UV shieldants

and the host polymer, thereby influencing the resultant properties of PNC systems [119]. Such multifunctional systems with improved material functionalities allow a whole new range of advanced techno-commercial applications, with the addition of even minute quantities of nano-sized fillers presenting a profound impact on the overall material functionalities of the host polymer. Nevertheless, in most cases, the observed amendment in the aspired functionality is a direct function of filler load, their relative dispersions, and the nature of the polymer-filler interface [3, 120].

3.7.1 Functional properties and related applications of PNCs

The introduction of inorganic nanofillers into a particle stabilizing organic host may offer high-performance multifunctional systems with versatile material properties that suit vivid technological applications

[3, 34, 121, 122]. However, the real-time outdoor applications of PNCs mandate a fundamental understanding of their inherent material functionalities. Consequently, some of the nanotechnology-enabled smart optical, optoelectronic, and energy storage functionalities of PNCs and their related applications are briefly highlighted in the sections that follow.

3.7.1.1 Optical properties and related applications

The optical applications of metal oxide nanofiller introduced PNCs take advantage of unique optical properties of metal oxide nanofillers, together with the ease of processing offered by host polymer.

Given that, most optical applications of PNCs demand effective engineering of the polymer refractive index (RI) with coeval preservation of optical transmittance. The size of the inorganic nanofiller becomes imperative in deciding the overall optical functionalities and hence, the resultant applications.

In general, 40 nm is the upper size limit for any inorganic nanostructure to be employed as an optically effective additive [34]. Additionally, the difference in RI between the inorganic filler and the organic polymer, the extent of filler dispersions, and the arrangement of fillers in the polymeric host are some of the essential factors that affect the optical characteristics of PNCs. Consequently, the random distribution of fillers favors optical transparency and UV absorption characteristics while an orderly arrangement induces optical dichroism [123]. Such polymer-based advanced functional materials are of significant interest toward a wide range of photonic and optoelectronic applications such as planar waveguides, flat panel displays, optical sensors, high-brightness LEDs, diffraction gratings, optical data storage systems, and many more.

UV-visible photonic absorption and related applications

The profound amplification in UV-radiation dosage has encouraged the scientific community to develop mechanically flexible PNC-based photo-protective materials [34, 83, 124–126]. An ideal UV-shielding material must present considerably high optical transparency in the visible range (> 400 nm), together with steep-absorption in the UV regions (200–400 nm).

Consequently, PNCs reinforced with TiO_2, ZnO, SiO_2, Al_2O_3, and CeO_2 (metal oxides with relatively higher UV absorption coefficients) are the most studied for UV shielding applications. The same was found true by Nithin et al., who extracted appreciable UV shielding abilities using PVA/Cs_2ZnO_2 NCs. The UV-visible spectral profiles (Fig. 3.6) justify the UV filtering abilities of the same. As can be seen from the figure, the UVC (290–100 nm) transmittance of PVA at 250 nm showed a considerable decrease upon the addition of 4 wt% Cs_2ZnO_2

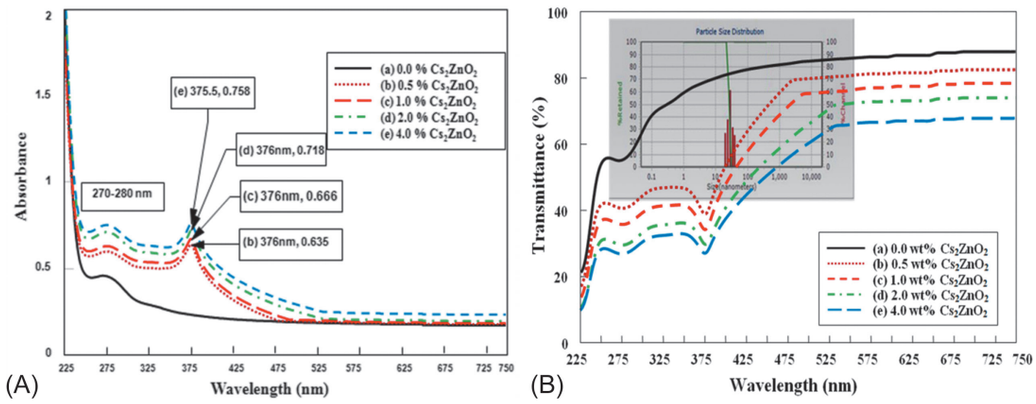


Fig. 3.6 UV-visible (A) absorbance; and (B) transmittance spectra of PVA/Cs_2ZnO_2 NCs (inset: dynamic light scattering profiles of Cs_2ZnO_2 NPs). Reproduced from reference K.S. Nithin, Siddaramaiah, Opto-electrical characteristics of poly (vinyl alcohol)/cesium zincate nanodielectrics, J. Phys. Chem. C 119 (2015) 20244–20255 with permission of The American Chemical Society.

NP. However, the change in optical transmittance in the visible region (> 400 nm) is only marginal. Further, they also opined that the observed retention in optical clarity of PVA NCs in visible regions may be owed to the smaller domain size (~ 44 nm) of Cs_2ZnO_2 NPs (inset to Fig. 3.6B). They also reported that the observed steep UV absorption coupled with high visible transparencies supported the possible application of PVA/Cs_2ZnO_2 NCs as visibly transparent and mechanically flexible UV shieldants [3].

Suma et al. reported mechanically flexible PVA/$Ce_{0.5}Zr_{0.5}O_2$ NC thick sheets that exhibit steep UV absorption at 380 nm. They opined that such PNC hybrids with appreciable photonic absorption at 380 nm are of significant interest as UV protective sunglasses. The said application was owed to the fact that white fluorescent and short wavelength (380 nm) radiations often induce retinal damage, which may in turn lead to visual disparity [104]. Similarly, Nithin et al. reported mechanically flexible and visibly clear UV filters with steep UV absorption and high visible transparencies (at 550 nm) using PVA/$Li_{0.4}Sn_{0.8}O$ NC films [83]. While, Shivanna et al. improved the UV endurance of polycarbonate (PC) films using solution combustion synthesized Cs_2ZnO_2 NPs. The augmented UV endurance in this case (PC/Cs_2ZnO_2 NC films) was analyzed via yellowing index quantification and Fourier transform infrared (FTIR) measurements at 1713 cm^1 (Fig. 3.7). Also, they observed that the foundation for improved UV stability was Cs_2ZnO_2 nanofiller induced lessening of undesirable photo-degradation reactions. They further opined that the introduced photo-active nanofillers can also act to dissipate the high-energy UV photons via polymer-nano metal oxide induced synergistic spectral downconversions [88, 89, 127]. The introduced metal oxide nanofiller offers protection against undesirable

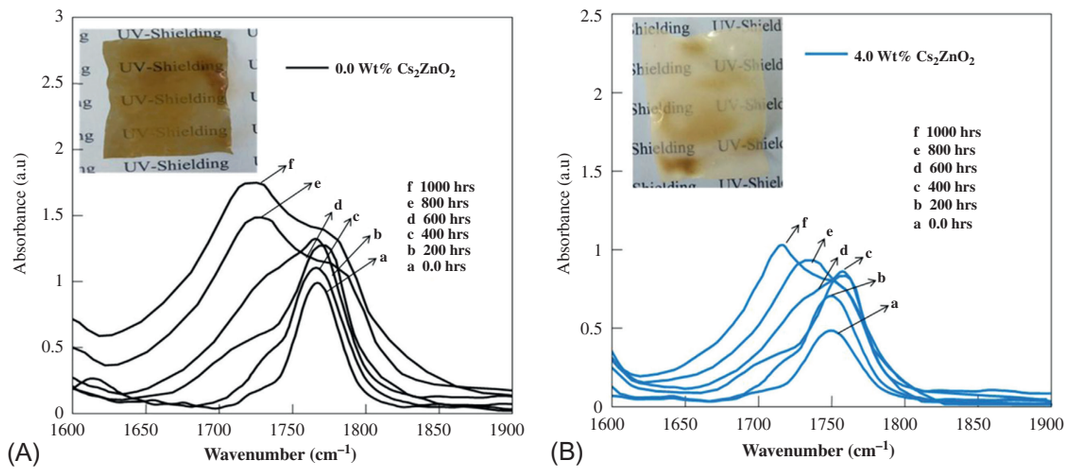


Fig. 3.7 FTIR spectra of irradiated (A) PC films; and (B) PC/4.0 wt% Cs_2ZnO_2 NC films in carbonyl region (inset: digital images of irradiated PC/Cs_2ZnO_2 NC films), toward establishing the UV endurance of PC films. Reproduced from reference S. Shivanna, K.S. Nithin, K.N. Shilpa, J.R.B. Mutturaj, S. Basavaraj, Patina-green coloured light emitting polycarbonate films: a synergistic extraction of improved UV endurance and considerate spectral down-conversion, J. Lumin. 210 (2019) 276–284 with permission of Elsevier.

photo-degradation reactions while the polymeric host guards the luminescence centers of nanostructured metal oxides.

Such photo-responsive polymer-based smart composites (PBSCs) with appreciable UV to visible photonic downconverting abilities are highly desirable for solar energy harvesting applications (toward augmenting the number of constructive photons entering the solar cells) [117]. All these studies submit that synergistic polymer-filler induced photo-responsive properties (the ability of PBSCs to absorb high-energy UV photons and reemit the same in visible regions via fluorescent emission) are the key toward developing mechanically flexible UV shieldants for various techno-commercial applications.

Additionally, optical transparency in photo-protective materials can only be retained in the form of films (μm thickness). An increase in PNC film thickness often leads to opaqueness/translucence, especially when the inorganic UV absorber is directly introduced into the polymer matrix through physical means [117, 128].

Thus, in recent years, chemical methods of PNC synthesis that take advantage of in situ polymerization techniques have attracted considerable technological interest. As a result, Liu et al. reported optically clear and UV shielding PMMA/ZnO NCs via in situ sol-gel polymerization [129]. The said PNCs were reported to retain their visible transparencies, even in their bulk size (thickness) of ~ 1 cm.

Further, Faubl and Quinn demonstrated that the UV-shielding efficacies of commercially available contact lenses are a direct function of their

thickness [130]. Jie Xiao et al. established that the encapsulation of TiO_2 NPs via a corona-shell-core structure using a poly (2-(dimethylamino) ethylmethacrylate) (PDMA) block copolymer eliminates the unwanted photo-catalytic degradation action of TiO_2 NPs, besides offering excellent UV-shielding effects [131]. Further, a few groups also tried the mechanically flexible UV shielding PNCs for food packaging and textile-related applications [132].

Eventually, increasing research efforts in this direction have also figured out that the size of the inorganic nanofiller, their relative dispersions, the nature of the polymer-filler interface, and the thickness of resultant PNC are instrumental toward the development of optically clear UV protective films [34, 83].

The visible light absorbing ability of PNCs is another imperative optical functionality, which may be considered exceedingly advantageous for various color applications. In simpler terms, PNCs could be obtained in different colors by mere variation in the size of nanofillers, as observed by Heffels et al. [133]. The as-developed PVA/AuNCs exhibited varying colors such as pink, purple, and blue upon tuning the particle diameter between 16, 43, and 79 nm, respectively. Kirchner and Zsigmondy demonstrated that interparticle distance also has a significant effect on the color of PBSCs, with the combination of gelatin and AuNPs exhibiting appreciable color switching (upon swelling) [134]. Accordingly, advanced PBSCs could be developed toward different color applications by the selective tuning of nanofiller size and the interparticle distance, as proposed by Maxwell Garnett [135].

Photoluminescence and related applications

Polymer-based photoluminescent (PL) composites are one such class of SCs that displays external light-dependent stimuli-responsive behaviors. Such luminescent PBSCs often display entirely new optical excitation and emission characteristics (which are significantly different from the introduced filler and base polymer (in isolation)) [136]. Accordingly, Lee et al. and Erskine et al. successfully implanted PL CdSe NPs in poly (lauryl methacrylate) (PLM) and poly styrene (PS) matrices [137, 138]. Peres et al. reported a bright green luminescence with CdSe/polybutylacrylate (PBA) NCs [139]. Farmer and Patten et al. developed PL films comprising core-shell CdS/SiO_2 nanofillers in PMMA [140]. Yordanov et al. reported photo-activated fluorescence from core/shell quantum dots of CdSe/CdS in poly(butylmethacrylate) [141]. Yet, the inherent toxicity issues of Cd, Se, and Pb limited the widespread applicability of such luminescent composites. This in turn paved the way for environmentally benign alternatives such as ZnO and CeO_2.

In general, PL in ZnO is said to be associated with two important cooperative phenomena, namely, exciton or near-band-edge emission leading to UV light and deep-level emission (related to oxygen vacancies)

leading to highly intense visible light [142]. Further, ZnO NPs are often encrusted with polymeric encapsulations to protect their optical functionality and also to improve their mechanical performance. However, during early attempts to protect ZnO via polymer capping, Guo et al. observed that PVP-capped ZnO exhibited appreciable UV emissions while their visible light emission intensities were relatively weaker [133, 143]. Similar results were also drawn from the studies of Chang et al., as they reported a strong UV emission in polyaniline-modified ZnO nanostructures [144]. However, if the polymer itself is luminescent, then the introduction of ZnO led to fluorescence quenching, as reported by Wang et al. and Ton-That et al. [145, 146].

In simpler terms, the fluorescent emission behaviors of ZnO mainly depend on the oxygen vacancies at the NP surface. Further, if the interactions between the polymeric matrix and the ZnO nanostructures are weak, the emission intensities are found to decrease significantly. A strong polymer/ZnO interaction often leads to guarded and in most cases augmented luminescence.

Going forward, a synergistic polymer/filler combination may lead to unique fluorescent behaviors in an otherwise nonfluorescent polymer or filler (in isolation), as reported by Sachhidananda et al. [89, 126, 127] (Fig. 3.8) and Suma et al. (Fig. 3.9) [47]. While, Nithin et al., extracted varying colored fluorescent emissions using alkali metal-doped ZnO NPs introduced PVA NC thick films (Fig. 3.10). They reported that the addition of alkali metal-doped ZnO (Cs_2ZnO_2, Rb_2ZnO_2, and Na_2ZnO_2) nanofillers induced blue-green, yellow-green, and orange-red emissions (upon UV excitation) in an otherwise nonfluorescent PVA [3, 89, 118, 127]. They also reported that the emission

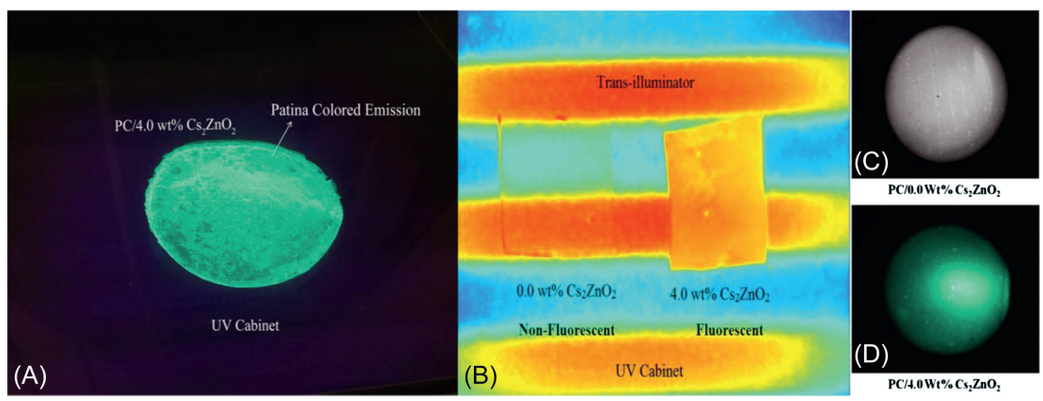


Fig. 3.8 (A) Digital photograph; (B) UVA-transilluminator recorded image; and (C) Fluorescence microscopic pictures of PC/Cs_2ZnO_2 NC thick films. Reproduced from reference S. Shivanna, K.S. Nithin, K.N. Shilpa, J.R.B. Mutturaj, S. Basavaraj, Patina-green coloured light emitting polycarbonate films: a synergistic extraction of improved UV endurance and considerate spectral down-conversion, J. Lumin. 210 (2019) 276–284 with permission of Elsevier.

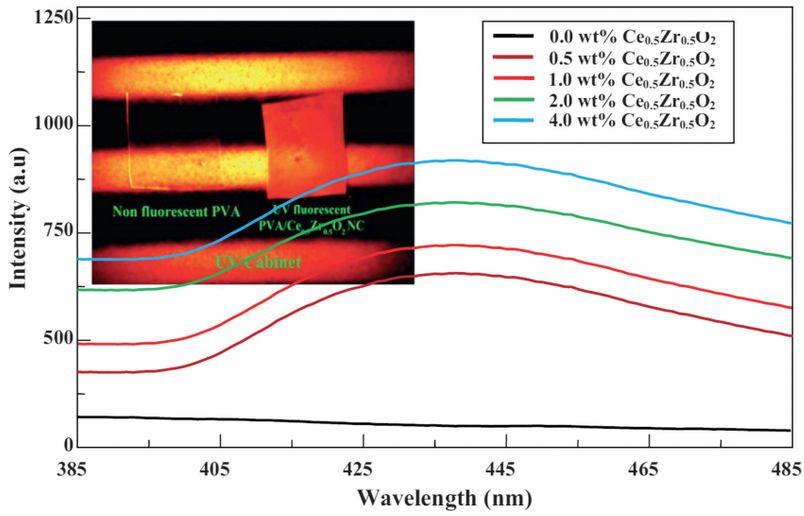


Fig. 3.9 Fluorescent emission spectrum of PVA/$Ce_{0.5}Zr_{0.5}O_2$ NC films (inset: UVA transilluminator images of UV fluorescent PVA/$Ce_{0.5}Zr_{0.5}O_2$). Reproduced from reference G.R. Suma, K.S. Nithin, K.N. Shilpa, S. Sachhidananda, V.S. Satyanarayana, Effect of $Ce_{0.5}Zr_{0.5}O_2$ nano fillers on structural and optical behaviors of poly (vinyl alcohol), J. Mater. Sci.: Mater. Electron. 28 (2017) 10707–10714 with permission of Springer.

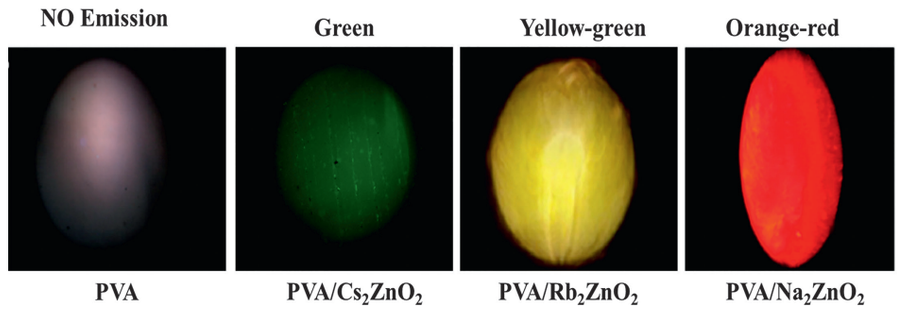


Fig. 3.10 Fluorescent microscopic images of PVA thick films introduced with various alkali metal-doped ZnO nanofillers.

wavelength of the as-developed PNC films displayed a considerable blue shift (orange-red to blue-green) as the ionization potential of the alkali metal dopant scales down (from Na to Cs).

They even submitted that the observed fluorescent emission behaviors of PVA NC films may be owed to the possible resonant energy transfer between the alkali metal-doped ZnO nanofillers and the PVA host. The photo-generated charge carriers (upon UV excitation) would occupy Zn vacancies and/or the shallow acceptor states on the alkali metal-doped ZnO nanofillers. This doable energy transfer may facilitate the transition of photo-generated electrons from the lowest unoccupied molecular orbital (LUMO) of the PVA to the surface of the mixed metal oxide nanofillers, thereby leading to fluorescent emission.

The luminescence behaviors of photo-active PBSC films may also depend on the electron donating tendencies of the polymeric

matrix, while a few polymers are known to trap photo-electrons from introduced nanofillers. A general concern in most of these PBSCs is the destruction in PL behaviors of semiconductor NPs upon loading to the polymer host. Suitable surface engineering of semiconductor NPs employing particle stabilizing polymers as host matrices and also making use of core-shell structures may enable protective effects and hence, preserve the PL behaviors.

Also, the novel fluorescent emission behaviors of polymer-nanofiller composite thick films depend on the nature of interfacial adhesions, the extent of filler dispersity, changes in the filler/polymer crystallinity (upon doping), and the relative energy levels of the polymeric matrix and the inorganic nanofillers (which may facilitate resonance energy transfer between the polymer-filler interface) (Fig. 3.11) [126].

Thus, polymer-based PL composites may offer prospective solutions to scores of pressing technological problems, especially where a noncontact form of stimulation and control is desired. Consequently, such designed flexible smart materials that bring about effective spectral downconversions are of considerable interest for solid-state lighting applications and as photo anodes in high-efficiency dye-sensitized solar cells, light-emitting diodes, and so forth.

Further, an electronics-free UV sensor is another such application domain that makes use of polymer-based PL composites which can selectively downconvert high-energy UV radiation into relatively lesser energy visible light. UV-responsive PBSCs are also explored toward augmenting the light-harvesting ability of solar cells. Diverse strategies have been proposed and numerous methods have been attempted to broaden the light-harvesting ability of solar cells. Some

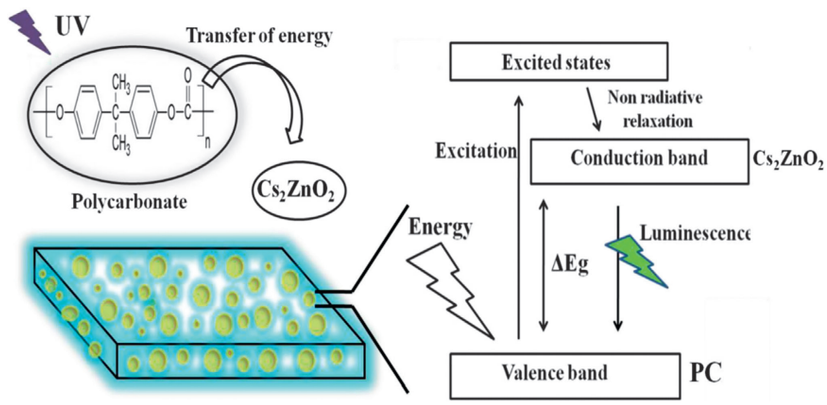


Fig. 3.11 Representative energy transfer in PC/Cs_2ZnO_2 NC thick films. Reproduced from reference S. Shivanna, K.S. Nithin, K.N. Shilpa, J.R.B. Mutturaj, S. Basavaraj, Patina-green coloured light emitting polycarbonate films: a synergistic extraction of improved UV endurance and considerate spectral down-conversion, J. Lumin. 210 (2019) 276–284 with permission of Elsevier.

of these include the harmonization of absorption response using multiple sensitizers (with complementary electronic band structures), the doping of the TiO_2 photo-anode with an UV-excited luminescent compound, and many more. Yet, of all the stratagems adopted, the most suitable, more expedient, and most viable strategy is the use of luminescent downshifting layers (LDS) that extend the short wavelength limit of solar cells. The said LDS layers act through the selective absorption of low-energy UV-photons and their reemission at longer wavelengths where the photoactive materials of the PV cell typically show optimal maximum spectral response.

To sum up, photo-responsive PBSCs as LDS layers take advantage of synergistic interactions between the opto-electronically effective inorganic fillers and the highly processable organic polymers. The same has been established by Nithin et al. using alkali metal-doped ZnO NP introduced PVA NCs and Sachhidananda et al. with alkali metal-doped ZnO NP introduced PC NCs [88, 89, 127].

3.7.1.2 Electrical properties and related applications

The science of dielectric materials has been pursued as a multidisciplinary research domain spread over the likes of physics and chemistry with close links to material technology and electrical/electronic engineering.

Dielectric science was chased for well over 100 years. It was only in recent decades that dielectric research has been broadened. This increasing technological interest in dielectric materials encouraged material scientists to expand their horizons from consumer products to the high technology arena. This led to noteworthy innovations in telecommunications, such as plastic fibers used for short optical data links and polymeric films employed for nonlinear optical applications.

The field of microelectronics experienced the formulation of radiation-sensitive polymers/photo-resists. Steady progress has also been reported in the field of passivation, with various PBSCs utilized for integrated circuits and the packages that house them.

Additionally, the science of dielectric materials is also of significant interest in applications involving electronic sensors and conduction isolators as well as power utilities, together with imperative advantages for applications involving communication devices and data storage systems [147, 148].

Electrical energy storage functionalities

Electrical energy storage is one of the key components toward the realization of numerous electronic devices, including portable electronic systems, hybrid electric vehicles, and pulse power applications [149, 150]. This wide application window of dielectric systems has

encouraged the materials research community to rely on nanostructured materials to develop novel dielectric systems for current and future commercial applications. The growing need for compact electrical and electronic power systems, aided by advanced energy storage devices that can accumulate a large quantity of charges and deliver the same nearly instantaneously (pulse power) has led to the development of nanotechnology-enabled mechanically flexible dielectric systems. The said hybrids take advantage of the high dielectric permittivity of inorganic nanostructures, alongside excellent process abilities offered by the polymeric domains. Such advanced energy storage devices demand higher power and energy densities in addition to greater charge-discharge current capabilities [151, 152].

Thus, in recent years, the dielectric properties of micro/nanofiller-reinforced PBCs have gained considerable scientific interest [153]. There are several reports on the dielectric behaviors of polymeric systems. The molecular orientation behaviors and their relaxation mechanisms have presented a complex view and hence, are yet to be fully understood [154, 155].

Further, one of the most convenient methods to establish the electronic band structure of polymeric composites is to establish the dielectric behaviors of composite films (as a function of applied frequency and temperature). Under the influence of an external electric field, the dielectric materials exhibit charge separation arising from electronic and/or ionic and/or dipolar polarization effects. Such dielectric materials may be employed to store electrical energy through electron distributions around the constituent atoms, caused by the external electric field. Besides, nanostructured inorganic systems are established dielectric materials displaying dielectric permittivity ranging from a few hundreds to thousands in magnitude. This in turn provides a virtuous possibility of engineering the dielectric behaviors of polymeric systems by the introduction of such inorganic nanofillers. Nevertheless, the dielectric behaviors of nanofiller-introduced polymeric systems generally fall short of expectations, owing to the greater permittivity of the filler than the polymer matrix. This leads to the storage of relatively lesser energy in the high permittivity phase. Thus, any further advancement in the area of PNC-based dielectric systems demands a fundamental understanding of the polymer-filler interface in addition to their processing and characterization techniques.

Advanced dielectric materials must offer relatively high energy densities, low dielectric loss, and good operational stabilities. In general, materials with increased saturated polarization and high breakdown strength together with smaller residual polarization are considered ideal for energy harvesting and storage applications.

Also, on the basis of energy storage time, commercially viable energy storage devices are categorized as short-duration and long-duration

energy storers. A battery represents a long-term storage unit and capacitors as short-term ones. Batteries are known to possess high energy density (10,300 W/kg) with relatively lesser power density (< 500 W/kg). Capacitors offer relatively higher power density, but suffer from low energy densities.

Lately, increasing demand for lighter, compact, flexible, and high energy density capacitors has motivated the scientific community toward the design and development of PNC-based energy storage systems. These coalesce excellent dielectric properties alongside appreciable thermal stability and increased mechanical strength [156–159]. Polymers as such are less suited for high energy density applications, owing to their low dielectric constants. Pristine inorganic nanofillers suffer from shortcomings associated with low breakdown strength. The inherent dielectric breakdown strengths of some of the most commonly studied polymeric matrices are presented in Table 3.5.

Further, the PNC approach capitalizes on the synergistic combination of inorganic nanostructures with large dielectric permittivity with organic matrices of high dielectric strength, thereby leading to augmented energy storage abilities [160]. Consequently, different types of nanofillers were explored toward the development of advanced PNC-based dielectrics with ceramic materials being considered as the vertebrae of electronic industries, following the unearthing of ferroelectricity in these wonder materials.

Accordingly, various research groups have focused on the development of hybrid polymer-ceramic NC systems with high-permittivity inorganic nanoceramics as reinforcements [161]. Since then, various ceramic fillers such as titanates ($BaTiO_3$ (BT), $Ba_{0.5}Sr_{0.5}TiO_3$ (BST)), zincates ($MgZnO_2$, $BaZnO_2$), zirconates ($PbZrO_2$, Na_2ZrO_2), and dielectric

Table 3.5 Dielectric breakdown strengths of some of the most commonly studied polymeric matrices.

Polymer type	Dielectric breakdown strength (V/μm)
Epoxy resin	25–45
Low density polyethylene	200
High density polyethylene	200
Polystyrene	200
Polypropylene	200
Polycarbonate	252
Polyimide	280
Polyester	300

ceramics with perovskite structures (very high dielectric constant) were continuously monitored for their inherent potential to augment the dielectric functionalities of PNCs.

In the case of ceramic filler-reinforced PNCs, the major objective of the dielectric system is to isolate two different electric potentials. Additionally, an ideal dielectric is also visualized to withstand appreciable electrical/thermal/mechanical stress besides presenting minimal dielectric loss.

Further, the recent literatures support that the addition of 30 vol% of calcium copper titanate increased the dielectric constant of polyimide by 14 times while the inherent breakdown strength was reduced by 36% [162]. However, the introduction of $BaTiO_3$ nanofillers (1 wt%) reduced the breakdown strength of LDPE by 16% [163]. Nevertheless, the polypropylene-$BaTiO_3$ NC developed by Guo et al. presented improved dielectric permittivity (~ 6.1 units), high breakdown strength (~ 2.6%), and higher energy density (~ 4.8 folds) [164]. The percolation thresholds of some of the important PNCs are presented in Table 3.6.

The observed reports speculate that in a well-dispersed PNC system, the interface between the inorganic nanofiller and the organic polymer may create effective charge transport centers, thereby avoiding premature electrical breakdown. Additionally, the dielectric loss of PNC is largely proportional to the surface area between the introduced nanofiller and the host polymer. However, a judicial tuning of the material parameters yields recoverable energy storage capacity as high as 2.05 J/cm^3 for MgO (6 vol%) loaded polypropylene NCs. Nevertheless, owing to the relatively higher dielectric constant of nanostructured ceramics, an appreciable magnitude of the electric field may be concentrated in the polymeric matrix. This often leads to decreased breakdown strength and hence, reduced energy storage

Table 3.6 Percolation thresholds of some of the important PNCs.

Polymer-filler combinations	Percolation threshold (wt%)
Epoxy + CNTs	0.004
Epoxy + MWCNTs	0.0025
PVOH + MWCNTs	5–10
PS + MWCNTs	2–3
PVOH + Cs_2ZnO_2	2–4
PVOH + C-ZnO	4
PVOH + $Ca_{0.2}Zn_{0.8}O_2$	2–4
PP + CNTs	2

densities. An additional complication is the high dielectric loss associated with polymer/ceramic NC films.

The field of PNC based dielectrics has witnessed appreciable progress over the last few years. However, there appears to be plenty of room for further improvisation as a number of issues remain to be addressed. An increase in dielectric constant without compromising the inherent dielectric breakdown strength, together with achieving low dielectric loss and lower leakage currents are some of the major confrontations. At present, a high volume percentage of ceramic loading is often required to bring about considerable improvements in the dielectric behaviors of PNCs. Nevertheless, at such high filler loadings, the inherent mechanical properties and the dielectric breakdown strength of PNCs are found to deteriorate. This may in turn scale down the energy storage abilities as the electrical energy storage density scales quadratically with the applied electric field.

However, a judicious combination of high dielectric constant inorganic nanofiller and particle stabilizing organic polymer may lead to appreciable changes in the polymer microstructure, thereby leading to better dielectric property tuning and hence, improved energy storage functionalities. Thus, the development of novel elastically yielding high energy density composites entails a strong interfacial adhesion and increased surface compatibilities between the inorganic filler and organic polymer [165].

3.8 Conclusions and future directions

PNC hybrids that fully exploit the unique material functionalities of inorganic nanofillers alongside the ease of processing and improved mechanical performance offered by the host polymer, would enable scores of productive applications. Besides, the effective realization of such PNC-based smart hybrids for advanced optical, optoelectronic, and energy storage applications demand a successful addressing of various data gaps. Further, the technological usefulness of such hybrids depend heavily on the synergism between the inorganic filler and the organic matrix (i.e., the nature of the filler, the filler morphology, the filler size, the filler composition, and the dispersion homogeneity) and their further scaling up.

Nevertheless, further translation of these advanced functional materials into commercial products rests on the ability to optimize the above-cited factors, together with adopting appropriate techno-commercially feasible fabrication techniques.

References

[1] K.S. Nithin, Polymer nanocomposites as luminescent down shifting layers, Res. Rev.: (Ed.) J. Mater. Sci. (2016).

[2] M.Q.A. Al-Gunaid, A.M.N. Saeed, K.S. Nithin, B.S. Madhukar, Siddaramaiah, Optical parameters, electrical permittivity and I–V characteristics of PVA/Cs_2CuO_2 nanocomposite films for opto-electronic applications, J. Mater. Sci.: Mater. Electron. 28 (2017) 8074–8086.

[3] K.S. Nithin, Siddaramaiah, Opto-electrical characteristics of poly (vinyl alcohol)/cesium zincate nanodielectrics, J. Phys. Chem. C 119 (2015) 20244–20255.

[4] F. Allhoff, P. Lin, D. Moore, What Is Nanotechnology and Why Does it Matter? From Science to Ethics, Wiley-Blackwell, Chichester, 2010.

[5] N. Staggers, T. McCasky, N. Brazelton, R. Kennedy, Nanotechnology: the coming revolution and its implications for consumers, clinicians, and informatics, Nurs. Outlook 56 (2008) 268–274.

[6] S. Sandeep, A.S. Santhosh, N.K. Swamy, G.S. Suresh, J.S. Melo, K.S. Nithin, Electrochemical detection of L-DOPA using crude polyphenol oxidase enzyme immobilized on electrochemically reduced RGO-Ag nanocomposite modified graphite electrode, Mater. Sci. Eng. B Solid-State Mater. Adv. Technol. 232 (2018) 15–21.

[7] H.B. Vasanth Patil, K.S. Nithin, S. Sachhidananda, Siddaramaiah, K.T. Chandrashekara, B.Y. Sathish Kumar, Mycofabrication of bioactive silver nanoparticle: photo catalysed synthesis and characterization to attest its augmented bio-efficacy, Arab J. Chem. 12 (2019) 4596–4611.

[8] G.R. Suma, N.K. Subramani, S. Sachhidananda, S.V. Satyanarayana Siddaramaiah, Nanotechnology enabled *E. coli* sensors: an opto-electronic study, Mater. Today Proc. 4 (10) (2017) 11300–11304.

[9] P. Sivadasu, D.V. Gowda, N.K. Subramani, B.M. Vishweshwaraiah, S. Shivanna, S. Hatna, Direct brain targeted nanostructured lipid carriers for sustained release of schizophrenic drug: formulation, characterization and pharmacokinetic studies, Indian J. Pharm. Educ. Res. 54 (2020) 73–84.

[10] M. Faraday, The Bakerian lecture: experimental relations of gold (and other metals) to light, Philos. Trans. R. Soc. Lond. 147 (1857) 145–181.

[11] R.P. Feynman, There's plenty of room at the bottom [data storage], J. Microelectromech. S 1 (1992) 60–66.

[12] N. Taniguchi, On the basic concept of nano-technology, in: Proceedings of the International Conference on Production, British Society of Precision Engineering, London, 1974.

[13] D.K. Eric, The coming era of nanotechnology, in: Engines of Creation, Anchor Book, 1986.

[14] S.K. Nagaraj, S. Shivanna, N.K. Subramani, H. Siddaramaiah, Revisiting powder X-ray diffraction technique: a powerful tool to characterize polymers and their composite films, J. Mater. Sci. 4 (2016) 1–5.

[15] K.N. Shilpa, H.B. Patil, P. Karthik, K. Mallikarjun, B.M. Jagajeevan Raj, S. Sharon, K.S. Nithin, Removal of Cu(II) from water using hydrothermally synthesized strontium doped zirconium oxide nano adsorbents, J. Mater. Sci. Eng. 1 (2016) 252–256.

[16] K.N. Shilpa, S.R. Urs, H.B. Patil, H.P. Jayadevappa, B.V. Latha, K.S. Nithin, S. Sachhidananda, Adsorptive removal of Cu(II) from aqueous solution using nanostructured lithium zincate, Int. J. Eng. Sci. Comput. 6 (2016) 8463–8468.

[17] E.C. Dreaden, M.A. Alaaldin, H. Xiaohua, J.M. Catherine, M.A. El-Sayed, The golden age: gold nanoparticles for biomedicine, Chem. Soc. Rev. 41 (2012) 2740–2779.

[18] K. Ibrahim, S. Khalid, I. Khan, Nanoparticles: properties, applications and toxicities, Arab. J. Chem. 12 (2019) 908–931.

[19] M.V. Bhavya, D.V. Gowda, S. Praveen, N.K. Subramani, H. Siddaramaiah, Cosmetics: polymers, in: Encyclopedia of Polymer Applications, First Edition T&F, 2018.
[20] K.N. Shilpa, K. Subramani, S. Sachhidananda, B.S. Madhukar, Visibly transparent PVA/sodium doped dysprosia ($Na_2Dy_2O_4$) nano composite films, with high refractive index: an optical study, J. Alloys Compd. 694 (2017) 884–891.
[21] K.S. Nithin, Nanotechnology enabled electrode materials for rechargeable sodium-ion batteries: an ideal resolution to global energy crisis, Res. Rev. J. Mater. Sci. 4 (4) (2016) 2–3.
[22] V.R. Gowariker, N.V. Viswanathan, J. Sreedhar, Polymer Science, New Age International, 1986.
[23] K.I. Winey, R.A. Vaia, Polymer nanocomposites, MRS Bull. 32 (2007) 314–322.
[24] B. Suresha, K. Adappa, N.K. Subramani, Mechanical and tribological behaviours of epoxy hybrid composites reinforced by carbon fibers and silicon carbide whiskers, Mater. Today: Proc. 5 (2018) 16658–16668.
[25] J.A. Diego, J. Sellares, A. Aragoneses, M. Mudarra, J.C. Canadas, J. Belana, TSDC study of the glass transition: correlation with calorimetric data, J. Phys. D. Appl. Phys. 40 (2007) 1138–1146.
[26] M.D. Migahed, M.T. Ahmed, A.E. Kotp, Computation of TSDC peak parameters in amorphous polymers using vogel-tammann-fulcher relaxation model, J. Macromol. Sci. B 44 (2005) 43–53.
[27] S. Cosnier, A. Karyakin (Eds.), Electro Polymerization: Concepts, Materials and Applications, John Wiley & Sons, 2011.
[28] G.G. Wallace, P.R. Teasdale, G.M. Spinks, L.A. Kane-Maguire, Conductive Electroactive Polymers: Intelligent Polymer Systems, CRC Press, 2008.
[29] C.K. Chiang, C.R. Fincher Jr., Y.W. Park, A.J. Heeger, H. Shirakawa, E.J. Louis, S.C. Gau, A.G. MacDiarmid, Electrical conductivity in doped polyacetylen, Phys. Rev. Lett. 39 (1977) 1098–1106.
[30] R.H. Friend, R.W. Gymer, A.B. Holmes, J.H. Burroughes, Electro-luminescence in conjugated polymers, Nature 397 (1999) 121–129.
[31] K.M. Mahesha, K.S. Subbaiah, B.M.J. Nithin, S.S. Raj, Highly flexible and conducting polymer nanocomposite films for selective gas sensing applications, Mater. Today Proc. 9 (2019) 515–521.
[32] R. Seto, T. Kojima, K. Hosokawa, Y. Koyama, G.I. Konishi, T. Takata, Synthesis and property of 9,9′-spirobifluorene-containing aromatic polyesters as optical polymers with high refractive index and low birefringence, Polymer 51 (2010) 4744–4749.
[33] J.G. Liu, M. Ueda, High refractive index polymers: fundamental research and practical applications, J. Mater. Chem. 19 (2009) 8907–8919.
[34] K.S. Nithin, S. Kasargod Nagaraj, S. Shivanna, H. Siddaramaiah, Highly flexible and visibly transparent poly (vinyl alcohol)/calcium zincate nanocomposite films for UVA shielding applications as assessed by novel ultraviolet photon induced fluorescence quenching, Macromolecules 49 (2016) 2791–2801.
[35] B. Suresha, R. Hemanth, K.S. Nithin, Automotive applications: reinforced material components, in: Encyclopedia of Polymer Applications, CRC Press, 2018.
[36] M. Tirumali, B. Kandasubramanian, A. Kumaraswamy, N.K. Subramani, B. Suresha, Fabrication, physicochemical characterizations and electrical conductivity studies of modified carbon nanofiber-reinforced epoxy composites: effect of 1-butyl-3-methylimidazolium tetrafluoroborate ionic liquid, Polym. Plast. Technol. Eng. 57 (2018) 218–228.
[37] S.A. Hallad, N.R. Banapurmath, D. Vishweshwar, S.A. Vivek, T.G. Malatesh, S.S. Ashok, Kevlar reinforced polymer matrix composite for structural application, IOP Conf. Series: Mater. Sci. Eng. 376 (2018), 012074.
[38] M. Manjunath, N.M. Renukappa, B. Suresha, Influence of micro and nanofillers on mechanical properties of pultruded unidirectional glass fiber reinforced epoxy composite systems, J. Comp. Mater. 50 (2015) 1109–1121.

[39] M. Hajian, G.A. Koohmareh, A. Mostaghasi, Investigation of the effects of titanate as coupling agent and some inorganic nanoparticles as fillers on mechanical properties and morphology of soft PVC, 2011, Int. J. Polym., Sci.
[40] N.B. Cramer, J.W. Stansbury, C.N. Bowman, Recent advances and developments in composite dental restorative materials, J. Dent. Res. 90 (2011) 402–416.
[41] G. Matthews, G.S. Plemper, Effects of calcium carbonate fillers on the behaviour of PVC in fires, Br. Polym. J. 13 (1981) 17–21.
[42] A. Wolska, M. Goździkiewicz, J. Ryszkowska, Thermal and mechanical behaviour of flexible polyurethane foams modified with graphite and phosphorous fillers, J. Mater. Sci. 47 (2012) 5627–5634.
[43] X. He, Y. Cai, Q. Wang, X. Qi, R. Guo, T. Yan, L. Boping, Improvement of mechanical properties and ultraviolet resistance of polyethylene pipe materials using high density polyethylene matrix grafted carbon black, J. Macromol. Sci. B 51 (2012) 298–312.
[44] A. Zimmermann, S. Jaerger, S.F. Zawadzki, F. Wypych, Synthetic zinc layered hydroxide salts intercalated with anionic azo dyes as fillers into high-density polyethylene composites: first insights, J. Polym. Res. 20 (2013) 224.
[45] C.P. Bergmann, in: M.J. Andrade (Ed.), Nanostructured Materials for Engineering Applications, Springer, Berlin, 2011.
[46] S. Sachhidananda, G.R. Suma, K.S. Nithin, S.V. Satyanarayana, Siddaramaiah, Tuning the electrical and thermal functionalities of mechanically flexible poly (vinyl alcohol) nanocomposites: effect of cerium zirconate nanofiller content, Int. J. Eng. Sci. 1 (2019) 8–14.
[47] B.M. Jagajeevanraj, S. Sachhidananda, K. Pushpalatha, K.S. Nithin, Nanostructured $Al_{0.2}Y_{1.8}O_3$ semiconductor assisted enhancement in PVOH fortitude to withstand high energy UV photons: an opto-mechanical study, Optik 182 (2019) 598–604.
[48] S. Granick, S.K. Kumar, E.J. Amis, M. Antonietti, A.C. Balazs, A.K. Chakraborty, G.S. Grest, C. Hawker, P. Janmey, E.J. Kramer, R. Nuzzo, Macromolecules at surfaces: research challenges and opportunities from tribology to biology, J. Polym. Sci. Part B: Polym. Phys. 41 (2003) 2755–2793.
[49] H. Althues, J. Henle, S. Kaskel, Functional inorganic nanofillers for transparent polymers, Chem. Soc. Rev. 36 (2007) 1454–1465.
[50] J. Karger-Kocsis, O. Gryshuk, J. Frohlich, R. Mulhaupt, Interpenetrating vinylester/epoxy resins modified with organophilic layered silicates, Compos. Sci. Technol. 63 (2003) 2045–2054.
[51] X. Huang, P.K. Jain, I.H. El-Sayed, M.A. El-Sayed, Gold nanoparticles: interesting optical properties and recent applications in cancer diagnostics and therapy, Nanomedicine 2 (2007) 681–693.
[52] F. Lambiase, M. Durante, A. Di Ilio, Fast joining of aluminum sheets with glass fiber reinforced polymer (GFRP) by mechanical clinching, J. Mater. Process. Technol. 236 (2016) 241–251.
[53] X. Qijie, L. Xiaohong, Z. Zhang, Preparation of copper nanoparticle improved polyamide 6 composites by an in-situ solution route with cupric oxide as the metallic copper source and investigation of their properties, New J. Chem. 39 (2015) 3015–3020.
[54] Y. Yanhong, J. Zhining, Y. Yulin, Preparation and mechanical properties of PTFE/nano-EG composites reinforced with nanoparticles, Procedia Environ. Sci. 10 (2011) 929–935.
[55] T.M. Madkour, A.A. Eman, T. Amr, M. Ghada, S. Rania, In-situ polymerization of polyurethane, silver nanocomposite foams with intact thermal stability, improved mechanical performance, and induced antimicrobial properties, J. Appl. Polym. Sci. 133 (2016) 11–20.
[56] H. Liu, S.J.S. Shang, Z. Song, D. Wang, Cellulose nanocrystal/silver nanoparticle composites as bifunctional nanofillers within waterborne polyurethane, ACS Appl. Mater. Interfaces 4 (2012) 2413–2419.

[57] D.R. Paul, M.R. Lioyd, Polymer nanotechnology: nanocomposites, Polymer 49 (2008) 3187–3204.
[58] A. Hatamie, A. Khan, M. Golabi, A.P. Turner, V. Beni, W.C. Mak, A. Sadollahkhani, H. Alnoor, B. Zargar, S. Bano, O. Nur, Zinc oxide nanostructure-modified textile and its application to biosensing, photocatalysis, and as antibacterial material, Langmuir 31 (2015) 10913–10921.
[59] J. Du, H. Sun, Polymer/TiO_2 hybrid vesicles for excellent UV screening and effective encapsulation of antioxidant agents, ACS Appl. Mater. Interfaces 6 (2014) 13535–13541.
[60] S. Kango, S. Kalia, A.J. Celli, Njuguna, Y. Habibi, R. Kumar, Surface modification of inorganic nanoparticles for development of organic-inorganic nanocomposites – a review, Prog. Polym. Sci. 38 (2011) 1232–1261.
[61] T.J. Pinnavaia, G.W. Beall (Eds.), Polymer-Clay Nanocomposites, John Wiley, 2000.
[62] J. Sommertune, A. Sugunan, A. Ahniyaz, R.S. Bejhed, A. Sarwe, C. Johansson, C. Balceris, F. Ludwig, O. Posth, A. Fornara, Polymer/iron oxide nanoparticle composites – a straight forward and scalable synthesis approach, Int. J. Mol. Sci. 16 (2015) 19752–19768.
[63] A. Krishnan, T.S. Sreeremya, S. Ghosh, Size-tunable hydrophilic cerium oxide nanoparticles as a 'turn-on' fluorescence sensor for the rapid detection of ultralow concentrations of vitamin C, RSC Adv. 6 (2016) 53550–53559.
[64] H. Wu, M. Rogalski, M.R. Kessler, Zirconium tungstate/epoxy nanocomposites: effect of nanoparticle morphology and negative thermal expansivity, ACS Appl. Mater. Interfaces 5 (2013) 9478–9487.
[65] X. Shi, H. Lian, X. Yan, R. Qi, N. Yao, T. Li, Fabrication and properties of polyimide composites filled with zirconium tungsten phosphate of negative thermal expansion, Mater. Chem. Phys. 179 (2016) 72–79.
[66] Y. Fan, X. Huang, G. Wang, P. Jiang, Core-shell structured biopolymer@$BaTiO_3$ nanoparticles for biopolymer nanocomposites with significantly enhanced dielectric properties and energy storage capability, J. Phys. Chem. C 119 (2015) 27330–27339.
[67] H. Luo, D. Zhang, C. Jiang, X. Yuan, C. Chen, K. Zhou, Improved dielectric properties and energy storage density of poly (vinylidene fluoride-co-hexafluoropropylene) nanocomposite with hydantoin epoxy resin coated $BaTiO_3$, ACS Appl. Mater. Interfaces 7 (2015) 8061–8069.
[68] Z. Pan, L. Yao, J. Zhai, D. Fu, B. Shen, H. Wang, High-energy-density polymer nanocomposites composed of newly structured one-dimensional $BaTiO_3$@Al_2O_3 nanofibers, ACS Appl. Mater. Interfaces 9 (2017) 4024–4033.
[69] H. Wei, H. Gu, J. Guo, S. Wei, J. Liu, Z. Guo, Silica doped nano polyaniline with endured electrochemical energy storage and the magnetic field effects, J. Phys. Chem. C 117 (2013) 13000–13010.
[70] C. Baur, Y. Zhou, J. Sipes, S. Priya, W. Voit, Organic, flexible, polymer composites for high-temperature piezoelectric applications, Energy Harvest. Syst. 1 (2014) 167–177.
[71] A. Manjunath, M. Irfan, K.P. Anushree, K.M. Vinutha, N. Yamunarani, Synthesis and characterization of CuO nanoparticles and CuO doped PVA nanocomposites, Adv. Chem. Phys. 6 (2016) 263.
[72] A.P. Wanninayake, S. Gunashekar, S. Li, B.C. Church, N. Abu-Zahra, Performance enhancement of polymer solar cells using copper oxide nanoparticles, Semicond. Sci. Technol. 30 (2015) 064004.
[73] H. Du, G.Q. Xu, W.S. Chin, L. Huang, W. Ji, Synthesis, characterization, and nonlinear optical properties of hybridized CdS-polystyrene nanocomposites, Chem. Mater. 14 (2002) 4473–4479.
[74] J.V. Antony, P. Kurian, N.P.N. Vadakkedathu, G.E. Kochimoolayil, In-situ synthesis of CdS quantum dot-partially sulfonated polystyrene composite: characterization and optical properties, Ind. Eng. Chem. Res. 53 (2014) 2261–2269.

[75] X.C. Wu, A.M. Bittner, K. Kern, Synthesis, photoluminescence, and adsorption of CdS/dendrimer nanocomposites, J. Phys. Chem. B 109 (2005) 230–239.
[76] J. Osuntokun, P.A. Ajibade, Structural and thermal studies of ZnS and CdS nanoparticles in polymer matrices, J. Nanomater. (2016) 1–14.
[77] A. Nasir, A. Kausar, A review on materials derived from polystyrene and different types of nanoparticles, Polym. Plast. Technol. Eng. 54 (2015) 1819–1849.
[78] J. Gong, L. Wang, D. Song, X. Zhu, L. Zhang, Stripping voltammetric analysis of organophosphate pesticides using Ni/Al layered double hydroxides as solid-phase extraction, Biosens. Bioelectron. 25 (2009) 493–496.
[79] F. Silverio, M.J. dos Reis, J. Tronto, J.B. Valim, Removal of aliphatic amino acids by hybrid organic-inorganic layered compounds, Appl. Surf. Sci. 253 (2007) 5756–5761.
[80] H. Abdolmohammad-Zadeh, Z. Rezvani, G.H. Sadeghi, E. Zorufi, Layered double hydroxides: a novel nano-sorbent for solid-phase extraction, Anal. Chim. Acta 685 (2011) 212–219.
[81] G. Fan, F. Li, D.G. Evans, X. Duan, Catalytic applications of layered double hydroxides: recent advances and perspectives, Chem. Soc. Rev. 43 (2014) 7040–7066.
[82] T. Champa, S. Sachhidananda, K.N. Shilpa, K.S. Nithin, Siddaramaiah, Optoelectronic behaviors of reversibly stretchable $Na_{0.8}Mn_{0.8}O_2$ reinforced poly(vinyl alcohol) nanocomposites, Int. J. Eng. Sci. Comput. 7 (2017) 14875–14879.
[83] K.S. Nithin, S. Sachhidananda, K.N. Shilpa, S. Chinmayee, S. Basavarajaiah, Poly (vinyl alcohol) decorated lithium doped stannous oxide nanocomposites as highly flexible UVA shieldants, Chem. Sci. J. 7 (2016) 121.
[84] C.S. Murthy, M.P. Nikolova, Metal oxide nanoparticles and their applications in nanotechnology, SN Appl. Sci. 1 (2019) 607.
[85] G.R. Suma, K.S. Nithin, B.V. Latha, S.K. Nagaraj, S. Shivanna, S.V. Sathyanarayana, Gent to refractive index engineering of strontium doped zirconium oxide (szo) reinforced poly vinyl pyrrolidone composite films: effect of dopant content and annealing temperature, Int. J. Eng. Sci. Comput. 6 (2016) 5703–5709.
[86] H. Tavakoli, P.S. Amir, S.J. Maram, J. Widgeon, K.V. Rufner, S. Benthem, S. Ushakov, A.N. Sen, Amorphous alumina nanoparticles: structure, surface energy, and thermodynamic phase stability, J. Phys. Chem. C 117 (2013) 17123–17130.
[87] C. Klingshirn, ZnO: from basics towards applications, Phys. Status Solidi B 244 (2007) 3027–3073.
[88] K.S. Nithin, S. Shivanna, S.K. Nagaraj, H. Siddaramaiah, Refractive index engineering of poly(vinylalcohol)/Li_2ZnO_2 nanocomposites: effect of filler content and annealing temperature, AIP Conf. Proc. 1943 (2018) 020127–020128.
[89] S. Sachhidananda, K.S. Nithin, K.N. Shilpa, H. Siddaramaiah, Orange-red fluorescent polymer nanocomposite films with large stokes shift: an opto-electronic exercise, J. Lumin. 208 (2018) 488–494.
[90] J. Fan, R. Freer, The roles played by Ag and Al dopants in controlling the electrical properties of ZnO varistors, J. Appl. Phys. 77 (1995) 4795–4800.
[91] Z.L. Wang, Zinc oxide nanostructures: growth, properties and applications, J. Condens. Matter Phys. 16 (2004) R829.
[92] A. Janotti, C.G. Van de Walle, Fundamentals of zinc oxide as a semiconductor, Rep. Prog. Phys. 72 (2009) 126501.
[93] H.N. Chandrakala, H. Shivakumaraiah, R. Somashekarappa, S. Somashekar, S. Chinmayee, Poly (vinyl alcohol)/zincoxide-ceriumoxide nanocomposites: electrical, optical, structural and morphological characteristics, Indian J. Adv. Chem. Sci. 2 (2014) 103–106.
[94] A. Rabenau, The role of hydrothermal synthesis in preparative chemistry, Angew. Chem. Int. Ed. 24 (1985) 1026–1040.

[95] R.W. Goranson, Solubility of water in granite magmas, EOS Trans. Am. Geophys. Union 12 (1931) 183.
[96] R.M. Barrer, Hydrothermal Chemistry of Zeolites, Academic Press, 1982.
[97] T.V. Anuradha, S. Ranganathan, T. Mimani, K.C. Patil, Combustion synthesis of nanostructured barium titanate, Scr. Mater. 44 (2001) 2237–2241.
[98] S.R. Jain, Energetics of propellants, fuels and explosives; a chemical valence approach, propellants, Explos Pyrotech. 12 (1987) 188–195.
[99] N. Millot, D. Aymes, F. Bernard, J.C. Niepce, A. Traverse, F. Bouree, B.L. Cheng, P. Perriat, Particle size dependency of ternary diagrams at the nanometer scale: evidence of TiO_2 clusters in Fe-based spinels, J. Phys. Chem. B 107 (2003) 5740–5750.
[100] J.M. McHale, A. Auroux, A.J. Perrotta, A. Navrotsky, Surface energies and thermodynamic phase stability in nanocrystalline aluminas, Science 277 (1997) 788–791.
[101] H.C. Yao, Y.Y. Yao, Ceria in automotive exhaust catalysts: I. Oxygen storage, J. Catal. 86 (1984) 254–265.
[102] H. Gu, P.L. Ho, E. Tong, L. Wang, B. Xu, Presenting vancomycin on nanoparticles to enhance antimicrobial activities, Nano Lett. 3 (2003) 1261–1263.
[103] L. Huang, D.Q. Li, Y.J. Lin, M. Wei, D.G. Evans, X. Duan, Controllable preparation of Nano-MgO and investigation of its bactericidal properties, J. Inorg. Biochem. 99 (2005) 986–993.
[104] P.L.S.G. Poizot, S. Laruelle, S. Grugeon, L. Dupont, J.M. Tarascon, Nano-sized transition-metal oxides as negative-electrode materials for lithium-ion batteries, Nature 407 (2000) 496.
[105] H. Huang, E.M. Kelder, J. Schoonman, Graphite-metal oxide composites as anode for Li-ion batteries, J. Power Sources 97 (2001) 114–117.
[106] M. Gratzel, Photoelectrochemical cells, Nature 414 (2001) 338–342.
[107] M. Mamak, N. Coombs, G. Ozin, Self-assembling solid oxide fuel cell materials: mesoporous yttria-zirconia and metal-yttria-zirconia solid solutions, J. Am. Chem. Soc. 122 (2000) 8932–8939.
[108] B. Sun, H. Sirringhaus, Solution-processed zinc oxide field-effect transistors based on self-assembly of colloidal nanorods, Nano Lett. 5 (2005) 2408–2413.
[109] Y. Sharma, N. Sharma, G.V. Subba Rao, B.V.R. Chowdari, Lithium recycling behaviour of nano-phase-$CuCo_2O_4$ as anode for lithium-ion batteries, J. Power Sources 173 (1) (2007) 495–501.
[110] S.J. Hwang, D.H. Park, J.H. Choy, G. Campet, Effect of chromium substitution on the lattice vibration of spinel lithium manganate: a new interpretation of the Raman spectrum of $LiMn_2O_4$, J. Phys. Chem. B 108 (2004) 12713–12717.
[111] M. Jayalakshmi, K. Balasubramanian, Solution combustion synthesis of Fe_2O_3/C, Fe_2O_3-SnO_2/C, Fe_2O_3-ZnO/C composites and their electrochemical characterization in non-aqueous electrolyte for supercapacitor application, Int. J. Electrochem. Sci. 4 (2009) 878–886.
[112] T.H. Shin, J.H. Myung, K.M. Naeem, C. Savaniu, J.T.S. Irvine, Ce(Mn,Fe)O_2(La,Sr)(Fe,Mn)O_3 composite as an active cathode for electrochemical reduction of CO_2 in proton conducting solid oxide cells, Solid State Ionics 275 (2015) 106–109.
[113] G.R. Suma, K.S. Nithin, S. Sachhidananda, S.V. Satyanarayana, Siddaramaiah, Optical and electrical evaluation of $Ag_{0.5}Cu_{0.75}O$ introduced poly (vinyl alcohol) based *E. coli* sensors, J. Mater. Sci.: Mater. Electron. 28 (2017) 13139–13148.
[114] A.M.N. Saeed, M.Q.A. Al-Gunaid, N.K. Subramani, B.S. Madhukar, S. Basavarajaiah, Effect of cesium aluminate nanofiller on optical properties of polyvinyl pyrrolidone nanocomposite films, Polym. Plast. Technol. Eng. 57 (2008) 1188–1196.
[115] Y. Kojima, A. Usuki, M. Kawasumi, A. Okada, Y. Fukushima, T. Kurauchi, O. Kamigaito, Mechanical properties of nylon 6-clay hybrid, J. Mater. Res. 8 (1993) 1185–1189.

[116] S.K. Kumar, B.C. Benicewicz, R.A. Vaia, K.I. Winey, 50th anniversary perspective: are polymer nanocomposites practical for applications? Macromolecules 50 (2017) 714–731.
[117] R.R. Dickerson, S. Kondragunta, G. Stenchikov, K.L. Civerolo, B.G. Doddridge, B.N. Holben, The impact of aerosols on solar ultraviolet radiation and photochemical smog, Science 278 (1997) 827–830.
[118] R. Hackam, Outdoor HV composite polymeric insulators, IEEE Trans. Dielectr. Electr. Insul. 6 (1999) 557–585.
[119] S. Prashanth, K.M. Subbaya, K.S. Nithin, S. Sachhidananda, Fiber reinforced composites – a review, J. Mater. Sci. Eng. 6 (2017) 1–6.
[120] K.S. Nithin, K.N. Shilpa, S. Sachhidananda, H. Siddaramaiah, Yellow-green luminescent poly (vinyl alcohol) nanocomposite thick films as effective spectral manipulators, J. Appl. Polym. Sci. 135 (2018) 46854.
[121] G.R. Suma, K.S. Nithin, K.N. Shilpa, S. Sachhidananda, V.S. Satyanarayana, Effect of $Ce_{0.5}Zr_{0.5}O_2$ nano fillers on structural and optical behaviors of poly (vinyl alcohol), J. Mater. Sci.: Mater. Electron. 28 (2017) 10707–10714.
[122] C. Kingston, R. Zepp, A. Andrady, D. Boverhof, R. Fehir, D. Hawkins, J. Roberts, P. Sayre, B. Shelton, Y. Sultan, V. Vejins, Release characteristics of selected carbon nanotube polymer composites, Carbon 68 (2014) 33–57.
[123] K.S. Nithin, S. Sachhidananda, K.N. Shilpa, B. Suresha, H. Siddaramaiah, Optoelectronic behaviours of UV shielding calcium zirconate reinforced polycarbonate nanocomposite films: an optical view, Mater. Today 5 (2018) 16626–16632.
[124] G. Ries, W. Heller, H. Puchta, H. Sandermann, H.K. Seidlitz, B. Hohn, Elevated UV-B radiation reduces genome stability in plants, Nature 406 (2000) 98–101.
[125] T. Masui, M. Yamamoto, T. Sakata, H. Mori, G. Adachi, Synthesis of BN-coated CeO_2 fine powder as a new UV blocking material, J. Mater. Chem. 10 (2000) 353–357.
[126] J. Zhang, S. Luo, L. Gui, Poly (methyl methacrylate)-titania hybrid materials by sol-gel processing, J. Mater. Sci. 32 (1997) 1469–1472.
[127] S. Shivanna, K.S. Nithin, K.N. Shilpa, J.R.B. Mutturaj, S. Basavaraj, Patina-green coloured light emitting polycarbonate films: a synergistic extraction of improved UV endurance and considerate spectral down-conversion, J. Lumin. 210 (2019) 276–284.
[128] V. Hrenov, M. Klapper, M. Koch, K. Mullen, Surface functionalized ZnO particles designed for the use in transparent nanocomposites, Macromol. Chem. Phys. 206 (2005) 95–101.
[129] P. Liu, P.Z. Su, Preparation and characterization of PMMA/ZnO nanocomposites via in-situ polymerization method, J. Macromol. Sci. B 45 (2006) 131–138.
[130] H. Faubl, M.H. Quinn, Spectra of UV-absorbing contact lenses: relative performance, Int. Contact Lens Clin. 27 (2000) 65–74.
[131] J. Xiao, W. Chen, F. Wang, J. Du, Polymer/TiO_2 hybrid nanoparticles with highly effective UV-screening but eliminated photocatalytic activity, Macromolecules 46 (2013) 375–383.
[132] E. Lizundia, L. Rubio-Ruiz, J.L. Vilas, L.M. León, Poly (L-lactide)/zno nanocomposites as efficient UV-shielding coatings for packaging applications, J. Appl. Poly. Sci. 133 (2016).
[133] J. Heffels, C.D. Friedrich, J. Teisen, K. Interewicz, C. Bastiaansen, W. Caseri, P. Smith, Polymers and metals: nanocomposites and complex salts with metallic chain structure, Recent Res. Dev. Macromol. Res. 2 (1997) 143–156.
[134] F. Kirchner, R. Zsigmondy, About the causes of the color changes of gold gelatin preparations, Ann. Phys. 320 (1904) 573.
[135] J.C. Maxwell Garnett, Colours in metal glasses and in metallic films, Philos. Trans. R. Soc. London 203 (1904) 385–420.

[136] W.C.W. Chan, S. Nie, Quantum dot bioconjugates for ultrasensitive non isotopic detection, Science 281 (1998) 2016–2018.
[137] J. Lee, V.C. Sundar, J.R. Heine, M.G. Bawendi, K.F. Jensen, Full color emission from II–VI semiconductor quantum dot-polymer composites, Adv. Mater. 12 (2000) 1102–1105.
[138] L. Erskine, T. Emrick, A.P. Alivisatos, J.M.J. Frechet, Preparation of semiconductor nanocrystal-polystyrene hybrid materials, Polym. Prep. 219 (2000) U413.
[139] M. Peres, L.C. Costa, A. Neves, M.J. Soares, T. Monteiro, A.C. Esteves, A. Timmons-Barros, T. Trindade, A. Kholkin, E. Alves, A green-emitting CdSe/poly (butyl acrylate) nanocomposite, Nanotechnology 16 (2005) 1969–1973.
[140] S.C. Farmer, T.E. Patten, Photoluminescent polymer/quantum dot composite nanoparticles, Chem. Mater. 13 (2001) 3920–3926.
[141] G.G. Yordanov, G.D. Gicheva, C.D. Dushkin, Optical memory based on photo-activated fluorescence of core/shell quantum dots embedded in poly(butylmethacrylate), Mater. Chem. Phys. 113 (2009) 507–510.
[142] H.M. Xiong, Photoluminescent ZnO nanoparticles modified by polymers, J. Mater. Chem. 20 (2010) 4251–4262.
[143] L. Guo, S. Yang, C. Yang, P. Yu, J. Wang, W. Ge, G.K. Wong, Highly monodisperse polymer-capped ZnO nanoparticles: preparation and optical properties, Appl. Phys. Lett. 76 (2000) 2901–2903.
[144] M. Chang, X.L. Cao, H. Zeng, L. Zhang, Enhancement of the ultraviolet emission of ZnO nanostructures by polyaniline modification, Chem. Phys. Lett. 446 (2007) 370–373.
[145] M. Wang, Y. Lian, X. Wang, PPV/PVA/ZnO nanocomposite prepared by complex precursor method and its photovoltaic application, Curr. Appl. Phys. 9 (2009) 189–194.
[146] C. Ton-That, M.R. Phillips, T.P. Nguyen, Blue shift in the luminescence spectra of MEH-PPV films containing ZnO nanoparticles, J. Lumin. 128 (2008) 2031–2034.
[147] H.M. Musal, H.T. Hahn, Thin-layer electromagnetic absorber design, IEEE Trans. Magn. 25 (1989) 3851–3853.
[148] C. Lu, C. Guan, Y. Liu, Y. Cheng, B. Yang, PbS/polymer nanocomposite optical materials with high refractive index, Chem. Mater. 17 (2005) 2448–2454.
[149] F. Papadimitrakopoulos, P. Wisniecki, D.E. Bhagwagar, Mechanically attrited silicon for high refractive index nanocomposites, Chem. Mater. 9 (1997) 2928–2933.
[150] T. Leodidou-Kyprianidou, W. Caseri, U.W. Suter, Size variation of PbS particles in high-refractive-index nanocomposites, J. Phys. Chem. 98 (1994) 8992–8997.
[151] W.D. Brown, D. Hess, V. Desai, M.J. Deen, Dielectric science and technology, Electrochem. Soc. Interface 15 (2006) 28–31. Spring.
[152] A.C. Arango, S.A. Carter, P.J. Brock, Charge transfer in photovoltaic consisting of interpenetrating networks of conjugated polymer and TiO_2 nanoparticles, Appl. Phys. Lett. 74 (1999) 1698–1700.
[153] H.S. Nalwa (Ed.), Handbook of Low and High Dielectric Constant Materials and Their Applications, Two-Volume Set, Academic Press, 1999.
[154] T. Osaka, M. Datta (Eds.), Energy Storage Systems in Electronics, CRC Press, 2000.
[155] B. Chu, X. Zhou, K. Ren, B. Neese, M. Lin, Q. Wang, F. Bauer, Q.M. Zhang, A dielectric polymer with high electric energy density and fast discharge speed, Science 313 (2006) 334–336.
[156] Z. Pu, X. Zheng, Y. Tian, L. Hu, J. Zhong, Flexible ultrahigh-temperature polymer-based dielectrics with high permittivity for film capacitor applications, Polymers 9 (2017) 596.
[157] O.G. Abdullah, D.S. Muhammad, Physical properties of pure and copper oxide doped polystyrene films, IJMSCI 5 (2010) 537–545.
[158] O.G. Abdullah, S.A. Hussen, A. Alani, Electrical characterization of polyvinyl alcohol films doped with sodium iodide, Asian Trans. Sci. Technol. 1 (2011) 01–04.

[159] B.C. Riggs, S. Adireddy, C.H. Rehm, V.S. Puli, R. Elupula, D.B. Chrisey, Polymer nanocomposites for energy storage applications, Mater. Today: Proc. 2 (2015) 3853–3863.
[160] Q. Wang, L. Zhu, Polymer nanocomposites for electrical energy storage, J. Polym. Sci. Part B: Polym. Phys. 49 (2011) 1421–1429.
[161] P. Barber, S. Balasubramanian, Y. Anguchamy, S. Gong, A. Wibowo, H. Gao, H.J. Ploehn, H.C. Zur Loye, Polymer composite and nanocomposite dielectric materials for pulse power energy storage, Materials 2 (2009) 1697–1733.
[162] Z.M. Dang, T. Zhou, S.H. Yao, J.K. Yuan, J.W. Zha, H.T. Song, J.Y. Li, Q. Chen, W.T. Yang, J. Bai, Advanced calcium copper titanate/polyimide functional hybrid films with high dielectric permittivity, Adv. Mater. 21 (2009) 2077–2082.
[163] M.S. Khalil, The role of BaTiO/sub 3/in modifying the dc breakdown strength of LDPE, IEEE Trans. Dielectr. Electr. Insul. 7 (2000) 261–268.
[164] N. Guo, S.A. DiBenedetto, D.K. Kwon, L. Wang, M.T. Russell, M.T. Lanagan, A. Facchetti, T.J. Marks, Supported metallocene catalysis for in situ synthesis of high energy density metal oxide nanocomposites, J. Am. Chem. Soc. 129 (2007) 766–767.
[165] B. Luo, X. Wang, Y. Wang, L. Li, Fabrication, characterization, properties and theoretical analysis of ceramic/PVDF composite flexible films with high dielectric constant and low dielectric loss, J. Mater. Chem. A 2 (2014) 510–551.

4

Tools and techniques toward characterizing polymer-based smart composites for optical, optoelectronic, and energy-related applications

K.S. Nithin[a], K.N. Shilpa[b], Rohini Thimmaiah[c], B.M. Jagajeevan Raj[a], S. Sachhidananda[b], and H. Siddaramaiah[d,†]

[a]Department of Chemistry, The National Institute of Engineering, Mysuru, India, [b]Department of Polymer Science and Technology, Sri Jayachamarajendra College of Engineering, JSS Science and Technology University, Mysuru, India, [c]Department of Chemistry, Coorg Institute of Technology, Ponnampet, India, [d]Vice-Chancellor of JSS Science and Technology University, Mysuru, India

4.1 Introduction

Mechanically flexible smart composites are polymer-based soft materials that change their physicochemical characteristics and hence the resultant material properties in response to an applied external stimulus.

Smartness in polymer-based smart composites (PBSCs) and/or nanocomposites (NCs) may be induced either by combinatorial effects or by the synergistic route [1, 2]. The ombinatorial route involves a thoughtful introduction of stimuli-responsive (functional materials) fillers into suitable polymeric host. Wherein, the introduced fillers serve as smartness causative agents, while the polymer handles the encapsulation role. However, in the case of PBSCs obtained via synergistic route, the exclusive physicochemical properties arising from the unique polymer-filler chemistries may induce novel material behaviors [3–6]. Also, even a small magnitude of external stimulus can bring about noticeable changes in their (PBSC) material functionalities (shape, size, color, conductivity, and so forth). Such design- flexible smart materials have attracted considerable technological interest in almost every walk of life [7, 8].

† Deceased.

Polymer-Based Advanced Functional Composites for Optoelectronic and Energy Applications
https://doi.org/10.1016/B978-0-12-818484-4.00012-4
Copyright © 2021 Elsevier Inc. All rights reserved.

Polymer nanocomposites (PNCs) are one such class of smart materials whose inherent physicochemical and resultant material functionalities could be effectively engineered using various filler-matrix combinations [9, 10]. Lately, the field of PNCs is at the forefront of vigorous research and developmental activities, owing to the early suggestions that these multifunctional hybrids would revolutionalize the materials world. Although PNC hybrids have been known for decades, the lack of effective characterization tools had limited the total understanding of their material behaviors, thereby narrowing the real-time applications [11, 12]. Further, the introduction of inorganic nanofillers into a particle stabilizing organic host may offer high-performance multifunctional systems with versatile material properties (mechanical, thermal, optical, magnetic, and dielectric) that suit vivid technological applications [13–15]. The wide-scale commercial exploitation of such multifunctional systems mandatea fundamental understanding of their inherent material functionalities. Accordingly, herein an attempt has been made to summarize some of the imperative tools and techniques adopted toward characterizing PBSCs (with special emphasis on metal oxide nanofillers loaded PNC thick films) for optical, optoelectronic, and energy-related applications.

4.2 Tools and techniques adopted for the characterization of polymer-based smart composites of optical, optoelectronic and electrical interest

4.2.1 Structural characterizations

The structural characterizations of PBSCs help to establish the success of composite formation via the thoughtful validation of filler-induced changes in electromagnetic radiation (depending on the nature of the characterization tool, say infrared (IR) in case of Fourier transform infrared (FTIR) spectroscopy, UV and visible photons in case of electronic spectroscopy, and so forth) absorption/transmittance/reflection characteristics of the host polymer.

4.2.1.1 Fourier transform infrared spectroscopy

FTIR spectroscopy is one such renowned characterization tool aimed at characterizing the structural changes in a molecule by producing an IR absorption/reflection (so as to identify their chemical functionalities).

In the IR region, the electromagnetic waves are known to couple with molecular vibrations and the IR frequency that corresponds to

the vibrational frequency of the chemical bond will be absorbed. In simpler terms, an IR frequency whose energy matches the vibrational energies of the chemical functionalities (functional groups) in the molecule will be strongly absorbed. Because each material is a unique combination of chemical groups, no two compounds can exhibit the same IR spectrum. Therefore, the FTIR technique stands tall as one of the most powerful tools that offers fingerprint information on the chemical functionalities of a material. The peak position, shape, and their relative intensities furnish a detailed account of the molecular structure under study. FTIR spectroscopy is majorly adopted for structural elucidation via functional group analysis because most functional groups present IR characteristic absorption at a specific frequency range (fingerprint regions) [16, 17].

In case of PBSCs (especially metal oxide nanofiller introduced polymer thick films), FTIR spectroscopy aims to establish the successfulness of introducing metal oxide nanofillers into the host polymer. That technique involves recording metal oxide nanofiller induced changes in the IR absorption/reflection characteristics of PNC thick films [18]. Additionally, FTIR spectroscopy also aids in a thorough understating of the nature of the interactions between the metal oxide nanofiller and the host polymer.

Accordingly, Shilpa et al. employed FTIR spectral studies to validate the successful formation of UV shielding poly vinyl alcohol (PVA)/$Na_2Dy_2O_4$ thick films (Fig. 4.1) [9]. They opined that the appearance of a new IR band at 520–540 cm^1 linked to metal-oxygen stretching [19]

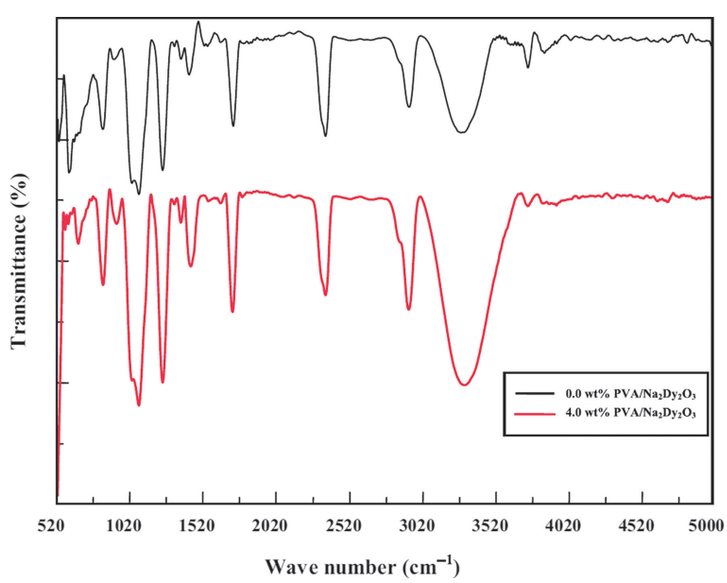


Fig. 4.1 FTIR spectrum of PVA/$Na_2Dy_2O_4$NC films. Reproduced from K.N. Shilpa, K. Subramani, S. Sachhidananda, B.S. Madhukar, Visibly transparent PVA/sodium doped dysprosia (Na2Dy2O4) nano composite films, with high refractive index: an optical study, J. Alloys Compd. 694 (2017) 884–891 with permission of Elsevier.

substantiated the presence of metal oxide nanofillers ($Na_2Dy_2O_4$) in the host polymer (PVA). The amalgamation of the asymmetric C-H stretching band (2920 cm^{-1}) with the -OH stretching vibrations (3690–3000 cm^{1}) and the notable reduction in the intensities of the -OH stretching vibrations of PVA (upon $Na_2Dy_2O_4$ nanofiller additions) justified the success of PVA/$Na_2Dy_2O_4$NC formation. Moving forward, they further opined that the relative broadening of the -OH stretching vibrations exemplified the electrostatic interactions between the surface charges on the metallic fractals of the $Na_2Dy_2O_4$ nanofillers and the hydroxyl dipoles of PVA [9, 20]. Correspondingly, FTIR spectroscopy has been widely employed toward establishing the physicochemical functionalities of numerous polymer/nanofiller combinations [21, 22]. Sachhidananda et al. employed an FTIR spectral tool to establish the UV endurance of polycarbonate (PC) films loaded with Cs_2ZnO_2 nanofillers. They used the quantification of the yellowing index and IR absorption at 1713 cm^{-1} to establish that the Cs_2ZnO_2 nanofillers induced improvement in the UV endurance of PC films (Figs. 4.2 and 4.3). In their combinatorial exploration using FTIR, UV-visible, and spectrofluorimetry studies combined with UV transilluminator measurements, they validated that Cs_2ZnO_2 nanofillers in PC dissipate the otherwise undesirable and high-energy UV radiation into relatively lesser energy visible light (spectral downconversion). This in turn guards the PC host from the high-energy UV

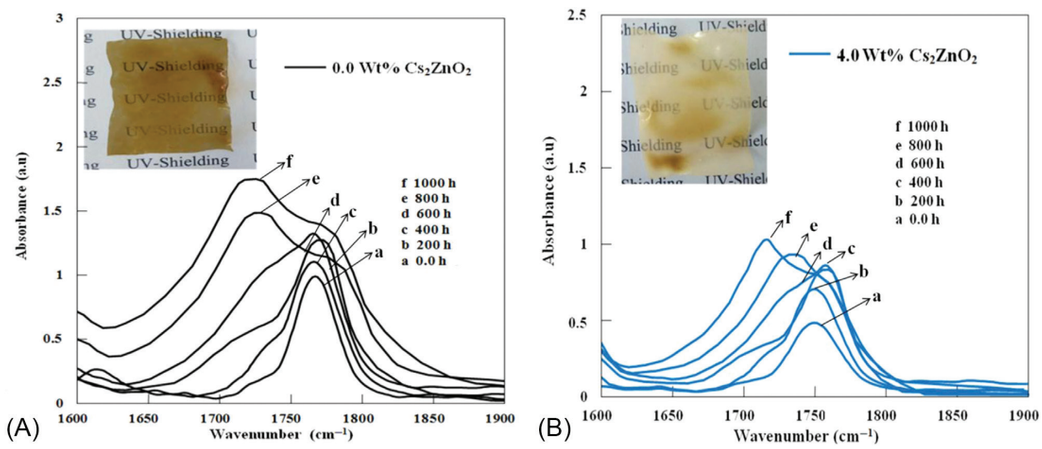


Fig. 4.2 FTIR spectra of irradiated (A) PC films; and (B) PC/4.0 wt% Cs_2ZnO_2 NC films in the carbonyl region (Inset: digital images of irradiated PC/Cs_2ZnO_2 NC films toward establishing the UV endurance of PC films). Reproduced from S. Shivanna, N.K. Subramani, S.K. Nagaraj, J.R.B. Mutturaj, S. Basavaraj, Patina-green coloured light emitting polycarbonate films: a synergistic extraction of improved UV endurance and considerate spectral down–conversion, J. Lumin. 210 (2019) 276–284 with permission of Elsevier.

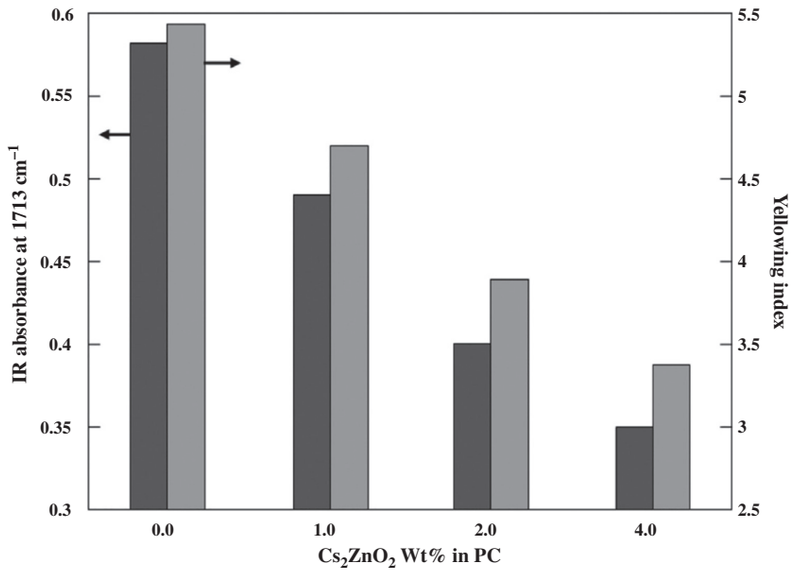


Fig. 4.3 Quantified yellowing index and IR absorption at 1713 cm^{1} for PC/Cs_2ZnO_2 NC films. Reproduced from S. Shivanna, N.K. Subramani, S.K. Nagaraj, J.R.B. Mutturaj, S. Basavaraj, Patina-green coloured light emitting polycarbonate films: a synergistic extraction of improved UV endurance and considerate spectral down–conversion, J. Lumin. 210 (2019) 276–284 with permission of Elsevier.

photon-induced adverse photo-degradation reactions. The same team also opined that the asynergistic combination of spectrally downconverting the nanofiller and particle stabilizing polymer is highly desirable for numerous photonic applications. The metal oxide nanofiller offers protection against undesirable photo-degradation reactions while the polymeric host guards the luminescence centers of the introduced nanofiller [23].

4.2.2 Microstructural characterizations

Polymers and their composite hybrids are of significant interest to material scientists, owing to their fascinating end product applications. As a consequence, advanced material characterization tools are in great demand for material scientists. Powder X-ray diffraction (P-XRD) is one such characterization tool that offers the advantage of simultaneously characterizing both the precursor and end product with a detailed qualitative presentation of their microstructural behaviors [24, 25].

4.2.2.1 Powder X-ray diffraction

P-XRD is a versatile nondestructive characterization tool that offers a detailed view of the chemical composition and crystallographic structure of the sample.

When X-rays are incident on crystalline solids, they are scattered in accordance with Bragg's law, which assumes the diffraction to take place only when the distance travelled by the rays reflected from successive planes of crystal differs by a complete number of wavelengths. Consequently, by scanning the sample through a range of 2θ angles, all possible diffractions could be achieved, owing to the random orientation of the powder or film. Plotting the angular positions and intensities of the resultant diffracted peaks produces the pattern characteristic to the sample. Finally, matching the resultant diffraction peaks to the characteristic d-spacing facilitates sample identification, as each system is essentially associated with a unique set of d-spacing. Finally, the resultant patterns are also studied for the position of diffraction maxima, peak intensities, and the intensity distribution as a function of the diffraction angle.

The results are then presented in the form of P-XRD diffractograms in the form of X-ray counts (intensity) as a function of 2θ. Additional functionalities such as average crystallite size (D), degree of PNC crystallinity, microstructural strain (ε), and dislocation density (δ) are computed using the following equations:

$$D = \frac{0.9\lambda}{\beta \cos\theta} \tag{4.1}$$

Where λ is the wavelength of the X-ray, β is the full width at half maximum, and Θ is the diffraction angle.

$$\text{Crystallinity}\,(\%) = \text{Total area of crystalline peaks} \Big/ \text{Total area of all peaks} \tag{4.2}$$

$$\varepsilon = \frac{\beta cos\theta}{4} \delta = 1/D^2 \tag{4.3}$$

Suma et al. employed the P-XRD technique to ascertain the successful development of PVA/$Ag_{0.5}Cu_{0.75}O$ NC films and also characterize their microstructural behaviors (Fig. 4.4). They reported that the P-XRD profiles of PVA/4 wt% $Ag_{0.5}Cu_{0.75}O$ NC film displayed additional Bragg's planes (upon nanofiller additions). This in turn ascertained the successful introduction of the $Ag_{0.5}Cu_{0.75}O$ nanofillers into the PVA while the changes in their degree of crystallization supported the possible charge transfer interactions between the metallic fractals of $Ag_{0.5}Cu_{0.75}O$ nanofillers and the -OH groups of the polymer backbone (Table 4.1). It is this charge transfer interaction that might have led to entirely new material functionalities in the resulting PNC thick films [26, 27].

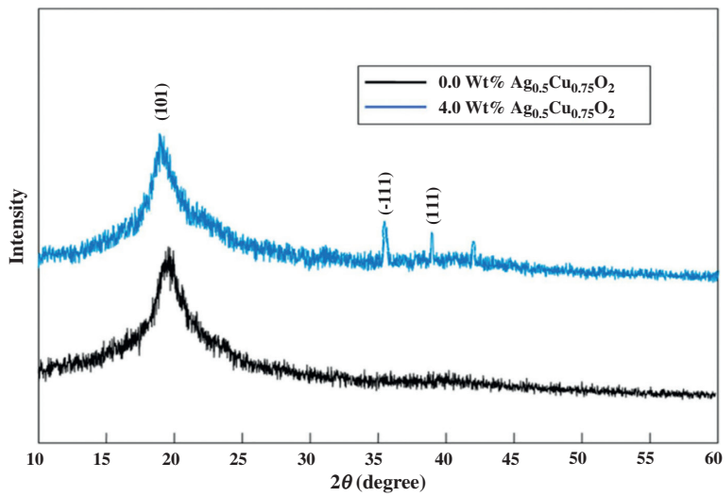


Fig. 4.4 P-XRD profiles of PVA and PVA/$Ag_{0.5}Cu_{0.75}O$ NC films. Reproduced from G.R. Suma, K.S. Nithin, S. Sachhidananda, S.V. Satyanarayana, Siddaramaiah, Optical and electrical evaluation of Ag0.5Cu0.75 O introduced poly (vinyl alcohol) based E. coli sensors. J. Mater. Sci. Mater. Electron. 28 (2017) 13139–13148 with permission of Springer.

Table 4.1 $Ag_{0.5}Cu_{0.75}O$ NP-induced changes in the degree of crystallinity and other microstructural parameters of PVA films.

Wt% of $Ag_{0.5}Cu_{0.75}O$ in PVA	c (%)	D (nm)	ε (10^{-3})	δ (10^{16} lines/m^2)
0.0	56.74	2.7	12.5	12.9
0.5	57.83	5.4	6.4	3.4
1.0	57.99	8.5	4.0	1.4
2.0	58.24	11.6	3.0	0.7
4.0	58.73	14.7	2.4	0.5

4.2.3 Optical and optoelectronic characterizations

4.2.3.1 UV-visible spectroscopy and photonic absorption/transmittance/reflectance related functionalities

Electronic spectroscopy deals with the interaction of UV-visible radiation (160–780 nm) with matter. In view of the fact that UV-visible spectroscopy involves incident photon-induced excitation of outer electrons, this spectral tool is rightly called electronic spectroscopy.

It is also well established that electronic energy levels in a material are quantized and only those photons that are sufficiently energized can bring about electronic excitations. Accordingly, when a sample is exposed to light (having photon energies ($h\nu$) resonating with the

energy requirements for electronic transitions), photonic absorption takes place and an electron is promoted from its highest occupied molecular orbital (HOMO) to its lowest unoccupied molecular orbital (LUMO).

A UV-visible spectrophotometer records the wavelength at which such photonic absorption occurs in conjunction with the degree of absorption at each wavelength. The resulting spectrum is a plot of optical absorbance (A) as a function of applied wavelength (λ), which in turn elucidates the optical absorption behaviors of the sample. This may then be correlated to the molecular structure and concentration of the light-absorbing species.

Similarly, the UV-visible transmittance values as a function of wavelength, quantifies their optical clarities. The data obtained from UV-visible absorbance and transmittance studies may further be processed to characterize the electronic band structure and hence, the optical constants such as the absorption coefficient (α), the optical bandgap (E_g), the Urbach energy (E_u), the refractive index (n), and the optical conductivity (σ_{opt}) using the following relations [9, 28, 29]:

(i) Absorption coefficient (α)

$$\alpha = (2.303)t \log \frac{I_t}{I_0} = \left(\frac{2.303}{t}\right)A \tag{4.4}$$

Where t is the film thickness and $I_0$and I_t are the intensities of the incident and transmitted light, respectively.

(ii) Optical bandgap (E_g)

$$\sqrt{\mathrm{B}}\left[\alpha h\nu - \mathrm{E_g}\right] = \sqrt{\alpha h\nu} \tag{4.5}$$

Where B is the proportionality constant.

The values of the optical bandgap are obtained from the plots of $(\alpha h\nu)^n$ as a function of photon energies ($h\nu$) where n can take up the value of 0.5 or 2 depending on whether the electronic transitions are indirect or direct, respectively.

(iii) Urbach energy (E_u)

$$\alpha = \alpha_0 \exp\left(h\nu / E_u\right) \tag{4.6}$$

Where α_0 is the proportionality constant and E_u is the energy of the band tail or Urbach energy. The logarithmic form of the above relation yields a straight line equation represented as:

$$\ln\alpha = \ln\alpha_0 + \left(h\nu / E_u\right) \tag{4.7}$$

Thus, Urbach energy is deduced from the slope of the straight line obtained from the plot of ln(α) as a function of $h\nu$.

(iv) Refractive index (n)

$$n(\lambda)=\sqrt{\left[\frac{4r}{(r-1)^2}-k^2\right]}-\frac{(r+1)}{(r-1)} \tag{4.8}$$

Where k is the extinction coefficient obtained from the relation $k=\frac{\alpha\lambda}{4\pi}$ and r is the material reflectance.

(v) Optical conductivity (σ_{opt})

$$\sigma_{opt}=\frac{\alpha nC}{4\pi} \tag{4.9}$$

Where n is the refractive index and C is the light velocity.

Accordingly, Nithin et al. employed a UV-visible spectral tool toward establishing Cs_2ZnO_2 nanofiller-induced changes in the optical functionalities of PVA NC thick films. They reported that the appearance of additional UV photonic absorption around 376 nm and a relative increase in their absorption intensities (with nanofiller content) justified successful composite formation (Fig. 4.5) [3]. Using the same tool, they also established that Cs_2ZnO_2 nanofillers can be effectively employed to tune the optical constants for PVA thick films (Table 4.2).

The UV-visible spectral tool was also used by Nithin et al. and Sachhidananda et al. to establish the UV shielding efficacies of metal oxide nanofiller introduced PVA and PC films (17, 11). Further, with the help of UV-visible transmittance measurements of PVA/$Ca_{0.2}Zn_{0.8}O$ NC films

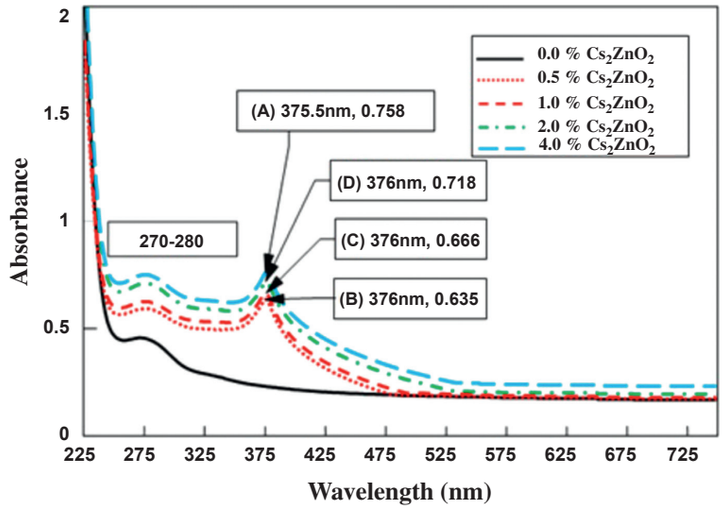


Fig. 4.5 UV-visible absorbance spectra of PVA NCs with (A) 0; (B) 0.5; (C) 1.0; (D) 2.0; and (E) 4.0 wt% of Cs_2ZnO_2 nanofillers. Reproduced from S. Prashanth, K.M. Subbaiah, K.S. Nithin, S. Sachhidananda, Fiber reinforced composites—a review, J. Mater. Sci. Eng. 6 (2017) 341–342 with permission of The American Chemical Society.

Table 4.2 Optical parameters of PVA/Cs_2ZnO_2 NC Films.

Cs_2ZnO_2 content in PVA (wt%)	Urbach energy (eV)	Absorption edge (eV)	Bandgap (eV)		Extinction coefficient (10^{-4})	Optical conductivity (μScm^{-1})
			Direct	Indirect	At band edge 376 nm	
0.0	0.48	4.80	4.59	4.50	0.52	0.82
0.5	0.53	4.72	4.47	4.37	1.26	1.78
1.0	0.57	4.62	4.42	4.30	1.28	1.83
2.0	0.75	4.52	4.25	4.20	1.34	2.18
4.0	0.83	4.40	4.00	4.12	1.53	2.27

Reproduced from K.S. Nithin, H. Siddaramaiah, Opto–electrical characteristics of poly (vinyl alcohol)/cesium zincate nanodielectrics, J. Phys. Chem. C 119 (2015) 20244–20255 with permission of The American Chemical Society.

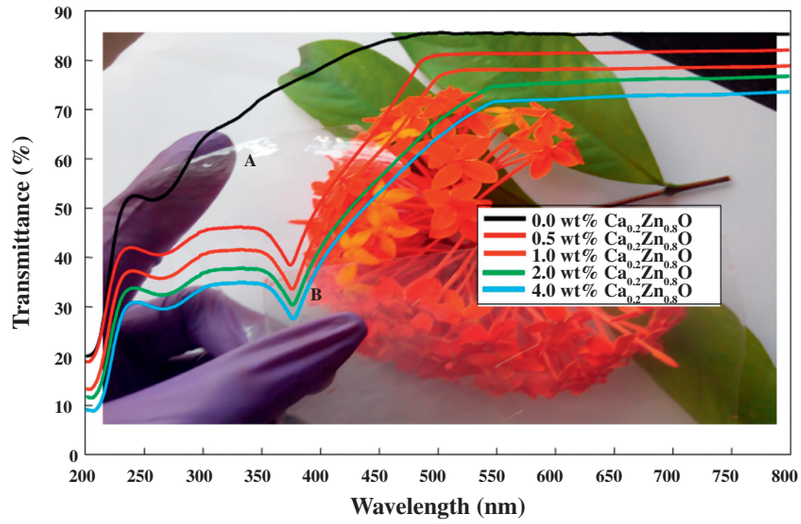


Fig. 4.6 UV-visible transmittance spectra of PVA/$Ca_{0.2}Zn_{0.8}O$ NC films. Background: digital photographs of 0.3 ± 0.03 mm thick PVA NC films depicting high visible transparencies. (A) 2 wt% PVA/$Ca_{0.2}Zn_{0.8}O$; and (B) 4 wt% PVA/$Ca_{0.2}Zn_{0.8}O$. Reproduced from K.S. Nithin, S.Kasargod Nagaraj, S. Shivanna, H. Siddaramaiah, Highly flexible and visibly transparent poly (vinyl alcohol)/calcium zincate nanocomposite films for UVA shielding applications as assessed by novel ultraviolet photon induced fluorescence quenching, Macromolecules. 49 (2016) 2791–2801 with permission of The American Chemical Society.

(Fig. 4.6), Nithin et al. proved that nanofillers with sizes less than 40 nm (which nullifies optical losses associated with Rayleigh scattering), near matching refractive indices (between the nanofiller and host polymer), and higher UV coupled with a lesser visible light absorption coefficient lead to the successful development of optically clear and UV shielding PNCs [4]. However, additional factors to be considered include the thickness of the resultant PNC film and the overall filler-matrix compatibilities [4].

Many researchers also used a UV-visible spectral tool to characterize the nature of the optical bandgaps (direct or indirect), which may lead to novel photo-chromic behaviors in such PBSCs [30–32]. The optical bandgap is essentially the energy switch that triggers the electronic excitations leading to stimulated photo-emissions [33]. The literature also supports that the best fit value of "n" in the plots of $(\alpha h\upsilon)^n$ vs. $(h\upsilon)$ decides the nature of the electronic excitations to be direct or indirect [34–36].

Nithin et al. and Sachhidananda et al. related the nature of the interband electronic excitation (direct or indirect) of PNCs to their photo-chromic (light-emitting) functionalities. They opined PBSCs with a direct bandgap relationship (which facilitates an efficient energy (E) and momentum (k) conserved electron-photon interactions). Where, the electron wave vectors will not change significantly (as represented in Fig.4.7) display an amplified fluorescent emission [23]. They also observed appreciable UV to visible spectral downconversion abilities and hence, augmented fluorescence (associated with the first-order luminescence phenomenon with a relatively shorter

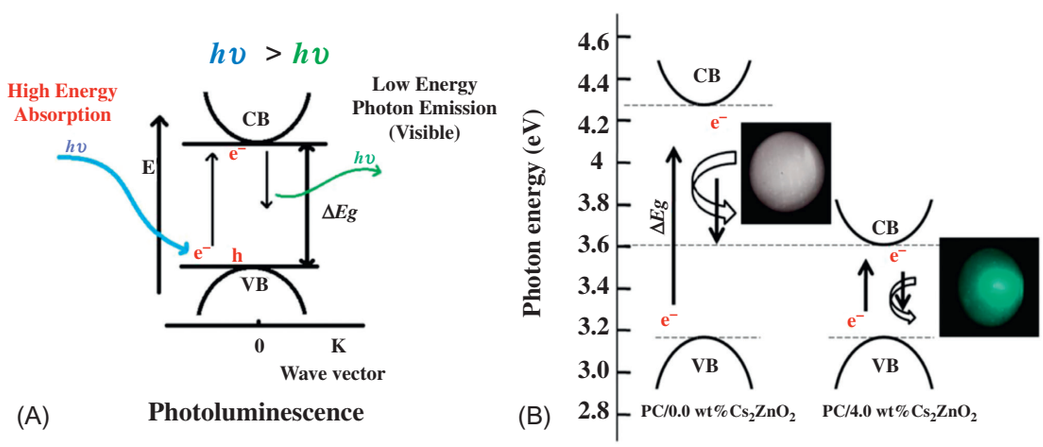


Fig. 4.7 Schematic representation of (A) quantum state energy (E) versus wave vector K; and (B) optical energy requirements leading to fluorescent emission in PC/Cs_2ZnO_2 NC films. Reproduced from S. Shivanna, N.K. Subramani, S.K. Nagaraj, J.R.B. Mutturaj, S. Basavaraj, Patina-green coloured light emitting polycarbonate films: a synergistic extraction of improved UV endurance and considerate spectral down–conversion, J. Lumin. 210 (2019) 276–284 with permission of Elsevier.

radiative lifetime leading to higher luminescence) in direct bandgap PNCs in contrast to indirect bandgap PNCs [3, 23, 33, 37].

4.2.3.2 Spectrofluorometry coupled with UVA transilluminator and related light-emitting functionalities

Fluorescence spectroscopy is an important analytical tool that characterizes the light emitting behaviors of materials upon photonic excitation.

Spectrofluorometers establish the fluorescence signature of molecules based on their photonic excitation (λ_{exi}) and emission (λ_{emi}) wavelengths [38–40]. Molecules in general have lower energy ground and higher energy excited electronic states, with various vibrational states in between. The electronic states of molecules are mainly classified into singlet and triplet based on the nature of spin states.

Also, molecules when excited with photons of appropriate energies will reside in one of the vibrational levels of the singlet excited state. The excited molecules may then travel down to the lowest vibrational state (in the excited electronic state) by losing some vibrational energy (through collision). The said molecule finally drops down to the more stable ground electronic state by energy dissipation through photonic emission.

Fluorescence spectroscopy is primarily concerned with the electronic and vibrational energy states of the molecules [40], which qualifies their light-emitting characteristics. Light-emitting behaviors in PBSCs are of significant interest for various optical and optoelectronic applications, especially when the absorbed radiation is high-energy UV and the emitted radiation is lower-energy visible light.

However, in atomic species, the emitted light is of the same energy as the absorbed radiation, owing to the lack of vibrational levels in atomic species. This type of fluorescence is termed resonance fluorescence.

Thus, fluorescence spectroscopy may be employed to determine both the excitation and emission characteristics of a sample under study. The plots of emission intensity as a function of wavelength (at fixed excitation) gives rise to the emission spectrum while emission intensity as a function of excitation wavelength gives rise to the excitation spectrum. Further, the excitation spectrum quantifies the energy requirement for electronic excitations while the emission spectrum establishes the light-emitting behaviors of PBSCs.

The literature on solar energy materials shows that the present generation of photovoltaic (PV) modules suffers from reduced quantum efficiencies, especially in the lower wavelength ($\lambda < 400\,\text{nm}$) regions (owing to the optical and recombination losses) [41]. However, an interesting solution is the effective integration of mechanically flexible polymer-based spectral manipulating layers into such PV modules. The introduced layers bring about an appreciable UV to visible photonic downconversion or photon cutting, thereby leading to an appreciable decline in the thermalization losses. It is for this reason that they are being increasingly investigated for solar cell applications [42].

Nithin et al. and Sachhidananda et al. employed fluorescence emission measurements coupled with a UVA transilluminator and fluorescence microscopic examination to qualify the UV to visible spectral downconversion abilities and hence, the suitability of PBSCs for solar cell applications [33, 39]. The fluorescence microscopic studies coupled with UVA-transilluminator measurements ascertained the photonic downconversion abilities of PBSCs (Fig. 4.8). The spectrofluorometric (excitation and emission spectrum) (Fig. 4.9) measurements quantified

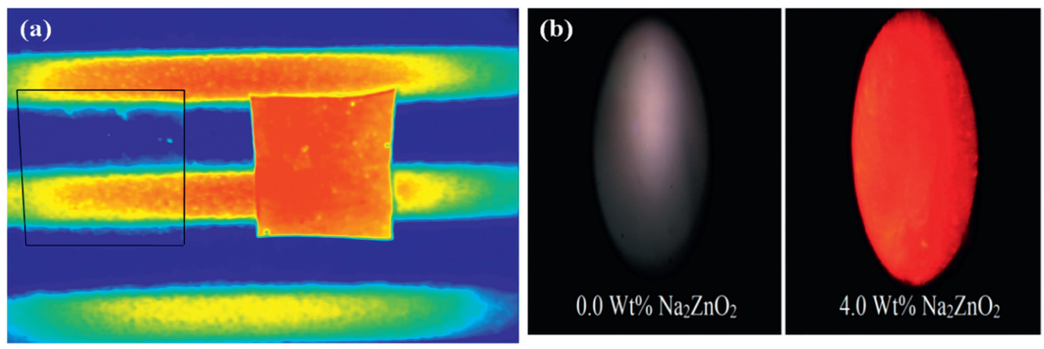


Fig. 4.8 Visible light-emitting behaviors of PVA/Na_2ZnO_2 NC films upon UV excitation. (A) Under UV-transillumination; and (B) Under a fluorescent microscope. Reproduced from S. Shivanna, K.S. Nithin, S. Kasargod Nagaraj, H. Siddaramaiah, Orange–red fluorescent polymer nanocomposite films with large stokes shift: an opto–electronic exercise, J. Lumin. 208 (2019) 488–494 with permission of Elsevier.

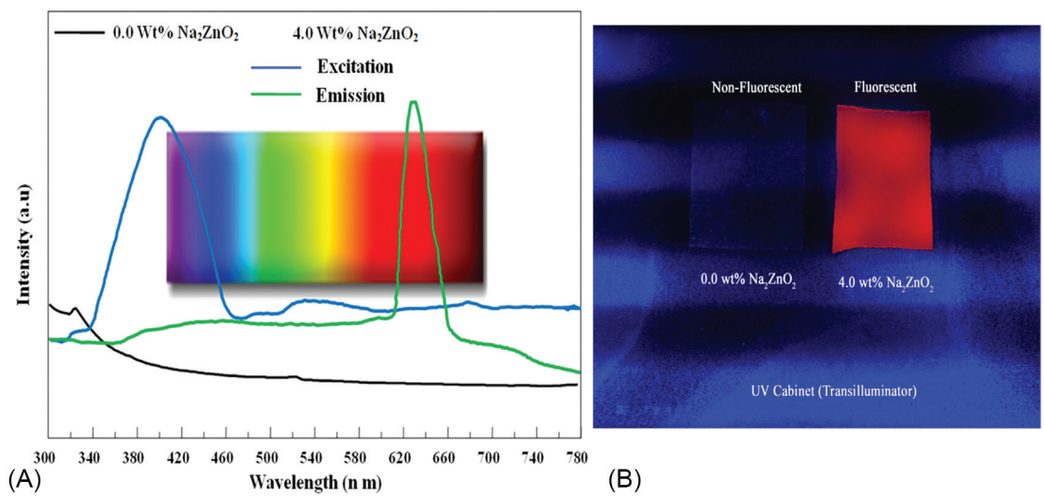


Fig. 4.9 (A) Synchronous excitation and emission (fluorescent) spectrum of PVA/Na_2ZnO_2 NC film depicting a large Stokes shift; and (B) UV-transilluminator images of NC films showing visible *orange-red* emission. Reproduced from S. Shivanna, K.S. Nithin, S. Kasargod Nagaraj, H. Siddaramaiah, Orange–red fluorescent polymer nanocomposite films with large stokes shift: an opto–electronic exercise, J. Lumin. 208 (2019) 488–494 with permission of Elsevier.

the Stokes shift values (in terms of wavelength), which in turn established the extent of the spectral downconversions [39].

4.2.4 Surface wettability measurements to characterize the weathering stabilities

4.2.4.1 Contact angle studies

Superhydrophobic surfaces are of significant technological interest, owing to their potential applications in self-cleaning, electro-wetting, and other related sectors [43, 44]. A wettability study often involves the measurement of static contact angles that specify the extent of wetting, with lower contact angles ($\leq$ 90 degree) signifying higher wettability and higher contact angles ($>$ 90 degree) supporting lower surface wetting. However, if the contact angles approach zero, it indicates complete wetting.

The contact angle (Θ) is the geometrical angle formed by the liquid droplet at the point of intersection with the solid surface. At lower Θ values, the probe liquid tends to spread, thereby indicating a higher degree of wetting. At higher Θ values, the extent of spreading (of the probe liquid) decreases, so lower wetting takes place.

As the real-time applications and shelf life of PBSCs depend largely on their surface characteristics, contact angle measurements of PBSCs have gained significant technological interest. For illustration, the lifetime of spectral manipulating layers coated over the solar cells depends on their surface wettabilities together with their weathering stabilities. In simpler terms, the real-time application of PBSCs often demands relatively hydrophobic and low surface energy layers so as to prevent the detrimental action of adverse weathering conditions on overall material performance.

The wetting behaviors of PNCs may, however, be valued by recording the digital images of static water contact with the solid surface and hence, the angle formed between them.

Further, the wetting behaviors of solids are also affected by their surface free energies, which are essentially computed using the following relation [45, 46]:

$$\gamma_L\left(1+\cos\theta\right)=2\left(\gamma_{sd}\gamma_{ld}\right)^{0.5}+2\left(\gamma_{sp}\gamma_{lp}\right)^{0.5} \tag{4.10}$$

Where γ_L is the liquid surface tension, γ_{ld} is the dispersive component of the liquid surface tension, γ_{sd} is the dispersive component of the solid surface tension, γ_{sp} is the polar component of the solid surface energy, and γ_{lp} is the polar component of the liquid surface energy.

The representative images toward contact angle measurements of PBSCs are given in Fig. 4.10 [33]. Further, several researchers have coupled contact angle measurements with scanning electronic microscopic (SEM) studies to validate the increase in water contact

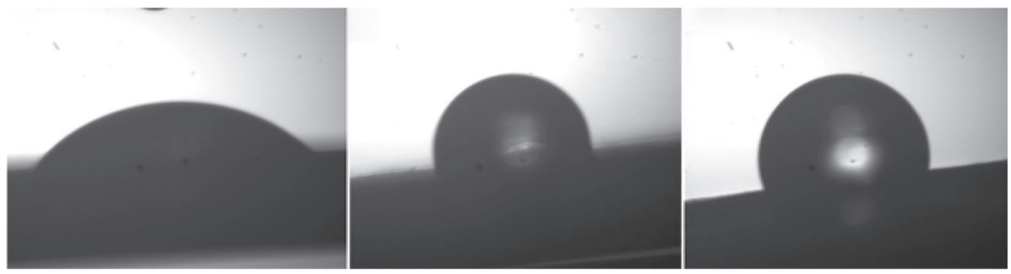


Fig. 4.10 Static contact angle images (water as probe liquid) of PVA NC films with (A) 0.0; (B) 2.0; and (C) 4 wt% of Rb_2ZnO_2. Reproduced from K.S. Nithin, S. Kasargod Nagaraj, S. Shivanna, H. Siddaramaiah, Yellow–green luminescent poly (vinyl alcohol) nanocomposite thick films as effective spectral manipulators, J. Appl. Polym. Sci. 135 (2018) 46854–46855 with permission of Wiley.

angle values of various polymers introduced with metal oxide NPs. They opined that metal oxides in polymers act to increase the surface roughness of polymers (established via SEM and atomic force microscopy (AFM) measurements), which may facilitate air entrapment between the surface voids of resultant PNCs. This in turn leads to a considerable reduction in adhesive forces (surface energies) between the liquid (water)/solid (film surface) interface, thereby enabling considerable enhancement in wetting resistance [9, 39, 47]. This increase in wetting resistance may also widen the application window of such mechanically flexible PBSCs.

4.2.5 Surface morphological behaviors

4.2.5.1 Scanning electron microscopy

The surface morphological featutes of PBSCs and filler introduced changes in the surface morphologies of polymers are often recorded using SEM [26, 48–50]. This analytical tool is extensively employed for various morphological measurements that demand greater resolutions (which cannot be achieved by conventional optical microscopes).

A typical electron microscopegenerates images of the specimen by scanning the surface with a focused electronic beam. Based on the interaction of the focused electron beam with the sample, useful information pertaining to the topological structure of the specimen and composition may be obtained. The most common mode of SEM image generation involves scanning a focused beam of electrons across the sample surface and recording the secondary electrons ejected by the specimen. Various researchers employed SEM studies to reflect and validate nanofiller morphology-dependent changes in the material functionalities of PBSCs.

Chien-Chong Hong et al. improved the piezoelectric output (210.4 pm/V) of PVDF by developing a PVDF-TrFE copolymer in

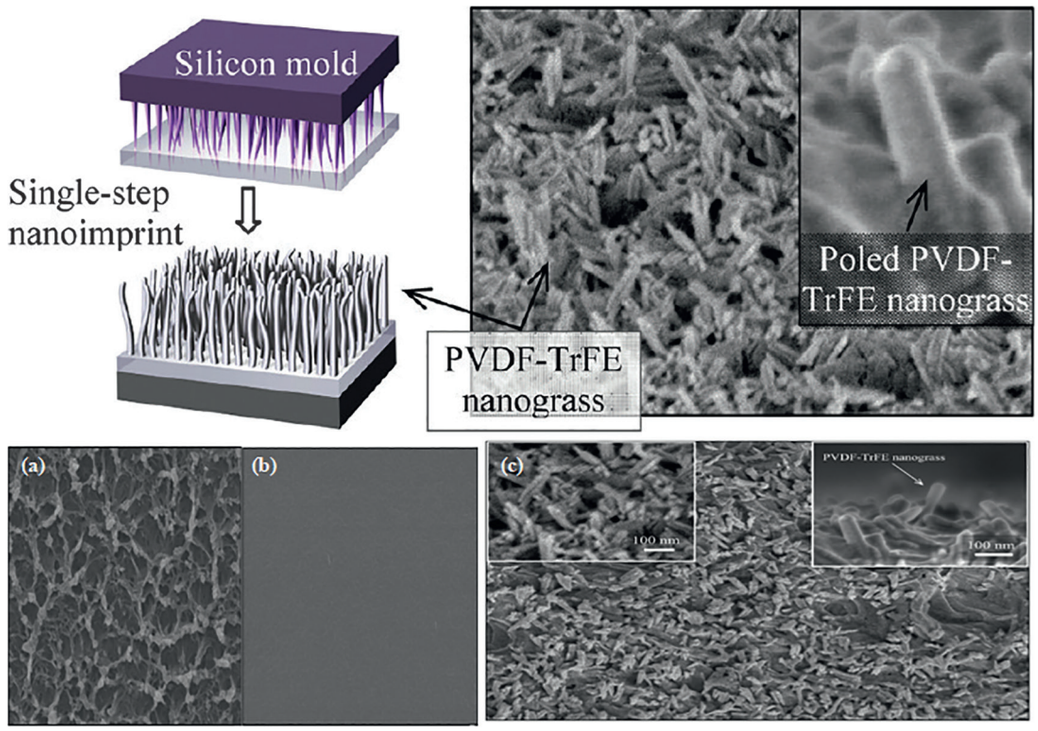


Fig. 4.11 Schematic representation of the fabrication process of PVDF-TrFE and SEM images of the as-fabricated PVDF-TrFE films. (A) Top view of cast-molded PVDF-TrFE nanostructures; (B) Top view of flat thin film (before thermal nanoimprint); and (C) Top view of PVDF-TrFE nanograss (after thermal nanoimprint) (*left inset*: inclined 70 degree view with high magnification; *right inset*: side view with high magnification). Reproduced from C.C. Hong, S.Y. Huang, J. Shieh, S.H. Chen, Enhanced piezoelectricity of nanoimprinted sub-20 nm poly (vinylidene fluoride–trifluoroethylene) copolymer nanograss, Macromolecules. 14 (2012) 1580–1586 with permission of The American Chemical Society.

nanograss morphologies. The morphology of the copolymer was ascertained using SEM. The same has been reproduced in Fig. 4.11 [51].

4.2.6 Thermo-analytical techniques

Thermo-analytical techniques such as differential scanning calorimetry (DSC) and a thermogravimetric analysis (TGA) offer useful information on various phase transitions. They offer continuous measurement of a physical change (weight, volume, heat capacity, and so forth) with an increase in the sample temperature at a predetermined rate.

As a consequence, thermo-analytical techniques have established themselves as very powerful tools to understand and quan-

tify the thermo-physical behaviors of materials. Thermo-analytical measurements of PBSCs also serve to establish the thermal performance of such smart materials to validate their real-time practical applicabilities.

4.2.6.1 Differential scanning calorimetry

Differential scanning calorimetry quantifies the heat flux corresponding to phase transitions in materials as a function of time and temperature. It involves the measurement of differences in heat requirements to increase the temperature of the sample, in contrast to the reference standard.

Further, both the sample and reference standard are maintained at near similar temperatures throughout the study. Thus, the basic operational principle of the DSC technique is the physical transformation-induced difference in the heat requirement of the sample. In simpler terms, when the system under study undergoes a physical change, more or less heat is required to flow to it than the reference standard. Such heat requirements of the sample depend on whether the physical change is exothermic or endothermic.

DSC can also be used to establish the heat requirements associated with thermal transitions such as glass transition temperature (T_g), crystalline melt (T_m), and curing temperature (T_{cure}) range of polymers and their composite hybrids. The temperature corresponding to a steep jump in specific heat capacity is considered to be the T_g of the sample.

4.2.6.2 Thermogravimetric analysis

Thermogravimetric analysis is one of the most useful thermo-analytical techniques, and it quantifies the changes in the physical and chemical properties of the material as a function of temperature or time (under controlled atmosphere) [52]. It is one of the most accepted tools for material characterization via decomposition pattern analysis.

When a sample is subjected to TGA, decomposition takes place at a very slow rate until a critical tenperature is reached. This is followed by very rapid pyrolysis and finally the sample disappears. Such behavior is a characteristic of a large number of decomposition processes of polymers and their composite systems. TGA can also be used to evaluate the introduced nanofiller-induced thermal stability changes in the polymeric matrix. That is, if the sample under study is thermally stable in the given temperature range, no mass change will be observed. Further, TGA also quantifies the upper temperature limit of materials beyond which the material thermally degrades.

4.2.7 Universal testing machine toward mechanical performance validations

The mechanical strength of PNC film is one of the prime factors that qualifies the suitability of materials for real-time outdoor operations. The word strength refers to the inherent ability of materials to resist mechanical load without failure.

A universal testing machine (UTM) is essentially a universal tester that equates the strength of the material before it fails. In a typical experimental procedure, the load cell and extensometer measure the mechanical force and deformation of the samples. A UTM may suitably be employed to test a number of various mechanical factors such as tensile, flexural, compression, shear, and fatigue cycling.

The load requirements to break the sample are measured as tensile strength while the distance between the machine grips during failure presents the elongation at break. Other parameters such as the elastic modulus, flexural strength, and so forth could be deduced using the software attachment provided. The mathematical expressions used to derive various tensile properties are presented below:

$$\text{Tensile strength} = \frac{\text{load at break}}{\text{cross sectional area}} \tag{4.11}$$

$$\text{Elongation at break} = \frac{\text{extended length at break}}{\text{original length}} \times 100\% \tag{4.12}$$

$$\text{Youngs modulus} = \frac{\text{tensile stress}}{\text{tensile strain}} \tag{4.13}$$

4.2.8 Electrical properties and determination of energy storage abilities

High dielectric constant (k) polymers are exceedingly attractive, owing to their potential applications in various electronic and electrical power systems [53–60]. However, highly processable polymers are known to present high breakdown strength and low dielectric loss [61, 62]. Yet, the low-k performance of polymers limits their broad utilization in dielectrics and other related energy storage applications.

Thus, the thoughtful introduction of ceramic nanomaterials (with a high dielectric constant) into particle stabilizing polymeric matrices is one of the most adapted approaches toward the development of energy storage composites, as they extract the merits of both components. Further, the right combination of nanostructured ceramics and polymer host, the nanofiller aspect ratio in the polymeric matrix, the optimal interfacial adhesion between the inorganic nanofiller and the organic polymer, and the improved dispersion stability of the

introduced nanofillers may all lead to increased dielectric constant, suppressed dielectric loss, and balanced dielectric breakdown, and hence high energy densities.

Every material is associated with its own unique set of electrical characteristics, the accurate measure of which may assist the technologists to suitably incorporate these materials for improved device performance. The dielectric behaviors and nature of charge transport prevalent in these heterogeneous systems may be deduced from the measured values of inductance (L), capacitance (C), and resistance (R). Accordingly, the material under study will be subjected to an alternating voltage source with an LCR meter measuring the voltage across the current flowing through it, the ratio of which determines the magnitude of impedance. Further, the equivalent capacitance, inductance, and resistance are also measured.

The dielectric parameter is essentially a function of applied frequency expressed by the complex permittivity as:

$$\varepsilon^*(\omega) = \varepsilon'(\omega) - \varepsilon''(\omega) \tag{4.14}$$

Where $\varepsilon'(\omega)$ and $\varepsilon''(\omega)$ are the real and imaginary parts of permittivity exhibiting energy storage (dielectric constant) and energy loss (dielectric loss) in each cycle of the electric field.

4.2.8.1 Dielectric constant

The dielectric constant ($\varepsilon'(\omega)$) is essentially a ratio between the permittivity of a system to the permittivity of vacuum. It quantifies the extent to which a material may concentrate the electric flux and is a relative measure of charge storage abilities.

The measured values of capacitance are employed to determine the dielectric constant using the following expression:

$$C(\omega) = \varepsilon_0 \varepsilon'(\omega) \frac{A}{d} \tag{4.15}$$

Where ε_0 is the permittivity of free space (8.85×10^{-12} F/m) while A is the area of the capacitor and d is the specimen thickness.

4.2.8.2 Loss tangent (Tan δ)

The loss tangent or dissipation factor quantifies the energy loss rate in a dissipative system under electrical oscillations or how lossy a material is for AC signals.

It is related to complex permittivity as:

$$\varepsilon''(\omega) = \varepsilon'(\omega) \tan\delta \tag{4.16}$$

Where δ is the phase angle.

4.2.8.3 AC conductivity (σ_{ac})

The nature of charge transport in multicomponent systems may be established by frequency-dependent conductivity measurements. The measured values of conductance are employed to determine the AC conductivity using the following expression:

$$\sigma_{ac} = d\frac{G(\omega)}{A} \tag{4.17}$$

4.2.8.4 Dielectric breakdown strength

The dielectric breakdown strength (E_b) is a factor of significant interest for energy storage applications, as it quantifies the operational electric field and maximum energy storage density of dielectrics [62, 63].

The dielectric breakdown strength of NCs can be extracted using the Weibull failure statistics:

$$P(E) = 1 - \exp\left[-\left(E/E_0\right)^{\beta}\right] \tag{4.18}$$

Where $P(E)$, E,and $\beta$are the cumulative electrical failure probability, the experimental breakdown strength, and the shape parameter, respectively. E_0 is the breakdown strength at 63.2% cumulative failure.

4.2.8.5 Theoretical maximum energy storage density

The theoretical maximum energy storage density (U_e),of a linear response dielectric system is a direct function of its dielectric permittivity and breakdown strength, expressed as [54]:

$$U_e = \frac{1}{2}\varepsilon_r\varepsilon_0\left(E_b\right)^2 \tag{4.19}$$

Where, ε_r is the relative dielectric constant and U_e is the theoretical maximum energy storage density.

4.2.8.6 Total stored energy density (U_{es})

For ferroelectric materials, the dielectric polarization is not necessarily a linear function of the applied electric field. The energy density in such heterogeneous systems can be deduced from electric displacement-electric field (D-E) loops and two probe current-voltage (I-V) measurements. The energy storage capabilities of PNCs can be deduced from the D-E loops using the Sawyer-Tower circuit, in accordance with the following integral:

$$U_{es} = \int EdD \tag{4.20}$$

4.2.8.7 Energy storage efficiency

The charge-discharge efficiency (η) is another imperative factor for evaluating the suitability of dielectric materials for energy storage applications. The energy storage efficiency of PNCs was obtained from the relation below:

$$\eta = \frac{U_{ed}}{U_{es}} \times 100\% \tag{4.21}$$

Where U_{ed} is the discharged energy density.

4.3 Conclusions and future directions

Given that the large-scale commercial exploitation of PBSCs mandates a fundamental understanding of their inherent material functionalities, the wide diversity in tools and techniques available for their structural, morphological, optical, electrical, mechanical, thermal, and other related characterizations plays an important role in deciding their commercial success.

Characterization is one of the most fundamental processes in materials research, in the absence of which no scientific understanding of engineering materials could be achieved. Moreover, the field of PNC-based smart materials offers both tremendous opportunities and significant new challenges for commercial exploitation. The further success of that exploitation depends on the possibility of developing advanced characterization tools aimed at understanding the critical nature of the interface, elucidating the interactions at the interface, and acquiring knowledge of the relationship between PNC properties and interfacial optimizations. Accordingly, progressive multidisciplinary research efforts will be required to bridge the gap in existing knowledge between technological developments and a fundamental understanding of PNC properties to improve their overall performance.

References

[1] S. Prashanth, K.M. Subbaiah, K.S. Nithin, S. Sachhidananda, Fiber reinforced composites—a review, J. Mater. Sci. Eng. 6 (2017) 341–342.
[2] M.V. Bhavya, D.V. Gowda, S. Praveen, N.K. Subramani, H. Siddaramaiah, Cosmetics: polymers, in: Encyclopedia of Polymer Applications, first ed., T&F, 2018.
[3] K.S. Nithin, H. Siddaramaiah, Opto–electrical characteristics of poly (vinyl alcohol)/cesium zincate nanodielectrics, J. Phys. Chem. C 119 (2015) 20244–20255.
[4] K.S. Nithin, S. Kasargod Nagaraj, S. Shivanna, H. Siddaramaiah, Highly flexible and visibly transparent poly (vinyl alcohol)/calcium zincate nanocomposite films for UVA shielding applications as assessed by novel ultraviolet photon induced fluorescence quenching, Macromolecules 49 (2016) 2791–2801.
[5] J.Y. Kim, H.M. Kim, D.H. Shin, K. Ihan, Synthesis of CdS nanoparticles dispersed within poly (urethane acrylate-co-styrene) films using an amphiphilic urethane acrylate nonionomer, J. Chem. Phys. 207 (2006) 925–932.

[6] K.S. Nithin, Polymer nanocomposites as luminescent down shifting layers, Res. Rev. J. Mater. Sci. 4 (2016).
[7] M. Tirumali, B. Kandasubramanian, A. Kumaraswamy, N.K. Subramani, B. Suresha, Fabrication, physicochemical characterizations and electrical conductivity studies of modified carbon nanofiber-reinforced epoxy composites: effect of 1-butyl-3-methylimidazolium tetrafluoroborate ionic liquid, Polym.-Plast. Technol. Eng. 57 (2018) 218–228.
[8] A.M.N. Saeed, M.Q.A. Al-Gunaid, N.K. Subramani, B.S. Madhukar, S. Basavarajaiah, Effect of cesium aluminate nanofiller on optical properties of polyvinyl pyrrolidone nanocomposite films, Polym.-Plast. Technol. Eng. 57 (2008) 1188–1196.
[9] K.N. Shilpa, K. Subramani, S. Sachhidananda, B.S. Madhukar, Visibly transparent PVA/sodium doped dysprosia ($Na_2Dy_2O_4$) nano composite films, with high refractive index: an optical study, J. Alloys Compd. 694 (2017) 884–891.
[10] T. Champa, S. Sachhidananda, K.N. Shilpa, K.S. Nithin, H. Siddaramaiah, Optoelectronic behaviors of reversibly stretchable $Na_{0.8}Mn_{0.8}O_2$ reinforced poly(vinyl alcohol) nanocomposites, Int. J. Eng. Sci. Comput. 7 (2017) 14875–14879.
[11] B. Suresha, R. Hemanth, K.S. Nithin, Automotive applications: reinforced material components, in: Encyclopedia of Polymer Applications, CRC Press, 2018.
[12] N.K. Subramani, K.N. Shilpa, S. Sachhidananda, B.M. Jagajeevan Raj, H. Siddaramaiah, Advances in polymer–based piezoelectric systems, in: Emergent Research on Polymeric and Composite Materials, IGI Global, 2018, pp. 139–157 (Chapter 6).
[13] Mahesha, K.M. Subbaiah, K.S. Nithin, B.M.J. Raj, S. Shivanna, Highly flexible and conducting polymer nanocomposite films for selective gas sensing applications, Mater. Today Proc. 9 (2019) 515–521.
[14] B.M. Jagajeevanraj, S. Sachhidananda, K. Pushpalatha, K.S. Nithin, Nanostructured Al0.2 Y1.8O3 semiconductor assisted enhancement in PVOH fortitude to withstand high energy UV photons: an opto–mechanical study, Optik 182 (2019) 598–604.
[15] P. Sivadasu, D.V. Gowda, N.K. Subramani, B.M. Vishweshwaraiah, S. Shivanna, S. Hatna, Direct brain targeted nanostructured lipid carriers for sustained release of schizophrenic drug: formulation, characterization and pharmacokinetic studies, Indian J. Pharm. Educ. Res. 54 (2020) 73–84.
[16] S. Sandeep, A.S. Santhosh, N.K. Swamy, G.S. Suresh, J.S. Melo, K.S. Nithin, Electrochemical detection of L–dopa using crude polyphenol oxidase enzyme immobilized on electrochemically reduced RGO–Ag nanocomposite modified graphite electrode, Mater. Sci. Eng. B Solid-State Mater. Adv. Technol. 232 (2018) 15–21.
[17] G.R. Suma, N.K. Subramani, S. Sachhidananda, S.V. Satyanarayana Siddaramaiah, Nanotechnology enabled E. coli sensors: an opto-electronic study, Mater. Today Proc. 4 (2017).
[18] P.B. Bhargav, V.M. Mohan, A.K. Sharma, V.V.R.N. Rao, Structural, electrical and optical characterization of pure and doped poly (vinyl alcohol) (PVA) polymer electrolyte films, Int. J. Polym. Mater. 56 (2007) 579–591.
[19] K.N. Shilpa, S.R. Urs, H.B. Patil, H.P. Jayadevappa, B.V. Latha, K.S. Nithin, S. Sachhidananda, Adsorptive removal of Cu (II) from aqueoussolution using nanostructured lithium zincate, Int. J. Eng. Sci. Comput. 6 (2016) 8463–8468.
[20] K.R. Reddy, A.V. Raghu, H.M. Jeong, Synthesis and characterization of novel polyurethanes based on 4,4′-{1,4-phenylenebis[methylylidenenitrilo]} diphenol, Poly. Bull. 60 (2008) 609–616.
[21] M.Q.A. Al-Gunaid, A.M.N. Saeed, K.S. Nithin, B.S. Madhukar, Siddaramaiah, Optical parmeters, electrical permittivity and I-V characterstics of PVA/Cs_2CuO_2 nanocomposite films for opto-electronic applications, J. Mater. Sci. Mater. Electron. 28 (2017) 8074–8086.

[22] J. Chamberain, J.E. Gibbs, H.E. Gebbie, The determination of refractive index spectra by fourier spectrometry, Infrared Phys. 9 (1969) 189–209.
[23] S. Shivanna, N.K. Subramani, S.K. Nagaraj, J.R.B. Mutturaj, S. Basavaraj, Patina-green coloured light emitting polycarbonate films: a synergistic extraction of improved UV endurance and considerate spectral down–conversion, J. Lumin. 210 (2019) 276–284.
[24] S.K. Nagaraj, S. Shivanna, N.K. Subramani, H. Siddaramaiah, Revisiting powder X–ray diffraction technique: a powerful tool to characterize polymers and their composite films, J. Mater. Sci. 4 (2016) 1–5.
[25] H.B. Vasanth Patil, K.S. Nithin, S. Sachhidananda, Siddaramaiah, K.T. Chandrashekara, B.Y.S. Kumar, Mycofabrication of bioactive silver nanoparticle: photo catalysed synthesis and characterization to attest its augmented bio-efficacy, Arab. J. Chem. 12 (2019) 4596–4611.
[26] G.R. Suma, K.S. Nithin, S. Sachhidananda, S.V. Satyanarayana, Siddaramaiah, Optical and electrical evaluation of $Ag_{0.5}Cu_{0.75}$ O introduced poly (vinyl alcohol) based E. coli sensors, J. Mater. Sci. Mater. Electron. 28 (2017) 13139–13148.
[27] G.R. Suma, K.S. Nithin, K.N. Shilpa, S. Sachhidananda, S.V. Satyanarayana Siddaramaiah, Effect of $Ce_{0.5}Zr_{0.5}O_2$ nano fillers on structural and optical behaviors of poly(vinyl alcohol), J. Mater. Sci. Mater. Electron. 28 (2017) 10707–10714.
[28] K.S. Nithin, Nanotechnology enabled electrode materials for rechargeable sodium–ion batteries: an ideal resolution to global energy crisis, Res. Rev. J. Mater. Sci. 4 (2016).
[29] V. Van, R.L.P. Henricus, J.C.M. Sterenborg, A. Pifferi, A. Torricelli, E. Chikoidze, R. Cubeddu, Determination of visible near-IR absorption coefficients of mammalian fat using time-and spatially resolved diffuse reflectance and transmission spectroscopy, J. Biomed. Opt. 10 (2005), 054004.
[30] G.R. Suma, K.S. Nithin, B.V. Latha, S.K. Nagaraj, S. Shivanna, S.V. Sathyanarayana, Gent to refractive index engineering of strontium doped zirconium oxide (szo) reinforced poly vinyl pyrrolidone composite films: effect of dopant content and annealing temperature, Int. J. Eng. Sci. Comput. 6 (2016) 5703–5709.
[31] H.N. Chandrakala, B. Ramaraj, Shivakumaraiah, Siddaramaiah, Optical properties and structural characteristics of zinc oxide-cerium oxide doped polyvinyl alcohol films, J. Alloys Compd. 586 (2014) 333–342.
[32] M. Sreemany, S. Sen, A simple spectrophotometric method for determination of the optical constants and band gap energy of multiple layer TiO2 thin films, Mater. Chem. Phys. 83 (2004) 169–177.
[33] K.S. Nithin, S. Kasargod Nagaraj, S. Shivanna, H. Siddaramaiah, Yellow–green luminescent poly (vinyl alcohol) nanocomposite thick films as effective spectral manipulators, J. Appl. Polym. Sci. 135 (2018) 46854–46855.
[34] K.S. Nithin, S. Shivanna, S.K. Nagaraj, H. Siddaramaiah, Refractive index engineering of poly(vinylalcohol)/Li_2ZnO_2 nanocomposites: effect of filler content and annealing temperature, AIP Conf. Proc. 1943 (2018) 020127–020128.
[35] B. Suresha, K. Adappa, N.K. Subramani, Mechanical and tribological behaviours of epoxy hybrid composites reinforced by carbon fibers and silicon carbide whiskers, Mater. Today: Proc. 5 (2018) 16658–16668.
[36] N. Kundachira Subramani, S. Shivanna, S. Kasargod Nagaraj, B. Suresha, B.M. Jagajeevan Raj, H. Siddaramaiah, Optoelectronic behaviours of UV shielding calcium zirconatereinforced polycarbonate nanocomposite films: an optical view, Mater. Today: Proc. 5 (2018) 16626–16632.
[37] A. Kitai, Luminescent Materials and Applications, John Wiley & sons, 2008.
[38] V.R. Gowariker, N.V. Viswanathan, J. Sreedhar, Polymer Science, New Age International, 1986.
[39] S. Shivanna, K.S. Nithin, S. Kasargod Nagaraj, H. Siddaramaiah, Orange–red fluorescent polymer nanocomposite films with large stokes shift: an opto–electronic exercise, J. Lumin. 208 (2019) 488–494.

[40] H. Yang, P. Jiang, Self-cleaning diffractive macroporous films by doctor blade coating, Langmuir 26 (2010) 12598–12604.
[41] R. Rothemund, Optical modelling of the external quantum efficiency of solar cells with luminescent down-shifting layers, Sol. Energy Mater. Sol. Cells 120 (2014) 621–622.
[42] H.Q. Wang, M. Batentschuk, A. Osvet, L. Pinna, C.J. Brabec, Rare-earth ion doped up-conversion materials for photovoltaic applications, Adv. Mater. 23 (2011) 2680–2681.
[43] A. Marmur, A Guide to the Equilibrium Contact Angles Maze, Contact Angle Wettability and Adhesion, CRS Press, T&F, 2009.
[44] B. Bhushan, Y.C. Jung, K. Koch, Self-cleaning efficiency of artificial superhydrophobic surfaces, Langmuir 25 (2009) 3240–3248.
[45] D.K. Owens, R.C. Wendt, Estimation of the surface free energy of polymers, J. Appl. Polym. Sci. 13 (1969) 1741–1747.
[46] M. Faraday, The Bakerian lecture: experimental relations of gold (and other metals) to light, Philos. Trans. R. Soc. Lond. 147 (1857) 145–181.
[47] K.M. Lang, D.A. Hite, R.W. Simmonds, R. McDermott, D.P. Pappas, J.M. Martinis, Conducting atomic force microscopy for nanoscale tunnel barrier characterization, Rev. Sci. Instrum. 75 (2004) 2726–2731.
[48] F. Hussain, M. Hojjati, M. Okamoto, R.E. Gorga, Polymer-matrix nanocomposites, processing, manufacturing, and application: an overview, J. Compos. Mater. 40 (2016) 1511–1575.
[49] A.W. Coats, J.P. Redfern, Thermogravimetric analysis: a review, Analyst 88 (1963) 906–924.
[50] K.N. Shilpa, H.B. Patil, P. Karthik, K. Mallikarjun, B.M. JagajeevanRaj, S. Sharon, K.S. Nithin, Removal of Cu (II) from water using hydrothermally synthesized strontium doped zirconium oxide nano adsorbents, J. Mater. Sci. Eng. 1 (2016) 252–256.
[51] C.C. Hong, S.Y. Huang, J. Shieh, S.H. Chen, Enhanced piezoelectricity of nanoimprinted sub-20 nm poly (vinylidene fluoride–trifluoroethylene) copolymer nanograss, Macromolecules 14 (2012) 1580–1586.
[52] Q. Li, K. Han, M.R. Gadinski, G. Zhang, Q. Wang, High energy and power density capacitors from solution-processed ternary ferroelectric polymer nanocomposites, Adv. Mater. 26 (2014) 6244–6249.
[53] C.G. Hardy, M.S. Islam, D. Gonzalez-Delozier, J.E. Morgan, B. Cash, B.C. Benicewicz, C. Tang, Converting an electrical insulator into a dielectric capacitor: end-capping polystyrene with oligoaniline, Chem. Mater. 25 (2013) 799–807.
[54] Q.M. Zhang, H. Li, M. Poh, F. Xia, Z.Y. Cheng, H. Xu, C. Huang, An all-organic composite actuator material with a high dielectric constant, Nature 419 (2002) 284–287.
[55] B. Chu, X. Zhou, K. Ren, B. Neese, M. Lin, Q. Wang, F. Bauer, Q.M. Zhang, A dielectric polymer with high electric energy density and fast discharge speed, Science 313 (2006) 334–336.
[56] Z.M. Dang, J.K. Yuan, S.H. Yao, R.J. Liao, Flexible nanodielectric materials with high permittivity for power energy storage, Adv. Mater. 25 (2013) 6334–6365.
[57] R.P. Ortiz, A. Facchetti, T.J. Marks, High-k organic, inorganic, and hybrid dielectrics for low-voltage organic field-effect transistors, Chem. Rev. 110 (2010) 205–239.
[58] S.S. Parizi, A. Mellinger, G. Caruntu, Ferroelectric barium titanate nanocubes as capacitive building blocks for energy storage applications, ACS Appl. Mater. Interfaces 6 (2014) 17506–17517.
[59] S.A. Paniagua, Y. Kim, K. Henry, R. Kumar, J.W. Perry, S.R. Marder, Surface-initiated polymerization from barium titanate nanoparticles for hybrid dielectric capacitors, ACS Appl. Mater. Interfaces 6 (2014) 3477–3482.

[60] C. Jason, L. Yingying, L. Kun, W. Wang, Electrical storage in poly (vinylidene fluoride) based ferroelectric polymers: correlating polymer structure to electrical breakdown strength, Chem. Mater. 20 (2008) 2078–2080.
[61] L. Zhu, Q. Wang, Novel ferroelectric polymers for high energy density and low loss dielectrics, Macromolecules 45 (2012) 2937–2954.
[62] Q. Li, G. Zhang, F. Liu, K. Han, M.R. Gadinski, C. Xiong, Q. Wang, Solution-processed ferroelectric terpolymer nanocomposites with high breakdown strength and energy density utilizing boron nitride nanosheets, Energy Environ. Sci. 8 (2015) 922–931.
[63] G. Wang, X. Huang, P. Jiang, Tailoring dielectric properties and energy density of ferroelectric polymer nanocomposites by high-k nanowires, ACS Appl. Mater. Interfaces 7 (2015) 18017–18027.

5

Mechanically flexible and visibly transparent polymer-based nanocomposites for UV-protective applications

B.M. Jagajeevan Raj[b], K.S. Nithin[b], K.N. Shilpa[a], S. Sachhidananda[a], S. Sandeep[c], H. Siddaramaiah[d,†] and K. Pushpalatha[b]

[a]Department of Polymer Science and Technology, Sri Jayachamarajendra College of Engineering, JSS Science and Technology University, Mysuru, India, [b]Department of Chemistry, The National Institute of Engineering, Mysuru, India, [c]Department of Chemistry, Sri Jayachamarajendra College of Engineering, JSS Science and Technology University, Mysuru, India, [d]Vice-Chancellor of JSS Science and Technology University, Mysuru, India

5.1 Introduction

Rapid changes in the global atmosphere and thinning of the ozone layer have all contributed to augmented research interest in UV-protective materials. Further, short-wavelength and high-energy UV radiations often damage both human and material health. That is to say, UV radiation acts as a stressor that promotes oxidative stress, a condition responsible for the aging of human skin [1]. Also, UV-induced photo-oxidative reactions lead to photo-aging associated severe deterioration in material health, especially of those compounds that are of organic origin [2].

Accordingly, organic matrices such as wood and polymer exhibit a drop in their mechanical strength and impact resistance upon UV exposure. However, dyes that are UV-sensitive undergo progressive fading and finally lose their original color, while UV light-induced weakening and embrittlement of cellulose fibers may cause the normal paper to bleach. The said detrimental effects may be owed to the high-energy UV radiation-induced photo-oxidative cleavage of chemical functionalities [3].

† Deceased.

Polymer-Based Advanced Functional Composites for Optoelectronic and Energy Applications
https://doi.org/10.1016/B978-0-12-818484-4.00003-3
Copyright © 2021 Elsevier Inc. All rights reserved.

UV radiation, also addressed as UV light, is invisible electromagnetic radiation similar to that of visible light but with shorter wavelengths and higher energies. This shorter wavelength and higher energy UV region is further subdivided into three regions, namely, UVC (100–290 nm), UVB (290–320 nm), and UVA (320–400 nm). Plus, light falling in the UVC regions and associated with higher photonic energies (4.43–12.4 eV), than UVB (3.94–4.43 eV) and UVA (3.10–3.94 eV) regions are the most dangerous and could cause more serious harm.

Although, all types of UV photons could cause potential damage to human skin. Nevertheless, each type will affect human skin differently. That is, UVA radiation, which accounts for 95% of the sun's radiation that reaches the Earth's surface, pierces deeper into human skin, leading to wrinkles, sun spots, and early aging. UVB radiation with relatively higher energy pierces only a few mm into skin and affects the skin's top layer, thereby leading to sunburns. The continued exposure of UVB rays, however, could significantly enhance the possibility of skin cancer. Finally, UVC photons associated with very high energy (higher than UVA rays and UVB radiation) are the most dangerous and extremely damaging, often leading to skin cancer. A pictorial representation on the penetration depth of UVA and UVB radiation on human skin is presented in Fig. 5.1.

It is for this reason that the development of advanced UV protective materials is an exciting area of research interest. Further, the fact that most optical applications of materials demand excellent design (mechanical) flexibilities and high optical clarities render polymer-based composites as the most sought after materials for UV protective applications. Additionally, materials in nanometric size offer unique end properties, owing to their ultrafine dimensions and high specific surface areas [5–8]. Plus, the ability of polymers to display dopant-dependent material property engineering has encouraged the

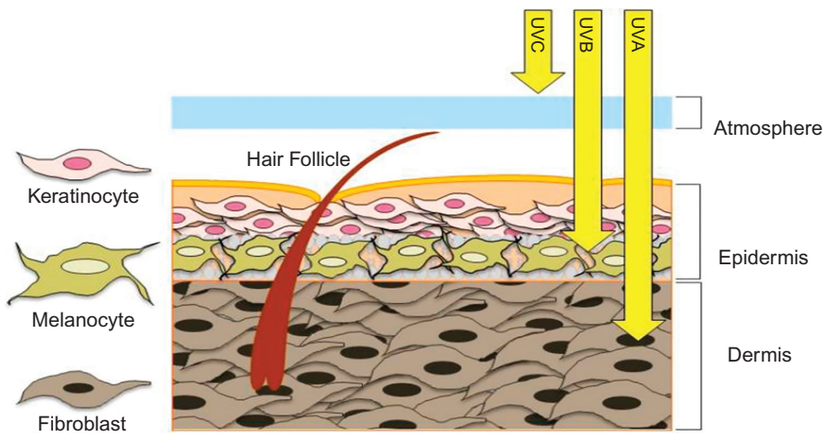


Fig. 5.1 Pictorial representation of UVB and UVA photons penetrating human skin [4].

scientific community to explore various nanofiller/polymer combinations for UV protective applications [3, 9, 10].

Herein, an attempt is made to summarize various filler, polymer, and composite related factors leading to the successful development of mechanically flexible and visibly transparent polymer-based UV-protective materials.

5.2 Classification of polymer-based UV-protective materials

In order to offer effective protection against UV radiation, one of the necessities of UV shielding molecules is their ability to transmute the absorbed higher energy radiation into relatively lesser energy via various photo-physical processes [11–16]. Generally, UV absorbers are either organic or inorganic colorless compounds with a strong absorption in the UV region of electromagnetic spectrum.

In addition, an ideal UV absorbent must satisfy the following conditions [17]:

- It must effectively absorb throughout the UV region, especially lesser wavelength and higher energy photons.
- It must be UV stable by itself.
- It must dissipate the absorbed energy via such an approach that causes no deterioratory changes in the medium it protects.

Such UV absorbent introduced polymer-based UV protective materials may be grouped into different types, based on the physical mechanism responsible for the protective effects and also on the nature of the UV absorbent used.

5.2.1 Based on physical mechanism responsible for protective effects

Based on the operating principle (i.e., whether optical absorption or reflection is responsible for protection effects), polymer-based UV-protective materials may be broadly classified into two types:

1. Optical absorption-supported polymer-based UV-protective materials.
2. Optical reflectance-supported polymer-based UV-protective materials.

Polymer-based UV-protective materials that take advantage of the optical absorption principle to eliminate UV photons from incoming light are either organic UV absorbent introduced or metal oxide nanofiller introduced polymer composites. However, when optical reflection is used to eliminate UV photons, more complex multilayered architectures must be employed, so that the interference effects contribute to the desired UV-protective behaviors [18]. In both cases, polymer serves the encapsulant role and offers processing ease and improved mechanical performance, while the additive enables UV blocking effects.

5.2.2 Based on the nature of the UV absorbent

Based on the nature of the UV absorbent, polymer-based UV-protective materials are classified as:

1. Polymer-based UV-protective materials containing organic UV absorbers.
2. Polymer-based UV-protective materials containing inorganic UV absorbers.

5.2.2.1 Polymer-based UV-protective materials containing organic UV absorbers

These materials are either developed by applying a polymer capping onto a UV absorbing molecule of organic origin or by suitably integrating an organic UV absorbent with an appropriate polymer host or by introducing organic UV stabilizers into the polymer host.

Such polymer-based organic UV blocking agents act via thoughtful dissipation of higher-energy UV photons into less damaging thermal phonons via various photo-physical processes. The said processes could effectively shield the host polymer, as it reduces the amount of UV light that can be absorbed by the chromophores present in the host polymer. The second type containing organic UV stabilizers acts as radical scavengers, that deactivate the products of photolysis, thereby decreasing the effectiveness of unwanted photo-oxidative polymer cleavage [19, 20].

Further, organic compounds with an inherent ability to form intramolecular hydrogen bonding present an effective radiationless means of energy dissipation and are the most preferred UV protective materials. Such materials include organic compounds with phenolic groups that could form O-H-O (salicylates, 2-hydroxybenzophenones, 2,2′-dihydroxybenzophenones and xantones) and/or O-H-N bridges (2-(2-hydroxyphenyl) benzotriazoles and 2-(2-hydroxyphenyl)-1, 3,5-triazines). Some of the most important nonphenolic UV absorbers include oxanilides and cyanoacrilates. Fig. 5.2 shows the chemical structures of some of the most commonly used phenolic-type UV absorbents.

Besides, the UV blocking effect in phenolic-type UV absorbents may be owed to excited state intramolecular proton transfer (ESIPT) (Fig. 5.3) effect induced radiationless energy dissipation [11, 12, 14, 15, 17, 21]. Nevertheless, in the case of nonphenolic-type UV absorbents, the energy dissipation may involve either ESIPT effects (in case of oxanilides) or the charge-separated species formed (in case of cyanoacrilates) losing energy via rotation or increased vibration about the central bond (Fig. 5.4).

Further, in the case of organic UV absorbents operating through ESIPT effects, the absorbed UV photons excite the UV absorb-

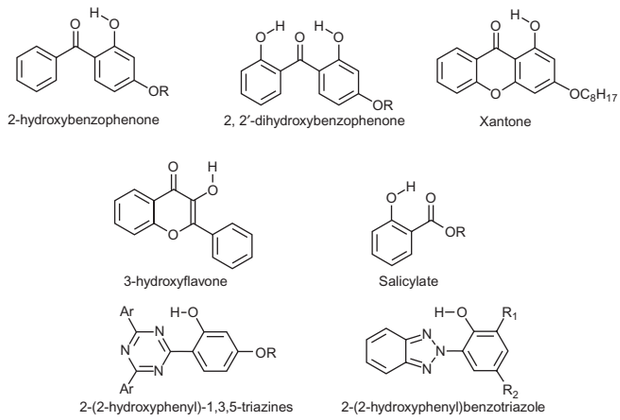


Fig. 5.2 Chemical structures of some of the important phenolic type UV absorbents. Reproduced from M. Zayat, P. Garcia-Parejo, D. Levy, Preventing UV-light damage of light sensitive materials using a highly protective UV-absorbing coating, Chem. Soc. Rev. 36 (2007) 1270–1281 with permission of the Royal Society of Chemistry.

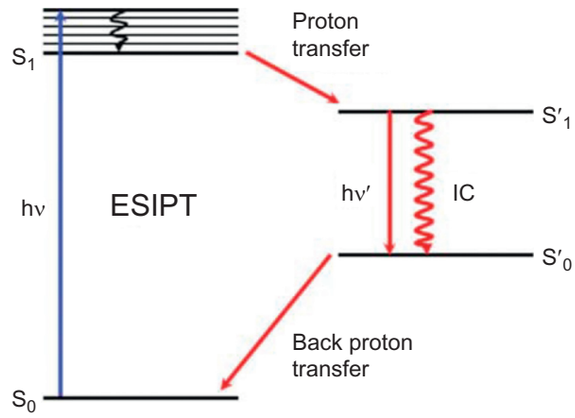


Fig. 5.3 Schematic representation of energy dissipation via ESIPT mechanism. Reproduced from M. Zayat, P. Garcia-Parejo, D. Levy, Preventing UV-light damage of light sensitive materials using a highly protective UV-absorbing coating, Chem. Soc. Rev. 36 (2007) 1270–1281 with permission of the Royal Society of Chemistry.

ing molecule from its ground state (S_0) to a higher energy singlet excited state (S_1). This electronic redistribution-induced higher acidity, prompts a proton transfer that in turn leads to the formation of a tautomeric species in its first excited singlet state (S_1'). It is this tautomeric species that loses the energy absorbed via nonradiative decay (Fig. 5.3). Also, in some cases, the tautomeric species formed may also dissipate the energy absorbed via fluorescent downconversions [13, 22]. Besides, the contribution of downconverted energy toward the degradation of material is very negligible, when compared to much stronger and higher energy reaching the sample from solar irradiation (in the absence of ESIPT effects).

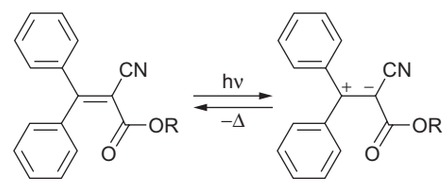


Fig. 5.4 Structural changes leading to energy dissipation in cyanoacrylates. Reproduced from M. Zayat, P. Garcia-Parejo, D. Levy, Preventing UV-light damage of light sensitive materials using a highly protective UV-absorbing coating, Chem. Soc. Rev. 36 (2007) 1270–1281 with permission of the Royal Society of Chemistry.

Although organic UV absorbents operating via ESIPT effects are known to offer high photo-stabilities. Yet, when these molecules are loaded into polar polymers, the intramolecular hydrogen bonding

within the organic molecules is distributed and new intermolecular hydrogen bonds are formed between the introduced UV absorbent and the polymer host. It is this disruption in intramolecular hydrogen bonding that leads to increased photo-reactivity and decreased photo-stability [17, 23].

Similarly, polymer films and/or sheets containing organic UV absorbents or stabilizers present high optical clarities and improved mechanical performance. Yet, they often suffer from low photo-stabilities and related photo-bleaching effects. In simpler terms, polymer-capped organic molecule associated UV-protective materials suffer from photo-stability issues, while organic UV absorbents, when integrated into the polymer host, may present inconvenience related to the photo-bleaching effects. However, in the case of polymers doped with organic UV stabilizers, the free radicals generated during the photo-oxidative reactions could destroy the active form of the stabilizer, thereby bringing down the effectiveness of the UV-protective material.

Even if mechanically flexible and visibly clear polymer-based UV-protective materials containing organic UV absorbers do not spoil the polymer host, the durability of the protective action is limited, which devalues its usefulness. This in turn has paved way for inorganic nanofiller introduced polymer-based mechanically flexible composites for optical and optoelectronic applications [10, 24, 25]. Besides, most optical applications demand UV shielding polymer nanocomposites with appreciable optical clarities. Consequently, various researchers have explored diverse inorganic filler/polymer combinations for UV shielding applications [26].

5.2.2.2 Polymer-based UV-protective materials containing inorganic UV absorbers

The tribulations related to photo-stabilities of organic UV absorbents paved the way for intensive research efforts on inorganic nanofiller introduced polymer-based mechanically flexible UV shieldants. Such organic (polymer)-inorganic (noncarbonaceous filler) nanocomposites (NCs) represent a new class of material hybrids that endows excellent optical, electrical, and mechanical behaviors [27–32].

The UV protective effects of inorganic materials are based on optical scattering and/or absorption principle. Further, UV protection via optical scattering is predominant when the size of the inorganic material is of the same order as that of the wavelength of incident light. However, optical absorption leading to the promotion of electrons from the conduction band of the inorganic UV absorbent to the valence band occurs when the photonic energy of the incident light is equal to the optical bandgap of the inorganic UV absorbent.

Of all the inorganic materials available, ceramic powders, including oxides, nitrides, and silicates, with superior phase homogeneities and lower densification temperatures are among the most attractive inorganic reinforcements. Of which, metal oxide nanofillers have attracted considerable research interest, owing to the fact that, they form a large diversity of oxides that can adopt varied structural geometries with unique electronic band structures [33]. Plus, with the decrease in particle size, the so-called quantum confinement effect also occurs, arising from the presence of atom-like electronic states, which brings about substantial changes in the electronic band structures and exciton energies [34, 35]. It is this opportunity to engineer the electronic band structures and hence, the resultant optical bandgap of metal oxides via thoughtful size and morphology tuning, that renders metal oxide nanofillers as among the most sought after inorganic UV absorbents. Table 5.1 presents the performance metrics of some of the important inorganic nanofiller introduced polymer-based UV protective materials.

However, the choice of appropriate metal oxide nanofiller for UV blocking applications depends on its optical energy gap (E_g), color, morphology, and average particle size. As E_g decides the wavelength of UV radiation to be filtered, color decides whether the developed UV protective material is optical clear while the particle size and morphology decide the nature and extent of the UV protective effects.

Further, most of the inorganic nanofiller loaded polymer-based UV protective materials operate via considerate downconversion of high-energy UV radiation into relatively lesser-energy visible light via fluorescent emission [50]. Such UV to visible photonic downconverting materials are established to operate on the basis of Förster resonant energy transfer (FRET) between the polymer host and the introduced nanofiller. One such freestanding UV protective polymer-based NC (PVA/Na_2ZnO_2) thick sheet that operates via the spectral downconversion principle was reported by Sachhidananda et al. [47]. They observed that the said NC selective converts high-energy UVA radiation (385 nm) to relatively lesser-energy visible light (630–660 nm) (Fig. 5.5).

Going forward, Nithin et al., Shilpa et al., and Suma et al. reported similar UV protective effects using PVA/Rb_2ZnO_2, $PVA/Na_2Dy_2O_4$, and $PVA/Ce_{0.5}Zr_{0.5}O_2$ NC thick films, respectively [48, 51, 52].

All these studies supported that upon excitation with UV radiations of appropriate energies, the doable energy transfer between the organic polymer and inorganic nanofiller may enable the transition of photo-generated electrons from the lowest unoccupied molecular orbital (LUMO) of the polymer to the conduction band (CB) of the nanofiller [53].

Further, Nithin et al. introduced a novel UVA-transilluminator-based visual inspection approach (the first of its kind) to establish

Table 5.1 Performance metrics of some of inorganic nanofiller introduced polymer-based UV protective materials.

Sl. No.	Polymer	Nanofiller	Emission maximum (nm)	Absorption maximum (nm)	Stokes shift (nm)	UV shielding efficacy (%)	Ref.
1.	Polyvinyl alcohol	ZnO	364	300	64	> 95	[36]
2.	Polyvinyl alcohol	Graphene Oxide (GO)	500	300	200	97.5	[37]
3.	Polyurethane	ZnO	500	360–460	40–140	45.16	[38]
4.	Epoxy	CeO_2	550	318	232	90	[39]
5.	Poly (L-lactide)	ZnO	360	315	45	61	[40]
6.	Fluorinated hyperbranched polyimides	TiO_2	800	665	135	27	[41]
7.	Polystyrene	ZnO	500	360	140	99	[42]
8.	Epoxy	ZnO	800	320	480	96	[42]
9.	Polyvinyl alcohol	S-GO	550	300	250	95	[43]
10.	Poly(methyl methacrylate)	ZrO_2	550	200–400	150–350	85	[43]
11.	PDMS	TiO_2	550	200–400	150–350	70	[43]
12.	Polystyrene	ZnO	550	200–300	250–350	50	[43]
13.	Poly(methyl methacrylate)	TiO_2	550	–	–	30	[43]
14.	Polyimide	TiO_2	550	–	–	–	[43]
15.	Poly(methyl methacrylate)	TiO_2	480–700	200–300	280–400	70	[44]
16.	Poly(methyl methacrylate)	ZnO	340	300	40	–	[45]
17.	PC	Cs_2ZnO_2	480	305	175	–	[46]
18.	Polyvinyl alcohol	Na_2ZnO_2	630	385	245	–	[47]
19.	Polyvinyl alcohol	Rb_2ZnO_2	584	380	196	–	[48]
20.	Polyvinyl alcohol	Cs_2ZnO_2	530	380	150	–	[49]

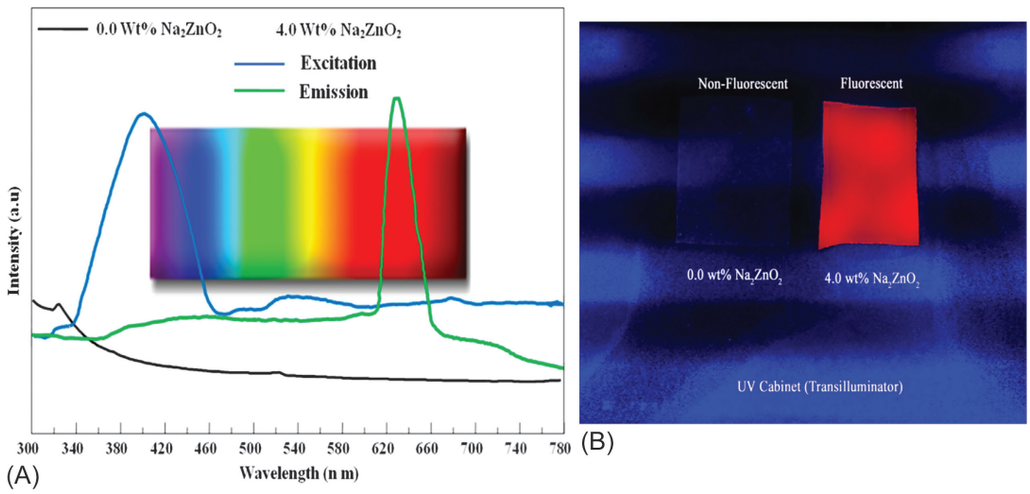


Fig. 5.5 UV protective PVA/Na_2ZnO_2 NC that operates via the fluorescent downconversion principle. (A) Synchronous excitation and emission (fluorescent) spectrum depicting large Stokes shift; and (B) UV-transilluminator images of NC films showing visible orange-red emission. Reproduced from S. Sachhidananda, K.S. Nithin, K.N. Shilpa, H. Siddaramaiah, Orange–red fluorescent polymer nanocomposite films with large stokes shift: an opto–electronic exercise, J. Lumin. 208 (2018) 488–494 with permission of Elsevier.

the spectral downconversion abilities and hence, the UV shielding efficacies of PVA NC films. The adopted approach offers clear visual evidence for the novel fluorescence behaviors of NC films. The UVA-transilluminator-based fluorescence measurements were well supported by fluorescence microscopic studies [54]. Fig. 5.6 supports the UV protective behaviors of PVA/4 wt% $Ca_{0.2}Zn_{0.8}O$ NC film, ascertained via fluorescence quenching of PVA/4 wt% Cs_2ZnO_2 NC film.

Similarly, Jagajeevanraj et al. and Sachhidananda et al. improved the UV endurance of PVA and PC using $Al_{0.2}Y_{1.8}O_3$ and Cs_2ZnO_2 nanofillers, respectively [46, 55]. Both these studies supported that the increase in UV endurance and reduced UV aging of the host polymer were due to the metal oxide nanofiller assisted energy drain. In simpler terms, when E_g of the inorganic nanofiller matches the photonic energy of UV light, it shields the polymer matrix from high-energy UV flux. It also offers a number of deexcitation pathways, which in turn brings down the probability of undesirable photo-activated reactions [46, 55].

Such designed flexible smart materials that bring about effective spectral downconversions are of considerable interest for solid-state lighting applications. Additionally, light-emitting polymer NC films also offer numerous promising applications similar to semiconductor nanoparticles, such as photo-anode in high-efficiency dye-sensitized solar cells, light-emitting diodes, mechanically flexible UV sensors, and so forth.

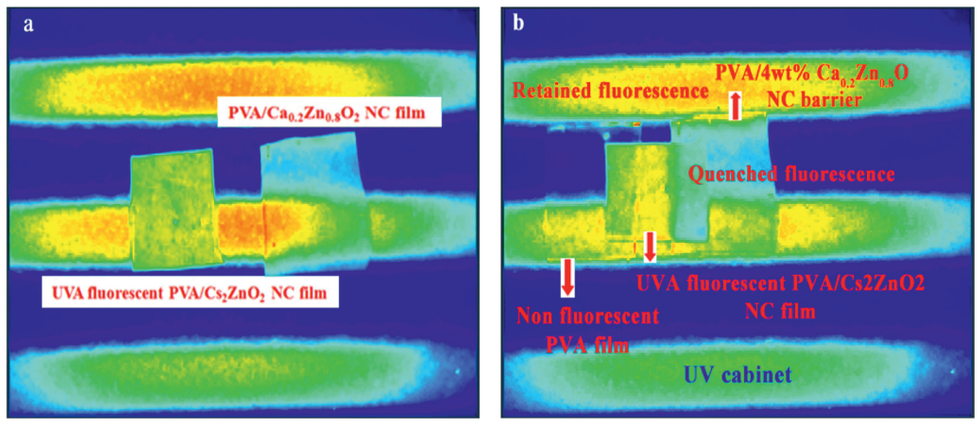


Fig. 5.6 UV protective behaviors of PVA/4 wt% $Ca_{0.2}Zn_{0.8}O$ NC film, ascertained via fluorescence quenching of PVA/4 wt% Cs_2ZnO_2 NC film. (A) UVA florescent PVA/4 wt% Cs_2ZnO_2 and PVA/4 wt% $Ca_{0.2}Zn_{0.8}O$ NC film; and (B) Demonstration of UVA shielding effects of PVA/4 wt% $Ca_{0.2}Zn_{0.8}O$ NC film via fluorescence quenching. Reproduced from K.S. Nithin, S. Kasargod Nagaraj, S. Shivanna, H. Siddaramaiah, Highly flexible and visibly transparent poly (vinyl alcohol)/calcium zincate nanocomposite films for UVA shielding applications as assessed by novel ultraviolet photon induced fluorescence quenching, Macromolecules 49 (2016) 2791–2801 with permission of The American Chemical Society.

Finally, an ideal polymer-based UV protective material must have high transparency in the visible regions and steep absorption in the UV regions. Thus, several factors such as the particle size of the inorganic nanofiller being introduced, the refractive index match between the inorganic nanofiller and the polymer host, optical absorption response of the inorganic nanofiller and the polymer host, and potential interaction of the components within the inorganic–organic hybrid decide the overall successfulness of the resulting inorganic nanofiller loaded polymer-based UV protective materials [56–60].

5.3 Imperative requirements toward developing mechanically flexible and visibly transparent UV protective materials

5.3.1 Inorganic nanofiller related factors

Most optical applications of UV protective materials demand high optical transparency in the visible region and steep absorption in the UV region. All factors that contribute to an increase in UV absorption and retention in visible transparencies (negligible visible light absorption and/or scattering) of the host polymer are of considerable interest.

Further, the optical clarity of polymer-based UV protective materials is measured via the transmission of visible light. Accordingly, various inorganic nanofiller-related factors such as optical response

(E_g, UV, and visible photonic absorption coefficient), particle size, and their relative dispersions in the host polymer are crucial in deciding the technological success of inorganic nanofiller introduced polymer-based UV protective materials.

5.3.1.1 Effect of nanofiller size and refractive index matching

The particle size and refractive index of inorganic nanofiller are very crucial towards developing optically transparent UV protective polymer nanocomposites (PNCs). As the intensity of scattered light is a direct function of particle size and difference in the refractive index between the inorganic nanofiller and the organic polymer, as described by Rayleigh's theory;

$$\frac{I_t}{I_o} = e^{-\left[\frac{3\phi_p x r^3}{4\lambda^4}\left(\frac{n_p}{n_m}-1\right)\right]} \tag{5.1}$$

where I_o and I_t are the intensity of incident and transmitted light, r is the radius of nanofiller (assuming it to be spherical), n_p and n_m are the refractive index of filler and matrix respectively. While, λ is the wavelength of incident light, ϕ_p is the volume fraction of the particle, and x is the path length of light.

Further, the matrix or host polymer could be treated as a nonabsorbing homogeneous medium, through which light passes through, without any deflection. However, the addition of inorganic nanofiller may lead to a refractive index difference, which in-turn leads to optical losses via absorption and/or scattering. Also, a higher scattering intensity of visible light is associated with turbid appearance of the resulting PNC, thereby limiting its optical applications.

In general a particle size of 40 nm is the upper-limit for inorganic nanofillers to avoid optical losses in the visible region via scattering. However, if the refractive index difference between the filler and matrix are negligible, then transparency could also be achieved, even with larger (> 40 nm) sized nanofillers [54].

That is to say, if the refractive indices between the inorganic nanofiller and organic polymer match, then the scattering intensity is very much negligible and hence, is independent of nanofiller size. The same was found true by Parlak and Demir, who successfully developed UV protective PS/CeO_2NCs with appreciable visible transparency, using refractive index matching approach [61].

5.3.1.2 Volume fraction of filler and its relative orientation or arrangement

Additional factors of interest includes volume fraction of the filler in the polymer host and path length (maximum distance through

which light has to pass through), as larger filler content and higher path length also leads to transparency loss.

The arrangement of nanofillers in host polymer is also of significant interest. As, random distribution favors optical transparency and UV absorption, orderly arrangement could lead to iridescence, while uniaxially oriented nanofillers induce optical dichroism [62].

5.3.1.3 Optical response of inorganic nanofiller

Owing to the fact that, wavelength of light being absorbed depends on the electronic band structure of the material, and electronic band structure of material may suitably engineered via thoughtful particle size engineering and introduction of suitable dopants. Ideal polymer-based UV protective materials may be suitably developed via thoughtful introduction of inorganic nanofillers with optimum optical response (wide optical band gap, high UV absorption coefficient and negligible visible light absorption coefficients).

5.3.2 Host polymer related factors

Polymers that may be employed as UV protective composite hosts, must present appreciable visible transmittance (absorb minimum light in visible regions). Besides, they must also show dopant dependent material property engineering, particle stabilizing effects and allow higher ease to be processed as flexible slabs. Also, UV absorption of such polymer host (within the composite) must be avoided to prevent undesirable photo-induced chemical reactions, that could otherwise lead to loss in elasticity or yellowing of composite.

5.3.3 Composite related factors

5.3.3.1 Filler-polymer compatibilities

As transparency in a composite film could be defined as the physical property of allowing light transmission through the composite. The noncompatible chemical functionality between the polymer and nanofiller could induce transparency loss due to agglomerization. Plus, the introduced filler or the potential interaction of the components within the composite must not induce undesirable functionalities such as photocatalytic effects. As some of the semiconductor nanofillers, when introduced into the polymer promotes unwanted photo-oxidative reactions. In such cases, the nature of filler-polymer interaction must be considerately engineered to induce photostabilization effects [63].

Besides, thickness of the resultant PNC is also critical, as increase in thickness is found to increase the path length of light and hence, lessen the transparency. Further, transparency could only be kept

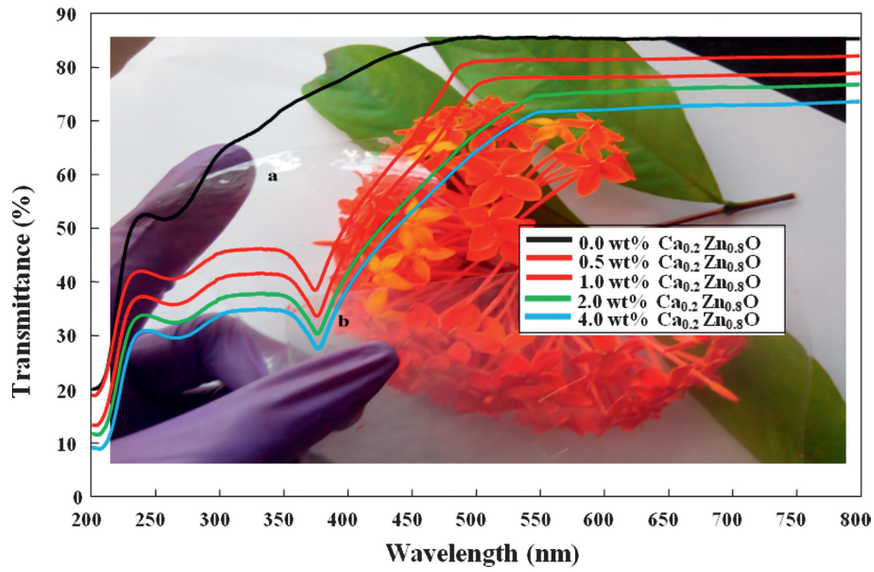


Fig. 5.7 Visibly transparent and UV protective PNC. Background: Digital photographs of 0.3 ± 0.03 mm thick (A) PVA/2 wt% $Ca_{0.2}Zn_{0.8}O$; and (B) PVA/4 wt% $Ca_{0.2}Zn_{0.8}O$NC film. Reproduced from K.S. Nithin, S. Kasargod Nagaraj, S. Shivanna, H. Siddaramaiah, Highly flexible and visibly transparent poly (vinyl alcohol)/calcium zincate nanocomposite films for UVA shielding applications as assessed by novel ultraviolet photon induced fluorescence quenching, Macromolecules 49 (2016) 2791–2801 with permission of The American Chemical Society.

in the form of films (mm scale thickness); but difficult in bulk form (cm scale thickness), as the increased thickness leads to opaqueness and/or translucence [64]. One such visibly clear UV protective PNC film of 0.33-mm thickness was developed by Nithin et al., using size reduced nanoparticles and particle stabilizing polymer approach (Fig. 5.7).

Further, dispersion of introduced filler is another imperative factor as homogeneous filler dispersions result in higher transparency and increased UV shielding effects. Also decrease in particle size, facilitates a more homogeneous filler distribution, larger filler/polymer interfacial area and hence, greater property enhancement. However, smaller size may lead to higher surface areas and hence, increased agglomerization and decreased transparency. Thus the development of synthetic methods avoiding the formation of inorganic filler aggregates, within the polymer is a key challenge.

The said challenge may be addressed either via suitable surface functionalization of nanofillers, to aid improved filler-matrix compatibilities or by adopting an in-situ polymerization approach, which allows the successful generation of particles and their subsequent embedding on the polymer host [65–67].

5.4 Surface engineering and in-situ polymerization approaches toward developing mechanically flexible and visibly transparent polymer-based UV protective materials

Owing to size reduction induced increased polymer-filler interfacial areas, surface energy adds an important contribution for stabilization phenomenon. It is this higher interfacial energies, that lead to inappropriate polymer-filler chemistries and hence, a loss is functional properties. Thus, in order to lessen the interface energies between nanofiller and the host polymer, various surface functionalization and stabilizing techniques are to be suitably adopted. Besides, an ideal surface modifier must possess an anchoring group, which binds the modifier on the nanofiller surface, while the other part of the modifier interact with the polymer and hence, reduce the surface energies. Such an energy reduction often leads to better filler-polymer chemistries and hence, augmented material performance.

The same has been found true by Matsuno et al., who reported 10 times more UV shielding effects with surface modified TiO_2 nanofillers in PS, in comparison to unmodified TiO_2 introduced PS [68]. While, Li et al. obtained thicker transparent ZnO/PMMA NC film, when dispersed in the presence of a coupling agent through sol-gel polymerization technique [69].

Besides, direct chemical mixing and melt processing of inorganic nanofillers with polymer often results in gradients of introduced fillers in the host polymer and hence, leads to agglomerization induced optical losses.

Thus, in-situ polymerization and in-situ nanoparticle formation techniques that provide an inherent homogeneity of the structures synthesized, overcoming the problem of agglomerization, even upon using higher concentration nanofillers are the most preferred.

However, the commercial success of this transparent PNC film development technique demands certain prerequisites. Which includes, a careful control of the interaction of inorganic building blocks with the host polymers, at molecular levels. Plus, improved compatibility of the particle synthesis media with the solvent, where the polymer is dissolved, which successfully avoids precipitation of the assembly and related agglomerizations.

5.5 Conclusions and future directions

Although the advent of nanotechnology, availability of advanced characterization tools and dopant dependent end properties of polymers offer enormous scope towards the development of various hybrid

inorganic-organic materials for UV protective applications. Yet, the successful development of mechanically flexible and visibly clear UV protective films demand various important filler, polymer and composite related properties to be suitably engineered. Thus, to draw the total commercial potential of such hybrids, future work should focus on scaling up these hybrid structures and evaluating the weathering stabilities of such materials to enable real-time operational applications.

References

[1] G.T. Wondrak, M.K. Jacobson, E.L. Jacobson, Endogenous UVA-photosensitizers: mediators of skin photodamage and novel targets for skin photoprotection, Photochem. Photobiol. Sci. 5 (2006) 215–237.

[2] E. Yousif, R. Haddad, Photodegradation and photostabilization of polymers, especially polystyrene, Springerplus 2 (2013) 398.

[3] K.S. Nithin, S. Sachhidananda, K.N. Shilpa, S. Chinmayee, S. Basavarajaiah, Poly (vinyl alcohol) decorated lithium doped stannous oxide nanocomposites as highly flexible UVA shieldants, Chem. Sci. J. 7 (2016) 121.

[4] A. Amaro-Ortiz, B. Yan, J.A. D'Orazio, Ultraviolet radiation, aging and the skin: prevention of damage by topical cAMP manipulation, Molecules 19 (2014) 6202–6219.

[5] K.N. Shilpa, H.B. Patil, P. Karthik, K. Mallikarjun, B.M. JagajeevanRaj, S. Sharon, K.S. Nithin, Removal of Cu (II) from water using hydrothermally synthesized strontium doped zirconium oxide nano adsorbents, J. Mater. Sci. Eng. 1 (2016) 252–256.

[6] K.N. Shilpa, S.R. Urs, H.B. Patil, H.P. Jayadevappa, B.V. Latha, K.S. Nithin, S. Sachhidananda, Adsorptive removal of Cu (II) from aqueous solution using nanostructured lithium zincate, Int. J. Eng. Sci. Comput. 6 (2016) 8463–8468.

[7] H.B.V. Patil, K.S. Nithin, S. Sachhidananda, Siddaramaiah, K.T. Chandrashekara, B.Y.S. Kumar, Mycofabrication of bioactive silver nanoparticle: photo catalysed synthesis and characterization to attest its augmented bio–efficacy, Arab. J. Chem. 12 (2019) 4596–4611.

[8] P. Sivadasu, D.V. Gowda, N.K. Subramani, B.M. Vishweshwaraiah, S. Shivanna, S. Hatna, Direct brain targeted nanostructured lipid carriers for sustained release of schizophrenic drug: formulation, characterization and pharmacokinetic studies, Indian J. Pharm. Educ. Res. 54 (2020) 73–84.

[9] G.R. Suma, K.S. Nithin, B.V. Latha, S.K. Nagaraj, S. Shivanna, S.V. Sathyanarayana, Gent to refractive index engineering of strontium doped zirconium oxide (szo) reinforced poly vinyl pyrrolidone composite films: effect of dopant content and annealing temperature, Int. J. Eng. Sci. Comput. 6 (2016) 5703–5709.

[10] M.Q.A. Al-Gunaid, A.M.N. Saeed, K.S. Nithin, B.S. Madhukar, Siddaramaiah, Optical parameters, electrical permittivity and I–V characteristics of PVA/Cs_2CuO_2 nanocomposite films for opto–electronic applications, J. Mater. Sci. Mater. Electron. 28 (2017) 8074–8086.

[11] M. Mosquera, J.C. Penedo, M.C. Ríos Rodríguez, F. Rodríguez-Prieto, Photoinduced inter-and intramolecular proton transfer in aqueous and ethanolic solutions of 2-(2′-hydroxyphenyl) benzimidazole: evidence for tautomeric and conformational equilibria in the ground state, J. Phys. Chem. 100 (1996) 5398–5407.

[12] G. Woessner, G. Goeller, P. Kollat, J.J. Stezowski, M. Hauser, U.K. Klein, H.E. Kramer, Photophysical and photochemical deactivation processes of ultraviolet stabilizers of the (2-hydroxyphenyl) benzotriazole class, J. Phys. Chem. 88 (1984) 5544–5550.

[13] W. Klöpffer, Intramolecular proton transfer in electronically excited molecules, Adv. Photochem. 10 (1977) 311–358.
[14] K.P. Ghiggino, A.D. Scully, I.H. Leaver, Effect of solvent on excited-state intramolecular proton transfer in benzotriazole photostabilizers, J. Phys. Chem. 90 (1986) 5089–5093.
[15] J.E.A. Otterstedt, Photostability and molecular structure, J. Chem. Phys. 58 (1973) 5716–5725.
[16] J. Keck, M. Roessler, C. Schroeder, G.J. Stueber, F. Waiblinger, M. Stein, D. Le-Gourrierec, H.E.A. Kramer, H. Hoier, S. Henkel, P. Fischer, H. Port, T. Hirsch, G. Rytz, P. Hayoz, Ultraviolet absorbers of the 2-(2-Hydroxyaryl)-1,3,5-triazine class and their methoxy derivatives: fluorescence spectroscopy and x-ray structure analysis, J. Phys. Chem. B 102 (1998) 6975–6985.
[17] J. Pospısil, S. Nespurek, Photostabilization of coatings. Mechanisms and performance, Prog. Polym. Sci. 25 (2000) 1261–1335.
[18] M.E. Calvo, J.R. Castro Smirnov, H. Míguez, Novel approaches to flexible visible transparent hybrid films for ultraviolet protection, J. Polym. Sci. B Polym. Phys. 50 (2012) 945–956.
[19] G. Rudko, A. Kovalchuk, V. Fediv, W.M. Chen, I.A. Buyanova, Enhancement of polymer endurance to UV light by incorporation of semiconductor nanoparticles, Nanoscale Res. Lett. 10 (2015) 1–6.
[20] N. Grassie, G. Scott, Polymer Degradation and Stabilisation, CUP Archive, 1988.
[21] S.H. Hamid, Handbook of Polymer Degradation, CRC Press, 2000.
[22] S. Carturan, A. Quaranta, G. Maggioni, A. Vomiero, R. Ceccato, G. Della Mea, Optical study of the matrix effect on the ESIPT mechanism of 3-HF doped sol-gel glass, J. Sol-Gel Sci. Technol. 26 (2003) 931–935.
[23] P.F. McGarry, J. Steffen, F. Yoshihisa, A.P. Nikolas, J.T. Nicholas, DMSO Solvent induced photochemistry in highly photostable compounds. The role of intermolecular hydrogen bonding, J. Phys. Chem. A 101 (1997) 764–767.
[24] S.K. Nagaraj, S. Shivanna, N.K. Subramani, H. Siddaramaiah, Revisiting powder X–ray diffraction technique: a powerful tool to characterize polymers and their composite films, J. Mater. Sci. 4 (2016) 1–5.
[25] T. Champa, S. Sachhidananda, K.N. Shilpa, K.S. Nithin, Siddaramaiah, Optoelectronic behaviors of reversibly stretchable $Na_{0.8}Mn_{0.8}O_2$ reinforced poly(vinyl alcohol) nanocomposites, Int. J. Eng. Sci. Comput. 7 (2017) 14875–14879.
[26] K.S. Nithin, S. Sachhidananda, K.N. Shilpa, B. Suresha, H. Siddaramaiah, Optoelectronic behaviours of UV shielding calcium zirconate reinforced polycarbonate nanocomposite films: an optical view, Mater. Today 5 (2018) 16626–16632.
[27] Mahesha, K.M. Subbaiah, K.S. Nithin, B.M.J. Raj, S. Shivanna, Highly flexible and conducting polymer nanocomposite films for selective gas sensing applications, Mater. Today Proc. 9 (2019) 515–521.
[28] B. Suresha, K. Adappa, N.K. Subramani, Mechanical and tribological behaviours of epoxy hybrid composites reinforced by carbon fibers and silicon carbide whiskers, Mater. Today Proc. 5 (2018) 16658–16668. Elsevier.
[29] S. Sachhidananda, G.R. Suma, K.S. Nithin, S.V. Satyanarayana, Siddaramaiah, Tuning the electrical and thermal functionalities of mechanically flexible poly (vinyl alcohol) nanocomposites: effect of cerium zirconate nanofiller content, Int. J. Eng. Sci. 1 (2019) 8–14.
[30] K.S. Nithin, S. Shivanna, S.K. Nagaraj, H. Siddaramaiah, Refractive index engineering of poly(vinylalcohol)/Li_2ZnO_2 nanocomposites: effect of filler content and annealing temperature, AIP Conf. Proc. 1943 (2018) 020127–020128.
[31] B. Suresha, R. Hemanth, K.S. Nithin, Automotive Applications: Reinforced Material Components, Encyclopedia of Polymer Applications, CRC Press, 2018.
[32] M.V. Bhavya, D.V. Gowda, S. Praveen, N.K. Subramani, H. Siddaramaiah, Cosmetics: polymers, in: Encyclopedia of Polymer Applications, first ed., T&F, 2018.

[33] S.S. Ray, Environmentally Friendly Polymer Nanocomposites: Types, Processing and Properties, Elsevier, 2013.
[34] T. Takagahara, K. Takeda, Theory of the quantum confinement effect on excitons in quantum dots of indirect-gap materials, Phys. Rev. B Condens. Matter 46 (1992) 15578.
[35] D.S. Kumar, B.J. Kumar, H.M. Mahesh, Quantum nanostructures (QDs): an overview, in: Synthesis of Inorganic Nanomaterials, Elsevier, Woodhead Publishing, 2018.
[36] M.S. Augustine, P.P. Jeeju, V.G. Sreevalsa, S. Jayalekshmi, Excellent UV absorption in spin-coated thin films of oleic acid modified zinc oxide nanorods embedded in polyvinyl alcohol, J. Phys. Chem. Solids 73 (2012) 396–401.
[37] S. Xie, J. Zhao, B. Zhang, Z. Wang, H. Ma, C. Yu, M. Yu, L. Li, J. Li, Graphene oxide transparent hybrid film and its ultraviolet shielding property, ACS Appl. Mater. Interfaces 7 (2015) 17558–17564.
[38] H. Wang, W. Lin, X. Qiu, F. Fu, R. Zhong, W. Liu, D. Yang, In situ synthesis of flowerlike lignin/ZnO composite with excellent UV-absorption properties and its application in polyurethane, ACS Sustain. Chem. Eng. 6 (2018) 3696–3705.
[39] N.N. Dao, M. Dai Luu, Q.K. Nguyen, B.S. Kim, UV absorption by cerium oxide nanoparticles/epoxy composite thin films, Adv. Nat. Sci. Nanosci. Nanotechnol. 2 (2011) 045013.
[40] E. Lizundia, L. Ruiz-Rubio, J.L. Vilas, L.M. Leon, Poly (l-lactide)/ZnO nanocomposites as efficient UV-shielding coatings for packaging applications, J. Appl. Polym. Sci. 133 (2016) 42426.
[41] L. Qing, S. Zhang, G. Liao, C. Yi, Z. Xu, Novel fluorinated hyperbranched polyimides with excellent thermal stability, UV-shielding property, organosolubility, and low dielectric constants, SAGE J. 30 (2017) 872–886.
[42] Y.Q. Li, S.Y. Fu, Y.W. Mai, Preparation and characterization of transparent ZnO/epoxy nanocomposites with high-UV shielding efficiency, Polymer 47 (2006) 2127–2132.
[43] Y. Wang, J. Su, T. Li, P. Ma, H. Bai, Y. Xie, M. Chen, W. Dong, A novel UV-shielding and transparent polymer film: when bioinspired dopamine–melanin hollow nanoparticles join polymers, ACS Appl. Mater. Interfaces 9 (2017) 36281–36289.
[44] X. Meng, Z. Zhang, N. Luo, S. Cao, M. Yang, Transparent poly (methyl methacrylate)/TiO_2 nanocomposites for UV-shielding applications, Polym. Sci. Ser. A 53 (2011) 977.
[45] Y. Zhang, S. Zhuang, X. Xu, J. Hu, Transparent and UV-shielding ZnO@ PMMA nanocomposite films, Opt. Mater. 36 (2013) 169–172.
[46] S. Shivanna, K.S. Nithin, K.N. Shilpa, J.R.B. Mutturaj, S. Basavaraj, Patina–green coloured light emitting polycarbonate films: a synergistic extraction of improved UV endurance and considerate spectral down–conversion, J. Lumin. 210 (2019) 276–284.
[47] S. Sachhidananda, K.S. Nithin, K.N. Shilpa, H. Siddaramaiah, Orange–red fluorescent polymer nanocomposite films with large stokes shift: an opto–electronic exercise, J. Lumin. 208 (2018) 488–494.
[48] K.S. Nithin, K.N. Shilpa, S. Sachhidananda, H. Siddaramaiah, Yellow–green luminescent poly (vinyl alcohol) nanocomposite thick films as effective spectral manipulators, J. Appl. Polym. Sci. 135 (2018) 46854.
[49] K.S. Nithin, Siddaramaiah, Opto–electrical characteristics of poly (vinyl alcohol)/cesium zincate nanodielectrics, J. Phys. Chem. C 119 (2015) 20244–20255.
[50] K.S. Nithin, Polymer nanocomposites as luminescent down shifting layers, Res. Rev. J. Mater. Sci. 4 (4) (2016) 6.
[51] K.N. Shilpa, K. Subramani, S. Sachhidananda, B.S. Madhukar, Visibly transparent PVA / sodium doped dysprosia ($Na_2Dy_2O_4$) nano composite films, with high refractive index: an optical study, J. Alloys Compd. 694 (2017) 884–891.

[52] G.R. Suma, K.S. Nithin, K.N. Shilpa, S. Sachhidananda, V.S. Satyanarayana, Effect of $Ce_{0.5}Zr_{0.5}O_2$ nanofillers on structural and optical behaviors of poly (vinyl alcohol), J. Mater. Sci. Mater. Electron. 28 (2017) 10707–10714.
[53] H.M. Xiong, Z.D. Wang, D.P. Xie, L. Cheng, Y.Y. Xia, Stable polymer electrolytes based on polyether-grafted ZnO nanoparticles for all-solid-state lithium batteries, J. Mater. Chem. 16 (2006) 1345–1349.
[54] K.S. Nithin, S. Kasargod Nagaraj, S. Shivanna, H. Siddaramaiah, Highly flexible and visibly transparent poly (vinyl alcohol)/calcium zincate nanocomposite films for UVA shielding applications as assessed by novel ultraviolet photon induced fluorescence quenching, Macromolecules 49 (2016) 2791–2801.
[55] B.M. Jagajeevanraj, S. Sachhidananda, K. Pushpalatha, K.S. Nithin, Nanostructured $Al_{0.2}Y_{1.8}O_3$ semiconductor assisted enhancement in PVOH fortitude to withstand high energy UV photons: an opto–mechanical study, Optik 182 (2019) 598–604.
[56] D. Kundu, R. Mukherjee, UV absorbing transparent sol-gel derived coatings on glass, J. Mater. Sci. Lett. 22 (2003) 1647–1649.
[57] H. Sakamoto, J. Qiu, A. Makishima, The preparation and properties of CeO_2–TiO_2 film by sol–gel spin-coating process, Adv. Mater. 4 (2003) 69–76.
[58] D. Levy, D. Avnir, F. Del Monte, Sunscreens for protection from sun irradiation, Intl. Patent Application PCT/IL/98/00021 WO 98/31333.
[59] N. Lapidot, O. Gans, F. Biagini, L. Sosonkin, C. Rottman, Advanced sunscreens: UV absorbers encapsulated in sol-gel glass microcapsules, J. Sol-Gel Sci. Technol. 26 (2003) 67–72.
[60] A. Jaroenworaluck, W. Sunsaneeyametha, N. Kosachan, R. Stevens, Characteristics of silica-coated TiO_2 and its UV absorption for sunscreen cosmetic applications, Surf. Interface Anal. 38 (2006) 473–477.
[61] O. Parlak, M.M. Demir, Toward transparent nanocomposites based on polystyrenematrixand PMMA-grafted CeO_2 nanoparticles, ACS Appl. Mater. Interfaces 3 (2011) 306–314.
[62] W. Caseri, Nanocomposites of polymers and metals or semiconductors: historical background and optical properties, Macromol. Rapid Commun. 21 (2000) 705–722.
[63] R. Yang, P.A. Christensen, T.A. Egerton, J.R. White, Degradation products formed during UV exposure of polyethylene ZnO nano-composites, Polym. Degrad. Stab. 95 (2010) 1533–1541.
[64] S. Li, M. Meng Lin, M.S. Toprak, D.K. Kim, M. Muhammed, Nanocomposites of polymer and inorganic nanoparticles for optical and magnetic applications, Nano Rev. 1 (1) (2010) 5214, https://doi.org/10.3402/nano.v1i0.5214.
[65] P.M. Ajayan, L.S. Schadler, P.V. Braun, Nanocomposite Science and Technology, Wiley-VCH, Weinheim, 2003.
[66] H.C. Van DeHulst, Light Scattering by Small Particles, John Wiley& Sons, New-York, 1957.
[67] G. Mie, Beiträge zur Optik trüber Medien, speziell kolloidaler Metallösungen, Ann. Phys. 330 (1908) 377–445.
[68] R. Matsuno, H. Otsuka, A. Takahara, Polystyrene-grafted titanium oxide nanoparticles prepared through surface-initiated nitroxide-mediated radical polymerization and their application to polymerhybrid thin films, Soft Matter 2 (2006) 415–421.
[69] S. Li, M.S. Toprak, Y.S. Jo, J. Dobson, D.K. Kim, M. Muhammed, Bulk synthesis of transparent and homogeneous polymeric hybrid materials with ZnO quantum dots and PMMA, Adv. Mater. 19 (2007) 4347–4352.

6

Photo-active polymer nanocomposite layer for energy applications

Arul Varman Kesavan and Praveen C. Ramamurthy
Department of Materials Engineering, Indian Institute of Science, Bangalore, India

6.1 Introduction

Electricity is an integral part of human society. Electricity can be obtained from both renewable and nonrenewable energy sources. Among all the renewable energy sources, solar energy technology offers numerous advantages over other renewable technologies. Organic photo-voltaic technology is one such upcoming solar energy technology aimed at satisfying the ever-mounting global energy demand. Also, the inherent advantages of organic photovoltaics, which includes flexibility to fabricate over a large area, a less-toxic fabrication process, lesser total device weight, and the ability of the device to be fabricated at relatively low temperature conditions [1–3] have all ensured increasing research on organic solar cells. Further, to achieve high power conversion efficacies, various polymer composites have been continuously explored as photoactive layers [4], charge transport layers, or charge collecting electrode materials in organic solar cells. Various materials that were explored to engineer the optoelectronic properties of solar cells include neat and functionalized graphene; graphene oxide [5]; reduced graphene oxide [6, 7]; metal nanoparticles (NPs) such as Ag, Au, Al, and so forth [8–10]; upconversion nanomaterials [11]; downconversion nanomaterials; quantum dots (CdSe, PbS); nanorods; and nanowires (NWs); of Ag and Cu, among others.

Further, the polymer composite used in organic solar cells must present appreciable optical, optoelectronic, and electrical properties, including high optical absorption, improved charge carrier mobility, appropriate spectral manipulation abilities, and so forth. Accordingly, this chapter presents the performance metrics of various natured

Polymer-Based Advanced Functional Composites for Optoelectronic and Energy Applications
https://doi.org/10.1016/B978-0-12-818484-4.00010-0
Copyright © 2021 Elsevier Inc. All rights reserved.

polymer composites (polymer-zero dimension (0D) materials, polymer-one dimensional (1D), and polymer-two dimensional (2D) materials) for solar cell applications.

6.2 Polymer-zero dimensional material composites

These composites are essentially polymer-based multiphase materials in which all dimensions of the fillers are in the nanoscale, or none of the (zero) dimensions of the filler exceed the nanometric scale. They include polymer composites containing quantum dots and/or inorganic semiconductor NPs. Some of the important polymer-zero dimensional material composites of interest in organic photovoltaics are cited below.

6.2.1 Polymer-PbS quantum dot composites

Semiconducting quantum dots are of significant interest for electronic device applications due to the fact that their physical properties may be appropriately engineered via thoughtful tuning of their size and shape. Further, the particle size and morphology of such semiconducting quantum dots may be successfully controlled by following suitable synthetic routes. Also, at the nanometric scale, these materials exhibit quantum confinement effects that in turn dictate the energy band structure and hence, the resultant optoelectronic behaviors [12]. Consequently, the appropriate size engineering of these nanomaterials may aid the quantum confinement effect controlled tuning of optical absorption and emission responses [13].

Polymer-quantum dot nanocomposites (NCs) are often adopted to achieve increased active layer mobility, to harvest infrared light, and to enhance the active layer stability in organic solar cells. Adding semiconducting nanomaterials in a polymer solar cell also reduces the mid-gap trap states, which in turn prevents bimolecular-type recombination in the device. However, care must be taken so that the optimum composition of the polymer/semiconducting quantum dots is used [14, 15]. One such hybrid polymer solar cell with a P3HT:PbS composite as the photo-active layer presented appreciable advantages over polymer/$PC_{61}BM$ or $PC_{70}BM$-based solar cells because, in the first case, the quantum dot material (PbS) also participated in the charge carrier generation.

In addition to this, the lead chalcogenide (PbS) also presents high charge carrier mobility, a broad absorption response (extends up to the infrared region), and multiple carrier generation [16–19]. Plus,

using inorganic quantum dots in a polymer solar cell increases the dielectric constant of the active layer. This enhancement prevents the recombination loss or, in other words, decreases the exciton binding energy because the current density (J) is directly related to the static dielectric constant (ε), in accordance with the Mott-Gurney equation. Also, the electron transfer time scale (a few 10^{-9} s to a few 10^{-15} s) across polymer:PbS is comparable with that of polymer:$PC_{61}BM$, which in turn favors the use of semiconducting quantum dots as an electron accepting material in hybrid polymer solar cells. Further, poly [{2,5-bis(2-hexyldecyl)-2,3,5,6-tetrahydro-3,6-dioxopyrrolo [3,4-c] pyrrole-1,4-diyl}-alt-{[2,2′-(1,4-phenylene)bis-thiophene]-5,5′-diyl} (PDPPTPT) was used as a donor material, along with a PbS quantum dot electron acceptor, for solar cell applications.

6.2.2 PEDOT:PSS-β-$NaYF_4$:Yb^{3+}/Er^{3+} upconversion NCs

Similar to any other composite studied in polymer solar cells, polymer upconversion NCs were studied in the active layer [20], transport layer [21], and the substrate [22]. The upconversion (UP) phenomenon was adopted in the polymer solar cells so as to tune the optical absorption response of the photo-active layer. This stratagem plays an important role in matching the active layer absorption response with the solar spectrum. The ITO/PEI/P3HT:$PCB_{61}M$/PEDOT:PSS:UCNP/Ag device structure was employed to investigate the upconversion process. Fig. 6.1 presents various optical responses of the said upconversion material and the corresponding device [21].

The photovoltaic properties of the device empowered with UCNCs are given in Fig. 6.2. From Fig. 6.2, it is evident that the device with a UC buffer layer shows a high short circuit current density with no change in the open circuit voltage. Herein, the polymer-UCNP composite buffer layer serves as the upconversion and light-scattering center. It is these dual phenomena at the interface that promote the light harvesting efficacies. Accordingly, the reference device showed 2.07% efficiency while the UC device showed 2.55% efficiency. Further, the detailed phenomena associated with the UC solar cell and also the particle-dependent UC process are thoughtfully presented elsewhere by Kesavan et al. [21].

6.2.3 PEDOT:PSS-aluminum NP composites

In polymer solar cells, metal NPs are continuously tried in various layers of the device, including the photo-active layer, the buffer layer, and the electrode. Plasmonic metal NPs such as Au [23, 24], Ag [25],

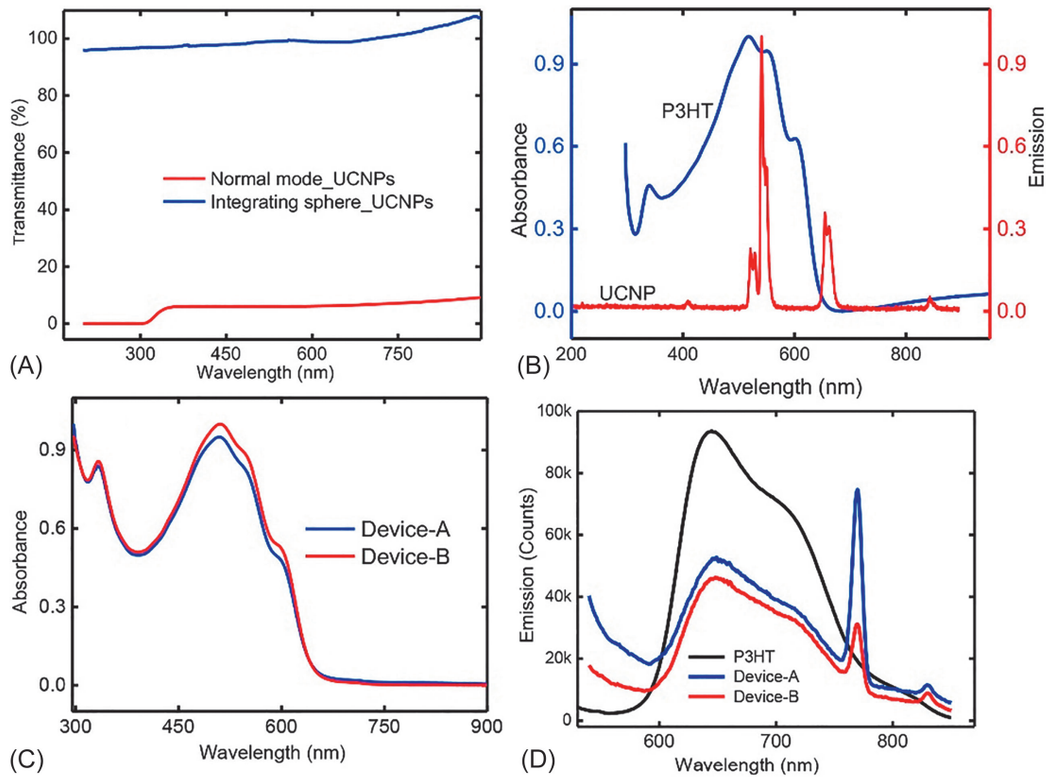


Fig. 6.1 (A) Transmittance spectra of glass/UCNPs by normal and integrated sphere mode; (B) absorption spectrum of P3HT and emission spectrum of β-$NaYF_4$:Yb^{3+}/Er^{3+} NPs; (C) UV-visible spectra of device (without Ag electrode); and (D) emission spectrum of P3HT and device (without Ag electrode). Reproduced with permission from A.V. Kesavan, M.P. Kumar, A.D. Rao, P.C. Ramamurthy, Light management through up-conversion and scattering mechanism of rare earth nanoparticle in polymer photovoltaics, Opt. Mater. 94 (2019) 286–293.

Cu [26], and Al [27] as well as the binary alloys [28] of these metals are extensively used to maximize the optical absorption responses [29]. Further, the size and shape of these NPs dictate their overall end properties; in turn, this facilitates material property engineering, supporting their increasing usage in various techno-commercial applications [30]. Figs. 6.3 and 6.4 present the performance metrics of one such device containing polymer-Al NP composites [31].

6.2.4 Polymer-silver NP composites

Silver NP is one of the most widely used materials to enable the plasmonic mechanism in solar cells. It is well known that by placing appropriate plasmonic materials, one could harness the synergistic

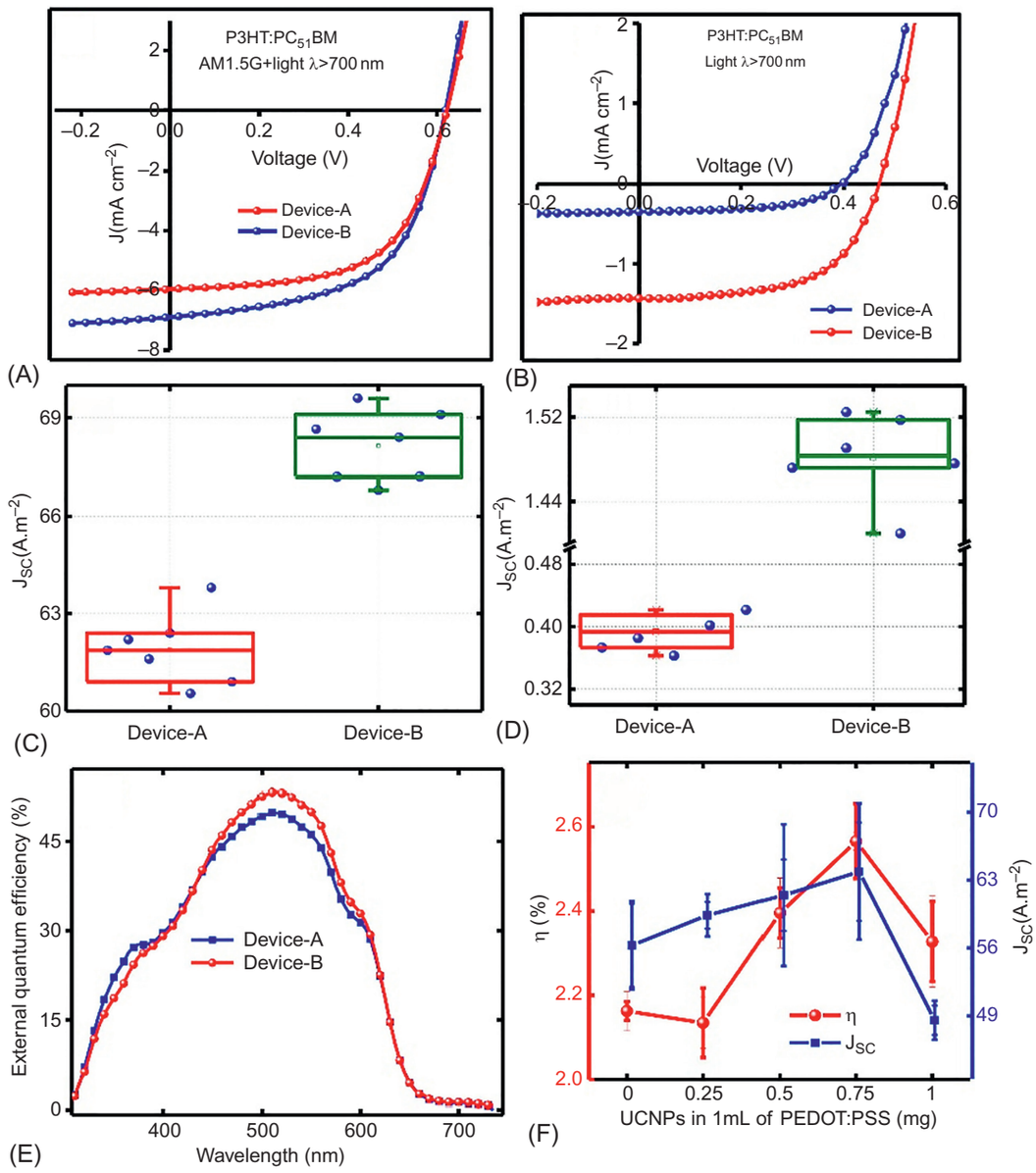


Fig. 6.2 (A) Photovoltaic characteristics of devices tested under AM1.5G + IR; (B) under IR light; (C) short circuit current density plot of devices under AM1.5G + IR; (D) under IR light; (E) EQE spectra of the devices; (F) J_{SC} and η with various β-$NaYF_4$:Yb^{3+}/Er^{3+} loading. Reproduced with permission from A.V. Kesavan, M.P. Kumar, A.D. Rao, P.C. Ramamurthy, Light management through up-conversion and scattering mechanism of rare earth nanoparticle in polymer photovoltaics, Opt. Mater. 94 (2019) 286–293.

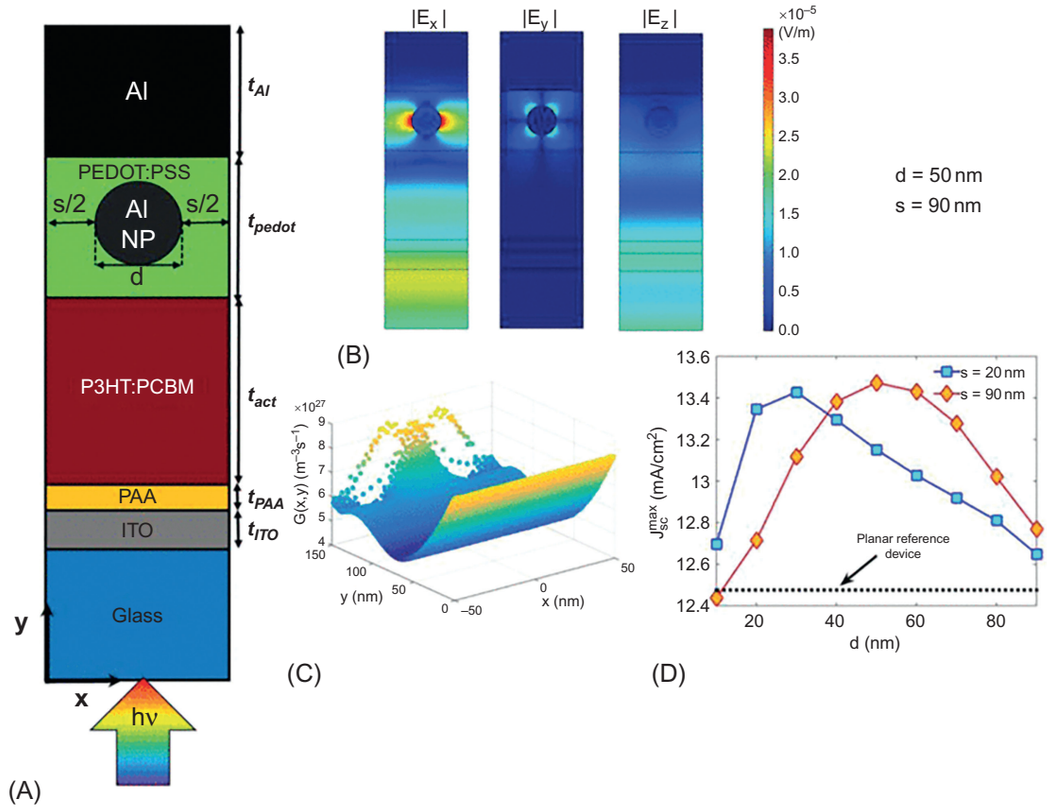


Fig. 6.3 (A) Two-dimensional device structure employed in the simulations; (B) absolute values of electric field components for $d = 50$ nm, $s = 90$ nm, and $\lambda = 500$ nm; (C) exciton generation rate profile for $d = 50$ nm and $s = 50$ nm ($x = 0$ corresponds to the bottom of the active layer); and (D) predicted maximum photo-current at short circuit for various s and d compared with the predictions for the planar reference device. Reproduced with permission from A.V. Kesavan, A.K. Jagdish, P.C. Ramamurthy, Organic inorganic hybrid hole transport layer for light management in inverted organic photovoltaic, IEEE J. Photovoltaics 7 (2017) 787–791.

advantage of far-field scattering and near-field light coupling, exhibited by the combinatorial effects of larger particles and smaller particles, respectively. Such Ag NPs were simultaneously employed in the active layer and also the buffer layer of polymer solar cells to enable the plasmonic effect [32]. One such solar cell combination that is adopted to explain the Ag NP plasmonics is presented in Fig. 6.5.

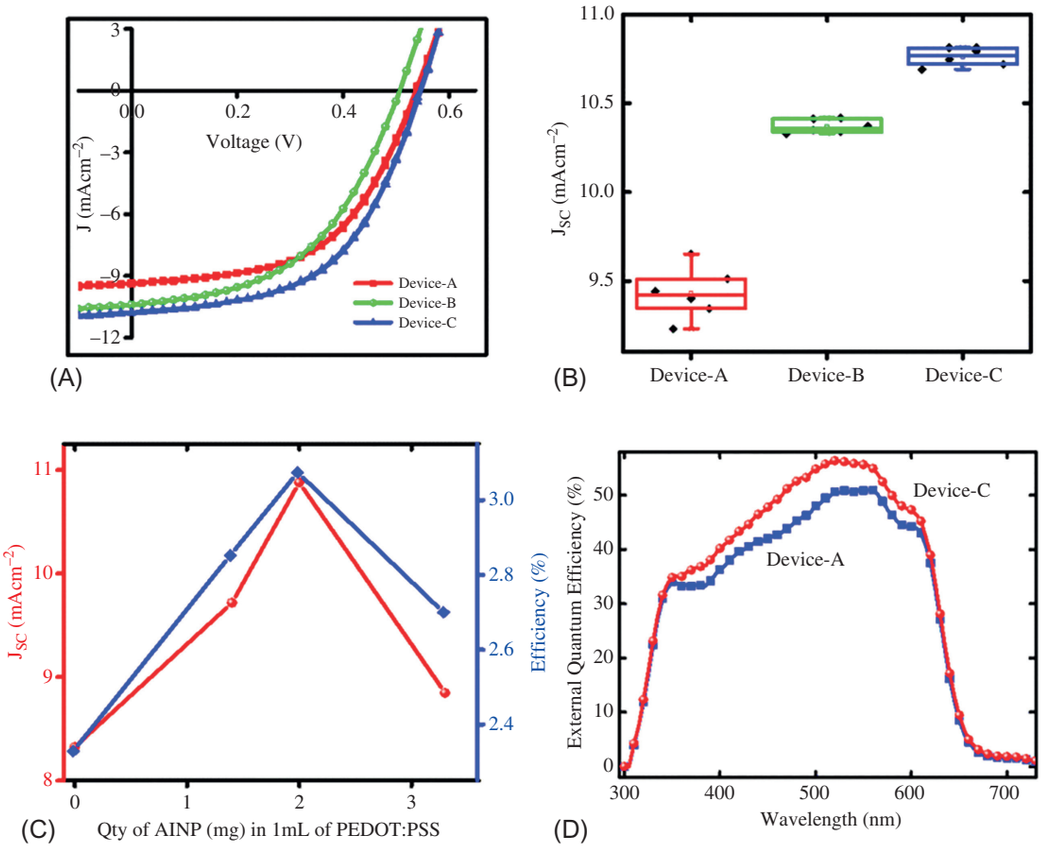


Fig. 6.4 (A) *J-V* curves of devices A, B, and C; (B) boxplot of J_{sc} for device-A, device-B, and device-C; (C) J_{sc} and efficiency of device with varying Al NP composition; and (D) external quantum efficiency spectra of device-A and device-C. Reproduced with permission from A.V. Kesavan, A.K. Jagdish, P.C. Ramamurthy, Organic inorganic hybrid hole transport layer for light management in inverted organic photovoltaic, IEEE J. Photovoltaics 7 (2017) 787–791.

The photovoltaic properties of the device with various Ag NP loadings are shown in Fig. 6.6. The 2:1 ratio PEDOT:PSS:AgNP composite offers better performance as presented by the *J-V* characteristics. Figs. 6.7 and 6.8 show the photovoltaic characteristics with the variation of Ag NPs in the active layer. From the figure, it was established that with 1% of Ag NPs in the active layer, the photovoltaic conversion efficiency was at the maximum. Fig. 6.9 depicts the EQE spectra of the devices.

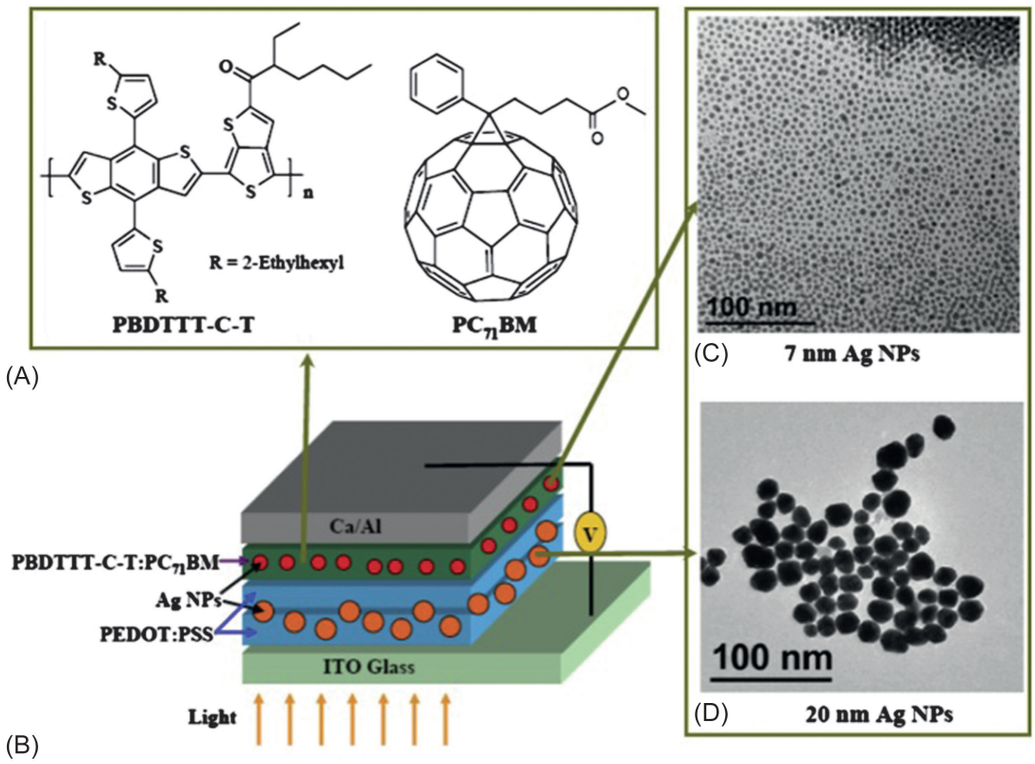


Fig. 6.5 (A) Chemical structures of PBDTTT-C-T and PC71BM; (B) schematic of the device structure; (C and D) TEM images of AgNPs; (C) 7 nm; and (D) 20 nm. Reproduced with permission from X.H. Liu, L.X. Hou, J.F. Wang, B. Liu, Z. Sen Yu, L.Q. Ma, S.P. Yang, G.S. Fu, Plasmonic-enhanced polymer solar cells with high efficiency by addition of silver nanoparticles of different sizes in different layers, Sol. Energy 110 (2014) 627–635.

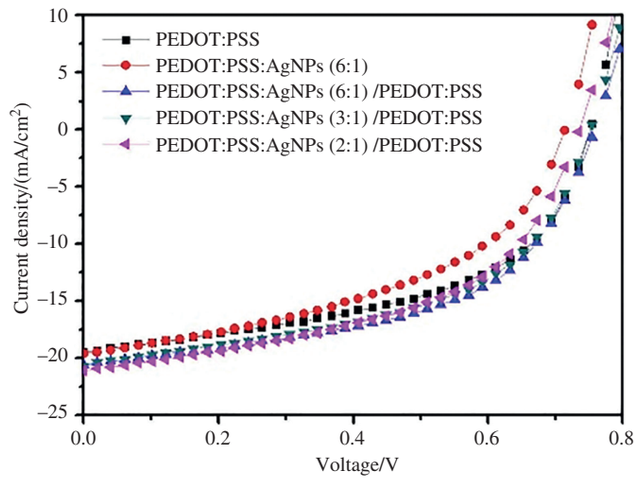


Fig. 6.6 The *J-V* curves of polymer solar cells embedded with Ag NPs (20 nm) into the anode buffer layer, measured under AM 1.5G illumination at 100 mW/cm^2. Reproduced with permission from X.H. Liu, L.X. Hou, J.F. Wang, B. Liu, Z. Sen Yu, L.Q. Ma, S.P. Yang, G.S. Fu, Plasmonic-enhanced polymer solar cells with high efficiency by addition of silver nanoparticles of different sizes in different layers, Sol. Energy 110 (2014) 627–635.

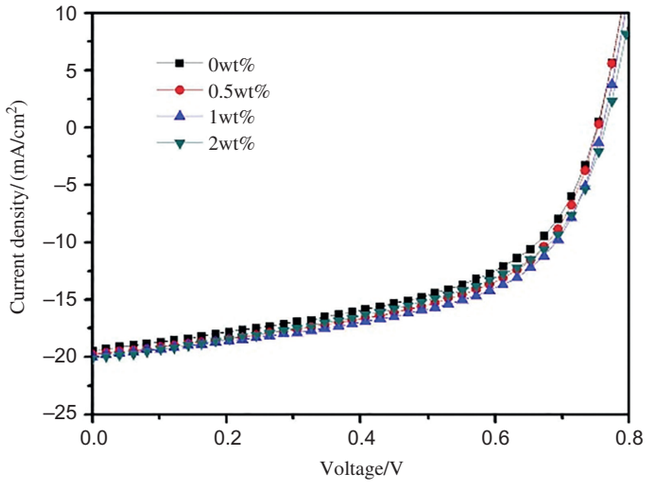


Fig. 6.7 The *J-V* curves of polymer solar cells embedded with Ag NPs (7 nm) into the active layer, measured under AM 1.5G illumination at 100 mW/cm^2. Reproduced with permission from X.H. Liu, L.X. Hou, J.F. Wang, B. Liu, Z. Sen Yu, L.Q. Ma, S.P. Yang, G.S. Fu, Plasmonic-enhanced polymer solar cells with high efficiency by addition of silver nanoparticles of different sizes in different layers, Sol. Energy 110 (2014) 627–635.

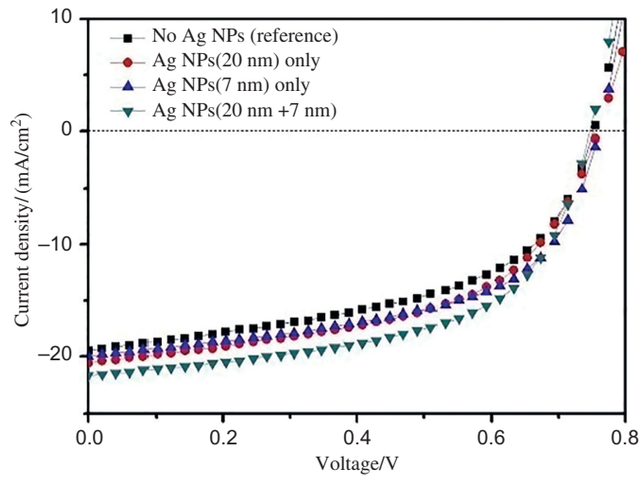


Fig. 6.8 The *J-V* curves of polymer solar cells with and without AgNPs. Reproduced with permission from X.H. Liu, L.X. Hou, J.F. Wang, B. Liu, Z. Sen Yu, L.Q. Ma, S.P. Yang, G.S. Fu, Plasmonic-enhanced polymer solar cells with high efficiency by addition of silver nanoparticles of different sizes in different layers, Sol. Energy 110 (2014) 627–635.

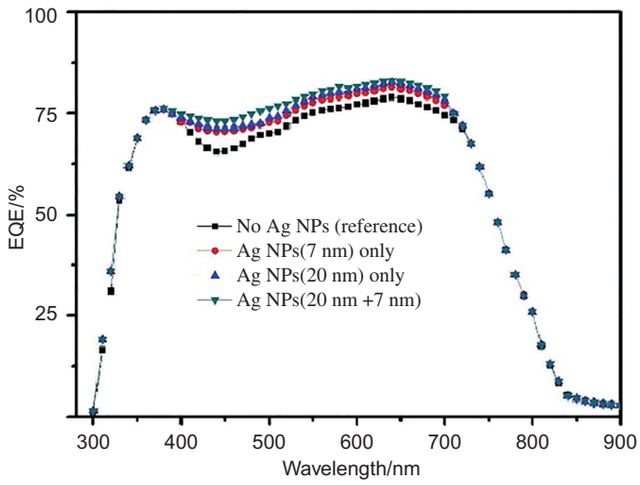


Fig. 6.9 The EQE spectra of polymer solar cells with and without AgNPs. Reproduced with permission from X.H. Liu, L.X. Hou, J.F. Wang, B. Liu, Z. Sen Yu, L.Q. Ma, S.P. Yang, G.S. Fu, Plasmonic-enhanced polymer solar cells with high efficiency by addition of silver nanoparticles of different sizes in different layers, Sol. Energy 110 (2014) 627–635.

6.3 Polymer one-dimensional material composites

These composites are essentially polymer-based multiphase materials in which one dimension of the filler is outside the nanoscale. They include polymer composites containing nanotubes, nanorods, and nanowires. Some of the important polymer 1D material composites of interest in organic photovoltaics are cited below.

6.3.1 Polymer-silver nanowire composites

Various polymer-nanowire composites have been explored for optoelectronic applications. As an alternate for the routinely used indium tin oxide (ITO) transparent conductor, polymer (PEDOT:PSS)-silver nanowire-based electrodes were utilized by Hong-Bo Sun et al. They established that the composite conductivity depends on the length and diameter of the silver nanowires used to prepare it. Also, the use of a longer and bigger diameter silver nanowire composite showed increased percentage transmittance over the smaller length and smaller diameter nanowires. For the longer nanowires (20–50 μm), transmittance in the visible light region was around 80%. It was also established that to obtain the densely packed composite electrode, the nanowire length should be small. Further, the length of the nanowire and the percolation limit for the polymer-nanowire composite matrix in the 1D case can be evaluated using the Equation [33, 34]:

$$N_c = 4.236 / \pi\, l^2 \tag{6.1}$$

where l and N_C are the length and percolation threshold density of the nanowires, respectively (Fig. 6.10).

From Eq. (6.1), it can be understood that the percolation threshold density is inversely related to the square of the nanowire length. It is also shown that an electrode with shorter nanowires (4–10 μm) shows a high fill factor and a low photo-current, whereas longer nanowires (> 20 μm) show a high photo-current and a low fill factor. Further, the lower photo-current of shorter nanowired device may be due to the loss of photons caused by the densely packed silver nanowires. Also, the high packing density of silver nanowire offers high conductivity while longer nanowires offer higher transmittance [34, 35] (Fig. 6.11).

Hong-Bo Sun et al. investigated a PEDOT:PSS-silver nanowire (AgNWs) electrode on the photopolymer substrate suitable for flexible and stretchable devices. These electrodes were fabricated by the template stripping method. The neat PEDOT:PSS and pure silver nanowire electrode offered low conductivity/high sheet resistance. The sheet resistance of the silver nanowire is the function of electrode thickness,

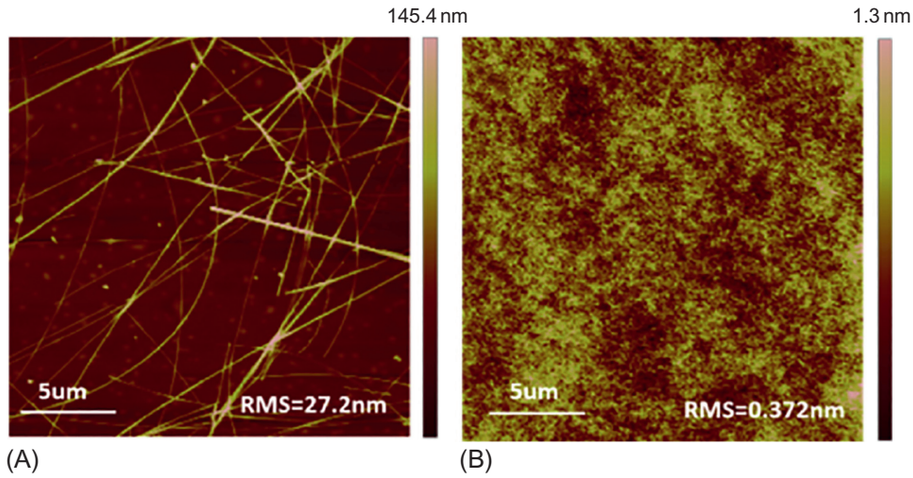


Fig. 6.10 AFM images of (A) the surface morphology of spin-coated composite film on the Si substrate, and (B) stripped-off composite film on the photopolymer substrate. Reproduced with permission from Y.S. Liu, J. Feng, X.L. Ou, H.F. Cui, M. Xu, H.B. Sun, Ultrasmooth, highly conductive and transparent PEDOT:PSS/silver nanowire composite electrode for flexible organic light emitting device, Org. Electron. 31 (2016) 247–252.

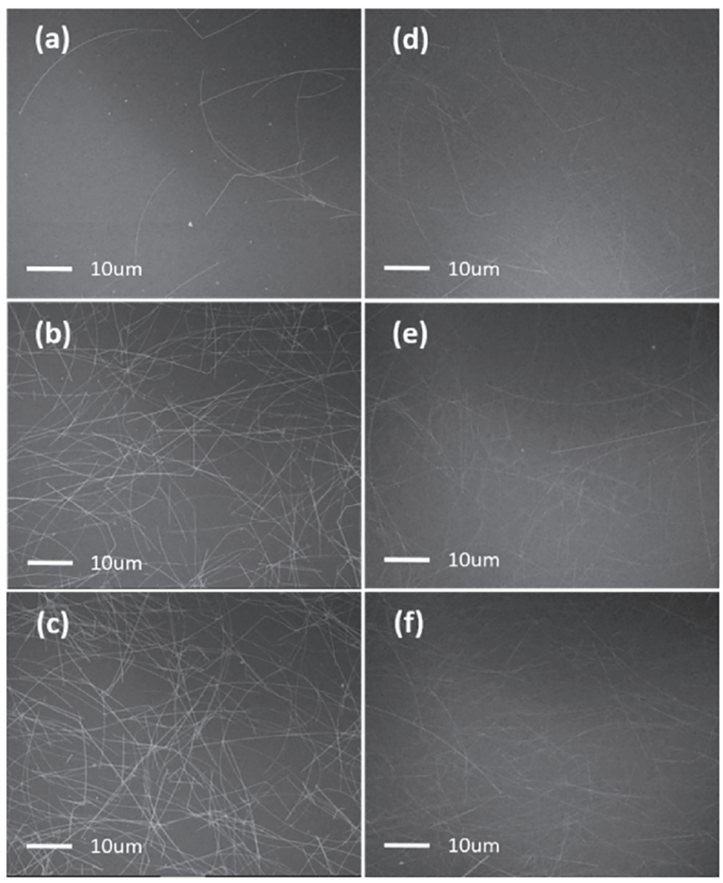


Fig. 6.11 SEM images of (A) the surfaces of spin-coated composite films on Si substrates with various concentrations of 0.1 mg/mL, (B) 0.5 mg/mL, and (C) 1.5 mg/mL; and stripped-off composite films on photopolymer substrates with various concentrations of (D) 0.1 mg/mL, (E) 0.5 mg/mL, and (F) 1.5 mg/mL. Reproduced with permission from Y.S. Liu, J. Feng, X.L. Ou, H.F. Cui, M. Xu, H.B. Sun, Ultrasmooth, highly conductive and transparent PEDOT:PSS/silver nanowire composite electrode for flexible organic light emitting device, Org. Electron. 31 (2016) 247–252.

the length of the silver nanowire, the diameter of the nanowire, and the packing density of the nanowire. The PEDOT:PSS conductivity/sheet resistance depends on the thickness. However, the composite electrode (PEDOT:PSS-AgNWs) utilizes short-range and long-range conductivity associated with PEDOT:PSS and AgNWs, respectively. A composite electrode also favors the improvement of transmittance and sheet resistance. Further, the stripping process gives rise to an ultrasmooth composite electrode. The electrode with a lower surface roughness improves the surface conductivity; the increase in conductivity should be associated with the reduced surface scattering of the electrode. The composite electrode with a low surface roughness show 25% improved OLED performance over the neat PEDOT:PSS electrode. This OLED performance is stable for more than 100 bending cycles [34, 36] (Fig. 6.12).

6.4 Polymer two-dimensional material composites

These composites are essentially polymer-based multiphase materials in which two dimensions of the filler are outside the nanoscale. They include polymer composites containing plate-like shaped nanomaterials such as graphene, nanofilms, nanolayers, and nanocoatings. Some of the important polymer 2D material composites of interest in organic photovoltaics are cited below.

6.4.1 Polymer-graphene composites

Continuous advancements in material synthesis and characterization techniques have offered numerous ways to explore various 2D materials. Also, 2D materials present many novel properties that are significantly different from their bulk counterparts. In the 2D material family, graphene and its derivatives were explored in various electronic device applications. This is because graphene presents high mobility (15,000 $cm^2/V/s$), large thermal conductivity (~ 3–6 kW/mK), a high surface area (~ 2600 m^2/g), appreciable electrical conductivity (~ $9 \times 10^7 Sm^{-1}$), a higher elastic modulus close to ~ 1 TPa, high ultimate strength (~ 130 GPa), and a breaking strength of ~ 40 Nm^{-1}.

Further, graphene/polymer NCs can serve in all three parts of polymer photovoltaics. That is, with an appropriate combination of graphene and polymer, one can use this type of composite as a transparent conducting electrode, an active layer, and an interface modifying layer. In addition to improving the optical and electrical properties, using these types of composite matrices also improves the flexibility and stretchability of the devices.

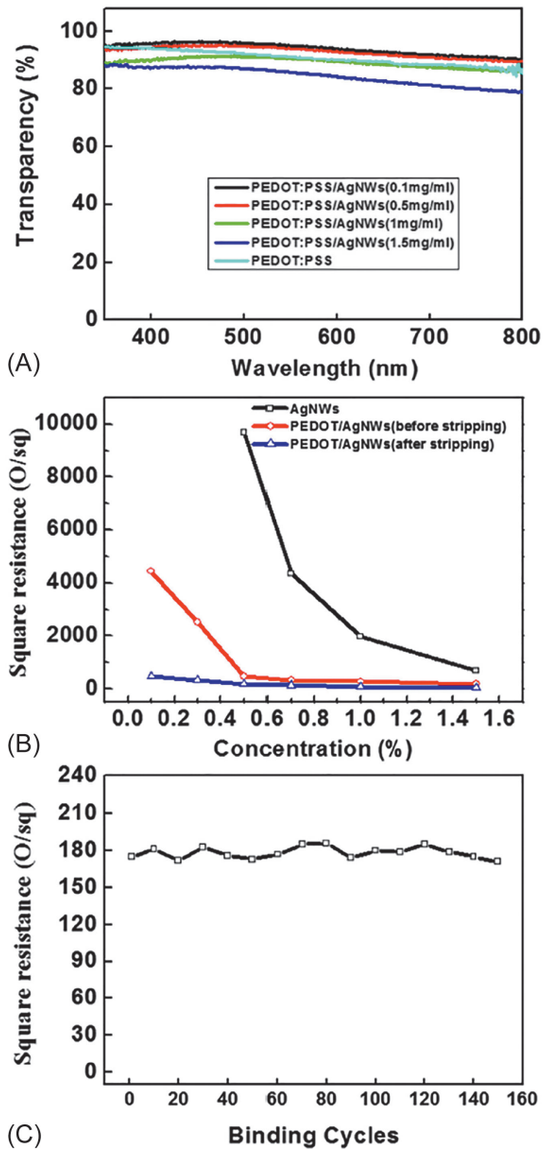


Fig. 6.12 (A) Transmittance spectra of composite films with different AgNW concentrations and pure PEDOT:PSS. (B) sheet resistance of composite films with different AgNW concentrations on Si and photopolymer substrates. (C) sheet resistance of the composite film (0.5 mg/mL) after 150 times of bending. Reproduced with permission from Y.S. Liu, J. Feng, X.L. Ou, H.F. Cui, M. Xu, H.B. Sun, Ultrasmooth, highly conductive and transparent PEDOT:PSS/silver nanowire composite electrode for flexible organic light emitting device, Org. Electron. 31 (2016) 247–252.

Moreover, such composites can be processed at low temperature, in contrast to conventional materials. Also, by suitably addressing the shortcomings of high defect density, which limit the power conversion efficiency of the device, one can fabricate highly efficient and stable photovoltaic devices. Further, it was also observed that the device using reduced graphene oxide (rGO) on a PET substrate as a transparent

electrode gave rise to improved device performance (without any change in the performance up to 1200 bending cycles). For the lowest sheet resistance (281 Ω/Sq) with the lowest transmittance (22.5%), the photovoltaic (active layer PCDTBT polymer) performance was 1.78%. However, in the high transmittance (84.6%), high sheet resistance (2850 Ω/Sq) zone, the performance was 0.74%. The highest performance (3.05%) was recorded for 59.1% optical transmittance and 565 Ω/Sq sheet resistance. Nevertheless, the V_{OC} remained nearly the same for all sheet resistance and all optical transmittance, which in turn supported that the energy level value does not show much difference with respect to thickness. Plus, the variation of rGO thickness does not have an appreciable effect on the V_{OC} of the PCDTBT polymer solar cells [37] (Fig. 6.13).

6.4.2 PTB7-MoS_2 composite

One of the important shortcomings of the polymer-based solar cell is its low electron mobility. Plus, the imbalance in charge carrier mobility (electron and hole mobility) induces undesirable recombinations during photovoltaic operation. To overcome these issues, various strategies were adopted in polymer solar cell design. One such strategy was embedding high electron mobility in the active layer. Further, the MoS_2 also acts as an effective charge transfer medium in ternary blend solar cells. The optical absorption properties of the PTB7, PTB7:MoS_2, and the corresponding devices are shown in Figs. 6.14A–C. Their photoluminescence characteristics are presented in Figs. 6.14B–D [38].

Further, an enhancement in charge carrier mobility (electron and hole mobility) is observed for the optimum loading of MoS_2. As the loading increases beyond the threshold limit, the electron mobility also increases. This results in an imbalance in the charge carrier transport and accelerates the unwanted recombination rate in the device. Plus, adding 2D material (MoS_2) with the PTB7 photo-active layer reduces the trap density and also supports the cascading effect of the energy level alignment with PTB7 and $PC_{70}BM$. This effect favors the high transport path across the PTB7 and $PC_{70}BM$ [38] (Figs. 6.15 and 6.16).

The ternary blend device PTB7:$PC_{70}BM$:MoS_2 showed enhanced device performance over the PTB7:$PC_{70}BM$ due to the reason stated earlier. From the detailed study of the ternary blend polymer composite system, it is noted that controlling the composite morphology is a prime factor in deciding the efficiency. The morphology controls the nanoscale phase separation, which decides the effective charge transfer across the donor and acceptor, in addition to the continuity of the active layer. The continuity of the active layer dictates the generated charge carriers to reach the corresponding electrode. The detailed mechanism of the ternary blend solar cells is reported elsewhere [38–42].

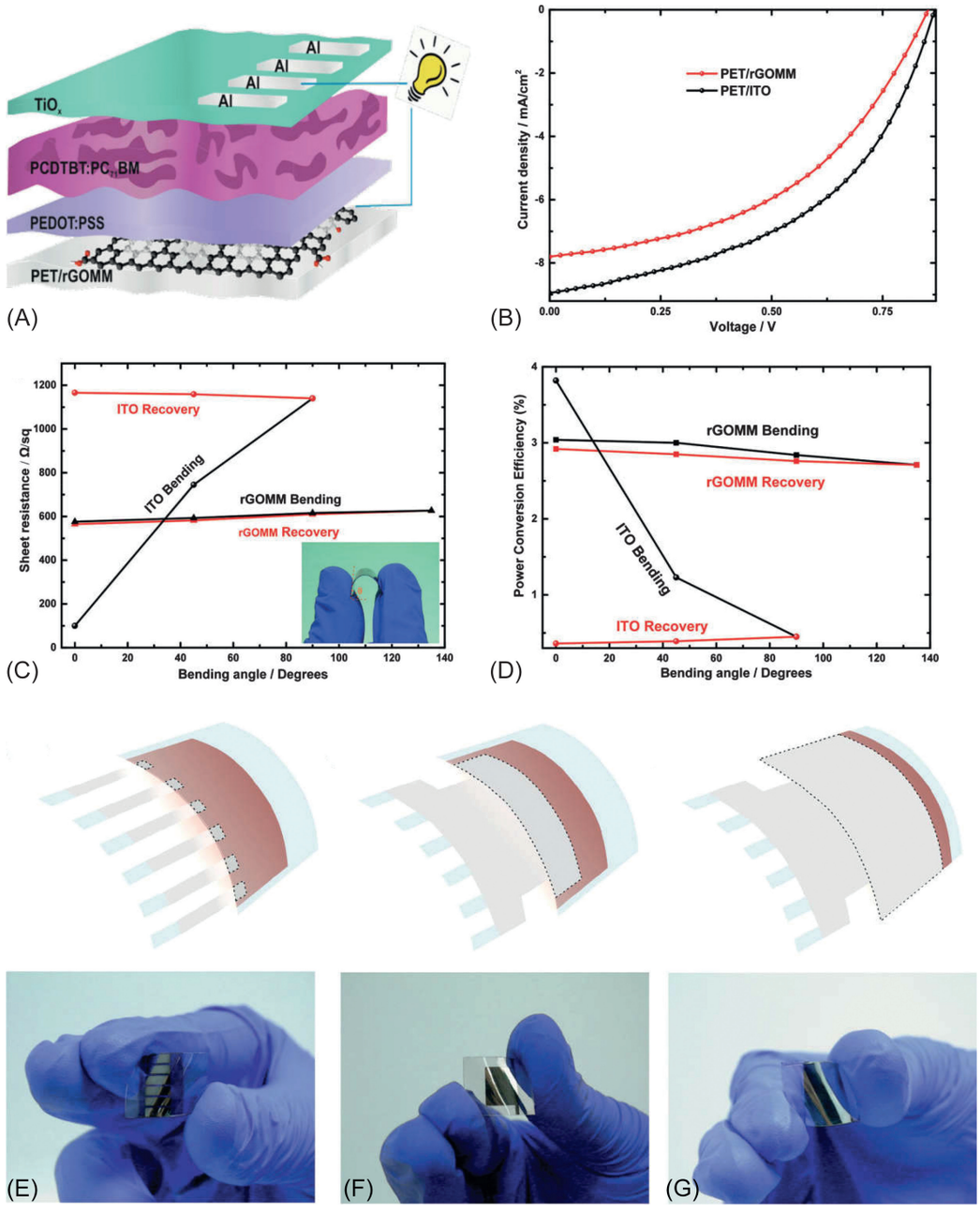


Fig. 6.13 (A) Schematic illustration of BHJ photovoltaic device with the laser-induced rGOMM as a transparent conducting electrode; (B) the illuminated current-voltage (*J-V*) curves of the solar cells with rGOMM *(red)* and ITO *(black)*; (C) sheet resistance versus device bending angle of rGOMM- and ITO-based solar cells. The inset photo represents an rGOMM-based device subjected to bending; (D) power conversion efficiency of rGOMM- and ITO-based flexible devices, after bending at certain angles; and (E–G) schematic illustration and photographs of devices exhibiting increased active areas; (E) 4, (F) 50, and (G) 135 mm^2. From D. Konios, C. Petridis, G. Kakavelakis, M. Sygletou, K. Savva, E. Stratakis, E. Kymakis, Reduced graphene oxide micromesh electrodes for large area, flexible, organic photovoltaic devices, Adv. Funct. Mater. 25 (2015) 2213–2221. https://doi.org/10.1002/adfm.201404046.

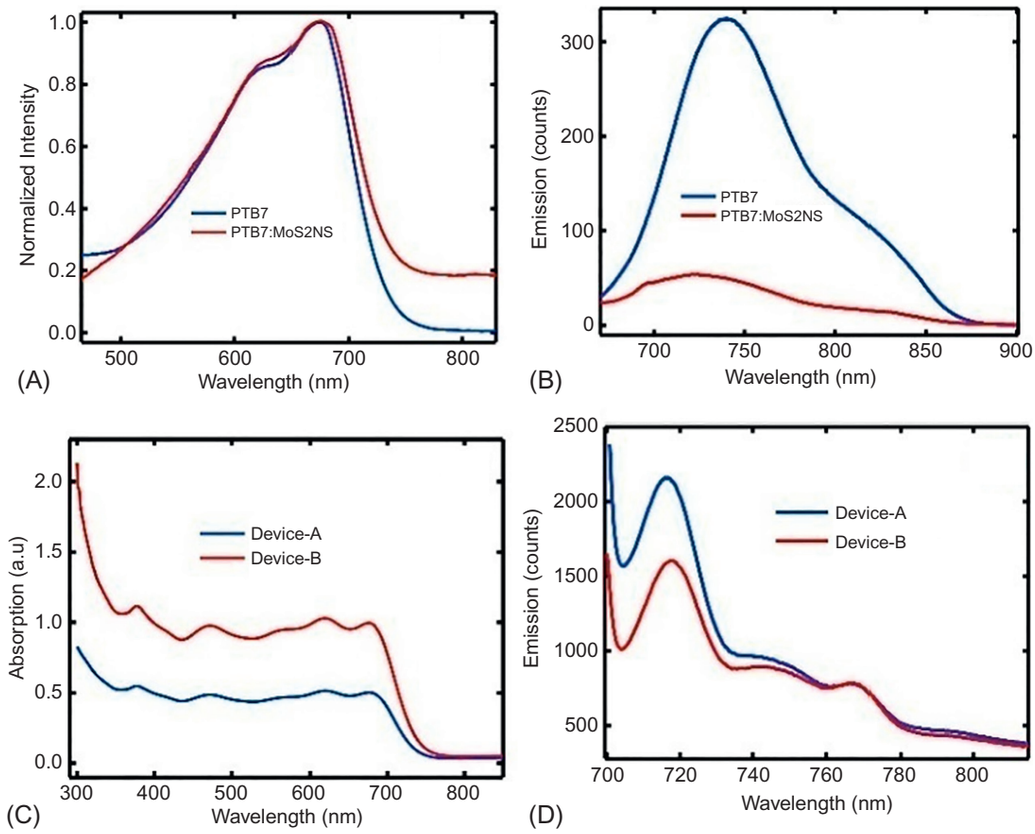


Fig. 6.14 (A) Optical absorption spectra of PTB7:MoS_2; (B) photoluminescence spectra of PTB7:MoS_2; (C) absorption spectra of the PTB7:$PC_{71}BM$ and PTB7:$PC_{71}BM$:MoS_2 active layer; (D) photoluminescence spectra of the PTB7:PC71BM and PTB7:PC71BM:MoS_2 active layer. Reproduced with permission from A.V. Kesavan, A.D. Rao, P.C. Ramamurthy, Optical and electronic property tailoring by MoS_2-polymer hybrid solar cell, Org. Electron. Phys. Mater. Appl. 48 (2017) 138–146.

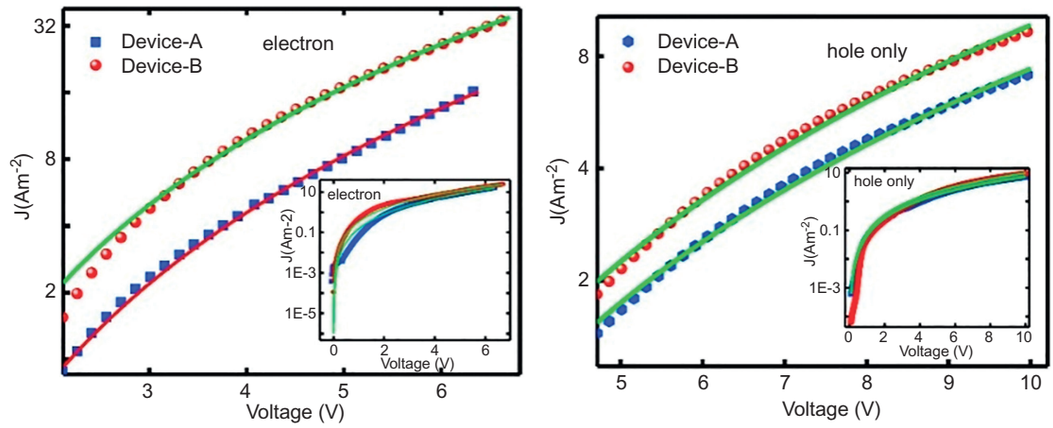


Fig. 6.15 Current-voltage characteristics of (A) electron-only device; and (B) hole-only device fitted using the modified space charge limited current equation. Reproduced with permission from A.V. Kesavan, A.D. Rao, P.C. Ramamurthy, Optical and electronic property tailoring by MoS_2-polymer hybrid solar cell, Org. Electron. Phys. Mater. Appl. 48 (2017) 138–146.

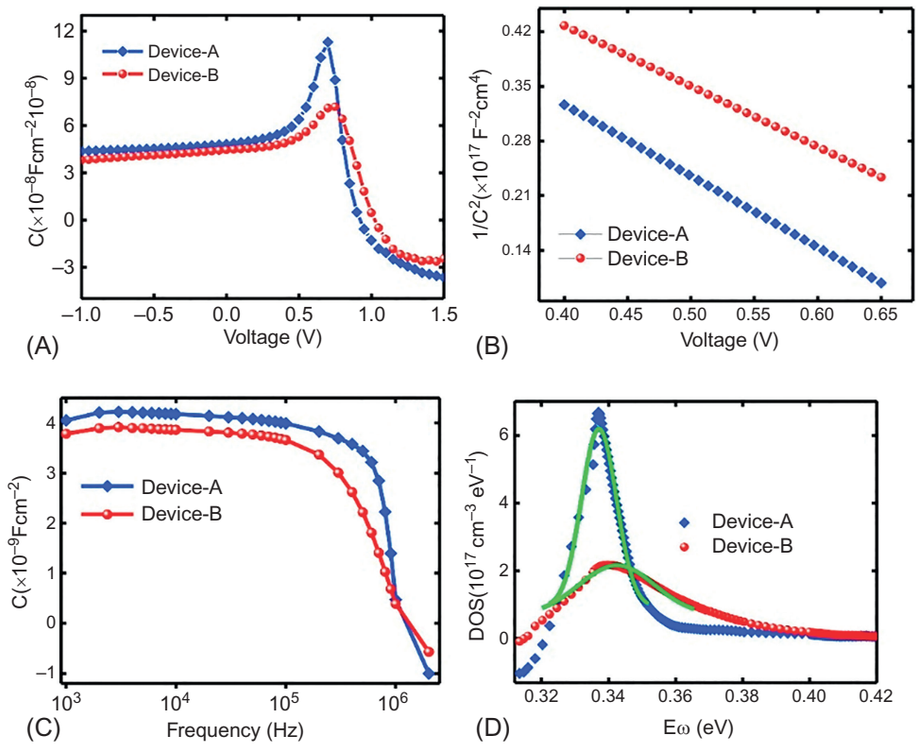


Fig. 6.16 (A) Capacitance-voltage spectra; (B) Mott-Schottky characteristics; (C) capacitance-frequency spectra; and (D) density of the state plots of the capacitance-voltage and the Mott-Schottky characteristics of a binary and ternary composite solar cell. Reproduced with permission from A.V. Kesavan, A.D. Rao, P.C. Ramamurthy, Optical and electronic property tailoring by MoS_2-polymer hybrid solar cell, Org. Electron. Phys. Mater. Appl. 48 (2017) 138–146.

6.4.3 Polymer-perovskite NCs

Many researchers are trying to develop conducting polymer-perovskite composites for optoelectronic applications, as they may enable the properties of individual components to be combined. Accordingly, to take advantage of the photo-active polymer and the perovskite semiconductors, PTB7-$CH_3NH_3PbI_3$NC was explored as a photo-active material for solar cell applications. PTB7 is one of the stable polymers that shows a power conversion efficiency of around ~9% with $PC_{70}BM$ and $CH_3NH_3PbI_3$. This study supported that the composite photo-active layer does not improve efficiency, but enables significant improvement in the stability of the solar cell. Also, the PTB7-$CH_3NH_3PbI_3$ composite active layer included device shows marginally high V_{OC}. This change in V_{OC} was reported to be the

consequence of PTB7 coverage over the $CH_3NH_3PbI_3$ grain boundary region and at the surface. The strong interaction of the CH_3NH_3 group with PTB7 and the coverage of PTB7 at the grain boundary and the surface of $CH_3NH_3PbI_3$ led to improved V_{OC}. Furthermore, the J_{SC} and V_{OC} of both the neat and composite active layer included devices were almost stable up to 400 h. However, thereafter, the V_{OC} and J_{SC} of the neat $CH_3NH_3PbI_3$ showed a decreasing trend. Plus, the J_{SC} and the fill factor of the PTB7-$CH_3NH_3PbI_3$ device was stable up to 900 h with only a small reduction, and the V_{OC} is almost stable. However, a continuous reduction in fill factor was observed, which in turn caused the neat $CH_3NH_3PbI_3$ solar cell efficiency to decrease. This study also supported that preventing grain boundary passivation helps in maintaining stable device performance [43].

Nevertheless, the presence of a small amount of poly(propylene carbonate) (PPC) in the perovskite active layer helps to remove the inherent shortcoming of the perovskite photovoltaics, which is the ambient stability (device stability against moisture, light, and heat). Using macromolecule-based grain boundary passivating over the small molecule technique overcomes the rapid nucleation in the grain boundaries. The macromolecular polymer chain leads to the formation of a perovskite-PPC composite by surrounding the polymer around the perovskite crystalline grain boundaries. This type of formation densifies the grain boundary region, which decreases the grain boundary defect, favors the charge carrier transport, or reduces the charge carrier losses at the grain boundaries. The defect density of the polycrystalline perovskite layer is 10^{16}–$10^{18}\,cm^{-3}$, which is double the defect density of single crystal perovskite (10^{9}–$10^{10}\,cm^{-3}$). Therefore, the effect of defect density on the device performance must be taken care of in the case of perovskite solar cells. Fig. 6.17 depicts the microstructural view of such a perovskite layer. The grain boundaries act as charge trapping states and the origin of the device degradation path. The presence of these macromolecular materials at the grain boundary also prevents the degradative attack of moisture and oxygen [44].

6.5 Conclusions and future directions

This chapter shed light on various polymer composites based on zero-, one-, and two-dimensional materials for solar cell applications. Such polymer-based composites are extensively studied in the active layer, as a buffer layer, as an electrode, and as the base substrate. Further, the detailed view on important polymer-nanomaterial composites revealed that a thoughtful combination of the appropriate polymer and right nanomaterial will pave the way for high efficiency and highly stable organic photovoltaics.

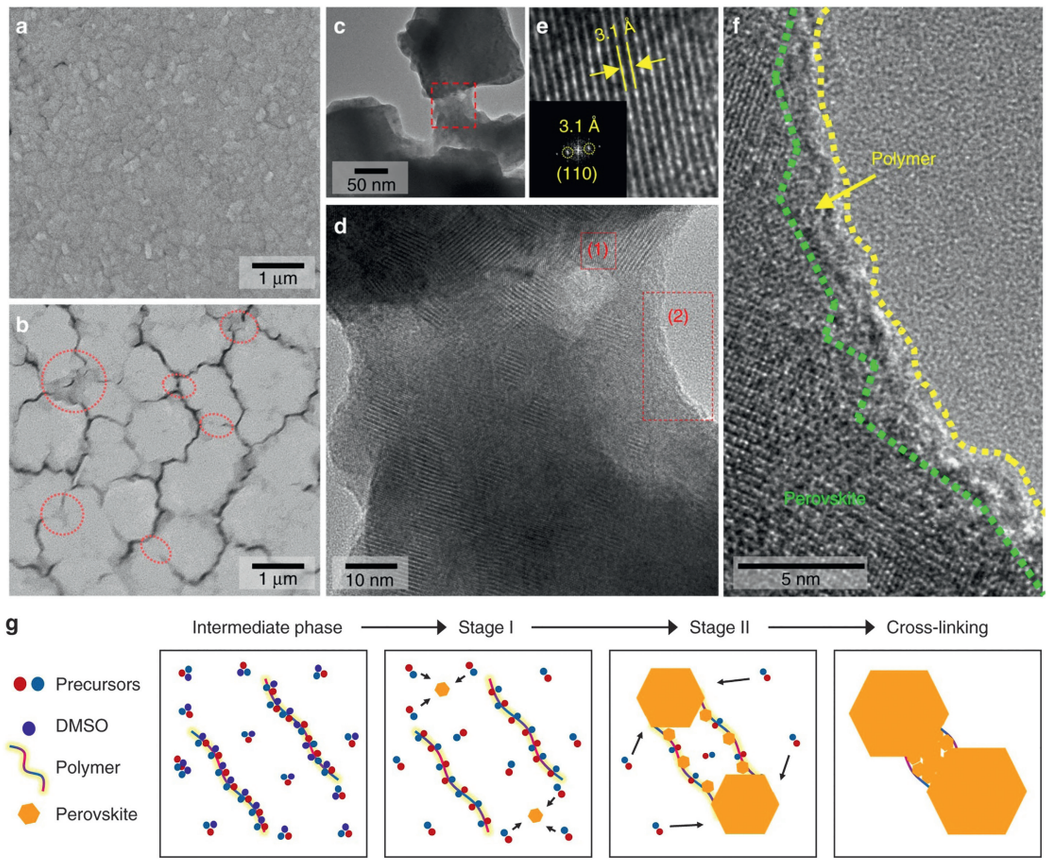


Fig. 6.17 (A and B) Scanning electron microscopy images of (A) $CH_3NH_3PbI_3$; (B) $CH_3NH_3PbI_3$:PPC film; (C and D) transmission electron microscopy (TEM) images of (C) cross-linked perovskite grains at lower magnification; (D) perovskite-polymer composite cross-linker between adjacent grains; (E) inverse fast Fourier transform (IFFT) images of the region-d (1) within the perovskite-polymer bridge (inset is FFT analysis); (F) boundary of the perovskite-polymer composite cross-linker region, highlighted in d (2) and (G), schematic drawing of the macromolecular intermediate phase induced crystallization and intergrain cross-linking. Reproduced with permission from T.H. Han, J.W. Lee, C. Choi, S. Tan, C. Lee, Y. Zhao, Z. Dai, N. De Marco, S.J. Lee, S.H. Bae, Y. Yuan, H.M. Lee, Y. Huang, Y. Yang, Perovskite-polymer composite cross-linker approach for highly-stable and efficient perovskite solar cells, Nat. Commun. 10 (2019) 1–10.

References

[1] G. Wang, F.S. Melkonyan, A. Facchetti, T.J. Marks, All-polymer solar cells: recent Progress, challenges, and prospects, Angew. Chem. Int. Ed. 58 (2019) 4129–4142.

[2] L.M. Chen, Z. Hong, G. Li, Y. Yang, Recent progress in polymer solar cells: manipulation of polymer: fullerene morphology and the formation of efficient inverted polymer solar cells, Adv. Mater. 21 (2009) 1434–1449.

[3] L. Meng, Y. Zhang, X. Wan, C. Li, X. Zhang, Y. Wang, X. Ke, Z. Xiao, L. Ding, R. Xia, H.L. Yip, Y. Cao, Y. Chen, Organic and solution-processed tandem solar cells with 17.3% efficiency, Science 361 (2018) 1094–1098.

[4] A.P. Litvin, I.D. Skurlov, I.G. Korzhenevskii, A. Dubavik, S.A. Cherevkov, A.V. Sokolova, P.S. Parfenov, D.A. Onishchuk, V.V. Zakharov, E.V. Ushakova, X. Zhang, A.V. Fedorov, A.V. Baranov, Ternary composites with PbS quantum dots for hybrid photovoltaics, J. Phys. Chem. C 123 (2019) 3115–3121.
[5] S.S. Li, K.H. Tu, C.C. Lin, C.W. Chen, M. Chhowalla, Solution-processable graphene oxide as an efficient hole transport layer in polymer solar cells, ACS Nano 4 (2010) 3169–3174.
[6] G.H. Jun, S.H. Jin, B. Lee, B.H. Kim, W.S. Chae, S.H. Hong, S. Jeon, Enhanced conduction and charge-selectivity by N-doped graphene flakes in the active layer of bulk-heterojunction organic solar cells, Energy Environ. Sci. 6 (2013) 3000–3006.
[7] S.I. Na, Y.J. Noh, S.Y. Son, T.W. Kim, S.S. Kim, S. Lee, H.I. Joh, Efficient organic solar cells with solution-processed carbon nanosheets as transparent electrodes, Appl. Phys. Lett. 102 (2013) 043304.
[8] K.S. Tan, M.K. Chuang, F.C. Chen, C.S. Hsu, Solution-processed nanocomposites containing molybdenum oxide and gold nanoparticles as anode buffer layers in plasmonic-enhanced organic photovoltaic devices, ACS Appl. Mater. Interfaces 5 (2013) 12419–12424.
[9] M. Stavytska-Barba, M. Salvador, A. Kulkarni, D.S. Ginger, A.M. Kelley, Plasmonic enhancement of Raman scattering from the organic solar cell material P3HT/PCBM by triangular silver nanoprisms, J. Phys. Chem. C 115 (2011) 20788–20794.
[10] A.V. Kesavan, A.K. Jagdish, P.C. Ramamurthy, Light Trapping and Management in Inverted Organic Solar Cells Employing Metal Nanoparticles, IEEE, 2017.
[11] J.C. Goldschmidt, S. Fischer, Upconversion for photovoltaics–a review of materials, devices and concepts for performance enhancement, Adv. Opt. Mater. 3 (2015) 510–535.
[12] G.R. Suma, K.S. Nithin, K.N. Shilpa, S. Sachhidananda, S.V. Satyanarayana, Effect of $Ce_{0.5}Zr_{0.5}O_2$ nano fillers on structural and optical behaviors of poly (vinyl alcohol), J. Mater. Sci. Mater. Electron. 28 (2017) 10707–10714.
[13] K.S. Nithin, Opto-electrical characteristics of poly (vinyl alcohol)/cesium zincate nanodielectrics, J. Phys. Chem. C 119 (2015) 20244–20255.
[14] Z. Yang, J.Z. Fan, A.H. Proppe, F.P.G. De Arquer, D. Rossouw, O. Voznyy, X. Lan, M. Liu, G. Walters, R. Quintero-Bermudez, B. Sun, S. Hoogland, G.A. Botton, S.O. Kelley, E.H. Sargent, Mixed-quantum-dot solar cells, Nat. Commun. 8 (2017) 1–8.
[15] R. Mastria, A. Rizzo, C. Giansante, D. Ballarini, L. Dominici, O. Inganäs, G. Gigli, Role of polymer in hybrid polymer/PbS quantum dot solar cells, J. Phys. Chem. C 119 (2015) 14972–14979.
[16] Y. Firdaus, E. Vandenplas, A. Khetubol, D. Cheyns, R. Gehlhaar, M. Van Der Auweraer, Charge transport and recombination in P3HT:PbS solar cells, J. Appl. Phys. 117 (2015) 095503.
[17] J. Seo, S.J. Kim, W.J. Kim, R. Singh, M. Samoc, A.N. Cartwright, Enhancement of the photovoltaic performance in PbS nanocrystal : P3HT hybrid composite devices by post-treatment-driven ligand exchange, Nanotechnology 20 (2009) 095202.
[18] J. Seo, M.J. Cho, D. Lee, A.N. Cartwright, P.N. Prasad, Efficient heterojunction photovoltaic cell utilizing nanocomposites of lead sulfide nanocrystals and a low-bandgap polymer, Adv. Mater. 23 (2011) 3984–3988.
[19] C. Piliego, M. Manca, R. Kroon, M. Yarema, K. Szendrei, M.R. Andersson, W. Heiss, M.A. Loi, Charge separation dynamics in a narrow band gap polymer-PbS nanocrystal blend for efficient hybrid solar cells, J. Mater. Chem. 22 (2012) 24411–24416.
[20] M. Kong, W. Hu, F. Cheng, Z. Huang, J. Zhang, Z. Han, N. Shi, Q. Fan, S. Chen, W. Huang, Efficiency enhancement in P3HT-based polymer solar cells with a NaYF 4:2% Er3 +, 18% Yb3 + up-converter, J. Mater. Chem. C 1 (2013) 5872–5878.
[21] A.V. Kesavan, M.P. Kumar, A.D. Rao, P.C. Ramamurthy, Light management through up-conversion and scattering mechanism of rare earth nanoparticle in polymer photovoltaics, Opt. Mater. 94 (2019) 286–293.

[22] K.M. Panidhara, A.K. Jagdish, A.V. Kesavan, P.C. Ramamurthy, Omnidirectional sub-bandgap photo-detection using functionalized moulded composite flexible platforms, Opt. Mater. 88 (2019) 359–365.
[23] A.S. Sarkar, A.D. Rao, A.K. Jagdish, A. Gupta, C.K. Nandi, P.C. Ramamurthy, S.K. Pal, Facile embedding of gold nanostructures in the hole transporting layer for efficient polymer solar cells, Org. Electron. Phys. Mater. Appl. 54 (2018) 148–153.
[24] J. Shin, M. Song, H. Hafeez, P.J. Jeusraj, D.H. Kim, J.C. Lee, W.H. Lee, D.K. Choi, C.H. Kim, T.S. Bae, S.M. Yu, K.H. Kim, H.G. Park, K.B. Chung, A. Song, Y.C. Kang, J. Park, C.S. Kim, S.Y. Ryu, Harvesting near- and far-field plasmonic enhancements from large size gold nanoparticles for improved performance in organic bulk heterojunction solar cells, Org. Electron. Phys. Mater. Appl. 64 (2019) 96–101.
[25] X. Li, W.C.H. Choy, H. Lu, W.E.I. Sha, A.H.P. Ho, Efficiency enhancement of organic solar cells by using shape-dependent broadband plasmonic absorption in metallic nanoparticles, Adv. Funct. Mater. 23 (2013) 2728–2735.
[26] L. Lu, Z. Luo, T. Xu, L. Yu, Cooperative plasmonic effect of Ag and Au nanoparticles on enhancing performance of polymer solar cells, Nano Lett. 13 (2013) 59–64.
[27] M. Sygletou, G. Kakavelakis, B. Paci, A. Generosi, E. Kymakis, E. Stratakis, Enhanced stability of aluminum nanoparticle-doped organic solar cells, ACS Appl. Mater. Interfaces 7 (2015) 17756–17764.
[28] H.C. Chen, S.W. Chou, W.H. Tseng, I.W.P. Chen, C.C. Liu, C. Liu, C.L. Liu, C.H. Chen, C.I. Wu, P.T. Chou, Large AuAg alloy nanoparticles synthesized in organic media using a one-pot reaction: their applications for high-performance bulk heterojunction solar cells, Adv. Funct. Mater. 22 (2012) 3975–3984.
[29] K.S. Nithin, K.N. Shilpa, S. Sachhidananda, H. Siddaramaiah, Yellow–green luminescent poly (vinyl alcohol) nanocomposite thick films as effective spectral manipulators, J. Appl. Polym. Sci. 135 (2018) 46854.
[30] A. Srivastava, D.P. Samajdar, D. Sharma, Plasmonic effect of different nanoarchitectures in the efficiency enhancement of polymer-based solar cells: a review, Sol. Energy 173 (2018) 905–919.
[31] A.V. Kesavan, A.K. Jagdish, P.C. Ramamurthy, Organic inorganic hybrid hole transport layer for light management in inverted organic photovoltaic, IEEE J. Photovoltaics 7 (2017) 787–791.
[32] X.H. Liu, L.X. Hou, J.F. Wang, B. Liu, Z. Sen Yu, L.Q. Ma, S.P. Yang, G.S. Fu, Plasmonic-enhanced polymer solar cells with high efficiency by addition of silver nanoparticles of different sizes in different layers, Sol. Energy 110 (2014) 627–635.
[33] C.H. Seager, G.E. Pike, Percolation and conductivity: a computer study. II, Phys. Rev. B 10 (1974) 1435–1446.
[34] Y.S. Liu, J. Feng, X.L. Ou, H.F. Cui, M. Xu, H.B. Sun, Ultrasmooth, highly conductive and transparent PEDOT:PSS/silver nanowire composite electrode for flexible organic light emitting device, Org. Electron. 31 (2016) 247–252.
[35] Z. Yu, L. Li, Q. Zhang, W. Hu, Q. Pei, Silver nanowire-polymer composite electrodes for efficient polymer solar cells, Adv. Mater. 23 (38) (2011) 4453–4457.
[36] S.N. Habisreutinger, T. Leijtens, G.E. Eperon, S.D. Stranks, R.J. Nicholas, H.J. Snaith, Carbon nanotube/polymer composites as a highly stable hole collection layer in perovskite solar cells, Nano Lett. 14 (2014) 5561–5568.
[37] D. Konios, C. Petridis, G. Kakavelakis, M. Sygletou, K. Savva, E. Stratakis, E. Kymakis, Reduced graphene oxide micromesh electrodes for large area, flexible, organic photovoltaic devices, Adv. Funct. Mater. 25 (2015) 2213–2221.
[38] A.V. Kesavan, A.D. Rao, P.C. Ramamurthy, Optical and electronic property tailoring by MoS_2-polymer hybrid solar cell, Org. Electron. Phys. Mater. Appl. 48 (2017) 138–146.
[39] L. Lu, T. Xu, W. Chen, E.S. Landry, L. Yu, Ternary blend polymer solar cells with enhanced power conversion efficiency, Nat. Photonics 8 (2014) 716.
[40] L. Lu, W. Chen, T. Xu, L. Yu, High-performance ternary blend polymer solar cells involving both energy transfer and hole relay processes, Nat. Commun. 6 (2015) 1–7.

[41] L. Lu, M.A. Kelly, W. You, L. Yu, Status and prospects for ternary organic photovoltaics, Nat. Photonics 9 (2015) 491–500.
[42] X. Liu, Y. Yan, Y. Yao, Z. Liang, Ternary blend strategy for achieving high-efficiency organic solar cells with nonfullerene acceptors involved, Adv. Funct. Mater. 28 (2018) 1802004.
[43] H. Wang, Y. Rahaq, V. Kumar, A composite light-harvesting layer from photoactive polymer and halide perovskite for planar heterojunction solar cells, Sci. Rep. 6 (2016) 1–9.
[44] T.H. Han, J.W. Lee, C. Choi, S. Tan, C. Lee, Y. Zhao, Z. Dai, N. De Marco, S.J. Lee, S.H. Bae, Y. Yuan, H.M. Lee, Y. Huang, Y. Yang, Perovskite-polymer composite cross-linker approach for highly-stable and efficient perovskite solar cells, Nat. Commun. 10 (2019) 1–10.

7

Shape memory polymers (SMP's) in optoelectronic devices

K. Anand[a] and Vaishak Nambiathody[b]

[a]Department of Basic Sciences, Amal Jyothi College of Engineering, Kanjirapally, Kerala, India, [b]Technical Consultancy Division, Rubber Research Institute of India, Kottayam, Kerala, India

7.1 Introduction

Optoelectronics is essentially the technological domain that includes the design and production of hardware devices that convert electrical energy into light and light into energy using semiconductors. Such semiconductors are solid crystalline materials that are lighter than metals and heavier than insulators. Further, these optoelectronic materials and/or devices are explored for various commercial applications, such as military services, telecommunications, automatic access control systems, medical equipment, and so forth. The said optoelectronic may be in the form of a photodiode, solar cell, light-emitting diode, optical fiber, laser diode, and other related systems.

7.2 Polymer as a material

Due to their versatility and adjustable chemical and physical properties combined with economical synthesis and processing techniques, polymers are considered the best suitable matrices for enabling new materials toward electronic and optoelectronic applications. Also, due to the high electro-optic (EO) coefficients, high thermal stability, good flexibility, and low dielectric constant, polymer materials are widely used for wide bandwidth and high-efficiency organic electro-optical modulation devices as well as flexible electronic circuits and microelectronic devices [1–4]. Devices based on low-cost polymer materials have been widely used in various fields such as optics, electromagnetics, and biomedicine [5]. Polymer-based optical materials have been commonly used in the fabrication of optical

Polymer-Based Advanced Functional Composites for Optoelectronic and Energy Applications
https://doi.org/10.1016/B978-0-12-818484-4.00009-4
Copyright © 2021 Elsevier Inc. All rights reserved.

waveguides, polymer fibers, and microoptics devices, owing to their high optical transmission properties, good plasticity, and excellent mechanical stability [6–9].

The major breakthrough in the properties of polymers was done by Alan Heeger, Alan MacDiarmid, and Hideki Shirakawa in 1977 with the discovery of the semiconducting properties of polyacetylene [10]. This earned them the Nobel prize in Chemistry [11–13]. Many more semiconducting and conducting polymers have been reported. Among these, small molecular weight semiconductors are more attractive as they can be efficiently handled and their ordered structure enables them to carry high charge. Also, their three-dimensional (3D) structure may be utilized as a template to fabricate a polymer matrix in solid electrolytes [14, 15]. In addition, semiconducting polymers and their composites may also be used for high-performance single component devices, hetero conjugation solar cells, organic electro-optical or magnetic components, and many more [16–18].

7.3 Solar cells

The conductive polymer substrate is responsible for supporting cells, transmitting light, and collecting and transmitting electrons in dye-sensitized solar cells (DSSCs). Indium-doped tin oxide (ITO) glass, fluorine-doped tin oxide (FTO) glass, ITO/polyethylene terephthalate (PET), and ITO/polyethylene naphthalate (PEN) are the common conductive substrates used in this device. Out of these, ITO/PET and ITO/PEN are the most widely used due to their high transparency, low cost, large flexibility, low sheet resistance, and light weight [19–21]. The charge carrier mobility is an important characteristic to be considered while designing the substrate. Consequently, several approaches have been developed to improve the charge carrying mobility of the substrate. A charge carrier mobility of ~ 1.1 cm^2 was achieved by using the polymers P3HT and PBTTT [22]. Also, the development of D-A polymers, which are copolymers with alternating electron-deficient and electron-rich units, along the polymer backbone have attracted significant interest for OFET and solar cell applications [23, 24]. The TiO_2 photoanodes in DSSC utilize polymers as a pore-forming reagent. A series of mesoporous TiO_2 anodes containing different ratios of poly vinyl pyrrolidone (PVP) was fabricated by Hou et al., wherein 20 wt% PVP was reported to give a higher conversion efficiency than the control sample. The catalytic reduction of I^{3-} in DSSC is brought out by the counter electrode system. Earlier, Pt-CE was commonly used. But due to its scarcity and corrosive nature, researchers are finding alternatives for this. Due to their low cost, translucence, simple synthesis, and high catalytical activity, conductive polymers are gaining momentum and can be used to replace Pt-CE

[25–27]. Poly(3,4-ethylenedioxythiophene): poly(styrene sulfonate) (PEDOT:PSS) is one of the most widely used conducting polymers. Its good film-forming properties, optical transparency, high electrical conductivity, and excellent mechanical stability render it the best candidate for transparent electrodes [28]. Baytron is the first commercialized trade name of PEDOT:PSS. This can replace the expensive ITO in organic solar cells [29]. Further, the use of cost-effective materials and fabrication techniques can achieve the goal of producing organic solar cells that can convert solar energy to electricity at a cost of less than $1 per watt [30–34].

Polymers are also attractive emissive materials in LEDs that can be operated at a very low cost and offer easier process ability, higher flexibility, and larger stability [35–38]. The performance metrics of one such (poly (3,4ethylenedioxythiophene): poly(styrene sulfonate) (PEDOT:PSS): graphene oxide: PEDOT oxide: (PEDOT GO) oxide (GO)) material are presented in Table 7.1 [39].

Cavendish Laboratory explored the electrode applications of polymers in an organic photodiode in 1999 [40]. A photodiode based on the polymer P1 was developed by Jinfeng Han et al. that was reported to present an external quantum efficiency of 7.8% at 1200 nm (Fig. 7.1), which is the best polymer photodiode so far [41, 42]. The blend between the derivatives of poly(thiophene) and poly(phenylene) has helped to accomplish a broad wavelength response. An external quantum yield of

Table 7.1 Device performances of PLEDs with the well-dispersed PEDOT:GO composite, the aggregated PEDOT:GO composite, and the PEDOT:PSS hole transport layers.

Device configuration	Luminance, L_{max} [cd/m^2] @ bias	Luminous efficiency, LE_{max} [cd/A] @ bias	Power efficacy, PE_{max} [lm/W] @ bias	External quantum efficiency, EQE_{max} [%] @ bias	Turn-on voltage [V]
ITO/PEDOT:PSS/SY/LiF/Al))	77,100 (11.0 V)	10.04 (7.4 V)	5.41 (4.4 V)	3.58 (7.2 V)	2.0
ITO/PEDOT:GO(pH 3)/SY/LiF/Al	105,300 (11.2 V)	14.63 (6.6 V)	9.06 (4.0 V)	5.17 (6.6 V)	2.0
ITO/PEDOT:C-GO(pH 9)/SY/LiF/Al)	106,700 (10.8 V)	21.74 (6.4 V)	13.38 (4.0 V)	7.48 (6.4 V)	2.0

Reproduced from J.C. Yu, J.I. Jang, B.R. Lee, G.-W. Lee, J.T. Han, M.H. Song, Highly efficient polymer-based optoelectronic devices using PEDOT:PSS and a GO composite layer as a hole transport layer, ACS Appl. Mater. Interfaces 6 (2014) 2067–2073.

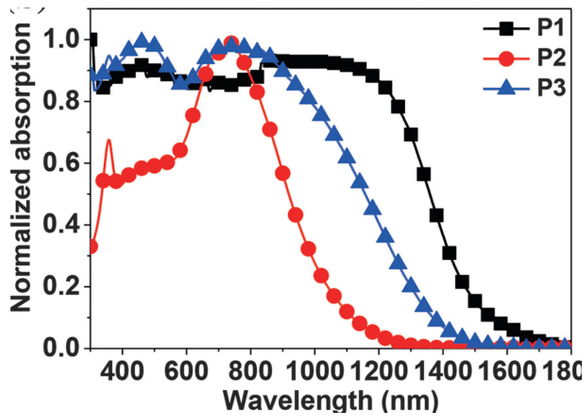


Fig. 7.1 External quantum efficiency (EQE) performance of no-gain photodiodes (P1–P3 were products synthesized by the Stille cross-coupling polymerization of DPP-2Br, TQ-2Br, BBT-2Br, and DTP-2Sn). Reproduced from J. Han, D. Yang, D. Ma, W. Qiao, Z.Y. Wang, Low-bandgap polymers for high-performance photodiodes with maximal EQE near 1200 nm and broad spectral response from 300 to 1700 nm, Adv. Opt. Mater. 6 (2018), 1800038 with permission of The Royal Society of Chemistry.

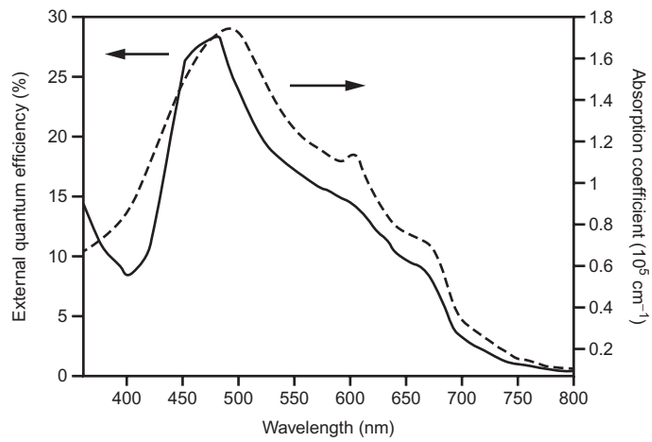


Fig. 7.2 Optical absorption of a POPT/MEH-CN-PPV double layer (-----) and EQE of an Au/PEDOT/POPT:MEH-CN-PPV (19: 1)/MEH-CN-PPV:POPT (19: l)/Ca device (——). From M. Granstrom, K. Petritsch, A.C Arias, R.H. Friend, High efficiency polymer photodiodes, Synth. Met. 102(1–3) (1999) 957–958.

4.5% was achieved under short circuit conditions, which was increased to 28% at 2V negative bias. Also, better results were obtained for double layers (Fig. 7.2) [43]. Linkoping University (Linkoping, Sweden) and the Chalmers University of Technology (Goeborg, Sweden) developed a photodiode from highly doped PEDOT-PSS with a donor layer of PTOPT and BEHP-PPV. They obtained a quantum efficiency of 35% while an additional layer of fullerene was added to improve absorption in the red and near-infrared wavelengths [44].

7.4 Shape memory polymers as a substrate for optoelectronics

Shape memory polymers (SMPs) were first discovered in 1980 and from that point, the shape-memory effect has been eyed by several

international researchers. Shape memory polymers (SMPs) are a novel class of smart materials that have developed rapidly in recent years. These materials have the ability to memorize and hence recover shapes under specific conditions. That behavior may be initiated using thermal, electrical, or environmental command [45–47]. They are associated with a broad range of application temperatures that can be tailored. They also have tunable stiffness and are easily processed. Polymers and metal alloys are the two materials used to realize such shape memory applications. Further, SMPs have been used in many areas, including biomedical science, deployable structures, actuators, sensors, optical and electrical devices, and smart fabrics [48–50].

Polymer-based shape memory materials possess the advantages of high elastic deformation (strain up to more than 200% for most of the materials), low cost, low density, and potential biocompatibility and biodegradability when compared to the alloy-based ones. They have been widely applied for aerospace, automobile, microelectronics, and optoelectronic applications, owing to their excellent mechanical properties, dielectric features, and high thermal and chemical resistance [51–53]. Plus, optoelectronic devices demand materials that are lighter, ultrathin, and flexible. Thus, alloys and glasses are not able to meet the requirements of optoelectronic devices. Therefore, optically transparent polymer is the most preferred substrate for future optoelectronic devices [54–57].

Optically transparent polyimides (PI) are one such transparent polymer matrix that has garnered significant interest toward flexible optoelectronic applications. This includes a plastic substrate of image displays, optical waveguides of communication interconnects, flexible printing circuit boards, and liquid crystal alignment layers. The optically transparent shape memory polyimide (TSMPI) has excellent shape memory effects with high thermal stabilities, good mechanical properties, and excellent optical transparency (Fig. 7.3) [58]. An optically transparent PI with a glass transition temperature (T_g) of 171°C, higher than any other SMP reported, has been successfully developed. The said 120 mm thick polyimide film was reported to have exhibited optical transmittance higher than 81% in the 450–800 nm region [58]. Compared with traditional optically important polymer films such as PET and poly(methyl methacrylate) (PMMA), PI with higher optical transparency, high thermal stability, and excellent mechanical properties has been continuously explored for flexible thin film transistors, flexible organic electroluminescent devices, and flexible solar cells [59–63].

Cross-linked glassy polymers are the simplest class of shape-polymeric materials. They have an excellent degree of shape recovery, rubber elasticity, adjustable rubbery modulus, and work capacity. A chemically cross-linked vinylidene random copolymer consisting of two vinylidene monomers (one being methyl methacrylate and the

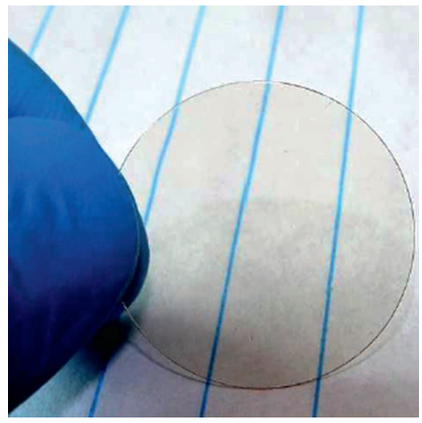


Fig. 7.3 Optical transparent film made from polyimide. From X. Qiu, D. Kong, W. Zhang, Y. Liu, J. Leng, Optically transparent high temperature shape memory polymers, Soft Matter. 12 (2016) 2894–2900.

other butyl methacrylate) is an example of this type of polymer. This thermoset shows complete shape fixing and fast, complete shape recovery in hot water at the stress-free stage. In addition, this polymer has the advantage of being stable and optically transparent. Prof. Larock's group worked on copolymerization and chemical cross-linking of renewable natural oils with a high degree of unsaturation with styrene and divinyl benzene to obtain random copolymer networks. These networks show tunable glass transitions and rubbery properties upon varying the monomer ratio [63–65]. Polynorbornene with $T_g = 40°C$ and high molecular weight poly(methyl methacrylate) (PMMA) with $T_g = 105°C$ have physical cross-links formed under deformed conditions. This will provide excellent elasticity above the glass transition [66–68].

Further, Yu et al., first reported the development of polymer light-emitting diodes on SMP substrates by using a single-walled carbon nanotube/polymer composite electrode as an ITO replacement [69, 70]. OLED devices have been successfully fabricated on flexible polymer substrates [such as polyether sulfone (PES)] and on recyclable nanocellulose/glycerol substrates in the past, which allowed for a limited deformation [71, 72]. Shape-memory polymer light-emitting diodes (PLEDs) using a new silver nanowire/polymer electrode have been reported. The electrode can be stretched by up to 16% with only a small increase in sheet resistance. The large deformation shape change and recovery of the PLEDs to various bi-stable curvatures have resulted in minimal loss of electro-luminescence performance [73]. On the other hand, UV curable shape memory polyesters have been used as substrates for the preparation of flexible OLEDs deformed to various stable shapes that recovered the initial plane shape. At the same time, the deformation caused little loss of the electroluminescent property [74–76]. OLEDs were fabricated using SMP substrates (1,3,5-triallyl-1,

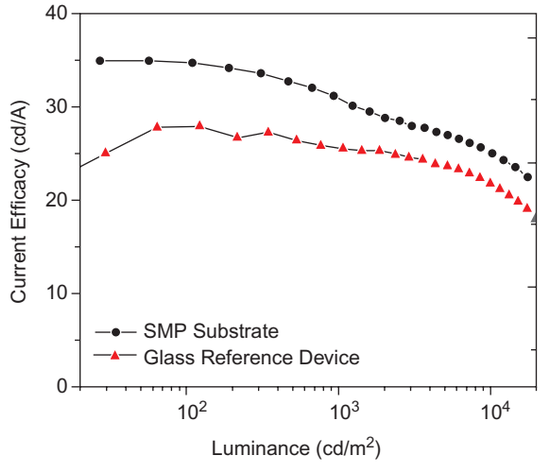


Fig. 7.4 Current efficacy versus luminance for 9-(3-(9H-Carbazol-9-yl)-5-(phenyl sulfonyl) phenyl)-9H-carbazole (mCPSOB-) and 4,4′-Bis(*N*-carbazolyl)-1,1′-biphenyl (CBP-) based OLEDs. From M.P. Gaj, A. Wei, C. Fuentes-Hernandez, Y. Zhang, R. Reit, W. Voit, S.R. Marder and B. Kippelen, Organic lightemitting diodes on shape memory polymer substrates for wearable electronics, Org. Electron. 25 (2015) 151–155.

3,5-triazine-2,4,6(1H,3H,5H)-tri-one (TATATO), tri-methylol propane tris(3-mercaptopropionate) (TMTMP), and tricyclodecane di-methanol di-acrylate (TCMDA)). It showed a low glass transition temperature of 43°C, a maximum efficacy of 33 cd/A (Fig. 7.4) measured at a luminance of 1000 cd/m^2, and a peak luminance of more than 30,000 cd/m^2 [76].

It was also observed that wrinkled nanoribbons and nanomembranes on PDMS offer stretchability to the brittle, inextensible semiconductor materials. Based on this method, stretchable electronics and optoelectronic systems are realized such as a silicon-based integrated circuit that is stretchable, twistable, and foldable [77–80].

7.5 Conclusions and future directions

To conclude, the field of optoelectronics is a fast emerging field. The scope has widened and includes electro-optics and photonics. It has wide applications in sourcing, detection, and light controls. The field also has large application in the military and aerospace industries. Because they use less power and provide a high bandwidth for communication, these devices have excellent application in designing the satellites of the future. It is reported that a GaN semiconductor is set up to make a great impact by 2025. The accelerated demand for energy efficient electronic devices by consumers might be the reason for the same. Apart from power efficiency, the material presents excellent chemical and mechanical properties, high saturation velocity, and voltage breakdown. With the emerging consumption of new fabricating and production technologies, the use of optoelectronic parts is rising high in the industrial sector.

References

[1] X. Zhang, C.J. Chung, A. Hosseini, H. Subbaraman, J. Luo, A.K.-Y. Jen, R.L. Nelson, C.Y.-C. Lee, R.T. Chen, High performance optical modulator based on electro-optic polymer filled silicon slot photonic crystal waveguide, J. Lightwave Technol. 34 (2016) 2941–2951.

[2] F. Wen, C. Hao, J. Xiang, L. Wang, H. Hou, Z. Su, W. Hu, Z. Liu, Enhanced laser scribed flexible graphene-based micro-supercapacitor performance with reduction of carbon nanotubes diameter, Carbon 75 (2014) 236–243.

[3] J. Gao, Y. Yang, Z. Zhang, J.Y. Yan, Z.H. Lin, X.Y. Guo, Bifacial quasi-solid-state dye-sensitized solar cells with poly (vinyl pyrrolidone)/polyaniline transparent counter electrode, Nano Energy 26 (2016) 123–130.

[4] C.P. Lee, C.A. Lin, T.C. Wei, M.L. Tsai, Y. Meng, C.T. Li, K.C. Huo, C.I. Wu, S.P. Lau, J.H. He, Economical low-light photovoltaics by using the Pt-free dye-sensitized solar cell with graphene dot/PEDOT:PSS counter electrodes, Nano Energy 18 (2015) 109–117.

[5] D. Jandura, D. Pudis, A. Kuzma, Fabrication technology for PDMS ridge waveguide using DLW, Optik Int. J. Light Electron. Opt. 127 (2016) 2848–2851.

[6] H. Ma, A.K.-Y. Jen, L.R. Dalton, Polymer-based optical waveguides: materials, processing, and devices, Adv. Mater. 14 (2002) 1339–1365.

[7] A.K. Das, Laser direct writing polymeric single-mode waveguide devices with a rib structure, Appl. Opt. 42 (2003) 1236–1243.

[8] H.H.D. Nguyen, U. Hollenbach, U. Ostrzinski, K. Pfeiffer, S. Hengsbach, J. Mohr, Freeform three-dimensional embedded polymer waveguides enabled by external-diffusion assisted two-photon lithography, Appl. Opt. 55 (2016) 1906–1912.

[9] J.W. David, Fibrebragg grating sensors in polymer optical fibres, Meas. Sci. Technol. 26 (2015) 6013.

[10] S. Cichosz, A. Masek, M. Zaborski, Polymer-based sensors: a review, Polym. Test. 67 (2018) 342–348.

[11] R. Kiebooms, R Menon, K Lee, Synthesis, electrical, and optical properties of conjugated polymers (Chapter 1), in: H.S. Nalwa (Ed.), Handbook of Advanced Electronic and Photonic Materials and Devices. Conducting Polymers, vol. 8, Elsevier, 2001.

[12] Proceedings of the 2000 International Conference on Science and Technology of Synthetic Metals, Synth. Met. 119–121(2001) 1–1905Proceedings of the 2000 International Conference on Science and Technology of Synthetic Metals, Synth. Met. 119–121(2001) 1–1905.

[13] S.R. Forrest, Active optoelectronics using thin-film organic semiconductors, IEEE J. Sel. Top. Quantum Electron. 6 (6) (2000) 1072–1083, https://doi.org/10.1109/2944.902156. IEEE J. Sel. Top. Quantum Electron. 6 (6) (2000) 1072–1083, https://doi.org/10.1109/2944.902156.

[14] M.M. Lee, J. Teeuscher, T. Miyasaka, T.N. Murakami, H.J. Snaith, Efficient hybrid solar cells based on meso-superstructured organometal halide perovskites, Science 338 (2012) 643–647.

[15] J. Wei, H. Li, Y.C. Zhao, W.K. Zhou, R. Fu, Y. Leprince-Wang, D.P. Yu, Q. Zhao, Suppressed hysteresis and improved stability in perovskite solar cells with conductive organic network, Nano Energy 26 (2016) 139–147.

[16] M. Cano-Garcia, A. Elmogi, M.-A. Mattelin, J. Missinne, M.A. Geday, J.M. Oton, G. Van Steenberge, X. Quintana, All-organic switching polarizer based on polymer waveguides and liquid crystals, Opt. Express 26 (2018) 9584–9594.

[17] A. Alfadhel, B. Li, J. Kosel, Magnetic polymer nanocomposites for sensing applications, in: Proceedings of the 2014 IEEE Sensors, Valencia, Spain, 2–5 November, 2014.

[18] C.-T. Wang, Y.-C. Li, J.-H. Yu, C.Y. Wang, C.-W. Tseng, H.-C. Jau, Y.-J. Chen, T.-H. Lin, Electrically tunable high Q-factor micro-ring resonator based on blue phase liquid crystal cladding, Opt. Express 22 (2014) 17776–17781.

[19] V. Zardetto, T.M. Brown, A. Reale, A.D. Carlo, Substrates for flexible electronics: a practical investigation on the electrical, film flexibility, optical, temperature, and solvent resistance properties, J. Polym. Sci., Part B: Polym. Phys. 49 (2011) 638–648.
[20] Q. Qin, R. Zhang, A novel conical structure of polyaniline nanotubes synthesized on ITO-PET conducting substrate by electrochemical method, Electrochim. Acta 89 (2013) 726–773.
[21] S.A. Agarkar, V.V. Dhas, S. Muduli, S.B. Ogale, Dye sensitized solar cell (DSSC) by a novel fully room temperature process: a solar paint for smart windows and flexible substrates, RSC Adv. 2 (2012) 11645–11649.
[22] H. Sirringhaus, 25th anniversary article: organic field-effect transistors: the path beyond amorphous silicon, Adv. Mater. 26 (2014) 1319–1335.
[23] Z. Yi, S. Wang, Y. Liu, Design of high-mobility diketopyrrolopyrrole-based π-conjugated copolymers for organic thin-film transistors, Adv. Mater. 27 (2015) 3589–3606.
[24] T. Lei, J.Y. Wang, J. Pei, Design, synthesis, and structure property relationships of isoindigo-based conjugated polymers, Acc. Chem. Res. 47 (2014) 1117–1126.
[25] Q.D. Tai, B.L. Chen, F. Guo, S. Xu, H. Hu, B. Sebo, X.Z. Zhao, In situ prepared transparent polyaniline electrode and its application in bifacial dye-sensitized solar cells, ACS Nano 5 (2011) 3795–3799.
[26] Z.Y. Tang, J.H. Wu, M. Zheng, Q.W. Tang, Q. Liu, J.M. Lin, J.L. Wang, High efficient PANI/Ptnanofibercounter electrode used in dye-sensitized solar cell, RSC Adv. 2 (2012) 4062–4064.
[27] J.W. Park, J. Jang, Fabrication of graphene/free-standing nanofibrillar PEDOT/P(VDF-HFP) hybrid device for wearable and sensitive electronic skin application, Carbon 87 (2015) 275–281.
[28] F. Zhang, M. Johansson, M.R. Andersson, J.C. Hummelen, O. Inganas, Polymer photovoltaic cells with conducting polymer anodes, Adv. Mater. 14 (2002) 662–665.
[29] R. Po, C. Carbonera, A. Bernardi, F. Tinti, N. Camaioni, Polymer- and carbon-based electrodes for polymer solar cells: toward low-cost, continuous fabrication over large area, Sol. Energy Mater. Sol. Cells 100 (2012) 97–114.
[30] H.H. Dam, K. Sun, E. Hanssen, J.M. White, T. Marszalek, W. Pisula, J. Czolk, J. Ludwig, A. Colsmann, M. Pfaff, D. Gerthsen, W.W.H. Wong, D.J. Jones, Morphology change and improved efficiency in organic photovoltaics via Hexa-peri-hexabenzocoronene templates, ACS Appl. Mater. Interfaces 6 (2014) 8824–8835.
[31] K. Sun, Z. Xiao, S. Lu, W. Zajaczkowski, W. Pisula, E. Hanssen, J.M. White, R.M. Williamson, J. Subbiah, J. Ouyang, A.B. Holmes, W.W.H. Wong, D.J. Jones, A molecular nematic liquid crystalline material for high-performance organic photovoltaics, Nat. Commun. 6 (2015) 6013.
[32] K. Sun, H. Zhang, J. Ouyang, Indium tin oxide modified with sodium compounds as cathode of inverted polymer solar cells, J. Mater. Chem. 21 (2011) 18339–18346.
[33] Z. Xiao, J. Subbiah, K. Sun, D.J. Jones, A.B. Holmes, W.W.H. Wong, Synthesis and photovoltaic properties of thieno[3,2-*b*]thiophenyl substituted benzo[1,2-*b*:4,5-*b*′]dithiophene copolymers, Polym. Chem. 5 (2014) 6710–6717.
[34] B. Zhao, K. Sun, F. Xue, J. Ouyang, Isomers of dialkyldiketo-pyrrolo-pyrrole: Electron-deficient units for organic semiconductors, Org. Electron. 13 (2012) 2516–2524.
[35] B.A. Al-Asbahi, Influence of SiO_2/TiO_2 nanocomposite on the optoelectronic properties of PFO/MEH-PPV-based OLED devices, Polymers 10 (2018) 800.
[36] K. Jokinen, A. Bykov, R. Sliz, K. Remes, T. Fabritius, R. Myllyla, Luminescence and spectrum variations caused by thermal annealing in undoped and doped polyfluorene OLEDs, Solid State Electron. 103 (2015) 184–189.

[37] C. Cuerva, J.A. Campo, M. Cano, B. Arredondo, B. Romero, E. Oton, J.M. Oton, Bis(pyridylpyrazolate)platinum(ii): A mechanochromic complex useful as a dopant for colour-tunable polymer OLEDs, New J. Chem. 39 (2015) 8467–8473.
[38] A.M. Assaka, P.C. Rodrigues, A.R. De Oliveira, L. Ding, B. Hu, F.E. Karasz, L. Akcelrud, Novel fluorine containing polyfluorenes with efficient blue electroluminescence, Polymer 45 (2004) 7071–7081.
[39] J.C. Yu, J. In Jang, B.R. Lee, G.-W. Lee, J.T. Han, M.H. Song, Highly efficient polymer-based optoelectronic devices using PEDOT:PSS and a GO composite layer as a hole transport layer, ACS Appl. Mater. Interfaces 6 (2014) 2067–2073.
[40] A.C. Arias, M. Granstrom, K. Petritsch, R.H. Friend, Organic photodiodes using polymeric anodes, Synth. Met. 102 (1999) 953–954.
[41] J. Han, D. Yang, D. Ma, W. Qiao, Z.Y. Wang, Low-bandgap polymers for high-performance photodiodes with maximal EQE near 1200 nm and broad spectral response from 300 to 1700 nm, Adv. Opt. Mater. 6 (2018) 1800038.
[42] J. Han, D. Yang, D. Ma, W. Qiao, Z.Y. Wang, Preparation of AZO:PDIN hybrid interlayer materials and application in high-gain polymer photodetectors with spectral response from 300 nm to 1700 nm, Org. Electron. 68 (2019) 953–954.
[43] M. Granstrom, K. Petritsch, A.C. Arias, R.H. Friend, High efficiency polymer photodiodes, Synth. Met. 102 (1999) 957–958.
[44] L.C. Chen, O. Inganas, L.S. Roman, M. Johansson, M. Andersson, Self organised polymer photodiodes for extended spectral coverage, Thin Solid Films 363 (2000) 286–289.
[45] T. Mu, L. Liu, X. Lan, Y. Liu, J. Leng, Shape memory polymers for composites, Compos. Sci. Technol. 160 (2018) 169–198.
[46] Y. Liu, H. Du, L. Liu, J. Leng, Shape memory polymers and their composites in aerospace applications: a review, Smart Mater. Struct. 23 (2014) 23001–23022.
[47] W. Wang, Y. Liu, J. Leng, Recent developments in shape memory polymer nanocomposites: actuation methods and mechanisms, Coord. Chem. Rev. 320–321 (2016) 38–52.
[48] J. Hu, Y. Zhu, H. Huang, J. Lu, Recent advances in shape-memory polymers: structure, mechanism, functionality, modeling and applications, Prog. Polym. Sci. 37 (2012) 1720–1763.
[49] Y. Zhang, Y. Li, W. Liu, Dipole-dipole and H-bonding interactions significantly enhance the multifaceted mechanical properties of thermoresponsive shape memory hydrogels, Adv. Funct. Mater. 25 (2015) 471–480.
[50] W.M. Sokolowski, S.C. Tan, Advanced self-deployable structures for space applications, J. Spacecr. Rockets. 44 (2007) 750–754.
[51] T. Sekitani, U. Zschieschang, H. Klauk, T. Someya, Flexible organic transistors and circuits with extreme bending stability, Nat. Mater. 9 (2010) 1015–1022.
[52] D. Liaw, K. Wang, Y. Huang, K. Lee, J. Lai, C. Ha, Advanced polyimide materials: synthesis, physical properties and applications, Prog. Polym. Sci. 37 (2012) 907–974.
[53] K. Min, T. Lee, C.P. Park, Z. Wu, H.H. Girault, I. Ryu, T. Fukuyama, Y. Mukai, D. Kim, Monolithic and flexible polyimide film microreactors for organic microchemical applications fabricated by laser ablation, Angew. Chem., Int. Ed. 49 (2010) 7063–7067.
[54] C. Yang, Y. Su, Colorless and high organosoluble polyimides from 2, 5-bis(3, 4-dicarboxyphenoxy)-tbutylbenzenedianhydride and aromatic bis(ether amine) bearing pendent trifluoromethyl groups, Polymer 46 (2005) 5778–5788.
[55] Z. Liu, J. Li, Z. Sun, G. Tai, S. Lau, F. Yan, The application of highly doped single-layer graphene as the top electrodes of semitransparent organic solar cells, ACS Nano 6 (2012) 810–818.
[56] J. Liu, T.M. Lee, C. Wen, C. Leu, High-performance organic–inorganic hybrid plastic substrate for flexible displays and electronics, J. Soc. Inf. Disp. 19 (2011) 63–69.

[57] M. Choi, J. Hwang, C. Kim, S. Ando, C. Ha, New colorless substrates based on polynorbornene-chlorinated polyimide copolymers and their application for flexible displays, J. Polym. Sci., Part A-1: Polym. Chem. 48 (2010) 1806–1814.
[58] X. Qiu, D. Kong, W. Zhang, Y. Liu, J. Leng, Optically transparent high temperature shape memory polymers, Soft Matter 12 (2016) 2894–2900.
[59] H. Ni, J. Liu, Z. Wang, S. Yang, A review on colorless and optically transparent polyimide films: chemistry, process and engineering applications, J. Ind. Eng. Chem. 28 (2015) 16–27.
[60] K. Sidler, N.V. Cvetkovic, V. Savu, D. Tsamados, A.M. Ionescu, J. Brugger, Organic thin film transistors on flexible polyimide substrates fabricated by full-wafer stencil lithography, Procedia Chem. 162 (2010) 155–159.
[61] H. Lim, W.J. Cho, C.S. Ha, S. Ando, Y.K. Kim, C.H. Park, K. Lee, Flexible organic electroluminescent devices based on fluorine-containing colorless polyimide substrates, Adv. Mater. 14 (2002) 1275–1279.
[62] J.W. Lim, D.Y. Cho, K. Eun, S.H. Choa, S.I. Na, J. Kim, H.K. Kim, Mechanical integrity of flexible Ag nanowire network electrodes coated on colorless PI substrates for flexible organic solar cells, Sol. Energy Mater. Sol. Cells. 105 (2012) 69–76.
[63] F. Li, A. Perrenoud, R.C. Larock, Thermophysical and mechanical properties of novel polymers prepared by the cationic copolymerization of fish oils, styrene and divinylbenzene, Polymer 42 (2001) 10133–10145.
[64] F. Li, R.C. Larock, New soybean oil–styrene–divinylbenzene thermosetting copolymers. v. shape memory effect, J. Appl. Polym. Sci. 84 (2002) 1533–1543.
[65] Z. Jing, S.S. Sergei, Reversible shape-shifting in polymeric materials, Polym.Phys. 54 (2016) 1365–1380.
[66] P.T. Mather, H.G. Jeon, T.S. Haddad, Strain recovery in POSS hybrid thermoplastics, American Chemical Society, polymer preprints, Div. Polym. Chem. 41 (2000) 528.
[67] H.G. Jeon, P.T. Mather, T.S. Haddad, Shape memory and nanostructure in-poly(norbornyl-POSS) copolymers, Polym. Int. 49 (2000) 453–457.
[68] H. Nagai, A. Ueda, S. Isomura, Shape-Memory Norbornene Polymer Molded Products, Jpn. Pat., 06080768, 1994.
[69] Z.B. Yu, Y. Zhibin, Z. Qingwu, L. Lu, C. Qi, N. Xiaofan, L. Jun, P. Qibing, Highly flexible silver nanowire electrodes for shape-memory polymer light-emitting diodes, Adv. Mater. 23 (2011) 664–668.
[70] Z.B. Yu, N. Xiaofan, L. Zhitian, P. Qibing, Intrinsically stretchable polymer light-emitting devices using carbon nanotube-polymer composite electrodes, Adv. Mater. 23 (2011) 3989–3994.
[71] K.A. Knauer, et al., Stacked inverted top-emitting green electrophosphorescent organic light-emitting diodes on glass and flexible glass substrates, Org. Electron. 14 (2013) 2418–2423.
[72] E. Najafabadi, et al., Efficient organic light-emitting diodes fabricated on cellulose nanocrystal substrates, Appl. Phys. Lett. 105 (2014), 063305.
[73] Y. Zhibin, Z. Qingwu, L. Lu, Q. Chen, N. Xiaofan, L. Jun, P. Qibing, Highly flexible silver nanowire electrodes for shape-memory polymer light-emitting diodes, Adv. Mater. 23 (2010) 664–668.
[74] H. Xu, C. Yu, S. Wang, V. Malyarchuk, T. Xie, J.A. Rogers, Deformable, programmable, and shape-memorizing micro-optics, Adv. Funct. Mater. 23 (2013) 3299–3306.
[75] T. Xie, X. Xiao, J. Li, R. Wang, Encoding localized strain history through wrinkle based structural colors, Adv. Mater. 22 (2010) 4390–4394.
[76] M.P. Gaj, A. Wei, C. Fuentes-Hernandez, Y. Zhang, R. Reit, W. Voit, S.R. Marder, B. Kippelen, Organic light emitting diodes on shape memory polymer substrates for wearable electronics, Org. Electron. 25 (2015) 151–155.
[77] Y. Sun, W.M. Choi, H. Jiang, Y.Y. Huang, J.A. Rogers, Controlled buckling of semiconductor nanoribbons for stretchable electronics, Nat. Nanotechnol. 1 (2006) 201–207.

[78] D.H. Kim, J.H. Ahn, W.M. Choi, H.S. Kim, T.H. Kim, J. Song, Y.Y. Huang, Z. Liu, C. Lu, J.A. Rogers, Stretchable and foldable silicon integrated circuits, Science 320 (2008) 507–511.
[79] I. Jung, J. Xiao, V. Malyarchuk, C. Lu, M. Li, Z. Liu, J. Yoon, Y. Huang, J.A. Rogers, Dynamically tunable hemispherical electronic eye camera system with adjustable zoom capability, Proc. Natl. Acad. Sci. U. S. A. 108 (2011) 1788–1793.
[80] D.Y. Khang, H. Jiang, Y. Huang, J.A. Rogers, A stretchable form of single-crystal silicon for high-performance electronics on rubber substrates, Science 311 (2006) 5.

8

π-Stacking, conjugated, polymer-supported carbon nanotubes (CNTs) composite materials for light-emitting diode (LED) application

V. Ramkumar[a], I.P. Bincy[b], D. Santhanaraj[c], M. Gopiraman[d], and Sellamuthu N. Jaisankar[a]

[a]Department of Polymer Science and Technology, Council of Scientific and Industrial Research (CSIR), Central Leather Research Institute (CLRI), Chennai, Tamilnadu, India, [b]Department of Physics, MES College, Nedumkandam, Kerala, India, [c]Department of Chemistry, Loyola College, Chennai, India, [d]Department of Applied Bioscience, College of Life and Environment Science, Konkuk University, Seoul, South Korea

8.1 Introduction

The term "optoelectronics" implies that, the studies of various optical devices and the electrical interaction on flow of light in a matter. The term "quantum electronics" means the device- and system-based interaction between light and material. Nowadays, novel photonics methods are developed through new technologies such as optoelectronics, quantum electronics, digital electronics [1–3], etc. The physico-chemical interaction between the light and system are stimulating factor of an optoelectronics, the important cases on semiconductor energy devices are light emitting diodes (LEDs), solar cell (SC) and the photodiodes (PDs) [4–6]. The new area of optoelectronics involves classical optics such as lenses, mirrors, and optical filters. The term photonics implies mixed electronics and optics. The modern discipline emphasizes the improvement in electronics, optical device and technologies. The electronics are considered as the flow of electrons and its controls by the photons. These areas are combined in many cases, due to the photons can be controlled by change of the electrons. As a final point, the applied

Polymer-Based Advanced Functional Composites for Optoelectronic and Energy Applications
https://doi.org/10.1016/B978-0-12-818484-4.00007-0
Copyright © 2021 Elsevier Inc. All rights reserved.

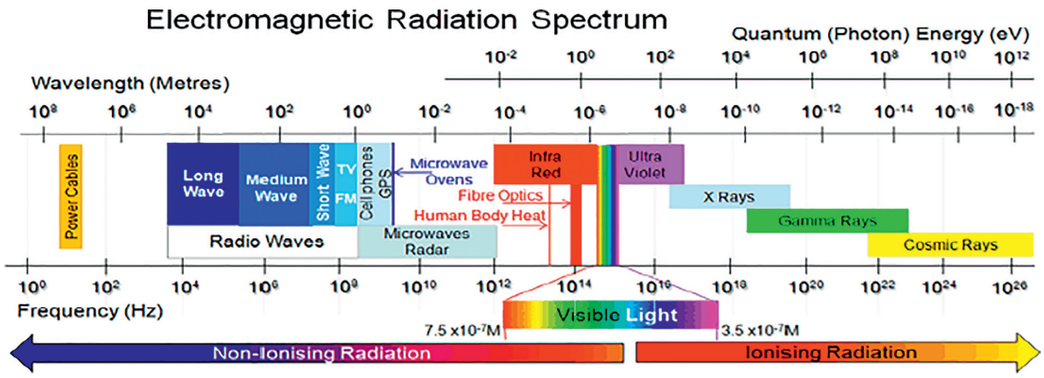


Fig. 8.1 Electromagnetic spectrum of radiation span.

research areas emerging from these domains include optical computing, optical sensing, optical processing, display technology, etc. An example of the emerging branch of optics that combines some of the above-mentioned disciplines is the field of integrated photonics [7–12]. The electromagnetic series range of the radiations span consists of wide range wavelengths from the cosmic ray to radio waves. The spectrum on a logarithmic scale is depicted in Fig. 8.1. In general, visible light lies within the narrow region of the spectrum with a wavelength from 0.4 to 0.7 m. This chapter deals with the interactions of visible light on the various carbon nanotube polymer composite materials and its power efficiency improvements.

8.2 π-Stacking and conjugation of polymers

Organic molecules generally exhibit a "π-electron" conjugated system through an electron acceptor and a donor group. This variation provides the push-pull conjugation effect, thus leading to an intramolecular charge transfer in the material [13–15]. The noncovalent attraction between the aromatic rings is called π stacking/π-π stacking. The noncovalent interaction involving an aromatic molecule permeates in the chemical process. The π-sigma interaction is weaker than π-π interaction, due to the geometry and electrostatic effect. The van der Waals forces mark the major contribution to the molecule of the pragmatic interactions. This report shows that the intramolecular charge transfer (ICT) behavior of a molecule depends upon the alignment and structure. The solid-state material ICT is mainly based on the π-π stacking of a molecule. These π-π stackings of the conjugated small molecules are influenced in a different angle of inter- and intramolecular interactions. The π-π

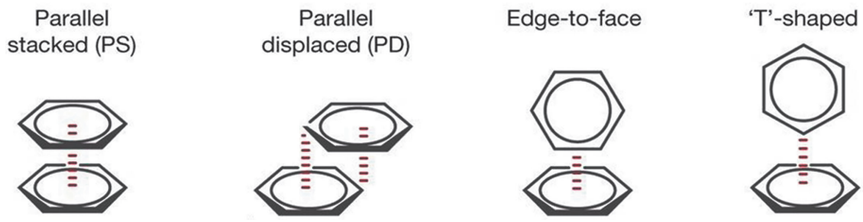


Fig. 8.2 Types of noncovalent π-π interactions in organic molecules.

stacking interactions are mentioned as a specific type of intermolecular attraction unique to aromatic molecules. The implicit understanding of distinct from the noncovalent interaction used to describe all the intermolecular complexes.

The best-studied interactions of π-systems are noncovalent interactions among neutral, closed-shell aromatic rings, and these are often characterized by the terms π-π interaction or π-stacking. The four types of π-π interactions are parallel stacked (PS), parallel displaced (PD), edge to face (EF), and T-shaped; they are shown in Fig. 8.2. This structural preference can be understood in terms of molecular quadruple movements. Considering how the π-π interaction can be played for ground-state stabilization, a large energy rise is caused by repulsive electrostatic interaction among the π—electrons of aromatic molecules.

Among the many known organic materials, some π -stacking conjugated polymer molecules exhibited extremely high energy conversion and fast charge transporting ability in their molecular structure. The π-stacking conjugated polymer molecules are widely used in frequency conversation, optical switching, and electrooptical applications. Commonly known as π-stacking conjugated polymers, these could enhance the delocalization of the electron system with strong donor and acceptor groups. The designing of molecules as π-stacking conjugated polymers greatly influences the molecular packing structure, which is highly required for electronics applications. On the other hand, π-stacking conjugated polymer molecules are much needed for optoelectronic applications.

8.3 The molecular photochemistry and photophysics

The photophysical process commences with the absorption of light in the form of electromagnetic radiation by a probe molecule. Following the initial act of light absorption, the molecule is lifted from the ground state to the singlet excited state, typically the HOMO to

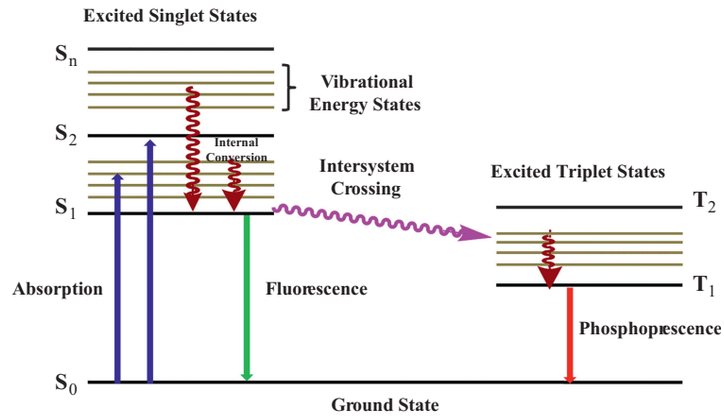


Fig. 8.3 Molecular mechanism of the Jablonski diagram.

LUMO level [16–18]. There are many ways to return to the ground state. The relative energy ordering of possible interconversions was summarized in the form of a Jablonski diagram, as shown in Fig. 8.3. The excitation of the molecule from the ground state to one of its excited electronic states of the same multiplicity results in the production of a vibrational excited state within the excited state. The molecule in the higher vibrational level of the excited state is to dissipate excess vibrational energy to the surroundings and arrive at the lowest vibrational level of the exciting level. This phenomenon is called vibrational relaxation within the excited state. This relaxation is very rapid, requiring less than 10^{-13} s for completion. Once the excited molecule has relaxed to the lowest vibrational level of the excited state, it can lose its excitation energy by several radiative and nonradiative processes. Photochemistry is a primary mechanism for all photobiology. When a molecule absorbs a photon of light, its electronic structure changes and reacts with the other molecules. The energy absorbed from light could rest in the photochemical change in the absorbed molecule. The energy could also be given off in the form of heat or lower-energy light such as fluorescence/phosphorescence to attain the ground state of the molecule. Each type of molecule has a different preference and mechanism its uses to get rid of the absorbed photon energy. The first law of photochemistry states that the light must be absorbed for a photochemical reaction to follow. This is a simple concept but it is the basis for the performance of photobiological and photochemical reactions. If the light of a particular wavelength is not absorbed by a system, the photochemical reaction will not occur. The second law of photochemistry describes each photon of light absorbed by a chemical system; only one molecule is activated for the photochemical reaction. This law is appropriate for an ordinary light intensity. However, with a high-power laser, the two photon reactions also can take place.

The molecule is raised to the higher energy state than that produced by the single-photon absorption.

Luminescence: The term luminescence describes a process in which materials absorb energy and instantly remit it as visible radiation. This occurs as a result of the excitation of electrons from the valence band into the conduction band of the materials. The source of the input energy may be higher energy levels. During the process, the excited electrons drops back to the lower energy levels. If the emission takes place within 10^{-8} s, it is called fluorescence; if the emission occurs more than 10^{-8} s, it is called phosphorescence. Luminescence takes place on the outer valance and conduction band. The luminescence does not occur in metals and certain materials. The energy gap between the valence and conduction band is designed such that an electron dropping through this gap produces a photon. Generally, pure materials do not exhibit this phenomenon. The luminescence process has been classified as three types, photoluminescence, cathode luminescence, and electroluminescence. Electroluminescence is used in LED devices, as the p-n resolving junctions are stimulated by an externally applied voltage. When a forward-biased voltage is applied across the device, the electrons and hole recombine at the junction and emit the photons in the visible range. The characteristic color of an LED depends upon the materials used from red to violet in the visible region.

8.4 The internal conversion and intersystem crossings

There are two types of mechanisms involved in the Jablonski diagram: internal conversion (IC) and intersystem conversion (ISC). The nonradioactive relaxation among two states of the same spin multiplicity is known as internal conversion. This can be accomplished in several ways. If the lower vibrational level of the first excited state overlaps with the higher vibrational level of the ground state, the excited and ground states will be in a transient thermal equilibrium and permit the deactivation of the excited and ground states. If there is no overlap between the upper and lower electronics states, internal conversion takes place by quantum mechanical tunneling. The nonradioactive transition between states with different spin multiplicities is called intersystem crossing.

8.5 Fluorescence and phosphorescence

The radioactive transition from the upper to lower states of the same multiplicity is termed fluorescence. Fluorescence is a comparatively fast process because of its spin allowed transition and fluorescence

lifetime, usually in the range of 10^{-8}–10^{-12} s. Fluorescence is generally observed in rigid framework organic molecules.

Phosphorescence emissions involve the transition between states of different multiplicities, usually T_1 and S_0. Direct excitation on the first excited triplet states is forbidden. This state is usually occupied only by intersystem crossing from the first excited singlet state. Phosphorescence is generally observed at liquid nitrogen temperature (77 K). The phosphorescence lifetime may range from 10^{-3} to several minutes, considerably longer than that of the excited state. Bimolecular reactions such as quenching of the excited state may occur either by a molecule in a ground state, termed self-quenching, or by physically added impurities, termed impurity quenching. Two important bimolecular reactions are energy transfer and electron transfer. In the energy transfer process, excited state molecules are capable of transferring their excited state energy to another molecule. Electron transfer occurs as a result of the transfer of an electron from or to an excited molecule. This simultaneously causes a reduction or oxidation of another species or another moiety in the same molecule, differentiated as inter- and intermolecular electron transfer, respectively.

Quantum yield: The energy of the absorbed light can be lost in many ways, as depicted in the figure (Jablonski diagram). The energy may be lost in the form of heat as it returns to the ground state level. Besides that, the energy can also be lost by the fluorescence (IC) and phosphorescence (ISC) processes; some energy can also be transferred to the neighbor molecule. The quantum yield is the probability that an absorbed photon undergoes one particular process. The quantum yield is typically a number between 0 and 1, except under unusual circumstances. The total of all the quantum yields for a particular absorption event should sum to 1. If the condition is altered such that the quantum yield for fluorescence gets increased, then the quantum yield for some other process obviously decreases.

8.6 The electron transfer reactions

The electron transfer reaction is the subject of extensive study because of its immense importance in chemistry and biology. In the past decades, electron transfer in particular has become a field of interest because of the tremendous progress in experimental and theoretical treatments. Electron transfer has a wide range of applications in photocatalysis, artificial photosynthesis, solar-energy storage, polymerization, photosensitization, etc. [19–22].

Intramolecular Electron Charge Transfer (ICT) Reactions: The excited state contributes in numerous inter- and intramolecular reactions. The intramolecular process may include decomposition to smaller fragments (photodecomposition), ejection of electrons

(photoionization), and isomerization (photoisomerization). The intermolecular reaction includes additional reactions where an excited molecule combines with the ground-state molecules to form a stable product.

Intramolecular Electron Transfer (IET) Reactions: The photoinduced intramolecular electron transfer process continues to be a focus of theoretical and experimental investigations. These studies have been motivated in part by a desire to understand biological systems and to mimic photosynthesis. The intramolecular electron transfer is a fascinating arena because of the presence of both the acceptor and donor within a single molecule. The exciting task in this area is to understand the design of spacers to increase the rate and efficiency of the electron transfer reaction. The spacers are rigid or flexible chain molecules and transfers the electron through the either conjugated bond or heteroatom. Electron transfer predominates in systems where there is an efficient overlap of the orbital between the donor and acceptor systems. In the case of organic systems, donor and acceptor molecules are linked by a long-chain flexible hydrocarbon. The chain length affects the reaction kinetics; similarly, the steric nature, temperature, solvent viscosity, and polarity influence the reaction kinetics. In selected cases, the hydrocarbon chain undergoes a twisted intramolecular electron transfer, which in turn leads to dual emissions.

Intermolecular Electron Transfer Processes: The intermolecular electron transfer reaction is a subject of great recognition, as it forms the basis for a variety of chemical reactions. In organic chemistry, it paved the way for the synthesis of different new organic compounds, and the product of electron transfer is used as a photoinitiator for polymerization. The intermolecular electron transfer reaction in inorganic complexes finds a vital place in solar-energy conversion. Intermolecular electron transfer is one of the major pathways of quenching. Excited-state quenching introduces the reactive of intermediates. The electron transfer can occur from both the singlet and triplet states of the molecule. Fluorescence quenching owing to exciplex formation and electron transfer has been studied extensively.

8.7 Determination of bandgap energy

Bandgap energy (E_g) is an essential tool for constructing optical devices such as LEDs, solar cells, thin-film transistors, etc. The determination of the energy gap of a material is necessary for display manufacturing [6, 8]. The bandgap energy is the most important factor to the materials, which defines the conductivity of corresponding compounds. The energy gap could define the conductor,

semiconductor and insulator property of the desire molecule. Chemists usually describe energy associated with light in terms of its wavelength in nanometers while physicists tend to refer to energy in electron volts (eV).

The color of emission depends upon the size of HOMO and LUMO energy gap to the visible light (380–780nm). LED efficiency depends greatly upon the choice of electrode materials, as the efficiency of the charge injection depends upon the size of the energy barrier between the work function of the electrode and the energy level of HOMO (for the anode) or LUMO (for cathode). Because balanced charge injection is required (the emission requires a hole and an electron to combine), energy barriers should also be of comparable sizes. As a result, in designing new materials for LED use, care must be taken to match the HOMO and LUMO energies as closely as possible to the electrode materials. The conjugated polymer material is an interesting one for all color emissions, as they exhibit good stability toward light, heat, and oxygen, despite their high tendency toward π-π^* aggregate formation with concomitant quenching of fluorescence. There are a lot of methods to predict the bandgap energy of a material; some simple methods are from the UV-visible spectra, cyclic voltammetry analysis, and theoretical (DFT) calculations. It is noteworthy to mention that these three obtained results exhibited a nearly similar value of the semiconducting level. Bandgap energy could obtain wavelength absorption from respective compounds. Semiconducting materials could play a role in optoelectronics applications.

8.8 Carbon nanotubes

Sumio Iijima et al. first discovered another allotrope of carbon and named it a carbon nanotube (CNT). CNTs are classified as two types: multiwalled carbon nanotubes (MWCNTs) and single-walled carbon nanotubes (SWCNTs) (Fig. 8.4). MWCNTs consist of two or more concentric cylindrical shells of graphene sheets coaxially arranged around a central hollow core with interlayer separations as in graphite. In contrast, SWCNT comprises a single graphene cylinder. Both SWCNTs and MWCNTs have physical characteristics of solids and are microcrystals with high aspect ratios of 1000 or more, although the diameter is close to molecular dimensions [23, 24]. CNTs are used as composite fibers in polymers to improve the optical, mechanical, thermal, and electrical properties of the bulk products. CNTs are used to control nanoscale structures due to their strength and flexibility; they also play very important roles in nanoelectronics.

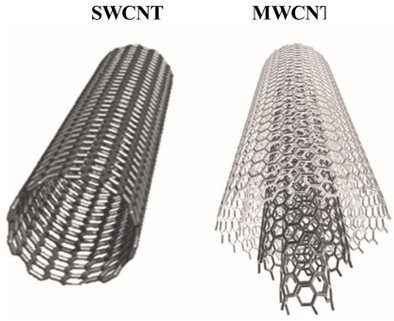


Fig. 8.4 Schematic structure of SWCNT and MWCNT.

8.9 CNT-polymer nanocomposites

CNT-polymer nanocomposites (CNT-PNC) are a combination of polymers with CNTs in a particular ratio (Fig. 8.5). The property of the polymers is improved by CNTs, and this plays a major role in the possession enhancement of the materials. CNT-PNC enhances the optical properties and conjugation of the material [25–29]. The optical properties of CNT-PNCs are considered important in flexible electronics. The dispersion of CNTs with a polymer matrix involves three important mechanisms of the interaction of the polymer matrix with carbon: (i) micromechanical interlocking: this could be difficult in nanotube composites due to their atomically smooth surface. Local nonuniformity along CNTs, including varying diameter and bends/kinks at places as a result of nonhexagonal defects, contributes to CNT-polymer adhesion by mechanical interlocking. (ii) Chemical bonding between the nanotubes and the matrix: this improves the interfacial interaction through an ionic or covalent bond that enables a stress transfer. (iii) Weak van der Waals bonding between the fiber and matrix: Under no chemical bonding between CNTs and the polymer, the origins of CNT-polymer interactions are electrostatic and van der Waals forces. Semiconducting CNTg CNT-PNCs are direct bandgap materials that possess free electron-hole pair excitations as well as strongly bound electron-hole pair states called excitation. The Van Hove singularities (nonsmooth point) of the density states are observed in the CNT-PNCs, thus leading to the strong absorption and emission nature of the material.

The density of electron desires the electrical and optical property of a materials, also plays a virtual role in fluorescence an electroluminescence behavior. CNT-PNCs have revealed clearly the property advantages that nanomaterials can provide in comparison to conventional CNTs and CNT-based polymers.

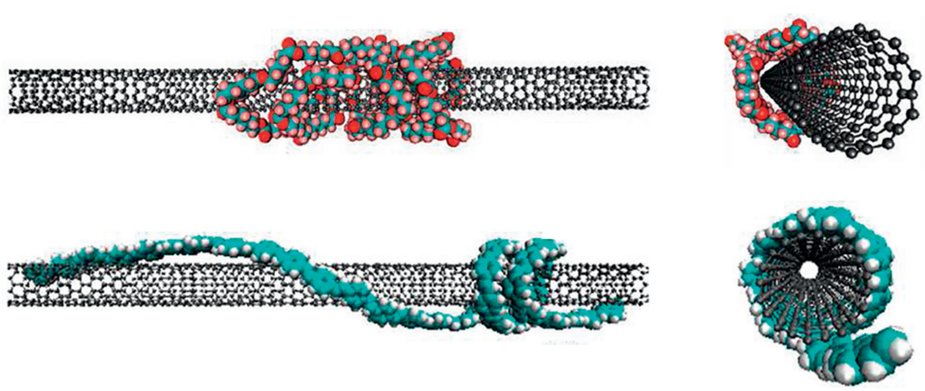


Fig. 8.5 Types of CNT-polymer composite formations.

8.10 Optoelectronic devices

The optoelectronic research area includes a wide range of devices containing LEDs, photodiodes, solar cells, information displays, image pick-up devices, optical storage, optical communication systems, and remote sensing systems. In addition, LED devices, telecommunication lasers, blue lasers, optical fiber photodiodes, and solar cells are the commercial examples of optoelectronic devices [2–6]. The mainstream of optoelectronic devices is the direct conversion between the electrons and photons, which are included in the LEDs, laser diodes, photodiodes, and solar cells.

LEDs: LEDs are commonly known as p-n semiconductor diodes in which electrons and holes recombine to yield photons. In this process, when a diode is electrically biased in the forward direction, it emits an incoherent narrow spectrum of light. In the light-emitting process, when voltage is applied to the lead material, the electrons can recombine easily with the holes within the device and release the energy in the form of photons. The resultant effect is called electroluminescence, and it is the conversion of electrical energy into light energy. The color of light is mainly governed by the bandgap energy of the material. Using an LED is more advantageous than any other type of emitting diode because it consumes less power and produces less heat. In general, LEDs last longer than incandescent lamps, and they could become the next generation of lighting. They could be widely used in any place such as in indication lights, computer components, watches, instrument panels, medical devices, switches, etc.

Solar Cells: The photovoltaic cell or solar cell is an electronic device that can directly convert sunlight radiation energy into electricity. When a photon falls from sunlight on a solar cell (p-n junction materials), it produces both the current and voltage to generate electric power. Sunlight consists of photons. When the photons hit the atoms of the solar cell, they transfer their energy to lose electrons. The electron flow converts as a current to an external circuit. The solar cell is made up of two layers bound together The first layer is loaded with free electrons, and these electrons are ready to jump from the first layer to the second layer. The second layer also has a few more electrons and they can be taken away from the surface easily. Therefore, it is ready to move a greater number of electrons from the top of the layer. The advantages of solar cells are that they require no fuel supply and they are not costly. They are also very dependable and require little maintenance.

Photodiode: The photodiode is a semiconductor light sensor device that generates a voltage or current when light radiation falls on the p-n junction material. The active p-n junction material might be operating in reverse bias mode during the irradiation process. A hole

or electron pair is created on the semiconductor materials when a photon with plenty of energy strikes the surface. The resultant electrons diffuse to the junctions to form an electric field. Due to this process, the electric field has developed across the depletion zone, and it is equal to a negative voltage across the unbiased diode. This method is popularly known as the inner photoelectric effect. This device can be widely used in three modes: photovoltaic as a solar cell, forward biased as an LED device, and reverse biased as a photodetector. Photodiodes are commonly employed in many types of circuits and different applications such as cameras, safety equipment, medical instruments, communication devices, and industrial applications.

Optical Fiber: An optical fiber or optic fiber is a plastic and transparent fiber material made of plastic or glass. It is somewhat thicker than a human hair, and it can function as a light pipe or waveguide to transmit light radiation between two ends of the fiber. The optical fiber material typically includes three concentric layers: a cladding, a core, and a jacket. The core part of the material is a light-transmitting region of the fiber in which the central section of the fiber is made up of silica material. Similarly, the cladding is a protective layer around the core also made up of silica, which generates an optical waveguide that limits the light in the core. However, the jacket is the nonoptical layer around cladding, which typically consists of one or more layers of a polymer that protects silica from physical or environmental damage. In general, jackets are available in different colors along with fiberoptic cable. These colors are used to recognize the fiber optic. For instance, an orange cable undoubtedly indicates a single modifier while a yellow one indicates a multimode fiber. For instance, an orange cable undoubtedly indicates a single modifier while a yellow one indicates a multimode fiber. In the single-mode fiber, one mode propagates and light rays travel through a straight cable. In a multimode cable, light rays travel all over the mode. These cables are broadly used in sensors, telecommunications, biomedical devices, fiber lasers, and many other industries. The advantages of using fiberoptic cable include their higher bandwidth, weightlessness, thinness, and less signal degradation than a copper wire. Moreover, they are cost-effective, flexible, and used in many medical and mechanical imaging systems.

Laser Diodes: A laser (light amplification by the stimulated emission of radiation) is a source of highly monochromatic, coherent, and directional light that operates under stimulated emission conditions. The function of a laser diode is to convert the electrical energy into light energy such as LEDs or infrared (IR) diodes. The beam of a typical laser is 4×0.6 mm and extends to a distance of up to 15 m. Most commonly, lasers are widely used as injection lasers or semiconductor lasers.

8.11 CNT-PNCs in optoelectronics

Polymer nanotechnology is enormously rooted in the design of advanced devices for electronic and optoelectronic applications. The dimensional scale for electronic devices has now entered the nanorange. The effectiveness of polymer-based nanocomposites in these areas is quite diverse, involving many prospective applications; they have been proposed for use in several applications. They are used in chemical sensors, electrocatalysis, electroluminescent devices, batteries, smart windows, and memory devices. Another potential application includes photovoltaic (PV) cells and photodiodes, printable conductors, supercapacitors, LEDs, and field effect transistors (FETs). The electrical conductivity of CNTs in insulating polymers has also been a topic of significant interest. The potential applications include electromagnetic interference protection, transparent conductive coatings, electrostatic dissipation, supercapacitors, electromechanical actuators, and several electrode applications.

The nano-sized CNTs are dispersed in polymers to improve their optical properties. The nanocomposite materials have a polymer matrix protected by a distinct nanomaterial to improve their properties. The polymers are occupied with particles that increase the stiffness and toughness of material, enhance barrier properties, and improve resistance to fire. The polymers are mostly enhanced by fillers to improve their mechanical, optical, and electrical properties and also to introduce antibacterial properties to the material. The nano-sized particles are distributed in the polymer to occupy a large number of sites in the polymer matrix to improve their strength and other properties. Enhancement with nanoparticles increases properties such as optical, modulus, heat resistance, electrical conductivity, and structural strength, but reduces gas permeability and flammability. Nanocomposite enhancement improves the luminescence, ultraviolet (UV) shielding, and UV resistance of transparent polymers. Nanoparticle agglomerations are avoided by incorporating them in the polymer matrix. The polymer nanocomposite has wide applications in the fields of microwave absorbing, sensors, data storage, and biomedical applications.

The amalgamation of CNTs into polymers advances their tensile strength, toughness, glass transition temperature, thermal conductivity, electrical conductivity, and optical properties. Recently, CNT-PNCs have garnered significant attention due to their unique mechanical, surface, and multifunctional properties as well as their robust interactions with the matrix resulting from the nanoscale microstructure and tremendously large interfacial area. However, CNTs are easy to agglomerate, bundle together, and entangle, leading to many defect sites in the composites and limiting the efficiency of CNTs on polymer matrices.

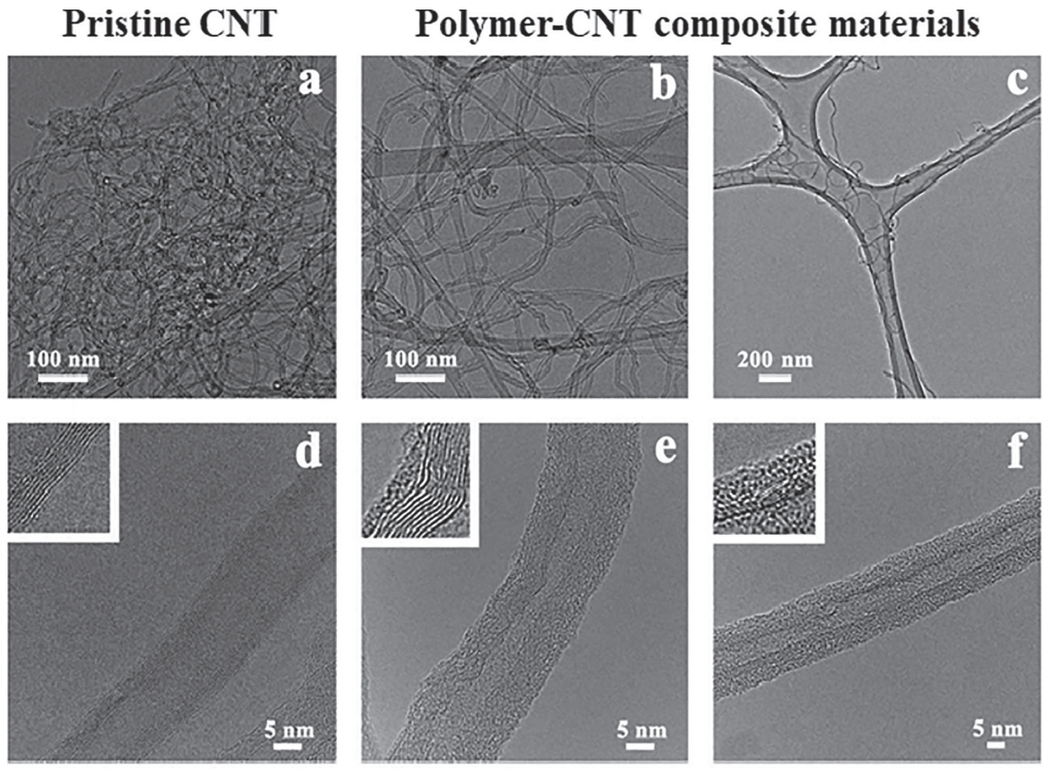


Fig. 8.6 TEM image of pristine CNTs (A, D) and polymer-modified CNTs (B–F).

There are numerous methods to enhance the diffusion of CNTs in a polymer matrix, including optimum physical blending, in situ polymerization, and chemical functionalization. A pristine CNT and a polymer-adapted CNT composite are depicted in Fig. 8.6 [30, 31].

Optimum physical blending: The broadly used compounding technique to prepare usually filled polymers is still the most convenient and practical way when nano-sized fillers are considered to replace micron-sized fillers for high-performance polymers. But the dispersion of nanofillers in a polymer matrix is more difficult than that of microfillers due to the strong tendency to agglomerate for the nanofillers. CNT-PNC dispersion can be done in several methods such as normal string, high power dispersion, ultrasound, and high speed sheering.

In situ polymerization: To develop the processability as well as the electrical, magnetic, and optical properties of CNTs, some conjugated or conducting polymers are attached to their surfaces by in situ polymerization. High-performance functioning composites based on

CNTs and polymers have also been prepared by in situ polymerization. The in situ polyimide PI/SWCNT composite films were antistatic and optically transparent with important conductivity improvement at a very low loading (0.1 vol.%). For PMMA/MWCNT composites consisting of 1 wt.% MWCNT, the storage modulus at 90°C is improved by an outstanding 1135% and the glass transition temperature is elevated exceptionally by about 40°C.

Chemical functionalization: In addition, the surfaces of CNTs have to be chemically functionalized (containing grafting copolymerization) to accomplish good dispersion in CNT-PNCs and solid interface adhesion between surrounding polymer chains, even though the interface area is very large. CNTs are accumulated as ropes or bundles. There are some catalyst residuals, bulky onions, spheroidal fullerenes, amorphous carbon, polyhedron graphite nanoparticles, and other forms of impurities in as-grown CNTs. Thus, purification, cutting/disentangling, and activation treatments are needed before chemical functionalization.

8.12 Polymer-CNT composite in LED application

CNT-PNCs are used as a versatile layered material in LED device fabrication. These CNT-Polymer composite materials is widely used in a device material such as cathode and anode, hole transporting layered (HTL), and emissive layer (EL). Also CNT-PNCs are excellent surface modifier materials for efficiency improvements in LED devices. Some of these materials are applied as a flexible material in electronic device applications [32–36].

8.13 CNT-PNCs as a stretchable electrode material

The CNT-PNC materials are used as both flexible and electrode materials in LEDs [37, 38]. CNT-PNCs demonstrate high flexibility for stretchable semiconductor devices. It's an easy method to fabricate a transparent device, and these devices are free from hazardous metal ions. The interpenetrating networks of CNT-PNCs have low sheet resistance, high compliance, high transparency, and low surface roughness. CNT-PNCs can reversibly be stretched and have a small change in sheet resistance. The electrode materials can work as both cathodes and anodes in LED devices. A metal-free device was fabricated by the roll lamination of two composite electrodes sandwiching an emissive polymer layer (EL). The devices distinctively combine mechanical

toughness and capability for large strain distortion because of the shape memory property of the CNT-PNC electrodes.

The in situ formation of a p-i-n junction during the LED process has been shown to permit the light-emitting polymer to form ohmic contacts with the electrodes and enable charge injections regardless of the electrode work function. Thus, the CNT-PNC electrode can be both a cathode and an anode material. The use of CNT-PNCs conveys shape memory properties to the LEDs. The devices can experience a large shape change at a preeminent temperature above the T_g of the polymer, and the new shape could be locked by cooling the device to the ambient temperature.

The suggested fluorescent polymer consists of a blue emission polyfluorene copolymer, an ionic conductor PEO-DMA, and a salt LiTf. The fluorescent polymer was further coated between two CNT-polymer electrodes. The chemical arrangements of the polyfluorene copolymer, ionic conductor, and salt are shown in Fig. 8.7. Thereafter, a scanning voltage at $0.1\,V\,s^{-1}$ was applied and the *L-I-V* characteristics were analyzed. The devices had a blue emission with CIE color coordinates at 0.22 and 0.37. The maximum efficiency was about $1.24\,cd\,A^{-1}$ at $200\,cd\,m^{-2}$.

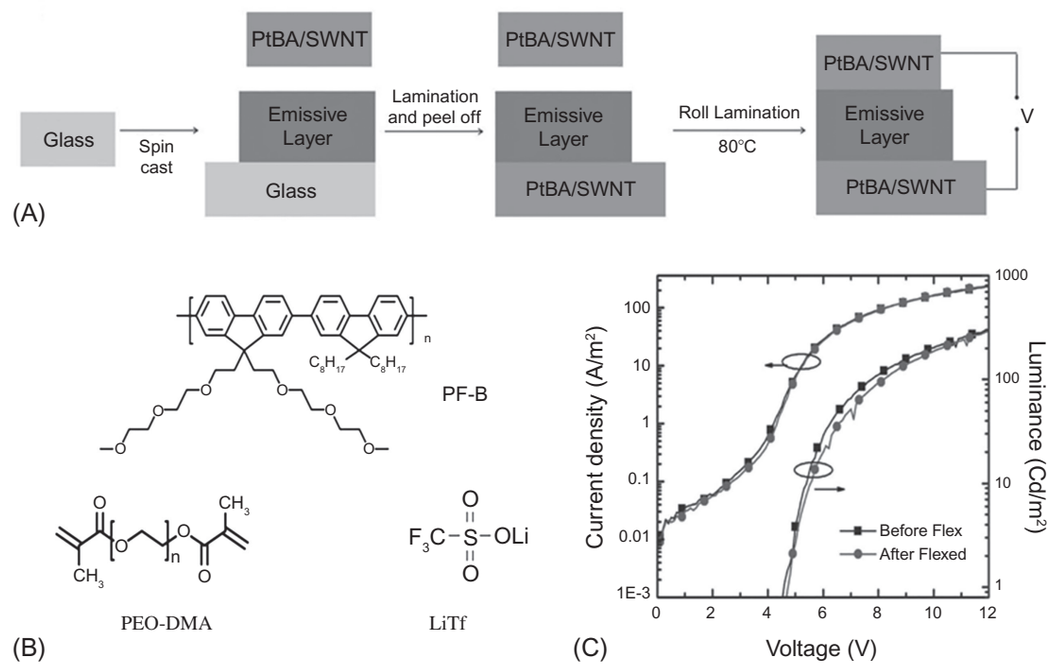


Fig. 8.7 Schematic diagram of fabricated device (A), molecular structure of the materials (B), efficiency graph of the device (C).

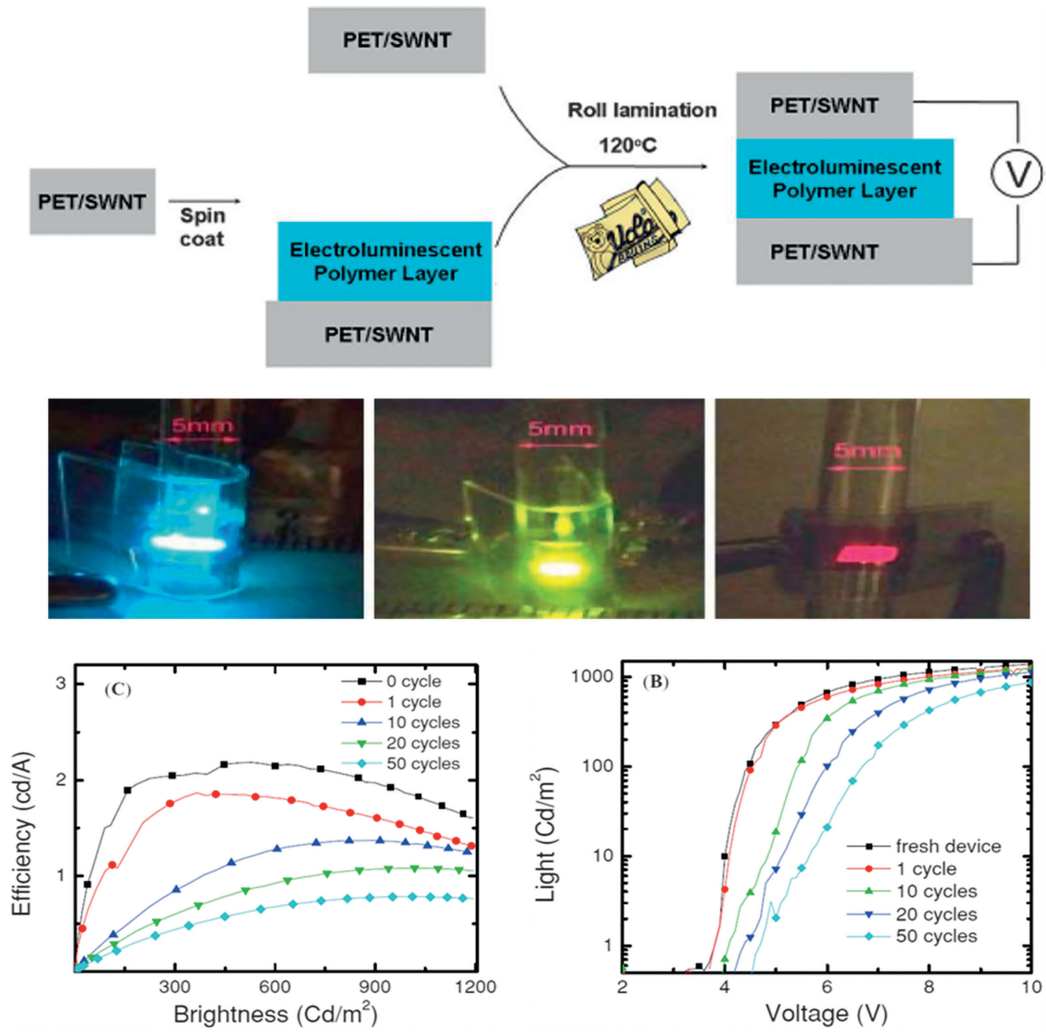


Fig. 8.8 CNT-PNCs as an electrode material in different color devices and their analysis.

Polymer LEDs (PLEDs) are based on the in situ formation of a p-i-n junction in a polymer blend that has been fabricated by roll lamination [37–40]. CNT-PNCs are used as both anodes and cathodes for the fabrication of a simple sandwich structure of polyester/CNT-PNCs/emissive polymer/CNT-PNCs/polyester (Fig. 8.8). The emissive polymer layer contains polyfluorene-based copolymers emitting red, yellow, and blue light. The device is semitransparent, with > 70% transmittance outside the wavelength range of the polymer π-π^* band-gap transition. The devices are also greatly flexible, as they can be bent

up to a 2.5 mm radius without producing permanent damage to device performance. Various mixed colors were obtained conveniently by stacking the semitransparent devices.

The device (1) displayed a blue emission with excellent electroluminescent performance, including a low turn-on voltage (3.8 V), a high efficiency of 2.2 cd A^{-1}, and excellent brightness of 1400 cd m^{-2} at 10 V. A yellow and red emissive device (2 and 3) also was fabricated and attained better performance. All the devices were extremely transparent with transmittance of > 70% in the wavelength range where the emissive polymer doesn't absorb. Stacking of the semitransparent devices was engaged to conveniently produce several mixed emission colors.

8.14 CNT-PNCs as an anode material

CNT-PNCs are also used as a potential anode material for LEDs. CNT films on flexible PET (polyethyneneterephthalate) substrates are used as transparent flexible anodes for LEDs. The CNT-PNC device has a skeleton of SWCNT/PEDOT-PSS:MeOH.TFB (poly(9,9-dioctylfluorene-*co*-*N*-(4-butylphenyl)diphenylamine)) + TPD-Si_2 (4,4c-bis[(*p*-trichlorosilyl propylphenyl)phenylamino]biphenyl)/BT (poly(9,9dioctylfluorene-*co*-benzothiadiazole))/CsF/Al, light production of 3500 cd m^{-2}, and a power efficiency of 1.6 cd A^{-1} [39]. The device's working lifetime is equivalent to devices with Sn-doped InO_3(ITO)/PET anodes (Fig. 8.9).

There are four categories of fabricated LED devices: Device 1: SWCNT/TFB + TPD-Si_2/TFB + BT/CsF/Al; Device 2: SWCNT/PEDOT-PSS/TFB + TPD-Si_2/TFB + BT/CsF/Al; Device 3: SWCNT/PEDOT;PSS:MeOH/TFB + TPD-Si_2/TFB + BT/Cs/Al; and Device 4:SWCNT/PEDOT:PSS-MeOH/TFB + TPD-Si_2/BT/CsF/Al. The characterization results suggest that CNT-PNCs are better than ITO for several reasons. (1) SWCNT films on PET exhibit sheet resistance with 80% transmittance, metrics comparable to marketable ITO on plastics. By doping SWCNT films with NO_2, a threefold reduction in sheet resistance without a change of transparency can be expected. (2) The exceptional mechanical flexibility of SWCNT films has been demonstrated. In contrast, ITO films on plastic crack after repeated blending. The SWCNT films on PET do not crack or crease after bending while ITO films become insulating. (3) The SWCNT films on PET show worthy acid resistance while ITO is rapidly corroded, even by a PEDOT:PSS solution. (4) Due to outstanding surface energy matching, SWCNT films adhere powerfully to PET and PMMA, passing the Scotch tape decohesion test. (5) SWCNT films, due to the nanoporous assembly, have a surface area as great as 1500 m^2/g, offering hole injection potential. (6) SWCNT film fabrication on PET, starting from SWCNT powders, is a room temperature process that is relatively

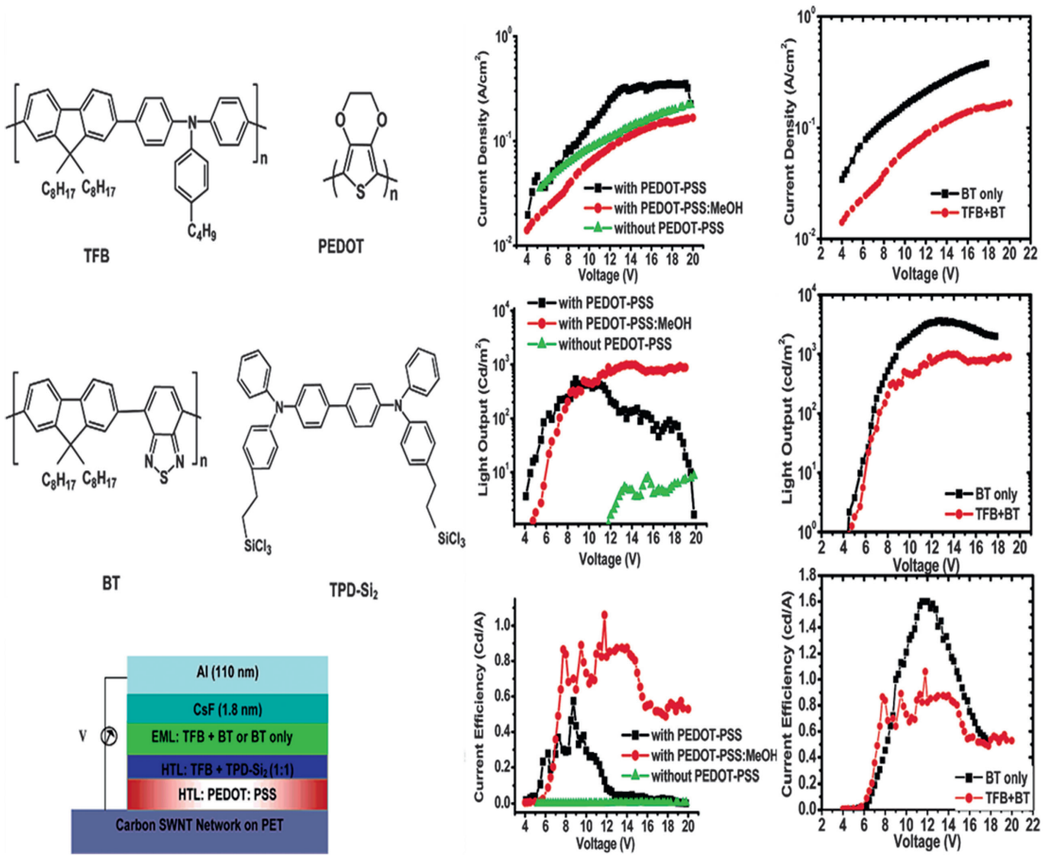


Fig. 8.9 The molecular and device structure of LEDs and its efficiency characterization. From J. Li, L. Hu, L. Wang, Y. Zhou, G. Gruner, T.J. Marks, Organic light-emitting diodes having carbon nanotube anodes, Nano Lett. 6(11) (2006) 2472–2477.

simple while ITO coating on a flexible substrate necessitates a vacuum and elaborate process equipment. Room temperature processing renders the SWCNT films suitable for use with a wide range of substrates for both top and bottom emission devices [39, 40].

8.15 CNT-PNCs as HTL and ETL

CNTs have been promised in LEDs as both hole-transporting and electron-transporting layers. The CNTs composites are usually affianced with the conjugated polymers towards the LED applications [40, 41]. The improvement of efficiency of the CNT-PNCs with several polymers and characterizations, which increases the efficiency of the CNT in LEDs. The CNT-PNC composites were prepared by combination of

CNT and conjugated polymer materials. The prepared CNT-PNCs are used as ETL and HTL materials in LEDs.

The first effort at utilizing CNTs in LEDs contained CNTs and poly(2,5-bis(cholestanoxy)-1-4-phenylvinelene) (BCHA-PPV), where the CNT was used as an HTL. The CNT-PNCs and PmPV significantly increase the electrical conductivity of the device; hence the composites exhibit the best output even in a lower concentration. Because of this, the composites possess ideal output, even in lower concentrations. The emission property of the material decreases because of the presence of CNT. The CNTs acts as a conductor and substrate-like the material in the device, which induces the electron transfer nature of the composites.

The MWCNTs-PmPV composite proposes as these materials could act as possible charge transporting material in LEDs. The device structure of HTL/M_3EHPPV/ETL, the HTL made by PVK, poly-TPF-DPX, and the poly-MWCNT-PmPV act as an ETL. The ETL composite concentration of 10% MWCNT showed the best result among the other concentrations.

The fabricated device (Fig. 8.10) with the structure of PET/ITO/MWCNT-PEDOT:PSS/AlQ_3/Al was optimized and used for further characterization. CNT mixing enhances the hole injection ability of PEDOT:PSS. The incorporation of TPD between the active and EL

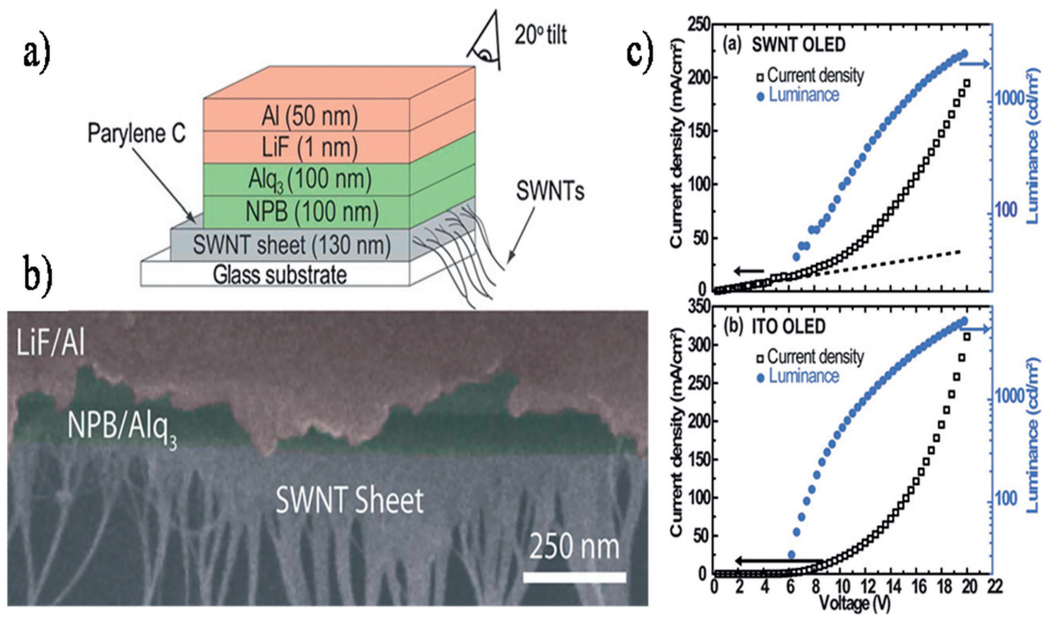


Fig. 8.10 Device structure of LED (A), cross cutting view of the device (B), and the efficiency characterization (C). From C.M. Aguirre, S. Auvray, S. Pigeon, R. Izquierdo, P. Desjardins, R. Martel, Carbon nanotube sheets as electrodes in organic light-emitting diodes, Appl. Phys. Lett. 88 (2006) 183104.

layer (PET/ITO/MWCNT-PEDOT:PSS/ TPD/Alq3/Al) possess the highest efficiency of 6800 cdm^{-2} at 15 V.

The typical structure of glass/MWCNT/PEDOT:PSS/MEH-PPV/Ca/Al shows a maximum efficiency of 500 cd m^{-2} at 2.4 V. The removal of the MWCNT layer in the device does not show any emission. Hence, the MWCNT acts a hole injector in the device. The MWCNT increases the recombination of electrons as well. Further advantages are that the material is quite flexible, transparent, porous in nature, and has a nanolayer thickness and high work function.

8.16 CNT-PNCs as an emissive layer

I: In recent research, CNT-PNCs are the possible emission materials in flexible LEDs. The EL property of the host MEH-PPV and PVK-based LEDs with and without mixing of CNTs are established in Fig. 8.11. For the MEH-PPV-coated devices, the maximum luminescence of the pristine and CNT-doped LEDs are 3900 cd m^{-2} at 5.0 V and 3600 cd m^{-2} at 5.4 V. For PVK-based devices, the maximum luminescence of the pristine, 0.05%, and 0.1% of CNT-doped LEDs are 3600 cd m^{-2} at 6.2 V, 7600 cd m^{-2} at 8.2 V, and 6800 cd m^{-2} at 9.1 V [42].

The performance of LEDs in EL has been revealed by the improvement of mixing CNTs in the polymer matrix. This may be because of the chemical interface bonding of CNTs and polymers. The mixing method is an effective method to improve color tuning as well as the physical and optical characteristic of LEDs. Many different LEDs were mixed and layered with polymer light-emitting material and technically fabricated into practical LEDs. The schematic energy level diagram of an individual film in PLEDs is shown in Fig. 8.11. The chemical solution of MEH-PPV is one of the PPV-based derivatives. The magnitudes of the HOMO and the LUMO of MEH-PPV are 4.9 eV and 2.8 eV, respectively. The work function of the LiF/Al bilayer-like film, the PEDOT film, and the ITO film are also estimated to be 3.2, 5.0, and 4.7 eV respectively. The built-in potential in MEH-PPV:CNT is formed in the energy gap between HOMO and LUMO in MEH-PPV. The results indicate that a typical relationship between the luminance and the applied voltage of the pristine and the 0.05% CNT-doped MEH-PPV-based PLEDs is 3900 cd m^{-2} at 5.0 V and 3600 cd m^{-2} at 5.4 V. The range of the enhancement on the maximum luminance for the CNT-incapacitated LED devices is considerably limited. Fig. 8.11 shows the illustrative correlation of the power efficiency vs the current efficiency vs the luminance of the pristine and the CNT-doped MEH-PPV-based PLEDs. The power efficiency is 0.1161 m/W at 1000 cd m^{-2} for the pristine and the CNT-doped MEH-PPV-based PLEDs. The improvement of CNT doping on the power efficiency of the equipped device is not

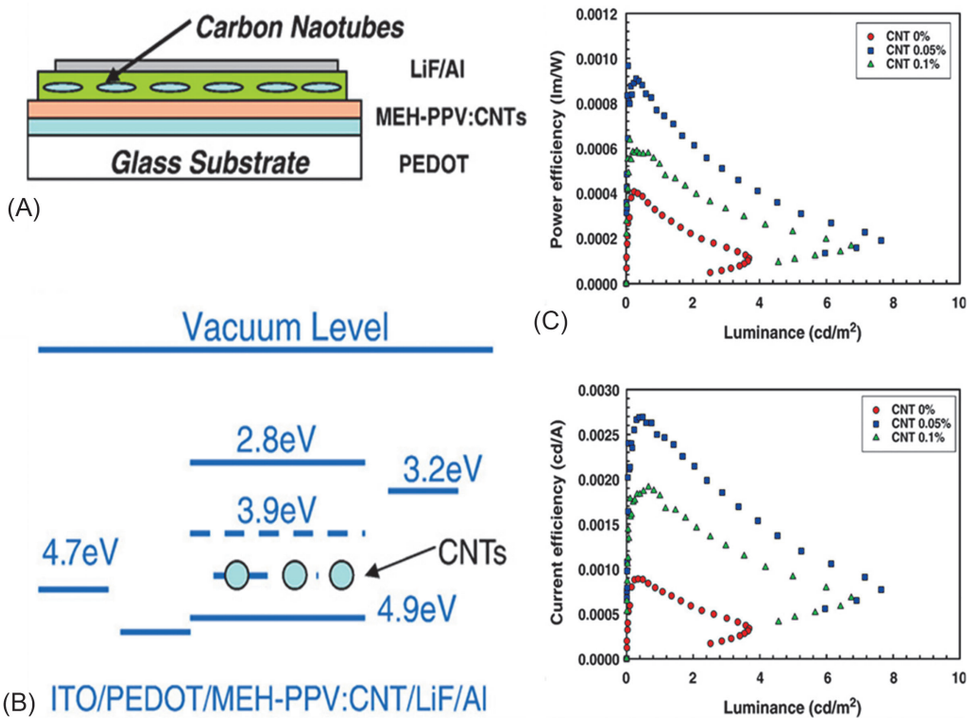


Fig. 8.11 Illustration of the device (A), energy level diagram (B), and the CNT-doped and undoped characterization results (C). From H.-S. Koo, M. Chen, H.-W. Yu, S.-K. Kwon, Y.-K. Lee, J. Jang, Electroluminescent characteristics of organic light-emitting diodes with doped carbon nanotubes, Diam. Relat. Mater. 16(4–7) (2007) 1162–1166. Copyright from Elsevier Publications.

deceptive. When the illumination is irradiated, the current efficiency at 2300 cd m^{-2} of the CNT-mixed device is 0.14 cd A^{-1}, higher than that of the pristine device with 0.12 cd A^{-1}. This shows that CNT doping can efficiently increase the current efficiency of PLEDs, but not the power efficiency of the devices. This may be due to the fact that the alignment of the dispersed CNTs in the matrix film facilitates the construction of the charge transfer complexes at the CNT surface, and the conductivity of the arranged film in the doped devices increases. Fig. 8.11 shows the typical relationships of power efficiency and current efficiency vs the luminance of the pristine and the CNT-mixed PVK-based PLEDs. When the illumination is treated, the power efficiencies at 1000 cdm^{-2} of the pristine, 0.05%, and 0.1% CNT-doped devices are 0.0003cdA^{-1}, 0.00074 cdA^{-1} and 0.0005cdA^{-1}, respectively. For irradiated illumination, the current efficiencies at 2300 cd m^{-2} of the 0.05% and 0.1% CNT-doped devices are 0.0020 cd A^{-1} and 0.0013cd A^{-1}, larger than the 0.0002 cd A^{-1} of the pristine device.

This also showed that the doping of CNTs at a suitable amount in PVK-based polymers can curiously improve the power efficiency and the current efficiency of PVK-based LEDs. PLEDs and the different amount of CNTs have been scientifically and technically synthesized by the chemical approach and the solution-based spin coating technique. The maximum luminance of PLEDs is initially enhanced with an increase in the doping amount of CNTs and then decreases at 5.0–5.4 V. The current efficiency of PLEDs is primarily enhanced with increasing the mixing of CNTs and then reductions as well. For MEH-PPV-based devices, the current efficiency at 2300 cd m^{-2} of a CNT-doped device is 0.14 cd A^{-1}, higher than the 0.12 cd A^{-1} of the pristine device. For PVK devices, the current efficiency at 2300 cd m^{-2} of the 0.05% and 0.1% CNT-doped device is larger than that of the pristine device. The optical performance of PLEDs in EL has effectively been demonstrated by the improvement of doping nanostructured carbon in the polymer matrix. This may be due to the chemical interaction bonding between CNTs and organic molecules in the polymer matrix.

II: The devices were constructed by the host molecule of the conjugated polymer MEH-PPV poly(2-methoxy-5-(2-ethylheyloxy)-1-4-phenylenevinylene). The MWCNTs were dispersed in DMF with the different volume ratio (0.05,0.15) and then added to polymer in chloroform solution. The composite materials acts as an active layer in LED device. The poly(3,4-ethylenedioythiophene): poly-(styrenesulfonate) (PEDOT:PSS) and (Tris-hydroxyquinoline) aluminum Alq_3 were used as the HTL and ETL, correspondingly, to enhance the injection charge from the electrodes to the active layer. The spin coating method was used to achieve facile and low-cost LEDs. The absorption spectrum of the active layer has studied by UV-Visible spectrophotometer. It clarified that the absorbance decreases with the increasing volume ratio of CNTs. The emission spectrum showed two peaks with respect to the quenching and recombination processes of mixing with CNTs. The AFM measurement displays increasing roughness average from 0.168 to 0.668 nm with increasing the volume percentage of CNTs.

The *I-V* properties of the composite materials were characterized; it has MEH-PPV-MWCNTs as the active layer. The threshold voltage of MEH-PPV is 2.5 V, and it decreases with increased CNT. The density of the current increases due to the tunneling majority charge at the interface among the HTL, ETL, and the active emissive layer. The CNT-PNC thin film at an 0.85:0.15 volume ratio of the composite (MEH-PPV:MWCNT) as the active EML emitted a tunable light color at a specific voltage. The organic semiconductor, oligomers, polymers, and dendrimers are all based on the π electron conjugated system. The π electron delocalization enhances the ICT and the efficiency of the LEDs.

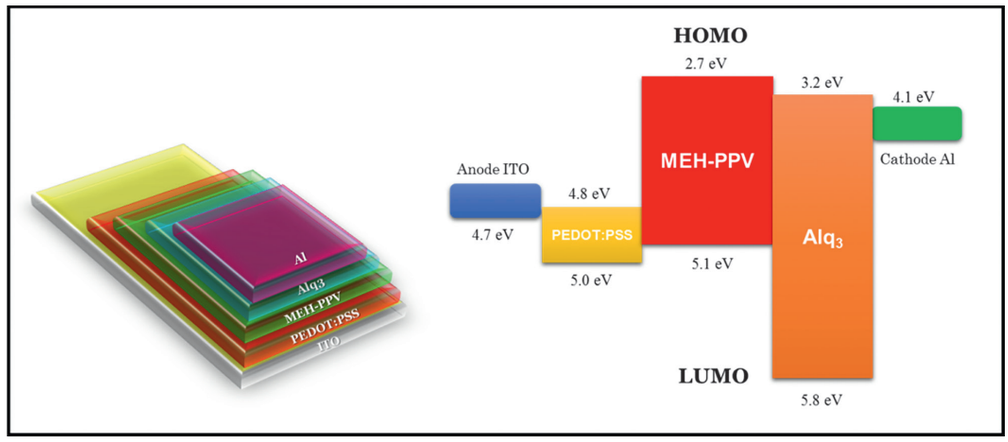


Fig. 8.12 Schematic representation of the fabricated LED device and the energy level diagram of the LEDs.

The device fabrication process: The structure of an LED device is of ITO/PEDOT:PSS/MEH-PPV:MWCNT/Alq_3/Al. The ITO-coated glass substrate was washed by a sequence step in acetone, ethanol, methanol, and deionized water in an ultrasonic bath for 10 min each. The HTL (PEDOT:PSS) was coated by spin coating at 4000 rpm for 1 min and dried at 150°C. The MEH-PPV:MWCNT solution was deposited at 1500 rpm for 1 min and then dried at 100°C to remove any residual solvent. The Alq3 solution was deposited at 1500 rpm for 1 min and then dried at 100°C. Finally, the Al metal was coated by thermal evaporation. The structure of the LED device is exposed in Fig. 8.12, which illustrates the energy diagram of these layers. The UV-visible absorption spectrum of MEH-PPV and MEH-PPV:MWCNT thin films with different volume ratios of 0.05 and 0.15 displayed two peaks at 338 and 510 nm. The spectra of all volume ratios of MWCNTs showed a linear dependence between the spectra of both the molecules MEH-PPV and MWCNT. This indicates that CNT is incorporated into the MEH-PPV matrix without modifying the chemical construction of the polymer. Therefore, it's likely that molecular orbital hybridization between the HOMO of the MEH-PPV and the LUMO of the MWCNTs is achieved by the mixing of MEH-PPV and MWCNTs [43].

The influence of CNTs through the organic active layer is described by the J-V characterization for both the pure polymer and that mixed with the MWCNT nanocomposite. The efficiency enhances about 103 and 105 times with amending by CNT of 0.05 and 0.15 volume ratio correspondingly. The emitted light contains orange and red color, with respect to MEH-PPV and MEH-PPV:MWCNTs nanocomposite. The orange light color dominate on red light color in both MEH-PPV and MEH-PPV:MWCNT nanocomposite, with volume ratio 0.05

of CNT as shown in Fig. 8.12. The EL spectra of orange and red light emitting color are independent on the applied voltage. The low and high voltage based on the J-V curve to parallel between MEH-PPV and MEH-PPV:MWCNTs OLED device, with different volume ratios of MWCNT (0.015, 0.15). The concentration level of the emission light at the volume ratio of 0.05 CNTs, the red light color control and at quantified and greater voltage like 6.5 V, the orange light color is dictate. The tuned color and the red shift in the EL spectrum, in addition to the fine band in all mixture curves, is due to the micro hollow effect. A microcavity is altered with the length of the light path, the refractive index, and the detection angle, and can be used to tune the light color of LEDs in addition to its efficiency.

8.17 Conclusion

In conclusion, the details of CNT-polymer nanocomposites and their applications on optoelectronics were studied and explained thoroughly. The basic concepts of optoelectronics and their applications were explained in a lucid manner. The CNT-PNC materials are potential materials for upcoming LED applications. Although there are some complications in PLEDs, the recent investigation is focused on the discovery of novel strategy to overcome those issues. The CNT-PNCs enhances the efficiency and reduces the cost of LEDs as well as optoelectronics devices.

Acknowledgment

The authors S.N.J and V.R gratefully acknowledge the DST-SERB-NPDF/2017, New Delhi, for providing the National Postdoctoral Fellowship (NPDF) to successful carry out this work.

References

[1] S.J. Benight, C.W. Jeffrey, B.H. Tok, Z. Bao, Stretchable and self-healing polymers and devices for electronic skin, Prog. Polym. Sci. 38 (12) (2013) 1961–1977.
[2] S. Henning, T. Nir, H.F. Richard, Integrated optoelectronic devices based on conjugated polymers, Science 280 (5370) (1998) 1741–1744.
[3] L.B. Jean, C. Jerome, B. David, A. Donizetti, S. Dos, S. Zhigang, Excited-state electronic structure of conjugated oligomers and polymers: a quantum-chemical approach to optical phenomena, Acc. Chem. Res. 32 (3) (1999) 267–276.
[4] X. Yan, X. Wei, L. Chun, L. Bo, Z. Li, P. Junbiao, C. Yong, W. Jian, Utilizing white OLED for full colour reproduction in flat panel display, Org. Electron. 9 (4) (2008) 533–538.
[5] G. Bernard, R. Philippe, P. Christophe, Organic light-emitting diode (OLED) technology: materials, devices and display technologies, Polym. Int. 55 (6) (2006) 572–582.

[6] V. Ramkumar, P. Kannan, Thiophene and furan containing pyrazoline luminescent materials for optoelectronics, J. Lumin. 169 (2016) 204–215.
[7] D. Jariwala, V.K. Sangwan, L.J. Lauhon, T.J. Mars, M.C. Hersam, Carbon nanomaterials for electronics, optoelectronics, photovoltaics and sensing, Chem. Soc. Rev. 42 (7) (2013) 2824–2860.
[8] V. Ramkumar, P. Kannan, Novel heterocyclic based blue and green emissive materials for opto-electronics, Opt. Mater. 46 (2015) 314–323.
[9] S. Libertino, A. Sciuto, Electro-optical modulators in silicon, Opt. Interconnects 119 (2006) 53–95.
[10] V. Ramkumar, S. Anandhi, P. Kannan, R. Gopalakrishnan, Synthesis, single crystal growth characterization and comparison of two new enone shifted chalcones and their NLO behaviour, Cryst. Eng. Commun. 15 (2013) 2438–2449.
[11] V. Ramumar, S. Anandhi, P. Kannan, R. Gopalakrishnan, Substitution effect on chalcone based materials for corrosion and photocrosslinking applications, RSC Adv. 5 (2014) 586–596.
[12] A.C. Grimsdale, K.L. Chan, R.E. Martin, P.G. Jokisz, A.B. Holmes, Synthesis of light-emitting conjugated polymers for application in electroluminescent devices, Chem. Rev. 109 (3) (2009) 897–1091.
[13] A.J. Neel, M.J. Hilton, M.S. Sigman, F.D. Toste, Exploiting non-covalent π-interactions for catalyst design, Nature 543 (2017) 637–646.
[14] C.R. Martinez, B.L. Iverson, Rethinking the term pi-stacking, Chem. Sci. 3 (2012) 2191–2201.
[15] Z.F. Yao, J.Y. Wang, J. Pei, Control of π-π stacking via crystal engineering in organic conjugated small molecule crystals, Cryst. Growth Des. 18 (1) (2018) 7–15.
[16] K. Tokumaru, J.D. Coyle, A collection of experiments for teaching photochemistry, Int. Union Pure Appl. Chem. 64 (9) (1992) 1343–1382.
[17] D. Bera, L. Qian, T.K. Tseng, P.H. Holloway, Quantum dots and their multimodal applications: a review, Materials (Basel) 3 (4) (2010) 2260–2345.
[18] D.F. Perepichka, R.B. Martin, Molecules with exceptionally small HOMO-LUMO gaps, Angew. Chem. Int. Ed. 44 (2005) 5370–5373.
[19] G.L. Closs, J.R. Miller, Intermolecular long distance electron transfers in organic molecules, Science 240 (4851) (1988) 440–447.
[20] Z.R. Grabowski, J. Dobkowski, Twisted intermolecular charge transfer (TICT) excited states: energy and molecular structure, Pure Appl. Chem. 55 (2) (1983) 245–252.
[21] S. Song, D. Ju, J. Li, D. Li, Y. Wei, C. Dong, P. Lin, S. Shuang, Synthesis and spectral characteristics of two novel intermolecular charge transfer fluorescent dyes, Talanta 77 (2009) 1707–1714.
[22] M. Wang, J. Zhang, J. Liu, C. Xu, H. Ju, Intermolecular energy and charge transfer in 5-(9-anthryl)-3-(4-nitrophenyl)-1-phenyl-2-pyrazoline, J. Lumin. 99 (2002) 79–83.
[23] E.C.W. Ou, L. Hu, G.C.R. Raymond, O.K. Soo, J. Pan, Z. Zheng, Y. Park, D. Hecht, G. Irvin, P. Drzaic, G. Gruner, Surface modified nanotube anodes for high performance organic light emitting diodes, ACS Nano 3 (8) (2009) 2258–2264.
[24] X.L. Xie, Y.W. Mai, X.P. Zhou, Dispersion and alignment of carbon nanotubes in polymer matrix: a review, Mater. Sci. Eng. R Rep. 49 (4) (2005) 89–112.
[25] S. Ghoshal, Polymer/carbon nanotubes (CNT) nanocomposites processing using additive manufacturing (three-dimensional printing) technique: an overview, Fibers 5 (2017) 40.
[26] R. Andrews, M.C. Weisenberger, Carbon nanotube polymer composites, Curr. Opinion Solid State Mater. Sci. 8 (2004) 31–37.
[27] J. Chen, L. Yan, Recent advances in carbon nanotube-polymer composites, Adv. Mater. 6 (6) (2017) 129–148.

[28] W.K. Maser, R. Sainz, M.T. Martinez, A.M. Benito, Electroactive polymer carbon nanotube composites: smart organic materials for optoelectronic application, Contrib. Sci. 4 (2) (2008) 187–192.
[29] G. Ajeesh, S. Bhowmik, S. Venugopal, L. Varshney, A. Baluch, Y. Park, S. Gilsang, C.G. Kim, Influence of chemically and plasma-functionalized carbon nanotubes on high-performance polymeric nanocomposites, High Perform. Polym. 28 (5) (2016) 570–580.
[30] S.K. Swain, I. Jena, Polymer/carbon nanotube nanocomposites: a novel material, Asian J. Chem. 22 (2010) 1–15.
[31] J. Chen, B. Liu, X. Gao, D. Xu, A review of the interfacial characteristics of polymer nanocomposites containing carbon nanotubes, RSC Adv. 8 (2018) 28048–28085.
[32] L. Dai, Light-emitting polymers and carbon nanotube electron emitters for optoelectronic displays, Smart Mater. Struct. 11 (2002) 645–651.
[33] M. Tyagi, D. Tyagi, Polymer nanocomposites and their applications in electronics industry, Int. J. Electron. Electr. Eng. 7 (6) (2014) 603–608.
[34] N. Sankar, M. Nagarjun Reddy, R.K. Prasad, Bull. Mater. Sci. 39 (1) (2016) 47–55.
[35] S. Scholz, D. Kondakov, B. Lussem, K. Leo, Degradation mechanisms and reactions in organic light-emitting devices, Chem. Rev. 115 (16) (2015) 8449–8503.
[36] M.A. Haase, J. Qiu, J.M. DePuydt, H. Cheng, Blue-green laser diodes, Appl. Phys. Lett. 59 (1991) 1272–1279.
[37] Z. Yu, X. Niu, Z. Liu, Q. Pei, Intrinsically stretchable polymer light-emitting devices using carbon nanotube-polymer composite electrodes, Adv. Mater. 23 (2011) 3989–3994.
[38] X. Fan, W. Nie, H. Tsai, N. Wang, H. Huang, Y. Cheng, R. Wen, L. Ma, F. Yan, Y. Xia, PEDOT:PSS for flexible and stretchable electronics: modifications, strategies and applications, Adv. Sci. 6 (2019) 1900813.
[39] J. Li, L. Hu, L. Wang, Y. Zhou, G. Gruner, T.J. Marks, Organic light emitting diodes having carbon nanotube anodes, Nano Lett. 6 (11) (2006) 2472–2477.
[40] Z. Yu, Z. Liu, M. Wang, M. Sun, G. Lei, Q. Pei, Highly flexible polymer light-emitting devices using carbon nanotubes as both anodes and cathodes, J. Photonics Energy 1 (2011). 011003-1-15.
[41] M. Bansal, R. Srivastava, C. Lal, M.N. Kamalasanan, L.S. Tanwar, Carbon nanotube based organic light emitting diodes, Nanoscale 1 (2009) 317–330.
[42] H.S. Koo, M. Chen, H.W. Yu, S.K. Kwon, Y. Lee, J. Jang, Electroluminescent characteristics of organic light-emitting diodes with doped carbon nanotubes, Diam. Relat. Mater. 16 (2007) 1162–1166.
[43] I.M. Ibrahim, A.H. Khalid, I.M. Ali, Colour tuneable of organic light emitting diode MEH-PPV: CNTS, J. Ovonic Res. 14 (2) (2018) 155–164.

9

Advances in polymer-based composites for solar energy conversion to chemical fuels

Anupma Thakur[a,b], Praveen Kumar[c], R.K. Sinha[b,d], and Pooja Devi[a,b]

[a]Academy of Scientific and Innovative Research (AcSIR), Ghaziabad, India, [b]CSIR-Central Scientific Instruments Organisation, Chandigarh, India, [c]School of Materials Science, Indian Association for the Cultivation of Science, Kolkata, India, [d]Department of Applied Physics, Delhi Technological University, Bawana Road, Delhi, India

9.1 Introduction

Fossil fuels as contemporary energy sources have been largely employed to meet the world's total energy demands for centuries. The upsurge in global population and economic development has caused extreme stress on these fuels, which has further aggravated the environmental concerns. Consequently, the echoes for clean and sustainable energy sources are being supported globally, which has encouraged extensive technological development toward harnessing clean energy. Among these, solar energy is the most promising because of its abundance and the fact that it could be stored as chemical or electrical energy for the future. The conversion of solar energy into hydrogen fuel through PC or PEC water splitting and finally to chemical fuel through CO_2 reduction is a promising approach. Hydrogen, a clean and energy efficient fuel, has found myriad applications ranging from low-powered devices to the aviation sector. Throughout the existence of life on Earth, Mother Nature has nourished humankind via various energy conversion processes. One such process involves solar-to-chemical energy conversion, with sunlight as the prime source of energy [1]. This natural mechanism of photosynthesis has inspired researchers and engineers to develop an artificial light-harvesting system for photosynthesis with engineered materials/nanomaterials [2]. In view of this, several successful and failed attempts have been made by researchers to understand the fundamental principles behind these processes as well as to innovate in material aspects related to the

Polymer-Based Advanced Functional Composites for Optoelectronic and Energy Applications
https://doi.org/10.1016/B978-0-12-818484-4.00004-5
Copyright © 2021 Elsevier Inc. All rights reserved.

conversion of solar energy into chemical energy to translate its success into user technologies. The captured solar radiation will provide the necessary energy to convert the chemical feedstocks such as water (H_2O) into clean chemical fuel such as hydrogen (H_2).

A range of solar energy harnessing systems based on various photocatalysts/photosensitizers [3, 4], narrow bandgap semiconductors [5, 6], bioproteins [7–9], dye sensitizers [10, 11], and plasmonic nanostructures [12, 13] has been developed and reported. Yet, lesser solar to hydrogen conversion efficiencies, higher cost, and stability issues present imperative challenges [14] toward broadening their application window.

However, over the recent past, conducting polymers such as polypyrrole (PPy) [15, 16], poly(3,4-ethylenedioxythiophene) (PEDOT) [17, 18], polythiophene (PTh) [19, 20], and porous organic polymers (POPs) such as covalent triazine frameworks (CTFs) [21, 22], covalent organic frameworks (COFs) [23, 24], and conjugated microporous polymers (CMPs) [25, 26] have become noticeable as low-cost and sustainable substitutes to traditional light absorbers. This is due to their facile synthetic techniques, higher mechanical flexibilities, tunable light absorption range, and larger weathering stabilities. Polymer-based materials are progressively finding their space in this domain, opening great avenues in clean-energy fuel technologies. Fig. 9.1 presents research timelines supporting the continuous advancements in polymer-based composite research for solar energy conversion to chemical fuel. Thus, this chapter sheds light on the advances in polymer-based materials toward the development of high-performance photocatalytic (PC) or photoelectrochemical (PEC) energy systems that can efficiently utilize solar energy to convert water to hydrogen in an economical manner.

Nevertheless, the solar to chemical energy conversion efficacies of polymeric materials are not commercially appreciable and hence, they require immediate and innovative technological intervention.

9.1.1 Energy crisis

Energy is a pedal to prompt progress in all sections of life to realize both social and economic stability. However, continuously escalating energy demands and depleting fossil fuel sources have contributed to an undesirable imbalance between energy demand and energy production (Fig. 9.2). This, in turn, has encouraged the scientific community to focus on alternative energy sources [28].

Also, the overdependence on fossil fuel-based energy sources has contributed to serious environmental effects, leading to global warming and thereby affecting the ecological balance [29]. Consequently, researchers, scientists, and technologists worldwide are vigorously searching for clean energy sources to meet the present as well as future energy demands.

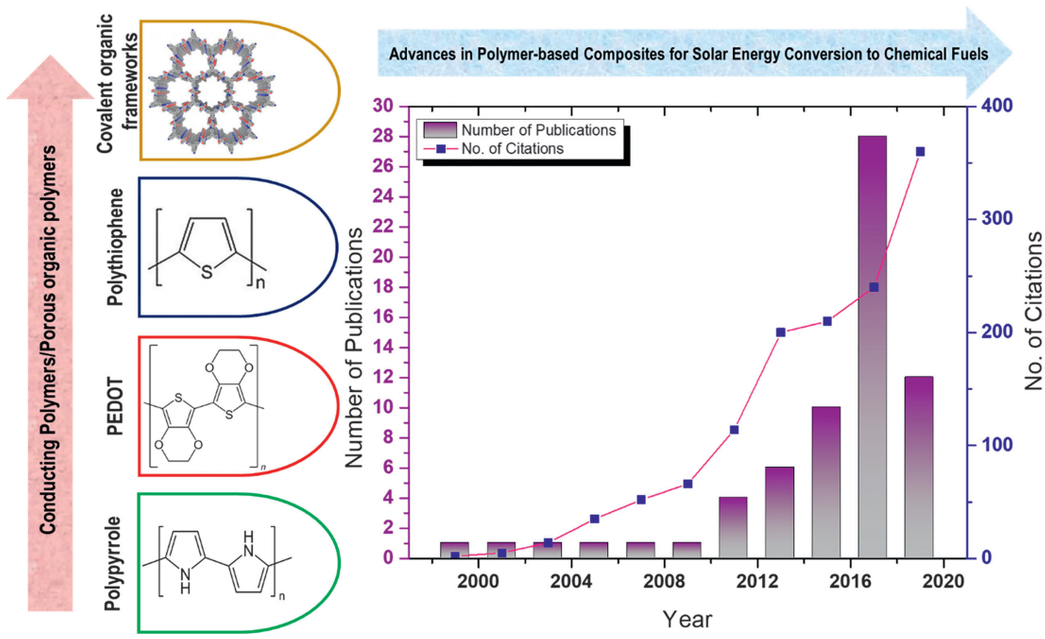


Fig. 9.1 Research timelines supporting the continuous advancements in polymer-based composite research for solar energy conversion to chemical fuel.

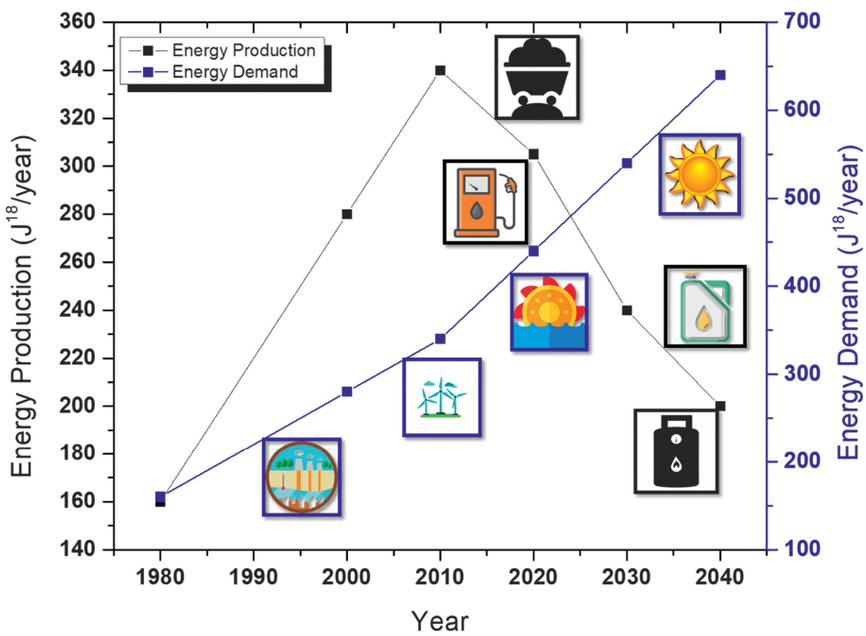


Fig. 9.2 Timeline of projection between energy production and demand [27].

9.1.2 Energy mitigation from fossil fuels to alternative fuels

Owing to the continuous exploitation of limited fossil fuel reserves and the negative environmental effects associated with them, the realization of a renewable energy-based economy is the need of the hour. Of all the renewable energy resources available, solar energy is one of the most promising because solar energy is relatively less capital- and technology-intensive in contrast to other renewable energy sources. Besides, it can also be converted into other energy forms such as electrical or chemical for future use.

Solar-driven (PC) water splitting is one such exclusive technique, wherein the solar radiation trapped from sunlight will bring about the conversion of H_2O into H_2. This hydrogen, the most elemental fuel in the universe, offers a number of advantages, including clean burning (the combustion of H_2 only yields ecofriendly byproducts) and ease of production. It is therefore viewed as a promising renewable chemical energy reserve of the future, when it could be generated resourcefully and stored easily. Besides, hydrogen as a clean fuel could yield 2.5-fold more energy per unit mass in comparison to fossil fuels [30].

Over the years, various researchers have made use of different renewables such as wind, sun, and biomass toward thermal, electrical, photonic, and biochemical energy production, which were then used as input for water splitting toward hydrogen production (Fig. 9.3) [31]. However, water electrolysis produces only 4% of the total hydrogen production, and it is the sole environmentally friendly practice for its production. Further, the process efficiency of this approach and the corrosion of electrodes used in this process (over time) limit its commercial viability. On the other hand, the water-splitting technique could be driven by solar energy using photoactive electrodes to realize cost-effective and efficient hydrogen production from water.

9.2 Fundamentals of solar energy conversion to chemical fuel

9.2.1 Solar spectrum of sun and its related energy profile

The ultimate solar power source, the Sun, is revealed as a 5900 K blackbody heater with an overall irradiance of 1366.1 W/m^2 at the Earth's atmosphere [32]. However, the solar radiation passing through the Earth's atmosphere gets attenuated by O_3, CO_2, water

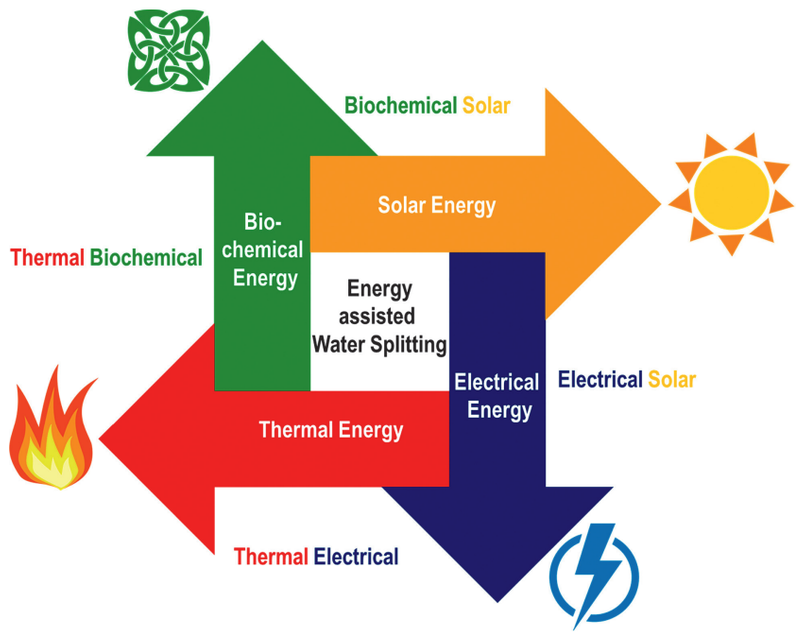


Fig. 9.3 Diverse forms of renewable energies driving water-splitting reactions [31].

vapor, and suspended particulates. It is for this reason that path length is the common factor to define the air mass (AM), which represents the amount of solar irradiance steered within the Earth's atmosphere. The AM number of the solar spectrum can be obtained from the zenith angle of the Sun by using the following mathematical expression:

$$\mathrm{AM} = {}^{1}\!/_{\cos\theta_{\mathrm{zenith}}}\,(\mathrm{number}) \tag{9.1}$$

where θ_{zenith} is the angle between the trajectory of the Sun and the local vertical vector gazing on the Earth's surface [33]. The AM numbers associated with the solar spectrum are widely known as AM 0, AM 1, and AM 1.5. These numbers can vary between 1 and 5 with respect to the time of day, the time of year, and the latitudinal location [34]. The standard solar spectrum preferred is AM 1.5, as it embodies nearly the average annual AM value received at diverse locations in the United States [35]. Generally, AM 1.5 is globally defined as the solar irradiance arriving at the zenith angle = 48.2 degrees, tilt angle = 37 degrees, the angle of incidence = 11.2 degrees, and the total irradiance (intensity) of 1000 W/m^2 (100 mW/cm^2) [36]. In AM 1.5, the G standard spectrum (where G denotes global), 90% of the solar intensity is owed to direct solar radiation and the other 10% is from diffuse solar radiation [37].

9.2.2 Hydrogen as a clean fuel and its economy

Hydrogen, the clean fuel, is a promising renewable energy carrier/fuel for the future, as it produces water as the combustion byproduct with zero carbon emissions, as portrayed in Fig. 9.4 [38, 39].

The key advantages of hydrogen include:

- It is the lightest element of all.
- It is abundantly available.
- It is ecologically and climatically clean at its point of use.

Hydrogen as a fuel is transformed to electricity and produced from water by means of a reversible solar-driven electrochemical reaction involving fuel cells and electrolyzers [40].

$$H_2 + \frac{1}{2}O_2 \xleftarrow{\text{Fuelcell/Electrolyzers}} \text{Electricity} + \text{Water} \tag{9.2}$$

Resembling any other energy transformation chain, the hydrogen energy chain entails five phases: production, storage, transport, dissemination, and finally utilization [41]. Currently, hydrogen is produced using thermal energy by steam reforming, as shown below [42]:

$$CH_4 + H_2O \rightarrow CO + 3H_2 \tag{9.3}$$

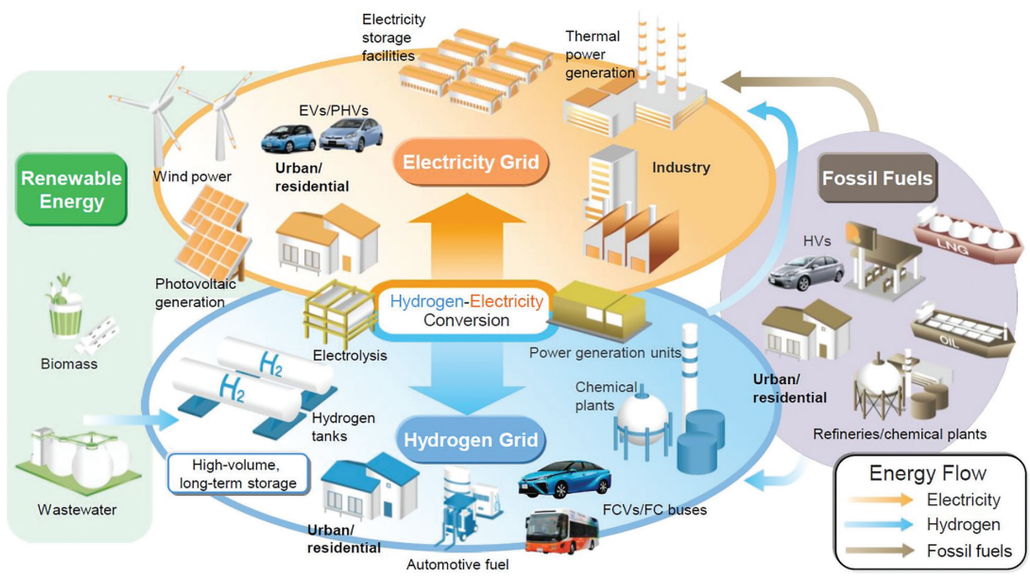


Fig. 9.4 Hydrogen as clean fuel: production and applications [38].

In the current hydrocarbon economy, gasoline is the primary fuel aiding the transportation sector. However, its combustion leads to toxic gas emissions into the environment [43]. Hydrogen as a fuel exhibits proficient comparative properties over gasoline, diesel, and compressed natural gas (CNG), as presented in Table 9.1 [44]. Thus, a gradual shuffling of these conventional energy sources to renewable hydrogen alternatives will result in 60% fuel efficiency.

9.2.3 Principle of PC and PEC processes

The solar water-splitting process is an uphill chemical reaction that involves the dissociation of water into hydrogen and oxygen. Generally, due to very low ionization power, the water-splitting reaction becomes thermodynamically unfavorable and critical (where $\Delta G = 237\,\text{kJ/mol}$) at standard temperature and pressure [45]. In the pursuit of carbon-free energy, electrical energy is favorably used to electrolyze water to hydrogen, which accounts for only 4% of the world's hydrogen production as compared to more than 90% driven by thermal energy [35]. The photolysis of water encompasses the complete decomposition of water into hydrogen and oxygen by means of photonic energy, as displayed in Fig. 9.5 [33]. Lately, there has been increased focus on photonic energy-driven hydrogen production.

9.2.3.1 Photochemical/PC water splitting

Photochemical/PC water splitting for hydrogen production is very similar to natural photosynthesis, as it can convert light energy to chemical energy. Here, a photocatalyst absorbs sunlight with an energy equivalent to or greater than its bandgap, thereby creating negative-electron (e^-) and positive-hole (h^+) pairs. Further, these electrons in the valence band of the photocatalyst get excited to the conduction band, and holes are left in the valence band. These photo-excited e^- and h^+ pairs are

Table 9.1 Comparative qualities of hydrogen with other fuels [44].

Fuel	Molecular weight	Density (g/L)	Ignition energy (MJ)	Diffusion coefficient (cm^3/s)	Energy density (kJ/kg)	Fuel efficiency (%)
Hydrogen	2	0.0893	0.017	0.61	142.00	60
CNG	16	0.7–0.9	0.28	1.90	45.30	–
Gasoline	100–105	710–770	0.24	21.34	48.6	22
Diesel	200–300	832	–	–	33.8	45

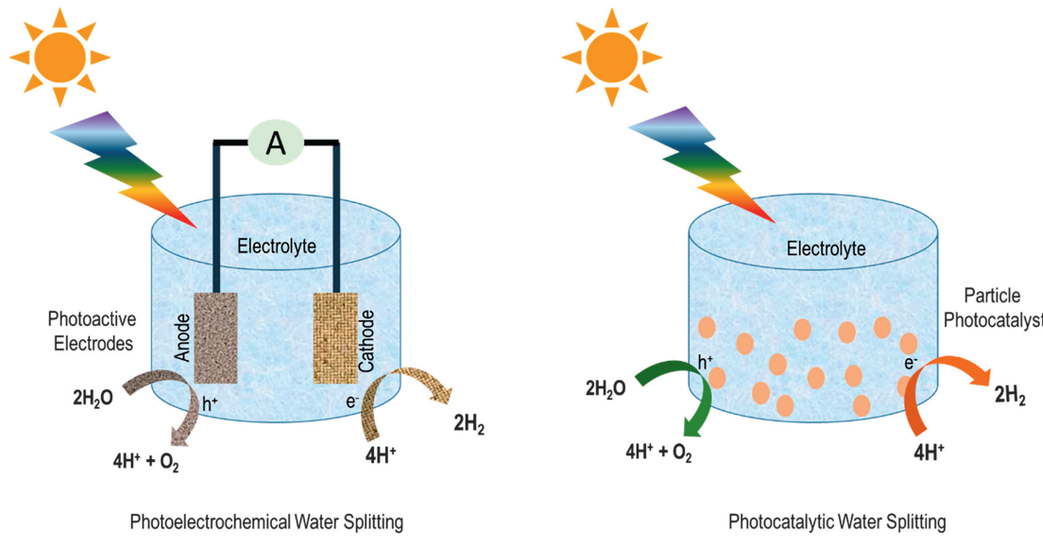


Fig. 9.5 Schematic depiction of PEC and PC water-splitting reactions.

consecutively conveyed to the surface of the photocatalyst for analogous reduction and oxidation chemical reactions, respectively [46].

9.2.3.2 PEC water splitting

The PEC water-splitting process, also called artificial photosynthesis, employs a photoactive anode/cathode and the other electrode that acts as the current collector; both are immersed in an aqueous electrolyte. For PEC water splitting, water is broken down by electrical charges (i.e., electron-hole pairs) in catalysts (upon light irradiation), which involves the electrochemical splitting of water into hydrogen and oxygen using the photo-generated electrons and holes, respectively [47]. A PEC reaction takes place in a PEC cell. The foremost difference between a PEC cell and an electrochemical cell is that in the first case, the electrodes are photoactive, thus requiring light absorption to drive the chemical reactions associated with water splitting. The water-splitting reactions are as follows [48];

$$2H^{+} + 2e^{-} \rightarrow H_2 \ldots\ldots\ldots\ldots \text{HER} \tag{9.4}$$

$$H_2O \rightarrow \frac{1}{2}O_2 + 2H^{+} + 2e^{-} \ldots\ldots\ldots\ldots \text{OER} \tag{9.5}$$

$$H_2O \rightarrow \frac{1}{2}O_2 + H_2 \ldots\ldots\ldots \text{Overall water splitting reaction} \tag{9.6}$$

Where the hydrogen evolution reaction and the oxygen evolution reaction are represented as HER and OER, respectively.

9.3 Advances in polymer-based composites as photoactive materials for clean-energy fuel systems

Polymer composite-based photoactive materials hold promise for cost-effective and lightweight solar energy conversion platforms that could benefit from simple fabrication procedures. In view of this, the first PEC water-splitting system, comprising TiO_2 as the photoanode and Pt as the counter electrode, was investigated by Honda and Fujishima in the early 1970s [49]. Since then, great research efforts have been made to reconnoiter numerous photoanodes for PEC water splitting, owing to their higher efficiency, larger aqueous stability, and cost-effectiveness.

Among the most intensely explored water-splitting systems, polymer-based photoelectrodes have established themselves to be more versatile, highly flexible, and ecofriendly materials of choice for water-splitting reactions.

9.3.1 Conducting polymer-based composites

Conducting polymers are conjugated carbon molecules with π-electron backbones. In these conjugated carbon molecules, electrons are able to travel through the backbone of the π-orbital system. Owing to this property, conducting polymers offer a number of interesting features, including tunable conductivity, low ionization potential, high electron affinity, visible light absorption capability, and facile synthetic protocols. Accordingly, these polymers are well explored in terms of designing photocatalysts/photoelectrodes for solar water-splitting processes (Table 9.2) [50–63].

Polypyrrole (PPy) was first studied more than 30 years ago as a PPy nanoparticle (NP) coating for a water oxidation catalytic reaction [50]. These researchers stated that when PPy NP modified CdS nanoparticles were designed, the PEC performance toward water oxidation improved and O_2 gas production was enhanced. They also testified as to the PC degradation performance of these PPy NP modified CdS nanoparticles. Their studies showcased the PEC behavior of PPy polymer- based composites [50]. Further, Tan and coworkers fabricated a PPy polymer-based photoelectrode for PEC water splitting [51]. A PPy modified TiO_2NP-based photoelectrode tailed the UV-to-visible light absorption. PPy decorated TiO_2NP-based photoelectrodes were fabricated in two surface morphologies: particulate natured and

Table 9.2 Conducting polymer-based composites for solar energy conversion to chemical fuel.

Sl. no.	Conducting polymers	Photocatalyst/ photoelectrode	Analytical characteristics	Ref.
1	Polypyrrole	PPy NP modified CdS nanoparticles	Enhanced water oxidation catalytic reaction	[50]
2		PPy modified TiO_2 nanoparticles (NPs)	Generated 0.04 mmol/min of hydrogen	[51]
3		TiO_2/PPy nanostructures	Enhanced PC effect toward the degradation of pollutants	[52]
4		PPy/CdS composite nanostructures	Enhanced rate of water oxidation reaction	[53]
5		PPy/ZnO photoanode	Enhanced PC effect toward the degradation of pollutants and rate of water oxidation reaction	[54]
6	Poly(3,4-ethylenedioxythiophene) (PEDOT)	AgNPs/PEDOT/SiNW arrays	Enhanced solar conversion efficiency of 2.86%	[55]
7		PEDOT- poly(styrene sulfonate)/Si nanocones	Enhanced rate of water oxidation reaction	[56]
8		PEDOT/nano-Ni/rGO thin film	Synergistically amplified the yielded photocurrent by 71%, as compared to bare	[57]
9		Pt/TiO_2/CdS/CdSe/PEDOT	Outstanding performance under visible-light irradiation with quantum efficiency of 6.9%, turnover number of 2210, and hydrogen production rate of 370 μmol/cm^2/h	[58]
10	Polythiophene (PTh)	TiO_2/Au/PTh photoelectrode	Photoelectric conversion of 0.11% and hydrogen production rate of 2.929 mmol/h/m^2 at 50 mW/cm^2	[59]
11		PTh-rGO-TiO_2 nanocomposite	Hydrogen production rate of 214.08 μmol/h with a quantum efficiency of 14.17% at 400 nm	[60]
12		PTh/Pd/TiO_2 nanocomposite	Showed photocurrent density of ~ 40 μA/cm^2 at 0.7 V	[61]
13		PTh-GO-CuO nanocomposite	Hydrogen production rate of 205.16 μmol/h and quantum efficiency of 12.96%	[62]
14		PTh-$CuBi_2O_4$ nanocomposite	Showed photocurrent density of 0.41 mA/cm^2 at 0.3 V	[63]

thin-film geometried. With the functionalization of TiO_2 NPs with PPy, a core-shell structure is formed. Plus, owing to the low bandgap of PPy (2.6 eV), it absorbs the visible light of solar irradiation and the photo-excited electrons get transferred to the conduction band of TiO_2 (3.2 eV). This leads to the subsequent electron-hole pair formation, which splits H_2O into H_2 and O_2 at the TiO_2 and PPy, respectively. The presented results demonstrated that this photoelectrode generated 0.04 mmol/min of hydrogen, which seemed to be comparable to other systems [51]. Similarly, Wang and coworkers investigated an in situ polymerization method to modify TiO_2 nanostructures with PPy. The synthesized TiO_2/PPy nanostructure showed enhanced photoactivity under irradiation, when studied for its PC effect toward degradation of pollutants [52]. Likewise, Zhang and co-workers reconnoitered an in situ polymerization method to modify CdS nanostructures with PPy polymer to improve the conductivity and light absorption spectrum. The presented results revealed that the PPy/CdS composite nanostructures showed greater performance with larger H_2 production rates [53]. Wang and coworkers fabricated a PPy polymer-based ZnO photoanode for PEC water splitting [54]. This work considered the vital characteristics of the PPy polymer that make it expedient in clean-fuel energy applications, including (i) a lower bandgap, (ii) larger conductivity, and (iii) higher stability in aqueous solutions. The PEC performance was, however, improved by employing the PPy polymer by increasing the gap in the Fermi levels so as to facilitate electron transfer from PPy to ZnO [54]. Equally, Ppy-based molecular composites, solid supports, and oligomers have also been reconnoitered for PEC water splitting [55, 56].

Poly(3,4-ethylenedioxythiophene) (PEDOT) is basically a functionalized thiophene, and it is considered to be paramount in conducting polymers in terms of greater conductivity, facile synthesis procedure, anticorrosion ability, transparency, aqueous stability, and fast redox kinetics [64]. PEDOT-based composites have stimulated the global research communities to enhance the performance of photoelectrodes for PEC water splitting. Accordingly, Duan and coworkers investigated PEDOT-decorated Ag nanoparticles functionalized with Si nanowires (AgNPs/PEDOT/SiNW arrays) for water splitting [57]. The fabricated nanoarrays displayed a stronger visible light absorption and obtained a solar-to-hydrogen conversion efficiency of 2.86% [57]. Likewise, Jeong and coworkers investigated Si nanocones with poly(styrenesulfonate) (PEDOT:PSS) for enhanced solar energy conversion applications [65]. Furthermore, Alsultan and coworkers reconnoitered a polymer-based composite of poly(3,4-ethylenedioxythiophene) (PEDOT)/nanoparticulate Ni (nano-Ni) and reduced graphene oxide (rGO). This composite is remarkably more catalytically active for hydrogen generation, as it synergistically amplified the photocurrent yield by 71% as compared to bare [58].

Srinivasan and coworkers fabricated a PC electrode based on a Pt/TiO_2/CdS/CdSe/PEDOT composite that exhibited efficient hydrogen generation through PC water splitting. Notably, the fabricated photoelectrode exhibited outstanding performance under visible-light irradiation with a quantum efficiency of 6.9%, a turnover number of 2210, and a hydrogen production rate of 370 μmol/cm^2/h [59]. Other conducting polymers such as polythiophene (PTh) have also been widely employed for solar conversion to chemical fuel applications. Fan and coworkers introduced an effective strategy to enhance the water-splitting performance by sandwiching Au plasmon in a TiO_2 and polythiophene (PTh) polymer, forming an inside inorganic-organic hybrid composite photoactive material [60]. The boosted water-splitting performance was backed by the optical transparency of the PTh nanowires, along with synergetic effects from plasmonic Au nanoparticles, as photosensitizers and electron-transporters. Outstandingly, the fabricated photoactive material exhibited enhanced performance with a photoelectric conversion of 0.11% and a hydrogen production rate of 2.929 mmol/h/m^2 at 50 mW/cm^2 [60]. The research findings employing the practice of conducting polymers recommend that organic polymers embrace the great potential for clean, stable, low-cost, and scalable solar-to-chemical fuel generation.

9.3.2 Porous organic polymer-based composites

Porous organic polymers (POPs) are covalently linked polymers with a large surface area and pores of nanodimensionality, which are favorable for catalytic conversions by exploiting their porous nature as active catalytic sites. Contrary to the other known porous materials such as metal-organic frameworks (MOFs) and nano-silica, POPs can be structurally designed and framed by varying the geometry and dimensions of the building blocks. Additionally, the strong covalent linkages in POPs offer high chemical and thermal stability, which is a primary criterion for water-splitting applications. POPs are mainly classified into covalent triazine frameworks (CTFs) and covalent organic frameworks (COFs). These covalently linked polymers are largely explored in terms of designing photocatalysts/photoelectrodes for solar water-splitting processes, as shown in Table 9.3 [66–73].

Dhanalaxmi and coworkers synthesized an $MnFe_2O_4$-porous organic polymer (POP) nanocomposite by means of N-rich benzene-benzylamine POP. The synthesized POP-based nanocomposite presented efficient PC water-splitting performance under AM 1.5 G sunlight irradiation. The portrayed results show that the obtained hydrogen evolution rate is 6.12 mmol/h/g in the absence of any noble metal cocatalyst, which is in itself the highest described for nonprecious metal catalysts [66]. Bi and coworkers synthesized covalent

Table 9.3 Porous organic polymer-based composites for solar energy conversion to chemical fuel.

Sl. no.	POPs Photocatalyst/ photoelectrode	Analytical characteristics	Ref.
1	$MnFe_2O_4$-porous organic polymer (POPs) nanocomposite	Obtained a hydrogen evolution rate of 6.12 mmol/h/g in the absence of any noble metal cocatalyst	[66]
2	Covalent triazine-based frameworks (CTFs) with platinum nanoparticles	Higher hydrogen evolution rate under visible light irradiation of $\lambda \geq 420$ nm	[67]
3	Bipyridine-containing covalent organic framework (TpBpy-COF) with its pores filled with Co(II)	Embraced a large surface area of 450 m^2/g with remarkable aqueous stability and overpotential of 400 mV at a current density of 1 mA/cm^2	[68]
4	2D covalent triazine-based frameworks (CTFs)	2D structure enhances the visible-light absorption due to interlayer coupling	[69]
5	Sulfur-doped CTFs	Enhanced adsorption of visible light and reduced recombination of free charge carriers due to sulfur doping	[70]
6	Ordered covalent triazine-based framework	Achieved 4% apparent quantum efficiency (AQE) at 420 nm	[71]
7	Hydrazone-based covalent organic framework (COFs)	These tunable scaffolds offer excellent PC hydrogen evolution	[72]
8	Covalent carbon nitride semiconductor with poly(triazineimide) (PTI) frameworks	Achieved 2.1% apparent quantum yield for the overall water splitting reaction	[73]
9	Photoluminescent porous CTF	A higher hydrogen evolution rate of 2370 μmol/g when irradiated for 20 h	[74]
10	Sulfone-containing covalent organic frameworks (COFs)	A higher hydrogen evolution rate of 16.3 mmol/g/h	[75]
11	Oriented films of 2D COFs	Higher visible light absorption, resulting in proton reduction and hydrogen evolution	[76]
12	CdS-2D COFs	Higher hydrogen evolution rate of 3678mmol/g/h	[77]

triazine-based frameworks (CTFs) with platinum nanoparticles. They displayed exceptional PC water-splitting activity and aqueous stability for hydrogen evolution in the presence of platinum under visible light irradiation of $\lambda \geq 420$ nm [67]. Additionally, Aiyappa and coworkers reported the synthesis of the bipyridine-containing covalent organic framework (TpBpy-COF), with its pores filled with Co (II), as an OER catalyst for electrocatalytic water splitting. The presented COF embraces a large surface area of 450 m^2/g with remarkable aqueous

stability and overpotential of 400 mV at a current density of 1 mA/cm^2 [68]. The research findings using porous organic polymers state that these organic polymers have prodigious potential for the realization of clean, stable, low-cost, and scalable energy systems for solar-to-chemical fuel generation.

9.3.3 Conjugated microporous polymer-based composites

Conjugated microporous polymers (CMPs) include a π-conjugated scaffold and a huge electron delocalized network assembly, and are favorable substitutes to inorganic semiconductor photoelectrodes for water splitting [74]. These polymers are well explored in terms of designing photocatalysts/photoelectrodes for solar water-splitting processes, as shown in Table 9.4 [74–78].

Wang and coworkers studied the overall water-splitting proficiency of conjugated microporous polymers [75]. They demonstrated the synthesis of nanosheets of a 1,3-diyne-linked conjugated microporous polymer (CMPs) from the oxidative coupling of 1,3,5-tris-(4-ethynylphenyl)-benzene (TEPB) and 1,3,5-triethynylbenzene (TEB). The results revealed that the CMP nanosheets showcased 10.3% and 7.6% quantum efficiencies at 420 nm, synthesized from TEPB and TEB, respectively [75]. Xu and coworkers proposed the synthesis of three perylene-containing conjugated microporous polymers (PrCMPs) by the Suzuki-Miyaura

Table 9.4 Conjugated microporous polymer-based composites for solar energy conversion to chemical fuels.

Sl. no.	CMPs Photocatalyst/ photoelectrode	Analytical characteristics	Ref.
1	Nanosheets of 1,3-diyne-linked CMPs	Showcased 10.3% and 7.6% quantum efficiencies at 420 nm, synthesized from TEPB and TEB, respectively	[74]
2	Perylene-containing conjugated microporous polymers (PrCMPs)	A hydrogen evolution rate of 12.1 μmol/h under UV-vis light irradiation	[75]
3	Planarized CMPs	Strongly enhanced hydrogen evolution	[76]
4	Extended CMPs	Showed the highest porosity and PC performance	[77]
5	Donor-π-acceptor (D-π-A) CMPs	Hydrogen evolution rate up to 106 μmol/h was achieved under UV-vis light irradiation ($\lambda > 300$ nm)	[78]

cross-coupling reaction from perylene with four polymerizable functional groups [76]. The results presented a hydrogen evolution rate of 12.1 μmol/h under UV-vis light irradiation because of their high surface area, broad light absorption, and the rational design of the conjugated microporous polymer photocatalysts [76]. Xu and coworkers studied the synthesis of donor-π-acceptor (D-π-A) conjugated microporous polymer (CMPs) photocatalysts. The donor and acceptor were pyrene, benzothiadiazole, and benzene (biphenyl), and π as the chelator units. The results presented a hydrogen evolution rate of 106 μmol/h, under UV-vis light irradiation of $\lambda > 300$ nm [78]. The research findings using conjugated microporous polymers show that these organic polymers have great potential for the realization of a clean, stable, low-cost, and scalable fuel cell system for solar-to-chemical fuel generation.

9.4 Conclusions and future directions

In summary, hydrogen as a future fuel has been gaining significant interest due to its potential applicability as a clean energy source. Solar energy harvesting and conversion techniques using PC or PEC splitting of water to hydrogen are a promising clean energy approach. The literature also support that polymers are progressively finding applications in the areas of solar energy conversion to hydrogen fuel and opening great avenues in clean-energy fuel technologies. The advances in polymeric science have led to extensive research efforts in the development of high-performance PC/photoelectrochemical energy systems that can efficiently convert solar energy to hydrogen fuel at low cost. The developments in conducting polymers and POPs for water-splitting applications are relatively promising. This chapter underlined the research findings and success stories of the design, synthesis, and fabrication of polymer-based composite materials as efficient photocatalysts/photoelectrodes for solar conversion to chemical fuel.

References

[1] H. Lambers, F.S. Chapin, T.L. Pons, Photosynthesis, in: Plant Physiological Ecology, Springer, 2008, pp. 11–99.
[2] S.A. Bonke, M. Wiechen, D.R. MacFarlane, L. Spiccia, Renewable fuels from concentrated solar power: towards practical artificial photosynthesis, Environ. Sci. 8 (2015) 2791–2796.
[3] S.T. Kochuveedu, PC and photoelectrochemical water splitting on TiO2 via photosensitization, J. Nanomater. 2016 (2016).
[4] Q. Liu, H. Lu, Z. Shi, F. Wu, J. Guo, K. Deng, L. Li, 2D ZnIn2S4 nanosheet/1D TiO2 nanorod heterostructure arrays for improved photoelectrochemical water splitting, ACS Appl. Mater. Interfaces 6 (2014) 17200–17207.

[5] L. Wang, W.A. Daoud, BiOI/TiO2-nanorod array heterojunction solar cell: growth, charge transport kinetics and photoelectrochemical properties, Appl. Surf. Sci. 324 (2015) 532–537.
[6] Y. Zhang, Q. Pei, J. Liang, T. Feng, X. Zhou, H. Mao, W. Zhang, Y. Hisaeda, X.M. Song, Mesoporous TiO2-based photoanode sensitized by BiOI and investigation of its photovoltaic behavior, Langmuir 31 (2015) 10279–10284.
[7] G. Dai, L.M. Chao, T. Iwasa, PC degradation of phenol with bacteriorhodopsin sensitized TiO2 nanoparticles, in: Advanced Materials Research, Trans Tech Publications, 2014, pp. 415–418.
[8] A. Molaeirad, S. Janfaza, A. Karimi-Fard, B. Mahyad, Photocurrent generation by adsorption of two main pigments of Halobacterium salinarum on TiO2 nanostructured electrode, Biotechnol. Appl. Biochem. 62 (2015) 121–125.
[9] L. Tsui, J. Huang, M. Sabat, G. Zangari, Visible light sensitization of TiO2 nanotubes by bacteriochlorophyll-C dyes for photoelectrochemical solar cells, ACS Sustain. Chem. Eng. 2 (2014) 2097–2101.
[10] J.R. Swierk, K.P. Regan, J. Jiang, G.W. Brudvig, C.A. Schmuttenmaer, Rutile TiO2 as an anode material for water-splitting dye-sensitized photoelectrochemical cells, ACS Energy Lett. 1 (2016) 603–606.
[11] N.S. McCool, J.R. Swierk, C.T. Nemes, C.A. Schmuttenmaer, T.E. Mallouk, Dynamics of electron injection in SnO2/TiO2 core/shell electrodes for water-splitting dye-sensitized photoelectrochemical cells, J. Phys. Chem. Lett. 7 (2016) 2930–2934.
[12] K. Qian, B.C. Sweeny, A.C. Johnston-Peck, W. Niu, J.O. Graham, J.S. DuChene, J. Qiu, Y.C. Wang, M.H. Engelhard, D. Su, Surface plasmon-driven water reduction: gold nanoparticle size matters, J. Am. Chem. Soc. 136 (2014) 9842–9845.
[13] L. Wang, Y. Wang, P. Schmuki, S. Kment, R. Zboril, Nanostar morphology of plasmonic particles strongly enhances photoelectrochemical water splitting of TiO2 nanorods with superior incident photon-to-current conversion efficiency in visible/near-infrared region, Electrochim. Acta 260 (2018) 212–220.
[14] M. Kibria, Z. Mi, Artificial photosynthesis using metal/nonmetal-nitride semiconductors: current status, prospects, and challenges, J. Mater. Chem. A 4 (2016) 2801–2820.
[15] J. Yang, X. Wang, B. Li, L. Ma, L. Shi, Y. Xiong, H. Xu, Novel iron/cobalt-containing polypyrrole hydrogel-derived trifunctional electrocatalyst for self-powered overall water splitting, Adv. Funct. Mater. 27 (2017) 1606497.
[16] J. Luo, Y. Ma, H. Wang, J. Chen, Preparation of polypyrrole sensitized TiO2 nanotube arrays hybrids for efficient photoelectrochemical water splitting, Electrochim. Acta 167 (2015) 119–125.
[17] X. Li, W. Lu, W. Dong, Q. Chen, D. Wu, W. Zhou, L. Chen, Si/PEDOT hybrid core/shell nanowire arrays as photoelectrodes for photoelectrochemical water-splitting, Nanoscale 5 (2013) 5257–5261.
[18] P. Bogdanoff, D. Stellmach, O. Gabriel, B. Stannowski, R. Schlatmann, R. van de Krol, S. Fiechter, Artificial leaf for water splitting based on a triple-junction thin-film silicon solar cell and a PEDOT: PSS/catalyst blend, Energ. Technol. 4 (2016) 230–241.
[19] K. Oka, O. Tsujimura, T. Suga, H. Nishide, B. Winther-Jensen, Light-assisted electrochemical water-splitting at very low bias voltage using metal-free polythiophene as photocathode at high pH in a full-cell setup, Energy Environ. Sci. 11 (2018) 1335–1342.
[20] X. Zong, X. Miao, S. Hua, L. An, X. Gao, W. Jiang, D. Qu, Z. Zhou, X. Liu, Z. Sun, Structure defects assisted PC H2 production for polythiophene nanofibers, Appl. Catal. Environ. 211 (2017) 98–105.
[21] L. Li, W. Fang, P. Zhang, J. Bi, Y. He, J. Wang, W. Su, Sulfur-doped covalent triazine-based frameworks for enhanced PC hydrogen evolution from water under visible light, J. Mater. Chem. A 4 (2016) 12402–12406.

[22] K. Schwinghammer, B. Tuffy, M.B. Mesch, E. Wirnhier, C. Martineau, F. Taulelle, W. Schnick, J. Senker, B.V. Lotsch, Triazine-based carbon nitrides for visible-light-driven hydrogen evolution, Angew. Chem. Int. Ed. 52 (2013) 2435–2439.
[23] V.S. Vyas, F. Haase, L. Stegbauer, G. Savasci, F. Podjaski, C. Ochsenfeld, B.V. Lotsch, A tunable azine covalent organic framework platform for visible light-induced hydrogen generation, Nat. Commun. 6 (2015) 8508.
[24] F. Haase, T. Banerjee, G. Savasci, C. Ochsenfeld, B.V. Lotsch, Structure–property–activity relationships in a pyridine containing azine-linked covalent organic framework for PC hydrogen evolution, Faraday Discuss. 201 (2017) 247–264.
[25] L. Li, R.G. Hadt, S. Yao, W.Y. Lo, Z. Cai, Q. Wu, B. Pandit, L.X. Chen, L. Yu, Photocatalysts based on cobalt-chelating conjugated polymers for hydrogen evolution from water, Chem. Mater. 28 (2016) 5394–5399.
[26] L. Li, W.Y. Lo, Z. Cai, N. Zhang, L. Yu, Donor–acceptor porous conjugated polymers for PC hydrogen production: the importance of acceptor comonomer, Macromolecules 49 (2016) 6903–6909.
[27] World Energy Outlook, The Global Energy Landscape Changing (2019).
[28] R. Lee, The outlook for population growth, Science 333 (2011) 569–573.
[29] M. Azwar, M. Hussain, A. Abdul-Wahab, Development of biohydrogen production by photobiological, fermentation and electrochemical processes: a review, Renew. Sustain. Energy Rev. 31 (2014) 158–173.
[30] K. Christopher, R. Dimitrios, A review on exergy comparison of hydrogen production methods from renewable energy sources, Energy Environ. Sci. 5 (2012) 6640–6651.
[31] S.Y. Tee, K.Y. Win, W.S. Teo, L.D. Koh, S. Liu, C.P. Teng, M.Y. Han, Recent progress in energy-driven water splitting, Adv. Sci. 4 (5) (2017), 1600337.
[32] D.E. Osborn, B.J. Thompson, Solar constant and air mass zero solar spectral irradiance tables, in: SPIE Milestone Series, vol. 54, SPIE, 1993, pp. 92–96.
[33] E. Glover, Design, Synthesis and Characterisation of Novel Materials for PC Water Splitting, UCL (University College London), 2017.
[34] R.J. Matson, K.A. Emery, R.E. Bird, Terrestrial solar spectra, solar simulation and solar cell short-circuit current calibration: a review, Sol. Cells 11 (1984) 105–145.
[35] I. Dincer, Green methods for hydrogen production, Int. J. Hydrogen Energy 37 (2012) 1954–1971.
[36] M.A. Green, Solar Cells: Operating Principles, Technology, and System Applications, Prentice-Hall, Inc, Englewood Cliffs, NJ, 1982.
[37] A. Murphy, P. Barnes, L. Randeniya, I. Plumb, I. Grey, M. Horne, J. Glasscock, Efficiency of solar water splitting using semiconductor electrodes, Int. J. Hydrogen Energy 31 (2006) 1999–2017.
[38] N.E.T.T.C.E. Revolution, Hydrogen Production in the Coming Hydrogen Economy, 2014.
[39] S.P. Badwal, S.S. Giddey, C. Munnings, A.I. Bhatt, A.F. Hollenkamp, Emerging electrochemical energy conversion and storage technologies, Front. Chem. 2 (2014).
[40] K. Zeng, D. Zhang, Recent progress in alkaline water electrolysis for hydrogen production and applications, Prog. Energy Combust. Sci. 36 (2010) 307–326.
[41] C.J. Winter, Hydrogen energy—abundant, efficient, clean: a debate over the energy-system-of-change, Int. J. Hydrogen Energy 34 (2009) S1–S52.
[42] K. Morganti, M. Al-Abdullah, A. Alzubail, G. Kalghatgi, Y. Viollet, R. Head, A. Khan, A. Abdul-Manan, Synergistic engine-fuel technologies for light-duty vehicles: fuel economy and greenhouse gas emissions, Appl. Energy 208 (2017) 1538–1561.
[43] L.F. Brown, A comparative study of fuels for on-board hydrogen production for fuel-cell-powered automobiles, Int. J. Hydrogen Energy 26 (2001) 381–397.
[44] E. Rincón-Mejía, A. de las Heras, Sustainable Energy Technologies, CRC Press, 2017.

[45] M.Z. Rahman, K. Davey, S. Qiao, Carbon, nitrogen and phosphorous containing metal-free photocatalysts for hydrogen production: progress and challenges, J. Mater. Chem. A 6 (2017) 1305–1322.
[46] Q. Wang, T. Hisatomi, Q. Jia, H. Tokudome, M. Zhong, C. Wang, Z. Pan, T. Takata, M. Nakabayashi, N. Shibata, Scalable water splitting on particulate photocatalyst sheets with a solar-to-hydrogen energy conversion efficiency exceeding 1%, Nat. Mater. 15 (2016) 611–615.
[47] J.W. Ager, M.R. Shaner, K.A. Walczak, I.D. Sharp, S. Ardo, Experimental demonstrations of spontaneous, solar-driven photoelectrochemical water splitting, Energy Environ. Sci. 8 (2015) 2811–2824.
[48] A.A. Ismail, D.W. Bahnemann, Photochemical splitting of water for hydrogen production by photocatalysis: a review, Sol. Energy Mater. Sol. Cells 128 (2014) 85–101.
[49] A. Fujishima, K. Honda, Electrochemical photolysis of water at a semiconductor electrode, Nature 238 (1972) 37–38.
[50] A.J. Frank, K. Honda, Polymer-modified electrodes, catalysis and water-splitting reactions, J. Photochem. 29 (1985) 195–204.
[51] Y. Tan, Y. Chen, Z. Mahimwalla, M.B. Johnson, T. Sharma, R. Brüning, K. Ghandi, Novel synthesis of rutile titanium dioxide–polypyrrole nano composites and their application in hydrogen generation, Synth. Met. 189 (2014) 77–85.
[52] D. Wang, Y. Wang, X. Li, Q. Luo, J. An, J. Yue, Sunlight PC activity of polypyrrole–TiO2 nanocomposites prepared by 'in situ' method, Catal. Commun. 9 (2008) 1162–1166.
[53] S. Zhang, Q. Chen, Y. Wang, L. Guo, Synthesis and photoactivity of CdS photocatalysts modified by polypyrrole, Int. J. Hydrogen Energy 37 (2012) 13030–13036.
[54] Z. Wang, P. Xiao, L. Qiao, X. Meng, Y. Zhang, X. Li, F. Yang, Polypyrrole sensitized ZnO nanorod arrays for efficient PEC splitting of water, Phys. B Condens. Matter 419 (2013) 51–56.
[55] R. Brimblecombe, G.C. Dismukes, G.F. Swiegers, L. Spiccia, Molecular water-oxidation catalysts for photoelectrochemical cells, Dalton Trans. 43 (2009) 9374–9384.
[56] J. Mola, E. Mas-Marza, X. Sala, I. Romero, M. Rodríguez, C. Vinas, T. Parella, A. Llobet, Ru-Hbpp-based water-oxidation catalysts anchored on conducting solid supports, Angew. Chem. Int. Ed. 47 (2008) 5830–5832.
[57] C. Duan, H. Wang, X. Ou, F. Li, X. Zhang, Efficient visible light photocatalyst fabricated by depositing plasmonic Ag nanoparticles on conductive polymer-protected Si nanowire arrays for photoelectrochemical hydrogen generation, ACS Appl. Mater. Interfaces 6 (2014) 9742–9750.
[58] M. Alsultan, J. Choi, R. Jalili, P. Wagner, G.F. Swiegers, Synergistic amplification of catalytic hydrogen generation by a thin-film conducting polymer composite, Cat. Sci. Technol. 8 (2018) 4169–4179.
[59] N. Srinivasan, Y. Shiga, D. Atarashi, E. Sakai, M. Miyauchi, A PEDOT-coated quantum dot as efficient visible light harvester for PC hydrogen production, Appl. Catal. Environ. 179 (2015) 113–121.
[60] W. Fan, C. Chen, H. Bai, B. Luo, H. Shen, W. Shi, Photosensitive polymer and semiconductors bridged by Au plasmon for photoelectrochemical water splitting, Appl. Catal. Environ. 195 (2016) 9–15.
[61] R. Kalyani, K. Gurunathan, PTh-rGO-TiO2 nanocomposite for PC hydrogen production and dye degradation, J. Photochem. Photobiol. A Chem. 329 (2016) 105–112.
[62] Y. Wang, W. Chu, S. Wang, Z. Li, Y. Zeng, S. Yan, Y. Sun, Simple synthesis and photoelectrochemical characterizations of polythiophene/Pd/TiO2 composite microspheres, ACS Appl. Mater. Interfaces 6 (2014) 20197–20204.

[63] R. Kalyani, K. Gurunathan, Intercalated network of graphene oxide (GO)–CuO–polythiophene (PTh) hybrid nanocomposite for PC applications, J. Mater. Sci. Mater. Electron. 27 (2016) 10634–10641.
[64] A. Elschner, S. Kirchmeyer, W. Lovenich, U. Merker, K. Reuter, PEDOT: Principles and Applications of an Intrinsically Conductive Polymer, CRC Press, 2010.
[65] S. Jeong, E.C. Garnett, S. Wang, Z. Yu, S. Fan, M.L. Brongersma, M.D. McGehee, Y. Cui, Hybrid silicon nanocone–polymer solar cells, Nano Lett. 12 (2012) 2971–2976.
[66] K. Dhanalaxmi, R. Yadav, S.K. Kundu, B.M. Reddy, V. Amoli, A.K. Sinha, J. Mondal, MnFe2O4 nanocrystals wrapped in a porous organic polymer: a designed architecture for water-splitting photocatalysis, Eur. J. Chem. 22 (2016) 15639–15644.
[67] J. Bi, W. Fang, L. Li, J. Wang, S. Liang, Y. He, M. Liu, L. Wu, Covalent triazine-based frameworks as visible light photocatalysts for the splitting of water, Macromol. Rapid Commun. 36 (2015) 1799–1805.
[68] H.B. Aiyappa, J. Thote, D.B. Shinde, R. Banerjee, S. Kurungot, Cobalt-modified covalent organic framework as a robust water oxidation electrocatalyst, Chem. Mater. 28 (2016) 4375–4379.
[69] X. Jiang, P. Wang, J. Zhao, 2D covalent triazine framework: a new class of organic photocatalyst for water splitting, Chem. Mater. 3 (2015) 7750–7758.
[70] L. Li, W. Fang, P. Zhang, J. Bi, Y. He, J. Wang, W. Su, Sulfur-doped covalent triazine-based frameworks for enhanced photocatalytic hydrogen evolution from water under visible light, J. Mater. Chem. A 4 (2016) 12402–12406.
[71] J. Xie, S.A. Shevlin, Q. Ruan, S.J. Moniz, Y. Liu, X. Liu, Y. Li, C.C. Lau, Z.X. Guo, J.J.E. Tang, Efficient visible light-driven water oxidation and proton reduction by an ordered covalent triazine-based framework, Energy Environ. Sci. 11 (2018) 1617–1624.
[72] L. Stegbauer, K. Schwinghammer, B.V. Lotsch, A hydrazone-based covalent organic framework for PC hydrogen production, Chem. Sci. 5 (2014) 2789–2793.
[73] L. Lin, C. Wang, W. Ren, H. Ou, Y. Zhang, X. Wang, PC overall water splitting by conjugated semiconductors with crystalline poly (triazine imide) frameworks, Chem. Sci. 8 (2017) 5506–5511.
[74] R.S. Sprick, B. Bonillo, R. Clowes, P. Guiglion, N.J. Brownbill, B.J. Slater, F. Blanc, M.A. Zwijnenburg, D.J. Adams, A.I. Cooper, Visible-light-driven hydrogen evolution using planarized conjugated polymer photocatalysts, Angew. Chem. Int. Ed. 55 (2016) 1792–1796.
[75] L. Wang, Y. Wan, Y. Ding, S. Wu, Y. Zhang, X. Zhang, G. Zhang, Y. Xiong, X. Wu, J.J.A.M. Yang, Conjugated microporous polymer nanosheets for overall water splitting using visible light, Adv. Mater. 29 (2017) 1702428.
[76] Y. Xu, N. Mao, S. Feng, C. Zhang, F. Wang, Y. Chen, J. Zeng, J.X. Jiang, Perylene-containing conjugated microporous polymers for PC hydrogen evolution, Macromol. Chem. Phys. 218 (2017) 1700049.
[77] R.S. Sprick, B. Bonillo, M. Sachs, R. Clowes, J.R. Durrant, D.J. Adams, A.I. Cooper, Extended conjugated microporous polymers for PC hydrogen evolution from water, Chem. Commun. 52 (2016) 10008–10011.
[78] Y. Xu, N. Mao, C. Zhang, X. Wang, J. Zeng, Y. Chen, F. Wang, J.X. Jiang, Rational design of donor-π-acceptor conjugated microporous polymers for PC hydrogen production, Appl. Catal. Environ. 228 (2018) 1–9.

10

Polymer nanocomposites for energy-related applications

Haradhan Kolya[a], Tapas Kuila[b], Nam Hoon Kim[a], and Joong Hee Lee[a,c]

[a]Department of Nano Convergence Engineering, Jeonbuk National University, Jeonju, Jeonbuk, Republic of Korea, [b]Surface Engineering and Tribology Division, CSIR-Central Mechanical Engineering Research Institute, Durgapur, India, [c]Carbon Composite Research Centre, Department of Polymer-Nano Science and Technology, Jeonbuk National University, Jeonju, Jeonbuk, Republic of Korea

10.1 Introduction

Lately, polymer nanocomposites (PNCs) have established themselves as an important class of advanced materials that is being tried for various techno-commercial applications. Various types of nanofillers, such as zero-dimensional (0D) particles (e.g., nanoscale, $CaCO_3$, and Al_2O_3), one-dimensional (1D) fibers (e.g., carbon nanotubes (CNTs) and Ag nanowires), two-dimensional (2D) sheets (e.g., graphene, boron nitride (BN), and MoS_2), and three-dimensional (3D) structures (e.g., graphite and montmorillonite) are used for preparing PNCs [1]. Also, PNCs are fast emerging as one of the most important divisions of the polymer industry, owing to the fact that nano-sized filler introduced polymers display unique and/or improved properties that are appreciably higher than the virgin polymers or their macro- and/or microcomposites. The observed property enhancements include improved modulus and strength, higher barrier properties, greater solvent and heat resistance, reduced flammability, better luminescence, larger conductivity, and unique optical absorption characteristics [2]. Accordingly, such PNCs are being increasingly applied in chemical sensors, fuel cells, electrocatalysis, supercapacitors, smart windows, batteries, and so forth [3, 4]. The resultant properties and corresponding applications are dependent on the types of fillers and polymers, the nature of dispersion, the interfacial behaviors, the preparation techniques, and the filler size and morphology [5, 6].

Polymer-Based Advanced Functional Composites for Optoelectronic and Energy Applications
https://doi.org/10.1016/B978-0-12-818484-4.00006-9
Copyright © 2021 Elsevier Inc. All rights reserved.

Silica (SiO_2) is one of the most widely used fillers, and it is commonly found in sand, quartz, and living organisms. It is an amorphous or polymorph material with low water solubility that depends on pH and temperature and is mostly used for construction applications. However, in recent decades, nano-sized silica has been extensively tried as a potential filler to prepare diverse PNCs for different domestic and industrial applications [7]. Also, polymer/SiO_2NCs have attracted significant research interest, owing to the wide diversity in their end properties [8].

In addition to SiO_2, CNTs have also attracted considerable scientific interest because of their extraordinary thermal conductivity and superior mechanical and electrical properties [9]. CNTs are essentially 1D carbon materials with sp^2 hybridized carbon. Further, the end properties of polymer/CNT NCs mainly depend on the dispersion of CNTs in the polymer host, in addition to the interfacial interactions between the introduced CNT and the host polymer. These NCs are mainly used in catalysis, energy harvesting, and energy storage applications [10].

Although promising, polymer/CNTNCs have difficulties in processing and suffer from both high material and manufacturing costs. To overcome these, various researchers have tried graphene as a filler. Graphene is essentially a characteristic planar single layer of sp^2-bonded carbon atoms [11]. It offers an improved capacitive performance owing to its enormous surface area, high electrical conductivity, prominent chemical stability, and high mechanical flexibility. In addition, graphene shows a good matrix for the synthesis of functional nanomaterials to enhance their electro-activity and electronic conductivity [12]. Polymer/graphene NCs and graphene transition metal oxide/hydroxide composites are widely studied as efficient conductor constituents for high-performance supercapacitors [12–14]. Polymer/graphene NCs also show increasing potential for energy harvesting applications, owing to the high permittivity and higher energy storage density of graphene together with the higher flexibility and improved thermal and mechanical properties of the host polymer. Although polymer/graphene NCs offer a high dielectric constant, they suffer limitations related to their higher dielectric loss and lower electric field strength. Nevertheless, the energy loss of polymer/graphene NCs could be minimized by insulating the graphene nanosheets with various ionic and nonionic reagents that act to lessen the direct interaction of the graphene nanosheets and hence, to decrease the motion of the π-orbital or moveable electrons in the polymer background. Yet, realizing PNCs with a high dielectric constant and a very low dielectric loss is a daunting challenge. Recently, Weng et al. [15] reported that the dielectric constant of a graphite microsheet introduced poly(vinylidene fluoride) NC film increased to 6.5×10^5 under a 100 Hz test frequency and with a field strength of 0.63 kV mm^{-1}. The film was also

reported to offer a specific energy storage of 2.07 J cm^{-3}, which is more than 120 times the pure poly(vinylidene fluoride) film [15]. Boron nitride (BN) was also tried as a special substrate for graphene. Hexagonal BN is structurally analogous to graphite with a smooth surface. It is an insulating isomorph of graphene with boron and nitrogen atoms occupying the inequivalent A and B sublattices in the Bernal structure. Plus, it has large optical phonon modes and a larger electrical bandgap [16]. The atomic planar surface of BN is expected to conquer rippling in a graphene sheet, thus having desirable in-plane physical properties. It also routinely conforms to both corrugated and flat surfaces. However, the major difference between BN and graphene is that graphene has nonpolar homonuclear C–C intralayer bonds, whereas hexagonal BN presents highly polar B–N bonds. Also, the immobile polarizabilities of the component atoms of B–N considerably differ from carbon-carbon atoms of graphene [16, 17].

This chapter offers a comprehensive review of the recent development and current state of PNC research for energy-related applications. Thus, the chapter sheds light on the synthetic routes for the preparation of PNCs and their related applications in supercapacitors, solar cells, lithium-ion batteries, lithium-sulfur batteries, lithium-air batteries, and so forth. This perspective on the energy-related applications of PNCs may offer a comprehensive vision on the current stage of energy harvesting research, thereby revealing the challenges and new directions for future development.

10.2 Preparation of polymer nanocomposites

Polymer/SiO_2NCs are prepared by one of three general preparative methods: blending, in situ polymerization, and the sol-gel process. The SiO_2 nanofiller can be introduced directly using in situ polymerization and blending methods, but in the sol-gel process, a SiO_2 precursor may be used [18] (Fig. 10.1).

The organic part can be introduced as a precursor, a linear polymer, or a semicrystalline linear polymer. The inorganic part can also be introduced in the same way. The characteristic properties of polymer/SiO_2NCs are found to be superior to the pure polymeric chain [18]. Recently, significant research efforts have been focused on figuring out the most effective synthetic routes to develop polymer/SiO_2NCs with tailored morphologies that represent a comparatively new category of NCs with advanced end properties.

On the other hand, to effectively fabricate polymer/CNT NCs with enhanced electrical performance, two major practical constraints are to be considered. The first constraint is dispersion-related issues, as it is very difficult to attain homogenous CNT dispersion in polymers because of their strong tendency to agglomerate due to higher van der

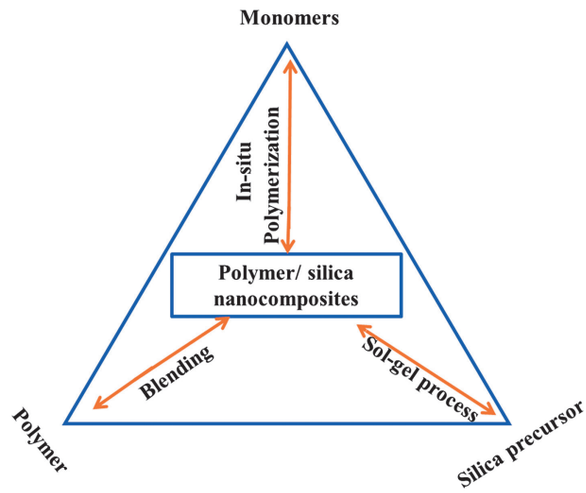


Fig. 10.1 Schematic representation of various preparation techniques of silica NCs.

Waals interactions. Second, the inert nature of the CNT surface (due to aromaticity) results in poor interfacial adhesion with the polymer host that in turn inhibits stress transfer at the time of loading [19]. Nevertheless, to overcome these challenges, many methods such as chemical modification involving either covalent or noncovalent bonding between nanotubes and polymers [20], ultrasonication [21], and ball milling [22] have been continuously explored. The noncovalent approach involves the physical adsorption or wrapping of conjugated polymers to the CNT surface via π-π stacking [23], as shown in Fig. 10.2. Physical methods take advantage of surfactants or macromolecules that are essentially adsorbed onto the surface of the CNT nanoparticles. Further, composites with nanoparticles containing an inorganic core and an organic shell or surface-modified nanoparticles can be considered a special type of NC and are often designated as hybrid nanoparticles [24].

Polymer/CNT NCs may be prepared by various methods, including in situ polymerizations [25], solution mixing [26], melt compounding [27], and milling [28]. Further, it is the in situ polymerization of monomers in the presence of CNTs that has been most widely explored for the synthesis of polymer-grafted CNT composites. Also, this technique works well with thermally less stable matrices. On the other hand, solution processing involves sonication or stirring aimed at dispersing the undesired CNT polymer solution, followed by solvent evaporation. Further, the melt-compounding technique is widely employed for the production of CNT-reinforced thermoplastic composites. Ball milling is the best adopted route to reduce the particle size, in addition to controlling the porosity and shape. Also, this technique is commonly used to prepare a fine polymer/CNT composite powder, which is subsequently melt-mixed with a twin roll.

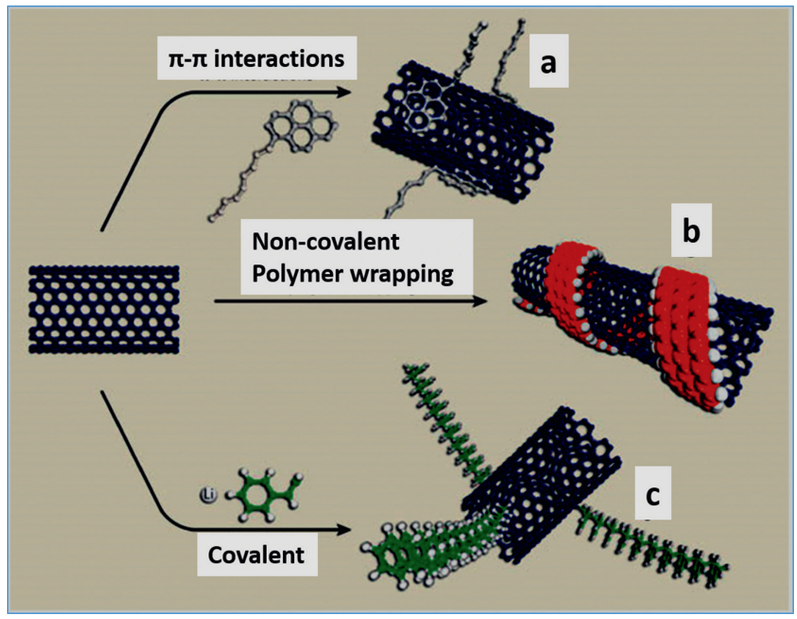


Fig. 10.2 Chemical modification of CNTs. Reproduced from P.M. Ajayan, J.M. Tour, Nanotube composites, Nature 447 (2007) 1066 with permission of the Nature Publishing Group.

To achieve higher compatibility and appreciable improvement in the end properties of polymer/GO composites, different routes of surface modification have been continuously tried. Many of these are similar to those used in polymer/CNTNC systems, such as chemical modification involving either covalent or noncovalent bonding (Fig. 10.2) [20], in situ polymerization, [25] solution mixing [26], melt compounding [27], and milling [28]. The solution mixing technique was successful enough to introduce GO nanofillers into a variety of polymers [29, 30]. Melt mixing was found to be more compatible and highly economical, as melt mixing is a solvent-free process [31]. However, melt mixing does not provide the same level of filler dispersion as that of solvent mixing or in situ polymerization [32]. Thus, solution mixing is the most widely adopted technique to prepare a wide diversity of PNCs [33, 34].

10.3 Energy-related applications of polymer nanocomposites

10.3.1 Supercapacitors

Supercapacitors are also known as ultracapacitors or electrical double-layer capacitors (EDLCs). An elementary capacitor generally

contains two metal plates divided by an insulator (air or film). At the time of charging, electrons are stored on the surface of one metal plate and depart from the other. Thus, one metal plate gains a negative charge while the other metal plate builds a positive charge. Nevertheless, it is the insulator that interrupts the natural attraction of the negative charge to the positive one, thereby generating an electric field. Further, discharge occurs when the two metal plates are connected with a circuit.

When supercapacitors consisting of two conductors finely coated with activated carbon are dipped in an electrolyte, one metal plate acquires a positive charge while the other acquires a negative charge. During charging, positive and negative ions from the electrolyte solution accumulate onto the surface of each carbon-coated metal plate and create an electric field. In this electric field, supercapacitors can store energy between the two oppositely charged electrodes through the electrolyte. Therefore, during charging, an electrical double layer is formed. Besides capacitors and supercapacitors, batteries can also store energy through appropriate chemical reactions. However, supercapacitors exhibit considerably higher power densities than batteries. Consequently, supercapacitors are excellent for numerous electronic devices and industrial applications, provided their energy densities are appreciably improved. Because the energy density (E) of a capacitor is ruled by $E = 1/2\,CV^2$, where C is the capacitance and V is the cell potential, increasing the potential/capacitance can lead to higher energy densities.

The best-used conductor material (porous carbon) typically possesses a double-layer capacitance of nearby $100\,\mathrm{F\,g^{-1}}$ and an energy density of $25\,\mathrm{Wh\,kg^{-1}}$. Generally, conducting polymer/CNT NCs show superior electrical and electro-chemical properties in comparison with a conducting polymer alone [35, 36]. That is, polyaniline (PANI), polypyrrole, and poly(3,4-ethylenedioxythiophene) with MWCNT NCs present higher capacitance values ($100–330\,\mathrm{F\,g^{-1}}$). Such materials are therefore used for various asymmetric configurations, with the capacitor voltage ranging from 0.6 to 1.8 V [37, 38]. Further, various researchers have observed and reported significant electrical performance enhancement with various PNCs. To name a few, MWCNTs and poly(*p*-phenylene vinylene) (PPV) with quantum effectiveness nearly twice that of the atypical ITO device have been reported [39]. Poly(vinylidene fluoride) (PVDF)/trifluorophenyl functionalized MWCNT NCs that exhibit enhanced dielectric permittivity that is close to the percolation threshold have also been developed [40, 41] (results of the same are shown in Fig. 10.3). PANI/MWCNT NCs prepared via in situ polymerization were reported by Potphode et al. to show a high energy density of $72.5\,\mathrm{Wh\,kg^{-1}}$ and a power density of $4.9\,\mathrm{kW\,kg^{-1}}$ [42].

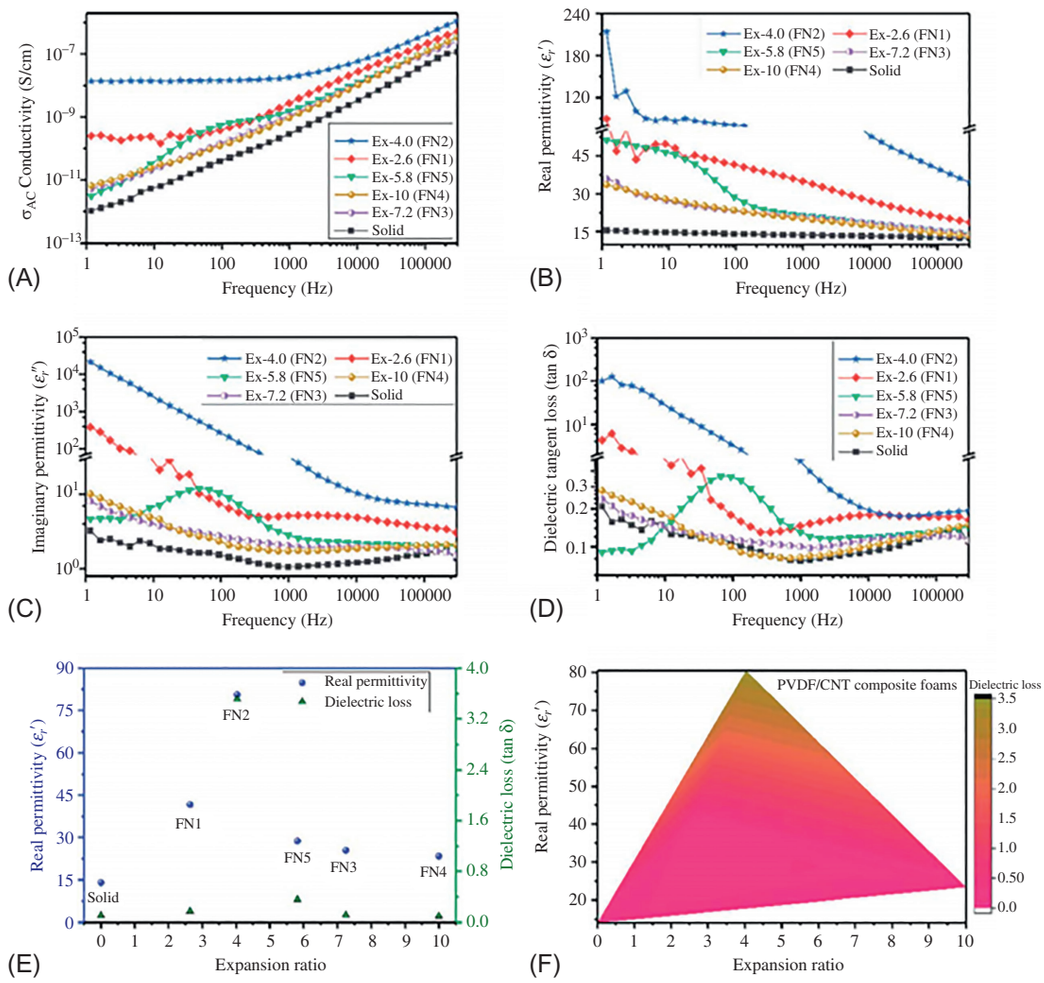


Fig. 10.3 (A) Frequency-dependent electrical conductivity of the solid and foamed PVDF/CNT composites; (B) Real permittivity; (C) Imaginary permittivity; (D) Dielectric loss of the solid and foamed PVDF/CNT composites as a function of the applied frequency ranging from 1 to 300,000 Hz, (E) Real permittivity and dielectric loss of the solid and foamed PVDF/CNT composites at 100 Hz frequency; and (F) Correlation between real permittivity, dielectric loss, and expansion ratio of the foamed PVDF/CNT composites at 100 Hz frequency. Reproduced from B. Zhao, M. Hamidinejad, C. Zhao, R. Li, S. Wang, Y. Kazemi, C.B. Park, A versatile foaming platform to fabricate polymer/carbon composites with high dielectric permittivity and ultra-low dielectric loss, J. Mater. Chem. A 7 (2018) 133–140 with permission of the Royal Society of Chemistry.

Ferroelectric-PNCs were reported to be associated with a high dielectric constant, high heat of the resistant, and higher chemical stabilities [43, 44]. PMMA/MWCNT NCs synthesized by Kim et al. via solution mixing were reported to show a significant enhancement in the electrical conductivity ($\approx 3000\,S\,m^{-1}$ at 0.4 wt% of MWCNT) [45]. Also, the amalgamation of CNTs with different metal oxides in a supercapacitor was reported to show a higher specific capacitance when compared to pristine CNTs [46].

Although promising, polymer/CNTNCs often suffer from both high cost and processing difficulties, which in turn lessen their applicability as commercial supercapacitors [47]. Nevertheless, in recent years, polymer/graphene NCs have been reported with increasing potential for energy conversion and storage applications. Also, PNC electrodes can combine both electrical double-layer capacitance from graphene and pseudocapacitance from polymers. Such a combination can increase the total electro-chemical performance of PNCs. Moreover, the presence of graphene in the polymer matrix can increase the mechanical stability and electrical conductivity of the host polymer. This higher electrical conductivity of graphene can further assist effective electron transfer (into conducting polymers) during the redox reactions. The presence of an sp^2 carbon lattice in graphene renders it highly suitable for energy applications, as established with PANI/graphene NCs [48]. In addition, PANI itself has a high theoretical specific pseudocapacitance of $2000\,F\,g^{-1}$, and exceptionally fast redox and acid-base doping and dedoping characteristics [48–52]. Further, 3D PANI/rGONCs possess an even higher specific capacitance of $385\,F\,g^{-1}$, a current density of $0.5\,A\,g^{-1}$, and a capacitance retention of 88% over 5000 cycles [53]. A hierarchical nanostructured PANI-rGO/cellulose fiber composite film showed a specific capacitance of $224\,F\,g^{-1}$, a current density of $0.1\,A\,g^{-1}$, and a capacitance retention of $\approx$89% over 1000 cycles [54] (results presented in Fig. 10.4). Further, the presence of sulfonic acid groups in the sulfonated PANI were reported to enhance the redox reaction and pseudocapacitance, thereby leading to a high specific capacitance of $1107\,F\,g^{-1}$ and a current density of $1\,A\,g^{-1}$ in a three-electrode set up. Also, when the sulfonated PANI was mixed with chemically reduced GO, it acted as an asymmetric supercapacitor with a specific capacitance of $157\,F\,g^{-1}$, a current density of $1.5\,A\,g^{-1}$, and a 94% retention in specific capacitance after 5000 charge-discharge cycles. The asymmetric supercapacitor exhibits a maximum energy density of $31.4\,Wh\,kg^{-1}$ and a large power density of $14.764\,kW\,kg^{-1}$ [55]. Besides PANI, polypyrrole/graphene NCs have also been employed as electrodes for high-performance supercapacitors [56, 57]. The 4,4′-diaminostilbene-2,2′-disulfonic acid functionalized r-GO electrode showed a high specific capacitance value of

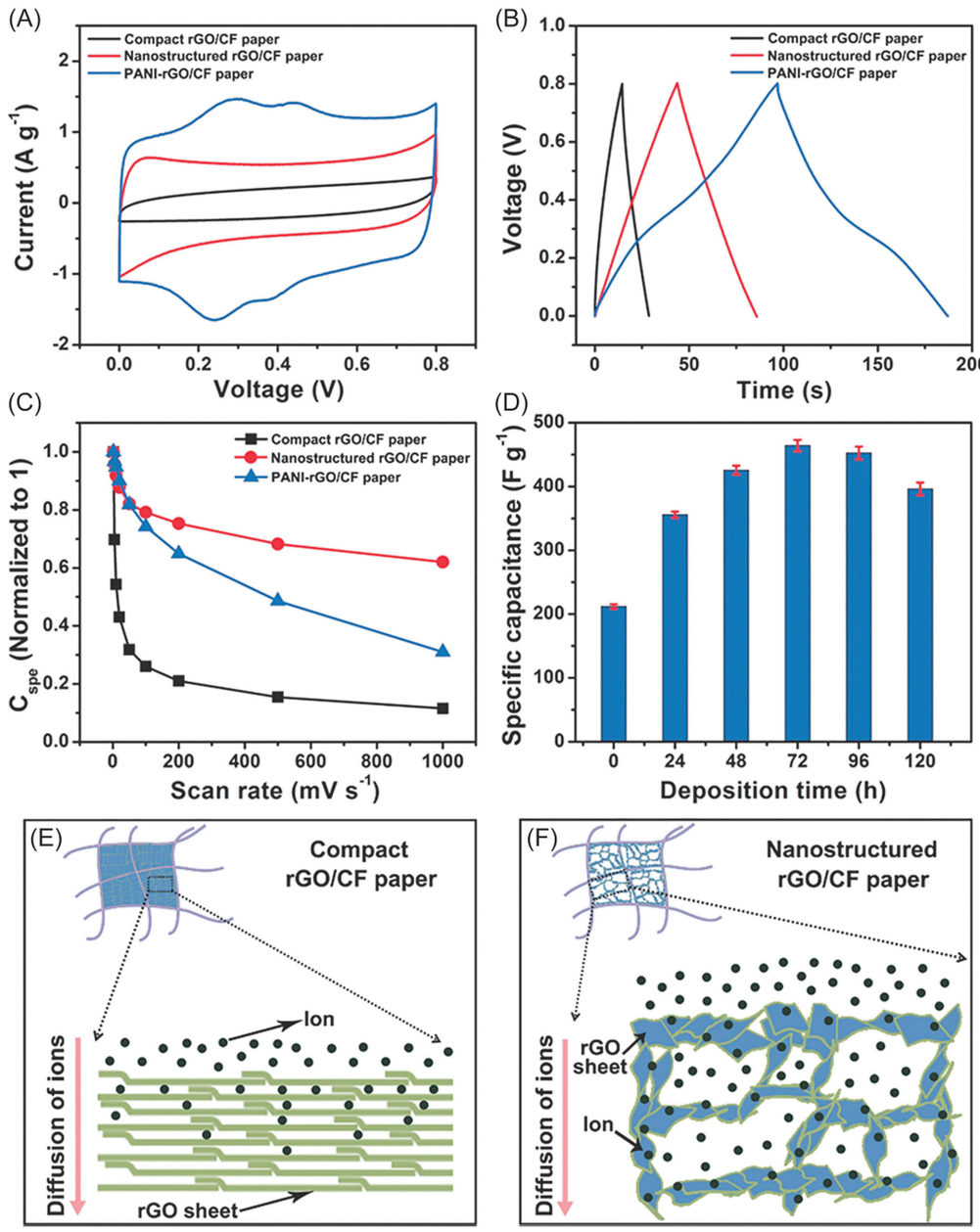


Fig. 10.4 (A) CV curves with a scan rate of 10 mV s^{-1}; (B) Charge/discharge curves at a current of 1 A g^{-1} of conventional supercapacitors based on compact r-GO/cellulose fiber composite paper, nanostructured r-GO/cellulose fiber composite paper, and PANI-r-GO/cellulose fibercomposite paper (PANI deposition time: 72 h); (C) Comparison of normalized specific capacitance between compact r-GO/cellulose fiber composite paper, nanostructured r-GO/cellulose fiber composite paper, and PANI-r-GO/cellulose fiber paper (PANI deposition time: 72 h at different scan rates); (D) Specific capacitance of the PANI-r-GO/cellulose fiber papers with different PANI deposition times; Schematic diagrams of ion diffusion in (E) Compact rGO/cellulose fiber composite paper; and (F) Nanostructured r-GO/cellulose fiber composite paper. Reproduced from L. Liu, Z. Niu, L. Zhang, W. Zhou, X. Chen, S. Xie, Nanostructured graphene composite papers for highly flexible and foldable supercapacitors, Adv. Mater. 26(2014) 4855–4862 with permission of Wiley.

1042 F g^{-1}, a current density of 1 A g^{-1}, and good cycling stability (95% capacitance retention after 3000 cycles in a three-electrode set up). The asymmetric supercapacitor showed a specific capacitance value of 159 F g^{-1}, a current density of 1 A g^{-1}, and an 86% retention in specific capacitance after 8500 cycles [58]. Other polymer/graphene NCs have also been used as electrode materials for high-performance supercapacitor devices [59–61]. Subsequently, the integration of fusion material as a positive electrode and r-GO as a negative electrode has resulted in asymmetric aqueous devices with a high specific energy of 27 Wh kg^{-1} [62].

A liquid electrode of polyoxometalate/r-GONC presented good cycling stability (~ 95%) and better Coulombic efficiency (~ 77%–79%) after 2000 cycles, with increasing suitability for energy storage applications [63] (results presented in Fig. 10.5). Polypyrrole/graphene NCs that present appreciable suitability for energy applications are often prepared via the in situ oxidative polymerization technique, with a varying wt% of graphene. The capacitance value of such NCs increased to a certain percentage of graphene, after which it showed a downward trend. The maximum capacitance value was, however, 409 F g^{-1} and the energy density was 227.2 Wh kg^{-1} at a 10 mV s^{-1} scan rate [63].

Polymer/silica NC film of poly(vinyl pyrrolidone) (PVP) and polyvinyl alcohol (PVA) displayed lessened optical energy gaps. The dielectric permittivity of such PNCs decreased with increasing SiO_2 loadings [64] (results presented in Fig. 10.6). Such PNC-based dielectric materials were also reported to enhance the performance of various microelectronic and organo-electronic devices [65]. Moreover, h-BN nanosheet-doped poly(vinyl alcohol) in a sulfuric acid gel polymer as an electrolyte and a separator of an asymmetric quasi-solid-state supercapacitor with activated carbon as the electrodes delivered a high specific capacitance, good rate capability, and excellent cycle stability at the current density of 0.5 A g^{-1}. This supercapacitor delivered an electrode specific capacitance of 124.5 F g^{-1} and retained 99.2% capacitance after 5000 charge-discharge cycles [66].

Recently, polymer/metal oxide NCs have been increasingly investigated as electrode materials for high-performance supercapacitors. Accordingly, Yang et al. reported that a hierarchical PANI/α-Fe_2O_3 nanostructure hydrogel prepared by in situ polymerization showed a specific capacitance of about 473.6 F g^{-1} and a current density of 1 A g^{-1} (388.0 F g^{-1} at 5 mV s^{-1}) [67]. Hu et al. synthesized PANI/SnO_2NCs with a specific capacitance of 305.3 F g^{-1}, a specific energy density of 42.4 Wh kg^{-1}, and a coulombic efficiency of 96% [68]. Further, Ghosh et al. reported that H^+ and Ni^{2+} codoped PANI on MWCNTs prepared by in situ polymerization presented a specific capacitance of 781 F g^{-1} at 0.5 A g^{-1} constant current and with 92% capacitance retention [69]. Su et al. reported PANI/TiO_2/GO composite prepared by in situ

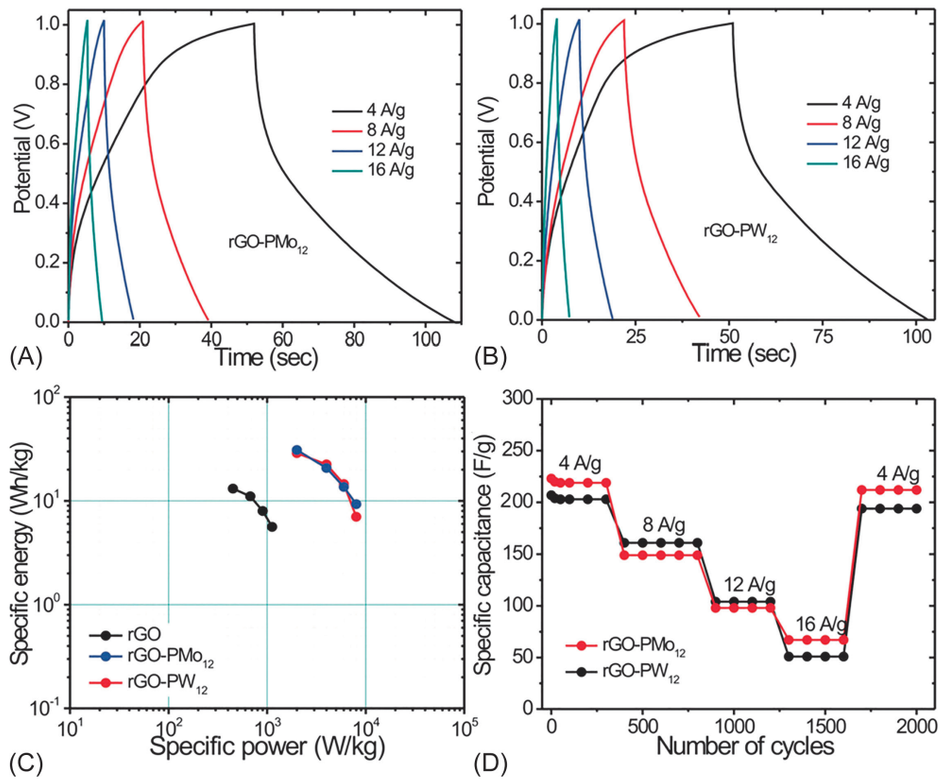


Fig. 10.5 (A, B) Galvanostatic charge/discharge curves for r-GO/phosphotungstate (rGO/PW_{12}) and rGO/phosphomolybdate (rGO/PMo_{12}) hybrid electro-active nanofluid (HENF) of 0.025% at different current densities in static condition; (C) Plot of specific energy versus specific power in the Ragone plot for r-GO, r-GO/PW_{12}, and r-GO/PMo_{12} in a flow cell; and (D) Galvanostatic charge/discharge cycling test for r-GO/polyoxometalates (POMs) HENFs of 0.025% at different current densities for 2000 cycles. Reproduced from D.P. Dubal, D. Rueda-Garcia, C. Marchante, R. Benages, P. Gomez-Romero, Hybrid graphene-polyoxometalates nanofluids as liquid electrodes for dual energy storage in novel flow cells, Chem. Rec. 18 (2018) 1076–1084 with permission of Wiley.

hydrolyzation of tetrabutyl titanate, which showed a specific capacitance of $430\,F\,g^{-1}$ at $1\,A\,g^{-1}$and with long cycle-life [70]. Similarly, Padmini et al. reported PANI/$CaCu_3Ti_4O_{12}$ composites via in situ polymerization that showed an appreciably high energy density of $30\,Wh\,kg^{-1}$ and excellent power density of $20\,kW\,kg^{-1}$ [71].

10.3.2 Solar cells

Lately, organic solar cells have received significant interest from both academia and industry, owing to their inherent advantages over conventional silicon-based devices such as light weight, higher

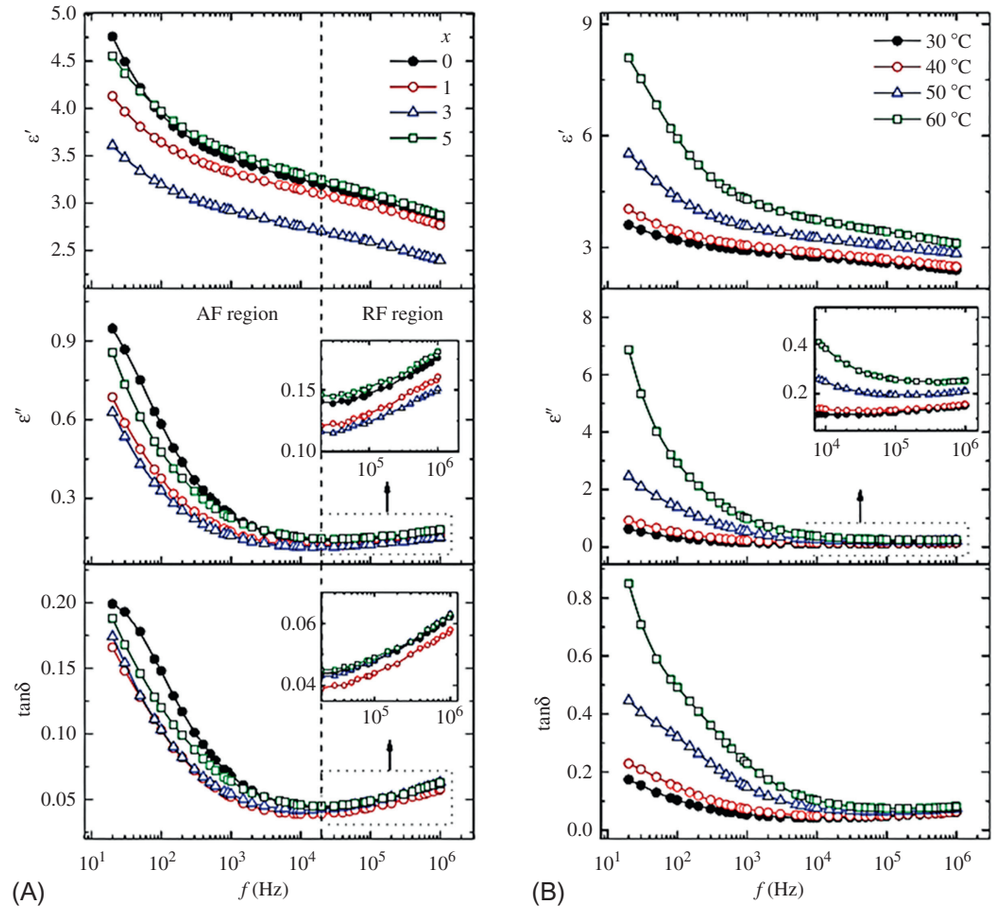


Fig. 10.6 Frequency-dependent real part (ε') and loss part (ε'') values of complex dielectric permittivity, and loss tangent ($\tan\delta$) of; (A) (PVA-PVP)-$x$wt% SiO_2NC films containing $x = 0$, 1, 3, and 5 at 30°C; and (B) (PVA-PVP)-3 wt% SiO_2NC film at temperatures of 30°C, 40°C, 50°C, and 60°C. (Inset: enlarged view of the spectra in the radio frequency (RF) region.) Reproduced from S. Choudhary, Characterization of amorphous silica nanofiller effect on the structural, morphological, optical, thermal, dielectric and electrical properties of PVA--PVP blend based polymer nanocomposites for their flexible nanodielectric applications, J. Mater. Sci. Mater. Electron. 29 (2018) 10517–10534 with permission of Springer Nature.

flexibility, lower processing cost, and lessened environmental impact. A typical representation of an organic solar cell is shown in Fig. 10.7A and that of a polymer solar cell is shown in Fig. 10.7B [72].

In recent years, CNTs have been explored as effective hole transporting ingredients for organic solar cells. Both single-walled and multiwalled CNT introduced conducting polymers possess conjugated π-systems, wherein electronic transitions are anticipated to

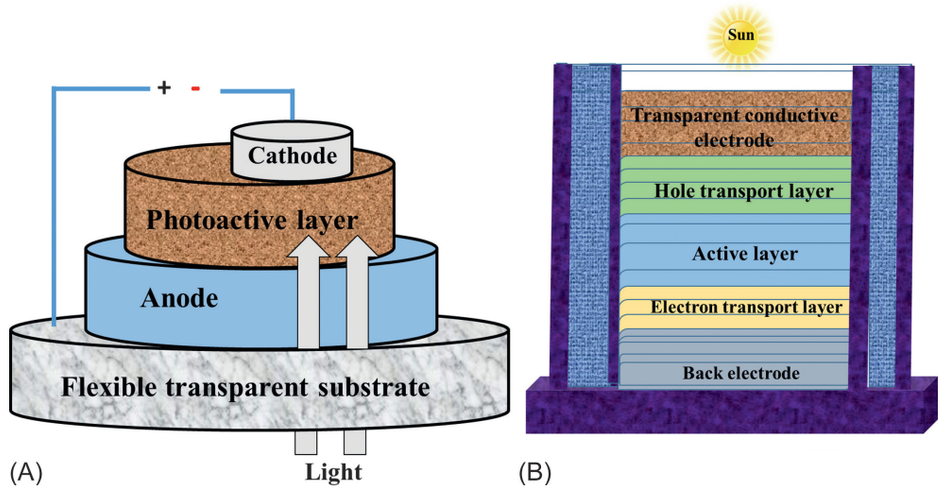


Fig. 10.7 Pictorial representation of; (A) An organic solar cell; and (B) A polymer solar cell.

occur via π-π interaction. Among 1D, 2D, and 3D structures of conducting polymers, 1D nanostructures (such as nanofibers, nanorods, nanotubes, and nanowires) are excellent applicants for nanoelectronic devices. Accordingly, a 3D interconnected network of polystyrene (PS)/MWCNTs showed excellent electrical conductivity, with 1.5 wt% nanotube loadings [73]. MWCNT-doped poly(3,4-ethylene dioxythiophene):poly(styrene sulfonate) composites showed higher out-of-plane conductivities for organic solar cell applications [74] while PANI/CNT NCs showed appreciable suitability for a wider range of applications (Fig. 10.8), including sensors, actuators, solar cells, fuel cells, and so on [75].

Perovskite solar cells have also received much consideration in recent years, owing to their extraordinary power conversion efficiency. For illustration, a simple glass encapsulation of carbon-sandwiched indium tin oxide/C_{60}/$CH_3NH_2PbI_3$/poly(3-hexylthiophene-2,5-diyl)/CNT devices showed excellent performance with stability maintained for up to 2200 h after constant illumination of one sun (100% light intensity) without a UV filter and under ambient conditions [76] (results are presented in Fig. 10.9). Also, fullerene, nonfullerene, and polymeric acceptor-based solar cells have been recently reported with futuristic practical applications [77].

Graphene-based PNCs with higher electrical conductivity, greater mobility, and high optical transmittance in the visible regions have been normally used as electrodes for dye-sensitized solar cells [78] and organic solar cells [56]. The r-GO/polyethylene terephthalate films (thickness 16 nm), when used in solar cells, displayed a power-conversion efficiency of 0.78%, an open-circuit voltage (V_{OC}) of 0.56 V,

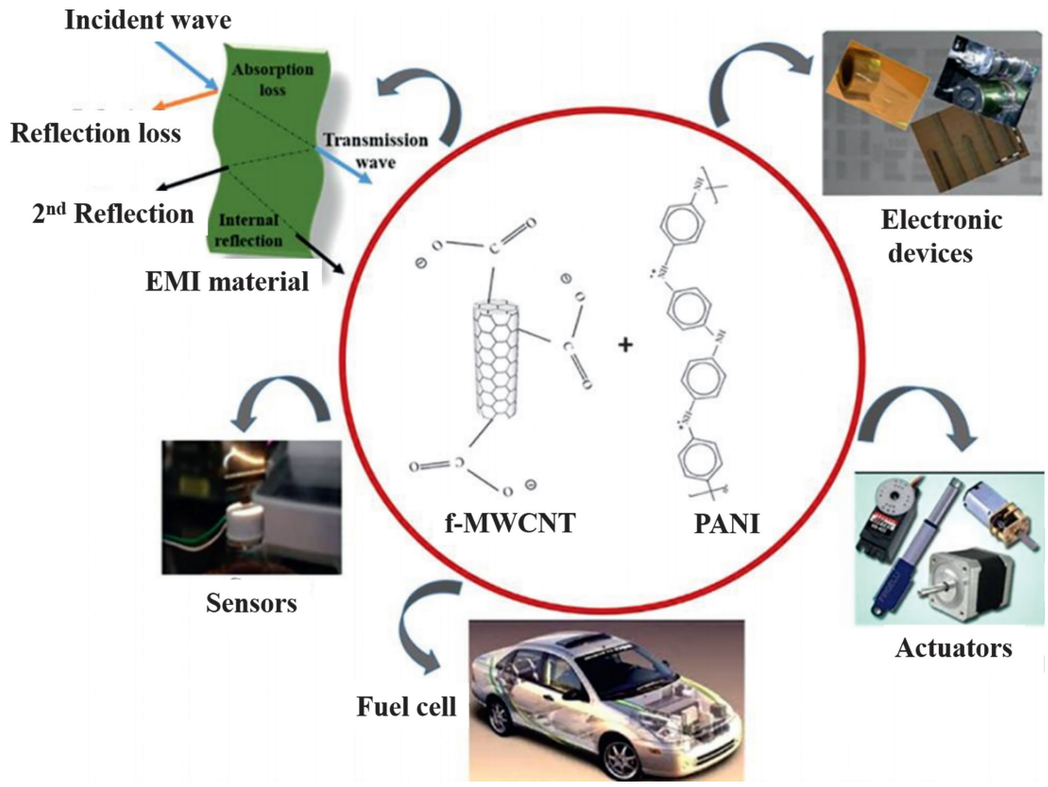


Fig. 10.8 Various application domains of PANI/CNT NCs. Reproduced from A. Kumar, V. Kumar, K. Awasthi, Polyaniline–carbon nanotube composites: preparation methods, properties, and applications, Polym.-Plast. Technol. Eng. 57 (2018) 70–97 with permission of Taylor and Francis.

a short-circuit current density (J_{sc}) of 4.39 mA cm^{-2}, and a transparency of 65% [79] (results presented in Fig. 10.10).

Poly(3,4-ethylenedioxythiophene) and poly(styrene sulfonate) composites are also explored as hole transport layers in polymer solar cells to facilitate the ease of hole extraction, owing to their high optical transparency, good conductivity, and smooth morphology. Also, a thin film of GO is found to be useful as an efficient hole transport layer in both conventional and inverted polymer solar cells [80] while ther-GO/poly(methyl methacrylate) NC film is found to be a suitable replacement as an electron conducting layer for perovskite solar cells in place of the traditionally used and expensive [6,6]-phenyl-C61-butyric acid methyl ester layer [81]. The polymer/graphene NCs show resistance in quenching by defeating the defect-induced carrier scattering in graphene while keeping the optical transmittance greater than 90%, which is the most desired aspect for many optoelectronic applications. Plus, polyethylene

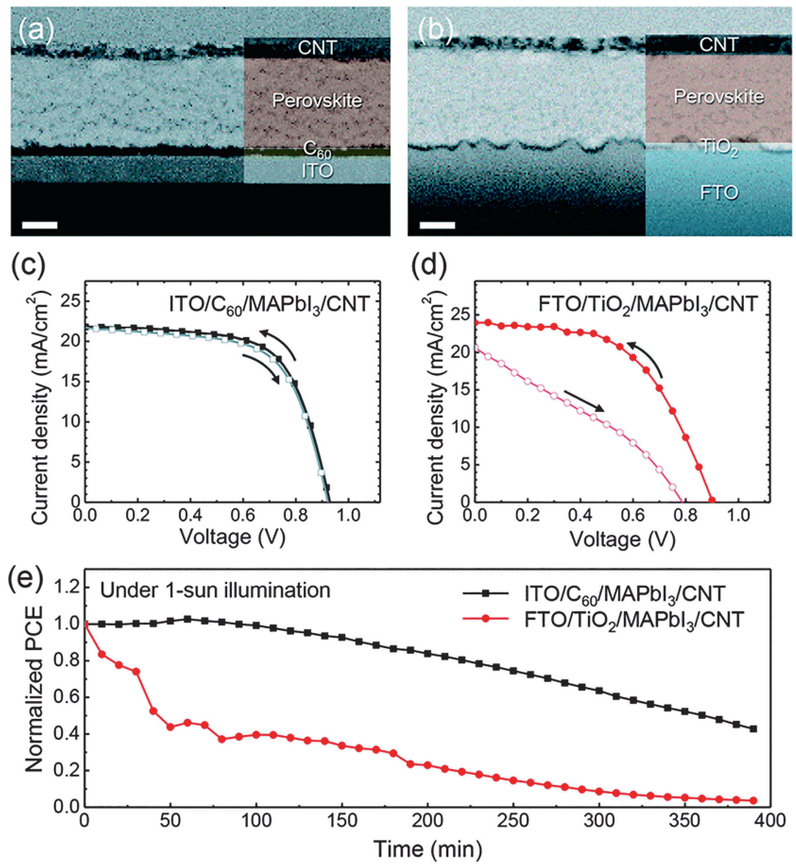


Fig. 10.9 Cross-sectional SEM images of (A) ITO/C_{60}/$MAPbI_3$/CNT device; (B) FTO/TiO_2/$MAPbI_3$/CNT. The forward and backward *J-V* curves of (C) C_{60}-based device; (D) TiO_2-based device; and (E) Time evolution of normalized PCEs of the C_{60}- and TiO_2-based devices, without encapsulation. Reproduced from N. Ahn, I. Jeon, J. Yoon, E.I. Kauppinen, Y. Matsuo, S. Maruyama, M. Choi, Carbon-sandwiched perovskite solar cell, J. Mater. Chem. A 6 (2018) 1382–1389 with permission of The Royal Society of Chemistry.

oxide and polyvinylidene fluoride-hexafluoropropylene with r-GO PNCs can act as high-performance polymer electrolytes for dye-sensitized solar cells [82]. Further, Kumar et al. reported that r-GO integrated poly [2-methoxy, 5-(2′-ethylhexyloxy)-*p*-phenylenevinylene] and poly(3-hexylthiophene) conducting polymer NCs showed more charge transfer capabilities and higher suitability for solar cell applications [83]. Also, PANI and PANI-grafted silica NCs can be used in ionic liquid electrolytes for dye-sensitized solar cells [84]. The thermal decomposition temperature of PANI/silica NCs is lower than that of pure PANI. However, it has a higher electrical conductivity at a low SiO_2 content. High SiO_2 content decreases its conductivity [85]. Li et al. have reported the graphene-on-silicon (Gr/Si) Schottky junction solar

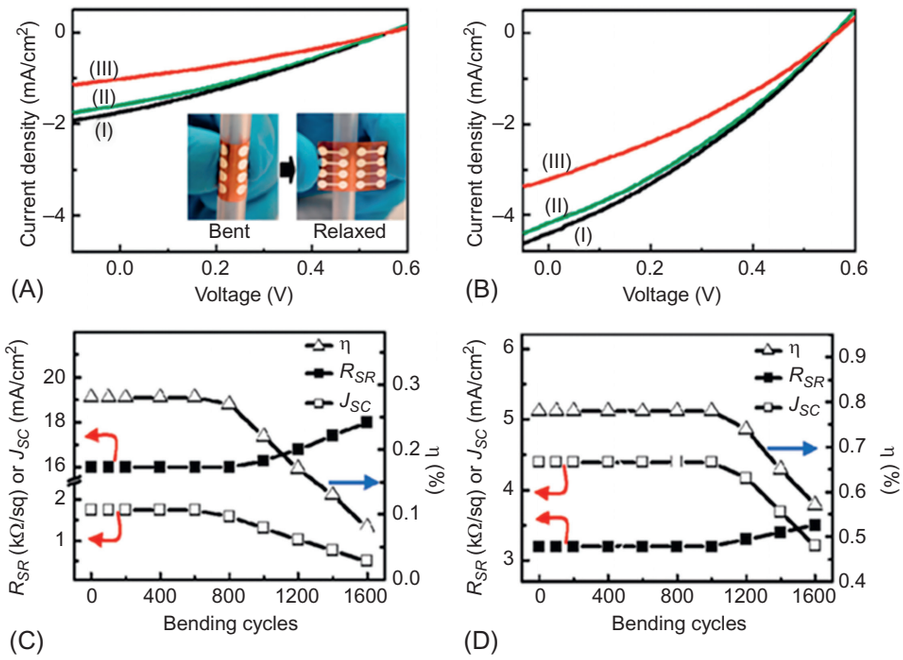


Fig. 10.10 *J-V* curves of (A) device 1 after applying (I) 400, (II) 800, and (III) 1200 cycles of bending; and (B) device 3 after applying (I) 800, (II) 1200, and (III) 1600 cycles of bending. The short-circuit current density (J_{sc}), overall power conversion efficiency (η), and the sheet resistance (RSR) of device 1 and device 3 are plotted as a function of bending cycles in (C) and (D), respectively. (Inset in (A): photograph of the bending relaxing experiments of the OPV device.) Reproduced from Z. Yin, S. Sun, T. Salim, S. Wu, X. Huang, Q. He, Y.M. Lam, H. Zhang, Organic photovoltaic devices using highly flexible reduced graphene oxide films as transparent electrodes, ACS Nano 4 (2010) 5263–5268 with permission of the American Chemical Society.

cells as promising candidates for low-cost photovoltaic applications [86]. Recently, Long et al. reported that a conjugated homopolymer based on the electron-deficient unit of double B⟵N bridged bipyridine (P-BNBP) can be used as an electron acceptor for all-polymer solar cells. P-BNBP showed a low-lying LUMO energy level of −3.59 eV, a high absorption coefficient of $1.6\times10^5\,\mathrm{L\,mol^{-1}\,cm^{-1}}$ at 626 nm, and moderate electron mobility of $4.37\times10^{-6}\,\mathrm{cm^2\,V^{-1}\,s^{-1}}$. All-polymer solar cell devices exhibit power conversion efficiencies of 2.44%–3.04%. These results demonstrated that conjugated homopolymers are promising as electron acceptor materials for all-polymer solar cells [87]. Maier et al. prepared $CuInS_2$-poly(3-(ethyl-4-butanoate)thiophene) NC layers via an in situ technique that showed an efficiency of about 0.4% when used in solar cells [88]. Polymer/copper indium sulfide NCs prepared via in situ polymerization by Rath et al. showed a good efficiency of up to 2.8% [89]. Similarly, Dayal et al. reported that poly [2,6-(4,4-bis-(2-ethylhexyl)-4*H*-cyclopenta [2,1-*b*;3,4-*b*′]dithiophene)-

alt-4,7-(2,1,3-benzothiadiazole)] and CdSe NPs exhibited an even higher power conversion efficiency of about 3.2% [90]. Wu et al. also reported poly [(9,9-bis(3′-(*N*,*N*-dimethylamino)propyl)-2,7-fluorene)-alt-2,7-(9,9-dioctyl)-fluorene]/ZnO NCs with appreciably higher solar cell performance [91].

10.3.3 Lithium-ion batteries

In recent decades, lithium-ion batteries have established themselves as the most dominant energy storage device for powerful portable electronic devices as well as electric vehicles. A polymer with highly electro-active functional groups and a stable skeleton can potentially be a powerful cathode contestant because its redox kinetics are intrinsically faster than those of inorganic intercalation cathodes. In addition, they can avoid undesirable dissolution in aprotic electrolytes, which is otherwise a common setback suffered by small organic molecules. On the other hand, CNTs are the most promising candidates to be used as anode materials, particularly in lithium-ion batteries (Fig. 10.11). Their powerful performance relies on the unique structural, mechanical, and electrical properties of CNTs.

Moreover, conductive CNTs can enrich the electronic transportation in nanostructured anode materials [92]. Hence, the applications of CNTs are expanding with time to serve as a multiskilled material in various ways because batteries can be used as a dominant energy storage

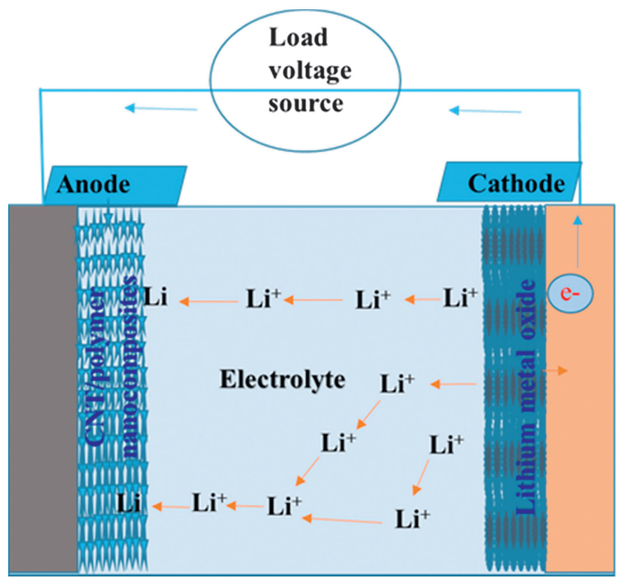


Fig. 10.11 Pictorial representation of a rechargeable lithium-ion battery.

device due to their large energy density compared to supercapacitors. PNCs, owing to their mechanical robustness, light weight, high conductivity, and higher flexibility, are increasingly being tried in battery applications. Consequently, PNCs of poly(3,4-ethylenedioxythiophene)/CNTs are directly applied as anode materials and easily fabricated into a rechargeable lithium-ion battery [93]. A conductive polymer/Jabuticaba (hybrid carbon) CNT NC with carbon black was reported to efficiently preserve its electrical conductivity, even when it was under a high strain of ≈ 200% [94]. Also, graphene-PNCs, when directly used without any binder as the cathode in a lithium ion battery, delivered a very high discharge capacity of 156 mAh g^{-1} at 0.1 C with an ultrahigh utilization of poly(anthraquinonylsulfide) (94.9%) and an impressive rate performance of 102 mAh g^{-1} at a high current density of 20°C [95]. 3D-muffled carbon domain-r-GO with PVA annealed at 700°C showed discharge capacities of 1395 mAh g^{-1} at 0.1 A g^{-1} and 606 mAh g^{-1} at 5 A g^{-1} [96]. It also has an excellent retentive capacity of 755 mAh g^{-1} after 600 cycles at a current density of 2 A g^{-1}. Additionally, more CO_2 activation was reported to boost the electro-chemical activation with exceptional discharge capacities of 1709 mAh g^{-1} at 0.1 A g^{-1} and 835 mAh g^{-1} at 2 A g^{-1} after 600 cycles [96]. It has been reported that 5-sulfoisophthalic acid coated with Si nanoparticle-doped PANI (core/shell) can also be used as an anode material for lithium-ion batteries [97]. Besides, poly(ethylene oxide) silicate@lithium also has excellent properties for battery applications [98]. Idrees et al. reported that a polyborosilazane derived ceramic-nitrogen sulfur doped graphene NC prepared via ball milling showed a reversible capacity of 785 mAh g^{-1} at a current density of 450 mA g^{-1} over 800 cycles, Hence, it is a promising anode material for lithium-ion batteries [99]. Zhao et al. reported that poly(vinylidene fluoride)/poly(vinyl chloride-*co*-vinyl acetate) (PVDF/P(VC-VAc)) blended polymer membranes prepared by phase inversion showed good electro-chemical performances as the polymer electrolyte for lithium-ion batteries [100]. Zhan et al. reported that the polymer/graphene NCs based on two different polymers such as poly(anthraquinonyl sulfide) (PAQS) and polyimide (PI) prepared by in situ polymerization showed ultrafast charging and discharging within a few seconds, and delivered capacities of 100 mAh g^{-1} (Fig. 10.12) [101]. Zhan et al. showed that the porous structure of the polymer layer is important for Li-ion conduction, as it helps to increase the contact area between the cathode electrode and the electrolyte. The homogeneously coated polymer particles on functionalized graphene surfaces were found from both SEM and TEM images (Fig. 10.12). This uniform polymer coating on the functionalized graphene surfaces and the equivalent higher dispersion of graphene in the NC facilitates better electro-chemical performance in Li-ion batteries.

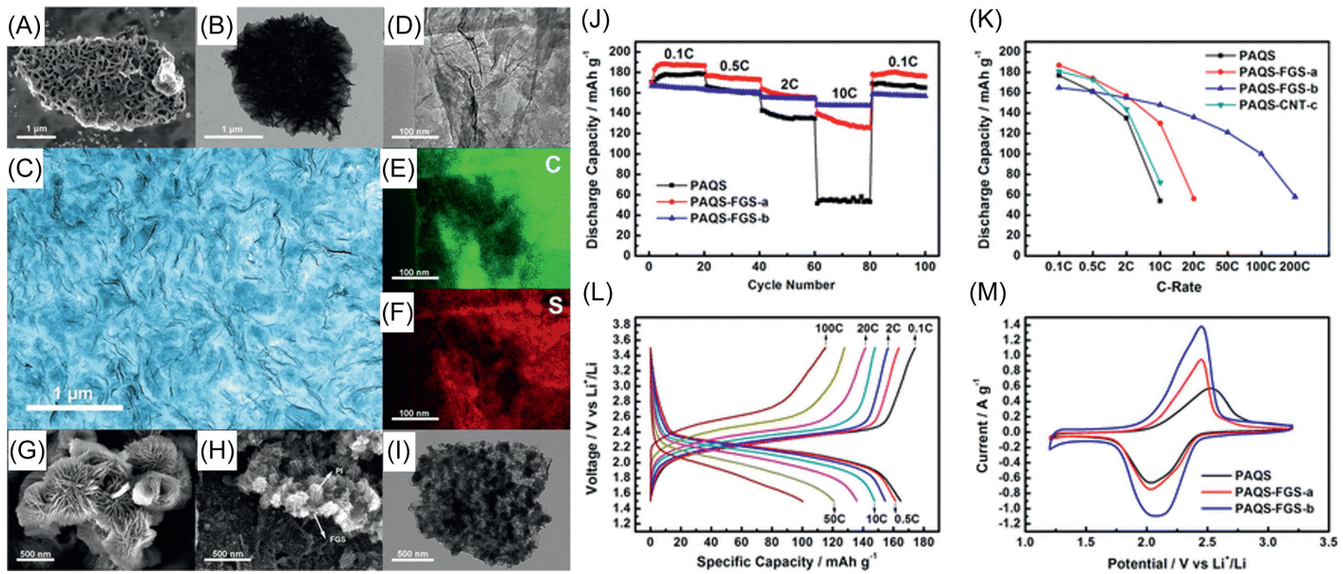


Fig. 10.12 (A) SEM image of PAQS-functionalized graphene sheets (FGS)-a; (B) Low-magnification TEM image of PAQS-FGS-a; (C) Cross-section TEM image of PAQS-FGS-b; (D) High-magnification TEM image of PAQS-FGS-b; (E,F) Corresponding carbon and sulfur elemental mapping images of PAQS-FGS-b; (G) SEM image of pure PI; (H) SEM image of PI-FGS-b; (I) Low-magnification TEM image of PI-FGS-b; (J) Cycling performance of PAQS and its composites at different C-rates; (1.5–3.5 V, 1 C = 225 mA g^{-1}). (K) Discharge specific capacity versus C-rate of PAQS and its composites; (L) Voltage profiles of PAQS-FGS-b at different C-rates; and (M) *C-V* curves of PAQS and its composites at a scan rate of 1 mV s^{-1}. The specific capacity is calculated based on the whole mass of the composite. Reproduced from Z. Song, T. Xu, M.L. Gordin, Y.-B. Jiang, I.-T. Bae, Q. Xiao, H. Zhan, J. Liu, D. Wang, Polymer–graphene nanocomposites as ultrafast-charge and discharge cathodes for rechargeable lithium batteries, Nano Lett. 12 (2012) 2205–2211 with permission of the American Chemical Society.

Lithium-ion batteries are one of the best illustrations for smaller and lighter batteries that require less charging time. However, the main disadvantages of Li-ion batteries are their expensive manufacturing, transportation restrictions, aging issues, protection levels, and difficulty in enhancing the energy density further. Consequently, alternative electrodes offering higher capacities at lesser costs and those addressing aging and safety issues are the need of the hour.

10.3.4 Lithium-sulfur batteries

Lithium-sulfur (Li-S) batteries are considered vital rechargeable batteries for the next-generation power supply [102], and PNCs play an important role in their construction and working. The Li-S battery is most important because of its high theoretical energy density (~ 2800 Wh L^{-1}) compared to Li-ion batteries. However, the insulating nature of sulfur, the polysulfide shuttle effect, and the formation and growth of lithium dendrites and their intermediates have lessened the wider applications of Li-S batteries. Nevertheless, using polymer materials, these issues may be effectively addressed and their electro-chemical performance efficiently controlled [103, 104]. Further, the applied energy density of Li-S batteries would be as high as 500 Wh kg^{-1}, which is about three times higher than that of a modern profitable Li-ion battery [105]. The Li-S cell essentially contains a cathode, an anode, and a separator immersed with electrolyte like a lithium-ion cell, wherein the electrical energy can be stored in sulfur electrodes. Mainly, lithium metal and sulfur are used as the anode and cathode, respectively. The separator used in such a battery is generally a microporous polypropylene film. The operating principle of an Li-S battery depends on the electro-chemical reactions between the sulfur and Li [106]. Generally, a cathode contains three components such as a conductive agent, a polymer binder, and an active material. Each component is responsible for determining the performance of the battery [107]. Wang et al. reported that a polypyrrole (PPY)/sulfur (50 wt%) composite electrode showed a higher discharge capacity of 1280 mAh g^{-1} at a current density of 50 mA g^{-1} than that of the virgin sulfur electrode (1100 mAh g^{-1}) [108]. The observed improvement in electro-chemical performance was reportedly due to the presence of conductive PPY absorbed with polysulfide onto the polymer matrix. Wang et al. also reported that PPY/S-CNT prepared by an in situ method showed an improved charge and discharge range (1.5–3.0 V at a current density of 50 mA g^{-1}), capacity (600 mAh g^{-1}), and cycling stability (40 cycles) [109]. FESEM images collected to investigate the surface and morphology of the synthesized materials and the resulted cell performance are shown in Fig. 10.13 [109]. The FESEM analysis revealed that the sulfur particles were found in irregular shapes and

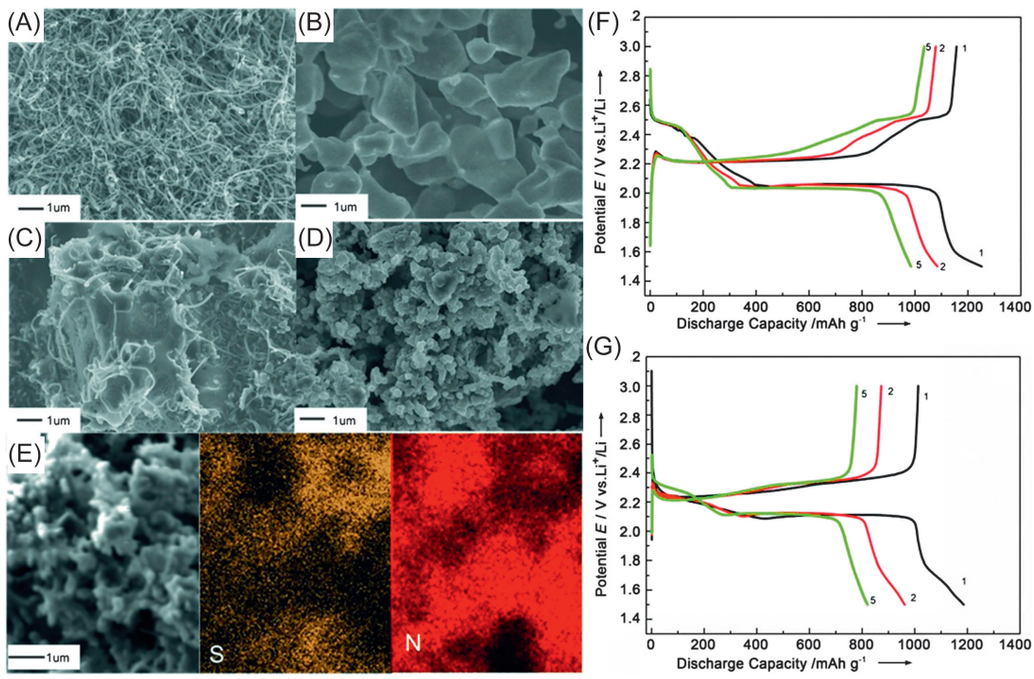


Fig. 10.13 FESEM images of (A) CNTs; (B) S; (C) S-CNTs; (D) S-CNT-PPY; (E) SEM image obtained from S-CNT-PPY composite with corresponding EDS maps of S and N; (F) Charge-discharge profiles of S-CNT-PPY composite electrode; and (G) S-CNT composite electrode. Reproduced from J. Wang, L. Lu, D. Shi, R. Tandiono, Z. Wang, K. Konstantinov, H. Liu, A conductive polypyrrole-coated, sulfur–carbon nanotube composite for use in lithium–sulfur batteries, ChemPlusChem 78 (2013) 318–324 with permission of ChemPlusChem.

sizes of 1–5 μm (Fig. 10.13B). In the PPY/S-CNT NC, the PPY nanoparticles were in the size range of 100–300 nm, which covered the surfaces of the S-CNT composites uniformly (Fig. 10.13D).

Similarly, Zhang et al. synthesized PPY/MWNT composites by in situ polymerization that showed good improvement in the cycle stability in Li-S batteries with a specific discharge capacity (960.7 mAh g^{-1}) after 40 cycles [110]. Wang et al. reported that the S-PPY/multilayer graphene composites showed an appreciably large discharge capacity and better cycle stability (60 cycles) due to the complex combination of both sulfur and amorphous PPY with multilayer graphene sheets. It was found that the maximum discharge capacity (852.4 mAh g^{-1}) was obtained with 70 wt% of sulfur [111]. Zhang et al. reported that the S/PPY-MnO_2 composites (70 wt% of S and 5 wt% of MnO_2) showed a stable Coulombic efficiency (~ 98.6%) and decay rate (0.07%) per cycle along with 500 cycles at the 1 C rate [112]. Li et al. reported that the PANI-@S/C composite prepared by ball milling and the thermal method showed good electro-chemical performance of the Li-sulfur

cell [113]. PANI-modified cetyltrimethylammonium bromide (CTAB)-GO-S NCs showed significantly improved performance in Li-sulfur batteries with high specific discharge capacities (~ 970 mAh g^{-1} at 0.2 C) and long-term cycling stabilities (300 cycles) [114].

10.3.5 Lithium-air battery

Among various metal-air batteries (lithium-air, zinc-air, and aluminum-air), the lithium-air (Li-air) battery has attracted significant technological attention since 2009 [115]. The basic difference between the Li-ion and the Li-air battery is their electrode configuration. The Li-air battery has a much higher energy density compared to all the other chemical batteries. Accordingly, Li-air batteries also play an important role in electronics, automobiles, remote sensors, robotic applications, and so forth. However, the Li-air battery technology is not matured yet and a number of critical issues must be appropriately addressed to make it commercially viable for future energy storage applications. Also, it is most essential to improve some of the factors of the Li-air battery such as the life cycle, the practical capacity, and the round-trip efficiency. In these batteries, O_2 is obtained from air and the pure Li is used as the electrode. Tentatively, the energy density of these batteries depends only on the Li electrode, by which it can be considerably improved. The important chemistry of Li-air batteries includes the lithium dissolution and deposition onto the anodic electrode (lithium), the oxygen reduction reaction (ORR), and the oxygen evolution reaction (OER) onto the cathodic electrode (air) [116]. Generally, four types of Li-air batteries have been developed, including solid-state lithium-air, nonaqueous or aprotic, mixed aprotic/aqueous, and aqueous (Fig. 10.14) [117].

Abraham et al. used the thin solid membrane of polyacrylonitrile (PAN)/carbon NCs for Li-air battery applications. The said electrolyte membrane functions both as the separator from the cathode or anode and the medium by which Li ions could reach the air cathode from the Li anode during discharging [118]. Porcarelli et al. reported a new type of polymer electrolyte prepared by the radical copolymerization of lithium 1-[3-(methacryloyloxy)propylsulfonyl]-1-(trifluoromethylsulfonyl)imide(LiMTFSI) with poly(ethylene glycol) methyl ether methacrylate (PEGM), bifunctional poly(ethylene glycol) methyl ether dimethacrylate (PEGDM), and a plasticizer of propylene carbonate (PC) [119]. Recently, Guo et al. reported that a polymer electrolyte with a low concentration of LiI (0.05 m) showed efficient activity in a Li-air battery [120]. The gel polymer electrolyte (GPE or 0.05 m LiI-GPE) contains the properties of the polymer matrix and the liquid electrolyte. The surface morphology of the polymer membrane presented regularly distributed elliptic micropores with an average diameter of 100 nm, showing good performance in the charge/discharge cycle of

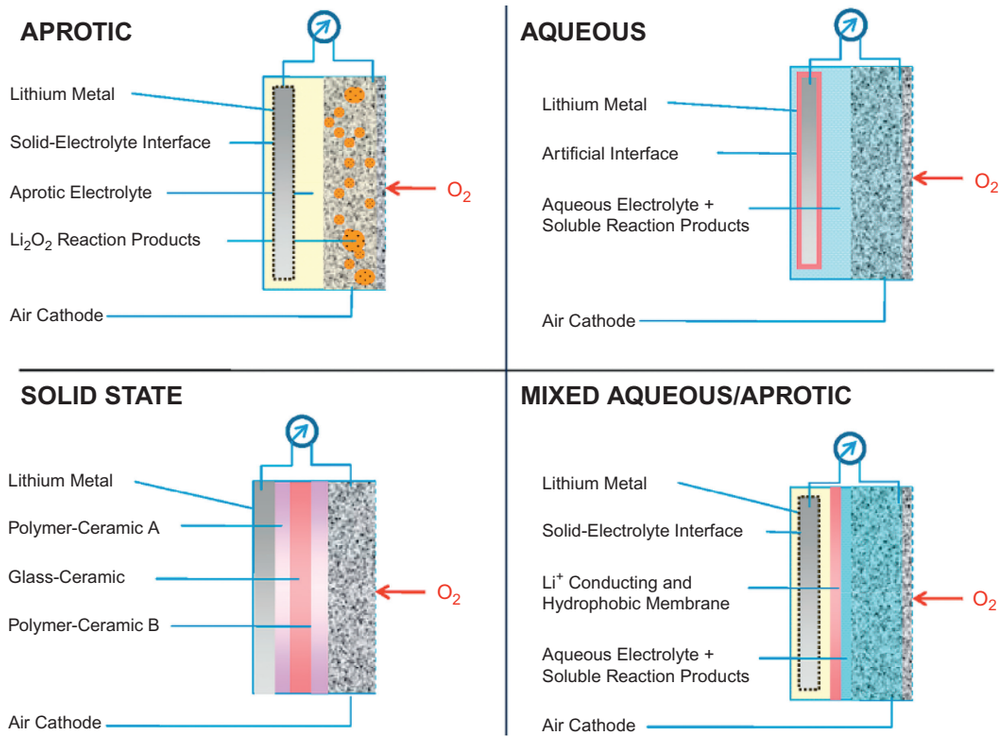


Fig. 10.14 Pictorial representation of four different architectures of Li-air batteries. Reproduced from G. Girishkumar, B. McCloskey, A.C. Luntz, S. Swanson, W. Wilcke, Lithium – air battery: promise and challenges, J. Phys. Chem. Lett. 1 (2010) 2193–2203 with permission of the American Chemical Society.

3500 mAh g^{-1} (liquid electrolyte-based cell), 3100 mAh g^{-1} (GPE-based cell), and 3400 mAh g^{-1} (0.05 m LiI-GPE-based cell) (Fig. 10.15) [120].

Yoon et al. reported that the NCs of CNT/Co_3O_4 show excellent catalytic activity for the air electrode of the Li-air battery due to the large surface area of the composite materials [121]. Zhang et al. prepared a new type of hydrophobic ionic liquid-silica-PVDF-hexafluoro propylene (HFP) polymer composite electrolyte with better discharge performance of the Li-air battery and higher capacity (2800 mAh g^{-1}) than the cell with pure ionic liquid as the electrolyte (1500 mAh g^{-1}) [122]. Li et al. reported that more and more systematic research is still essential for the potential application of hybrid polymer electrolytes in Li-air batteries [123].

10.3.6 Fuel cells

Nowadays, research related to fuel cells is gaining increasing interest, owing to the pressing need to generate more power without the emission of toxic gases. Fuel cells convert chemical energy into electrical

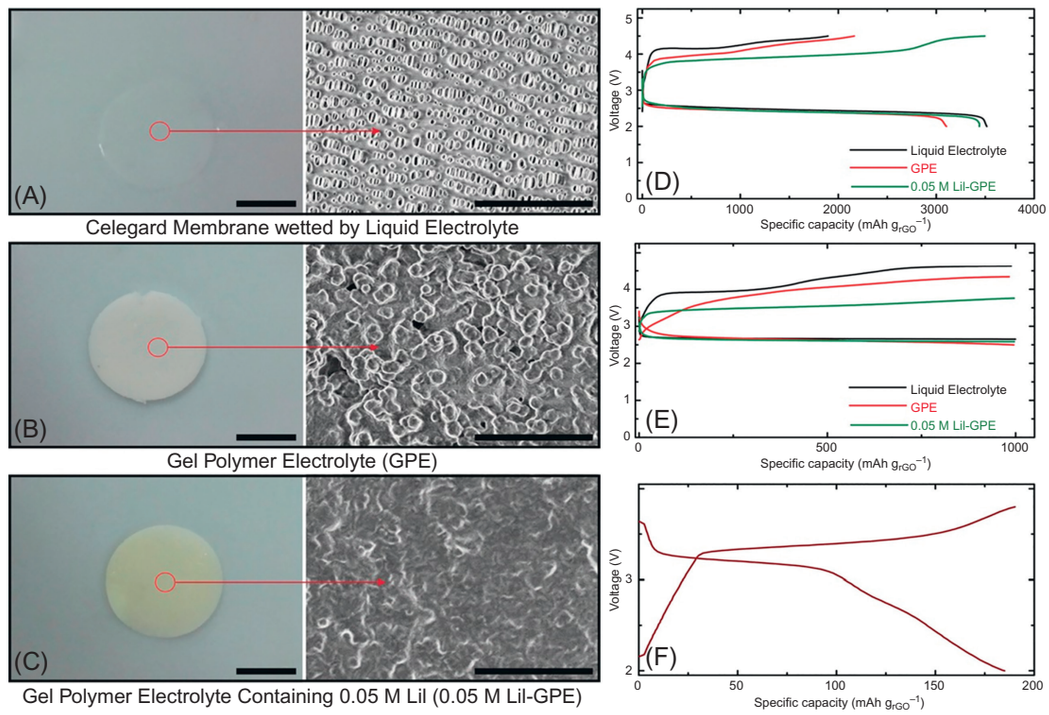


Fig. 10.15 Photographic and SEM images of (A) Celgard membrane wetted by a liquid electrolyte; (B) Gel polymer electrolyte (GPE); and (C) Gel polymer electrolyte containing 0.05 m LiI (0.05 m LiI-GPE); (D) Full discharge/charge curves with an applied current density of 1000 mA g^{-1} of the Li-air batteries using GPE, 0.05 m LiI-GPE, and liquid electrolyte; (E) Discharge/charge curves with a fixed capacity of 1000 mAh g^{-1} and an applied current density of 1000 mA g^{-1} of the Li-air batteries using GPE, 0.05 m LiI-GPE, and a liquid electrolyte; (F) Charge/discharge profile of the 0.05 m LiI-GPE-based Li-air battery tested without any O_2 atmosphere at an applied current density of 1000 mA g^{-1}, within the voltage window from 2 to 3.8 V. Reproduced from Z. Guo, C. Li, J. Liu, Y. Wang, Y. Xia, A long-life lithium–air battery in ambient air with a polymer electrolyte containing a redox mediator, Angew. Chem. Int. Ed. 56(2017) 7505–7509 with permission of Angewandte Chemie.

energy with much less power loss through electro-chemical oxidation. It was Sir William Robert Grove in 1839 who first reported the electro-chemical conversions in fuel cells [124]. Different types of fuel cells were reported that included proton exchange membrane fuel cells, polymer electrolyte membrane fuel cells, phosphoric acid fuel cells, ammonia-air fuel cells, alkaline fuel cells, direct solid oxide fuel cells, methanol fuel cells, and molten carbonate fuel cells [125]. Among these, polymer electrolyte membrane fuel cells have drawn more attention due to their chemical stability, efficient proton conductivity, and outstanding mechanical properties. Also, some perfluorinated polymer electrolyte (Nafion, Aciplex, and Flemion) membranes are considered the most promising electrolyte membranes for polymer electrolyte fuel cells [126],

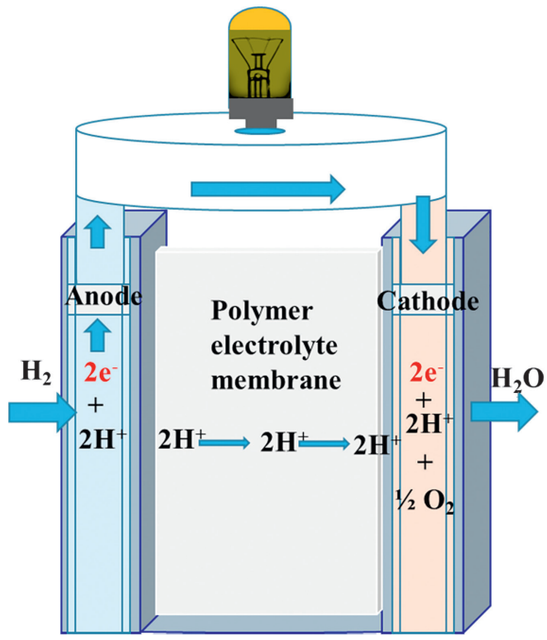


Fig. 10.16 Pictorial representation of a polymer electrolyte fuel cell and its electrochemical reactions.

owing to their efficient water uptake and proton transport properties. The important electro-chemical reactions that occur at the cathode and anode are shown in Fig. 10.16.

A good polymer electrolyte membrane in the fuel cell should meet the following requirements; low cost, efficient proton conductivity (over 100 and below 0°C), good water uptake above 100°C, and durability for 10 years. Nowadays, many polymers are tried as polymer electrolyte membrane in fuel cells, which include poly(trifluorostyrene sulfonic acid), poly(styrene), poly(oxy-1,4-phenyleneoxy-1,4-phenylenecarbonyl-1,4-pheneylene), poly(1,4-phenylene), poly(oxy-1,4-phenylene), poly(phenylene sulfide), and so forth [126]. Polymer/silica NCs are also explored for fuel cell applications, as the presence of silica in the polymer increases the water uptake capacity at high temperature (80°C) more than its virgin polymer. Thus, sulfonated silica to Nafion has improved the water uptake due to the presence of silica in the ionic culture of Nafion [127].

Also, the addition of hydrophilic phosphosilicate to Nafion@silica NC was found to improve the water uptake capacity of the membrane; however, the higher content of the nanofiller reduces the water uptake capacity of the PNCs [128]. The membrane of the Nafion-silica-ZrO_2 composite showed high proton conductivity compared to the virgin

Nafion and Nafion-ZrO_2 membranes at 120°C because of the better water-retention ability of silica and the good proton conductivity of ZrO_2 [129]. Recently, Alam et al. reported that the NC containing a 5% metal-organic framework/$SiSO_3H$ showed improved proton conductivity (17 mS cm^{-1} at 70°C) and a power density of 40.80 mW cm^{-2} at a peak current density of 100.30 mA cm^{-1}. Modification of the polymer with CNT (SWT/MWT) has been reported to be an ideal strategy to improve the fuel cell properties of polymer electrolyte membranes [130]. Accordingly, sulfonated graphene nanoribbons were used to prepare NCs with sulfonated MWCNTs via the hydrothermal route. The said PNC showed a current density of 840 mA cm^{-2} at 0.6 V [131]. Similarly, Quin et al. reported the successful development of a hierarchically porous organic metal framework using titanium-metal with nitrogen-doped graphene NC [132]. Uadah et al. reported the free radical polymerization of butylvinylimidazolium in the presence of modified GO to develop NC membranes with a high proton conductivity of 78.5 and 26.5 mS cm^{-1} at 100 and 25°C, respectively [133]. The improved properties of the polymer with different filler NC membranes depend highly on the extent of filler dispersions in the polymer host and the corresponding surface modifications.

10.3.7 Conclusions and future directions

In summary, the PNC-based electro-active materials show huge potential for supercapacitors, solar cells, Li-ion batteries, Li-S batteries, Li-air batteries, and fuel cell applications. Different types of PNC-based electro-active materials such as polymers mixed with silica, CNTs, graphene, BN, and metal oxides can be fabricated by various techniques, including solid-state reactions, mechanical mixing, ball milling, sol-gel, in situ polymerization, and wet-chemical synthesis. Also, significant improvement in the specific surface area, electrical and ionic conductivities, specific capacitance, cyclic stability, energy efficiency, and power density can be achieved using various PNCs and different preparation techniques. The reinforcement of polymeric structures with nano-sized fillers has shown considerable improvement for energy applications of composites, even with very low content of introduced fillers. Nevertheless, the degree of reinforcement depends on the type of filler, the nature of the functional groups, the quantitative ratio of the filler, the amount of filler, the type of polymer, and the method of processing. Also, an ideal polymer-filler combination must offer uniform filler dispersion in addition to strong interfacial interactions. However, a high nanofiller content could lessen the composite properties, owing to the poor dispersion of nanofillers in the host polymer. Also, the orientation of the nano-sized fillers in the polymer host is critical in deciding their overall optical and electrical

properties. Further, covalently functionalized CNTs could deliver superior polymer reinforcement, owing to their better stress transfer behaviors. PNCs demonstrate unique electronic characteristics, owing to their high specific surface area, low mass density, good compatibility, excellent conductivity, and elegant flexibility. Accordingly, different types of PNCs have been broadly designed, developed, and studied for practical applications in supercapacitors, solar cells, and lithium batteries.

PNCs offer potential gains in supercapacitor performance as well as the energy efficiency of solar cells, fuel cells, and batteries. Yet, the superiority and hence the suitability of PNCs depend on various fillers, polymers, and interface-related factors. Thus, more research needs to be done in the future to realize the ideal PNC combinations for energy-related applications.

Acknowledgments

The authors acknowledge support from the X-mind Corps program (2017H1D8A2030449) through the National Research Foundation (NRF), funded by the Ministry of Science and ICT of the Republic of Korea.

References

[1] Y. Liu, S. Kumar, Polymer/carbon nanotube nano composite fibers–a review, ACS Appl. Mater. Interfaces 6 (2014) 6069–6087.
[2] T. Sridhar, A.U. Kini, A. Hiremath, A review on nanoparticle filled polymer nanocomposites, Int. J. Eng. Technol. 7 (2018) 169–173.
[3] F. Leroux, J.-P. Besse, Polymer interleaved layered double hydroxide: a new emerging class of nanocomposites, Chem. Mater. 13 (2001) 3507–3515.
[4] T. Kuila, S.K. Srivastava, A.K. Bhowmick, A.K. Saxena, Thermoplastic polyolefin based polymer – blend-layered double hydroxide nanocomposites, Compos. Sci. Technol. 68 (2008) 3234–3239.
[5] J.L. Vickery, A.J. Patil, S. Mann, Fabrication of graphene–polymer nanocomposites with higher-order three-dimensional architectures, Adv. Mater. 21 (2009) 2180–2184.
[6] S. Shivanna, K.S. Nithin, S.K. Nagaraj, J.R.B. Mutturaj, S. Basavaraj, Patina-green coloured light emitting polycarbonate films: a synergistic extraction of improved UV endurance and considerate spectral down-conversion, J. Lumin. 210 (2019) 276–284.
[7] S. Prashanth, K.M. Subbaya, K.S. Nithin, S. Sachhidananda, Fiber reinforced composites - a review, J. Mater. Sci. Eng. 6 (2017) 1–6.
[8] P. Hajji, L. David, J.F. Gerard, J.P. Pascault, G. Vigier, Synthesis, structure, and morphology of polymer-silica hybrid nanocomposites based on hydroxyethyl methacrylate, J. Polym. Sci. Part B Polym. Phys. 37 (1999) 3172–3187.
[9] S.H. Liao, C.Y. Yen, C.C. Weng, Y.F. Lin, C.C.M. Ma, C.H. Yang, M.C. Tsai, M.Y. Yen, M.C. Hsiao, S.J. Lee, X.F. Xie, Y.H. Hsiao, Preparation and properties of carbon nanotube/polypropylene nanocomposite bipolar plates for polymer electrolyte membrane fuel cells, J. Power Sources 185 (2008) 1225–1232.
[10] Z. Spitalsky, D. Tasis, K. Papagelis, C. Galiotis, Carbon nanotube–polymer composites: chemistry, processing, mechanical and electrical properties, Prog. Polym. Sci. 35 (2010) 357–401.

[11] B. Sun, Formulation of 2D graphene deformation based on chiral-tube base vectors, J. Nanomater. 3 (2010).
[12] J. Zhu, D. Yang, Z. Yin, Q. Yan, H. Zhang, Graphene and graphene-based materials for energy storage applications, Small 10 (2014) 3480–3498.
[13] S. Stankovich, D.A. Dikin, G.H.B. Dommett, K.M. Kohlhaas, E.J. Zimney, E.A. Stach, R.D. Piner, S.T. Nguyen, R.S. Ruoff, Graphene-based composite materials, Nature 442 (2006) 282.
[14] B. Ravi, B. Rajender, S. Palaniappan, Improving the electrochemical performance by sulfonation of polyaniline-graphene-silica composite for high performance supercapacitor, Int. J. Polym. Mater. Polym. Biomater. 65 (2016) 835–840.
[15] L. Weng, T. Wang, L. Liu, A study on the structure and properties of poly(vinylidene fluoride)/graphite micro-sheet composite films, J. Compos. Mater. 51 (2017) 3769–3778.
[16] L. Pauling, The structure and properties of graphite and boron nitride, Proc. Natl. Acad. Sci. U. S. A. 56 (1966) 1646–1652.
[17] O. Hod, Graphite and hexagonal boron-nitride have the same interlayer distance. Why? J. Chem. Theory Comput. 8 (2012) 1360–1369.
[18] H. Zou, S. Wu, J. Shen, Polymer/silica nanocomposites: preparation, characterization, properties, Chem. Rev. 108 (2008) 3893–3957.
[19] J.M. Gonzalez-Dominguez, A. Anson-Casaos, A.M. Diez-Pascual, B. Ashrafi, M. Naffakh, D. Backman, H. Stadler, A. Johnston, M. Gomez, M.T. Martinez, Solvent-free preparation of high-toughness epoxy–SWNT composite materials, ACS Appl. Mater. Interfaces 3 (2011) 1441–1450.
[20] N. Karousis, N. Tagmatarchis, D. Tasis, Current progress on the chemical modification of carbon nanotubes, Chem. Rev. 110 (2010) 5366–5397.
[21] P.-C. Ma, N.A. Siddiqui, G. Marom, J.-K. Kim, Dispersion and functionalization of carbon nanotubes for polymer-based nanocomposites: a review, Compos. Part A Appl. Sci. Manuf. 41 (2010) 1345–1367.
[22] Y.B. Li, B.Q. Wei, J. Liang, Q. Yu, D.H. Wu, Transformation of carbon nanotubes to nanoparticles by ball milling process, Carbon N. Y. 37 (1999) 493–497.
[23] P.M. Ajayan, J.M. Tour, Nanotube composites, Nature 447 (2007) 1066.
[24] T. Hanemann, D.V. Szabo, Polymer-nanoparticle composites: from synthesis to modern applications, Materials 3 (2010) 3468–3517.
[25] W. Wang, L. Xu, F. Liu, X. Li, L. Xing, Synthesis of isocyanate microcapsules and micromechanical behavior improvement of microcapsule shells by oxygen plasma treated carbon nanotubes, J. Mater. Chem. A 1 (2013) 776–782.
[26] T. Wu, Y. Pan, H. Bao, L. Li, Preparation and properties of chitosan nanocomposite films reinforced by poly(3,4-ethylenedioxythiophene)-poly(styrenesulfonate) treated carbon nanotubes, Mater. Chem. Phys. 129 (2011) 932–938.
[27] T. Liu, I.Y. Phang, L. Shen, S.Y. Chow, W.D. Zhang, Morphology and mechanical properties of multiwalled carbon nanotubes reinforced nylon-6 composites, Macromolecules 37 (2004) 7214–7222.
[28] P.S. Rama Sreekanth, S. Kanagaraj, Assessment of bulk and surface properties of medical grade UHMWPE based nanocomposites using nanoindentation and microtensile testing, J. Mech. Behav. Biomed. Mater. 18 (2013) 140–151.
[29] M. Fang, K. Wang, H. Lu, Y. Yang, S. Nutt, Covalent polymer functionalization of graphene nanosheets and mechanical properties of composites, J. Mater. Chem. 19 (2009) 7098–7105.
[30] B. Das, K. Eswar Prasad, U. Ramamurty, C.N.R. Rao, Nano-indentation studies on polymer matrix composites reinforced by few-layer graphene, Nanotechnology 20 (2009) 125705.
[31] D.R. Paul, L.M. Robeson, Polymer nanotechnology: nanocomposites, Polymer (Guildf) 49 (2008) 3187–3204.
[32] H. Kim, Y. Miura, C.W. Macosko, Graphene/polyurethane nanocomposites for improved gas barrier and electrical conductivity, Chem. Mater. 22 (2010) 3441–3450.

[33] R. Naresh Muthu, S. Rajashabala, R. Kannan, Synthesis and characterization of polymer (sulfonated poly-ether-ether-ketone) based nanocomposite (h-boron nitride) membrane for hydrogen storage, Int. J. Hydrog. Energy 40 (2015) 1836–1845.
[34] R. Jan, P. May, A.P. Bell, A. Habib, U. Khan, J.N. Coleman, Enhancing the mechanical properties of BN nanosheet–polymer composites by uniaxial drawing, Nanoscale 6 (2014) 4889–4895.
[35] C. Peng, S. Zhang, D. Jewell, G.Z. Chen, Carbon nanotube and conducting polymer composites for supercapacitors, Prog. Nat. Sci. 18 (2008) 777–788.
[36] S. Bhadra, D. Khastgir, N.K. Singha, J.H. Lee, Progress in preparation, processing and applications of polyaniline, Prog. Polym. Sci. 34 (2009) 783–810.
[37] E. Frackowiak, V. Khomenko, K. Jurewicz, K. Lota, F. Béguin, Supercapacitors based on conducting polymers/nanotubes composites, J. Power Sources 153 (2006) 413–418.
[38] O.K. Park, T. Jeevananda, N.H. Kim, S. Kim, J.H. Lee, Effects of surface modification on the dispersion and electrical conductivity of carbon nanotube/polyaniline composites, Scr. Mater. 60 (2009) 551–554.
[39] H. Ago, K. Petritsch, M.S.P. Shaffer, A.H. Windle, R.H. Friend, Composites of carbon nanotubes and conjugated polymers for photovoltaic devices, Adv. Mater. 11 (1999) 1281–1285.
[40] Z.M. Dang, L. Wang, Y. Yin, Q. Zhang, Q.Q. Lei, Giant dielectric permittivities in functionalized carbon-nanotube/electroactive-polymer nanocomposites, Adv. Mater. 19 (2007) 852–857.
[41] B. Zhao, M. Hamidinejad, C. Zhao, R. Li, S. Wang, Y. Kazemi, C.B. Park, A versatile foaming platform to fabricate polymer/carbon composites with high dielectric permittivity and ultra-low dielectric loss, J. Mater. Chem. A 7 (2018) 133–140.
[42] D.D. Potphode, L. Sinha, P.M. Shirage, Redox additive enhanced capacitance: Multi-walled carbon nanotubes/polyaniline nanocomposite based symmetric supercapacitors for rapid charge storage, Appl. Surf. Sci. 469 (2019) 162–172.
[43] N. Mukhin, V. Afanasjev, I. Sokolova, D. Chigirev, R. Kastro, L. Rudaja, G. Lebedeva, A. Oseev, A. Tumarkin, Heat-resistant ferroelectric-polymer nanocomposite with high dielectric constant, Materials 11 (2018) 1439.
[44] S. Jiang, L. Jin, H. Hou, L. Zhang, Polymer-based nanocomposites with high dielectric permittivity, in: Polymer-Based Multifunctional Nanocomposites and Their Applications, Elsevier, 2019, pp. 201–243.
[45] H.M. Kim, K. Kim, S.J. Lee, J. Joo, H.S. Yoon, S.J. Cho, S.C. Lyu, C.J. Lee, Charge transport properties of composites of multiwalled carbon nanotube with metal catalyst and polymer: application to electromagnetic interference shielding, Curr. Appl. Phys. 4 (2004) 577–580.
[46] H. Chu, L. Wei, R. Cui, J. Wang, Y. Li, Carbon nanotubes combined with inorganic nanomaterials: preparations and applications, Coord. Chem. Rev. 254 (2010) 1117–1134.
[47] N. Liu, F. Luo, H. Wu, Y. Liu, C. Zhang, J. Chen, One-step ionic-liquid-assisted electrochemical synthesis of ionic-liquid-functionalized graphene sheets directly from graphite, Adv. Funct. Mater. 18 (2008) 1518–1525.
[48] J. Wu, Q. Zhang, A. Zhou, Z. Huang, H. Bai, L. Li, Phase-separated polyaniline/graphene composite electrodes for high-rate electrochemical supercapacitors, Adv. Mater. 28 (2016) 10211–10216.
[49] H. Fan, N. Zhao, H. Wang, J. Xu, F. Pan, 3D conductive network-based free-standing PANI–RGO–MWNTs hybrid film for high-performance flexible supercapacitor, J. Mater. Chem. A 2 (2014) 12340–12347.
[50] P. Sekar, B. Anothumakkool, S. Kurungot, 3D polyaniline porous layer anchored pillared graphene sheets: enhanced interface joined with high conductivity for better charge storage applications, ACS Appl. Mater. Interfaces 7 (2015) 7661–7669.

[51] Y. Xu, Y. Tao, X. Zheng, H. Ma, J. Luo, F. Kang, Q.-H. Yang, A metal-free supercapacitor electrode material with a record high volumetric capacitance over 800 F cm(-3), Adv. Mater. 27 (2015) 8082–8087.
[52] T. Kuilla, S. Bhadra, D. Yao, N.H. Kim, S. Bose, J.H. Lee, Recent advances in graphene based polymer composites, Prog. Polym. Sci. 35 (2010) 1350–1375.
[53] Y. Meng, K. Wang, Y. Zhang, Z. Wei, Hierarchical porous graphene/polyaniline composite film with superior rate performance for flexible supercapacitors, Adv. Mater. 25 (2013) 6985–6990.
[54] L. Liu, Z. Niu, L. Zhang, W. Zhou, X. Chen, S. Xie, Nanostructured graphene composite papers for highly flexible and foldable supercapacitors, Adv. Mater. 26 (2014) 4855–4862.
[55] P. Bandyopadhyay, T. Kuila, J. Balamurugan, T.T. Nguyen, N.H. Kim, J.H. Lee, Facile synthesis of novel sulfonated polyaniline functionalized graphene using m-aminobenzene sulfonic acid for asymmetric supercapacitor application, Chem. Eng. J. 308 (2017) 1174–1184.
[56] J. Cao, Y. Wang, J. Chen, X. Li, F.C. Walsh, J.-H. Ouyang, D. Jia, Y. Zhou, Three-dimensional graphene oxide/polypyrrole composite electrodes fabricated by one-step electrodeposition for high performance supercapacitors, J. Mater. Chem. A 3 (2015) 14445–14457.
[57] X. Yang, A. Liu, Y. Zhao, H. Lu, Y. Zhang, W. Wei, Y. Li, S. Liu, Three-dimensional macroporous polypyrrole-derived graphene electrode prepared by the hydrogen bubble dynamic template for supercapacitors and metal-free catalysts, ACS Appl. Mater. Interfaces 7 (2015) 23731–23740.
[58] P. Bandyopadhyay, T.T. Nguyen, N.H. Kim, J.H. Lee, Facile synthesis of 4,4′-diaminostilbene-2,2′-disulfonic-acid-grafted reduced graphene oxide and its application as a high-performance asymmetric supercapacitor, Chem. Eng. J. 333 (2018) 170–184.
[59] X. Zhang, A. Ciesielski, F. Richard, P. Chen, E.A. Prasetyanto, L. De Cola, P. Samori, Modular graphene-based 3D covalent networks: functional architectures for energy applications, Small 12 (2016) 1044–1052.
[60] N.Q. Tran, B.K. Kang, S.N. Tiruneh, D.H. Yoon, Design of advanced MnO/N-Gr 3D walls through polymer cross-linking for high-performance supercapacitor, Chemistry 22 (2016) 1652–1657.
[61] L. Mao, Y. Li, C. Chi, H.S. On Chan, J. Wu, Conjugated polyfluorene imidazolium ionic liquids intercalated reduced graphene oxide for high performance supercapacitor electrodes, Nano Energy 6 (2014) 119–128.
[62] J.S. Sanchez, A. Pendashteh, J. Palma, M. Anderson, R. Marcilla, Porous NiCoMn ternary metal oxide/graphene nanocomposites for high performance hybrid energy storage devices, Electrochim. Acta 279 (2018) 44–56.
[63] D.P. Dubal, D. Rueda-Garcia, C. Marchante, R. Benages, P. Gomez-Romero, Hybrid graphene-polyoxometalates nanofluids as liquid electrodes for dual energy storage in novel flow cells, Chem. Rec. 18 (2018) 1076–1084.
[64] S. Choudhary, Characterization of amorphous silica nanofiller effect on the structural, morphological, optical, thermal, dielectric and electrical properties of PVA-PVP blend based polymer nanocomposites for their flexible nanodielectric applications, J. Mater. Sci. Mater. Electron. 29 (2018) 10517–10534.
[65] S. Sun, C. Li, L. Zhang, H.L. Du, J.S. Burnell-Gray, Effects of surface modification of fumed silica on interfacial structures and mechanical properties of poly(vinyl chloride) composites, Eur. Polym. J. 42 (2006) 1643–1652.
[66] J. Hu, K. Xie, X. Liu, S. Guo, C. Shen, X. Liu, X. Li, J. Wang, B. Wei, Dramatically enhanced ion conductivity of gel polymer electrolyte for supercapacitor via h-BN nanosheets doping, Electrochim. Acta 227 (2017) 455–461.
[67] Z. Yang, L. Tang, J. Ye, D. Shi, S. Liu, M. Chen, Hierarchical nanostructured α-Fe2O3/polyaniline anodes for high performance supercapacitors, Electrochim. Acta 269 (2018) 21–29.

[68] Z.A. Hu, Y.L. Xie, Y.X. Wang, L.P. Mo, Y.Y. Yang, Z.Y. Zhang, Polyaniline/SnO2 nanocomposite for supercapacitor applications, Mater. Chem. Phys. 114 (2009) 990–995.
[69] D. Ghosh, S. Giri, A. Mandal, C.K. Das, Supercapacitor based on H+ and Ni2+ co-doped polyaniline–MWCNTs nanocomposite: synthesis and electrochemical characterization, RSC Adv. 3 (2013) 11676–11685.
[70] H. Su, T. Wang, S. Zhang, J. Song, C. Mao, H. Niu, B. Jin, J. Wu, Y. Tian, Facile synthesis of polyaniline/TiO2/graphene oxide composite for high performance supercapacitors, Solid State Sci. 14 (2012) 677–681.
[71] M. Padmini, P. Elumalai, P. Thomas, Symmetric supercapacitor performances of CaCu3Ti4O12 decorated polyaniline nanocomposite, Electrochim. Acta 292 (2018) 558–567.
[72] A.M. Bagher, Introduction to organic solar cells, Sustain. Energy 2 (2014) 85–90.
[73] Q. Adler, Carbon nanotube-polymer composites for solar cell applications, SURF. (2011) 22373.
[74] D. Mombru, M. Romero, R. Faccio, A.W. Mombru, Raman microscopy insights on the out-of-plane electrical transport of carbon nanotube-doped PEDOT:PSS electrodes for solar cell applications, J. Phys. Chem. B 122 (2018) 2694–2701.
[75] A. Kumar, V. Kumar, K. Awasthi, Polyaniline–carbon nanotube composites: preparation methods, properties, and applications, Polym.-Plast. Technol. Eng. 57 (2018) 70–97.
[76] N. Ahn, I. Jeon, J. Yoon, E.I. Kauppinen, Y. Matsuo, S. Maruyama, M. Choi, Carbon-sandwiched perovskite solar cell, J. Mater. Chem. A 6 (2018) 1382–1389.
[77] N. Zheng, Z. Wang, K. Zhang, Y. Li, F. Huang, Y. Cao, High-performance inverted polymer solar cells without electron extract layer via one-step coating of cathode buffer and active layer, J. Mater. Chem. A 7 (2019) 1429–1434.
[78] X. Wang, L. Zhi, K. Müllen, Transparent, conductive graphene electrodes for dye-sensitized solar cells, Nano Lett. 8 (2008) 323–327.
[79] Z. Yin, S. Sun, T. Salim, S. Wu, X. Huang, Q. He, Y.M. Lam, H. Zhang, Organic photovoltaic devices using highly flexible reduced graphene oxide films as transparent electrodes, ACS Nano 4 (2010) 5263–5268.
[80] X. Liu, H. Kim, L.J. Guo, Optimization of thermally reduced graphene oxide for an efficient hole transport layer in polymer solar cells, Org. Electron. 14 (2013) 591–598.
[81] T. Sakorikar, M.K. Kavitha, S.W. Tong, P. Vayalamkuzhi, K.P. Loh, M. Jaiswal, Graphene: polymer composites as moisture barrier and charge transport layer toward solar cell applications, AIP Conf. Proc. 1953 (2018), 100029.
[82] K. Prabakaran, P.J. Jandas, S. Mohanty, S.K. Nayak, Synthesis, characterization of reduced graphene oxide nanosheets and its reinforcement effect on polymer electrolyte for dye sensitized solar cell applications, Sol. Energy 170 (2018) 442–453.
[83] S. Kumar, J. Kumar, S. Narayan Sharma, S. Srivastava, rGO integrated MEHPPV and P3HT polymer blends for bulk hetero junction solar cells: a comparative insight, Optik (Stuttg) 178 (2019) 411–421.
[84] P. Ma, J. Tan, H. Cheng, Y. Fang, Y. Wang, Y. Dai, S. Fang, X. Zhou, Y. Lin, Polyaniline-grafted silica nanocomposites-based gel electrolytes for quasi-solid-state dye-sensitized solar cells, Appl. Surf. Sci. 427 (2018) 458–464.
[85] M. Babazadeh, F. Zalloi, A. Olad, Fabrication of conductive polyaniline nanocomposites based on silica nanoparticles via in-situ chemical oxidative polymerization technique, Synth. React. Inorg. Met. Nano-Metal Chem. 45 (2015) 86–91.
[86] X. Li, H. Zhu, K. Wang, A. Cao, J. Wei, C. Li, Y. Jia, Z. Li, X. Li, D. Wu, Graphene-on-silicon schottky junction solar cells, Adv. Mater. 22 (2010) 2743–2748.
[87] X. Long, C. Dou, J. Liu, L. Wang, A homopolymer based on double B⟵N bridged bipyridine as electron acceptor for all-polymer solar cells, Chin. Chem. Lett. 29 (2018) 1343–1346.

[88] E. Maier, T. Rath, W. Haas, O. Werzer, R. Saf, F. Hofer, D. Meissner, O. Volobujeva, S. Bereznev, E. Mellikov, H. Amenitsch, R. Resel, G. Trimmel, CuInS2–Poly(3-(ethyl-4-butanoate)thiophene) nanocomposite solar cells: preparation by an in situ formation route, performance and stability issues, Sol. Energy Mater. Sol. Cells 95 (2011) 1354–1361.
[89] T. Rath, M. Edler, W. Haas, A. Fischereder, S. Moscher, A. Schenk, R. Trattnig, M. Sezen, G. Mauthner, A. Pein, D. Meischler, K. Bartl, R. Saf, N. Bansal, S.A. Haque, F. Hofer, E.J.W. List, G. Trimmel, A direct route towards polymer/copper indium sulfide nanocomposite solar cells, Adv. Energy Mater. 1 (2011) 1046–1050.
[90] S. Dayal, N. Kopidakis, D.C. Olson, D.S. Ginley, G. Rumbles, Photovoltaic devices with a low band gap polymer and CdSe nanostructures exceeding 3% efficiency, Nano Lett. 10 (2010) 239–242.
[91] N. Wu, Q. Luo, Z. Bao, J. Lin, Y.-Q. Li, C.-Q. Ma, Zinc oxide: conjugated polymer nanocomposite as cathode buffer layer for solution processed inverted organic solar cells, Sol. Energy Mater. Sol. Cells 141 (2015) 248–259.
[92] B.J. Landi, M.J. Ganter, C.D. Cress, R.A. DiLeo, R.P. Raffaelle, Carbon nanotubes for lithium ion batteries, Energy Environ. Sci. 2 (2009) 638–654.
[93] J. Chen, Y. Liu, A.I. Minett, C. Lynam, J. Wang, G.G. Wallace, Flexible, aligned carbon nanotube/conducting polymer electrodes for a lithium-ion battery, Chem. Mater. 19 (2007) 3595–3597.
[94] W.J. Song, J. Park, D.H. Kim, S. Bae, M.J. Kwak, M. Shin, S. Kim, S. Choi, J.H. Jang, T.J. Shin, S.Y. Kim, K. Seo, S. Park, Jabuticaba-inspired hybrid carbon filler/polymer electrode for use in highly stretchable aqueous Li-ion batteries, Adv. Energy Mater. 8 (2018), 1702478.
[95] Y. Zhang, Y. Huang, G. Yang, F. Bu, K. Li, I. Shakir, Y. Xu, Dispersion–assembly approach to synthesize three-dimensional graphene/polymer composite aerogel as a powerful organic cathode for rechargeable Li and Na batteries, ACS Appl. Mater. Interfaces 9 (2017) 15549–15556.
[96] Y. Zhang, Q. Ma, S. Wang, X. Liu, L. Li, Poly(vinyl alcohol)-assisted fabrication of hollow carbon spheres/reduced graphene oxide nanocomposites for high-performance lithium-ion battery anodes, ACS Nano 12 (2018) 4824–4834.
[97] H.Y. Lin, C.H. Li, D.Y. Wang, C.C. Chen, Chemical doping of a core-shell silicon nanoparticles@polyaniline nanocomposite for the performance enhancement of a lithium ion battery anode, Nanoscale 8 (2016) 1280–1287.
[98] Y.W. Chen-Yang, Y.L. Wang, Y.T. Chen, Y.K. Li, H.C. Chen, H.Y. Chiu, Influence of silica aerogel on the properties of polyethylene oxide-based nanocomposite polymer electrolytes for lithium battery, J. Power Sources 182 (2008) 340–348.
[99] M. Idrees, S. Batool, J. Kong, Q. Zhuang, H. Liu, Q. Shao, N. Lu, Y. Feng, E.K. Wujcik, Q. Gao, T. Ding, R. Wei, Z. Guo, Polyborosilazane derived ceramics - nitrogen sulfur dual doped graphene nanocomposite anode for enhanced lithium ion batteries, Electrochim. Acta 296 (2019) 925–937.
[100] M. Zhao, X. Zuo, X. Ma, X. Xiao, J. Liu, J. Nan, Self-supported PVdF/P(VC-VAc) blended polymer electrolytes for LiNi0.5Mn1.5O4/Li batteries, J. Membr. Sci. 532 (2017) 30–37.
[101] Z. Song, T. Xu, M.L. Gordin, Y.-B. Jiang, I.-T. Bae, Q. Xiao, H. Zhan, J. Liu, D. Wang, Polymer–graphene nanocomposites as ultrafast-charge and discharge cathodes for rechargeable lithium batteries, Nano Lett. 12 (2012) 2205–2211.
[102] X. Ji, K.T. Lee, L.F. Nazar, A highly ordered nanostructured carbon–sulphur cathode for lithium–sulphur batteries, Nat. Mater. 8 (2009) 500.
[103] J. Zhu, P. Zhu, C. Yan, X. Dong, X. Zhang, Recent progress in polymer materials for advanced lithium-sulfur batteries, Prog. Polym. Sci. 90 (2018) 118–163.
[104] R. Bouchet, A stable lithium metal interface, Nat. Nanotechnol. 9 (2014) 572.

[105] N.S. Choi, Z. Chen, S.A. Freunberger, X. Ji, Y.K. Sun, K. Amine, G. Yushin, L.F. Nazar, J. Cho, P.G. Bruce, Challenges facing lithium batteries and electrical double-layer capacitors, Angew. Chem. Int. Ed. 51 (2012) 9994–10024.
[106] Z. Lin, Z. Liu, W. Fu, N.J. Dudney, C. Liang, Phosphorous pentasulfide as a novel additive for high-performance lithium-sulfur batteries, Adv. Funct. Mater. 23 (2013) 1064–1069.
[107] X. Zhang, H. Xie, C.S. Kim, K. Zaghib, A. Mauger, C.M. Julien, Advances in lithium—sulfur batteries, Mater. Sci. Eng. R. Rep. 121 (2017) 1–29.
[108] J. Wang, J. Chen, K. Konstantinov, L. Zhao, S.H. Ng, G.X. Wang, Z.P. Guo, H.K. Liu, Sulphur-polypyrrole composite positive electrode materials for rechargeable lithium batteries, Electrochim. Acta 51 (2006) 4634–4638.
[109] J. Wang, L. Lu, D. Shi, R. Tandiono, Z. Wang, K. Konstantinov, H. Liu, A conductive polypyrrole-coated, sulfur–carbon nanotube composite for use in lithium–sulfur batteries, ChemPlusChem 78 (2013) 318–324.
[110] Y. Zhang, Y. Zhao, T.N.L. Doan, A. Konarov, D. Gosselink, H.G. Soboleski, P. Chen, A novel sulfur/polypyrrole/multi-walled carbon nanotube nanocomposite cathode with core–shell tubular structure for lithium rechargeable batteries, Solid State Ionics 238 (2013) 30–35.
[111] W. Wang, G. Li, Q. Wang, G. Li, S. Ye, X. Gao, Sulfur-polypyrrole/graphene multi-composites as cathode for lithium-sulfur battery, J. Electrochem. Soc. 160 (2013) A805–A810.
[112] J. Zhang, Y. Shi, Y. Ding, W. Zhang, G. Yu, In-situ reactive synthesis of polypyrrole-MnO2 coaxial nanotubes as sulfur hosts for high-performance lithium–sulfur battery, Nano Lett. 16 (2016) 7276–7281.
[113] G.-C. Li, G.-R. Li, S.-H. Ye, X.-P. Gao, A polyaniline-coated sulfur/carbon composite with an enhanced high-rate capability as a cathode material for lithium/sulfur batteries, Adv. Energy Mater. 2 (2012) 1238–1245.
[114] Y. Qiu, W. Li, G. Li, Y. Hou, L. Zhou, H. Li, M. Liu, F. Ye, X. Yang, Y. Zhang, Polyaniline-modified cetyltrimethylammonium bromide-graphene oxide-sulfur nanocomposites with enhanced performance for lithium-sulfur batteries, Nano Res. 7 (2014) 1355–1363.
[115] B. Chen, D.Y.C. Leung, J. Xuan, H. Wang, A mixed-pH dual-electrolyte microfluidic aluminum–air cell with high performance, Appl. Energy 185 (2017) 1303–1308.
[116] P.G. Bruce, S.A. Freunberger, L.J. Hardwick, J.-M. Tarascon, Li–O2 and Li–S batteries with high energy storage, Nat. Mater. 11 (2011) 19.
[117] G. Girishkumar, B. McCloskey, A.C. Luntz, S. Swanson, W. Wilcke, Lithium—air battery: promise and challenges, J. Phys. Chem. Lett. 1 (2010) 2193–2203.
[118] K.M. Abraham, Z. Jiang, A polymer electrolyte-based rechargeable lithium/oxygen battery, J. Electrochem. Soc. 143 (1996) 1–5.
[119] L. Porcarelli, A.S. Shaplov, F. Bella, J.R. Nair, D. Mecerreyes, C. Gerbaldi, Single-ion conducting polymer electrolytes for lithium metal polymer batteries that operate at ambient temperature, ACS Energy Lett. 1 (2016) 678–682.
[120] Z. Guo, C. Li, J. Liu, Y. Wang, Y. Xia, A long-life lithium–air battery in ambient air with a polymer electrolyte containing a redox mediator, Angew. Chem. Int. Ed. 56 (2017) 7505–7509.
[121] T.H. Yoon, Y.J. Park, Carbon nanotube/Co3O4 composite for air electrode of lithium-air battery, Nanoscale Res. Lett. 7 (2012) 28.
[122] D. Zhang, R. Li, T. Huang, A. Yu, Novel composite polymer electrolyte for lithium air batteries, J. Power Sources 195 (2010) 1202–1206.
[123] B. Li, Y. Liu, X. Zhang, P. He, H. Zhou, Hybrid polymer electrolyte for Li–O_2 batteries, Green Energy Environ. 4 (2019) 3–19.
[124] W.R. Grove, XLII. On a small voltaic battery of great energy; some observations on voltaic combinations and forms of arrangement; and on the inactivity of a copper positive electrode in nitro-sulphuric acid, Lond. Edin. Dubl. Philos. Mag. J. Sci. 15 (1839) 287–293.

[125] S.M.J. Zaidi, M.A. Rauf, in: S.M.J. Zaidi, T. Matsuura (Eds.), Fuel Cell Fundamentals BT - Polymer Membranes for Fuel Cells, Springer US, Boston, MA, 2009, pp. 1–6.
[126] M. Rikukawa, K. Sanui, Proton-conducting polymer electrolyte membranes based on hydrocarbon polymers, Prog. Polym. Sci. 25 (2000) 1463–1502.
[127] Y. Jin, S. Qiao, L. Zhang, Z.P. Xu, S. Smart, J.C.D. da Costa, G.Q. Lu, Novel nafion composite membranes with mesoporous silica nanospheres as inorganic fillers, J. Power Sources 185 (2008) 664–669.
[128] A.K. Mishra, S. Bose, T. Kuila, N.H. Kim, J.H. Lee, Silicate-based polymer-nanocomposite membranes for polymer electrolyte membrane fuel cells, Prog. Polym. Sci. 37 (2012) 842–869.
[129] K.T. Park, U.H. Jung, D.W. Choi, K. Chun, H.M. Lee, S.H. Kim, ZrO2–SiO2/Nafion® composite membrane for polymer electrolyte membrane fuel cells operation at high temperature and low humidity, J. Power Sources 177 (2008) 247–253.
[130] M. Carmo, V.A. Paganin, J.M. Rosolen, E.R. Gonzalez, Alternative supports for the preparation of catalysts for low-temperature fuel cells: the use of carbon nanotubes, J. Power Sources 142 (2005) 169–176.
[131] A. Shukla, S.D. Bhat, V.K. Pillai, Simultaneous unzipping and sulfonation of multi-walled carbon nanotubes to sulfonated graphene nanoribbons for nanocomposite membranes in polymer electrolyte fuel cells, J. Membr. Sci. 520 (2016) 657–670.
[132] X. Qin, Y. Huang, K. Wang, T. Xu, Y. Wang, P. Liu, Y. Kang, Y. Zhang, Novel hierarchically porous Ti-MOFs/nitrogen-doped graphene nanocomposite served as high efficient oxygen reduction reaction catalyst for fuel cells application, Electrochim. Acta 297 (2019) 805–813.
[133] A. Ouadah, T. Luo, J. Wang, S. Gao, X. Wang, X. Zhang, Z. Fang, Z. Wu, J. Wang, C. Zhu, Imidazolium-grafted graphene oxide via free radical polymerization: an efficient and simple method for an interpenetrating polymer network as electrolyte membrane, Compos. Sci. Technol. 164 (2018) 204–213.

11

Influence of polymers on carbon-based composites in energy storage applications

Manu Patel U.M.
Scientist, Hollingsworth and Vose, Mysuru, India

11.1 Introduction

11.1.1 Lithium-sulfur battery

A lithium-sulfur (Li-S) battery is a new class of rechargeable battery that is currently under research. This type of battery can be used in electric automobiles such as cars as well as scooters and aviation. Sulfur is considered a potential cathode material because of its high theoretical capacity ($1672\,mA\,h\,g^{-1}$) and higher energy density ($2500\,Wh\,kg^{-1}$). The high capacity is associated with the conversion of elemental sulfur to lithium sulfide (Li_2S) by reversibly accommodating two electrons per sulfur atom. This is an order of magnitude higher when compared to current commercial Li-ion technology. In addition, Li-S batteries also present many other advantages: sulfur is a waste material of the petroleum industry, which makes it an inexpensive raw material, and Li-S can be operated under a wide range of temperatures and hence is considered safe [1–4]. Despite having many advantages, the Li-S system does have its shortcomings such as the insulating nature of sulfur and the shuttling of lithium polysulfide during battery cycling. Sulfur by nature is a very poor electrical conductor; this is one of the most import drawbacks that needs to be addressed if sulfur is to be used as a commercial cathode material in the Li-S battery. Researchers have addressed this issue by introducing a conductive carbon matrix in different forms to obtain the required electrical conductivity in the electrode. Although the introduction of carbon to the cathode electrodes addresses the conductivity of the sulfur cathode, it also reduces the overall particle energy density of the system. The other major issue of the Li-S system is the shuttling of lithium polysulfides. Most of the intermediates (lithium polysulfides) formed during battery cycling are soluble in electrolytes. After entering the electrolyte, the polysulfides

Polymer-Based Advanced Functional Composites for Optoelectronic and Energy Applications
https://doi.org/10.1016/B978-0-12-818484-4.00008-2
Copyright © 2021 Elsevier Inc. All rights reserved.

shuttle between the anode and cathode electrodes, resulting in active material loss in the cathode and undesired side reactions on the anode. The shuttling mechanism in the Li-S system results in rapid capacity fading and battery failure in a short duration [5–7]. A schematic representation of the shuttling mechanism is shown in Fig. 11.1. Apart from these issues, the cathode electrode undergoes volume change by up to 50% during battery cycling, resulting in the mechanical failure of the cathode electrode. The expansion of the cathode occurs at the end of discharge when Li_2S is formed from sulfur, and contraction at the end of the charge when sulfur is formed from Li_2S [5–7]. All these factors have acted as a bottleneck for the commercialization of the Li-S system.

To overcome these obstacles, recent research efforts have been focused on reducing the adverse effects associated with the shuttling of polysulfides by developing a new type of S cathode [8, 9]. The most common types of cathodes in use today include carbon nanotube (CNT)/S composites [10], graphene/S composites [11–15], and conductive polymer/S composites [16–19].

Going forward, conductive polymers are considered promising candidates to obtain improved electronic conductivity in the Li-S battery, as they encapsulate the surface of the carbon/S composite and provide a continuous electron transfer pathway. In addition, they also help in maintaining the structural integrity of the electrode by accommodating large volume changes during cycling. Also, the polymer-encapsulated layer serves as a physical barrier to prevent the diffusion of soluble long-chain lithium polysulfides from the cathode, thereby improving the cycle performance and reversible capacity of the Li-S battery. Several conductive polymers such as polydopamine (PDA),

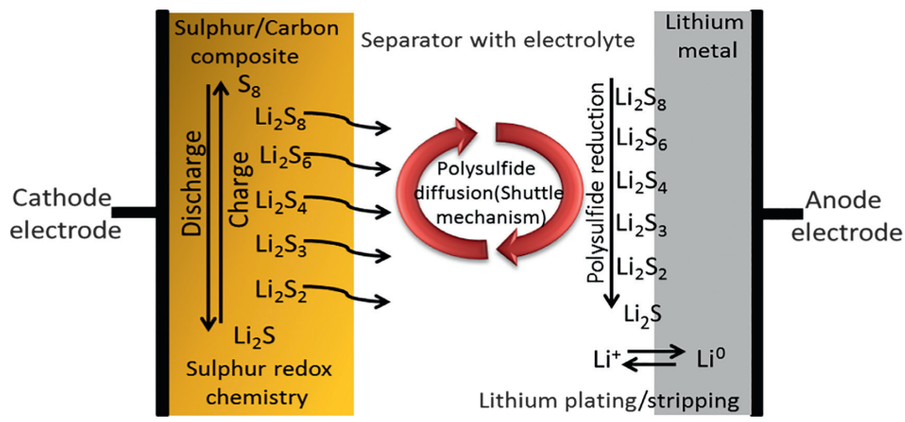


Fig. 11.1 Schematic representation of the workings of an Li-S battery and the lithium-polysulfide shuttling mechanism inside the Li-S battery (during battery cycling).

polypyrrole (PPy), polyaniline (PANI), polythiophene, poly(3,4-ethylene dioxythiophene) (PEDOT), and polyacrylonitrile have been used in S cathodes, and improved cell performance has been reported [20–25]. The high mechanical flexibility of PDA allows the S@PDA cathode to accommodate volumetric variation during the discharge/charge processes along with good lithium-ion conductivity [20]. An S/PPy composite cathode was reported to successfully reduce the solubility of polysulfides and minimize the loss of active material during cycling [21]. A strategy of wrapping fine S particles with a dual-shell hollow PANI resulted in improved cycle performance [22]. Both S/polythiophene and S/polyacrylonitrile composite cathodes were shown to eliminate polysulfide dissolution and the shuttle effect between the Li anode and S cathode [23, 24]. PEDOT is likely one of the most promising coating materials for S cathodes because of its high electronic conductivity, which ensures good long-term cycle and rate performances [25, 26]. In this chapter, we discuss a few such examples to show and understand how the presence of a conductive polymer in carbon/S composites influences the battery performance.

11.1.2 Li-ion battery

Lithium-ion (Li-ion) batteries are rechargeable batteries with high energy density that are commonly used in consumer electronics ranging from smartwatches to large applications such as electric vehicles [27]. Unlike the disposable lithium primary battery, a secondary Li-ion battery uses an intercalated lithium compound instead of metallic lithium as its electrode. Just as batteries in general come in all shapes, sizes, and chemistries, so do Li-ion batteries. Their various chemistries and structures offer different features, often with trade-offs between efficiency, cost, and safety [27–30].

The Li-ion battery is made of an anode electrode, a cathode electrode, and a separator. The separator acts as an electron flow inhibitor between the anode and cathode electrodes and holds the electrolyte. The Li-ion batteries can use several different materials as electrodes. The most common combination is that of lithium iron phosphate (cathode) and graphite (anode), which is most commonly found in portable electronic devices such as cell phones and laptops. Other cathode materials include lithium manganese oxide (used in hybrid electric and electric automobiles) and lithium cobalt oxide. Li-ion batteries typically use ether-based organic solvents (diethyl carbonate, dimethyl carbonate, ethylene carbonate, and so forth) and noncoordinating inorganic salts ($LiBF_4$, $LiPF_6$, $LiClO_4$, and so forth) in their electrolyte [28–30].

Further, to understand the importance of the binder in the Li-ion battery electrode, one needs to understand the working principle of

the Li-ion battery. During Li-ion battery cycling, the intercalation and deintercalation of Li ions occur. Intercalation is when Li ions move into an electrode (during battery discharge, the Li ion moves into the cathode from the anode) and deintercalation is where Li ions move out of the electrode (during battery discharge, the Li ion moves out of the anode) [27]. A reverse of the above process takes place when the battery is charged. During the charge and discharge cycles, electrons flow in the same direction of the Li ions, and the movement of the Li ions during the battery cycling leads to volume changes in the electrode.

Fig. 11.2 shows the working mechanism of the Li-ion battery. For the below process to occur efficiently, the electrode should have very good interparticle electronic contact along with good electrode mass contact to the current collector (on which the active material, carbon black, and binder are coated). The binder is the only component in the electrode that facilities the above process and hence, the absence of a good binder in the electrode will be detrimental for battery performance [31–34].

The battery electrode is composed of three important components: the active material, the carbon additive, and the polymer binder in the ratio of nearly 90:7:3, respectively [31–34]. (i) First, the active material, which in the electrode is responsible for the high potential and high gravimetric energy densities, is obtained from the battery. The active material is the largest component in the electrode, ranging from 90% to 95% of the total electrode composition; (ii) Second, carbon black is added to the electrode to enhance the electronic conductivity between the active material particles. The carbon in the electrode is very crucial for the optimum performance of the battery, and its ratio ranges from 3% to 5%; (iii) Finally, although the ratio of the polymer binder in the electrode is the least (2%–3%), the binder plays a very important role in keeping the electrode together. In the absence of a binder, the active material and the carbon particles will not be held together, nor will they stick to the current collector [31].

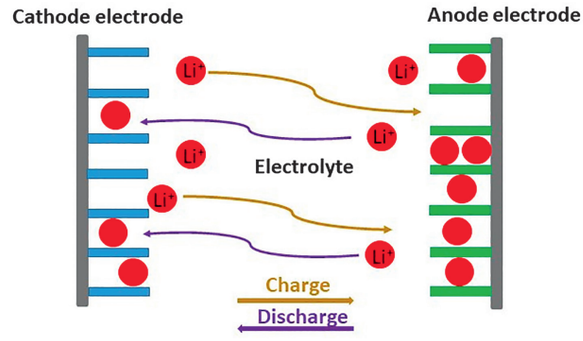


Fig. 11.2 Schematics of the working mechanism of a Li-ion battery during battery cycling.

11.2 Polymer-based binders for a Li-ion battery

The polymer should have certain properties so that it can be used as a binder in a Li-ion battery. The binder used in the electrode should not react with the active material and the electrolyte. It should be electrochemically stable and should provide mechanical strength to the electrode [35]. Above all, it should satisfy all the above properties when used in a very small quantity in the electrode. If too much of the conductive additives and polymer binder are added to the electrode, they degrade the total capacity of the cell. If too little is added, the electronic conductivity and the mechanical integrity of the electrode will be reduced. The absence of adequate contact between the electrode components (active material, carbon black, and binder) and contact between the electrode components and the current collector will have a detrimental effect on the battery performance [35].

Polymer binders are used in both cathode and anode electrodes, but the amount of carbon content in the cathode electrode is far less (3%–5%) in comparison to the amount of carbon content in the anode electrode (90%–95% in the form of graphite or graphene) [36, 37]. Further, mechanical interlocking between the electrode particles arises when a binder solution penetrates the pores of a particular surface (or surfaces) and is subsequently hardened. During the drying process, the binder solution solidifies in situ and the embedded film remains in the pores of the material, leading to adhesion. The strength of this adhesion is influenced by the roughness of a particular surface, which allows for a higher area for bonding [38] as well as the nature of the binder itself. Various binding mechanisms have been proposed that occur at the interface between the binder and the active material surface [39]. The most commonly accepted mechanisms are those that include intermolecular forces, electrostatic forces, and covalent bonding, which occur at the binder/surface interface. In the case of intermolecular forces, the adhesive strength between two materials can be improved if the ever-present van der Waals forces are supplemented by hydrogen bonding between the binder and substrate [40]. Similarly, further improvements in adhesive strength can be achieved if either electrostatic [41] or covalent bonds [42] occur at the interface.

The most conventional binder used for composite electrodes for Li-ion batteries is polyvinylidene fluoride (PVDF). PVDF shows superior chemical and electrochemical stability, but this does not eliminate Li-ion battery-related problems such as having to use toxic organic solvents such as *N*-methylpyrrolidone (NMP), which are indispensable for dissolving the polymer. Besides, the cost of PVDF-based electrodes is still a concern in the battery industry [43–47]. Plus, PVDF also tends to swell in organic solvents, which can lead to the active mass breaking away from the electrode current collector during the working of the

battery [48]. Thus, a large amount of effort has been put into the creation of an environmentally friendly and cost-effective binder for Li-ion batteries. Consequently, extensive research has been conducted in this field.

Accordingly, Broniarz et al. [49] in their study investigated aqueous-based polyvinyl alcohol (PVA), CMC binders, and organic-based PVDF for spherical structure graphite (MCMB) electrodes. The physical and chemical properties of the pristine binders were examined. Then, MCMB-based anodes with different binders were prepared to examine the effect of water-based binders on electrochemical characteristics, which were compared with the PVDF-based binder system. This study showed how the water-based binders (CMC and PVA) were applied as effective binders for the graphite anode with spherical structure graphite (MCMB) for Li-ion batteries, in comparison with the organic solvent-based binder PVDF.

Based on their study, the authors concluded that the surface of the graphite electrodes with MCMB showed a higher homogeneity level for compounds prepared with water-based CMC and PVA polymers, compared with the organic solvent-based PVDF polymer. The authors also showed that the most satisfying adhesion was observed for all graphite electrodes with water-based binders (CMC and PVA). The authors attributed the good adhesion by the water-based binder to the structure of the polymer binders and their ability to swell in liquid electrolyte. It was also shown that the swelling of the polymer binder highly influences the mechanical properties of the graphite electrodes, especially the adhesion strength between the active materials and the current collector. Plus, the influence of the binder structure on the battery performance was also higher in the case of water-based binders. The performance of the electrodes with water-based binders was profoundly superior after 10 cycles of charging and discharging with a current density of $150\,mA\,g^{-1}$. The reason for such a superior performance by water-based binder electrodes is because the electrode mass did not separate from the current collector, providing better contact between the active material and the current collector. In PVDF-based electrodes, the adhesion of the active material mass to the current collector was weak because of binder swelling in the liquid electrolyte [49].

Further, Wang et al. [50], in their study, performed a scratch test to assess the binding mechanism of adhesion between the binders and a copper (Cu) current collector. Their results showed the better binding affinity of xanthan gum (XG) than PVDF, and the electrochemical impedance spectroscopy (EIS) test showed good electronic and ionic conductivity of the graphite anode with the XG. The natural graphite electrode fabricated with the XG binder presented a remarkable electrochemical performance. Compared with the conventional

PVDF-based anode, the initial Coulombic efficiency, cycling stability, and rate capability were substantially improved. The wear tests not only demonstrated that the XG film has a higher elasticity than the PVDF film, but it also proved to have better adhesion strength between the XG binder and the Cu foil substrate than the PVDF/Cu coating. EIS measurements showed that the graphite electrode using XG as a binder had a lower charge transfer resistance and more active kinetics on the electrode/electrolyte surface than the electrode using a PVDF binder. Also, the graphite electrode with XG as the binder not only can reduce cost and environmental pollution, but also can enhance the electrochemical performance [50].

Although the polymer binder in the anode electrode is present in a small ratio, it can influence the battery performance to a great extent. The ability of the polymer binder to bind itself to the active anode material along with the current collector is very important to obtain optimum performance. While binding the active material, the binder should not plug the porous structure of the active material. Apart from binding properties, the polymer binder should not react with the active material and the electrolyte used in the battery. Any side reaction between the binder and other electrode components can be detrimental to battery performance. An ideal binder will facilitate good adhesion, accommodate volume changes taking place in the electrode during battery cycling, and remain inert toward the electrolyte and active material.

11.3 Polymer-based binders for an Li-S battery

The polymer-based binder plays an important role in the electrochemical performances of Li-S batteries. A good binder in cathode preparation should not only be a high-adhesion agent, but also be a strong dispersion medium. This is beneficial for having a complete electrode structure and favors uniform distribution between the insulating S particles and the conductive carbon additives, which in turn ensures good electrical contact and results in high S utilization. During electrochemical reactions (battery cycling), binders can become inactive sites, leading to the deterioration of battery performance. So, a selective and functional binder is extremely important in a battery.

The early research on binders for Li-S batteries was mostly focused on polymers such as PVDF, poly(tetrafluoroethylene) (PTFE), and poly(ethylene oxide) (PEO) [51–53], commonly used in Li-ion batteries too. However, these Li-ion binders cannot solve the problem of polysulfide diffusion and dissolution, and these binders can affect the conductivity of the cathode. Meanwhile, PVDF usually needs NMP to dissolve, but NMP is poisonous and difficult in volatilization because of

its high melting point. Thus, many other materials have been explored as binders to achieve more functionality for Li-S battery cathodes such as poly(vinylpyrrolidone) (PVP) [54], gelatin [55], styrene-butadiene rubbers (SBR) [56], carboxyl methyl cellulose (CMC) [57], and functional water-soluble binders [7].

Obtaining a high S-loaded electrode is always a concern as many times the cathode electrode contains an excess amount of binder and conductive additives that bring the overall S loading in the electrode. Zhang et al. [58] proposed a dual binder system in which they were able to obtain a high S-loaded cathode. The authors used a combination of poly(acrylamide-*co*-diallyldimethylammonium chloride) (AMAC) and poly(acrylonitrile-methyl methacrylate) (ANMMA) as the second binder. AMAC is insoluble in the organic solvents that help in retaining the binding properties inside the battery that contains organic solvents. The ANMMA binder in the electrode binds the cathode components to the current collector and also avoids the current collector corrosion.

Binders are mostly nonconductors of electrons. When added to the electrodes, it brings down the overall electronic conductivity of the cathode. Because binders are homogenously dispersed connecting cathode particles in the electrode, they reduce the interparticle electronic conductivity that increases the overall resistance of the battery. Researchers have been looking for binders that inherit all the properties that are required by the binder along with electronic conductivity. When polymers such as PAA, PEDOT, and PSS were mixed, a very high conductive binder material was obtained. That obtained binder showed the synergistic effects of different functional groups that proved to be advantageous for battery performance. The developed binder not only facilitated efficient electron transfer among the electrode particles, but also inhibited the polysulfide dissolution in the electrolyte [59]. Bhattacharya et al. prepared polyamidoamine (PAMAM) dendrimers as a functional binder for high-performance Li-S batteries [60]. The authors showed that a high sulfur-loading cathode was obtained when they used such a binder. The electrodes obtained showed stable, high capacity and rate capability along with long cycling life. It was found that the stable high performance was due to the strong wettability of the cathode with the electrolyte as well as the interfacial interaction between the dendrimers and the cathode materials.

Although the polymer binder's ratio in the electrode is very small, it has a very important role in obtaining an electrode that gives optimum performance. As seen from some of the discussions above, it is clear that binders in the electrode need to be optimized according to the requirement of the Li-S battery. The S electrode undergoes extreme volume changes along with the diffusion of polysulfides from the

electrode. The binder needs to have properties where it can not only withstand the volume changes taking place during battery cycling, but the overall conductivity of the electrode must not be decreased; this is very crucial for battery performance. To summarize, current research is ongoing to develop an ideal Li-S cathode binder that has the required properties.

11.4 Conductive polymer/carbon composites in Li-S cathode electrode

Conductive polymers have free electrons (conjugated electrons) that are helpful in enhancing electronic conductivity when they are mixed with poor electron-conducting materials such as sulfur [61]. When sulfur particles are mixed with conductive polymers, they improve the electronic conductivity of the cathode electrode. The presence of a conductive polymer around the sulfur matrix is also known to keep the volume changes and sulfur particle aggregation in check. The most important observation is that when conductive polymers are added to the sulfur cathode, they act as a barrier for the dissolved lithium polysulfides that are coming out of the cathode electrode during battery cycling (Fig. 11.3).

The most commonly used conductive polymer composites in Li-S batteries include PPy, PANI, polythiophene (PTh), polyacrylonitrile (PAN), polyaniline nanotubes (PANI-NT), and PEDOT [61, 62]. The conductivity of the sulfur cathode improved and the diffusion of polysulfides from the cathode electrode was reduced when Yuan et al. [63] and Zhang et al. [64] introduced a conductive polymer PPy to the sulfur/carbon matrix core-shell matrix. The improvements were reflected in the better performance of the battery.

Chung and coworkers [65] proposed an S polymer composite with poly(sulfur-random-1,3-diisopropenylbenzene) (poly(S-r-DIB)) copolymers as an example to highlight the impact of copolymer structure-composition on the electrochemical properties of the Li-S battery. The obtained organosulfur cathode delivered an initial specific discharge capacity of 823 $mA\,h\,g^{-1}$ after 100 cycles at 0.1 C. The authors claimed that polyolefin with unsaturated carbon-carbon covalent bonds and a stable C-S bond encapsulates the S into the polymer matrix and the obtained copolymer facilitates the effective trapping of polysulfides, leading to improved electrochemical properties. Furthermore, they optimized the capacity to 1005 $mA\,h\,g^{-1}$ at the same condition [66]. The organosulfur unit serves as a plasticizer in the insoluble dispersed Li_2S_3/Li_2S_2 discharge product phase, as it is capable of suppressing the irreversible deposition of these discharge products with the result of limiting the capacity loss.

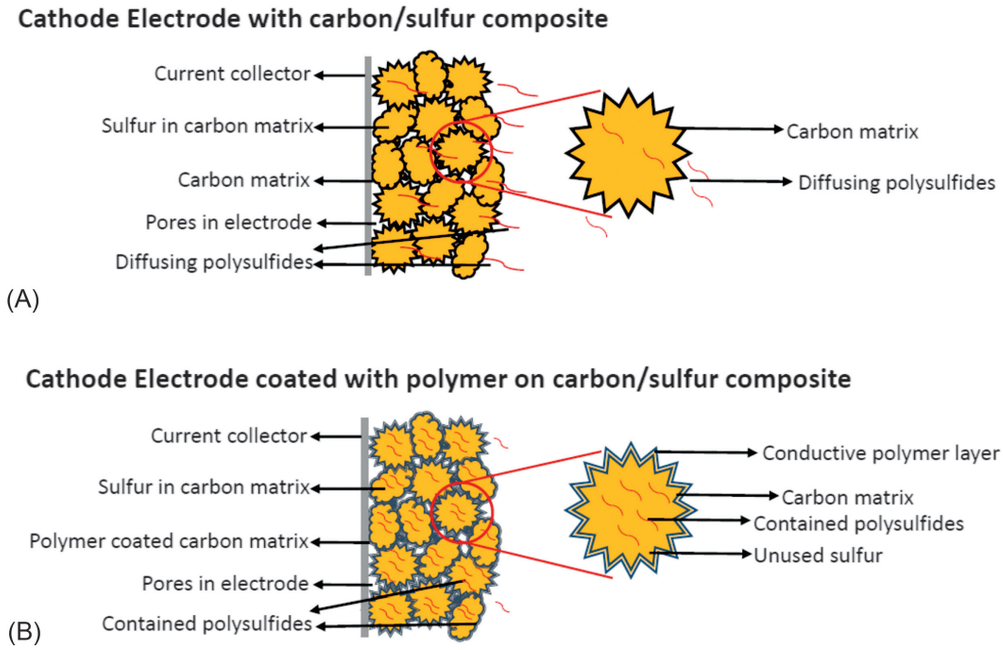


Fig. 11.3 (A) Carbon/S composite electrode without a polymer barrier showing the diffusion of dissolved polysulfides that leads to battery capacity fading; (B) carbon/S composite electrode with a conductive polymer barrier showing the prevention of polysulfide diffusion from the cathode electrode.

PEDOT, a conductive polymer, was used to enhance the performance of the sulfur cathode by increasing the electronic conductivity and entrapping the polysulfides. Chen et al. [17] reported a discharge capacity of $1117\,\mathrm{mA\,h\,g^{-1}}$ and a stable $930\,\mathrm{mA\,h\,g^{-1}}$ capacity after 50 cycles. The authors reported an S/carbon/PEDOT core/shell structure that acted as a barrier for the diffusion of polysulfides while retaining the active material in the cathode electrode, which resulted in the improved performance of the battery.

To achieve a high-loading sulfur cathode with high conductivity, hybrid polymers possessing both high ionic and electronic conductivities were recently developed [67]. An example is the multifunctional copolymer poly(styrene-4-sulfonate) (PSS)/PPy, which is able to greatly enhance the redox kinetics. In particular, the conductive PPy is capable of immobilizing the diffusing sulfur species in the cathode through the formation of a polysulfide-H-N interaction (hydrogen bond) while the PSS with fixed sulfonate groups can provide fast ionic diffusion. The PSS/PPy-cell could provide an initial discharge capacity as high as $1108\,\mathrm{mA\,h\,g^{-1}}$ at a C/10 rate with a capacity retention of 64%

after 200 cycles. Remarkably, it could also reach an 80 wt% sulfur content with a surface sulfur loading of 6.0 mg cm^{-2}.

Some of the most commonly used conductive polymers are PPy, PANI, and PEDOT. The high conductivity and polysulfide encapsulation nature of these polymers make them the most common pick among researchers. Liu et al. [18] compared the electrochemical performances of the batteries using these conductive composite polymers as a coating material on S nanospheres. The authors reported that among the three conductive polymers used, PEDOT showed the best performance. In the presence of PEDOT, the shuttling mechanism was the least that resulted in enhancing the battery performance.

Conducting polymers such as PPy, PTh, poly(3,4-ethylenedioxythiophene)-poly(styrene sulfonate) (PEDOT:PSS), and PANI have been successfully used in sulfur composites to improve the cycle performance and the rate capacity of Li-S batteries. The conducting polymers are used as physical barriers for clogging polysulfides or sulfur absorbents by thermal treatment. Sulfur and polysulfides cannot easily escape from the composite with a conducting polymer coating. Moreover, the conductive feature of polymers facilitates the lithium ion and electron transport in the Li/S cells and high-rate charge/discharge capability can be expected [68–71].

Conductive polymer materials have been modified to mimic the properties of carbon nanotubes. Carbon nanotubes are highly conductive and have pores or tunnels that can encapsulate the S and its intermediates when used as a conductive matrix in the S cathode electrode. Researchers such as Xioa et al. [18] reported a PANI nanotube that can encapsulate S and its polysulfide intermediates. The modified polymer nanotubes not only provided the required electronic conductivity in the cathode electrode, but also trapped the polysulfides inside the pores by means of electrostatic forces. The authors showed a life cycle of 500 cycles and attributed the long cycling to efficient active material encapsulation during cycling.

PEG-wrapped graphene-S nanocomposites were reported by Wang et al. [12]. The synthesized submicrometer S particles are coated with PEG surfactants and graphene sheets, which function as a chemical and physical protective coating for trapping the polysulfide intermediates. The soft PEG coating further accommodated the volume change of the wrapped S particles during cell cycling. The conductive graphene coating offered the encapsulated S particles a robust and electrically conductive shell. Therefore, PEG/graphene-S nanocomposites showed high and stable discharge capacities up to 600 mA h g^{-1} over more than 100 cycles. This was a significant improvement in the cyclability of polymer-coated S-carbon nanocomposites from 20 cycles (at a C/10 rate) to 140 cycles (at a C/2 rate).

11.5 Conclusions and future directions

In summary, many researchers have demonstrated that the conductive polymer coating on the surface of carbon/S composites effectively encapsulates the polysulfides and minimizes the diffusion of dissolved polysulfides and the loss of active mass in the cathodes, which leads to a notable improvement in the performance of Li-S batteries. In some of the above examples, the initial discharge capacity reached as high as $1140\,mA\,h\,g^{-1}$ against the theoretical capacity of $1675\,mA\,h\,g^{-1}$, which is ~ 10% higher than that of the bare counterpart without a polymer coating. More significantly, the discharge capacity of the batteries with polymer coating remained significantly high and showed improved life cycle and Coulomb efficiency. Also, a selective and functional polymer binder is extremely important to improve the electrochemical performances of Li-S batteries. Plus, the strategy of a conductive polymer coating on the exterior surface of active electrodes can be potentially generalized for improving the performance of other electrode materials in lithium-sulfur batteries.

References

[1] A. Manthiram, Y. Fu, Y.S. Su, Challenges and prospects of lithium–sulfur batteries, Acc. Chem. Res. 46 (2013) 1125–1134.
[2] S. Evers, L.F. Nazar, New approaches for high energy density lithium–sulfur battery cathodes, Acc. Chem. Res. 46 (2013) 1135–1143.
[3] J. Wang, S.Y. Chew, Z.W. Zhao, S. Ashraf, D. Wexler, J. Chen, S.H. Ng, S.L. Chou, H.K. Liu, Sulfur–mesoporous carbon composites in conjunction with a novel ionic liquid electrolyte for lithium rechargeable batteries, Carbon 46 (2008) 229–235.
[4] Y.S. Su, A. Manthiram, Lithium–sulphur batteries with a microporous carbon paper as a bifunctional interlayer, Nat. Commun. 3 (2012) 1166–1169.
[5] Y.V. Mikhaylik, J.R. Akridge, Polysulfide shuttle study in the Li/S battery system, J. Electrochem. Soc. 151 (2004) A1969–A1976.
[6] L. Yin, J. Wang, F. Lin, J. Yang, Y. Nuli, Polyacrylonitrile/graphene composite as a precursor to a sulfur-based cathode material for high-rate rechargeable Li–S batteries, Energy Environ. Sci. 5 (2012) 6966–6972.
[7] S.S. Zhang, Liquid electrolyte lithium/sulfur battery: fundamental chemistry, problems, and solutions, J. Power Sources 231 (2013) 153–162.
[8] C. Zhang, H.B. Wu, C. Yuan, Z. Guo, X.W. Lou, Confining sulfur in double-shelled hollow carbon spheres for lithium–sulfur batteries, Angew. Chem. Int. Ed. 51 (2012) 9592–9595.
[9] Y.S. Su, A. Manthiram, A new approach to improve cycle performance of rechargeable lithium–sulfur batteries by inserting a free-standing MWCNT interlayer, Chem. Commun. 48 (2012) 8817–8819.
[10] S. Dorfler, M. Hagen, H. Althues, J. Tubke, S. Kaskel, M.J. Hoffmann, High capacity vertical aligned carbon nanotube/sulfur composite cathodes for lithium–sulfur batteries, Chem. Commun. 48 (2012) 4097–4099.
[11] J. Guo, Y. Xu, C. Wang, Sulfur-impregnated disordered carbon nanotubes cathode for lithium–sulfur batteries, Nano Lett. 11 (2011) 4288–4294.

[12] H. Wang, Y. Yang, Y. Liang, J.T. Robinson, Y. Li, A. Jackson, Y. Cui, H. Dai, Graphene wrapped sulfur particles as a rechargeable lithium–sulfur battery cathode material with high capacity and cycling stability, Nano Lett. 11 (2011) 2644–2647.
[13] L. Ji, M. Rao, H. Zheng, L. Zhang, Y. Li, W. Duan, J. Guo, E.J. Cairns, Y. Zhang, Graphene oxide as a sulfur immobilizer in high performance lithium/sulfur cells, J. Am. Chem. Soc. 133 (2011) 18522–18525.
[14] S. Evers, L.F. Nazar, Graphene-enveloped sulfur in a one pot reaction: a cathode with good coulombic efficiency and high practical sulfur content, Chem. Commun. 48 (2012) 1233–1235.
[15] M.U.M. Patel, N.D. Luong, J. Seppala, E. Tchernychova, R. Dominko, Low surface area graphene/ cellulose composite as a host matrix for lithium sulphur batteries, J. Power Sources 254 (2014) 55–61.
[16] Y. Yang, G.H. Yu, J.J. Cha, H. Wu, M. Vosgueritchian, Y. Yao, Z. Bao, Y. Cui, Improving the performance of lithium-sulfur batteries by conductive polymer coating, ACS Nano 5 (2011) 9187–9193.
[17] H. Chen, W. Dong, J. Ge, C.H. Wang, X.D. Wu, W. Lu, L.W. Chen, Ultrafine sulfur nanoparticles in conducting polymer shell cathode materials for high performance lithium/sulfur batteries, Sci. Rep. 3 (2013) 1910–1915.
[18] L.F. Xiao, Y.L. Cao, J. Xiao, B. Schwenzer, M.H. Engelhard, L.V. Saraf, Z.M. Nie, G.J. Exarhos, J. Liu, A soft approach to encapsulate sulfur: polyaniline nanotubes for lithium-sulfur batteries with long cycle life, Adv. Mater. 24 (2012) 1176–1181.
[19] W. Li, G. Zheng, Y. Yang, Z.W. Seh, N. Liu, Y. Cui, High-performance hollow sulfur nanostructured battery cathode through a scalable, room temperature, one-step, bottom-up approach, Proc. Natl. Acad. Sci. U. S. A. 110 (2013) 7148–7153.
[20] Y. Deng, H. Xu, Z. Bai, B. Huang, J. Su, G. Chen, Durable polydopamine-coated porous sulfur core–shell cathode for high performance lithium–sulfur batteries, J. Power Sources 300 (2015) 386–394.
[21] J. Shao, X.Y. Li, L. Zhang, Q.T. Qu, H.H. Zheng, Core–shell sulfur@ polypyrrole composites as high-capacity materials for aqueous rechargeable batteries, Nanoscale 5 (2013) 1460–1464.
[22] Y. An, P. Wei, M. Fan, D. Chen, H. Chen, Q. Ju, G. Tian, K. Shu, Dual-shell hollow polyaniline/sulfur-core/polyaniline composites improving the capacity and cycle performance of lithium–sulfur batteries, Appl. Surf. Sci. 375 (2016) 215–222.
[23] Y. Liu, A.K. Haridas, K.K. Cho, Y. Lee, J.H. Ahn, Highly ordered mesoporous sulfurized polyacrylonitrile cathode material for high-rate lithium sulfur batteries, J. Phys. Chem. C 12 (2017) 26172–26179.
[24] B. Oschmann, J. Park, C. Kim, K. Char, Y.E. Sung, R. Zentel, Copolymerization of polythiophene and sulfur to improve the electrochemical performance in lithium–sulfur batteries, Chem. Mater. 27 (2015) 7011–7017.
[25] H. Li, M.Q. Sun, T. Zhang, Y.Q. Fang, G.C. Wang, Improving the performance of PEDOT-PSS coated sulfur@ activated porous graphene composite cathodes for lithium–sulfur batteries, J. Mater. Chem. A 2 (2014) 18345–18352.
[26] M. Zhang, Q. Meng, A. Ahmad, L. Mao, W. Yan, Z. Wei, Poly (3, 4-ethylenedioxythiophene)-coated sulfur for flexible and binder-free cathodes of lithium–sulfur batteries, J. Mater. Chem. A 5 (2017) 17647–17652.
[27] B. Dunn, H. Kamath, J.M. Tarascon, Electrical energy storage for the grid: a battery of choices, Science 334 (2011) 928–935.
[28] Z. Yang, J. Zhang, M.C.W. Kintner-Meyer, X. Lu, D. Choi, J.P. Lemmon, J. Liu, Electrochemical energy storage for green grid, Chem. Rev. 111 (2011) 3577–3613.
[29] D. Andre, S.J. Kim, P. Lamp, S.F. Lux, F. Maglia, O. Paschos, B. Stiaszny, Future generations of cathode materials: an automotive industry perspective, J. Mater. Chem. A 3 (2015) 6709–6732.

[30] D. Bresser, K. Hosoi, D. Howell, H. Li, H. Zeisel, K. Amine, S. Passerini, Perspectives of automotive battery R&D in China, Germany, Japan, and the USA, J. Power Sources 382 (2018) 176–178.
[31] K.P. Lee, N.C. Chromey, R. Culik, J.R. Barnes, P.W. Schneider, Toxicity of N-methyl-2-pyrrolidone (NMP): teratogenic, subchronic, and two-year inhalation studies, Fundam. Appl. Toxicol. 9 (1987) 222–235.
[32] D.E. Malek, L.A. Malley, T.W. Slone, G.S. Elliott, G.L. Kennedy, W. Mellert, K. Deckardt, C. Gembardt, B. Hildebrand, S.R. Murphy, D.B. Bower, G.A. Wright, Repeated dose toxicity study (28 days) in rats and mice with N-methylpyrrolidone (NMP), Drug Chem. Toxicol. 20 (1997) 63–77.
[33] W. Zhu, D.R. Schmehl, C.A. Mullin, J.L. Frazier, Four common pesticides, their mixtures and a formulation solvent in the hive environment have high Oral toxicity to honey bee larvae, PLoS One 9 (2014) e77547.
[34] F.M. Courtel, S. Niketic, D. Duguay, Y. Abu-Lebdeh, I.J. Davidson, Water-soluble binders for MCMB carbon anodes for lithium-ion batteries, J. Power Sources 196 (2011) 2128–2134.
[35] D. Bresser, D. Buchholz, A. Moretti, A. Varzi, S. Passerini, Alternative binders for sustainable electrochemical energy storage—the transition to aqueous electrode processing and bio-derived polymers, Energy Environ. Sci. 11 (2018) 3096–3127.
[36] J. Drofenik, M. Gaberscek, R. Dominko, F.W. Poulsen, M. Mogensen, S. Pejovnik, J. Jamnik, Cellulose as a binding material in graphitic anodes for Li ion batteries: a performance and degradation study, Electrochim. Acta 48 (2003) 883–889.
[37] J.H. Lee, S. Lee, U. Paik, Y.M. Choi, Aqueous processing of natural graphite particulates for lithium-ion battery anodes and their electrochemical performance, J. Power Sources 147 (2005) 249–255.
[38] A.N. Gent, C.W. Lin, Model studies of the effect of surface roughness and mechanical interlocking on adhesion, J. Adhes. 32 (1990) 113–125.
[39] D.J. Gardner, M. Blumentritt, L. Wang, N. Yildirim, Adhesion Theories in Wood Adhesive Bonding, Scrivener Publishing, Beverly, 2015.
[40] A. Magasinski, B. Zdyrko, I. Kovalenko, B. Hertzberg, R. Burtovyy, C.F. Huebner, T.F. Fuller, I. Luzinov, G. Yushin, Toward efficient binders for Li-ion battery Si-based anodes: polyacrylic acid, ACS Appl. Mater. Interfaces 2 (2010) 3004–3010.
[41] B.V. Derjaguin, I.N. Aleinikova, Y.P. Toporov, On the role of electrostatic forces in the adhesion of polymer particles to solid surfaces, Powder Technol. 2 (1969) 154–158.
[42] J. Song, M. Zhou, R. Yi, T. Xu, M.L. Gordin, D. Tang, Z. Yu, M. Regula, D. Wang, Interpenetrated gel polymer binder for high-performance silicon anodes in lithium-ion batteries, Adv. Funct. Mater. 24 (2014) 5904–5910.
[43] M. Yoo, C.W. Frank, S. Mori, Interaction of poly (vinylidene fluoride) with graphite particles. 1. Surface morphology of a composite film and its relation to processing parameters, Chem. Mater. 15 (2003) 850–861.
[44] M. Yoo, C.W. Frank, S. Mori, S. Yamaguchi, Interaction of poly(vinylidene fluoride) with graphite particles. 2. Effect of solvent evaporation kinetics and chemical properties of PVDF on the surface morphology of a composite film and its relation to electrochemical performance, Chem. Mater. 16 (2004) 1945–1953.
[45] M.H.T. Nguyen, E.S. Oh, Application of a new acrylonitrile/butylacrylate water-based binder for negative electrodes of lithium-ion batteries, Electrochem. Commun. 35 (2013) 45–48.
[46] J. Chong, S. Xun, H. Zheng, X. Song, G. Liu, P. Ridgway, W.J. Qiang, V.S. Battaglia, A spherical natural graphite/LiFePO4 electrodes and cells, J. Power Sources 196 (2011) 7707–7714.
[47] S.F. Lux, F. Schappacher, A. Balducci, S. Passerini, M. Winter, Low cost, environmentally benign binders for lithium-ion batteries, J. Electrochem. Soc. 157 (2010) A320–A325.

[48] V. Barsykov, V. Khomenko, The influence of polymer binders on the performance of cathodes for lithium-ion batteries, Mater. Sci. Appl. Chem. 21 (2010) 67–71.
[49] M.O. Broniarz, A. Martyla, L. Majchrzycki, M. Nowicki, A. Sierczynska, Influence of polymer binder structure on the properties of the graphite anode for lithium-ion batteries, Eur. J. Chem. 7 (2016) 182–186.
[50] Z. Wang, G. Dang, Q. Zhang, J. Xie, Xanthan gum as a potential binder for graphite anode in lithium-ion batteries, Int. J. Electrochem. Sci. 12 (2017) 7457–7468.
[51] L. Chen, L.L. Shaw, Recent advances in lithium-sulfur batteries, J. Power Sources 267 (2014) 770–783.
[52] Z. Lin, C. Liang, Lithium-sulfur batteries: from liquid to solid cells, J. Mater. Chem. A 3 (2015) 936–958.
[53] M.J. Lacey, F. Jeschull, K. Edstrom, Why PEO as a binder or polymer coating increases capacity in the Li-S system, RSC Adv. 49 (2013) 8531–8533.
[54] Z.W. Seh, Q. Zhang, W. Li, G. Zheng, H. Yao, Y. Cui, Stable cycling of lithium sulfide cathodes through strong affinity with a bifunctional binder, Chem. Sci. 4 (2013) 3673–3677.
[55] Y. Wang, Y. Huang, W. Wang, Structural change of the porous sulfur cathode using gelatin as a binder during discharge and charge, Electrochim. Acta 54 (2009) 4062–4066.
[56] M.K. Song, Y. Zhang, E.J. Cairns, A long-life, high-rate lithium/sulfur cell: a multifaceted approach to enhancing cell performance, Nano Lett. 13 (2013) 5891–5899.
[57] M. He, L.X. Yuan, W.X. Zhang, Enhanced cyclability for sulfur cathode achieved by a water-soluble binder, J. Phys. Chem. 115 (2011) 15703–15709.
[58] S.S. Zhang, Binder based on polyelectrolyte for high capacity density lithium/sulfur battery, J. Electrochem. Soc. 159 (2012) A1226–A1229.
[59] J. Pan, G.Y. Xu, B. Ding, Z. Chang, A.X. Wang, H. Douand, X.G. Zhang, PAA/PEDOT:PSS as a multifunctional, water-soluble binder to improve the capacity and stability of lithium–sulfur batteries, RSC Adv. 6 (2016) 40650–40655.
[60] P. Bhattacharya, M.I. Nandasiri, D.P. Lv, A.M. Schwarz, J.T. Darsell, W.A. Henderson, D.A. Tomalia, J. Liu, J.G. Zhang, J. Xiao, Polyamidoamine dendrimer-based binders for high-loading lithium-sulfur battery cathodes, Nano Energy 19 (2016) 176–186.
[61] W. Kang, N. Deng, J. Ju, Q. Li, D. Wu, X. Ma, L. Li, M. Naebe, B. Cheng, A review of recent developments in rechargeable lithium–sulfur batteries, Nanoscale 8 (2016) 16541–16588.
[62] Y. Yang, G. Zheng, Y. Cui, Nanostructured sulfur cathodes, Chem. Soc. Rev. 42 (2013) 3018–3032.
[63] G. Yuan, H. Wang, Facile synthesis and performance of polypyrrole-coated sulfur nanocomposite as cathode materials for lithium/sulfur batteries, J. Energy Chem. 23 (2014) 657–661.
[64] Y. Zhang, Z. Bakenov, Y. Zhao, A. Konarov, T.N.L. Doan, M. Malik, T. Paron, P. Chen, One-step synthesis of branched sulfur/polypyrrole nanocomposite cathode for lithium rechargeable batteries, J. Power Sources 208 (2012) 1–8.
[65] W.J. Chung, J.J. Griebel, E.T. Kim, H. Yoon, A.G. Simmonds, H.J. Ji, P.T. Dirlam, R.S. Glass, J.J. Wie, N.A. Nguyen, The use of elemental sulfur as an alternative feedstock for polymeric materials, Nat. Chem. 5 (2013) 518.
[66] A.G. Simmonds, J.J. Griebel, J. Park, K.R. Kim, W.J. Chung, V.P. Oleshko, J. Kim, E.T. Kim, R.S. Glass, C.L. Soles, Inverse vulcanization of elemental sulfur to prepare polymeric electrode materials for Li–S batteries, ACS Macro Lett. 3 (2014) 229.
[67] P. Han, S.-H. Chung, A. Manthiram, Designing a high-loading sulfur cathode with a mixed ionic-electronic conducting polymer for electrochemically stable lithium-sulfur batteries, Energy Storage Mater. 17 (2019) 317–327.
[68] X. Liang, Y. Liu, Z. Wen, L. Huang, X. Wang, H. Zhang, A nano-structured and highly ordered polypyrrole-sulfur cathode for lithium–sulfur batteries, J. Power Sources 196 (2011) 6951–6955.

[69] F. Wu, J. Chen, R. Chen, S. Wu, L. Li, S. Chen, T. Zhao, Sulfur/polythiophene with a core/shell structure: synthesis and electrochemical properties of the cathode for rechargeable lithium batteries, J. Phys. Chem. C 115 (2011) 6057–6063.
[70] L. Duan, J. Lu, W. Liu, P. Huang, W. Wang, Z. Liu, Fabrication of conductive polymer-coated sulfur composite cathode materials based on layer-by-layer assembly for rechargeable lithium–sulfur batteries, Colloid Surf. A Physicochem. Eng. Asp. 414 (2012) 98–103.
[71] Y. Fu, Y.S. Su, A. Manthiram, Sulfur-polypyrrole composite cathodes for lithium-sulfur batteries, J. Electrochem. Soc. 159 (2012) A1420–A1424.

Further reading

Y.Z. Fu, A. Manthiram, Enhanced cyclability of lithium–sulfur batteries by a polymer acid-doped polypyrrole mixed ionic–electronic conductor, Chem. Mater. 24 (2012) 3081–3087.

12

Recent advances in conjugated polymers for lithium-ion and supercapacitor applications

U.T. Uthappa[a,b], Ho-Young Jung[b], and Mahaveer D. Kurkuri[a]

[a]Centre for Nano and Material Sciences, Jain University, Jain Global Campus, Bengaluru, Karnataka, India, [b]Department of Environment and Energy Engineering, Chonnam National University, Buk-gu, Gwangju, Republic of Korea

12.1 Introduction

Energy storage systems are necessary for the storage of generated energy, either from traditional thermal and nuclear power generation methods or from renewable energy sources such as wind, solar, tidal, electronic vehicles, individual gadgets, and other portable electronics [1, 2]. These energy storage systems must possess high storage capacity, faster charge-discharge rates, flexibility, long life cycle stability, utility, light weight, and flexibility for their use in future applications [3]. Presently, energy storage systems such as batteries and supercapacitors have been researched and fabricated for commercialization. To resolve the setbacks of the existing energy storage materials, various researchers have explored diverse innovative and challenging approaches [4–11]. As organic redox-active materials are compelling materials for subsequent energy storage systems, the scientific community must concentrate on them as they possess great advantages such as better chemical and physical properties, enticing molecular structures, and enhanced electrochemical storage performances [12]. Further, redox-active polymers have been specifically used over single organic molecules due to their excellent properties such as good stability, excellent processability, easy and quick manufacturing of devices, etc. [13].

A new class of materials called conjugated polymers (CPs) was first discovered in 1977 [14]. The electronic properties of CPs vary significantly from well-established inorganic semiconductors [15]. Accordingly, over the last few decades, CPs have gained significant research interest that in turn led to a number of publications. Research in this area has provided a fundamental understanding of these

Polymer-Based Advanced Functional Composites for Optoelectronic and Energy Applications
https://doi.org/10.1016/B978-0-12-818484-4.00001-X
Copyright © 2021 Elsevier Inc. All rights reserved.

materials in chemistry and material science while also enabling the commercialization and industrial growth of these polymer goods [16, 17]. The mechanical properties of CPs are identical to plastic properties, allowing them to be flexed, bent, and even extended [18–24]. The electrodes of conjugated polymers can be easily incorporated in textiles, structural panels, electronic papers, and so forth [25–27]. CPs also offer additional benefits in addition to their mechanical versatility, such as synthetic tailorability and processability, which make them acceptable entrants for electrochemical applications. In addition, it is possible to change the physical and electrochemical properties of CPs through appropriate synthetic routes [28–30].

New synthetic methods have upgraded the processability, so most CPs are now processed through screen printing or inkjet printing [31–33]. In conjunction with negative metal electrodes, CPs have recently been widely explored in anion-based lithium battery designs [34]. Most mainstream rechargeable battery systems currently depend on high-energy Li-ion battery technology. They are also potentially high-power density rivals for pseudocapacitor and supercapacitor applications [34–38]. Some review papers have integrated different redox-active polymers with their electrochemical efficiency into unique energy storage applications [12, 13, 39]. Therefore it is appreciated that the recent research progress for new and precise molecular scheme for recently advanced CPs in energy storage systems is summarized and hosted to deliver extensive and new innovative perceptions in this field. We anticipate that this chapter and the research papers cited would enable material scientists, electrochemists, and engineers to further advance CPs for high-performance Li-ion battery and supercapacitor applications.

12.2 Operating principles of conjugated polymers

We must first consider the basic properties of CPs themselves in order to grasp the working theory of CPs within the battery and supercapacitor electrode system. The conductive and charge storage skills of CPs depend on their electronic characteristics and are the basis of the interesting electronic and optical properties of CPs. The arrangement of the molecular orbitals along with the conjugated polymer backbone leads to a band structure identical to that of inorganic semiconductors [40]. The effectiveness of the conjugation length at which no additional monomer units are auxiliary to the chain affects the polymer's electronic properties [41–43]. Polymers are categorized as n-type and p-type, respectively, constructed on their ability to quickly undergo oxidation or reduction. Structures with electron-rich species have

inflated HOMO levels to generate solid p-type materials because of their ability to stabilize the positive charge, whereas those structures with weak electron species produce n-type material by stabilizing their negative charges at lower LUMO levels [44].

12.3 Applications of conjugated polymers

12.3.1 Conjugated polymers as electrode materials for lithium-ion batteries

Higgins et al. fabricated silicon (Si) nanoparticle (NP) lithium-ion battery negative electrodes. By using the conducting polymer PEDOT:PSS system, they demonstrated a first cycle lithiation capacity of 3685 mAh/g and a cycle efficiency of ~78%. Subsequently, after 100 repeated cycles at 1 A/g, this electrode was static to store a remarkable 1950 mAh/g normalized to Si mass analogous to 1542 mAh/g [45].

Going forward, poly(1,4-dihydro-11Hpyrazino[2′,3′:3,4]cyclopenta[1,2-*b*]quinoxalin-11-one) (PPCQ) as an anode material with a new coupled ladder-like oligomer with a rich amount of hetero atoms was built. The synthetic protocol is shown in Fig. 12.1. In addition to this impressive lithium storage of 972 mAh/g after 120 cycles demonstrated by ultralong tests of 1000 cycles at an excessive current density of 2.5 A/g [46].

Xie et al. developed poly (2,3-dithiino-1,4-benzoquinone) (PDB) with a structured polymer over a facile dual step polymerization process. After 100 cycles, the PDB could achieve a better reversible basic capacity of 681 mAh/g with 98.4% capacity retention. A good rate performance was also achieved, with a rapid capacity recovery, next testing at various current densities [46].

In other studies, the phthalocyanine-conjugated system replaced by tetra-carboxyl and octa-carboxyl groups was used as the cathode content in Li-B. The electrochemical properties of the microparticles were studied, considering lithium as the counter-electrode, and the electrochemical mechanism of carboxyl groups substituted with phthalocyanines was analyzed. The results indicate that

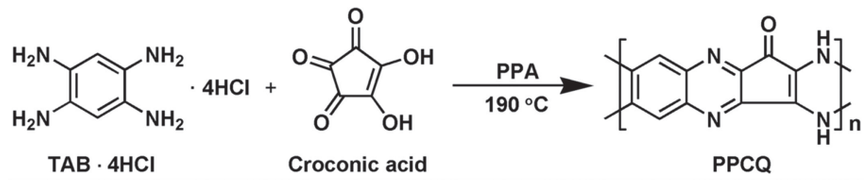


Fig. 12.1 Synthetic root of PPQ. Reproduced with permission J. Xie, Z. Wang, P. Gu, Y. Zhao, Z.J. Xu, Q. Zhang, A novel quinone-based polymer electrode for high performance lithium-ion batteries, Sci. China Mater. 59 (2016) 6–11.

phthalocyanines substituted for carboxyl have a high specific ability. They still maintain power after 20/50 cycles while retaining capacities of about 300 and 500 mAh/g [47].

A composite material has been obtained consisting of radical polymer-modified graphene sheets, G-g-PTMA, and RGO. In this work, the multirole of G-g-PTMA in G-g-PTMA/RGO composites gave a cathode with peak specific power up to 466 mAh/g, and good cycle efficiency with a rapid one-electrode PTMA redox reaction [48].

In addition, another work revealed that conjugated copolymers consisting of cyclopentadithiophene (CPDT) and methyl benzoate were synthesized through the direct arylation polymerization method of easy synthesis monitored by saponification in order to record high-yield polymers with high molecular weight. The polymers were combined with Si NPs to be used in the development of an anode electrode in Li-Bs as conducting binders. The electrode battery containing the saponified polymer showed greater definite capacity of up to 1820 mAh/g and superior stability prior to saponification matched to the battery comprising the polymer [49].

To synthesize flexible polypyrrole (PPy) films as free-standing anodes for Li-Bs, a simple vapor phase polymerization (VPP) method was also explored. The development of PPy graphic film is shown in Fig. 12.2. For Li-Bs, and even after 1000 cycles, the basic capacity was retained at 216.7 mAh/g. Importantly, repetitive discharge/charge processes did not alter the PPy film's orderly structure [50].

As the cathode material of Li-Bs, the hetero aromatic organic compound *N*,*N*′-diphenyl-1,4,5,8-naphthalenetetra-carboxylic diimide (DP-NTCDI-250) was formed via a simple one-pot *N*-acylation reaction. Electrochemical calculations showed that the DP-NTCDI-250 could supply a primary discharge power of 170 mAh/g at a current density of 25 mAh/g. A power of 119 mAh/g was also retained after 100 cycles [51].

Hierarchical $MnCO_2O_4$/PPy composites were fabricated by a simple solvothermal method. To boost the conductivity, the PPy layer

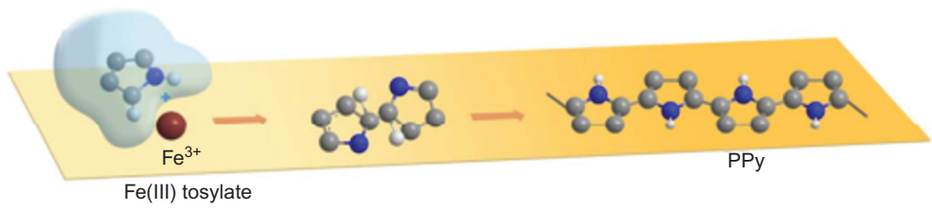


Fig. 12.2 Schematic of PPy film fabrication. Reproduced with permission J.R.T. Yuan, W. Zhang, Z. Tan, J. Yang, Z.F. Ma, S. Zheng, Flexible overoxidized polypyrrole films with orderly structure as high-performance anodes for Li-ion and Na-ion batteries, ACS Appl. Mater. Interfaces 8 (2016) 35114–35122.

acted as a conductive agent and could adjust the volume of the buffer during cycling. These composites of $MnCO_2O_4$/PPy showed stronger electrochemical properties than those of pristine $MnCO_2O_4$. The discharge capacity of $MnCO_2O_4$/PPy at a current density of 200 mAh/g was 910 mAh/g after 100 cycles. The discharge capacity was still maintained at 598 mAh/g after 50 cycles, even at a current density of approximately 2000 mA/g [52].

Yang et al. formed a highly conductive 2D COF (covalent organic structure) and polyporphyrin (TThPP) bound to the surface of copper foil by 4-thiophenephenyl groups. The anode and TThPP showed high specific capacities and outstanding rate efficiency, indicated with a reversible capacity of up to 666 mAh/g. As a lithium-ion capacitor anode, the specific capacitance reached 82.79 F/g at a current density of 50 mA/g [53].

Park et al. established polydopamine (PDA) coating as an extraordinary method for improving the thermal stability of graphite anodes, which, due to the conflicting existence of the two variables, was difficult to achieve simultaneously. The PDA coating significantly improved the storage performance and rate performance of the 60°C cycle and 90°C, primarily as a result of the Lewis basicity of PDA [54].

In another study, natural graphite composites (SANGs) were fabricated by spray drying and the subsequent pyrolysis of the granulation of natural graphite and styrene/acrylonitrile copolymer (SAN) particles. These SANGs have shown better kinetic properties when used as anodes in Li-Bs than those of natural graphite [55].

Another study demonstrated perylene diimide dyes, a bulky family of small conjugated fragments with redox-active carbonyl/hydroxyl groups that can reversibly absorb and discharge Li-ions. They have been investigated as cost-effective organic materials for Li-Bs of the next generation. Accordingly, a series of perylene diimide dyes was examined as Li-storable cathodes. The designed perylene diimides displayed a beginning reversible capacity of ~ 100 mAh/g with exceptional cyclability and rate capability. As simplest perylene diimide, 119 mAh/g redox capacity with ~ 96% capacity retention over 200 cycles [56].

For better-performance Li-B anodes, PEI-derived MnO_2-GO was reported; it enabled high reversible capacities of 880 mAh/g at a current density of 0.1 A/g. In addition, the combined location of the PEI interfacial layer and the conductive reduced graphene oxide permitted a unique level of 460 mAh/g at current densities of up to 5 A/g and a normalized capacity variance of 0.67 at current densities of 100–3000 mA/g [57].

Wang et al. proposed poly (methyl methacrylate) (PMMA) for rechargeable Li-Bs. The specially designed thin film PMMA electrode had a high reversible capacity of 343 mAh/g at C/25 and retained 82.6%

of the capacity retention obtained at C/25 when cycled at a rate of 1°C. Meanwhile, this pristine PMMA electrode without a binder or conductive agents demonstrated a high reversible ability of 196.8 mAh/g after 150 cycles at 0.2°C with a power retention of 73.5% [58].

On the other hand, tin dioxide (SnO_2) has drawn considerable interest in Li-Bs. With a reversible definite capability approximately 770 mAh/g at 2000 mA/g and notable cyclability for robust PP nanotubes (NTs) as the anode, mesoporous SnO_2 showed excellent rate performance, accompanied by a high specific capacity of approximately 790 mAh/g at 200 mA/g after 200 cycles [59]. The schematic of SnO_2@PPy NT fabrication and their TEM images are represented in Fig. 12.3.

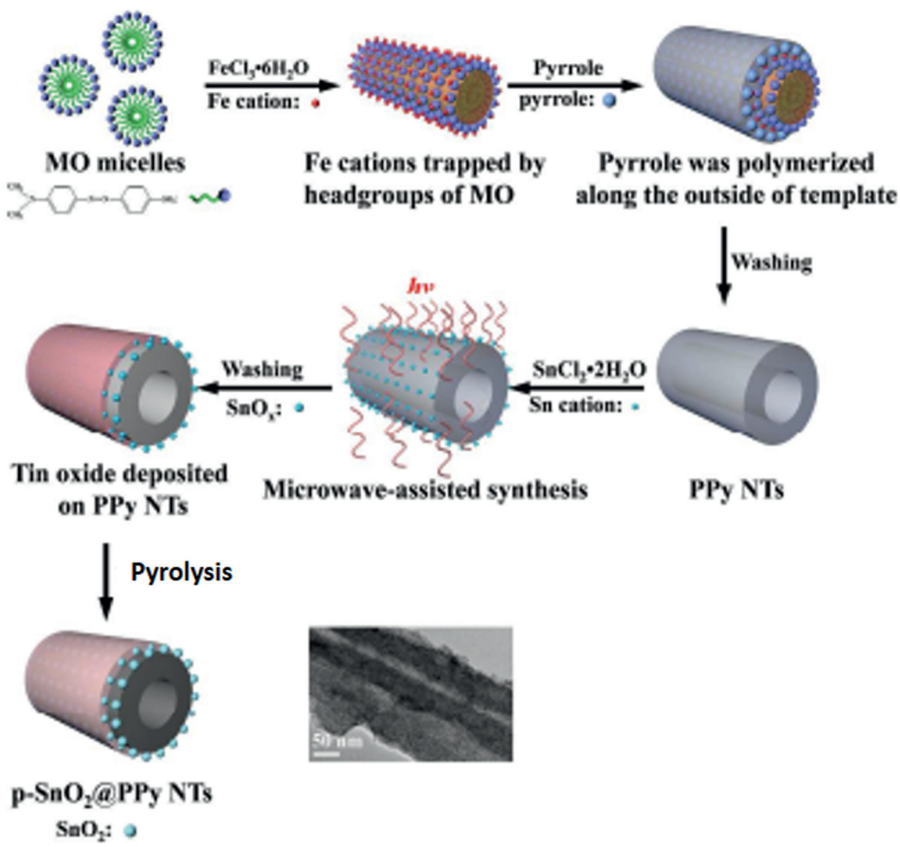


Fig. 12.3 Diagram of manufacturing SnO_2@PPy NTs through the soft polymerization of the template and assisted synthesis by microwave. Inset: SnO_2@PPy NTs' TEM images. Reproduced with permission X. Du, T. Yang, J. Lin, T. Feng, J. Zhu, L. Lu, Y. Xu, J. Wang, Microwave-assisted synthesis of SnO2@ polypyrrole nanotubes and their pyrolyzed composite as anode for lithium-ion batteries, ACS Appl. Mater. Interfaces 8 (2016) 15598–15606.

A novel hypercrosslinked polymer of poly-Pillar 5 quinone (Poly-P5Q) was applied as the electrode material to Li-Bs. The Poly-P5Q cathode's initial discharge capacity was up to 105 mAh/g while 82.3% of its initial discharge capacity was maintained in the theoretical window between 1.75 and 3.25 V after 100 charge-discharge cycles [60].

In addition, a versatile composite of $NH_4V_4O_{10}$@PPy@MnO_2 nanowire arrays was manufactured for use in Li-Bs as an electrode material. The experimental results showed that the nanowire arrays of $NH_4V_4O_{10}$@PPy@MnO_2 had better electrochemical efficiency than the nanowire arrays of $NH_4V_4O_{10}$/$NH_4V_4O_{10}$@PPy. The conductive PPy shell effectively tolerated the volume shift resulting from the insertion/deinsertion of Li^+ into the electrode material and prevented the $NH_4V_4O_{10}$ from detaching and agglomerating at the $NH_4V_4O_{10}$ core during cycling [61]. The fabrication of the $NH_4V_4O_{10}$@PPy@MnO_2 nanowire array on a Ti film is shown in Fig. 12.4.

In another study, N-substituted naphthalene tetra carboxylic diimide (NTCDI) was used in lithium half-cells as a positive electrode active material. These two NTCDI products have a fairly steady electrochemical behavior after cycling at a mean potential of 2.3 V vs Li^+/Li^0, resulting in 147 mAh/g and 113 mAh/g specific capacity values for dicarboxylate and disulfonate derivatives, respectively [62].

Hu et al. reported a hierarchical PMo_{12}/PANI/MWNT nanocomposite material as an anode material in Li-Bs. It showed an inclusive discharge capacity of 1000 mAh/g for 100 cycles at a current density of 0.5 mA/cm^2. The synergistic effect of PMo_{12}, PANI, and MWNTs has been described as the main component responsible for improving the discharge and rate capacity as well as improving the overall stability [63].

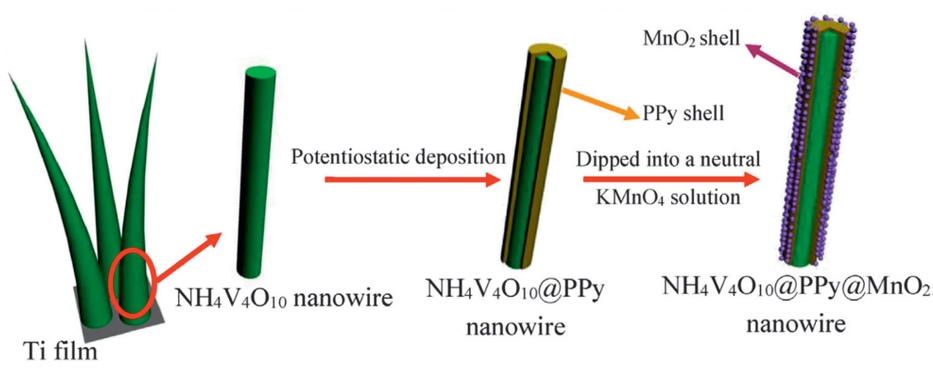


Fig. 12.4 Fabrication of $NH_4V_4O_{10}$@PPy@MnO_2 nanowires array on Ti film. Reproduced with permission C. Wang, H. Liu, M. Jiang, Y. Wang, R. Liu, Z. Luo, X. Liu, W. Xu, C. Xiong, D. Fang, Ammonium vanadate@ polypyrrole@ manganese dioxide nanowire arrays with enhanced reversible lithium storage, Appl. Surf. Sci. 416 (2017) 402–410.

In another work, the three-dimensional (3D) composite EG-SnO_2-PANI (expanded graphite) was developed by means of a solvothermal process, monitored by in situ oxidative polymerization. The rate efficiency and cycle stability of the EG-SnO_2-PANI sample were advanced in combination with pristine SnO_2 and EG-SnO_2 samples. As a result, at a current density of 0.1 A/g, the 3D EG-SnO_2-PANI not only provided a greater primary columbic efficiency of 77.8% and an outstanding preliminary reversible power of 1021 mAh/g, but also retained at 408 mAh/g after 100 cycles [64].

Another work represented, 1,4-diaminoanthraquinone (14DAAQ) and *p*-phthalaldehyde (PPD), an extremely conjugated Schiff polymer base (PSB). At a current density of 10 mA/g, PSB exhibited a reversible basic capacity of 175 mAh/g. In addition, cycling stability with 90% power retention was preserved after 100 cycles [65]. The synthetic protocol and SEM images of the final product are shown in Fig. 12.5.

In another work, CNTs were embedded with PEDOT:PSS conducting polymer aerogels. Using iron(III) chloride hexahydrate as crosslinkers, these aerogels were prepared. The effects of CNTs and their electrochemical efficiency on aerogel morphology were also investigated. The increase in CNT content has been found to offer improved electrochemical efficiency with a specific capacitance of 35 F/g and a cycling stability of more than 1000 cycles [66].

Wang et al. developed two new porous organic frameworks using hexaazatrinaphthalene (HATN) cores as cathode materials for Li-Bs. HATNPF polymers, an enhancement over earlier described porous organic polymers and HATN monomers, have demonstrated high specific capacity (309 mAh/g) and excellent long-term cycling stability [67].

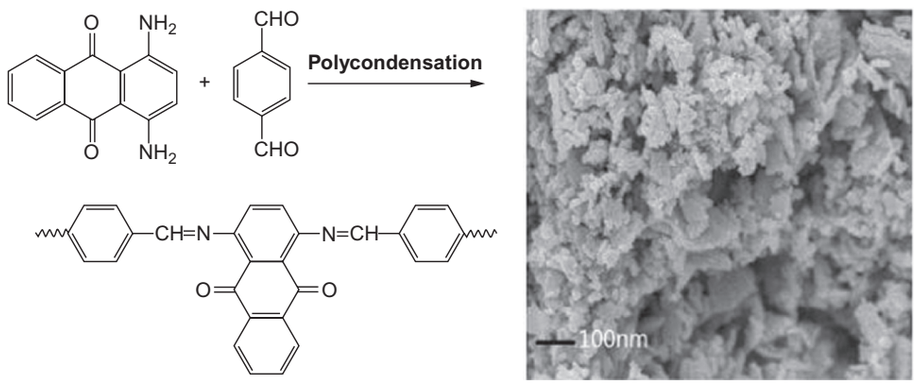


Fig. 12.5 Synthetic route of; (A) SSB; and (B) SEM images of SSB. Reproduced with permission F.J. Haijun Yea, L. Hongqin, X. Zheng, Y. Jiao, Z. Hui, Facile synthesis of conjugated polymeric Schiff base as negative electrodes for lithium ion batteries, Electrochim. Acta 253 (2017) 319–323.

By chemical oxidative polymerization, mesoporous interlinked polymer-Poly (4,4′,4″-tris(*N*,*N*-diphenyl-amino) triphenylamine) (PTDATA) was prepared. PTDATA showed a well-defined multistage discharge voltage plateau and an improved capacity of 133.1 mAh/g when studied as the cathode material for organic free radical batteries, which was equal to 92% of its theoretical capacity (143.5 mAh/g) [68].

A series of hydrogel alginate (alg) binders for the Si anode of Li-Bs was obtained by coordinating alginate molecule chains with dissimilar cations. The Si anodes with Al-alg or Ba-alg both delivered their power to around 2100 mAh/g after 300 cycles at 420 mA/g [69].

By adapting a simple synthetic process prepared with 2,6-dibromo-*N*,*N*′-bis(2-ethylhexyl)-1,4,5,8-naphthalene diimide and (*E*)-1,2-bis(tributylstannyl) ethene via the Stille coupling reaction, a large flat-conjugated copolymer poly[ethylene-*N*,*N*′-bis(2-ethylhexyl)-1,4,5,8-naphthalene diimide] (PENDI) was synthesized. The results of the electrochemical production showed that the reversible power of PENDI can be maintained at 85% of its original theoretical capacity [70].

In another research, two types of naphthalene-based polyimide derivatives were successfully engineered by the condensation polymerization of NT with two different diamines. At 20 mA/g, with an average discharge power of 174.5 mAh/g, a high value of 133.5 mAh/g at 500 mA/g and a strong cycle stability of 153 mAh/g at 50 mA/g after 60 cycles were observed [71].

A nitrogen-doped porous carbon nanoparticle (NPCN) resulted in another work by pyrolyzing nitrogen comprising conjugated microporous polymer nitrogen (NCMP). BET research has shown that the NPCN-specific KOH surface area is 1845 $m^2 g^{-1}$, considerably greater than NPCN. In addition, the KOH NPCN has the ability to cycle at 1°C for 600 cycles, which is extraordinary as 527 mAh/g, with a 97.6% power retaining ratio [72]. Fig. 12.6 demonstrates the cycling efficiency of the NPCN and NPCN-KOH.

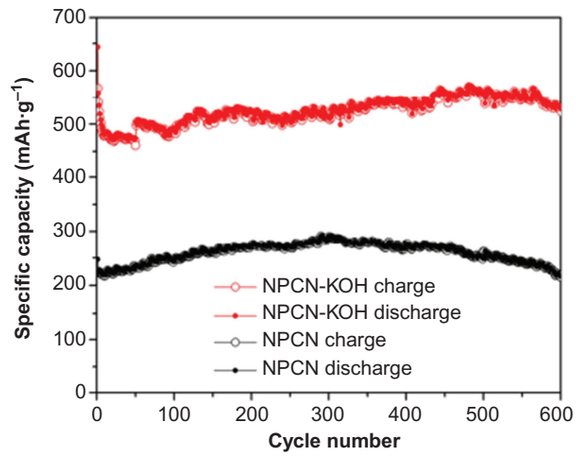


Fig. 12.6 Cycling performance of NPCN and NPCN-KOH. Reproduced with permission Q. Zhang, Q. Dai, C. Yan, C. Su, A. Li, Nitrogen-doped porous carbon nanoparticle derived from nitrogen containing conjugated microporous polymer as high performance lithium battery anode, J. Alloys Compd. 714 (2017) 204–212.

Jin et al. developed a simple hydrothermal system, chemical solution, and sintering process through which they successfully manufactured MnO_x/Fe_2O_3 NTs through three phases. At a current density of 200 mA/g, the MnO_x/Fe_2O_3/PPy NT electrode showed a discharge capacity of 1060 mAh/g after 100 cycles, which is far greater than that of the bare MnO_2, MnO_x/Fe_2O_3, and MnO_2/PPy NT electrodes [73].

Xu et al. produced PPy-co-PPy-C-TEMPO single-step electrodes synthesized by in situ electrochemical polymerization. They had a discharge capacity of 62.6 mAh/g

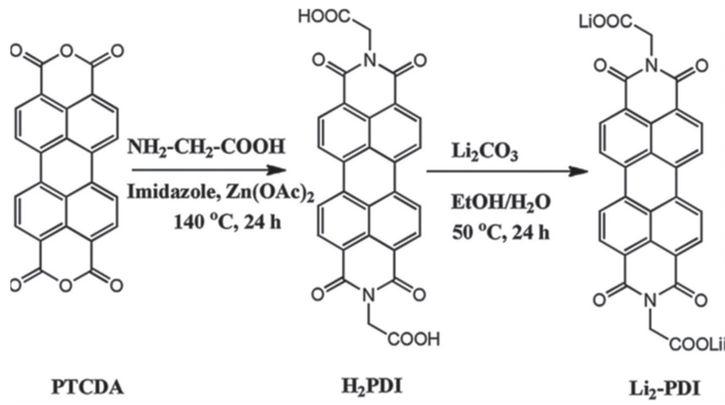


Fig. 12.7 Synthetic protocol of Li_2-PDI. Reproduced with permission M. Veerababu, R. Kothandaraman, Rational functionalization of perylene diimide for stable capacity and long-term cycling performance for Li-ion batteries, Electochim. Acta 232 (2017) 244–253.

compared to the pure PPy electrode while PPy-co-PPy-C-TEMPO (4:1) had a discharge capacity of up to 70.9 mAh/g. The use of in situ electrochemical polymerization in the existence of a functional monomer enclosed in TEMPO may be due to the improved discharge capability [74].

In this report, *N*,*N*′-bis (glycinyl) perylene diimide (Li_2-PDI) perylene-based dilithium salt was synthesized; the synthetic protocol is shown in Fig. 12.7. The $-CH_2-COO-Li$ modification of perylene diimide is a modest approach to lessen the dissolution of the monomer in the electrolyte. The Li_2-PDI electrode exhibited excellent capacity retention behavior at a current density of 17 mA/g, which is 98% of the theoretical specific capacity, and gave a stable specific capacity of 101 mAh/g even after 100 cycles [75].

Lin et al. well-defined 2D single-layer hole conjugated polymers (HCP). Due to the synergistic impact of better porosity, hetero atomic doping, and the virtuous dispersity of NGHCP nanosheets, they are appropriate as exceptional anode materials for Li-Bs. The designed material showed a greater reversible ability of 1320 mAh/g (at 20 mA/g), a reasonable performance rate, and an outstanding cycle life for more than 600 cycles with an approximate 100% Coulombic efficiency [76].

Ma et al. formed PTCDA composites of MnO and carbon pyrolysis synthesized through simple adsorption of Mn^{2+} on 3,4,9,10-perylene tetracarboxylic dianhydride (PTCDA), trailed by thermal annealing. In this work, the used anode materials for Li-Bs, electron transport, and cycling stability were encouraged by this interesting and novel construction. A responsive reversible capacity of 1066 mAh/g was retained after 100 cycles under the current density of 100 mA/g [77].

In another part of the work, maleic acid was also tried as the anode for lithium ion batteries without alteration. It showed an ultrahigh reversible capacity of 1500 mAh/g at 46.2 mA/g current density.

The electrode still delivers a power of 570.8 mAh/g, also at a high current density of 46.2 A/g. After 500 cycles, power retention of 98.1% is achieved after cycling at 2.31 A/g [78].

Lyu et al. developed composites based on aromatic polyimide (PI) as extremely conductive graphene for application in Li-Bs. In addition to a better reversible capacity of 232.6 mAh/g at a C/10 charge-discharge rate, the synergistic behavior among PI and graphene has allowed extremely high cycle stability [79].

In this work, a conjugated porous polymer (CPP-1) and carbonized porous material (CPP-1-C) of boron dipyrromethene (BODIPY) were synthesized and characterized by doping with hetero atoms to boost the property of Li-ion storage. In Li-Bs, CPP-1 and CPP-1-C were then tried as anode materials. Long-term cyclical output at 0.1 and 1 A/g was achieved with a simple capacity of 273.2 mAh/g at 0.1 A/g after 100 cycles and 250.8 mAh/g at 1 A/g after 300 cycles. These findings showed that as next-generation electrode materials, BODIPY-based CPPs could be ideal [80].

A novel, thiophene-rich conjugated microporous polymer of poly tetra (2-thienyl) ethylene (PTTE) was synthesized and used as an anode material for Li-Bs via $FeCl_3$-catalyzed oxidative polymerization. The assembled Li-Bs showed a superior specific capacitance of 973 mAh/g at 100 mA/g with an outstanding level of efficiency, exceptional degree capability, and better cycling stability [81].

Xu et al. designed a simple one-pot reaction using two isomeric pairs of poly (anthraquinonyl imide)s (PAQIs) and investigated their electrochemical properties as Li-B cathodes. The PAQI materials have demonstrated a high reversible capacity of 202 mAh/g and constant cyclability, with a capacity retention of 80% over 200 cycles and a significant efficiency speed [82].

Wei et al. fabricated an anode material for Li-Bs using $FeCl_3$-promoted oxidative coupling polymerization; this formed indole-based conjugated microporous poly (bis-indolyl maleimide) (PBIM) with higher electrochemical efficiency. High capacity (1172 mAh/g, 50 mA/g), excellent cycle life (1000 cycles), and improved rate efficiency (214 mAh/g, 2.5 C C) were shown by the prepared PBIM anode, aided by the reversible cation-π interaction and unique aromatic structure containing the N-heteroatom [83].

In another analysis, the combination of emulsion polymerization and the subsequent Friedel-Crafts reaction formed hypercross-connected polystyrene (HPS) nanospheres. The initial discharge and charge capacities of HPS were 533 and 262 mAh/g while a constant capacity of 356 mAh/g was supplied at 0.2 A/g for 100 times after repeated charge-discharge. The capability remained at 222 mAh/g even when cycled 1000 times at 2 A/g [84].

A new, thiophene-rich conjugated microporous polymer of poly tetra(2-thienyl)ethylene (PTTE) was also synthesized and discovered

as an anode material for Li-B applications using $FeCl_3$-catalyzed oxidative polymerization. The assembled Li-Bs had a superior specific capacitance of 973 mAh/g at 100 mA/g after 100 cycles with outstanding speed performance [81].

Shen et al. developed a thin flexible nanofiber paper electrode of solid-state supercapacitors by combining the beneficial features of exceedingly well-arranged conductive polymer chains of polyethylene dioxythiophene (PEDOT). This versatile, symmetrical supercapacitor system assembled with paper electrodes displayed a specific volumetric capacitance of approximately 106.3 F cm^{-3}, a current density of 0.83 A cm^{-3}, and excellent cyclic stability [85].

12.3.2 Conjugated polymers as electrode materials for supercapacitors

The honeycomb-shaped nanocomposites of graphene oxide/polyaniline/metal hydroxide (GO/PANI/metal hydroxide) with nickel or cobalt ions were obtained by in situ polymerization in one stage. The electrochemical results of this work indicated that the exact capacitance of the composite was 743 F/g. At a 20 mA current, the Cp and Ep of the supercapacitors were found to be 26.45 F/g and 3.56 Wh/kg, respectively. This hybrid supercapacitor exhibited excellent life cycle measurements, with a degradation capacitance of 15.6% over 2000 cycles [86].

Nanocomposites were obtained via the in situ polymerization of a 3D interconnected honeycomb structure with porous nitrogen-doped carbon (HPC)/polyaniline (PANI) nanowire arrays. The well-organized PANI nanowire arrays associated both on the interior and exterior surface of the porous HPC demonstrated a high specific capacitance of 1080 F/g. The integrated asymmetric supercapacitor based on HPC/PANI and HPC had a better energy density value of approximately 60.3 Wh/kg and a power density value of approximately 18 Wh/kg, with a strong cyclic constancy of 91.6% specific capacitance, in a neutral aqueous solution [87].

In another study, the core-shell structures of MWCNT@MnO_2@PPy were analyzed as a standard protocol for the abundant production of electrodes toward supercapacitor applications. The relative concentration of CNTs in this composite was changed to optimize the double-layer capacitance. The obtained structures exhibited capacitance on the order of 272.7 F/g, with a reasonable cyclic performance [88].

A successful approach was developed toward the fabrication of core-shell nanocomposites of NiO/PANI-MWCNT by two stages of in situ polymerization. The core-shell structure and the surface behavior of the nanocomposites were confirmed using TEM and SEM analysis.

The specific capacitance of this material with 7% of MWCNT was found to be 356.54 F/g [89].

In another work, a poly (3,4-ethylene dioxythipohene) (PEDOT) hybrid with the carbon-based material graphene oxide (GO) was synthesized by the electrochemical process. In this study, the moderate electropolymerization potential was found to upshot in a higher definite capacitance of 115.15 F/g by an energy density of 13.60 Wh/kg and a power density of 139.09 W/kg at a current density of 0.3 A/g [90].

Free-standing carbon nanofibers/carbon nanotubes/polyaniline (CNFs/CNTs/PANI) ternary combinations were efficiently developed in another study. As anticipated, the ternary combinations as electrodes showed superior specific capacitance (315 F/g at 1 A/g), intense rate capacity (235 F/g at 32 A/g), high energy/power density (5.1 Wh/kg at 10.1 kW/kg), and notable cycling constancy (91% capacitance retention after 10,000 cycles at 2 A/g), as expected [91]. Fig. 12.8 shows the cycling stability and efficiency of the Coulomb system.

The poly(*N*-methyl-3,4-dihydrothieno[3,4-*b*][1,4]oxazine) (PMDTO) and novel nitrogen poly(3,4-ethyl-endioxythiophene) (PEDOT) analogues were obtained. This work showed that at a discharge current density of 3 A/g, the as-prepared PMDTO electrode had a definite capacitance of 154.3 F/g and exhibited cycling constancy at a high current density of 10 A/g with a maximum capacitance retention of nearly 71% for the next 500 cycles [92].

RGO-I was an important 2D template in this study for the progression of porous CMPs on the graphene surface. The G-CMPs might easily be transformed into porous carbon materials by thermal carbonization while preserving their 2D morphology. As electrode materials for supercapacitors, the carbonized hybrid materials were tested, resulting in a maximum energy of 9.3 Wh/kg and a power compactness of 9581 W/kg [93].

In another study, PEDOT nanodendrites and nanospheres were synthesized. With a specific capacitance of 284 F/g with a superior energy density of 39.44 Wh/kg and outstanding cycling constancy, which is among the maximum described to date, the PEDOT nanodendrites obtained were potentially tested as supercapacitor electrodes [94].

Current work has shown the efficiency of electropolymerized polypyrrole (e-PPy) supercapacitors, which have ultrahigh capacitance retention rates of more than 97%, 91%, and 86% after 15,000, 50,000, and 100,000 charging/discharging cycles,

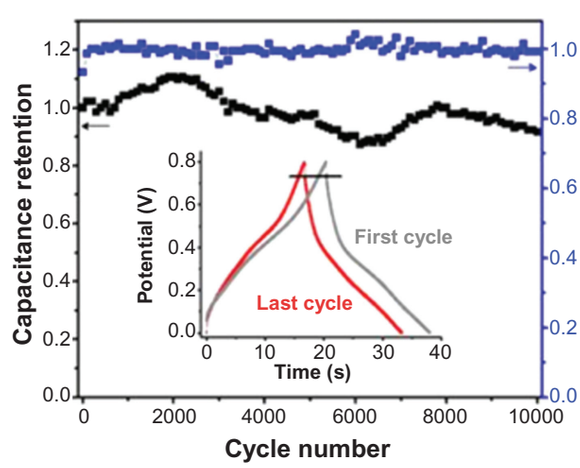


Fig. 12.8 Cycling stability and Coulomb efficiency of the device. Reproduced with permission F. Miao, C. Shao, X. Li, K. Wang, N. Lu, Y. Liu, Electrospun carbon nanofibers/carbon nanotubes/polyaniline ternary composites with enhanced electrochemical performance for flexible solid-state super capacitors, ACS Sustain. Chem. Eng. 4 (2016) 1689–1696.

respectively. They could also withstand more than 230,000 charge/discharge cycles, with around half of the initial capacitance still retained [95].

Tang et al. developed an easy method for preparing composites of $FeCl_3$-doped PANI/SSCNTs (PANI/SSCNTs/Fe^{3+}) as a superelectrode with remarkable enactment. In the designed nanocomposite, the role of Fe^{3+}-doped PANI is to form a charge transfer complex and confirm a greater specific capacitance of 727 F/g [96].

In another analysis, through the oxidative polymerization of pyrrole in an aqueous Ag^{+} comprising solution, spherical silver-incorporated conductive PPy composites were primed in the existence of trisodium citrate. The charge-discharge amounts showed a determined exact capacitance of 315.8 F/g for the Ag/PPy electrode, greater than that of the pristine PPy electrode [97].

A high-performance polyaniline-based electrode material doped with graphene oxide sheets was manufactured by oxidative in situ polymerization. The gap in the PA/GO composite band was reduced from 2.06 to 1.94 eV and the gap in the electrochemical band declined from 2.94 to 2.17 eV (1%, 3%, and 5%). In comparison to the conductivity of pristine PA (0.075 S/m), composite electrical conductivity improved starting 47 to 84 S/m, with an increase in GO and temperature respectively [98].

Another research showed the oxidative chemical and electrochemical polymerization of EDOT in the presence of lignin sulfonate by PEDOT/lignin biocomposites. In addition, after 1000 charge/discharge cycles, PEDOT/lignin was a highly stable biocomposite, maintaining about 83% of its electroactivity. These findings demonstrated that the redox doping approach was a simple and straightforward way to boost PEDOT electroactive efficiency [99].

In another part of the work, due to the synergetic effect of the PPy@$MnMoO_4$ components, PPy produced superior capacitance, even through thousands of charge-discharge cycles; the $MnMoO_4$ nanorods helped to increase the stability of PPy. The strong synergetic effect enabled the MMP2 to display a greater particular capacitance of 374.8 F/g at a current density of 0.2 A/g and durable cycling stability [100].

For instance, the in situ decrease of graphene oxide in the existence of PPy NTs, as spacers, by nanocomposites of reduced graphene oxide (RGO) nanosheets and PPy NTs was obtained. With the rise in RGO feeding, the actual capacitance progressively increased to 281 F/g. At 1000 cycles, the capacitive retention was nearby 77.28% of the initial capacitance. Using PPy NT as spacers, the surface area of RGO nanosheets achieved a determined energy compactness of 39 Wh/kg and a power density of 3105 W/kg using RGO nanosheets [101].

Other electrochemical studies have shown that the basic capacitance of RGO-g-NPAN hybrids for conventional physical mixtures is 654.3 F/g at 1 A/g and 418.5 F/g at 1 A/g. The covalent grafting hybrids

could also decrease the interface resistance between RGO and NPAN polymers to increase the transfer of charge in the NPAN phase of faradaic transformation. The basic capacitance of the RGO-g-NPAN-based capacitor maintained 79% of its initial capacitance under 1000 successive charge/discharge cycles while the typical physical mixture showed 67% of its initial capacitance, indicating a strong cycling stability for RGO-g-NPAN hybrids [102].

In aqueous symmetric supercapacitors, conjugated ladder polymers constructed on phenoxazine have been synthesized. The acid-induced polymer prominently outperformed the inherent ones due to virtuous hydrophilicity and impeccably supported conjugation. It realized a precise capacitance of 311 F/g with an energy density of 10.1 Wh/kg at a current density of 1 A/g in an aqueous sulfuric acid electrolyte [103].

In another research, gadolinium oxide (Gd_2O_3) was obtained by the pulse electrochemical method and hybrid poly (*o*-aminophenol) (POAP)/Gd_2O_3 films were then manufactured as active electrodes by the electropolymerization of *o*-aminophenol (OAP) in the *manifestation* of Gd_2O_3 nanoparticles. Surface and electrochemical tests were used to classify composite films containing Gd_2O_3 and POAP/Gd_2O_3. The specific composite film capacitance, specific energy, and specific power were determined to be 300 F/g, 41.66 Wh/kg, and 833.22 W/kg, respectively [104].

An easy methodology for the development of binder-free PANI and PANI-CNT nanofiber electrodes was obtained in other work. A particular capacitance of up to 385 F/g was disclosed by the formed electrodes. By combining low electrochemical impedance and noble inter- and intrafiber porosity, the high electrochemical performance of the manufactured electrode facilitated ion diffusion to the PANI active sites [105].

A new b-ketoenamine conjugated microporous polymer (KECMP) was produced with condensation among 1,3,5-triformyl-phloroglucinol and *m*-phenylenediamine without a template via Schiff base microwave-assisted condensation. The resulting KECMP demonstrated a better retention capacity potential of up to 200 A/g [106].

For the coating of poly(3,4-ethylenedioxythiophene)-poly(styrenesulfonate) (PEDOT:PSS) on an MWCNT thin film, a quick and cost-effective "dip and dry" approach was shown in another work. The electrochemical output of the electrode PEDOT:PSS/MWCNT was evaluated using the techniques of cyclic voltammetry and galvanostatic charge-discharge. Within the 0–0.9 V potential range of 1 M aqueous H_2SO_4 electrolytes, a precise capacitance of 235 F/g at 5 mV s^{-1} was achieved [107].

In another part of the work, fullerene C60 whisker (FW)/polyaniline emeraldine base (PANI-EB) composites were synthesized by directly mixing the FW toluene suspension and the PANI-EB/*N*-methyl-2-pyrrolidone colloid. The execution of FW/PANI-EB derived from these

systems showed superior exact capacitance (813 F/g at current density 1 A/g), short electrical resistance, and better cycling stability [108].

For flexible energy storage applications, a flexible 2D molybdenum disulfide (MoS_2)-based electrode was tested. MoS_2 is a durable hybrid film integrated with high PEDOT:PSS. This film has outstanding mechanical properties with a breakage strength of 18.0 MPa and a Young's modulus of 2.0 GPa. After 5000 charge/discharge cycles, it can provide a wide 141.4 F cm^{-3} volumetric capacitance and a high 4.9 mWh cm^{-3} volumetric energy density [109].

The development of standalone polyaniline (PANI)-based film electrodes with polyvinyl chloride (PVC) and aniline reformed PVC (PVC-An) films as elastic substrates was designed by Wang et al. The PVC-g-PANI film with a loose surface affected improved large concert due to the embedding of PANI from the PVC-An film as substrate, correlated with superior precise capacitance 645.3 F/g at a current density of 1 A/g, strong capacitance holding 63.2% of the inventive value at a current density of 10 A/g and 52.0% at a scan rate of 100 mV s^{-1}, with reasonable cycle stability [110]. Fig. 12.9 displays the fabrication aspect of the flexible PVC-g-PANI.

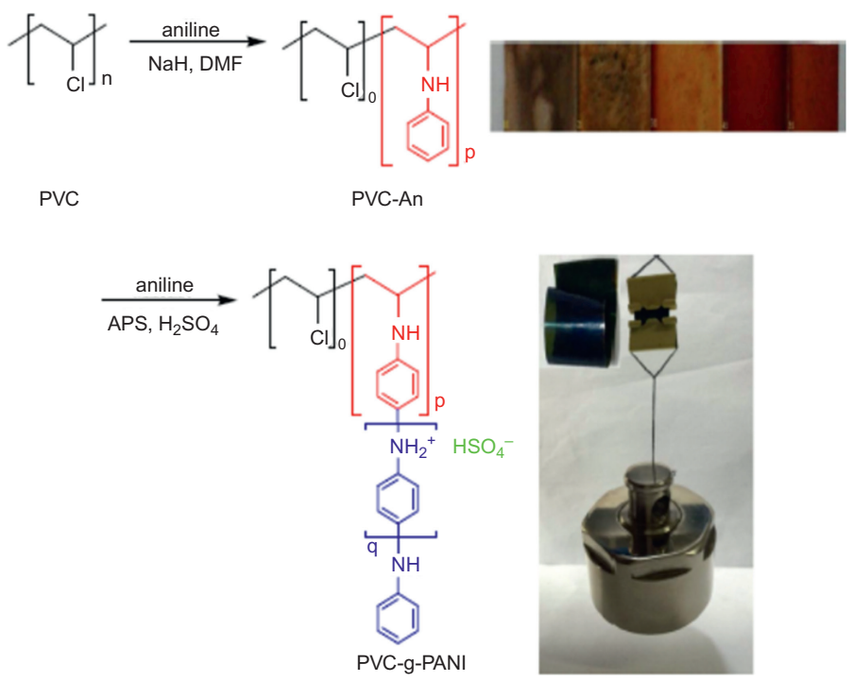


Fig. 12.9 Illustration of the fabrication of flexible PVC-g-PANI. Reproduced with permission H. Wang, D. Liu, P. Du, W. Wei, Q. Wang, P. Liu, Comparative study on polyvinyl chloride film as flexible substrate for preparing free-standing polyaniline-based composite electrodes for super capacitors, J. Colloid Interface Sci. 506 (2017) 572–581.

Das et al. designed electrochemically 2D π-conjugated covalent organic frameworks (COFs) for high-fperformance supercapacitor applications. These COFs were constructed based on the periodic organization of organic building blocks. By utilizing the solvothermal Schiff base condensation process, porous π-conjugated TFP (1,3,5-triformylphloroglucinol)-NDA (1,5-diaminonaphthalene)-COF (TFP-NDA-COF) was prepared. The designed COFs showed an energy packing of up to 379 F/g at a 2 mV s^{-1} scan rate, 348 F/g at 0.5 A/g, and after 800 charge discharge cycles, an outstanding specific capacitance of 75% [111]. The cyclic routine of TFP-NDA-COF is shown in Fig. 12.10.

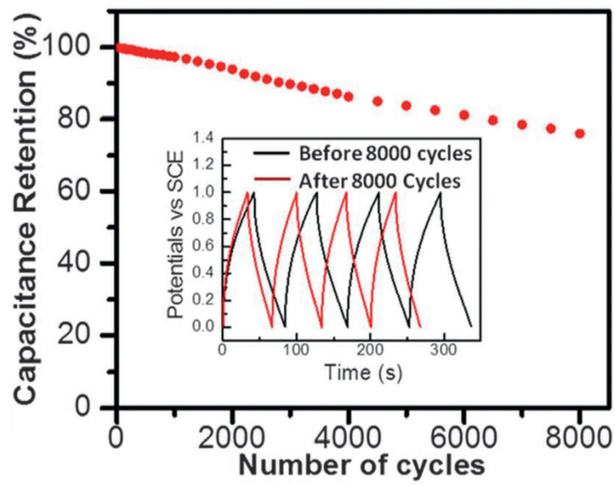


Fig. 12.10 Cyclic performance of TFP-NDA-COF. Reproduced with permission S.K. Das, K. Bhunia, A. Mallick, A. Pradhan, D. Pradhan, A. Bhaumik, A new electrochemically responsive 2D π-conjugated covalent organic framework as a high performance super capacitor, Microporous Mesoporous Mater. 266 (2018) 109–116.

In other studies, reduced graphene oxide (rGO), Ag nanoparticles, and polythiophene (PTh) ternary nanocomposites with diverse initial feeding ratios of 0.2, 0.3, and 0.4, respectively, were reported. The preparation of nanocomposites was through in situ polymerization and the chemical reduction of rGO. Better capacitive efficiency with a high specific capacitance in acid electrolyte solution (953.13 F/g at 4 mV s^{-1} scan rate) was shown by the electroactive nanocomposite material (0.2 feed ratio). It also demonstrated elevated strength with 91.88% detailed capacitance after 1000 charge/discharge cycles as well as important energy density (28.8 Wh/kg at 5 mV s^{-1} scan rate) and power compactness (2843.3 W/kg at 1000 mV s^{-1} scan rate) [112].

In this research, carbon film prepared from electrochemically synthesized poly(3,4-ethylenedioxythiophene) (PEDOT) film and carbon film arranged from chemically synthesized polyacetylene (PA) film demonstrated highly ordered porous structures with granule and fibril morphologies. The average electrical conductivity of the carbonized PEDOT and PA films at 1100°C was 2.1 S cm^{-1} and 9.9 S cm^{-1}, respectively [113].

For high-performance electrodes using in situ polymerization, a highly ordered PANI nanocone on bare GO. The schematic representation of the GO-PANI hybrid is shown in Fig. 12.11. The basic electrode capacitance systems was as great as 481 F/g at a current density of 1 A/g. The distinctive assembly of PANI showed additional charge transmission trails, rapid charge allocation, and quickness of electrons to the bare GO due to its wide surface area manifested to the electrolyte [114].

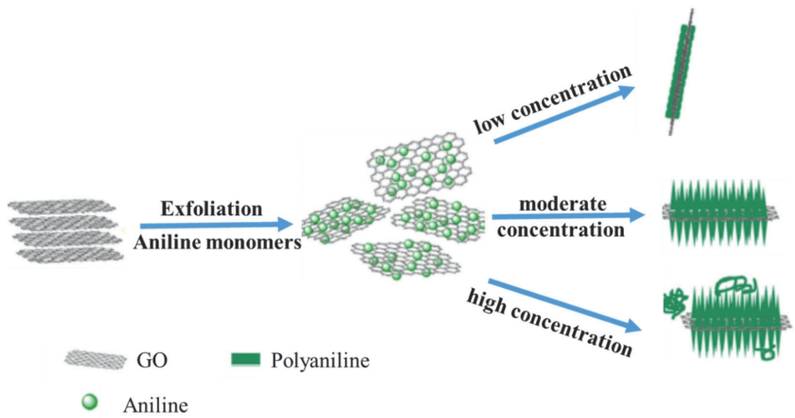


Fig. 12.11 Schematic representation of GO-PANI hybrid preparation. Reproduced with permission N. Song, W. Wang, Y. Wu, D. Xiao, Y. Zhao, Fabrication of highly ordered polyaniline nanocone on pristine graphene for high-performance super capacitor electrodes, J. Phys. Chem. Solids 115 (2018) 148–155.

In another work, Wang et al. developed PANI spheres in two different approaches. In this work, identical poly (methyl methacrylate-butyl methacrylate-methacrylic acid) (PMMA-PMBA-PMAA) microspheres obtained as self-sacrificial templates by the emulsion polymerization technique were reported. The developed H-PANI unveiled a particular capacitance of 485.5 F/g at 1 A/g and around 60% of performance was retained in spite of 500 cycles [115].

12.4 Conclusions and future directions

In this chapter, we discussed the latest developments of CPs alone and CPs combined with other materials as promising electrode materials for Li-ion and supercapacitor applications. The potential of the conjugated polymers is well known due to the ease of processability, flexibility, and exciting morphologies. Further, conjugated polymers are combined with other efficient materials such as GO, RGO, $MnCO_2O_4$, MnO_2, SnO_2, MWCNT, MnO, Fe_2O_3, NiO, carbon nanofibers, fullerene C60 whiskers, MoS_2, and lignin for the effective interaction of one component with another, which leads to synergistic properties and improved results. In addition, the electrochemical performances such as specific capacity, cyclic stability, and Coulombic efficiency are precisely elucidated. Finally, in the near future, we believe that this chapter will encourage material scientists, electrochemists, and engineers to further advance conjugated polymers for high-performance, next-generation Li-Bs and supercapacitor applications.

Acknowledgments

The authors greatly thank DST Nanomission, India (SR/NM/NS-20/2014); DST, India (DST-TM-WTI-2K14-213); and DST, India (DST/BDTD/EAG/2019) for financial support. Prof. Ho-Young-Jung acknowledges financial support from Chonnam National University (Grant number: 2018-3274), South Korea.

References

[1] N.S. Lewis, Research opportunities to advance solar energy utilization, Science 351 (2016) 1920.
[2] C.P. Grey, J.M. Tarascon, Sustainability and in situ monitoring in battery development, Nat. Mater. 16 (2016) 45–56.
[3] D. Larcher, J.M. Tarascon, Towards greener and more sustainable batteries for electrical energy storage, Nat. Chem. 7 (2015) 19–29.
[4] P.B. Tchounwou, C.G. Yedjou, A.K. Patlolla, D.J. Sutton, Heavy metal toxicity and the environment, Exp. Suppl. 101 (2012) 133–164.
[5] X. Lu, M. Yu, G. Wang, Y. Tong, Y. Li, Flexible solid-state super capacitors: design, fabrication and applications, Energy Environ. Sci. 7 (2014) 2160.
[6] M.S. Park, J. Kim, K.J. Kim, J.W. Lee, J.H. Kim, Y. Yamauchi, Porous nanoarchitectures of spinel-type transition metal oxides for electrochemical energy storage systems, Phys. Chem. Chem. Phys. 17 (2015) 30963–30977.
[7] B. Anothumakkool, S. Bhange, R. Soni, S. Kurungot, Novel scalable synthesis of highly conducting and robust PEDOT paper for high performance flexible solid-super capacitor, Energy Environ. Sci. 8 (2015) 1339–1347.
[8] D. Dubal, O. Ayyad, V. Ruiz, P. Gómez-Romero, ChemInform abstract: hybrid energy storage: the merging of battery and super capacitor chemistries, Chem. Soc. Rev. 44 (2015) 1777–1790.
[9] J. Kim, C. Young, J. Lee, Y.P. Heo, M.S. Park, S. Hossain, Nanoarchitecture of MOF-derived nanoporous functional composites for hybrid super capacitors, J. Mater. Chem. A 5 (2017) 15065–15072.
[10] M. Armand, J.M. Tarascon, Building better batteries, Nature 451 (2008) 652–657.
[11] V.R. Stamenkovic, D. Strmcnik, P.P. Lopes, N.M. Markovic, Energy and fuels from electrochemical interfaces, Nat. Mater. 16 (2016) 57–69.
[12] T.B. Schon, B.T. McAllister, P.F. Li, D.S. Seferos, The rise of organic electrode materials for energy storage, Chem. Soc. Rev. 45 (2016) 6345–6404.
[13] N. Casado, G. Hernandez, H. Sardon, D. Mecerreyes, Current trends in redox polymers for energy and medicine, Prog. Polym. Sci. 52 (2016) 107–135.
[14] M.J. Taghizadeh, S. Afghihi, H. Saidi, Superhydrophobic surface based silica nanoparticle modified with diisocyanate and short and long normal chain alcohols, Asian J. Nanosci. Mater. 1 (2018) 74–80.
[15] A. Kausar, M. Siddiq, Conducting polymer/graphene filler–based hybrids: energy and electronic applications, in: Polymer Science: Research Advances, Practical Applications and Educational Aspects, Formatex Research Center, 2016.
[16] D.D. Borole, U.R. Kapadi, P.P. Mahulikar, D.G. Hundiwale, Electrochemical behaviour of polyaniline, poly(o–toluidine) and their copolymer in organic sulphonic acids, Mater. Lett. 58 (2004) 3816–3822.
[17] J.A. Dominis, M.G. Spinks, A.P.L. Kane-Maguire, G.G. Wallace, A de-doping/re-doping study of organic soluble polyaniline, Synth. Met. 129 (2002) 165–172.
[18] S.M. Kyu, J.I. Won, R.H. Woo, Flexible polymer battery with conducting polymer as a cathode, Mol. Cryst. Liq. Cryst. Sci. Technol. 316 (2006) 337–340.

[19] J.Z. Wang, S.L. Chou, J. Chen, S.Y. Chew, G.X. Wang, K. Konstantinov, J. Wu, S.X. Dou, H.K. Liu, Paper-like free standing polypyrrole and polypyrrole. LiFePO4 composite films for flexible and bendable rechargeable battery, Electrochem. Commun. 10 (2008) 1781–1784.
[20] J. Wang, S. Chou, H. Liu, G.X. Wang, C. Zhong, S.Y. Chew, H.K. Liu, Highly flexible and bendable free-standing thin film polymer for battery application, Mater. Lett. 63 (2009) 2352–2354.
[21] C. Wang, W. Zheng, Z. Yue, C.O. Too, G.G. Wallace, Buckled, stretchable polypyrrole electrodes for battery applications, Adv. Mater. 23 (2011) 3580–3584.
[22] W. Hu, S. Chen, Z. Yang, L. Liu, H. Wang, Flexible electrically conductive nanocomposite membrane based on bacterial cellulose and polyaniline, J. Phys. Chem. B 115 (2011) 8453–8457.
[23] B. Yue, C. Wang, X. Ding, G.G. Wallace, Polypyrrole coated nylon lycra fabric as stretchable electrode for super capacitor applications, Electrochim. Acta 68 (2011) 18–24.
[24] D. Wei, D.P.J. Cotton, T. Ryhanen, All-solid-state textile batteries made from nano-emulsion conducting polymer inks for wearable electronics, Nanomaterials 2 (2011) 268–274.
[25] K. Bock, Polymer electronics systems-polytronics, Proc. IEEE 93 (2005) 1400–1406.
[26] F.D. Carpi, Electroactive polymer-based devices for e-textiles in biomedicine, IEEE Trans. Inf. Technol. Biomed. 9 (2005) 295–318.
[27] C.Y. Wang, A.M. Ballantyne, S.B. Hall, C.O. Too, D.L. Officer, G.G. Wallace, Functionalized polythiophene-coated textile: a new anode material for a flexible battery, J. Power Sources 156 (2006) 610–614.
[28] L. Nyholm, G. Nystrom, A. Mihranyan, M. Stromme, Toward flexible polymer and paper-based energy storage devices, Adv. Mater. 23 (2011) 3751–3769.
[29] Y.G. Kim, B. Thompson, N. Ananthakrishnan, G. Padmanaban, S. Ramakrishnan, J. Reynolds, Variable band gap conjugated polymers for optoelectronic and redox applications, J. Mater. Res. 20 (2005) 3188–3198.
[30] G. Snook, P. Kao, A. Best, Conducting polymer based super capacitor devices and electrodes, J. Power Sources 196 (2011) 1–12.
[31] S.R. Forrest, The path to ubiquitous and low-cost organic electronic appliances on plastic, Nature 428 (2011) 911–918.
[32] T. Tsutsui, K. Fujita, The shift from “hard” to “soft” electronics, Adv. Mater. 14 (2002) 949–952.
[33] C. Amb, S. Rasmussen, Synthesis of metal thiophenedithiolenes for the production of magnetic conducting polymers, Polym. Prepr. 48 (2007) 128–129.
[34] P. Novak, K. Muller, K.S.V. Santhanam, O. Haas, Electrochemically active polymers for rechargeable batteries, Chem. Rev. 97 (1907) 207–282.
[35] J. Xie, Zhang, Recent progress on rechargeable lithium batteries with organic materials as promising electrodes, J. Mater. Chem. A 4 (2016) 7091–7106.
[36] A.M. Bryan, L.M. Santino, Y. Lu, S. Acharya, J.M. D’Arcy, Conducting polymers for pseudocapacitive energy storage, Chem. Mater. 28 (2016) 5989–5998.
[37] C.R. Mulzer, L. Shen, R.P. Bisbey, J.R. McKone, N. Zhang, H.D. Abruna, et al., Superior charge storage and power density of a conducting polymer-modified covalent organic framework, ACS Cent. Sci. 2 (2011) 667–673.
[38] Q. Zhao, Y. Lu, J. Chen, Advanced organic electrode materials for rechargeable sodium-ion batteries, Adv. Energy Mater. 7 (2017) 1601792.
[39] S. Muench, A. Wild, C. Friebe, B. Haupler, T. Janoschka, U.S. Schubert, Polymerbased organic batteries, Chem. Rev. 116 (2011) 9438–9484.
[40] A. Moliton, R.C. Hiorns, Review of electronic and optical properties of semiconducting π-conjugated polymers: applications in optoelectronics, Polym. Int. 53 (2011) 1397–1412.
[41] G. Klaerner, R.D. Miller, Polyfluorene derivatives: effective conjugation lengths from well-defined oligomers, Macromolecules 31 (1998) 2007–2009.

[42] J. Rissler, Effective conjugation length of π-conjugated systems, Chem. Phys. Lett. 395 (2004) 92–96.
[43] M. Wohlgenannt, X.M. Jiang, Z.V. Vardeny, Confined and delocalized polarons in π-conjugated oligomers and polymers: a study of the effective conjugation length, Phys. Rev. B 69 (2004) 241204.
[44] Q.T. Zhang, J.M. Tour, Alternating donor/acceptor repeat units in polythiophenes, intramolecular charge transfer for reducing band gaps in fully substituted conjugated polymers, J. Am. Chem. Soc. 120 (1998) 5355–5362.
[45] T.M. Higgins, S.H. Park, P.J. King, C. Zhang, N. McEvoy, N.C. Berner, D. Daly, A. Shmeliov, U. Khan, G. Duesberg, V. Nicolosi, J.N. Coleman, A commercial conducting polymer as both binder and conductive additive for silicon nanoparticle-based lithium-ion battery negative electrodes, ACS Nano 10 (2016) 3702–3713.
[46] J. Xie, Z. Wang, P. Gu, Y. Zhao, Z.J. Xu, Q. Zhang, A novel quinone-based polymer electrode for high performance lithium-ion batteries, Sci. China Mater. 59 (2016) 6–11.
[47] J. Chen, Q. Zhang, M. Zeng, N. Ding, Z. Li, S. Zhong, et al., Carboxyl-conjugated phthalocyanines used as novel electrode materials with high specific capacity for lithium-ion batteries, J. Solid State Electrochem. 20 (2016) 1285–1294.
[48] Z.J.Y. Li, M. Lang, C. Zhang, X. Huang, Covalently functionalized graphene by radical polymers for graphene-based high-performance cathode materials, ACS Appl. Mater. Interfaces 8 (2016) 17352–17359.
[49] K.L. Wang, T.H. Kuo, C.F. Yao, S.W. Chang, Y.S. Yang, H.K. Huang, C.J. Tsai, M. Horie, Cyclopentadithiophene-benzoic acid copolymers as conductive binders for silicon nanoparticles in anode electrodes of lithium ion batteries, Chem. Commun. 53 (2017) 1856–1859.
[50] J.R.T. Yuan, W. Zhang, Z. Tan, J. Yang, Z.F. Ma, S. Zheng, Flexible overoxidized polypyrrole films with orderly structure as high-performance anodes for Li-ion and Na-ion batteries, ACS Appl. Mater. Interfaces 8 (2016) 35114–35122.
[51] M. Lv, F. Zhang, Y. Wu, M. Chen, C. Yao, J. Nan, D. Shu, R. Zeng, H. Zeng, S.L. Chou, Heteroaromatic organic compound with conjugated multi-carbonyl as cathode material for rechargeable lithium batteries, Sci. Rep. 6 (2016) 23515.
[52] R. Jina, Y. Menga, Y. Maa, H. Lia, Y. Suna, G. Chen, Hierarchical MnCo2O4 constructed by mesoporous nanosheets@polypyrrole composites as anodes for lithium ion batteries, Electrochim. Acta 209 (2016) 163–170.
[53] S.Z.H. Yang, S. Zhang, L. Han, Z. Zhang, Z. Xue, J. Gao, C. Huang, Y. Yi, H. Liu, Y. Li, High conductive two-dimensional covalent organic frame work for lithium storage with large capacity, ACS Appl. Mater. Interfaces 8 (2016) 5366–5375.
[54] S.H. Park, H.J. Kim, J. Lee, Y.K. Jeong, J.W. Choi, H. Lee, Mussel-inspired polydopamine coating for enhanced thermal stability and rate performance of graphite anodes in Li-ion batteries, ACS Appl. Mater. Interfaces 8 (2016) 13973–13981.
[55] M. Chen, A. Wang, W. Li, X. Liu, L. Fu, W. Huanga, Novel self-assembled natural graphite based composite anodes with improved kinetic properties in lithium-ion batteries, J. Mater. Chem. A 4 (2016) 9865–9872.
[56] X. Zhu, X. Liu, W. Deng, L. Xiao, H. Yang, Y. Cao, Perylenediimide dyes as a cheap and sustainable cathode for lithium ion batteries, Mater. Lett. 175 (2016) 191–194.
[57] C. Chae, K.W. Kim, Y.J. Yun, D. Lee, J. Moon, Y. Choi, S.S. Lee, S. Choi, S. Jeong, Polyethylenimine mediated electrostatic assembly of MnO2 nanorods on graphene oxides for use as anodes in lithium-ion batteries, ACS Appl. Mater. Interfaces 8 (2016) 11499–11506.
[58] Y. Wang, L. Zhang, L. Zhang, F. Zhang, P. He, H. Zheng, H. Zhou, Reversible lithium-ion uptake in poly (methylmethacrylate) thin-film via lithiation/delithiation at in situ formed intramolecular cyclopentanedione, Adv. Energy Mater. 6 (2016) 1601375.

[59] X. Du, T. Yang, J. Lin, T. Feng, J. Zhu, L. Lu, Y. Xu, J. Wang, Microwave-assisted synthesis of SnO2@ polypyrrole nanotubes and their pyrolyzed composite as anode for lithium-ion batteries, ACS Appl. Mater. Interfaces 8 (2016) 15598–15606.
[60] A. Ahmad, Q. Meng, S. Melhi, L. Mao, M. Zhang, B.H. Han, K. Lu, Z. Wei, A hierarchically porous hypercrosslinked and novel quinone based stable organic polymer electrode for lithium-ion batteries, Electrochim. Acta 255 (2017) 145–152.
[61] C. Wang, H. Liu, M. Jiang, Y. Wang, R. Liu, Z. Luo, X. Liu, W. Xu, C. Xiong, D. Fang, Ammonium vanadate@ polypyrrole@ manganese dioxide nanowire arrays with enhanced reversible lithium storage, Appl. Surf. Sci. 416 (2017) 402–410.
[62] A.E. Lakraychi, K. Fahsi, L. Aymard, P. Poizot, F. Dolhem, J.-P. Bonnet, Carboxylic and sulfonic N-substituted naphthalene diimide salts as highly stable nonpolymeric organic electrodes for lithium batteries, Electrochem. Commun. 76 (2017) 47–50.
[63] F.J. Jun Hu, Y.F. Song, Engineering high-performance polyoxometalate/PANI/MWNTs nanocomposite anode materials for lithium ion batteries, J. Chem. Eng. 326 (2017) 273–280.
[64] L. Yi, L. Liu, G. Guo, X. Chen, Y. Zhang, S. Yu, X. Wang, Expanded graphite@ SnO2@ polyaniline composite with enhanced performance as anode materials for lithium ion batteries, Electrochim. Acta 240 (2017) 63–71.
[65] F.J. Haijun Yea, L. Hongqin, X. Zheng, Y. Jiao, Z. Hui, Facile synthesis of conjugated polymeric Schiff base as negative electrodes for lithium ion batteries, Electrochim. Acta 253 (2017) 319–323.
[66] H. Cheng, L. Medina, H.M. Duong, Free-standing PEDOT:PSS/CNT aerogels and their electrochemical performance, Mater. Technol. 32 (2017) 622–629.
[67] J. Wang, C.S. Chen, Y. Zhang, Hexaazatrinaphthylene-based porous organic polymers as organic cathode materials for lithium ion battery, ACS Sustain. Chem. Eng. 2 (2017) 1772–1779.
[68] C. Su, H. He, L. Xu, K. Zhao, C. Zheng, C. Zhang, Mesoporous conjugated polymer based on high free radical density polytriphenylamine derivative: its preparation and electrochemical performance as cathode material for Li-ion batteries, J. Mater. Chem. A 5 (2017) 2701–2709.
[69] Z.-Y. Wua, L. Deng, J.-T. Lia, Q.-S. Huang, Y.-Q. Lu, J. Liub, T. Zhanga, L. Huang, S.-G. Sun, Multiple hydrogel alginate binders for Si anodes of lithium-ion battery, Electochim. Acta 245 (2017) 371–378.
[70] H. Zhang, Y. Xie, X. Chen, T. Jia, W. Huang, S. Luo, Q. Hou, R.-H. Zeng, Z. Sun, Naphthalene diimide-ethylene conjugated copolymer as cathode material for lithium ion batteries, J. Electrochem. Soc. 164 (2017) 290–294.
[71] C. Chen, X. Zhao, H.-B. Li, F. Gan, J. Zhang, J. Dong, Q. Zhang, Naphthalene-based polyimide derivatives as organic electrode materials for lithium-ion batteries, Electrochim. Acta 229 (2017) 387–395.
[72] Q. Zhang, Q. Dai, C. Yan, C. Su, A. Li, Nitrogen-doped porous carbon nanoparticle derived from nitrogen containing conjugated microporous polymer as high performance lithium battery anode, J. Alloys Compd. 714 (2017) 204–212.
[73] R. Jin, Q. Wang, H. Li, Y. Ma, Y. Sun, G. Li, Polypyrrole layer coated MnOx/Fe2O3 nanotubes with enhanced electrochemical performance for lithium ion batteries, Appl. Surf. Sci. 403 (2017) 62–70.
[74] L. Xu, C. Zhang, Preparation of TEMPO-contained pyrrole copolymer by in situ electrochemical polymerization and its electrochemical performances as cathode of lithium ion batteries, Ionics 23 (2017) 1375–1382.
[75] M. Veerababu, R. Kothandaraman, Rational functionalization of perylene diimide for stable capacity and long-term cycling performance for Li-ion batteries, Electochim. Acta 232 (2017) 244–253.

[76] Z.Q. Lin, J. Xie, B.-W. Zhang, J.-W. Li, J. Weng, R.-B. Song, X. Huang, H. Zhang, H. Li, Y. Liu, Z.J. Xu, W. Huang, Q. Zhang, Solution-processed nitrogen-rich graphene-like holey conjugated polymer for efficient lithium ion storage, Nano Energy 41 (2017) 117–127.
[77] J. Ma, H. Wang, X. Liu, L. Lu, L. Nie, X. Yang, Y. Chai, R. Yuan, Synthesis of tube shape MnO/Cp composite from 3,4,9,10-perylenetetracarboxylic dianhydride for lithium ion batteries, Chem. Eng. 309 (2017) 545–551.
[78] Y. Wang, Y. Deng, Q. Qu, X. Zheng, J. Zhang, G. Liu, V.S. Battaglia, H. Zheng, Ultrahigh-capacity organic anode with high-rate capability and long cycle life for lithium-ion batteries, ACS Energy Lett. 2 (2017) 2140–2148.
[79] H. Lyu, P. Li, J. Liu, S. Mahurin, J. Chen, D.K. Hensley, G.M. Veith, Z. Guo, S. Dai, X.-G. Sun, Aromatic polyimide/graphene composite organic cathodes for fast and sustainable lithium-ion batteries, ChemSusChem 11 (2018) 763–772.
[80] G. Li, J.-F. Yin, H. Guo, Z. Wang, Y. Zhang, X. Li, J. Wang, Z. Yin, G.-C. Kuang, BODIPY-based conjugated porous polymer and its derived porous carbon for lithium-ion storage, ACS Omega 3 (2018) 7727–7735.
[81] X. Wang, C. Zhang, Y. Xu, Q. He, P. Mu, Y. Chen, J. Zeng, F. Wang, J. Xing, Conjugated microporous polytetra(2-Thienyl)ethyleneas high performance anode material for lithium and sodium-ion batteries, Macromol. Chem. Phys. 219 (2018) 1700524.
[82] F. Xu, H. Wang, M. Wu, J. Nan, T. Li, S. Cao, Electrochemical properties of poly(anthraquinonyl imide)s as high-capacity organiccathode materials for Li ion batteries, Mater. Chem. Phys. 214 (2018) 120–125.
[83] W. Wei, Y. Xua, L. Yang, Indole-based conjugated microporous polymer: a new and stable lithium storage anode with high-capacity and long-life induced by cation-π interaction and N-rich aromatic structure, J. Mater. Chem. A 214 (2018) 120–125.
[84] Z. Li, W. Zhong, A. Cheng, Z. Li, L. Li, H. Zhang, Novel hyper-crosslinked polymer anode for lithium-ion batteries with highly reversible capacity and long cycling stability, Electrochim. Acta 281 (2018) 162–169.
[85] Y. Bu, M. Cao, Y. Jiang, L. Gao, Z. Shi, X. Xiao, M. Wang, G. Yang, Y. Zhou, Y. Shen, Ultra-thin bacterial cellulose/poly(ethylenedioxythiophene) nanofibers paper electrodes for all-solid-state flexible super capacitor supercapacitors, Electrochim. Acta 271 (2018) 624–631.
[86] L. Ma, L. Su, J. Zhang, D. Zhao, C. Qin, Z. Jin, K. Zhao, A controllable morphology GO/PANI/metal hydroxide composite for super capacitor, J. Electroanal. Chem. 777 (2016) 75–84.
[87] P. Yu, Z. Zhang, L. Zheng, F. Teng, L. Hu, X. Fang, A novel sustainable flour derived hierarchical nitrogen-doped porous carbon/polyaniline electrode for advanced asymmetric super capacitors, Adv. Energy Mater. 6 (2016) 1–10.
[88] A.H.P. de Oliveiraa, M.L.F. Nascimento, H.P. de Oliveiraa, Carbon nanotube@MnO2@polypyrrole composites: chemical synthesis, characterization and application in super capacitors, Mater. Res. 19 (2016) 1080–1087.
[89] D. Das, L.J. Borthakur, B.C. Nath, B.J. Saikia, K.J. Mohan, S.J. Dolui, Designing of hierarchical NiO/PAni-MWCNT core-shell nanocomposites for high performance super capacitor electrode, RSC Adv. 6 (2016) 44878–44887.
[90] N.H.N. Azman, H.N. Lim, Y. Sulaiman, Effect of electropolymerization potential on the preparation of PEDOT/graphene oxide hybrid material for super capacitor application, Electochim. Acta 188 (2015) 785–792.
[91] F. Miao, C. Shao, X. Li, K. Wang, N. Lu, Y. Liu, Electrospun carbon nanofibers/carbon nanotubes/polyaniline ternary composites with enhanced electrochemical performance for flexible solid-state super capacitors, ACS Sustain. Chem. Eng. 4 (2016) 1689–1696.
[92] Z. Feng, D. Mo, W. Zhou, Q. Zhou, J. Xu, B. Lu, S. Zhen, Z. Wang, X. Ma, Electrosynthesis and electrochemical capacitive behavior of a new nitrogen PEDOT analogue based polymer electrode, New J. Chem. 40 (2016) 2304–2314.

[93] K. Yuan, T. Hu, Y. Xu, R. Graf, G. Brunklaus, M. Forster, Y. Chen, U. Scherf, Engineering the morphology of carbon materials: 2D porous carbon nanosheets for high-performance super capacitors, ChemElectroChem 3 (2016) 1–8.
[94] M. Rajesha, C.J. Raj, B.C. Kim, R. Manikandana, S.-J. Kim, S.Y. Park, K. Lee, K.H. Yu, Expeditious and eco-friendly hydrothermal polymerization of PEDOT nanoparticles for binder free high performance super capacitor electrodes, RSC Adv. 6 (2016) 110433–110443.
[95] Y. Huang, M. Zhu, Z. Pei, Y. Huang, H. Geng, C. Zhi, Extremely stable polypyrrole achieved from molecular ordering for highly flexible super capacitors, ACS Appl. Mater. Interfaces 3 (2016) 2435–2440.
[96] L. Tang, F. Duan, M. Chen, Fabrication of ferric chloride doped polyaniline/multilayer super-short carbon nanotube nanocomposites for super capacitor applications, J. Solid State Electrochem. 20 (016) (2016) 2805–2816.
[97] L. Yuan, C. Wan, X. Ye, F. Wu, Facial synthesis of silver-incorporated conductive polypyrrole submicron spheres for super capacitors, Electrochim. Acta 213 (2016) 115–123.
[98] S. Konwer, Graphene oxide-polyaniline nanocomposites for high performance super capacitor and their optical, electrical and electrochemical properties, J. Mater. Sci. 27 (2016) 4139–4146.
[99] F.N. Ajjan, T. Rebis, A. Elfwing, N. Solin, D. Mecerreyes, O. Inganas, High performance PEDOT/lignin biopolymer composites for electrochemical super capacitor supercapacitors, J. Mater. Chem. A 4 (2016) 1838–1847.
[100] H. Wang, Y. Song, J. Zhou, X. Xu, W. Hong, J. Yana, R. Xuea, H. Zhaoa, Y. Liua, J. Gao, High-performance super capacitor materials based on polypyrrole composites embedded with core-sheath polypyrrole@MnMoO4nanorods, Electochim. Acta 212 (2016) 775–783.
[101] M. Devi, A. Kumar, In-situ reduced graphene oxide nanosheets–polypyrrole nanotubes nanocomposites for super capacitor applications, Synth. Met. 222 (2016) 318–329.
[102] J. Zhang, J. Gao, Q. Song, Z. Guo, A. Chen, G. Chen, S. Zhou, N-substituted carboxyl polyaniline covalent grafting reduced graphene oxide nanocomposites and its application in super capacitor, Electochim. Acta 199 (2016) 70–89.
[103] X. Gong, Y. Zhang, H. Wen, Y. Fan, P. Han, Y. Sun, X. Zhang, H. Yang, B. Lin, Phenoxazine based conjugated ladder polymers as novel electrode materials for super capacitors, ChemElectroChem 3 (2016) 1837–1846.
[104] H.M. Shiri, A. Ehsani, Pulse electrosynthesis of novel wormlike gadolinium oxide nanostructure and its nanocomposite with conjugated electroactive polymer as a hybrid and high efficient electrode material for energy storage device, J. Colloid Interface Sci. 484 (2016) 70–76.
[105] S.K. Simotwo, C. DelRe, V. Kalra, Super capacitor electrodes based on high-purity electrospun polyaniline and polyaniline-carbon nanotube nanofibers, ACS Appl. Mater. Interfaces 33 (2016) 21261–21269.
[106] S. Chai, N. Hu, Y. Han, X. Zhang, Z. Yang, L. Wei, L. Wang, H. Wei, The microwave-assisted solvothermal synthesis of a novel b-ketoenamine-linked conjugated microporous polymer for super capacitors, RSC Adv. 6 (2016) 49425–49428.
[107] S.S. Karade, B.R. Sankapal, Room temperature PEDOT:PSS encapsulated MWCNT's thin film for electrochemical super capacitor, J. Electroanal. Chem. 771 (2016) 80–86.
[108] H. Wang, X. Yan, G. Piao, A high-performance super capacitor based on fullerene C60 whisker and polyaniline emeraldine base composite, Electrochim. Acta 231 (2017) 264–271.
[109] Y. Ge, R. Jalili, C. Wang, T. Zheng, Y. Chao, G.G. Wallace, A robust free-standing MoS2/poly(3,4-ethylenedioxythiophene):poly(styrenesulfonate) film for super capacitor applications, Electochim. Acta 235 (2017) 348–355.

[110] H. Wang, D. Liu, P. Du, W. Wei, Q. Wang, P. Liu, Comparative study on polyvinyl chloride film as flexible substrate for preparing free-standing polyaniline-based composite electrodes for super capacitors, J. Colloid Interface Sci. 506 (2017) 572–581.
[111] S.K. Das, K. Bhunia, A. Mallick, A. Pradhan, D. Pradhan, A. Bhaumik, A new electrochemically responsive 2D π-conjugated covalent organic framework as a high performance super capacitor, Microporous Mesoporous Mater. 266 (2018) 109–116.
[112] M. Ates, S. Caliskan, E. Ozten, A ternary nanocomposite of reduced graphene oxide, Ag nanoparticle and polythiophene used for super capacitors, Fullerenes Nanotubes Carbon Nanostruct. 26 (2018) 360–369.
[113] S. Matsushita, B. Yan, T. Matsui, J.D. Kim, K. Akagi, Conjugated polymer-based carbonaceous films as binder-free carbon electrodes in super capacitors, RSC Adv. 8 (2018) 19512–19523.
[114] N. Song, W. Wang, Y. Wu, D. Xiao, Y. Zhao, Fabrication of highly ordered polyaniline nanocone on pristine graphene for high-performance super capacitor electrodes, J. Phys. Chem. Solids 115 (2018) 148–155.
[115] Z. Wang, H. Qiang, C. Zhang, Z. Zhu, M. Chen, C. Chen, D. Zhang, Facile fabrication of hollow polyaniline spheres and its application in super capacitor, J. Polym. Res. 25 (2018) 129.

13

Polymer-based electro-active smart composites as stretchable strain sensors

K.S. Nithin[a], K.R. Prakash[b], V. Ravi Kumar[b,c], M.V.S. Deepak[d], B.J. Kishen Karumbaiah[e], S. Sachhidananda[f], K.N. Shilpa[f], B.M. Jagajeevan Raj[a], and H. Siddaramaiah[g,†]

[a]Department of Chemistry, The National Institute of Engineering, Mysuru, India, [b]Department of Mechanical Engineering, The National Institute of Engineering, Mysuru, India, [c]Department of Mechanical Engineering, Amrita School of Engineering, Amrita Vishwa Vidyapeetham, Bengaluru, India, [d]Department of Mechanical Engineering, ATME College of Engineering, Mysuru, India, [e]Department of Mechanical Engineering, Coorg Institute of Technology, Ponnampet, India, [f]Department of Polymer Science and Technology, Sri Jayachamarajendra College of Engineering, JSS Science and Technology University, Mysuru, India, [g]Vice-Chancellor of JSS Science and Technology University, Mysuru, India

13.1 Introduction

The advent of mobile Internet era and the ever accumulating interest in Internet of Things (IOT), have encouraged the scientific community to develop portable electronic devices with smart material functionalities. This in turn has created a sharp demand for smart electronic devices with enhanced mechanical flexibilities, thereby initiating a vibrant technological area called flexible electronics [1].

While, constantly increasing apprehension of personalized medicine, continuously scaling up computing platforms, and augmented human-machine interactivity have all contributed to increased interest in wearable electronics. Additionally, mechanically flexible electronic systems integrated to device-engineering technologies enable the effective fabrication of slender, lighter, stretchable, and foldable sensors and/or actuators.

Further, conventional electronics developed with rigid and planar silicon wafers often suffer from tribulations related to aptness

[†] Deceased.

Polymer-Based Advanced Functional Composites for Optoelectronic and Energy Applications
https://doi.org/10.1016/B978-0-12-818484-4.00014-8
Copyright © 2021 Elsevier Inc. All rights reserved.

(inability to fit into irregular contours and/or moving objects) [2]. This is particularly in the case of wearable devices for predictive analytics and treatment, which involves continuous physiological monitoring [3]. Thus, polymer-based mechanically flexible electro-active materials have attracted considerable scientific interest. Such flexible materials empowered with smart electro-active functionalities are projected to revolutionize the global flexible electronics market with a wide range of techno-commercial products, including electronic skin for robotics and prosthetics [4–6], wearable sensors for structural health monitoring, biosensors for preliminary medical diagnosis [5–9], and so forth.

In simpler terms, polymer-based electro-active smart composites with their unique molecular architectures, dopant-dependent electro-active characteristics, and inherent abilities to withstand relatively large mechanical stress (without disturbing their unique electronic properties) have revolutionized the human lifestyle [8, 10].

Herein, an attempt is made to highlight various types of polymer composite-based stretchable strain sensors, their operating mechanisms, the performance metrics that validate the suitability of material for stretchable strain sensing, and factors that decide the strain sensing performance of polymer-based conductive composites.

13.2 Classification of polymer-based strain sensors based on operating mechanism

There are several types of strain sensors (fiber Bragg grating (FBG), Raman shift, tribo, and piezo) that transduce mechanical deformations into electrical signals [11, 12]. Yet, only piezo-based (piezoresistive, piezoelectric, and piezocapacitive) strain sensors are the most widely investigated, owing to their relatively simple read-out systems [13]. A schematic depiction of different types (based on their operating mechanism) of piezo-based strain sensors is given in Fig. 13.1.

13.2.1 Piezoresistive strain sensors

Piezoresistivity is essentially the change in electrical resistance (to the flow of current) of the material that is being mechanically stressed. That is to say, when mechanical force is applied to piezoresistive materials, the electrical resistance to current passing through it shows an appreciable change [14].

This relative change in electrical resistance $\left(\frac{\Delta R}{R}\right)$ under various mechanical excitations is given as:

$$\frac{\Delta R}{R} = (GF)\,\varepsilon \tag{13.1}$$

Where R_0 is the electrical resistance of the material at the unstretched state, R is the difference in resistance at the stretched state, GF is the gauge factor, and ε is the applied strain.

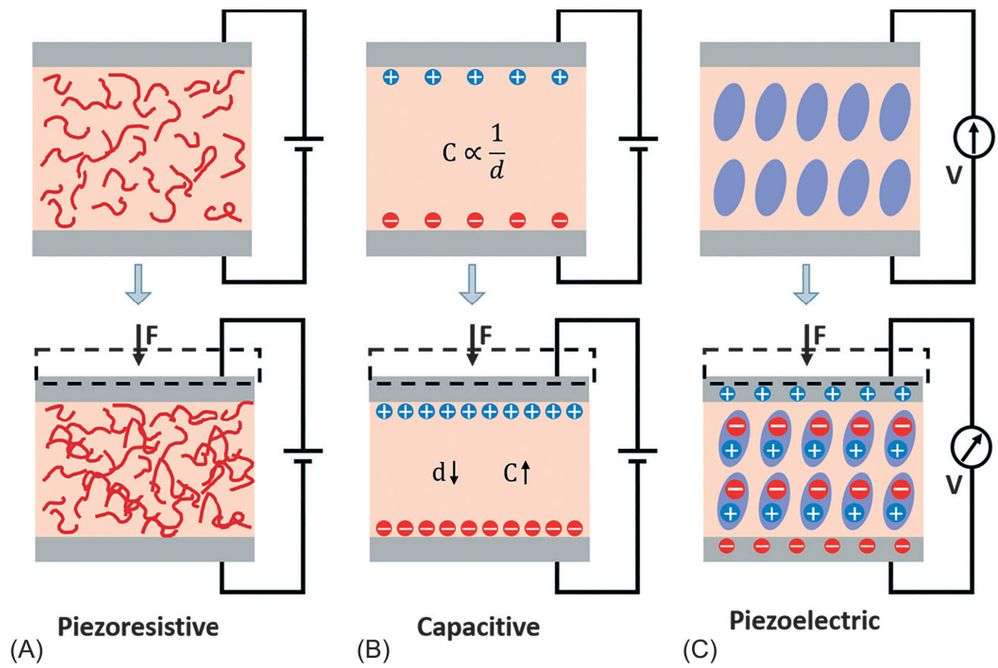


Fig. 13.1 Schematic illustration of three important operating mechanisms in piezo-based strain sensors. (A) Piezoresistive; (B) Piezocapacitive; and (C) Piezoelectric. Reproduced from Yaping Zang, Fengjiao Zhang, Chong-an Di and Daoben Zhu, Advances of flexible pressure sensors toward artificial intelligence and health care applications, Mater. Horiz. 2 (2015) 140–156.

Although a large number of piezoresistive (PR) materials have been continuously reported, only a few present the required aptness for stretchable sensor applications [14].

Such polymer-based electro-active composites operating via PR mode are mostly developed by introducing conductive fillers (particles, wires, tubes, or flakes) into insulating polymers to induce current percolating pathways [15, 16]. Consequently, piezoresistivity in such polymer composites arises from changes in the interfiller distance upon being stressed [17, 18].

In addition to mechanical stimulus-induced contact variations in fillers, PR behaviors can also be enabled via the tunnelling effect (which involves crossing electrons between two disconnected fillers within a certain cut-off distance). Initially (before applying load), the fillers are in total contact with each other and hence, the resistance between the fillers is dominated by contact-type resistance. However, upon applying the mechanical load, they (fillers) are separated (well within a certain distance) by the applied stress and hence, the tunneling resistance becomes more dominating. Thus, in such cases

(dominated by the tunneling effect), the GF or sensitivity of the strain sensors would be several magnitudes higher than that due to contact resistance variations alone.

The advent of nanotechnology and the inherent ability of polymers to display dopant-dependent electrical property engineering have all contributed to rising interest in polymer composites for various techno- commercial applications [19, 20], which also includes pressure or strain sensing applications [13].

One such PR polymer nanocomposite (PNC) made of reduced graphene oxide (rGO) ink mixed with multiwalled carbon nanotubes (MWCNTs) [(MWCNT-rGO@PU)] introduced polyurethane (PU) foams was tried for small-scale motion-monitoring applications (Fig. 13.2) by Amit Tewari et al. [21].

Zhonglei Ma et al. reported PR sensors made by dip-coating conductive MWCNTs and graphene to PU sponges. They reported that the electrical conductivities of such PR sensors showed a monotonic dependence on the number of dip-coating cycles. Further, they also observed that conductive sponges with more dip-coating cycles exhibited a larger change in electrical resistance (upon repeated compression) [22]. Going forward, they also demonstrated that the said PR sponge exhibited excellent responsiveness and appreciable stability in various sensor-related applications ranging from lighting LED lamps (Fig. 13.3) to detecting human body movements (Fig. 13.4).

However, in the case of elastic polymer composites loaded with conducting fillers, the PR effect is relatively lesser, mostly due to the large mismatch of elasticities between the conductive network and the elastomeric polymer, which in turn results in relatively lesser adhesion.

13.2.2 Piezoelectric strain sensors

The piezoelectric (PE) effect involves the thoughtful conversion of applied stress into usable voltage. It is essentially an electromechanical interaction in noncentrosymmetric crystal structures. This in turn leads to the generation of electrical charges upon being subjected to mechanical loads.

Conventionally, PE effects were often reported in ceramic-based materials. Although promising, conventional peizoceramics often suffered from tribulations related to their mechanical performance and hence, were less chosen for wearable sensor applications. Consequently, polymer-based PE materials have gained substantial scientific interest, wherein an applied mechanical stimulus leads to redistribution of the electrical dipoles and the subsequent generation of charges [14, 23]. Such polymer-based PE composites may be successfully developed by suitably inducing material asymmetry, either by introducing noncentrosymmetric crystalline fillers into the

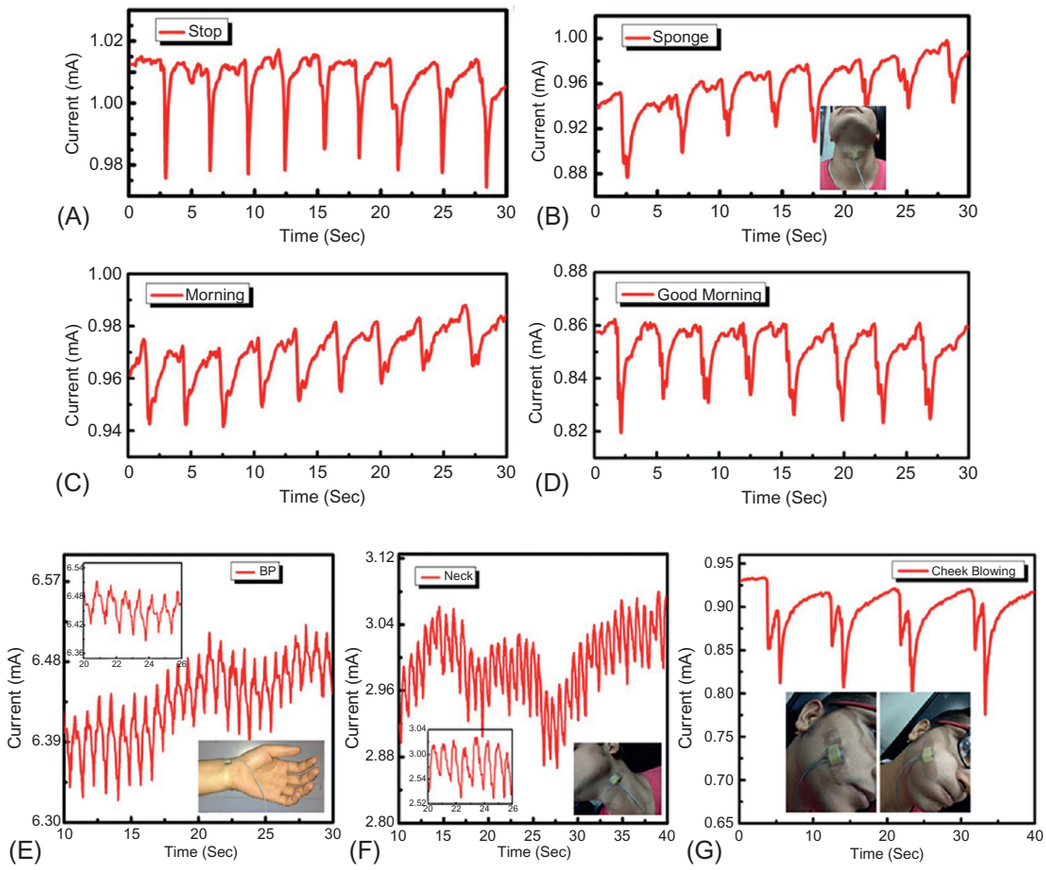


Fig. 13.2 Real-time response (current vs. time) profiles of an MWCNT-rGO@PU PR sensor for various small-scale motion monitoring applications. (A–D) Voice detection through the throat while pronouncing different words such as; (A) Stop; (B) Sponge; (C) Morning; and (D) Good morning. (E) Blood pulse detection through the wrist; (F) Neck; and (G) Checking cheek bulging. Reproduced from A. Tewari, G. Srinivas, B. Siva, C.R. McNeill, G. Dipti, Highly exfoliated MWNT–rGO ink-wrapped polyurethane foam for piezoresistive pressure sensor applications, ACS Appl. Mater. Interfaces 10 (2018) 5185–5195 with permission of The American Chemical Society.

polymeric host or by extracting filler/polymer synergistic effect introduced PE effects. Table 13.1 presents some of the most common ceramic-polymer combinations operating via PE mode and their performance metrics.

Further, Gullapalli et al. reported mechanically flexible PE polymer composites developed by embedding zinc oxide (ZnO) NPs in cellulose fibers [24]. Zefeng Chen et al. reported PDMS-based $PbTiO_3$ nanowires (PTNWs)/graphene NCs (fabricated via the layer-by-layer approach) with appreciable GF and rapid response time (when compared to PDMS/graphene and PDMS/PTNW composites) [25].

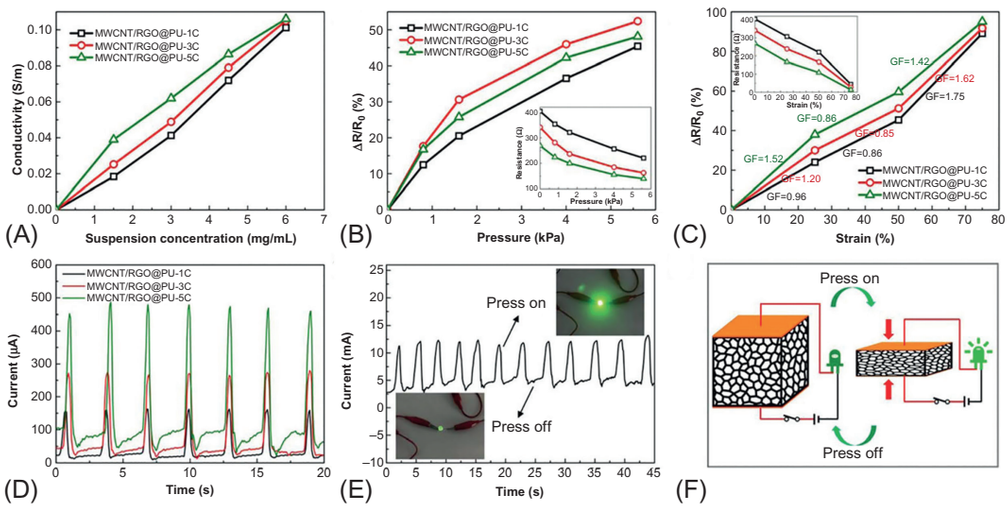


Fig. 13.3 (A) Electrical conductivities of the MWCNT/RGO@PU sponges with 1, 3, and 5 dip-coating cycles as a function of suspension concentration; (B) Relative resistance changes of the MWCNT/RGO@PU sponges with 1, 3, and 5 dip-coating cycles at different applied pressures; (C) Different applied strains; (D) Responsive current curve of the sensors during repeated compression and recovery processes with an applied strain of 25%; (E) Electric current variation cycles with repeated press on and off; and (F) Illustration for the brightness variations of the LED lamp during repeated compression and recovery processes. Reproduced from Z. Ma, A. Wei, J. Ma, L. Shao, H. Jiang, D. Dong, Z. Ji, Q. Wang, S. Kang, Lightweight, compressible and electrically conductive polyurethane sponges coated with synergistic multiwalled carbon nanotubes and graphene for piezoresistive sensors, Nanoscale 10 (2008) 7116–7126 with permission of The Royal Society of Chemistry.

Park et al. adopted a sandwich approach and successfully developed PE mats of electrospun (poly(vinylidenefluoride-co-trifluoroethylene)) nanofiber, sandwiched between two sheets of elastomer. Such an approach was found to yield highly sensitive PEs with improved microstrain measurement properties [26]. Luana et al. developed multilayered sheets of electrospun poly(vinylidenefluoride-co-trifluoroethylene) fibers, with polymer chains adopting a strong preferential orientation. They also demonstrated that such a sensor offers excellent potential for electronic skin-related applications [27].

Polymer-based PE composites have also tried for monitoring dynamic pressure changes related to human body movements. One such self-powered sensor with a hybridized combination of both PE PVDF fibers and triboelectric Cu-PTFE was reported by Yiin-Kuen Fuh et al. [28].

PE sensors also help in understanding the human body mechanics and hence, offer productive input on how to address those problems related to body mechanics (Fig. 13.5). In addition, the knowledge of PE properties can also aid disease detection or injury analysis. Moreover,

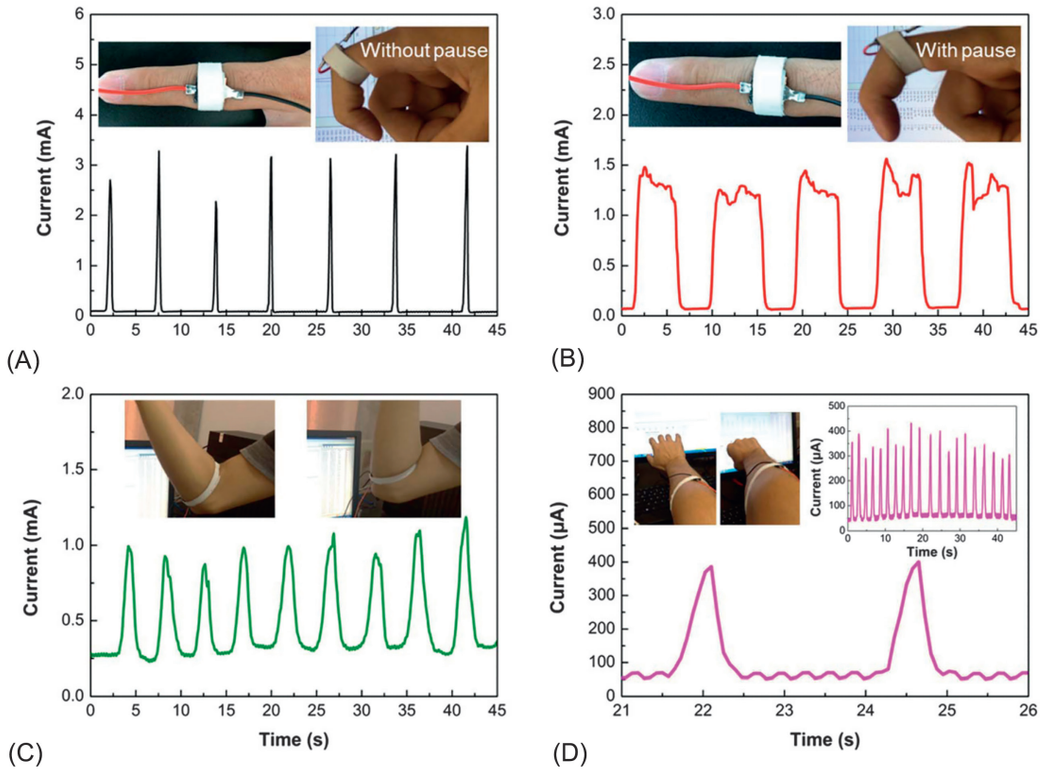


Fig. 13.4 Human motion detection using the MWCNT/RGO@PU sponge-based PR sensors. (A–D) Changes in current output of the sensor in response to finger bending. (A) Without pause; (B) With pause in the bending state; (C) With elbow bending; and (D) Muscle contraction. Reproduced from Z. Ma, A. Wei, J. Ma, L. Shao, H. Jiang, D. Dong, Z. Ji, Q. Wang, S. Kang, Lightweight, compressible and electrically conductive polyurethane sponges coated with synergistic multiwalled carbon nanotubes and graphene for piezoresistive sensors, Nanoscale 10 (2008) 7116–7126 with permission of The Royal Society of Chemistry.

Table 13.1 PE performance of some of the most common ceramic-polymer combinations (composites).

Introduced ceramic	Volume (%)	Host polymer	d_{33}
PTCa	50	Epoxy	22
PTCa	65	P(VDF-TrFE)	28
PTCa	20–50	Rubber	17–44
PT	70	Acrylic	32
PZT	67	PVDF	48

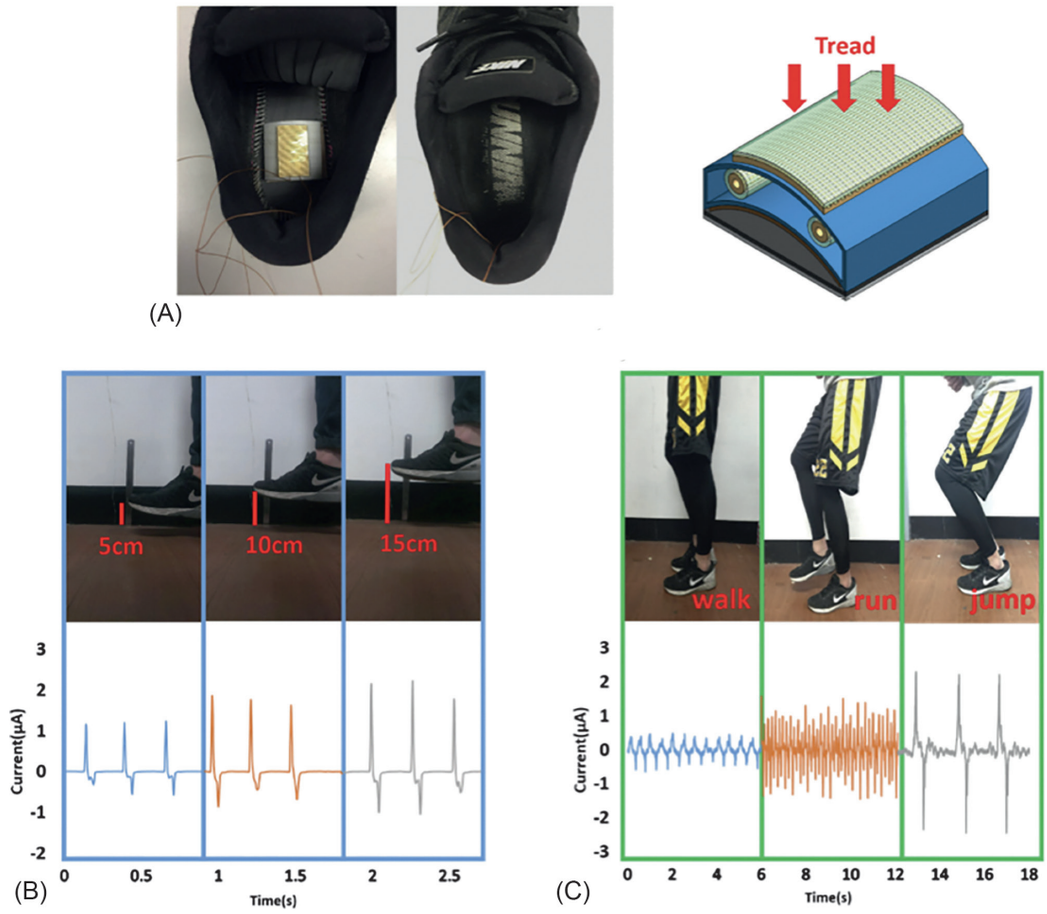


Fig. 13.5 Photographs of HSPS (hybridized self-powered sensor) fixed to (A) Shoe sole; (B–C) Relative changes in current versus time for various biomechanical motions; (B) Treading; and (C) walking, running, and jumping. Reproduced from F. Yiin-Kuen, L. Shan-Chien, C. Chun-Yu, Piezoelectrically and triboelectrically hybridized self-powered sensor with applications to smart window and human motion detection, APL Mater. 5 (2017) 074202.

based on the fact that the PE tissue properties are determined by proteins, diseases that affect the amount or distribution of proteins could be easily validated and hence, reported using PE sensors [29]. Although a number of materials with potential PE properties have been reported so far, they are mostly structured in arrays, which often leads to tribulations related to crosstalk. It is during this crosstalk that the neighboring units in the array are affected (by the unit undergoing force), which in turn send their own signals, thereby disturbing the device sensitivity [30].

13.2.3 Piezocapacitive strain sensors

Piezocapacitive (PC) sensing involves the quantification of applied mechanical stress by measuring the capacitance change of the dielectric layer (upon applying stress) sandwiched between the conductive electrodes.

Herein, the applied stress (between the conductive layers) is expected to bring the layers closer and hence, a corresponding change in electric capacitance is observed.

This change in electrical capacitance $\left(\frac{\Delta C}{C}\right)$ under various mechanical excitations is given as:

$$\frac{\Delta C}{C} = (GF)\,\varepsilon \tag{13.2}$$

Where C_0 is the electrical capacitance of the sensor at the unstretched state and C is the difference in capacitance at the stretched state.

In PC-based strain sensors, applied mechanical load induced material compressibility is the key factor that determines the deformation resistibility of the sensors and hence, is directly correlated to measurement sensitivity or GF.

Although resistive-type strain sensors exhibit high sensitivity, they often suffer from large hysteresis and nonlinear responses [31]. On the other hand, capacitive-type strain sensors offer relatively small hysteresis and linear response, thus making them extremely promising for soft matter-based stretchable strain sensing applications.

Accordingly, various researchers reported PC strain sensors using solid elastomeric dielectric layers. However, the said sensors often suffered from low sensitivity (mainly due to the viscoelastic property of the elastomer). This issue was addressed using low modulus materials and introducing microstructures into dielectric layers. Consequently, Tee et al. tried a porous matrix based approach and reported PC elastomeric dielectric layers with micro and/or 3D porous structures. Voids in the said structure empowered the dielectric layer to elastically deform (with applied stress), and hence, to present improved GF [32]. Lipomi et al. developed PC sensors using dielectric layers of silicone elastomer (Ecoflex) and two PDMS-coated single-walled carbon nanotube (SWCNT) electrodes. Using elastomers, which were as soft as dielectrics, the authors were able to draw improved conductivity coupled with high mechanical strechabilities [33], although the sensitivities were not appreciably improved.

Cohen et al. demonstrated SWCNT-based percolation electrodes separated by a elastomeric layer (dielectric) using vacuum filtration and hydrophobic patterning of silicone. The as-developed PC sensor displayed good linearity with a GF of 0.99 [34]. Darren et al. produced

spring -like PC structures that displayed increased conductivity at the strained state [33]. Further, a PC touch sensor capable of both contact and noncontact sensing was reported by Kang et al. using patterned graphene electrodes (doped with bis(trifluoromethane) sulfonamide (TFSA)) structured on a polyethylene terephthalate (PET) substrate. The said sensor was capable of sensing both the distance and shape of approaching objects [35].

Thus, from the available literature, it is quite evident that most PC strain sensors offer high linearity, low hysteresis, and long-term cyclic stability (which are very much decisive for stretchable strain sensing applications). Yet, they suffer from lesser GFs and a limited sensing range. Consequently, more research and developmental efforts are required to fabricate effective PC strain sensors with higher GFs and an improved sensing range. One such approach was successfully explored by Nur et al. and Shintake et al., who tried auxetic structures to improve the sensitivity of the stretchable PC strain sensors [36, 37]. They reported that the said sensors took advantage of the negative Poisson ratio auxetic structures, which brings about an increase in the width of the sensor (in response to applied strain) contrary to conventional sensors that show a decrease in width [38]. Besides, it is this deformation characteristic of the negative Poisson ratio auxetic structure that brings about a larger capacitive change and hence, improved sensitivity. Although promising, the said stratagem is in its infancy and requires further research to be industry ready.

13.3 Factors validating the suitability of materials for stretchable strain sensing and their related performance metrics

The suitability of any material for strain sensing applications depends on two important sets of performance metrics: the basic ones (sensitivity, strechability, linearity, hysteresis, response time, and related aspects) and the specific ones (self-power, wireless communication, biodegradability, and related aspects).

13.3.1 Basic metrics

13.3.1.1 Sensitivity and strechability

The basic performance metric is the sensitivity of the material, often expressed as GF, which presents the slope of the relative changes in electrical functionalities (of the sensor) as a function of applied strain. It is calculated using the relation:

$$GF = \frac{\Delta R}{R_0 \varepsilon}, GF = \frac{\Delta C}{C_0 \varepsilon} \tag{13.3}$$

$$GF = \frac{\Delta x}{x_0 \varepsilon} \tag{13.4}$$

Where x is the change in electrical functionality (capacitance or resistance) and x_0 is the initial electrical functionality at strain $(\varepsilon) = 0$.

GF is one of the major criteria that qualifies the suitability of a given material for strain sensing applications.

Although customary metallic foils and semiconductor-based strain sensors present relatively high GF, they often suffer from tribulations related to their mechanical performance. This in turn limits their wearable and/or stretchable sensor related applications.

It is these limitations that have paved the way for polymer composite-based stretchable strain sensors. Further, the GF and the sensitivity of the strain sensor depend on the functional sensing material, the mechanism involved in sensing, and the structural configuration. In stretchable strain sensors operating via PC mode, the fundamental detecting component is the geometric impact. In resistive-type strain sensors, the observed sensing effect is due to the separation between the conductive squares and/or the break engendering in the slender movies and/or the burrowing impact [39]. Thus, in PC-type strain sensors operating via the geometrical effect, the theoretical maximum GF is limited to 1. However, in the PR-type, the GF values are relatively much higher, owing to the fact that PR strain sensors exhibit highly appreciable changes in resistance with considerable structural changes (upon being mechanically stressed).

Moving forward, stretchability is another important performance metric of mechanically adaptive strain sensors. Such stretchable strain sensors may be successfully developed by one of the following techniques, which involves either synchronous mixing of conductive materials and a stretchable network (or) the fabrication of a stretchable conductive system implanted inside a flexible lattice.

While the first approach is simple and scalable, it presents tribulations related to linearity (as high linearity demands improved filler dispersions) and the percolation threshold (as a high percolation threshold demands higher filler content, which may lead to filler agglomerizations) [16, 40, 41].

The second approach addresses the limitations presented by the first approach. Yet, fabrication techniques associated with the second approach are relatively more complex and mechanical performance may be limited, owing to poor adhesion between the conductive system and the flexible lattice. Besides, various strain sensors present diverse strechabilities depending on the nature of the strain sensing material, the sensor fabrication process, and other related aspects.

Also, 1D nanomaterials (carbon nanotubes (CNTs) and silver nanowires (AgNWs)), with high aspect ratios [42–46] and inherent

abilities to sustain a percolation network at large strains are preferred over other nanomaterials, such as carbon blacks (CBs), graphene, and silver nanoparticles (NPs). Also, high aspect ratio nanofillers induce the effective formation of percolation networks, which in turn enables stable electro-mechanical performance even at high strain levels. The lack of robust percolating networks in low aspect ratio nanofillers leads to lessened strechabilities [47, 48]. Table 13.2 summarizes some of the important polymer/filler composite combinations as well as their strain sensing mechanisms, GFs, and overall strechabilities.

Table 13.2 Some important polymer composite-based strain sensors, their operating mechanisms, and related performance metrics.

Polymer/filler combination	Operating mechanism	Strechability (%)	GF	Ref.
Ag NW-PDMS	PR	35	20	[49]
Ag-PU fiber	PR	150	211	[50]
Crumpled graphene-PDMS	PR	100	7.1	[51]
PEDOT: PSS-PU	PR	350	6	[52]
Ag NP/CNT-PDMS	PR	2.4	95	[53]
PEDOT:PSS-polyvinylpyrrolidone (PVP)	PR	4	360	[54]
Graphene-Plastic	PR	2	150	[55]
Ag NW-Hydrogel	PR	460	1.52	[56]
Pt-PUA	PR	2	2000	[57]
Graphene Mesh-PDMS	PR	8	6×10^6	[58]
Au NW-Latex Rubber	PR	350	9.9	[59]
Ag NW-Eco-flex	PC	50	0.7	[60]
CNT-silicone	PC	100	0.99	[34]
Ionic fluid-silicone	PC	700	0.35	[61]
CNT-Eco-flex	PR	500	1–2.5	[12]
Aligned CNT-PDMS	PR	280	0.82	[62]
ZnO NW-PDMS	PR	50	114	[63]
CNT-Dragon-skin elastomer	PC	300	0.97	[64]
Graphene foam-PDMS	PR	70	15–29	[65]
CBs-TPE	PR	80	20	[66]
CBs-PDMS	PR	10	1.8–5.5	[67]
CNTs-Eco-flex	PC	150	1	[68]
CBs-Eco-flex	PR	400	3.8	[69]
Platinum (Pt)-PDMS	PR	2	2000	[57]
Au NW-PANI-rubber	PR	149.6	20.4–61.4	[70]
Ag NW-PEDOT: PSS/PU	PR	100	1.07–12.4	[71]
CNTs-PEDOT: PSS/PU	PR	100	8.7–62.3	[72]

As can be seen from the table, most highly sensitive sensors can only maintain their superiority in a limited strain range, and the search for advanced sensors with mutually high stretchability and augmented sensitivity is still on.

13.3.1.2 Linearity

Linearity in electro-active strain sensors is a performance metric that characterizes the proportionality relationship between the electrical output (response) and the mechanical input (stimulus).

Besides, a linear fit of GF for a particular strain sensor could simplify the calibration and also ensure ease in data processing [73]. However, most strain sensors, especially those operating via PR mode, undergo applied strain-induced changes in their microstructures from homogeneous to nonhomogeneous morphology, which in turn leads to undesirable nonlinearity in their GFs [74]. Table 13.3 presents the proportionality relationship between the electrical output and

Table 13.3 Proportionality relationship between the electrical output and mechanical input (linearity) of some important electro-active polymer-based smart composites.

Polymer/filler combination	Proportionality relationship	Ref.
Ag NWs-PDMS	Linear upto 40%	[74]
CNT-Ecoflex	Linear	[12]
CB-PDMS	Linear	[67]
Aligned CNT-PDMS	Two linear regions	[62]
ZnO NWs-PDMS	Linear	[63]
CNT-Dragon-skin elastomer	Linear	[64]
Graphene foam-PDMS	Linear	[65]
CB-TPE	Nonlinear	[66]
CB-PDMS	Two linear regions	[67]
CNT-Ecoflex	Linear	[68]
CB-Ecoflex	Nonlinear	[69]
CNT-silicone elastomer	Linear	[34]
Graphene-rubber	Nonlinear	[75]
Ag NW-Ecoflex	Linear	[76]
Platinum (Pt)–PDMS	Nonlinear	[57]
Au NW-PANI-rubber	Linear	[70]
Ag NW-PEDOT: PSS/PU	Nonlinear	[71]
Au NW-latex rubber	Linear	[59]
CNT-PEDOT:PSS/PU	Nonlinear	[72]

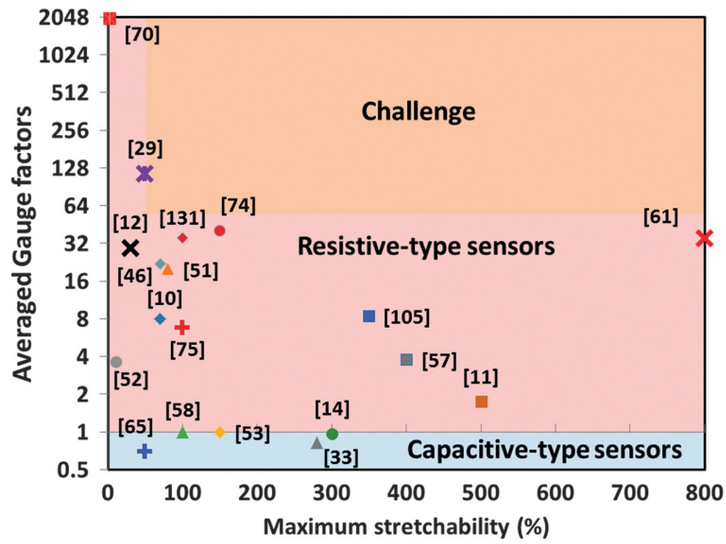


Fig. 13.6 Average GF as a function of the maximum stretchability of some of the recently reported PR-type and PC-type strain sensors. The *orange*-colored region represents that scientifically challenging space that presents an optimal balance of stretchability, sensitivity, and linearity. Reproduced from M. Amjadi, K.U. Kyung, I. Park, M. Sitti, Stretchable, skin-mountable, and wearable strain sensors and their potential applications: a review, Adv. Funct. Mater. 26 (2016) 1678–1698 with permission of Wiley.

mechanical input (linearity) of some of the important electro-active polymer-based smart composites.

Although polymer composite-based strain sensors operating via PC mode exhibit excellent linearity, they often suffer from low sensitivities. Also, high GF (highly sensitive) strain sensors must present considerable structural deformations (upon stretching). Also, the fact that highly stretchable strain sensors must be morphologically intact (upon large stretching) leads to significant trade-offs between high sensitivity, higher linearity, and increased stretchability. A pictorial depiction of the average GF as a function of maximum strechabilities in various PR and PC strain sensors is presented in Fig. 13.6. It is therefore the simultaneous promotion of sensitivity (GFs $\geq$ 50), linearity, and strechability ($\varepsilon \geq 100\%$), a grand scientific challenge that requires pressing scientific consideration.

13.3.1.3 Hysteresis, response time, and recovery time

Hysteresis is an important performance metric that qualifies the suitability of a sensor for wearable and/or skin-mountable applications, particularly when unique movements are to be sensed and recorded.

The response time quantifies how fast a given strain sensor moves toward a steady-state response (upon applying the desired stimulus). In general, a 90% time constant ($\tau_{90\%}$) is used as the standard response time value for stretchable strain sensors [74].

PC-type strain sensors with an immediate response to applied strain often present relatively low hysteresis. PR-type strain sensors

Table 13.4 Recovery time of some of the important polymer composite-based strain sensors.

Polymer/filler combination	Recovery time (ms)	Ref.
Ag NW-PDMS	200	[11]
ZnO NW-polystyrene	140	[63]
CNT-Ecoflex	332	[12]
Ag NW	50	[76]
CNT	100	[64]
CNT thin films-PDMS	5	[62]
CB-elastomer composites	100	[66]

with a hindered recovery of the filler position (owing to interfacial slide under weak binding) lead to high hysteresis.

Further, the interfacial binding between the introduced filler and the polymer substrate (using a low viscoelastic polymer and improved sensor configuration) is critical toward hysteresis optimizations. The higher viscoelasticity of the polymeric matrix leads to a delayed response time [59]. The response times of some of the important polymer/filler combinations are presented in Table 13.4.

Further, PR-type polymer-based composites require more time to reestablish the percolation network and hence, display larger response times than the PC-type. The same holds for the recovery time, as PC-type sensors present a recovery time in the subsecond scale while it is a few seconds for PR-type sensors.

13.3.1.4 Self-healing

Stretchable strain sensors with excellent self-mending abilities offer tremendous potential for wearable sensor applications [77, 78]. Although the most functional polymer composite-based strain sensing matrix may present excellent GF and improved strechabilities, scratches and damage are inevitable in daily use, which may in turn lessen the device functionality and service lifetime. It is for this reason that self-healing polymer-based composites that recover their fundamental functions (postdamage) have attracted significant technological interest. Besides, self-healing materials could reduce undesirable mechanical damage and thereby extend the sensor stability and durability.

Self-healing polymer-based strain sensing composites are further categorized as intrinsic self-healing polymer composites and extrinsic self-healing polymer composites [79]. Intrinsic self-healing polymer composites can heal themselves (via dynamic physical or chemical

interactions) without the aid of any additional self-healing agent. Extrinsic self-healing polymer composites rely on external healing agents [80].

13.3.2 Specific metrics

The specific performance metrics of stretchable strain sensors depend on the desired application. Accordingly, one expects biocompatibility and biodegradability for applications involving direct human contact, such as skin-mountable electronics [81] while wireless communication-supported strain sensors are desired for wearable health monitoring units [82]. However, self-powering abilities are desired for those biomedical applications that demand energy-free health monitoring characteristics [83].

13.4 Stretchable elastomer-based conductive polymer composites

Of all the available polymer composite types, conductive filler introduced stretchable elastomer-based flexible conductive polymer composites (FCPCs) have attracted intensive technological interest due to their high stretchability, excellent flexibility, tunable strain sensing functionalities, and ease of processing [14, 64, 84]. Further, based on the configuration and mode of operation, such FCPCs are grouped into (1) Filled-type, (2) Sandwich-type, and (3) Adsorption-type strain sensors.

13.4.1 Filled-type FCPC-based strain sensors

Filled-type strain sensors are essentially developed via the direct dispersion of conductive fillers (often carbonaceous) in a mechanically flexible polymer matrix. The said sensors are mostly developed either via melt compounding or by solution mixing.

However, filled-type FCPC-based strain sensors often demand relatively high filler loadings, which in turn may result in low flexibility, complex processing techniques, and high production costs [85]. Besides, the higher filler loading may also affect sensitivity, especially under low and/or small strain range. Consequently, this type of strain sensor is mostly preferred for detecting large strains.

13.4.2 Sandwich-type FCPC-based strain sensors

This type of strain sensor is developed by considerately sandwiching a conductive network or conductive layer between two flexible or

stretchable polymer layers. Such strain sensors are mostly fabricated by depositing, transferring, or printing a conductive layer on a prefabricated flexible substrate and finally coating another flexible polymer as the protective thin layer.

Consequently, the preparation of such sensors presents cumbersome processing techniques, that often check their mass production abilities. Moreover, repeatability in such sensors is also an issue, owing to the difficulties encountered in controlling the thickness and microstructures via depositions [86]. Nevertheless, sandwich-structured strain sensors present higher GFs, and hence, are mostly suitable for validating microstrains.

13.4.3 Adsorption-type FCPC-based strain sensors

FCPC-based adsorption-type strain sensors are composited by coating a layer of conductive materials over a flexible nonconductive substrate [87]. Further, this type of strain sensor demands improved adhesion between the conductive coating and flexible substrate (polymer).

Thus, conductive materials are often surface-treated to induce strong surface interactions. Further, adsorption-type strain sensors are endowed with superstretchability, excellent sensitivity, high durability, and fast response rates.

13.5 Material selection for stretchable strain sensors and their related applications

Lately, rapid development in flexible electronics has created enormous demand for mechanically flexible strain sensors [88]. While, the advent of nanotechnology and significant advancements in composite material research are known to offer augmented potential toward the effective fabrication of advanced functional materials [89–93]. Nevertheless, to extract ideal performance, it is critical to choose reasonably utilitarian materials and rationally structure their models. This approach involves a thoughtful combination of electrically conductive fillers with an elastomeric matrix, wherein the fillers serve the sensing role while the elastomeric lattice supplies the desirable mechanical functionalities [94–96]. Fig. 13.7 presents one such strain sensor. While, Tables 13.5–13.9 present some of the most commonly explored polymer composite-based strain sensors, their material functionalities, fabrication techniques, performance metrics, and related applications.

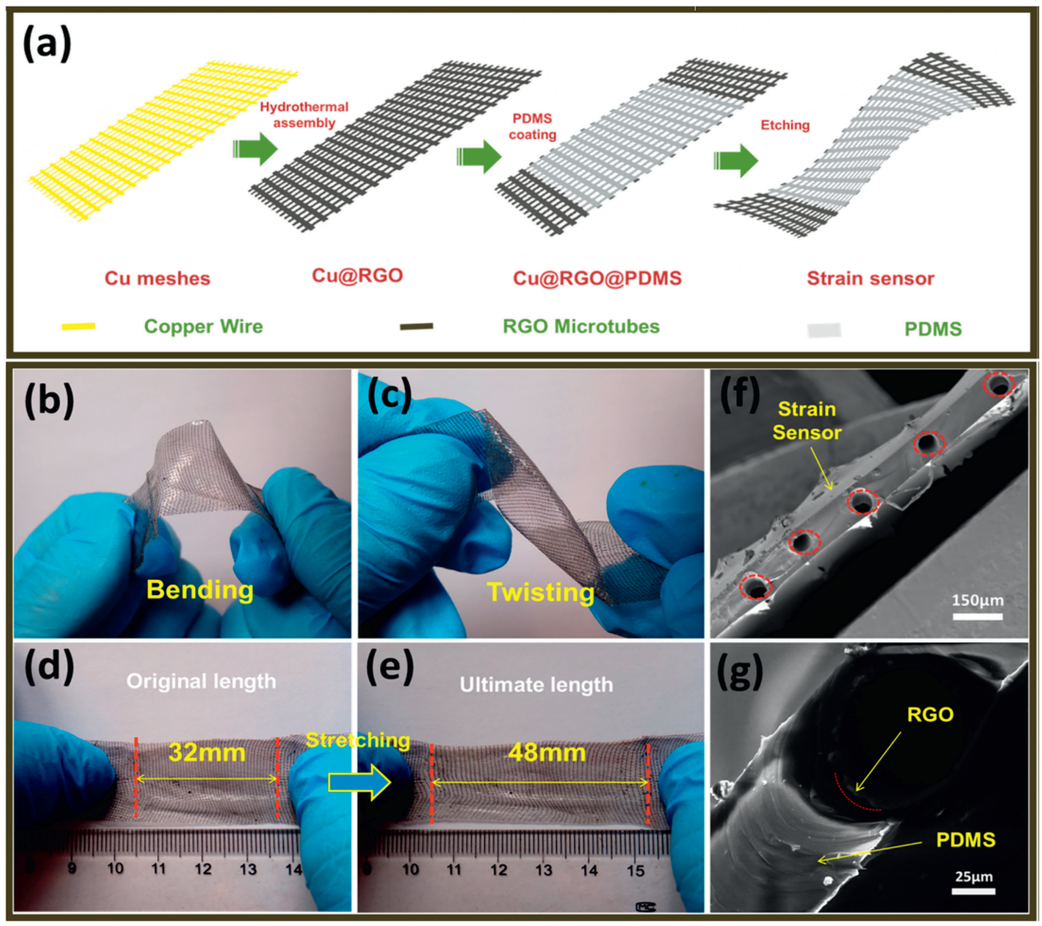


Fig. 13.7 (A) Fabrication steps of RGO microtube elastomer strain sensor. (B–C) Digital photographs of (B) Arbitrarily bended; and (C) Twisted strain sensor (D–E). Images supporting excellent stretchability (~ 50% strain) of the said strain sensor. (F–G) SEM images with different magnification. Reproduced from Y. Tang, Z. Zhao, H. Hu, Y. Liu, X. Wang, S. Zhou, J. Qiu, Highly stretchable and ultrasensitive strain sensor based on reduced graphene oxide microtubes–elastomer composite, ACS Appl. Mater. Interfaces 49 (2015) 27432-27439 with permission of The American Chemical Society.

Table 13.5 PDMS-based flexible sensors, their performance metrics, and related applications.

Polymer/filler combinations	Fabrication technique	Performance		Linearity	Related applications	Ref.
		Stretchability (%)	GF			
EGaIn/PDMS	Printing technique	350	1.6–3.2	Partially linear	Electronic skin, wearable devices, and robots	[97]
AgNW/PDMS	Micromolding method	70	2–14	Partially linear	Virtual reality and motion detection	[11]
CNT, CB/PDMS	Micromolding method	22.6	29	Nonlinear	Wound monitoring and human-machine interfacing	[67]
CB/PDMS	Liquid phase mixing	10	5.5	Linear	Real-time health monitoring	[98]
Graphene/PDMS	Coating technique	7.1	2.4–14	Two linear areas	Multiple-parameter health monitoring	[99]
GWF/PDMS	Coating technique	30	~ 106	Nonlinear	Fatigue detection and advanced therapies	[100]
MWCNT/PDMS	Liquid phase mixing	45	1.2	Nonlinear	Biomedical applications	[101]
MWNT, GNP/PDMS	Printing technique	40	> 100	Partially linear	Health monitoring and diagnostics	[102]
AgNP/PDMS	Printing technique	20	4.7–12.5	Two linear area	Force and pressure measurement devices	[103]
CNT/PDMS	Printing technique	100	$2–10^4$	Nonlinear	Measuring joint motions in real time	[104]
CNT/PDMS	Liquid-induced densification	–	200	Nonlinear	Human motion including blood pulsing and breath monitoring	[105]
CNT/PDMS	Cast coating	280	0.06–0.82	Nonlinear	–	[62]
CNT/PUPEDOT:PSS/PDMS	Spin coating	100	62	Nonlinear	–	[72]
RGO/PDMS	Cast coating	50	630	–	–	[106]
Graphene Fabric/PDMS	Spin coating	–	35	–	–	[100]
GO/PDMS	Filtration	Bending radii (2.5–5 cm)	-	Nonlinear	–	[107]
Graphene nanocellulose/PDMS	Filtration	100	7.1	Partially linear	Human-machine interfacing	[108]
Ti/Au/PDMS	Micromolding method	–	–	Nonlinear	Measuring drug-induced changes in cell parameters	[109]
GnPs/PDMS	Micromolding method	< 10	27.7–164.5	Nonlinear	Human-machine interface, health monitoring, and electronic skin-related applications	[110]
CP/PDMS	Layer-by-layer technique	3	25.3	Partially linear	Robot controlling and breath monitoring	[111]

Table 13.6 Polyimide-based flexible sensors, their performance metrics, and related applications.

Polymer/ filler combinations	Fabrication technique	Performance		Linearity	Related applications	Ref.
		Stretching (%)	GF			
Polyimide/Si wafer	Inverted fabrication technique	17	1.3	Linear	Wearable devices, soft robots, and electronic skin applications	[112]
Polyimide/ SWCNN	Micromanufacturing	–	7.67	Nonlinear	Real-time bone strain sensing	[113]
Polymide/Gold	Sputtering of thin film	–	4.9–6.6	Linear	Robotic and pressure-mapping applications	[114]
Polymide/ Nickel-chrome alloy	Inverted fabrication technique	66	0.61	Linear	Robotic applications	[112]

Table 13.7 Parylene C-based flexible sensors, their performance metrics, and related applications.

Polymer/filler combinations	Fabrication technique	Performance		Linearity	Related applications	Ref.
		Stretching (%)	GF			
Thin-film metal gauge encapsulated between two layers of parylene-C	Layer by layer	2.2	2.56	Linear	Measure bone surface strain	[115]
SWCNNs encapsulated between two layers of Parylene-C	Layer by layer	–	4.58–6.44	Linear	Measure bone surface strain	[116]
Carbon nanotube networks encapsulated between two layers of Parylene-C	Layer by Layer	2	–	Linear	Wearable smart textiles	[117]

Table 13.8 Polyurethane-based flexible sensors, their performance metrics, and related applications.

Polymer/filler combinations	Fabrication technique	Performance		Linearity	Related applications	Ref.
		Stretching (%)	GFs			
Polyurethane/CB	Layer by layer	0.1	39	–	Wearable devices	[118]
Polyurethane/CNT	Diffusion process	400	–	Nonlinear	Wearable devices	[119]
Polyurethane/ Graphine	Coating/hot pressing	30	0.78–17.7	Partly linear	Wearable devices	[120]
Polyurethane/PPy	In situ Polymerization	100	–	–	Wearable devices	[121]
Polyurethane/ PEDOT:PSS	Fiber wet spinning	160	–	–	Wearable devices	[52]

Table 13.9 Ecoflex-based flexible sensors, their performance metrics, and related applications.

Polymer/ filler combinations	Fabrication technique	Performance		Linearity	Related applications	Ref.
		Stretching (%)	GF			
Ecoflex/gold	Contact transfer	–	37.8–70.3	Linear	–	[122]
CNT-Ecoflex	–	510	0.61	Linear	Motion detection of finger and wrist joints	[123]
CNT fiber/ Ecoflex	Spinning	200–900	0.24–64	Linear	Motion detecting systems	[124]
CNT/Ecoflex	Printing Technique	300	1–1.5	Linear	Wearable electronics and soft robots with high stretchability and low hysteresis	[125]
Sliver Nanowire/ Ecoflex	Screen printed	50	0.7	Bilinear	Monitoring thumb movement, sensing the strain of the knee joint in the patellar reflex (knee-jerk), and other human motions	[76]

13.6 Factors affecting the strain sensing performance of polymer-based conductive composites

The strain sensing performance of FCPCs is related to those functionalities that influence the strain sensing mechanisms such as the tunnelling effect, the overlapping area of conductive fillers, and/or crack propagation during mechanical operation.

In general, these functionalities include the size and shape of the conductive fillers, their dispersions, the nature and extent of the interactions between the conductive filler and the polymeric host, and other related aspects.

13.6.1 Dispersion and morphology of conductive nanofillers

The size and extent of conductive filler dispersions decide the overall material functionalities of FCPCs [126–128]. Generally, an improved filler dispersion helps to lower the conductive percolation threshold of composites. Their (conductive fillers) morphology may directly affect the destruction and reconstruction of conductive paths (during stretching-releasing cycles), thereby influencing the strain sensing behaviors.

13.6.2 Interactions between conductive nanofillers and the polymer matrix

The nature and extent of the interactions between the conductive nanofillers and the polymer matrix plays a critical role in deciding their overall strain sensing performance. Strong interfacial interaction often results in higher GFs, owing to the effective transfer of the applied mechanical load from the weak elastomeric substrate to strong conductive networks, which in turn enables them (sensors) to be destroyed more easily [129, 130].

Also, in adsorption-type FCPCs, a strong conductive layer and elastomeric substrate interactions stabilize the strain sensor by preventing the conductive particles from falling off the substrate. The said effect therefore ensures excellent stability and higher reproducibility in adsorption-type FCPC-based strain sensors.

In addition to the above-cited factors, other factors such as the tunnelling barrier height, the viscoelastic properties of the polymeric substrate, the strain rate, and the filler content are also crucial in deciding the strain sensing behavior of FCPCs.

Further, an increased tunnelling barrier height in FCPCs leads to higher strain sensitivity, while a higher elasticity in polymer substrates results in better repeatability. Whereas, the electrical response of composites elevate, upon increasing the strain rate, while their strain sensitivity lessens with increasing filler content.

13.7 Conclusions and future directions

Electro-active polymer-based composite materials with excellent strechability and appreciable mechano-electrical response present increased aptness for strain sensing applications. Although such piezo-based strain sensors could operate via different mechanisms, each of these types present their own advantages and tribulations. That is to say, piezocapacitive-type strain sensors offer excellent stretchability, linearity, and hysteresis performance, while suffering from low sensitivity. The piezoresistive-type strain sensors present higher sensitivity and increased stretchability, but suffer from their hysteresis and nonlinearities.

Further, a thoughtful selection of functional fillers and flexible substrates may enable high-performance strain sensors. Such thoughtfully developed electro-active polymer-based strain sensors offer many potential applications that cover the biomedical, robotics, and entertainment sectors.

However, the future commercial success of such materials depends on the successfulness in addressing challenges such as attaining a certain degree of hysteresis, high dynamic responses with low overshoot and decay, robust and flexible packaging, and conformal attachment to the human body.

Acknowledgment

Dr. Nithin K.S., wholeheartedly acknowledges the funding support received under NIE-CRD Research Promotion Scheme.

References

[1] W. Gao, O. Hiroki, K. Daisuke, T. Kuniharu, J. Ali, Flexible electronics towards wearable sensing, ACS Chem. Res. 52 (2019) 523–533.
[2] G.R. Suma, N.K. Subramani, S. Sachhidananda, S.V. Satyanarayana Siddaramaiah, Nanotechnology enabled E. coli sensors: an opto-electronic study, Mater. Today Proc. 4 (2017).
[3] Y. Yang, W. Gao, Wearable and flexible electronics for continuous molecular monitoring, Chem. Soc. Rev. 48 (2019) 1465–1491.
[4] T. Someya, T. Sekitani, S. Iba, Y. Kato, H. Kawaguchi, T. Sakurai, A large-area, flexible pressure sensor matrix with organic field-effect transistors for artificial skin applications, Proc. Natl. Acad. Sci. 101 (2004) 9966–9970.

[5] J. Park, Y. Lee, J. Hong, M. Ha, Y.D. Jung, H. Lim, S.Y. Kim, H. Ko, Giant tunneling piezoresistance of composite elastomers with interlocked microdome arrays for ultrasensitive and multimodal electronic skins, ACS Nano 8 (2014) 4689–4697.
[6] A. Chortos, J. Liu, Z. Bao, Pursuing prosthetic electronic skin, Nat. Mater. 15 (2016) 937.
[7] H. Zhu, X. Wang, J. Liang, H. Lv, H. Tong, L. Ma, Y. Hu, G. Zhu, T. Zhang, Z. Tie, Z. Liu, Versatile electronic skins for motion detection of joints enabled by aligned few-walled carbon nanotubes in flexible polymer composites, Adv. Funct. Mater. 27 (2017) 1606604.
[8] K. Wang, Q. Liu, Q.M. Guan, J. Wu, H.N. Li, J.J. Yan, Enhanced direct electrochemistry of glucose oxidase and biosensing for glucose via synergy effect of graphene and CdS nanocrystals, Biosens. Bioelectron. 26 (2011) 2252–2257.
[9] S. Alwarappan, C. Liu, A. Kumar, C.Z. Li, Enzyme-doped graphene nanosheets for enhanced glucose biosensing, J. Phys. Chem. C 14 (2010) 12920–12924.
[10] J. Zhang, J. Ma, S. Zhang, W. Wang, Z. Chen, A highly sensitive nonenzymatic glucose sensor based on CuO nanoparticles decorated carbon spheres, Sensors Actuators B Chem. 211 (2015) 385–391.
[11] M. Amjaid, A. Pichitpajongkit, S. Lee, S. Ryu, I. Park, Highly stretchable and sensitive strain sensor based on silver nanowire–elastomer nanocomposite, ACS Nano 8 (2014) 5154–5163.
[12] M. Amjadi, Y.J. Yoon, I. Park, Ultra-stretchable and skin-mountable strain sensors using carbon nanotubes–Ecoflex nanocomposites, Nanotechnology 26 (2015) 375501.
[13] K.S. Nithin, Polymer based piezoelectric energy harvesters, Res. Rev. J. Mater. Sci. 4 (2016).
[14] F. Aviles, I.A.O. Aviles, C.P. Marco, Piezoresistivity, strain, and damage self-sensing of polymer composites filled with carbon nanostructures, Adv. Eng. Mater. 20 (2018) 1701159.
[15] K.S. Nithin, Siddaramaiah, Opto-electrical characteristics of poly (vinyl alcohol)/cesium zincate nanodielectrics, J. Phys. Chem. C 119 (2015) 20244–20255.
[16] G. Georgousis, E. Kontou, A. Kyritsis, P. Pissis, M. Micusik, M. Omastova, Piezoresistivity of conductive polymer nanocomposites: experiment and modeling, J. Reinf. Plast. Compos. 37 (2018) 1085–1098.
[17] S. Sachhidananda, G.R. Suma, K.S. Nithin, S.V. Satyanarayana, S. Siddaramaiah, Tuning the electrical and thermal functionalities of mechanically flexible poly (vinyl alcohol) nanocomposites: effect of cerium zirconate nanofiller content, Int. J. Eng. Sci. 1 (2019) 8–14.
[18] M.Q.A. Al-Gunaid, A.M.N. Saeed, K.S. Nithin, B.S. Madhukar, Siddaramaiah, Optical parameters, electrical permittivity and I-V characteristics of PVA/Cs2CuO2 nanocomposite films for opto-electronic applications, J. Mater. Sci. Mater. Electron. 28 (2017) 8074–8086.
[19] K.S. Nithin, S. Kasargod Nagaraj, S. Shivanna, H. Siddaramaiah, Highly flexible and visibly transparent poly (vinyl alcohol)/calcium zincate nanocomposite films for UVA shielding applications as assessed by novel ultraviolet photon induced fluorescence quenching, Macromolecules 49 (2016) 2791–2801.
[20] S. Prashanth, K.M. Subbaiah, K.S. Nithin, S. Sachhidananda, Fiber reinforced composites—a review, J. Mater. Sci. Eng. 6 (2017) 341–342.
[21] A. Tewari, G. Srinivas, B. Siva, C.R. McNeill, G. Dipti, Highly exfoliated MWNT–rGO ink-wrapped polyurethane foam for piezoresistive pressure sensor applications, ACS Appl. Mater. Interfaces 10 (2018) 5185–5195.
[22] Z. Ma, A. Wei, J. Ma, L. Shao, H. Jiang, D. Dong, Z. Ji, Q. Wang, S. Kang, Lightweight, compressible and electrically conductive polyurethane sponges coated with synergistic multiwalled carbon nanotubes and graphene for piezoresistive sensors, Nanoscale 10 (2008) 7116–7126.

[23] H. Kaczmarek, K. Bogusław, K. Ewa, C. Marta, B. Dagmara, Advances in the study of piezoelectric polymers, Russ. Chem. Rev. 88 (2019) 749.
[24] H. Gullapalli, V.S. Vemuru, A. Kumar, A. Botello-Mendez, R. Vajtai, M. Terrones, S. Nagarajaiah, P.M. Ajayan, Flexible PE ZnO–paper nanocomposite strain sensor, Small 6 (2016) 1641–1646.
[25] Z. Chen, Z. Wang, X. Li, Y. Lin, N. Luo, M. Long, N. Zhao, J.B. Xu, Flexible PE-induced pressure sensors for static measurements based on nanowires/graphene heterostructures, ACS Nano 11 (2007) 4507–4513.
[26] S.H. Park, H.B. Lee, S.M. Yeon, J. Park, N.K. Lee, Flexible and stretchable PE sensor with thickness-tunable configuration of electrospun nanofiber mat and elastomeric substrates, ACS Appl. Mater. Interfaces 8 (2016) 24773–24781.
[27] L. Persano, C. Dagdeviren, Y. Su, Y. Zhang, S. Girardo, D. Pisignano, Y. Huang, J.A. Rogers, High performance PE devices based on aligned arrays of nanofibers of poly (vinylidenefluoride-co-trifluoroethylene), Nat. Commun. 4 (2013) 1633.
[28] F. Yiin-Kuen, L. Shan-Chien, C. Chun-Yu, Piezoelectrically and triboelectrically hybridized self-powered sensor with applications to smart window and human motion detection, APL Mater. 5 (2017), 074202.
[29] M. Minary-Jolandan, M.F. Yu, Uncovering nanoscale electromechanical heterogeneity in the subfibrillar structure of collagen fibrils responsible for the piezoelectricity of bone, ACS Nano 3 (2009) 1859–1863.
[30] M. Chen-Glasser, P. Li, J. Ryu, S. Hong, in: S.G. Vassiliadis, D. Matsouka (Eds.), Piezoelectric Materials for Medical Applications, Piezoelectricity—Organic and Inorganic Materials and Applications, IntechOpen, 2018.
[31] J. Shintake, E. Piskarev, S.H. Jeong, D. Floreano, Ultrastretchable strain sensors using carbon black-filled elastomer composites and comparison of capacitive versus resistive sensors, Adv. Mater. Technol. 3 (2018) 1700284.
[32] B.C.-K. Tee, A. Chortos, R.R. Dunn, G. Schwartz, E. Eason, Z. Bao, Tunable flexible pressure sensors using microstructured elastomer geometries for intuitive electronics, Adv. Funct. Mater. 24 (2014) 5427.
[33] D.J. Lipomi, V. Michael, C.K.T. Benjamin, L.H. Sondra, A.L. Jennifer, H.F. Courtney, B. Zhenan, Skin-like pressure and strain sensors based on transparent elastic films of carbon nanotubes, Nat. Nanotechnol. 6 (2011) 788.
[34] D.J. Cohen, D. Mitra, K. Peterson, M.M. Michel, A highly elastic, capacitive strain gauge based on percolating nanotube networks, Nano Lett. 12 (2012) 1821–1825.
[35] M. Kang, J. Kim, B. Jang, Y. Chae, J.H. Kim, J.H. Ahn, Graphene-based three-dimensional Cp touch sensor for wearable electronics, ACS Nano 11 (2017) 7950–7957.
[36] R. Nur, N. Matsuhisa, Z. Jiang, M.O. Nayeem, T. Yokota, T. Someya, A highly sensitive capacitive-type strain sensor using wrinkled ultrathin gold films, Nano Lett. 18 (9) (2018) 5610–5617.
[37] J. Shintake, V. Cacucciolo, D. Floreano, H. Shea, Soft robotic grippers, Adv. Mater. 30 (2018) 1707035.
[38] J. Shintake, T. Nagai, K. Ogishima, Sensitivity improvement of highly stretchable capacitive strain sensors by hierarchical auxetic structures, Front. Robot. AI. 6 (2019) 127.
[39] Y. Lu, M.C. Biswas, Z. Guo, J.W. Jeon, E.K. Wujcik, Recent developments in bio-monitoring via advanced polymer nanocomposite-based wearable strain sensors, Biosens. Bioelectron. 123 (2019) 167–177.
[40] Mahesh, K.M. Subbaiah, K.S. Nithin, B.M.J. Raj, S. Shivanna, Highly flexible and conducting polymer nanocomposite films for selective gas sensing applications, Mater. Today Proc. 9 (2019) 515–521.
[41] K.N. Shilpa, K. Subramani, S. Sachhidananda, B.S. Madhukar, Visibly transparent PVA/sodium doped dysprosia (Na2Dy2O4) nano composite films, with high refractive index: an optical study, J. Alloys Compd. 694 (2017) 884–891.

[42] S. Sandeep, A.S. Santhosh, N.K. Swamy, G.S. Suresh, J.S. Melo, K.S. Nithin, Electrochemical detection of L–dopa using crude polyphenol oxidase enzyme immobilized on electrochemically reduced RGO–Ag nanocomposite modified graphite electrode, Mater. Sci. Eng. B Solid-State Mater. Adv. Technol. 232 (2018) 15–21.
[43] K.N. Shilpa, S.R. Urs, H.B. Patil, H.P. Jayadevappa, B.V. Latha, K.S. Nithin, S. Sachhidananda, Adsorptive removal of Cu (II) from aqueous solution using nanostructured Lithium Zincate, Int. J. Eng. Sci. Comput. 6 (2016) 8463–8468.
[44] K.N. Shilpa, H.B. Patil, P. Karthik, K. Mallikarjun, B.M. JagajeevanRaj, S. Sharon, K.S. Nithin, Removal of Cu (II) from water using hydrothermally synthesized strontium doped zirconium oxide nano adsorbents, J. Mater. Sci. Eng. 1 (2016) 252–256.
[45] G.R. Suma, K.S. Nithin, B.V. Latha, S.K. Nagaraj, S. Shivanna, S.V. Sathyanarayana, Gent to refractive index engineering of strontium doped zirconium oxide (SZO) reinforced poly vinyl pyrrolidone composite films: effect of dopant content and annealing temperature, Int. J. Eng. Sci. Comput. 6 (2016) 5703–5709.
[46] B. Suresha, R. Hemanth, K.S. Nithin, Automotive Applications: Reinforced Material Components, Encyclopedia of Polymer Applications, CRC Press, 2018.
[47] A.M.N. Saeed, M.Q.A. Al-Gunaid, N.K. Subramani, B.S. Madhukar, S. Basavarajaiah, Effect of cesium aluminate nanofiller on optical properties of polyvinyl pyrrolidone nanocomposite films, Polym.-Plast. Technol. Eng. 57 (2008) 1188–1196.
[48] S. Shivanna, N.K. Subramani, S.K. Nagaraj, J.R.B. Mutturaj, S. Basavaraj, Patina–green coloured light emitting polycarbonate films: a synergistic extraction of improved UV endurance and considerate spectral down–conversion, J. Lumin. 210 (2019) 276–284.
[49] K.K. Kim, S. Hong, H.M. Cho, J. Lee, Y.D. Suh, J. Ham, S.H. Ko, Highly sensitive and stretchable multidimensional strain sensor with prestrained anisotropic metal nanowire percolation networks, Nano Lett. 15 (2015) 5240–5247.
[50] R. Ma, B. Kang, S. Cho, M. Choi, S. Baik, Extraordinarily high conductivity of stretchable fibers of polyurethane and silver nanoflowers, ACS Nano 9 (2015) 10876–10886.
[51] C. Yan, J. Wang, W. Kang, M. Cui, X. Wang, C.Y. Foo, K.J. Chee, P.S. Lee, Highly stretchable piezoresistive graphene–nanocellulose nanopaper for strain sensors, Adv. Mater. 26 (2014) 2022–2027.
[52] M.Z. Seyedin, J.M. Razal, P.C. Innis, G.G. Wallace, Strain-responsive polyurethane/PEDOT:PSS elastomeric composite fibers with high electrical conductivity, Adv. Funct. Mater. 24 (2014) 2957–2966.
[53] K. Takei, Z. Yu, M. Zheng, H. Ota, T. Takahashi, A. Javey, Highly sensitive electronic whiskers based on patterned carbon nanotube and silver nanoparticle composite films, Proc. Natl. Acad. Sci. U. S. A. 111 (2014) 1703–1707.
[54] B. Sun, Y.Z. Long, S.L. Liu, Y.Y. Huang, J. Ma, H.D. Zhang, G. Shen, S. Xu, Fabrication of curled conducting polymer microfibrous arrays via a novel electrospinning method for stretchable strain sensors, Nanoscale 5 (2013) 7041–7045.
[55] M. Hempel, D. Nezich, J. Kong, M. Hofmann, A novel class of strain gauges based on layered percolative films of 2D materials, Nano Lett. 12 (2012) 5714–5718.
[56] P. Lee, J. Lee, H. Lee, J. Yeo, S. Hong, K.H. Nam, D. Lee, S.S. Lee, S.H. Ko, Highly stretchable and highly conductive metal electrode by very long metal nanowire percolation network, Adv. Mater. 24 (2012) 3326–3332.
[57] D. Kang, P.V. Pikhitsa, T.W. Choi, C. Lee, S.S. Shin, L. Piao, B. Park, K.Y. Suh, T.I. Kim, M. Choi, Ultrasensitive mechanical crack-based sensor inspired by the spider sensory system, Nature 516 (2014) 222–226.
[58] X. Li, R. Zhang, W. Yu, K. Wang, J. Wei, D. Wu, A. Cao, Z. Li, Y. Cheng, Q. Zheng, R.S. Ruoff, H. Zhu, Stretchable and highly sensitive graphene-on-polymer strain sensors, Sci. Rep. 2 (2012) 870.

[59] S. Gong, D.T.H. Lai, B. Su, K.J. Si, Z. Ma, L.W. Yap, P. Guo, W. Cheng, Highly stretchy black gold E-skin nanopatches as highly sensitive wearable biomedical sensors, Adv. Electron. Mater. 1 (2015) 1400063.
[60] X. Yang, Y. Zhao, J. Xie, X. Han, J. Wang, C. Zong, H. Ji, J. Zhao, S. Jiang, Y. Cao, Bioinspired fabrication of free-standing conducting films with hierarchical surface wrinkling patterns, ACS Nano 10 (2016) 3801–3808.
[61] A. Frutiger, J.T. Muth, D.M. Vogt, Y. Mengüç, A. Campo, A.D. Valentine, C.J. Walsh, J.A. Lewis, Capacitive soft strain sensors via multicore-shell fiber printing, Adv. Mater. 27 (2015) (2015) 2440–2446.
[62] Y. Takeo, H. Yuhei, Y. Yuki, Y. Yoshiki, I. Ali, N.F. Don, H. Kenji, A stretchable carbon nanotube strain sensor for human-motion detection, Nat. Nanotechnol. 6 (2011) 296–301.
[63] X. Xiao, L. Yuan, J. Zhong, T. Ding, Y. Liu, Z. Cai, Y. Rong, H. Han, J. Zhou, Z.L. Wang, High-strain sensors based on ZnO nanowire/polystyrene hybridized flexible films, Adv. Mater. 23 (2011) 5440–5444.
[64] L. Cai, L. Song, P. Luan, Q. Zhang, N. Zhang, Q. Gao, D. Zhao, X. Zhang, M. Tu, F. Yang, W. Zhou, Q. Fan, J. Luo, W. Zhou, P.M. Ajayan, S. Xie, Super-stretchable, transparent carbon nanotube-based capacitive strain sensors for human motion detection, Sci. Rep. 3 (2013) 1–9.
[65] Y.R. Jeong, H. Park, S.W. Jin, S.Y. Hong, S.S. Lee, J.H. Sook, Highly stretchable and sensitive strain sensors using fragmentized graphene foam, Adv. Funct. Mater. 25 (2015) 4228–4236.
[66] C. Mattmann, F. Clemens, G. Troster, Sensor for measuring strain in textile, Sensors 8 (2008) 3719–3732.
[67] N. Lu, C. Lu, S. Yang, J. Rogers, Highly sensitive skin-mountable strain gauges based entirely on elastomers, Adv. Funct. Mater. 22 (2012) 4044–4050.
[68] U.H. Shin, D.W. Jeong, S.M. Park, S.H. Kim, H.W. Lee, J.M. Kim, Highly stretchable conductors and piezocapacitive strain gauges based on simple contact-transfer patterning of carbon nanotube forests, Carbon 80 (2014) 396–404.
[69] J.T. Muth, D.M. Vogt, R.L. Truby, Y. Menguç, D.B. Kolesky, R.J. Wood, J.A. Lewis, Embedded 3D printing of strain sensors within highly stretchable elastomers, Adv. Mater. 26 (2014) 6307–6312.
[70] S. Gong, T.H.L. Daniel, Y. Wang, L.W. Yap, K.J. Si, Q. Shi, N.N. Jason, T. Sridhar, H. Uddin, W. Cheng, Tattoolike polyaniline microparticle-doped gold nanowire patches as highly durable wearable sensors, ACS Appl. Mater. Interfaces 7 (2015) 19700–19708.
[71] B.U. Hwang, J.H. Lee, T.Q. Trung, E. Roh, D.I. Kim, S.W. Kim, N.E. Lee, Transparent stretchable self-powered patchable sensor platform with ultrasensitive recognition of human activities, ACS Nano 9 (2015) 8801–8810.
[72] E. Roh, B.U. Hwang, D. Kim, B.Y. Kim, N.E. Lee, Stretchable, transparent, ultrasensitive, and patchable strain sensor for human-machine interfaces comprising a nanohybrid of carbon nanotubes and conductive elastomers, ACS Nano 9 (2015) 6252–6261.
[73] Y. Liu, H. Wang, W. Zhao, M. Zhang, H. Qin, Y. Xie, Flexible, stretchable sensors for wearable health monitoring: sensing mechanisms, materials, fabrication strategies and features, Sensors 18 (2018) 645.
[74] M. Amjadi, K.U. Kyung, I. Park, M. Sitti, Stretchable, skin-mountable, and wearable strain sensors and their potential applications: a review, Adv. Funct. Mater. 26 (2016) 1678–1698.
[75] C.S. Boland, U. Khan, C. Backes, A. O'Neill, J. McCauley, S. Duane, R. Shankar, Y. Liu, I. Jurevicz, A.B. Dalton, J.N. Coleman, Sensitive, high-strain, high-rate bodily motion sensors based on graphene-rubber composites, ACS Nano 8 (2014) 8819–8830.
[76] S. Yao, Y. Zhu, Wearable multifunctional sensors using printed stretchable conductors made of silver nanowires, Nanoscale 6 (2014) 2345–2352.

[77] X. Kuang, K. Chen, C.K. Dunn, J. Wu, V.C. Li, H.J. Qi, 3D printing of highly stretchable, shape-memory and self-healing elastomer toward novel 4D printing, ACS Appl. Mater. Interfaces 10 (2018) 7381–7388.
[78] S. Liu, O. Oderinde, I. Hussain, F. Yao, G. Fu, Dual ionic cross-linked double network hydrogel with self-healing, conductive, and force sensitive properties, Polymer 144 (2018) 111–120.
[79] S. Liu, Y. Lin, Y. Wei, S. Chen, J. Zhu, L. Liu, A high performance self-healing strain sensor with synergetic networks of poly (ε-caprolactone) microspheres, graphene and silver nanowires, Compos. Sci. Technol. 146 (2017) 110–118.
[80] J.C. Lai, J.F. Mei, X.Y. Jia, C.H. Li, X.Z. You, Z. Bao, A stiff and healable polymer based on dynamic-covalent boroxine bonds, Adv. Mater. 28 (2016) 8277–8282.
[81] C.A. Poland, R. Duffin, I. Kinloch, A. Maynard, W.A. Wallace, A. Seaton, V. Stone, S. Brown, W. MacNee, K. Donaldson, Carbon nanotubes introduced into the abdominal cavity of mice show asbestos-like pathogenicity in a pilot study, Nat. Nanotechnol. 3 (2008) 423.
[82] J. Eom, R. Jaisutti, H. Lee, W. Lee, J.S. Heo, J.Y. Lee, S.K. Park, Y.H. Kim, Highly sensitive textile strain sensors and wireless user-interface devices using all-polymeric conducting fibers, ACS Appl. Mater. Interfaces 9 (2017) 10190–10197.
[83] M. Shi, H. Wu, J. Zhang, M. Han, B. Meng, H. Zhang, Self-powered wireless smart patch for healthcare monitoring, Nano Energy 32 (2017) 479–487.
[84] Y. Tang, Z. Zhao, H. Hu, Y. Liu, X. Wang, S. Zhou, J. Qiu, Highly stretchable and ultrasensitive strain sensor based on reduced graphene oxide microtubes–elastomer composite, ACS Appl. Mater. Interfaces 49 (2015) 27432–27439.
[85] X. Yangyang, J. Zhou, R. Tao, X. Xu, G. Lubineau, Making a bilateral compression/tension sensor by pre-stretching open-crack networks in carbon nanotube papers, ACS Appl. Mater. Interfaces 10 (2018) 33507–33515.
[86] S. Zhang, H. Deng, Q. Zhang, Q. Fu, Formation of conductive networks with both segregated and double-percolated characteristic in conductive polymer composites with balanced properties, ACS Appl. Mater. Interfaces 6 (2014) 6835–6844.
[87] Y. Wei, S. Chen, X. Yuan, P. Wang, L. Liu, Multiscale wrinkled microstructures for piezoresistive fibers, Adv. Funct. Mater. 26 (2016) 5078–5085.
[88] J. Wang, F. Tang, Y. Wang, Q. Lu, S. Liu, L. Li, Self-healing and highly stretchable gelatin hydrogel for self-powered strain sensor, ACS Appl. Mater. Interfaces 12 (2020) 1558–1566.
[89] S.K. Nagaraj, S. Shivanna, N.K. Subramani, H. Siddaramaiah, Revisiting powder X–ray diffraction technique: a powerful tool to characterize polymers and their composite films, J. Mater. Sci. 4 (2016) 1–5.
[90] K.S. Nithin, S. Shivanna, S.K. Nagaraj, H. Siddaramaiah, Refractive index engineering of poly(vinylalcohol)/Li2ZnO2 nanocomposites: effect of filler content and annealing temperature, AIP Conf. Proc. 1943 (2018) 020127–020128.
[91] B.M. Jagajeevanraj, S. Sachhidananda, K. Pushpalatha, K.S. Nithin, Nanostructured $Al_{0.2}Y_{1.8}O_3$ semiconductor assisted enhancement in PVOH fortitude to withstand high energy UV photons: an opto–mechanical study, Optik 182 (2019) 598–604.
[92] B. Suresha, K. Adappa, N.K. Subramani, Mechanical and tribological behaviours of epoxy hybrid composites reinforced by carbon fibers and silicon carbide whiskers, Mater. Today Proc. 5 (2018) 16658–16668.
[93] K.S. Nithin, S. Kasargod Nagaraj, S. Shivanna, H. Siddaramaiah, Yellow–green luminescent poly (vinyl alcohol) nanocomposite thick films as effective spectral manipulators, J. Appl. Polym. Sci. 135 (2018) 46854–46855.
[94] K. Muller, E. Bugnicourt, M. Latorre, M. Jorda, Y.E. Sanz, J.M. Lagaron, O. Miesbauer, A. Bianchin, S. Hankin, U. Bolz, G. Perez, M. Jesdinszki, M. Lindner, Z. Scheuerer, S. Castello, M. Schmid, Review on the processing and properties of

polymer nanocomposites and nanocoatings and their applications in the packaging, automotive and solar energy fields, Nanomaterials. 7 (2017) 74.
[95] M. Tirumali, B. Kandasubramanian, A. Kumaraswamy, N.K. Subramani, B. Suresha, Fabrication, physicochemical characterizations and electrical conductivity studies of modified carbon nanofiber-reinforced epoxy composites: effect of 1-butyl-3-methylimidazolium tetrafluoroborate ionic liquid, Polym.-Plast. Technol. Eng. 57 (2018) 218–228.
[96] S. Shivanna, K.S. Nithin, S. Kasargod Nagaraj, H. Siddaramaiah, Orange–red fluorescent polymer nanocomposite films with large stokes shift: an opto–electronic exercise, J. Lumin. 208 (2019) 488–494.
[97] H. Yan, Y. Chen, Y. Deng, L. Zhang, X. Hong, W. Lau, J. Mei, D. Hui, H. Yan, Y. Liu, Coaxial printing method for directly writing stretchable cable as strain sensor, Appl. Phys. Lett. (2016).
[98] J.H. Kongh, N.S. Jang, S.H. Kim, J.M. Kim, Simple and rapid micropatterning of conductive carbon composites and its application to elastic strain sensors, Carbon 77 (2014) 199–207.
[99] S.H. Bae, Y. Lee, B.K. Sharma, H.J. Lee, J.H. Kim, J.H. Ahn, Graphene-based transparent strain sensor, Carbon 51 (2013) 236–242.
[100] W. Yan, W. Li, T. Yang, X. Li, X. Zang, M. Zhu, K. Wang, D. Wu, H. Zhu, Wearable and highly sensitive graphene strain sensors for human motion monitoring, Adv. Funct. Mater. 24 (2014) 4666–4670.
[101] C.X. Liu, J.W. Choi, Analyzing resistance response of embedded PDMS and carbon nanotubes composite under tensile strain, Microelectron. Eng. 117 (2014) 1–7.
[102] C. Lee, L. Jug, E. Meng, High strain biocompatible polydimethylsiloxane-based conductive graphene and multiwalled carbon nanotube nanocomposite strain sensors, Appl. Phys. Lett. 102 (2013) 183511.
[103] J.H. Lee, D. Yang, S. Kim, I. Park, Stretchable Strain Sensor Based on Metal Nanoparticle Thin Film for Human Motion Detection & Flexible Pressure Sensing Devices, IEEE, 2013.
[104] R. Rahimi, O. Manuel, Y. Wuyang, Z. Babak, Highly stretchable and sensitive unidirectional strain sensor via laser carbonization, ACS Appl. Mater. Interfaces 7 (2015) 4463–4470.
[105] G. Yang, F. Xiaoliang, T. Jianping, L. Ting, P. Likun, X. Fuzhen, Highly sensitive strain sensors based on fragmentized carbon nanotube/polydimethylsiloxane composites, Nanotechnology 29 (2018) 235501.
[106] H. Du, C. Zhao, J. Lin, Z. Hu, Q. Shao, J. Guo, B. Wang, D. Pan, E.K. Wujcik, Z. Guo, Carbon nanomaterials in direct liquid fuel cells, Chem. Rec. 18 (2018) 1365–1372.
[107] J. Ren, C. Wang, X. Zhang, T. Carey, K. Chen, Y. Yin, F. Torrisi, Environmentally-friendly conductive cotton fabric as flexible strain sensor based on hot press reduced graphene oxide, Carbon 111 (2017) 622–630.
[108] C. Yan, J. Wang, W. Kang, M. Cui, X. Wang, C.Y. Foo, K.J. Chee, P.S. Lee, Graphene: highly stretchable piezoresistive graphene–nanocellulose nanopaper for strain sensors, Adv. Mater. 26 (2014) 1950.
[109] D.S. Kim, Y.J. Jeong, B.K. Lee, A. Shanmugasundaram, D.W. Lee, Piezoresistive sensor-integrated PDMS cantilever: a new class of device for measuring the drug-induced changes in the mechanical activity of cardiomyocytes, Sensor. Actuat. B Chem. 240 (2017) 566–572.
[110] S. Ge, Z. Zhao, J.H. Pai, I. Lee, L. Zhang, C. Stevenson, K. Ishara, R. Zhang, H. Zhu, J. Ma, Highly sensitive, wearable, durable strain sensors and stretchable conductors using graphene/silicon rubber composites, Adv. Funct. Mater. 26 (2016) 7614–7625.
[111] Y. Li, Y.A. Samad, T. Taha, G. Cai, S.Y. Fu, K. Liao, Highly flexible strain sensor from tissue paper for wearable electronics, ACS Sustain. Chem. Eng. 4 (2016) 4288–4295.

[112] J. Engel, J. Chen, C. Liu, B.R. Flachsbart, J.C. Selby, M.A. Shannon, Development of polyimide-based flexible tactile sensing skin, MRS (OPL) Arch. (2002) 736.
[113] Y.T. Huang, S.C. Huang, C.C. Hsu, R.M. Chao, Polyimide-based Single-walled carbon nanonets (SWCNNs) flexible strain sensor for bone, in: International Conference on Bioinformatics and Biomedical Technology, 2010.
[114] T. Han, A. Nag, N. Afsarimanesh, F. Akhter, H. Liu, S. Sapra, S. Mukhopadhyay, Y. Xu, Gold/Polyimide based resistive SRs, Electronics 8 (2019) 565.
[115] G.Y. Yang, G. Johnson, W.C. Tang, J.H. Keyak, Parylene-based strain sensors for bone, IEEE Sensors J. 7 (2007) 1693–1697.
[116] Y.T. Huang, S.C. Huang, C.C. Hsu, R.M. Chao, T.K. Vu, Design and fabrication of single-walled carbon nanonet flexible strain sensors, Sensors 12 (2012) 3269–3280.
[117] C.L. Chen, E. Lopez, Y.J. Jung, S. Muftu, S. Selvarasah, M.R. Dokmeci, Mechanical and electrical evaluation of parylene-C encapsulated carbon nanotube networks on a flexible substrate, Appl. Phys. Lett. 93 (2008), 093109.
[118] W. Xiaodong, Y. Han, X. Zhang, C. Lu, Highly sensitive, stretchable, and wash-durable strain sensor based on ultrathin conductive layer@polyurethane yarn for tiny motion monitoring, ACS Appl. Mater. Interfaces 8 (2016) 9936–9945.
[119] Q. Fan, Z. Qin, S. Gao, Y. Wu, J. Pionteck, E. Mäder, M. Zhu, The use of a carbon nanotube layer on a polyurethane multifilament substrate for monitoring strains as large as 400%, Carbon 50 (2012) 4085–4092.
[120] Y. Li, K. Dai, G. Zheng, C. Liu, C. Shen, X. Yan, J. Guo, Z. Guo, Electrically conductive thermoplastic elastomer nanocomposites at ultralow graphene loading levels for strain sensor applications, J. Mater. Chem. C 4 (2016) 157–166.
[121] M. Li, H. Li, W. Zhong, Q. Zhao, D. Wang, Stretchable conductive polypyrrole/polyurethane (PPy/PU) strain sensor with netlike microcracks for human breath detection, ACS Appl. Mater. Interfaces 6 (2014) 1313–1319.
[122] G.H. Lim, N.E. Lee, B. Lim, Highly sensitive, tunable, and durable gold nanosheet strain sensors for human motion detection, J. Mater. Chem. C 4 (2016) 5642–5647.
[123] M. Amjadi, I. Park, Carbon nanotubes-ecoflex nanocomposite for strain sensing with ultra-high stretchability, in: IEEE International Conference on Micro Electro Mechanical Systems (MEMS), 2015.
[124] T. Giffney, E. Bejanin, A.S. Kurian, J. Travas-Sejdic, K. Aw, Highly stretchable printed strain sensors using multi-walled carbon nanotube/silicone rubber composites, Sens. Actuators A Phys. 259 (2017) 44–49.
[125] S. Ryu, P. Lee, J.B. Chou, R. Xu, R. Zhao, A.J. Hart, S.G. Kim, Extremely elastic wearable carbon nanotube fiber strain sensor for monitoring of human motion, ACS Nano 9 (2015) 5929–5936.
[126] G.R. Suma, K.S. Nithin, S. Sachhidananda, S.V. Satyanarayana, Siddaramaiah, Optical and electrical evaluation of $Ag_{0.5}Cu_{0.75}O$ introduced poly (vinyl alcohol) based E. coli sensors, J. Mater. Sci. Mater. Electron. 28 (2017) 13139–13148.
[127] G.R. Suma, K.S. Nithin, K.N. Shilpa, S. Sachhidananda, S.V. Satyanarayana, Siddaramaiah, Effect of Ce0.5Zr0.5O2 nano fillers on structural and optical behaviors of poly(vinyl alcohol), J. Mater. Sci. Mater. Electron. 28 (2017) 10707–10714.
[128] K.S. Nithin, S. Shivanna, S. Nagaraj, S. Chinmayee, S. Basavarajaiah, Poly (vinyl alcohol) decorated lithium doped stannous oxide nanocomposites as highly flexible UVA shieldants, Chem. Sci. J. 7 (2016) 121–122.
[129] X. Cui, G. Zhu, Y. Pan, Q. Shao, M. Dong, Y. Zhang, Z. Guo, Polydimethylsiloxane-titania nanocomposite coating: fabrication and corrosion resistance, Polymer 138 (2018) 203–210.
[130] C. Jianwen, Q. Yu, X. Cui, M. Dong, J. Zhang, C. Wang, J. Fan, Y. Zhu, Z. Guo, An overview of stretchable strain sensors from conductive polymer nanocomposites, J. Mater. Chem. C 7 (2019) 11710–11730.

14

Nanotechnology-enabled polymer-based flexible electronics and their potential applications

B.J. Kishen Karumbaiah[a,b], K.S. Nithin[c], K.R. Prakash[d], V. Ravi Kumar[d,e], K.N. Shilpa[f], T. Basava[b], P. Shruthi[c], and S. Sachhidananda[f]

[a]Department of Mechanical Engineering, Coorg Institute of Technology, Ponnampet, India, [b]Department of Mechanical Engineering, Sri Dharmasthala Manjunatheshwara Institute of Technology, Ujire, India, [c]Department of Chemistry, The National Institute of Engineering, Mysuru, India, [d]Department of Mechanical Engineering, The National Institute of Engineering, Mysuru, India, [e]Department of Mechanical Engineering, Amrita School of Engineering, Amrita Vishwa Vidyapeetham, Bengaluru, India, [f]Department of Polymer Science and Technology, Sri Jayachamarajendra College of Engineering, JSS Science and Technology University, Mysuru, India

14.1 Introduction

Smart materials represent an important class of advanced material systems with stimuli-responsive material properties [1]. Smartness refers to the ability of material to sense, adapt, memorize, and exhibit the appropriate response [2]. These advanced functional materials often present intelligent functionalities that display a reversible dependence on external stimulus [3]. Consequently, such stimuli-responsive materials offer diverse techno-commercial applications, that covers aerospace, robotics, optoelectronics, biomedical, structural health monitoring, self-healing, and other related sectors [4–6].

Although a number of ceramic-based smart materials have been continuously reported, they often suffer from a low coefficient of friction and therefore fall short for those applications that demand high dimensional tolerance [7]. Which in-turn paved the way for polymer-based smart materials. Stretchable electronics is one such fast-emerging technological sector that demand high dimensional tolerance. As a

Polymer-Based Advanced Functional Composites for Optoelectronic and Energy Applications
https://doi.org/10.1016/B978-0-12-818484-4.00013-6
Copyright © 2021 Elsevier Inc. All rights reserved.

consequence, polymer-based electro-active materials have gained significant technological interest. Further, there also exists a vast chemical design space to molecularly engineer the material functionalities of polymers [8]. Going forward, the possibility of introducing nanostructured materials with important cooperative physicochemical phenomena, has opened up diverse opportunities in the field of electro-active polymer composite-based flexible electronics [5, 6, 9]. Additionally, conventional rigid wafer-based electronics are intrinsically noncompatible with curvilinear and deformable architectures. While, mechanically flexible and wearable electronics enable facile interaction with both the human body and materials, in addition to offering long-term health monitoring abilities, with minimum discomfort [10–13]. Consequently, nanotechnology-enabled polymer-based electro-active smart materials show promising implications in structural health monitoring and human motion monitoring applications.

Human skin presents multiple advanced functionalities such as an adequate response to external stimulus, imparting elasticity to joints and muscle activity, and autonomous self-healing [14]. Such significant inspirations drawn from the multiple functionalities offered by human skin and the closeness in properties of polymer nanocomposites (PNCs) with human skin have prompted the scientific community to explore and integrate functions of skin into electronic devices [15, 16]. This is thanks to the particle size and morphology-dependent end properties of nanomaterials, together with the processing ease, mechanical flexibility, and skin-like material behaviors of polymers [17, 18]. Thus, in recent years, the scientific community has witnessed the development of a number of mechanically flexible and wearable electronics-based sensors and actuators. Such flexible electro-active materials were made possible from a thoughtful combination of functional nanofillers introduced, embedded, and/or mounted on flexible polymers. Herein, an attempt is made to summarize some of the latest breakthrough research outcomes on nanotechnology-enabled polymer-based electro-active smart materials and their related applications. Plus, special emphasis is paid to nanotechnology-enabled polymer-based electro-active smart composites as skin-inspired electronics.

14.2 Polymer-based electro-active smart composites

Polymer-based smart materials are mostly mechanically flexible soft materials that display reversibly large physical or chemical changes in response to an external stimulus. Based on the actual stimulus they respond to, such polymer-based soft material-enabled smart composites are classified as thermo-active (temperature as the

stimulus), photo-active (light as the stimulus), electro-active (electric field as the stimulus), and other stimuli-active materials. Accordingly, electro-active polymer-based smart composites (EAPBSCs) show an inherent ability to reversibly change their physicochemical functionalities with applied electric fields. Of all the stimuli-active materials available, EAPBSCs stand tall,as among the most preferred smart materials with potential sensor- and actuator-related applications. That privilege may be owed to their large active deformation potential, high response speed, low density, and improved resilience [19].

In addition, these materials are also extremely fracture-tolerant, lighter, and can withstand large mechanical stress [20]. EAPBSCs may be further classified as ionic EAPBSCs and electronic EAPBSCs. While ionic EAPBSCs have the advantage of being actuated with low voltages (as low as 1–2 V), they demand that the electrolyte maintain its wetness during operation. It is this demand for wetness (during operation) that renders ionic EAPBSCs commercially less viable [21]. On the other hand, electronic or dielectric EAPBSCs operate under very high activation electrical fields and in dry conditions. Additionally, the fact that electronic EAPBSCs can respond very quickly to voltage stimuli and can retain their induced deformations, even with relatively large stress [22], make them the preferred EAPBSCs.

EAPBSCs respond to an applied electrical signal either via a thoughtful display of mechanical actuation and/or stress within the material or show a change in electrical response (capacitance, resistance, and conductance) corresponding to the applied mechanical load or pressure. It is the second type of EAPBSCs that are preferred for wearable sensor applications. Although many different strain sensors transduce mechanical stimulus into electrical signals, only the piezo-based (piezoresistive, piezoelectric, and piezocapacitive) EAPBSCs are being extensively investigated for skin-mountable and wearable strain sensors. This is because they offer relatively simple read-out systems and high design flexibilities (improved mechanical flexibility and strechability). Further, an ideal sensor must present a linear correlation in sensing response (resistance or capacitance) with the applied strain. In addition, the changes in their sensing response (with applied pressure) must be large enough to be easily quantified.

14.3 Applications of nanotechnology-enabled polymer smart composite-based flexible electronics

Mechanically flexible, soft electronic devices enable numerous interesting applications, including personalized patient care, soft robotics, human-machine interfaces, and so forth [23–25]. Thus, materials

that are relatively less strain-sensitive could be used for structural health monitoring, mass measurement, and pressure sensing applications [26–28]. While, materials that offer high strain sensitivity and improved mechanical flexibility could be utilized as body-integrated electronic devices. However, polymer-based electro-active soft materials would be more beneficial for soft-bodied robotic applications. Fig. 14.1 gives the pictorial representation of diverse applications, that take advantage of polymer-based electro-active smart materials. While, Table 14.1 presents some of the important polymer smart composite-based electro-active materials, their performance metrics, and related applications.

14.3.1 Sports performance monitoring

Polymer-based electro-active smart composites that offer wearable and skin-mountable features could serve in sports performance monitoring applications. Piezo-resistive smart composites mounted on a wrist, elbow, or joint that show a change in resistance upon bending may be employed toward body movement analysis during various sport activities. Polymer-based Rosette type-strain sensors, which are capable of sensing the direction of strain under in-plane deformations, may be used to monitor tissue swelling and/or expansion during various physical activities to compute body fitness and/or wellness analysis [17, 71–75].

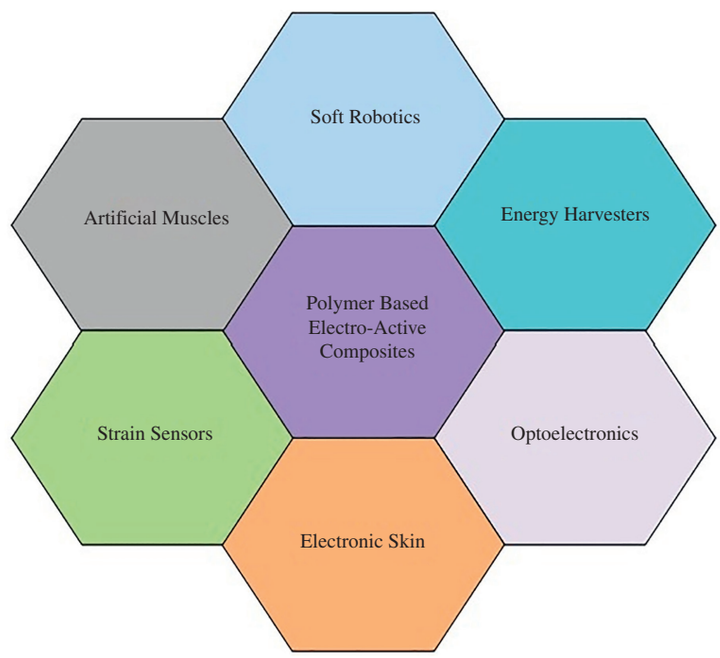


Fig. 14.1 Pictorial representation of diverse application domains of polymer-based electro-active smart materials.

Table 14.1 Some of the important polymer-based electro-active materials, their performance metrics, and related applications.

Material	Related application	Target Signal	Output magnitude	Stretchability (%)	Ref.
Rare earth salt (Er^{+}+PVDF)	Voice sensor	Conductivity	$0.125\,W\,m^{-2}$	–	[29]
Nano barium ferrite/PAA hydogel	Flexible, wearable	Conductivity	$1.22\times10^{-2}\,S\,cm^{-1}$	–	[30]
Ag-PDMS	Flexible antenna	Conductivity	$1000\,S\,cm^{-1}$	20	[31]
STEP microfibers	Smart fabrics	Conductivity	$3.27\,MS\,m^{-1}$	120	[32]
Electrically conductive hydrogel	Implantable microelectronics	Conductivity	$47.4\,S\,cm^{-1}$	–	[33]
Ag-Au nanowires/elastomer	Wearable bioelectronic devices	Conductivity	$41{,}850\,S\,cm^{-1}$	266	[34]
Fluoro-carbon elastomer	Wearable sensors	Conductivity	$10^{-3}\,S\,cm^{-1}$	2000	[35]
AgF/AgNP/MPU/IU/PDMS	Robots and ultrastrechable self-healing	Conductivity	$3086\,S\,cm^{-1}$	3500	[36]
CBS/DPP	Flexible electronics	Conductivity	$6.2\,S\,cm^{-1}$	180	[37]
NaCl/PEGDA/$FeCl_3$/hydrogel	Wearable sensors	Ionic conductivity	$5.5\times10^{-3}\,S\,cm^{-1}$	–	[38]
MWCNT/silicone	Bending motion monitors	Strain sensitivity	1.5 (GF)	300	[39]
MXene(Ti_3C_2T)/hydrogel	Wearable electronics	Strain sensitivity	80 (GF)	3400	[40]
PVDF/PU/MWCNT(PPM) aerogels	Pressure sensing	Strain sensitivity	157 (GF)	–	[41]
MOF nanofilm	Flexible sensors	Strain sensitivity	10000 (GF)	–	[42]
DPP-TVT-PDCA/PDMS-PDCA	Skin-like active strain sensors	Strain sensitivity	5.75×10^{5} (GF)	1500	[43]
$Ti_3C_2T_x$ MXene nanostacks/CNT	Health and sporting	Strain sensitivity	772.6 (GF)	130	[44]
PDA-talc/PAM hydrogel	Human-friendly biological devices	Strain sensitivity	0.693 (GF)	1000	[45]
Agar/NaCl/PAM DN ionic hydrogel	Transparent strain sensors	Strain sensitivity	2.1 (GF)	1920	[46]
ACNF/PDMS	Flexible electronics	Strain sensitivity	180 (GF)	30	[47]
(IL)/PMMA-r-PBA	Healthcare devices and smart textiles	Strain sensitivity	2.73 (GF)	850	[48]

Continued

Table 14.1 Some of the important polymer-based electro-active materials, their performance metrics, and related applications—cont'd

Material	Related application	Target Signal	Output magnitude	Stretchability (%)	Ref.
PVA/glycerol/NaCl/ ionic hydrogel	Wearable sensors	Strain sensitivity	4.01 (GF)	570	[49]
Eutectic gallium indium/elastomer microtubes	Motion sensors	Resistivity	$2.9\times10^{-6}\,\Omega$cm	600	[50]
Rare earth salt (Er^{3+}+PVDF)	Energy harvesting	Current output	15.5 μA	–	[29]
Reduced graphene oxide/polyaniline nanowires	Pressure sensors	Current output	300 μA	–	[51]
MBAA/EG/PVA/ PAA/hydrogel	Self-healing	Healing efficiency	90.4%	550	[52]
Graphene oxide/ polyimide	Sweat sensors	Ampermoteric sensitivity	48 μA/mMcm^2	–	[53]
Supermolecular polymer materials	Flexible electronics	Fracture toughness	30,000 J m^{-2}	400	[54]
PDMS oligomers/ hydrogen bonding	E-skin and wearable electronics	Fracture toughness	12,000 J m^{-2}	1200	[55]
PVA/glycerol/NaCl (PGN) ionic hydrogel	Biomimetic prostheses	Mechanical toughness	8.65 MJ m^{-3}	570	[49]
TA/CNC ionic gels	Health care monitoring	Mechanical toughness	5.60 MJ m^{-3}	2900	[56]
(IL)/PMMA-r-PBA	Healthcare devices and smart textiles	Elastic modulus	3.1×10^5 Pa	850	[48]
Chitosan/TA/CNC/ nanocomposite hydrogel	Adhesives	Fracture strength	1.2 MPa	800	[57]
Supermolecular polymer materials	Flexible electronics	Tensile strength	3.74 MPa	17000	[54]
Zwitterionic hydrogel	Mechano sensory electronics	Compressive strength	7.5 MPa	1000	[58]
Agar/NaCl/PAM DN ionic hydrogel	Transparent strain sensors	Tensile strength and compressive strength	400 kPa and 2.7 MPa	1920	[46]
Acrylamide and polyvinyl alcohol hydrogel	Pressure sensors	Pressure sensitivity	0.02 kPa^{-1} for pressure range (3.27–6.85 kPa)	500	[59]

Table 14.1 Some of the important polymer-based electro-active materials, their performance metrics, and related applications—cont'd

Material	Related application	Target Signal	Output magnitude	Stretchability (%)	Ref.
Graphene film/ PDMS	Pulse monitoring	Sensitivity/linear detection range	1875.53 kPa^{-1} for pressure range (0–40 kPa)	–	[60]
Ag NP/Polyimine nanocomposites	E-skin and tactile sensing	Pressure sensitivity	0.0067 kPa^{-1} for pressure range (0–3.27 kPa)	500	[61]
PPDL/PS/ITO/PET/ PDMS	E-skin and pressure sensing	Capacitive pressure sensitivity	449 kPa^{-1} for pressure range (0–100 kPa)	–	[62]
β-phase PVDF/TrFE polymer	Piezoelectric energy harvesting	Output power density	16.4 mW cm^{-2}	–	[63]
Ag-doped PEDOT:PSS/CNT composites	Stretchable energy storage units	Capacitance	64 mF cm^{-2}	480	[64]
Graphene film/ PDMS	Pulse monitoring	Stability under noise	78 dB	–	[60]
NaCl/PEGDA/$FeCl_3$/ hydrogel	Wearable and Self-healable materials	Self-healing	97% recovery in 10 min	–	[38]
PAA/Ca^{2+}/TATPE	Wearable electronics	Self-healing	100% recovery in 1 min	1350	[65]
Gel/TA/Ag NW/ hydrogel	Self-healable materials	Self-healing	95% recovery in 0.65 sec	1600	[66]
Ag-NW/h-PDMS	Transparent Self-healable materials	Self-healing	100% recovery in 3 min	350	[67]
p-PVDF-HFP-DBP complex	Industrial applications	Self-healing	68.84% recovery in 24 h	800	[68]
EPDM/ZDMA/ rubber	Self-healable materials	Mechanically self-healing	95% recovery in 1 h	450	[69]
TA/CNC ionic gels	Healthcare monitoring	Self-healing	92% recovery in 30 min	2900	[56]
(G/CNT) Polyaniline	Stretchable energy storage units	Energy storage	1.9 times (higher than the substrate)	270	[70]

14.3.2 Virtual reality and entertainment technology

Polymer-based smart composite-enabled wearable motion sensors and input gears can also be used for virtual reality and interactive gaming applications. The wearable movement sensors and input gear-based approach have numerous advantages over the vision-based approach (using a set of cameras and image processing) for motion detection, with reference to mobility, space requirement, cost, and resolution [76–79]. Accordingly, Amjadi et al. effectively controlled an avatar in a virtual environment using a smart glove composed of five wearable strain sensors that were integrated with a custom-made data acquisition (DAQ) chip [80] (Fig. 14.2).

14.3.3 Human-machine interfaces, soft robotics, and haptics

Electro-active polymer-based smart composites can also be utilized to build intelligent human-machine interfaces, and the signals generated using such wearable sensors may be utilized to actuate smart robots. Accordingly, S. Gong et al. used one such wearable strain sensor mounted on the fingers to remote control a gripper robot (Fig. 14.3). The robotic movements toward performing various tasks were controlled via the bending and subsequent straightening of fingers mounted with wearable strain sensors [81]. Further, it is to be noted that such an approach could be beneficial in performing those complicated surgical procedures that may otherwise be out of reach for the human body [80, 82–84].

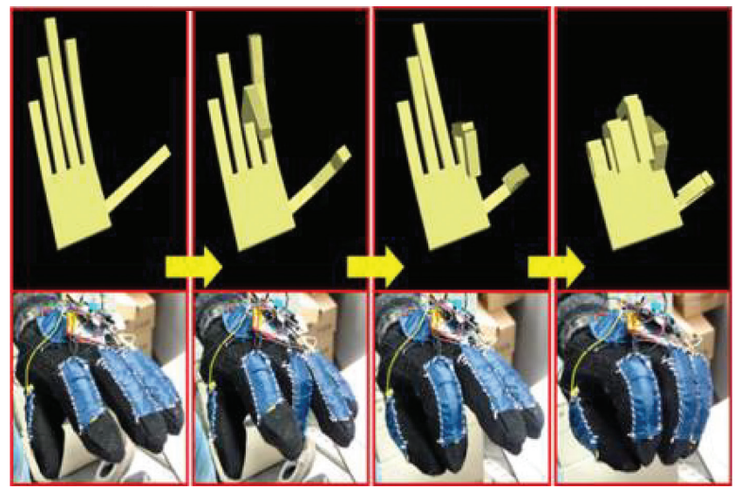


Fig. 14.2 Wearable sensor mounted smart glove controlled avatar in the virtual environment. Reproduced with permission from M. Amjadi, A. Pichitpajongkit, S. Lee, S. Ryu, I. Park, Highly stretchable and sensitive strain sensor based on silver nanowire–elastomer nanocomposite, ACS Nano 8 (2014) 5154–5163. Copyright 2014, American Chemical Society.

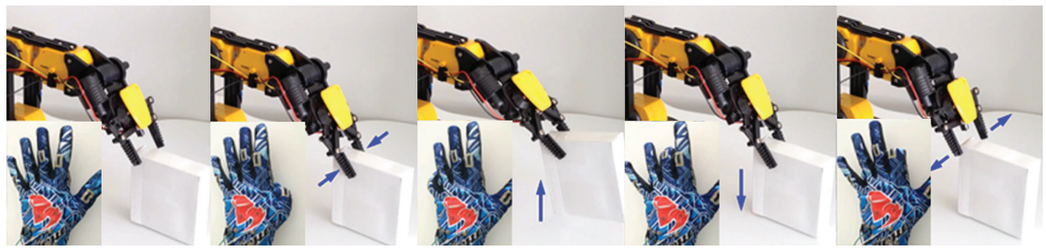


Fig. 14.3 Pictorial representation of wearable sensor mounted smart glove controlled gripper robot, supporting the robotic application of polymer-based flexible electronics. Reproduced with permission from S. Gong, D. Lai, Y. Wang, L. W. Yap, K. J. Si, Q. Shi, N. N. Jason, T. Sridhar, H. Uddin, W. Cheng, Tattoolike polyaniline microparticle-doped gold nanowire patches as highly durable wearable sensors, ACS Appl. Mater. Interfaces 7 (2015) 19700–19708. Copyright 2015, American Chemical Society.

Smart gloves controlled using wearable sensors are very advantageous over those that are controlled using optical fibers or metal-strain gauges (cyber glove), with respect to their mechanical performance, strain sensitivity, fabrication cost, and ease of operation [74, 85]. Such sensors can also be used as sensory artificial skins for robots to allow soft robots to sense and interact with the outer environment [86, 87].

14.3.4 Biomedical

Because of the fact that polymer smart composite-based wearable sensors offer increased operational ease and long-term real-time data acquisition, such materials are increasingly employed for various biomedical applications [88,89]. Fig. 14.4 presents a pictorial representation of remote and personalized health monitoring using wearable sensors. Such skin-mountable sensors acquire physiological data from the human body such as the heart rate, body movements, the breathing rate, blood pressure and so forth [82, 90]. This acquired data may then be transmitted from the sensor to any access point such as a mobile phone, a computer, and beyond. This will enable health-care professionals to remotely monitor the health conditions of the patient and to take desirable medical decisions. Further, of all the electro-active smart composites used for biomedical applications, resistive-type sensors with high sensitivity are used to monitor low-strain motions, while capacitive-type sensors with low hysteresis and fast response are used to compute high-strain motions.

14.4 Skin-inspired electronics

The naturally derived multiple functionalities of human skin serve as the framework toward engineering skin-inspired electronic devices. Such skin-inspired electronic materials must be lighter in weight,

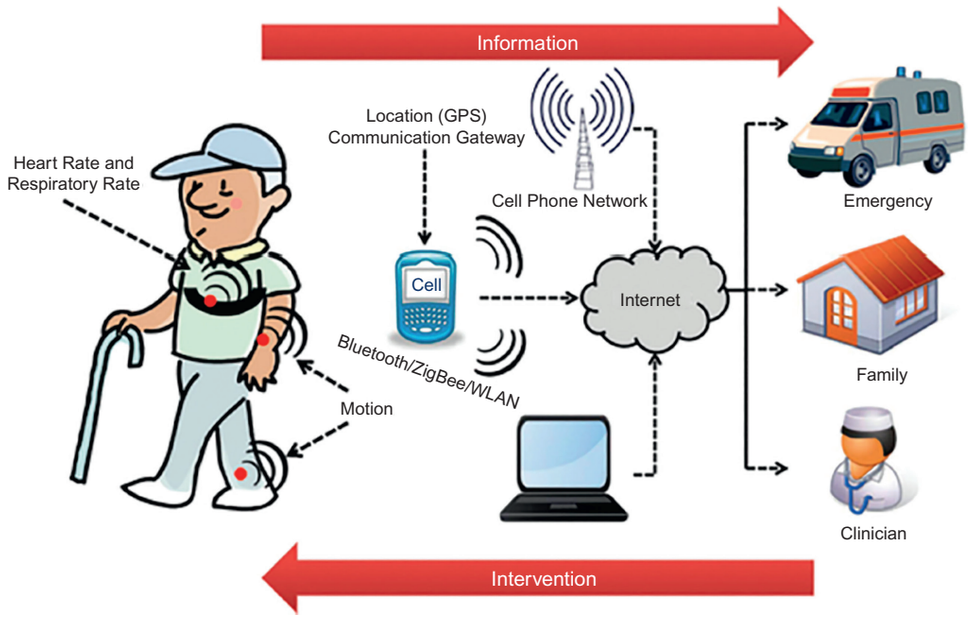


Fig. 14.4 A schematic representation of remote and personalized healthcare systems. Reproduced with permission from S. Patel, H. Park, P. Bonato, L. Chan, M. Rodgers, A review of wearable sensors and systems with application in rehabilitation, J. Neuroeng. Rehabil. 9 (2012) 21. Copyright 2012, BioMed Central.

mechanically flexible, and seamlessly conformable while functioning reliably [91]. Consequently, polymer-based composite materials with filler-related advanced electronic functionalities and polymer offered improved mechanical properties are the most widely investigated skin-inspired electronic materials. Table 14.2 presents some of the most desirable properties in polymer-based skin-inspired electronic materials and how they are achieved [98]. Table 14.3 sheds light on nanotechnology-enabled functional materials in dynamically cross-linked polymer matrices and their performance efficacies toward various skin-inspired electronic applications.

14.5 Conclusions and future directions

Nanotechnology-enabled polymer-based electro-active soft materials have emerged as great candidates for next-generation stretchable and wearable electronics. This chapter has highlighted various important polymer/nanomaterial combinations explored for flexible electronic applications. This chapter also sheds light on the function-

Table 14.2 Most desirable properties in polymer-based skin-inspired electronic materials and how they are achieved.

Desired property	What is to look at?	How is it achieved?
Stretchability and elasticity	Ability to consistently adapt to dynamic motions	1. Polymer-based materials may be molecularly designed to either include inherent cross-links or used in conjunction with reactive additives, which could generate cross-linking sites [92] 2. Using conjugated polymer-based materials with amorphous regions imparting stretchability while interconnected semicrystalline and crystalline domains facilitate high mobilities and improved conductivities [93, 94]
Self-healing and regeneration	Aptitude to autonomously repair itself and regenerate functionality in response to external damage	1. Shape memory polymer-based materials to be introduced as substrates, which may autonomously reunite crack interfaces via entropy-driven recovery of original structures [71, 95]
Transience and biodegradability	Ability to be transient, recyclable, and form nontoxic byproducts	1. Polymer-based materials with chemical moieties (especially one with labile bonds), which are susceptible to controlled hydrolysis or oxidation are used as substrates [96]
Envisaged functionalities: (Conformability and adhesion)	Be able enough to make stable, conformal contact with biological tissues to achieve improved signal integrity and long-term usability	1. Making devices ultrathin, this increases the magnitude of secondary forces between devices and skin, thereby offering improved conformability and adhesion [97]

ality requirements of materials for flexible electronics, and the most feasible way of achieving them. Further, it was also found that in many tailored composite materials, there is a trade-off between stretchability and electrical conductivity, which is an important research gap that requires immediate consideration. Also, there exixts significant scope for considerate improvement in the biocompatibility, biodegradability, self-healing, transparency, chemical stability, and weathering stability of materials for next-generation flexible electronics. Further, we strictly believe that by addressing all these functionalities, nanotechnology-enabled soft materials may open up a huge commercial market in the field of clinical medicine, sports, military equipment, and next-generation wearable electronics.

Table 14.3 Some of the important combinations of polymer-based soft materials as skin-inspired electronics.

Skin-like conductors: Materials that offer adequate power and data transfer for large-scale sensing circuits and displays				
Composite type	**Mechanical performance**	**Electrical performance**	**Optical performance**	**Ref.**
Ag NP/formed on the surface of electrospun poly(styrene-block-butadiene-block styrene) fibers	Stretchability: up to 100%	Conductivity: 2200 S cm^{-1}	–	[99]
Aligned AuNPs loaded in polyurethane using layer-by-layer technique	Stretchability: up to 110%	Conductivity: 2400 S cm^{-1}	–	[100]
Aligned AuNPs loaded in polyurethane using vacuum-assisted flocculation technique	Stretchability up to 480%	Conductivity: 35 S cm^{-1}	–	[100]
Ag (NPs) applied on fluorine rubber aligned in the direction of tensile strain	Stretchability up to 400%	Conductivity: 935 S cm^{-1}	–	[101]
Buckled structure strained carbon nanotube (CNT) electrodes with elastomeric substrates	Stretchability up to 150%	Conductivity: 2200 S cm^{-1}	Transperancy: greater than 79%	[102]
CNT electrodes with embedded Ag nanowires into PUA	Stretchability up to 20%	Resistivity: 15 Ω sq^{-1}	Transperancy: greater than 90%	[103]
Graphene sheets using transfer printing technique on branched plasticizers	Stretchability up to 120%	Resistivity: 200 Ω sq^{-1}	Transperancy: greater than 88%	[104]
Ionic liquids with (PEDOT:PSS)	Stretchability up to 100%	Conductivity: 4100 S cm^{-1}	Transperancy: greater than 95%	[105]
Ionic liquids with (PEDOT:PSS)	Stretchability up to 800%	Conductivity: 56 S cm^{-1}	Transperancy: greater than 95%	[105]
Unsorted metallic CNTs with insulating (SEBS)	Stretchability up to 60%	–	Field effect mobility of 15.4 $cm^2(V\,s)^{-1}$	[106]
(FT4-DPP) with (PEO)	Stretchability up to 100%	–	Field effect mobility of 8.45 $cm^2(V\,s)^{-1}$	[107]
(PDCA) with (DPP)	Stretchability up to 100%	–	Field effect mobility of 1.12 $cm^2(V\,s)^{-1}$	[108]
(DPPT-TT) with (SEBS) elastomer	Stretchability up to 100%	–	Field effect mobility of 1.32 $cm^2(V\,s)^{-1}$	[109]

Table 14.3 Some of the important combinations of polymer-based soft materials as skin-inspired electronics—cont'd

Skin-like conductors: Materials that offer adequate power and data transfer for large-scale sensing circuits and displays				
Composite type	**Mechanical performance**	**Electrical performance**	**Optical performance**	**Ref.**
Au-coated Ag NWs in SBS elastomer	Stretchability up to 266%	Conductivity: 41,850 S cm^{-1}	–	[34]
Nickel microparticles with urea-based H-bonding super molecular polymer	–	Conductivity: 40 S cm^{-1}	–	[110]
Silver flakes with SPMs	Stretchability up to 900% fracture strain	Conductivity: 46.5 S cm^{-1}	–	[111]
SWCNTs with ionic liquid in fluorinated copolymer matrix	Stretchability up to 134%	Conductivity: 57 S cm^{-1}	–	[112]
SWCNTs with jet milling technique in rubber matrix	Stretchability up to 118%	Conductivity: 102 S cm^{-1}	–	[113]
Au NPs deposited with layer-by-layer technique on PU	Stretchability up to 115%	Conductivity: 11,000 S cm^{-1}	–	[100]
Au NPs deposited with vaccum-assisted floccuation technique on PU	Stretchability up to 486%	Conductivity: 1800 S cm^{-1}	–	[100]
Ag Nps with electrospun SBS rubber fibers	Stretchability up to 100%	Conductivity: 2200 S cm^{-1}	–	[99]
Ag NWs with elastomeric copolymer	–	Conductivity: 10,000 S cm^{-1}	–	[114]
PANI covalently grafted into SEBS-g-MA	Stretchability up to 40%	Conductivity: 1.5×10^{4} S cm^{-1}	–	[115]
Borate network polypyrrole/PCTC composite	Stretchability up to 25.21%	Conductivity: 116.3 S cm^{-1}	–	[116]
Ag NW-cotton PU fiber with PDMS	Stretchability up to 500%	Conductivity: 688 S cm^{-1}	–	[117]
Ag NPs into Rubber matrix with sintering process	Stretchability up to 400%	Conductivity: 6168 S cm^{-1}	–	[101]
Nano barium ferrite/PAA hydogel	Stretchability up to 100%	Conductivity: 1.22×10^{-2} S cm^{-1}	–	[118]
AgFs/AgNPs/MPU/IU/PDMS	Stretchability upto 3500%	Conductivity: 3086 S cm^{-1}	–	[36]

Acknowledgment

Dr. Nithin K.S., wholeheartedly acknowledges research funding support from NIE-CRD under Research Promotion Scheme 2019.

References

[1] C.A. Rogers, Proceedings U.S. Army Research Office Workshop on Smart Materials, Structures and Mathematical Issues, Technomic Publishing Co., 1988.
[2] S. Kamila, Introduction, classification and applications of smart materials: an overview, Am. J. Appl. Sci. 10 (8) (2013) 876–880.
[3] T. Takagi, A concept of intelligent materials, J. Intell. Mater. Syst. Struct. 1 (1990) 149–156.
[4] N.K. Subramani, S. Shivanna, S.K. Nagaraj, B. Suresha, B.M.J. Raj, H. Siddaramaiah, Optoelectronic behaviours of UV shielding calcium zirconate reinforced polycarbonate nanocomposite films, Mater. Today Proc. (2018).
[5] G.R. Suma, N.K. Subramani, S. Sachhidananda, S.V. Satyanarayana, H. Siddaramaiah, Optical and electrical evaluation of Ag 0.5 Cu 0.75 O introduced poly(vinyl alcohol) based E. coli sensors, J. Mater. Sci. Mater. Electron. 22 (2017) 13139–13148.
[6] K. Mahesh, M. Subbaiah, K.S. Nithin, B.M.J. Raj, S. Shivanna, Highly flexible and conducting polymer nanocomposite films for selective gas sensing applications, Mater. Today Proc. 9 (2019) 515–521.
[7] G.R. Suma, N.K. Subramani, K.N. Shilpa, S. Sachhidananda, S.V. Satyanarayana, H. Siddaramaiah, Effect of Ce0.5Zr0.5O2 nano fillers on structural and optical behaviors of poly(vinyl alcohol), J. Mater. Sci. Mater. Electron. 14 (2017).
[8] N.K. Subramani, S.K. Nagaraj, S. Shivanna, H. Siddaramaiah, Yellow–green luminescent poly(vinyl alcohol) nanocomposite thick films as effective spectral manipulators, J. Appl. Polym. Sci. 135 (2018) 47.
[9] S. Shivanna, N.K. Subramani, S.K. Nagaraj, J.R.B. Mutturaj, S. Basavaraj, Patina-green coloured light emitting polycarbonate films: a synergistic extraction of improved UV endurance and considerate spectral down-conversion, J. Lumin. 210 (2019).
[10] S. Shivanna, N.K. Subramani, K. Swamy, S.K. Nagaraj, J.R.B. Muthuraj, H. Siddaramaiah, Orange-red fluorescent polymer nanocomposite films with large stokes shift: an opto-electronic exercise, J. Lumin. 208 (2019) 488–494.
[11] R.C. Webb, A.P. Bonifas, A. Behnaz, Y. Zhang, K.J. Yu, H. Cheng, M. Shi, Z. Bian, Z. Liu, Y.S. Kim, Ultrathin conformal devices for precise and continuous thermal characterization of human skin, Nat. Mater. 12 (10) (2013) 938–944.
[12] X. Wang, Y. Gu, Z. Xiong, Z. Cui, T. Zhang, Silk-moulded flexible, ultrasensitive, and highly stable electronic skin for monitoring human physiological signals, Adv. Mater. 26 (2014) 1336–1342.
[13] P. Bingger, M. Zens, P. Woias, Highly flexible capacitive strain gauge for continuous long-term blood pressure monitoring, Biomed. Microdevices 14 (2012) 573–581.
[14] D. Son, Z. Bao, Nanomaterials in skin-inspired electronics: toward soft and robust skin-like electronic nanosystems, ACS Nano 12 (2018) 11731–11739.
[15] A. Chortos, J. Liu, Z. Bao, Pursuing prosthetic electronic skin, Nat. Mater. 15 (2016) 937–950.
[16] D.H. Kim, N. Lu, R. Ma, Y.S. Kim, R.H. Kim, S. Wang, J. Wu, S.M. Won, H. Tao, A. Islam, K.J. Yu, T.I. Kim, R. Chowdhury, M. Ying, L. Xu, M. Li, H.J. Chung, H. Keum, M. McCormick, P. Liu, Y.W. Zhang, F.G. Omenetto, Y. Huang, T. Coleman, J.A. Rogers, Epidermal Electronics, Science 333 (2011) 838–843.

[17] M. Amjadi, Y.J. Yoon, I. Park, Ultra-stretchable and skin-mountable strain sensors using carbon nanotubes-Ecoflex nanocomposites, Nanotechnology 26 (2015).
[18] C. Pang, C. Lee, K.Y. Suh, Recent advances in flexible sensors for wearable and implantable devices, J. Appl. Polym. Sci. 130 (2013) 1429–1441.
[19] N.K. Subramani, K.N. Shilpa, S. Shivanna, J. Raj, S. Hatna, Advances in polymer-based piezoelectric systems, in: Emergent Research on Polymeric and Composite Materials, IGI Global, 2018.
[20] Y.B. Cohen, Electroactive Polymer (EAP) Actuators as Artificial Muscles: Reality, Potential, and Challenges, SPIE Press, Bellingham WA, 2004.
[21] M. Kretzer, Article in materiability.com, Portfolio, and Electro Active-Polymers, 2013.
[22] L.J. Romasanta, M.A.L. Manchado, R. Verdejo, Increasing the performance of dielectric elastomer actuators: a review from the materials perspective, Prog. Polym. Sci. 51 (2015) 188–211.
[23] Z. Bao, X. Chen, Flexible and stretchable devices, Adv. Mater. 28 (2016).
[24] J. Rogers, G. Malliaras, T. Someya, Biomedical devices go wild, Sci. Adv. 4 (2018).
[25] M. Amjadi, K.U. Kyung, I. Park, M. Sitti, Stretchable, skin-mountable, and wearable strain sensors and their potential applications: a review, Adv. Funct. Mater. 15 (2016) 1678–1698.
[26] I. Kang, M.J. Schulz, J.H. Kim, V. Shanov, D. Shi, A carbon nanotube strain sensor for structural health monitoring, Smart Mater. Struct. 15 (2006) 737.
[27] J. Zhang, J. Liu, R. Zhuang, E. Mäder, G. Heinrich, S. Gao, Single MWNT-glass fiber as strain sensor and switch, Adv. Mater. 23 (2011) 3392–3397.
[28] L. Wang, Y. Li, Semisupervised distance-preserving self-organizing map for machine-defect detection and classification, IEEE Trans. Instrum. Meas. 62 (2013).
[29] S.K. Gosh, A Hybrid strain and thermal energy harvester based on an infra-red sensitive Er3 + modified poly(vinylidene fluoride) ferroelectret structure, Sci. Rep. 7 (2017) 1–13.
[30] H. Gu, H. Zhang, C. Ma, H. Sun, C. Liu, K. Dai, J. Zhang, R. Wei, T. Ding, Z. Guo, Smart strain sensing organic-inorganic hybrid hydrogels with nano barrium ferrite as cross-linker, J. Mater. Chem. 7 (2019) 2353–2360.
[31] Z. Chen, J. Xi, W. Huang, M.M. Yuen, Stretchable conductive elastomer for wireless wearable communication applications, Sci. Rep. 7 (2017) 10958.
[32] L. Yu, J.C. Yeo, R.H. Soon, T. Yeo, H.H. Lee, C.T. Lim, Highly stretchable, weavable, and washable piezoresistive microfiber sensors, ACS Appl. Mater. Interfaces 10 (2018) 12773–12780.
[33] Y. Liu, J. Liu, S. Chen, T. Lei, Y. Kim, S. Niu, H. Wang, X. Wang, A.M. Foudeh, J.B.H. Tok, Z. Bao, Soft and elastic hydrogel-based microelectronics for localized low-voltage neuromodulation, Nat. Biomed. Eng. 3 (2019) 58–68.
[34] S. Choi, S.I. Han, D. Jung, H.J. Hwang, C. Lim, S. Bae, O.K. Park, C.M. Tschabrunn, M. Lee, S.Y. Bae, J.W. Yu, J.H. Ryu, S.-W. Lee, K. Park, P.M. Kang, W.B. Lee, R. Nezafat, T. Hyeon, D.H. Kim, Highly conductive, stretchable and biocompatible Ag–Au core–sheath nanowire composite for wearable and implantable bioelectronics, Nat. Nanotechnol. 13 (2018) 1048–1056.
[35] Y. Cao, Y.J. Tan, S. Li, W.W. Lee, H.C. Guo, Y. Cai, C. Wang, Self-healing electronic skins for aquatic environments, Nat. Electron. 2 (2019) 75–82.
[36] S.H. Kim, H. Seo, J. Kang, J. Hong, D. Seong, H.J. Kim, J. Kim, J. Mun, I. Youn, J. Kim, Y.C. Kim, H.K. Seok, C. Lee, J.B.H. Tok, Z. Bao, D. Son, An ultrastretchable and self-healable nanocomposite conductor enabled by autonomously percolative electrical pathways, ACS Nano 13 (2019) 6531–6539.
[37] Y. Zhao, A. Gumyusenge, J. He, G. Qu, W.W. McNutt, Y. Long, Continuous melt-drawing of highly aligned flexible and stretchable semiconducting microfibers for organic electronics, Adv. Funct. Mater. 28 (2018) 1705584.

[38] S. Park, B.G. Shin, S. Jang, K. Chung, Three-dimensional self-healable touch sensing artificial skin device, ACS Appl. Mater. Interfaces 12 (2020) 3953–3960.
[39] T. Giffney, E. Bejanin, A.S. Kurian, S.J. Travas, K. Aw, Highly stretchable printed strain sensorsusing multi-walled carbon nanotube/silicone rubber composites, Sens. Actuators A Phys. 259 (2017) 44–49.
[40] Y.Z. Zhang, K.H. Lee, D.H. Anjum, MXenes stretch hydrogel sensor performance to new limits, Sci. Adv. 6 (2018), eaat0098.
[41] F.X. Wang, S.H. Zhang, L.J. Wang, Y.L. Zhang, J. Lin, X.H. Zhang, T. Chen, Y.K. Lai, G.P. Pan, L.N. Suna, An ultrahighly sensitive and repeatable flexible pressure sensor based on PVDF/PU/MWCNT hierarchical framework-structured aerogels for monitoring human activities, J. Mater. Chem. 46 (2018) 12575–12583.
[42] L. Pan, G. Liu, W. Shi, J. Shang, W.R. Leow, Y. Liu, Y. Jiang, S. Li, X. Chen, R.W. Li, Mechano-regulated metal-organic framework nanofilm for ultrasensitive and anti-jamming strain sensing, Nat. Commun. 9 (2018) 1–10.
[43] J.Y. Oh, D. Son, T. Katsumata, Y. Lee, Y. Kim, J. Lopez, H.C. Wu, J. Kang, J. Park, X. Gu, J. Mun, N.G.J. Wang, Y. Yin, W. Cai, Y. Yun, J.B.H. Tok, Z. Bao, Stretchable self-healable semiconducting polymer film for active-matrix strain-sensing array, Sci. Adv. 5 (2019), eaav3097.
[44] Y. Cai, J. Shen, G. Ge, Y. Zhang, W. Jin, W. Huang, J. Shao, J. Yang, X. Dong, Stretchable Ti3C2Tx MXene/Carbon nanotube composite based strain sensor with ultrahigh sensitivity and tunable sensing range, ACS Nano 12 (2018) 56–62.
[45] X. Jing, H.Y. Mi, Y.J. Lin, E. Enriquez, X.F. Peng, L.S. Turng, Highly stretchable and biocompatible strain sensors based on mussel-inspired super-adhesive self-healing hydrogels for human motion monitoring, ACS Appl. Mater. Interfaces 10 (2018) 20897–20909.
[46] W. Hou, N. Sheng, X. Zhang, Z. Luan, P. Qi, M. Lin, Y. Tan, Y. Xia, Y. Li, K. Sui, Design of injectable agar/NaCl/polyacrylamide ionic hydrogels for high performance strain sensors, Carbohydr. Polym. 211 (2019) 322–328.
[47] J. Hun, L.J. Kim, D. Liu, F. Guo, X. Shen, Q. Zheng, S. Jeon, J.-.K. Kim, Highly aligned, anisotropic carbon nanofiber films for multidirectional strain sensors with exceptional selectivity, Adv. Funct. Mater. 29 (2019) 1901623.
[48] Y.M. Kim, H.C. Moon, Ionoskins: nonvolatile, highly transparent, ultrastretchable ionic sensory platforms for wearable electronics, Adv. Funct. Mater. 30 (2020) 1907290.
[49] S. Pan, M. Xia, H. Li, X. Jiang, P. He, Z. Sun, Y. Zhang, Transparent, high-strength, stretchable, sensitive and anti-freezing poly(vinyl alcohol) ionic hydrogel strain sensors for human motion monitoring, J. Mater. Chem. C 8 (2020) 2827–2837.
[50] T.N. Do, Y. Visell, Stretchable, twisted conductive microtubules for wearable computing, robotics, electronics and healthcare, Sci. Rep. 7 (2018) 1753.
[51] G. Ge, Y. Cai, Q. Dong, Y. Zhang, J. Shao, W. Huang, X. Dong, A flexible pressure sensor based on rGO/polyaniline wrapped sponge with tunable sensitivity for human motion detection, Nanoscale 10 (2018) 10033.
[52] G. Ge, W. Yuan, W. Zhao, Y. Lu, Y. Zhang, W. Wang, P. Chen, W. Huang, W. Si, X. Dong, Highly stretchable and autonomously healable epidermal sensor based on multi-functional hydrogel frameworks, J. Mater. Chem. A 7 (2019) 5949–5956.
[53] X. Xuan, H.S. Yoon, J.Y. Park, A wearable electrochemical glucose sensor based on simple and low-cost fabrication supported micro-patterned reduced graphene oxide nanocomposite electrode on flexible substrate, Biosens. Bioelectron. 109 (2018) 75–82.
[54] X. Yan, Z. Liu, Q. Zhang, J. Lopez, H. Wang, H.C. Wu, S. Niu, H. Yan, S. Wang, T. Lei, J. Li, D. Qi, P. Huang, J. Huang, Y. Zhang, Y. Wang, G. Li, J.B.H. Tok, X. Chen, Z. Bao, Quadruple H-bonding cross-linked supramolecular polymeric materials as substrates for stretchable, anti-tearing, and self-healable thin film electrodes, J. Am. Chem. Soc. 140 (2018) 5280–5289.

[55] J. Kang, D. Son, G.N. Wang, Y. Liu, J. Lopez, Y. Kim, J.Y. Oh, T. Katsumata, J. Mun, Y. Lee, L. Jin, J.B.H. Tok, Z. Bao, Tough and water-insensitive self-healing elastomer for robust electronic skin, Adv. Mater. 30 (2018) 1706846.
[56] C. Shao, M. Wang, L. Meng, H. Chang, B. Wang, F. Xu, J. Yang, P. Wan, Musselinspired cellulose nanocomposite tough hydrogels with synergistic self-healing, adhesive and strain-sensitive properties, Chem. Mater. 30 (2018) 3110–3121.
[57] C. Cui, C. Shao, L. Meng, J. Yang, High-strength, self-adhesive, and strain-sensitive Chitosan/Poly(acrylic acid) double-network nanocomposite hydrogels fabricated by salt-soaking strategy for flexible sensors, ACS Appl. Mater. Interfaces 11 (2019) 39228–39237.
[58] B. Yang, W. Yuan, Highly stretchable, adhesive, and mechanical zwitterionic nanocomposite hydrogel biomimetic skin, ACS Appl. Mater. Interfaces 11 (2019) 40620–40628.
[59] G. Ge, Y. Zhang, J. Shao, W. Wang, W. Si, W. Huang, X. Dong, Stretchable, transparent, and self-patterned hydrogel-based pressure sensor for human motions detection, Adv. Funct. Mater. 28 (2018) 1802576.
[60] J. He, P. Xiao, W. Lu, J. Shi, L. Zhang, Y. Liang, C. Pan, S.W. Kuo, T. Chen, A Universal high accuracy wearable pulse monitoring system via high sensitivity and large linearity graphene pressure sensor, Nano Energy 59 (2019) 422–433.
[61] Z. Zou, C. Zhu, Y. Li, X. Lei, W. Zhang, J. Xiao, Rehealable, fully recyclable, and malleable electronic skin enabled by dynamic covalent thermoset nanocomposite, Sci. Adv. 4 (2018), eaaq0508.
[62] J.C. Yang, J.O. Kim, J. Oh, S.Y. Kwon, J.Y. Sim, D.W. Kim, H.B. Choi, S. Park, Microstructured porous pyramid-based ultrahigh sensitive pressure sensor insensitive to strain and temperature, ACS Appl. Mater. Interfaces 11 (2019) 19472–19480.
[63] X. Yuan, X. Gao, J. Yang, X. Shen, Z. Li, S. You, Z. Wanga, S. Dong, The large piezoelectricity and high power density of a 3D-printed multilayer copolymer in a rugby ball-structured mechanical energy harvester, Energy Environ. Sci. 13 (2019) 152–161.
[64] Y. Zhu, N. Li, T. Lv, Y. Yao, H. Peng, J. Shi, S. Cao, T. Chen, Ag-doped PEDOT:PSS/CNT composites for thin-film all-solid-state supercapacitors with a stretchability of 480%, J. Mater. Chem. A 6 (2018) 941–947.
[65] H. Zhoua, S. Zhenga, C. Qub, D. Wangb, C. Liub, Y. Wanga, X. Fana, W. Xiaob, H. Lib, D. Zhaob, J. Changb, C. Chenc, X. Zhaoc, Simple and environmentally friendly approach for preparing high performance polyimide precursor hydrogel with fully aromatic structures for strain sensor, Eur. Polym. J. 114 (2019) 346–352.
[66] J. Wang, F. Tang, Y. Wang, Q. Lu, S. Liu, L. Li, Self-healing and highly stretchable gelatin hydrogel for self-powered strain sensor, ACS Appl. Mater. Interfaces 12 (2020) 1558–1566.
[67] S.O. Kim, C.J. Han, Y. Kim, K.S. Kim, D.U. Kim, C.R. Lee, J.W. Kim, Fabrication of a bending-insensitive in-plane strain sensor from a reversible cross-linker-functionalized silicone polymer, ACS Appl. Mater. Interfaces 12 (2020) 6516–6524.
[68] Y. Cao, H. Hu, S.I. Allec, B.M. Wong, D.S. Nguyen, C. Wang, A highly stretchy, transparent elastomer with the capability to automatically self-heal underwater, Adv. Mater. 30 (2018) 1804602.
[69] Z.F. Zhang, K. Yang, S.G. Zhao, L.N. Guo, Self-healing behavior of ethylene propylene diene rubbers based on ionic association, Chin. J. Polym. Sci. 37 (2019) 700–707.
[70] Z. Chen, T. Lv, Y. Yao, H. Li, N. Li, Y. Yang, K. Liu, G. Qian, X. Wang, T. Chen, Three-dimensional seamless graphene/carbon nanotube hybrids for multifunctional energy storage, J. Mater. Chem. A 7 (2019) 24792–24799.

[71] B. Jeong, A. Gutowska, Lessons from nature: stimuli responsive polymers and their biomedical applications, Trends Biotechnol. 20 (2002) 305–310.
[72] N. Lu, C. Lu, S. Yang, J. Rogers, Highly sensitive skin-mountable strain gauges based entirely on elastomers, Adv. Funct. Mater. 22 (2012) 4044–4050.
[73] J.H. Kong, N.S. Jang, S.H. Kim, J.M. Kim, Simple and rapid micro patterning of conductive carbon composites and its application to elastic strain sensors, Carbon 77 (2014) 199–207.
[74] S.H. Bae, Y. Lee, B.K. Sharma, H.J. Lee, J.H. Kim, J.H. Ahn, Graphene-based transparent strain sensor, Carbon 51 (2013) 236–242.
[75] M.M. Rodgers, V.M. Pai, R.S. Conroy, Big data, big challenges: a healthcare perspective: background, issues, IEEE Sensors J. 15 (2015) 3119.
[76] M. Amjadi, A. Pichitpajongkit, S. Ryu, I. Park, IEEE 27th International Conference on Micro Electro Mechanical Systems (MEMS), IEEE, Picastaway, NJ, USA, 2014.
[77] R. Poppe, A survey on vision-based human action recognition, Image Vis. Comput. 28 (2010) 976–990.
[78] S.S. Rautaray, A. Agrawal, Real time hand gesture recognition system for dynamic applications, Artif. Intell. Rev. 43 (2012) 1–54.
[79] E. Roh, B.U. Hwang, D. Kim, B.Y. Kim, N.E. Lee, Stretchable, transparent, ultrasensitive, and patchable strain sensor for human-machine interfaces comprising a nanohybrid of carbon nanotubes and conductive elastomers, ACS Nano 9 (2015) 6252–6261.
[80] M. Amjadi, A. Pichitpajongkit, S. Lee, S. Ryu, I. Park, Highly stretchable and sensitive strain sensor based on silver nanowire–elastomer nanocomposite, ACS Nano 8 (2014) 5154–5163.
[81] S. Gong, D. Lai, Y. Wang, L.W. Yap, K.J. Si, Q. Shi, N.N. Jason, T. Sridhar, H. Uddin, W. Cheng, Tattoolike polyaniline microparticle-doped gold nanowire patches as highly durable wearable sensors, ACS Appl. Mater. Interfaces 7 (2015) 19700–19708.
[82] T. Yamada, Y. Hayamizu, Y. Yamamoto, Y. Yomogida, A.I. Najafabadi, D.N. Futaba, K. Hata, A stretchable carbon nanotube strain sensor for human-motion detection, Nat. Nanotechnol. 6 (2011) 296–301.
[83] L. Cai, L. Song, P. Luan, Q. Zhang, N. Zhang, Q. Gao, D. Zhao, X. Zhang, M. Tu, F. Yang, Super-stretchable, transparent carbon nanotube-based capacitive strain sensors for human motion detection, Sci. Rep. 3048 (2013).
[84] C. Yan, J. Wang, W. Kang, M. Cui, X. Wang, C.Y. Foo, K.J. Chee, P.S. Lee, Highly stretchable piezoresistive graphene-nanocellulose nanopaper for strain sensors, Adv. Mater. 26 (2013) 2022–2027.
[85] X. Li, R. Zhang, W. Yu, K. Wang, J. Wei, D. Wu, A. Cao, Z. Li, Y. Cheng, Q. Zheng, Stretchable and highly sensitive graphene-on-polymer strain sensors, Sci. Rep. 870 (2012).
[86] M. McEvoy, N. Correll, Materials that couple sensing, actuation, computation, and communication, Mater. Sci. 347 (2015) 1261689.
[87] C. Majidi, Soft Robotics: A Perspective-Current Trends and Prospects for the Future, Mary Ann Liebert, Inc, 2014.
[88] S. Patel, H. Park, P. Bonato, L. Chan, M. Rodgers, J. Neuroeng, Rehabil., A review of wearable sensors and systems with application in rehabilitation, J. Neuroeng. Rehabil. 9 (21) (2012).
[89] A. Pantelopoulos, N.G. Bourbakis, Systems, man, and cybernetics, part C: applications and reviews, IEEE Trans. 32 (2010).
[90] S. Gong, W. Schwab, Y. Wang, Y. Chen, Y. Tang, J. Si, B. Shirinzadeh, W. Cheng, A wearable and highly sensitive pressure sensor with ultrathin gold nanowires, Nat. Commun. 5 (2014) 3132.
[91] M. Amjadi, K.U. Kyung, I. Park, M. Sitti, Stretchable, skin-mountable, and wearable strain sensors and their potential applications, Adv. Funct. Mater. 26 (2019) 1678–1698.

[92] C. Mattmann, F. Clemens, G. Troster, Sensor for measuring strain in textile, Sensors 8 (2008) 3719.
[93] Y. Wang, L. Wang, T. Yang, X. Li, X. Zang, M. Zhu, K. Wang, D. Wu, H. Zhu, Wearable and highly sensitive graphene strain sensors for human motion monitoring, Adv. Funct. Mater. 24 (2014) 4666.
[94] J.T. Muth, D.M. Vogt, R.L. Truby, Y. Mengüç, D.B. Kolesky, R.J. Wood, J.A. Lewis, Embedded 3D printing of strain sensors within highly stretchable elastomers, Adv. Mater. 26 (2014) 6307–6312.
[95] J. You, D. Almeda, G.J.C. Ye, D.T. Auguste, Bioresponsive matrices in drug delivery, J. Biol. Eng. 4 (2010) 1–12.
[96] M. Zrinyi, L. Barsi, A. Buki, Deformation of ferrogels induced by nonuniform magnetic fields, J. Chem. Phys. 104 (1996) 8750–8756.
[97] P. Dames, B. Gleich, A. Flemmer, K. Hajek, N. Seidl, F. Wiekhorst, D. Eberbeck, I. Bittmann, C. Bergemann, T. Weyh, L. Trahms, J. Rosenecker, C. Rudolph, Targeted delivery of magnetic aerosol droplets to the lung, Nat. Nanotechnol. 2 (2007) 495–499.
[98] H. Tran, V.R. Feig, K. Liu, Y. Zheng, Z. Bao, Polymer chemistries underpinning materials for skin-inspired electronics, Macromolecules 52 (2019) 3965–3974.
[99] M. Park, J. Im, M. Shin, Y. Min, J. Park, H. Cho, S. Park, M.B. Shim, S. Jeon, D.Y. Chung, J. Bae, J. Park, U. Jeong, K. Kim, Highly stretchable electric circuits from a composite material of silver nanoparticles and elastomeric fibres, Nat. Nanotechnol. 7 (2012) 803–809.
[100] Y. Kim, Z. Zhu, B. Yeom, M. Di Prima, X. Su, J.G. Kim, S.J. Yoo, C. Uher, N.A. Kotov, Stretchable nanoparticle conductors with self-organized conductive pathways, Nature 500 (2013) 59–63.
[101] N. Matsuhisa, D. Inoue, P. Zalar, H. Jin, Y. Matsuba, A. Itoh, T. Yokota, D. Hashizume, T. Someya, Printable elastic conductors by in situ formation of silver nanoparticles from silver flakes, Nat. Mater. 16 (2017) 834–840.
[102] D.J. Lipomi, M. Vosgueritchian, B.C.K. Tee, S.L. Hellstrom, J.A. Lee, C.H. Fox, Z. Bao, Skin-like pressure and strain sensors based on transparent elastic films of carbon nanotubes, Nat. Nanotechnol. 6 (2011) 788–792.
[103] J. Liang, L. Li, D. Chen, T. Hajagos, Z. Ren, S.Y. Chou, W. Hu, Q. Pei, Intrinsically stretchable and transparent thin-film transistors based on printable silver nanowires, carbon nanotubes and an elastomeric dielectric, Nat. Commun. 6 (2015) 7647.
[104] N. Liu, A. Chortos, T. Lei, L. Jin, T.R. Kim, W.G. Bae, C. Zhu, S. Wang, R. Pfattner, X. Chen, R. Sinclair, Z. Bao, Ultratransparent and stretchable graphene electrodes, Sci. Adv. 3 (2017), e1700159.
[105] Y. Wang, C. Zhu, R. Pfattner, H. Yan, L. Jin, S. Chen, F. Molina-Lopez, F. Lissel, J. Liu, N.I. Rabiah, Z. Chen, J.W. Chung, C. Linder, M.F. Toney, B. Murmann, Z. Bao, A highly stretchable, transparent, and conductive polymer, Sci. Adv. 3 (2017), e1602076.
[106] A. Chortos, C. Zhu, J.Y. Oh, X. Yan, I. Pochorovski, J. W. F. To, N. Liu, U. Kraft, B. Murmann, Z. Bao, Investigating limiting factors in stretchable all-carbon transistors for reliable stretchable electronics, ACS Nano 11 (2017) 7925–7937.
[107] Y. Lee, J.Y. Oh, T.R. Kim, X. Gu, Y. Kim, G.J.N. Wang, H.C. Wu, R. Pfattner, J. W. F. To, T. Katsumata, D. Son, J. Kang, J.R. Matthews, W. Niu, M. He, R. Sinclair, Y. Cui, J.B.H. Tok, T.W. Lee, Z. Bao, Deformable organic nanowire field-effect transistors, Adv. Mater. 30 (2018) 1704401.
[108] J.Y. Oh, S. Rondeau-Gagne, Y.C. Chiu, A. Chortos, F. Lissel, G.J.N. Wang, B.C. Schroeder, T. Kurosawa, J. Lopez, T. Katsumata, J. Xu, C. Zhu, X. Gu, W.G. Bae, Y. Kim, L. Jin, J.W. Chung, J.B.H. Tok, Z. Bao, Intrinsically stretchable and healable semiconducting polymer for organic transistors, Nature 539 (2016) 411–415.

[109] J. Xu, S. Wang, G.J.N. Wang, C. Zhu, S. Luo, L. Jin, X. Gu, S. Chen, V.R. Feig, W.F.J. To, S. Rondeau-Gagne, J. Park, B.C. Schroeder, C. Lu, J.Y. Oh, Y. Wang, Y.H. Kim, H. Yan, G. Sinclair, D. Zhou, G. Xue, B. Murmann, C. Linder, W. Cai, J.B.H. Tok, J.W. Chung, Z. Bao, Highly stretchable polymer semiconductor films through the nanoconfinement effect, Science 355 (2017) 59–64.

[110] B.C.K. Tee, C. Wang, R. Allen, Z. Bao, An electrically and mechanically self-healing composite with pressure and flexion-sensitive properties for electronic skin applications, Nat. Nanotechnol. 7 (2012) 825–832.

[111] Q. Zhang, S. Niu, L. Wang, J. Lopez, S. Chen, Y. Cai, R. Du, Y. Liu, J.C. Lai, L. Liu, C.H. Li, X. Yan, C. Liu, J.B.H. Tok, X. Jia, Z. Bao, An elastic autonomous self-healing capacitive sensor based on a dynamic dual crosslinked chemical system, Adv. Mater. 30 (2018) 1801435.

[112] T. Sekitani, Y. Noguchi, K. Hata, T. Fukushima, T. Aida, T. Someya, A rubberlike stretchable active matrix using elastic conductors, Science 321 (2008) 1468–1472.

[113] T. Sekitani, H. Nakajima, H. Maeda, T. Fukushima, T. Aida, K. Hata, T. Someya, Stretchable active-matrix organic light-emitting diode display using printable elastic conductors, Nat. Mater. 8 (2009) 494–499.

[114] J. Park, S. Choi, A.H. Janardhan, S.Y. Lee, S. Raut, J. Soares, K. Shin, S.X. Yang, C. Lee, K.W. Kang, H.R. Cho, S.J. Kim, P. Seo, W. Hyun, S. Jung, H.J. Lee, N. Lee, S.H. Choi, M. Sacks, N.S. Lu, M.E. Josephson, T. Hyeon, D.H. Kim, H.J. Hwang, Electromechanical cardioplasty using a wrapped elasto-conductive epicardial mesh, Sci. Transl. Med. 8 (2016), 344ra386.

[115] H. Stoyanov, M. Kollosche, S. Risse, R. Wache, G. Kofod, Soft conductive elastomer materials for stretchable electronics and voltage controlled artificial muscles, Adv. Mater. 25 (2013) 578–583.

[116] L. Guo, M. Ma, N. Zhang, R. Langer, D.G. Anderson, Stretchable polymeric multielectrode array for conformal neural interfacing, Adv. Mater. 26 (2014) 1427–1433.

[117] R. Ma, J. Lee, D. Choi, H. Moon, S. Baik, Knitted fabrics made from highly conductive stretchable fibers, Nano Lett. 14 (2014) 1944–1951.

[118] H. Gu, H. Zhang, C. Ma, H. Sun, C. Liu, K. Dai, J. Zhang, R. Wei, T. Ding, Z. Guo, Smart strain sensing organic-inorganic hybrid hydrogels with nano barium ferrite as cross-linker, J. Mater. Chem. C 7 (2019) 2353–2360.

Index

Note: Page numbers followed by *f* indicate figures and *t* indicate tables.

A

Absorption, 37
Active material, 252
Adsorption-type flexible conductive polymer composite (FCPC)-based strain sensors, 307
Advanced materials, 52–53
Ag nanoparticles, 281
Anode material, 185–186, 186*f*

B

Bandgap energy (E_g), determination of, 175–176
Batteries, 180
  electrode, 252
Bimolecular reactions, 174
Biomedical, 329
Boron dipyrromethene (BODIPY), 275
Bottom-up approach, 61–62
Bulk oxides, 59, 65

C

Carbon-based materials, 38
Carbon black, 252
Carbon composites
  in Li-S cathode electrode, 257–259, 258*f*
Carbonized porous material (CPP-1-C), 275
Carbon nanotube-polymer nanocomposites (CNT-PNCs), 177, 177*f*
  anode material, 185–186, 186*f*
  chemical bonding between nanotubes and matrix, 177
  electron-transporting layers (ETL), 186–188
  emissive layer, 188–192, 189*f*
  hole-transporting layers (HTL), 186–188
  in LED application, 182
  micromechanical interlocking, 177
  in optoelectronics, 180–182, 181*f*
  stretchable electrode material, 182–185, 183–184*f*
  weak van der Waals bonding between fiber and matrix, 177
Carbon nanotubes (CNTs), 176, 219*f*, 259, 272
  amalgamation of, 180–181
Carbon quantum dots (CQDs), 38
Cathode luminescence, 173
Ceramic-based smart materials, 321–322
Ceramic powders, 59
Characterization, 92–111
Chemical functionalization, 182
Chemical sensors, 180
Clean-energy fuel systems
  conducting polymer-based composites, 203–206
  conjugated microporous polymers (CMPs), 208–209
  porous organic polymers (POPs), 206–208
CNTs. *See* Carbon nanotubes (CNTs)
COF. *See* 2D covalent organic framework (COF)
COFs. *See* Covalent organic frameworks (COFs)
Color switching, 11–13
Combustion synthesis. *See* Solution combustion synthesis (SCS)
Composites, 128–129
Conducting polymer, 151–152
Conductive nanofillers
  dispersion, 312
  morphology, 312
  polymer matrix, 312–313
Conductive polymer
  in Li-S cathode electrode, 257–259, 258*f*
Conjugated microporous polymers (CMPs), 208–209
Conjugated polymer-based composites
  inorganic-organic composites, 45–46
Conjugated polymer-based smart materials, 31–32
Conjugated polymers (CPs), 38–43, 265–266
  applications of, 267–282
  electronic properties of, 265–266
  lithium-ion (Li-ion) batteries, 267–276, 267–268*f*, 270–274*f*
  mechanical properties of, 265–266
  operating principles of, 266–267
  supercapacitors, 276–282, 277*f*, 280–282*f*
Conjugated porous polymer (CPP-1), 275
Conjugation of polymers, 170–171, 171*f*
Contact angles, 104–105
Covalent bonding, 253
Covalent organic frameworks (COFs), 281
CPDT. *See* Cyclopentadithiophene (CPDT)
CPs. *See* Conjugated polymers (CPs)
CQDs. *See* Carbon quantum dots (CQDs)
Critical solution temperatures (CSTs), 7
CSTs. *See* Critical solution temperatures (CSTs)

Cyclic voltammetry technique, 279
Cycling stability, 254–255
Cyclopentadithiophene (CPDT), 268

D

Device fabrication process, 191
Dielectric elastomer-based smart composites, 20
Differential scanning calorimetry (DSC), 107
Dip and dry approach, 279
Direct arylation polymerization method, 268
Discharge capacity, 260
Dispersion, 312
DP-NTCDI-250. *See* N,N'-diphenyl-1,4,5,8-naphthalenetetra-carboxylic diimide (DP-NTCDI-250)
DSC. *See* Differential scanning calorimetry (DSC)

E

Edge to face (EF), 171
EDLCs. *See* Electrical double-layer capacitors (EDLCs)
Electrical double-layer capacitors (EDLCs), 219–220
Electrical energy storage
  dielectric breakdown strengths, 78*t*
  percolation thresholds, 79*t*
Electrical properties, 76–80
  AC conductivity, 110
  dielectric breakdown strength, 110
  dielectric constant, 109
  energy storage efficiency, 111
  loss tangent, 109
  theoretical maximum energy storage density, 110
  total stored energy density, 110
Electro-active, 322–323
Electrocatalysis, 180
Electrochemical calculations, 268
Electrochemical impedance spectroscopy (EIS) test, 254–255
Electrochemical reactions, 255
Electrochemical tests, 279
Electroluminescence, 173, 178
Electroluminescent devices, 180
Electromagnetic spectrum, of radiation span, 170*f*
Electronic-type electro-responsive dielectric elastomer-based smart composites, 20
  piezoelectric (PE), 19
Electron microscopes, 54
Electron transfer reactions, 174–175
Electron-transporting layers (ETL), 186–188
Electropolymerized polypyrrole (e-PPy) supercapacitors, 277–278
Electro-responsive
  advantages and disadvantages, 16–17*t*
  classification of, 15–20
  conducting, 18
  electronic-type electro-responsive, 19–20
  gels, 17–18
  ionic polymer-metal composites (IPMCs), 18–19
  ionic-type electro-responsive, 17–19
Electrostatic forces, 253
Emulsion polymerization technique, 282
Energy storage systems, 265
Entertainment technology, 328
e-PPy. *See* Electropolymerized polypyrrole (e-PPy) supercapacitors
Excitation, 177
External quantum efficiency (EQE), 159–160, 160*f*

F

FCPCs. *See* Flexible conductive polymer composites (FCPCs)
Field effect transistors (FETs), 180
Filled-type FCPC-based strain sensors, 306
Filler orientation, 127–128
Filler-polymer compatibilities, 128–129
Fillers, 56–67
Flexible conductive polymer composites (FCPCs), 306–307
Flexible electronics, 330–331
Fluorescence, 173–174
Fluorescent polymer, 183
Fourier transform infrared spectroscopy (FTIR), 69–70, 71*f*, 92–95
Friedel-Crafts reaction, 275
Fuel cells, 237–240
Functional additives, 56–67

G

Gadolinium oxide (Gd_2O_3), 279
Galvanostatic charge/discharge
  curves, 225*f*
  technique, 279
Graphene-based PNCs, 227–228
Graphite (anode), 251

H

Haptics, 328–329
HATN. *See* Hexaazatrinaphthalene (HATN)
Heat-sensitive, 6–13
Hexaazatrinaphthalene (HATN), 272
Hole-transporting layers (HTL), 186–188
Host polymer, 57*t*, 128
HSPS. *See* Hybridized self-powered sensor (HSPS)
Human-machine interfaces, 328–329
Hybridized self-powered sensor (HSPS), 298*f*
Hybrid materials, 36
Hydrogen
  clean and energy efficient fuel, 195–196
  clean fuel and its economy, 200–201
  elemental fuel, 198
  solar-to-hydrogen conversion efficiency, 205–206

Hydrothermal growth process, 62
Hypercross-connected polystyrene (HPS), 275
Hysteresis, 304–305

I

Impurity quenching, 174
Initial Coulombic efficiency, 254–255
Inner photoelectric effect, 178–179
Inorganic materials, 34–35
Inorganic nanofiller related factors
  nanofiller size and refractive index matching, 127
  optical response, 128
  volume fraction, 127–128
Inorganic nanofillers, 59
Inorganic UV absorbers, 122–126
In-situ polymerization, 130, 181–182
Intermolecular electron transfer processes, 175
Intermolecular forces, 253
Internal conversion (IC), 173
Intersystem conversion (ISC), 173
Intersystem crossings, 173
Intramolecular charge transfer (ICT), 170–171
Intramolecular electron charge transfer (ICT) reactions, 174–175
Intramolecular electron transfer (IET) reactions, 175
Ionic-type electro-responsive
  electro-responsive conducting, 18
  electro-responsive gels, 17–18
  electro-responsive ionic polymer-metal composites (IPMCs), 18–19

J

Jablonski diagram
  molecular mechanism of, 171–173, 172*f*

K

β-Ketoenamine conjugated microporous polymer (KECMP), 279

L

Laser diodes, 179
LCST. *See* Lower critical solution temperature (LCST)
Li-air battery. *See* Lithium-air (Li-air) battery
Light-emitting diodes (LEDs), 159, 169–170, 178, 180
  polymer-CNT composite in, 182
  structure of, 187–188, 187*f*, 191, 191*f*
Light-emitting functionalities, 102–104
Linearity, 303–304
Li-S batteries. *See* Lithium-sulfur (Li-S) battery
Li-S cathode electrode, conductive polymer/carbon composites in, 257–259, 258*f*
Lithium-air (Li-air) battery, 236–237
Lithium insertion metal oxides, 66
Lithium-ion (Li-ion) batteries, 231–234
  conjugated polymers (CPs), 267–276, 267–268*f*, 270–274*f*
  polymer-based binders, 253–255
  working mechanism of, 252*f*
Lithium iron phosphate (cathode), 251
Lithium-sulfur (Li-S) battery, 234–236, 249–251, 250*f*
  polymer-based binders, 255–257
Low-cost conjugated polymer-based opto-electronic materials, 40
Lower critical solution temperature (LCST), 6–7, 8*f*
Luminance, 162–163, 163*f*
Luminescence, 173

M

Magneto-responsive, 20–21
Maleic acid, 274–275
Memory devices, 180
Metal oxide nanofillers, 59–61
  synthetic techniques, 61–64
Metal oxides, 59
Methyl benzoate, 268
Microstructural characterizations, 95–96
Molecular photochemistry, 171–173
Molybdenum disulfide (MoS_2), 148, 150–151*f*
Morphology, 312
Multiwalled carbon nanotubes (MWCNTs), 176, 176*f*

N

Nanocomposites (NCs), 276
  PEDOT:PSS-β-$NaYF_4$:Yb^{3+}/Er^{3+} upconversion NCs, 137, 139*f*
  polymer-perovskite, 151–152, 153*f*
  polymer-quantum dot, 136
Nanofillers
  classification of, 58–67
  nanometric fillers, 57
  size, 127
Nanomaterials, 55*f*
Nanometric fillers, 57
Nanoscale, 53–54
Nano-sized metal oxides
  applications of, 65
  properties of, 65
Nanostructured porous materials, 66
Nanotechnology
  definition, 52–53
  history of, 53
Nanotechnology-enabled, 323–329
Naphthalene-based polyimide, 273
Natural graphite composites (SANGs), 269
Natural rubber (NR), 55
Nitrogen-doped porous carbon nanoparticle (NPCN), 273
N-methylpyrrolidone (NMP), 253–254
N,N'-diphenyl-1,4,5,8-naphthalenetetra-carboxylic diimide (DP-NTCDI-250), 268
Novel photonics methods, 169–170

NPCN. *See* Nitrogen-doped porous carbon nanoparticle (NPCN)
NR. *See* Natural rubber (NR)
N-substituted naphthalene tetra carboxylic diimide (NTCDI), 271
NTCDI. *See* N-substituted naphthalene tetra carboxylic diimide (NTCDI)

O

OFETs. *See* Organic field-effect transistors (OFETs)
Optical absorption, 69–72
Optical characterizations, 97–104
Optical fiber/optic fiber, 179
Optical properties, 69–76
Optical response, 128
Optimum physical blending technique, 181
Opto-electronic characterizations, 97–104
Opto-electronic devices
  applications, 157–158
  shape memory polymers (SMPs), 160–163
Opto-electronic materials
  applications of, 33*f*
  categories of, 35*f*
  energy applications, 37–46
  hybrid materials, 36
  importance of, 32–33
  inorganic materials, 34–35
  organic materials, 35–36
  radiative transitions, 36–37
Optoelectronics, 169–170
  CNT-polymer nanocomposites (CNT-PNCs) in, 180–182, 181*f*
  devices, 178–179
Organic field-effect transistors (OFETs), 41–42
Organic materials, 35–36
Organic ultraviolet absorbers, 120–122
Organo gel fiber-embedded polymer composite film, 12*f*
Organosulfur unit, 257

P

PAAc. *See* Polyacrylic acid (PAAc)
PAAm. *See* Polyacrylamide (PAAm)
P(AAm-co-DADMAC). See Poly(acrylamide-co-diallyl dimethyl ammonium chloride) (P(AAm-co-DADMAC))
PANI. *See* Polyaniline (PANI)
PAQIs. *See* Poly (anthraquinonyl imide)s (PAQIs)
Parallel displaced (PD), 171
Parallel stacked (PS), 171
PBIM. *See* Poly(bis-indolyl maleimide) (PBIM)
PBSCs. *See* Polymer-based smart composites (PBSCs)
PDA. *See* Polydiacetylene (PDA); Polydopamine (PDA) coating
PDB. *See* Poly (2, 3-dithiino-1, 4-benzoquinone) (PDB)
PDMA. *See* Poly (2-(dimethylamino) ethylmethacrylate) (PDMA)
PE. *See* Piezoelectric (PE)
PEDOT. *See* Poly(3,4-ethylenedioxythiophene) (PEDOT)
PENDI. *See* Poly(ethylene-N, N′-bis(2-ethylhexyl)-1, 4,5,8-naphthalene diimide) (PENDI)
Perovskite solar cells, 227
Perylene diimide dyes, 269
Phosphorescence, 173–174
Photo-active polymer nanocomposite layer
  electricity, 135
  material composites
    polymer one-dimensional, 144–146
    polymer two-dimensional, 146–152
    polymer-zero dimensional, 136–141
  organic photovoltaics, 135
  polymer composite, 135–136
Photocatalytic (PC) energy systems, 201–202
Photochemistry, 171–173
Photodiodes, 169–170, 178–180
Photoelectrochemical (PEC) water splitting, 202–203
Photoluminescence, 173
Photoluminescent (PL), 72
Photonic absorption, 97–102
Photonic emission, 69–72
Photonics, 169–170
Photophysical process, 171–173
Photophysics, 171–173
Photo-responsive, 13–15
Photo-responsive smart composites, 13
Photovoltaic (PV) cells, 180
π-Conjugated polymers, 42
π-electron, 170–171
π-π stacking, 170–171
π-stacking, 170–171, 171*f*
π-stacking conjugated polymers, 171
Piezocapacitive strain sensors, 299–300
Piezoelectric (PE), 19
Piezoelectric strain sensors, 294–298
Piezoresistive strain sensors, 292–294
PL. *See* Photoluminescent (PL)
Plastic optical fibers (POFs), 32, 42–43
PMDTO. *See* Poly(N-methyl-3,4-dihydrothieno [3,4-b][1,4] oxazine) (PMDTO)
PMMA. *See* Poly (methyl methacrylate) (PMMA)
PNCs. *See* Polymer nanocomposites (PNCs)
PNIPAm. *See* Poly(N-isopropylacrylamide) (PNIPAm)
P-n junction material, 178–179
P-n semiconductor diodes, 178
POFs. *See* Plastic optical fibers (POFs)

Poly (2,3-dithiino-1,4-benzoquinone) (PDB), 267
Poly (2-(dimethylamino) ethylmethacrylate) (PDMA), 71–72
Poly(3,4-ethylene dioxythiophene) (PEDOT), 220–222, 228–231, 250–251, 258, 277
Poly(acrylamide-*co*-diallyl dimethyl ammonium chloride) (AMAC), 256
Poly(acrylonitrile-methyl methacrylate) (ANMMA), 256
Poly (bis-indolyl maleimide) (PBIM), 275
Poly[ethylene-*N*,*N*′-bis(2-ethylhexyl)-1,4,5,8-naphthalene diimide] (PENDI), 273
Poly(ethylene oxide) (PEO), 255–256
Poly (methyl methacrylate) (PMMA), 269–270
Poly(*N*-isopropylacrylamide) (PNIPAm), 7
Poly(*N*-methyl-3,4-dihydrothieno[3,4-*b*][1,4] oxazine) (PMDTO), 277
Poly(styrene sulfonate), 228–231
Poly(tetrafluoroethylene) (PTFE), 255–256
Poly(vinyl pyrrolidone) (PVP), 224
Poly(vinylidene fluoride) (PVDF), 221*f*
Polyacrylamide (PAAm), 7
Polyacrylic acid (PAAc), 7
Polyacrylonitrile, 250–251
Polyaniline (PANI), 220–222, 250–251
Polydiacetylene (PDA), 12*f*, 250–251
Polydopamine (PDA) coating, 269
Polymer-based binders
  lithium-ion (Li-ion) battery, 253–255
  lithium-sulfur (Li-S) battery, 255–257
Polymer-based composites
  clean-energy fuel systems, 203–209
  conducting polymers, 196
  energy crisis, 196
  energy mitigation from fossil fuels, 198, 199*f*
  fossil fuels, 195–196
  photocatalysts/photosensitizers, 196
  research timelines, 196, 197*f*
  solar-to-chemical energy conversion, 195–196
Polymer-based photo-responsive materials, 13
Polymer-based shape memory materials, 11
Polymer-based smart composites (PBSCs)
  classification of, 3
  electrical properties, 108–111
  electro-chromic and thermo-chromic display, 1
  fillers, 2
  microstructural characterizations, 95–96
  optical and opto-electronic characterizations, 97–104
  stimuli-responsive, 3–21
  stimuli-responsive practices, 2*f*
  structural characterizations, 92–95
  surface morphological behaviors, 105–106
  surface wettability measurements, 104–105
  thermo-analytical techniques, 106–107
  universal testing machine (UTM), 108
Polymer-based strain sensors
  piezocapacitive strain sensors, 299–300
  piezoelectric strain sensors, 294–298
  piezoresistive strain sensors, 292–294
Polymer-based UV-protective materials, 119
  imperative requirements, 126–129
  inorganic UV absorbers, 122–126
  in-situ polymerization, 130
  organic UV absorbers, 120–122
  physical mechanism, 119
  surface engineering, 130
  types, 119
  UV absorbent, 120–126
Polymer-graphene, 146–148
Polymer light-emitting diodes (PLEDs), 159, 159*t*, 162–163, 184–185, 190
Polymer nanocomposites (PNCs), 92
  commercial exploits, 68*t*
  electrical properties and applications, 76–80
  energy-related applications, 219–241
  optical properties and applications, 69–76
  preparation of, 217–219
Polymer nanotechnology, 180
Polymer one-dimensional material composites
  polymer-based multiphase, 144
  polymer-silver nanowire, 144–146, 145*f*, 147*f*
Polymer-PbS quantum dot, 136–137
Polymer-perovskite, 151–152, 153*f*
Polymer-Poly (4,4',4"-tris(*N*,*N*-diphenyl-amino) triphenylamine) (PTDATA), 273
Polymers, 54–56
Polymer-silver nanowire composites, 144–146, 145*f*, 147*f*
Polymer two-dimensional material composites
  polymer-graphene composites, 146–148, 149*f*
  polymer-perovskite NCs, 151–152, 153*f*
  PTB7-MoS_2 composite, 148, 150–151*f*

Polymer-zero dimensional material composites
PEDOT:PSS-aluminum NP composites, 137–138, 140–141*f*
PEDOT:PSS-β-$NaYF_4$:Yb^{3+}/Er^{3+} upconversion NCs, 137, 139*f*
polymer-PbS quantum dot, 136–137
polymer-silver NP composites, 138–141, 142–143*f*
Poly-P5Q. *See* Poly-Pillar 5 quinone (Poly-P5Q)
Poly-Pillar 5 quinone (Poly-P5Q), 271
Polypyrrole (PPy), 220–222, 250–251
films, 268
Poly (anthraquinonyl imide)s (PAQIs), 275
Poly tetra(2-thienyl)ethylene (PTTE), 275–276
Polythiophene (PTh), 250–251, 281
Polyvinyl chloride (PVC), 280
Polyvinylidene fluoride (PVDF), 253–256
Porous organic polymers (POPs), 206–208
Powder X-ray diffraction (P-XRD), 95–96
Printable conductors, 180
PTDATA. *See* Polymer-Poly (4,4',4"-tris(*N,N*-diphenyl-amino) triphenylamine) (PTDATA)
PTTE. *See* Poly tetra(2-thienyl) ethylene (PTTE)
Pulse electrochemical method, 279
PVA/Cs_2ZnO_2 NC thick films, 14*f*
PVC. *See* Polyvinyl chloride (PVC)
PVDF. *See* Poly(vinylidene fluoride) (PVDF); Polyvinylidene fluoride (PVDF)
PVDF-TrFE copolymer, 106*f*
P-XRD. *See* Powder X-ray diffraction (P-XRD)

Q

Quantum confinement, 59
Quantum dots
polymer composites, 136
polymer-PbS quantum dot, 136–137
Quantum efficiency, 159–160, 160*f*
Quantum electronics, 169–170
Quantum yield, 174

R

Radiative transitions
absorption, 37
spontaneous emission, 37
stimulated emission, 37
Rate capability, 254–255
Recovery time, 304–305
Reduced graphene oxide (RGO), 278, 281
Reflectance, 97–102
Refractive index matching, 127
Remote and personalized health monitoring, 330*f*
Response time, 304–305
RGO. *See* Reduced graphene oxide (RGO)

S

Sandwich-type FCPC-based strain sensors, 306–307
Scanning electron microscopy (SEM), 105–106
Scratch test, 254–255
SCS. *See* Solution combustion synthesis (SCS)
Self-healing, 305–306
Self-quenching, 174
SEM. *See* Scanning electron microscopy (SEM)
Sensitivity, 300–303
Separator, 251
Shape memory effect (SME), 8
Shape memory polymers (SMPs)
polymer as material, 157–158
solar cells, 158–160
as substrate, 160–163
Shape memory PU/nickel (SMPU/Ni), 10*f*
Shuttling mechanism, 249–250, 250*f*
Single-walled carbon nanotubes (SWCNTs), 176, 176*f*
Silica (SiO_2), 216
Silver nanowires, 138–141, 142–143*f*
SiO_2. *See* Silica (SiO_2)
Skin-inspired electronics, 329–330
Smart composite, 323–329
Smart polymer-based materials, 37–46
Smart windows, 180
SME. *See* Shape memory effect (SME)
SMPU/Ni. *See* Shape memory PU/nickel (SMPU/Ni)
SnO_2. *See* Tin dioxide (SnO_2)
Soft robotics, 328–329
Solar cells, 41–42, 169–170, 178, 225–231
charge carrier mobility, 158–159
conductive polymer substrate, 158–159
device performances, 159, 159*t*
electrode applications, 159–160
external quantum efficiency (EQE), 159–160, 160*f*
optical absorption, 159–160, 160*f*
polymers, 159
Solar energy
conversion to chemical fuel
hydrogen, 200–201
photocatalytic (PC)/photoelectrochemical (PEC), 201–203
sun, 198–199
harnessing systems, 196
hydrogen fuel, 195–196
water-splitting technique, 198
Sol-gel technique, 62–64
Solution-based spin coating technique, 190
Solution combustion synthesis (SCS), 64
Solvothermal method, 268–269
Spectrofluorometry, 102–104
Spin coating method, 190
S/polyacrylonitrile composite cathodes, 250–251

S/polythiophene composite cathodes, 250–251
Spontaneous emission, 37
Sports performance monitoring, 324
Stimulated emission, 37
Stimuli-responsive
  biological stimuli, 3
  chemical stimuli, 3
  physical stimuli, 3
  responses, 5*t*
  synthetic techniques and applications, 4–5*t*
Strain sensing performance, 312–313
Strain sensors
  basic metrics, 300–306
  material selection, 307
  specific metrics, 306
Strechability, 300–303
Stretchable electrode material, 182–185, 183–184*f*
Stretchable electronics, 321–322
Structural characterizations, 92
Sulfur, 249–250
Supercapacitors, 180, 219–225
  conjugated polymers (CPs), 276–282, 277*f*, 280–282*f*
Surface engineering, 130
Surface morphological behaviors, 105–106
Surface tests, 279
Surface wettability, 104–105
Synthetic protocol, 267*f*

T

TCE. *See* Transparent conducting electrodes (TCE)
Temperature-induced color switching-type polymer-based smart composites (PBSCs), 11–13
Temperature-induced shape memory-type polymer-based smart composites (PBSCs), 8–11
TGA. *See* Thermogravimetric analysis (TGA)
Thermo-analytical techniques
  differential scanning calorimetry (DSC), 107
  thermogravimetric analysis (TGA), 107
Thermogravimetric analysis (TGA), 107
Thermo-mechanical cycle, 9*f*
Thermo-responsive, 6–13
Thermo-responsive smart colorimetric patch, 9*f*
Tin dioxide (SnO_2), 270
Tools and technique, 92–111
Top-down approach, 61–62
TPA. *See* Triphenylamine (TPA)
T-shaped interactions, 171
Transmittance, 97–102
Transparent conducting electrodes (TCE), 42
Triphenylamine (TPA), 40–41

U

UCST. *See* Upper critical solution temperature (UCST)
Ultracapacitors, 219–220
Ultraviolet
  absorbent, 120–126
  protective materials, 126–129
  visible photonic absorption, 69–72
  visible spectral tool, 99
  visible spectrophotometer, 98
  visible spectroscopy, 97–102
  visible transmittance values, 98
Universal testing machine (UTM), 108
Upconversion, 135, 137
Upper critical solution temperature (UCST), 6–7
UTM. *See* Universal testing machine (UTM)

V

van der Waals forces, 170–171
Vapor phase polymerization (VPP) method, 268
Vibrational relaxation, 171–173
Virtual reality, 328
Volume fraction, 127–128
VPP. *See* Vapor phase polymerization (VPP) method

W

Wearable sensors, 328–329*f*
Wear tests, 254–255

X

Xanthan gum (XG), 254–255

Z

Zinc oxide (ZnO), 12*f*
Zinc oxide nanofillers, 59–61
ZnO. *See* Zinc oxide (ZnO)